

https://dspace.org/

Mathematical modelling, design, and optimization of electrochemical capacitor cells

Ike, Innocent Sunday

2017

https://hdl.handle.net/10539/24089

Ike, Innocent Sunday (2017) Mathematical modelling, design and optimization of electrochemical capacitor cells, University of the Witwatersrand, Johannesburg, https://hdl.handle.net/10539/24089

Downloaded from a DSpace repository. https://dspace.org/

Mathematical Modelling, Design, and Optimization of Electrochemical Capacitor Cells



INNOCENT SUNDAY, IKE

A thesis submitted to the Faculty of Engineering and the Built Environment, University of the Witwatersrand, Johannesburg, in fulfilment of the requirements for the degree of Doctor of Philosophy in Engineering (Chemical Engineering).

Johannesburg, 2017

DECLARATION

I declare that this thesis is my own unaided work. It is being submitted for the degree of Doctor of Philosophy in Engineering to the University of the Witwatersrand, Johannesburg. It has not been submitted before for any degree or examination to any other university.

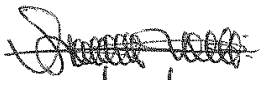

Innocent Sunday, IKE

19th...day of …June... Year …2017

ABSTRACT

The effects of self-discharge on the performance of symmetric electric double layer capacitors (EDLCs) and active electrolyte enhanced supercapacitors (AEESCs) were examined by incorporating self-discharge into electrochemical capacitor (EC) models during charging and discharging. The effects of self-discharge on the performance of asymmetric ECs were also studied by including applicable self-discharge mechanisms into mass transfer and charge conservation equations during charging and discharging. Sources of self-discharge in capacitors are several impurities, side-reactions, redox reactions and electric double layer's (EDL's) instability. Incorporation of self-discharge into symmetric and asymmetric EC models, created a platform to reduce the number of experiments to determine the minimum allowable amount of impurities and redox species in components of the device for maximum performance. It was observed that key self-discharge parameters to be tuned in order to suppress the EC self-discharge rate are concentration of the shuttle impurities, concentration of redox species, and the thickness of the separator. Tuning key self-discharge parameters of a symmetric device with both side-reactions/redox reactions and EDLs instability self-discharges, improved first and second charge-discharge cycle efficiency η_{E1} and η_{E2}. Thes charge-discharge cycle efficiencies (η_{E1} and η_{E2})were enhanced from 38.13% and 38.14% to 80.54% and 81.56% respectively, compared with 84.24% and 84.25%, respectively in similar capacitor without self-discharge. The tuning process also improved the energy efficiencies η_{E1} and η_{E2} of the asymmetric device with both side-reactions/redox reactions and EDL's instability self-discharges from 67.21% and 75.00% to 87.21% and 88.70% respectively, compared with 90.72% and 90.82%, respectively in a similar capacitor without self-discharge. Energy loss by self-discharge in the symmetric capacitor with tuned key self-discharge parameters was reduced from 28.38Wh in untuned to 5.60Wh, while that of the asymmetric capacitor with tuned key self-discharge parameters was reduced from

59.53Wh in untuned to 7.43Wh. Fast charging and discharging of the EC greatly reduced the self-discharge rate, compared with slow charging and discharging. In symmetric and asymmetric capacitors, both EDL's instability and side-reactions and/or reactions self-discharges occurs in significant measure but side-reactions or reactions contributed to the majority of the self-discharges. It was shown that models that incorporated self-discharge give more practical evaluation of voltage decay and energy dissipation during self-discharge. The influence of different charging current densities, charging times and several structural designs on symmetric EC performance such as capacitance, energy density and power density was investigated through modelling and simulation. The effects of different charging current densities, charging times and several structural designs on asymmetric EC performance via modelling and simulation can be investigated, and the results would be similar. The difference between symmetric and asymmetric ECs is that symmetric use the same type of electrode while asymmetric use different types of electrodes. Clear understanding of the effects of different structural design variables and operating conditions on capacitors' performance will guide in optimal design and fabrication of high performance ECs. The operating conditions and design configurations examined are charging current density, charging times, electrode and electrolyte effective conductivity, electrode thickness and electrode porosity. It was revealed that ECs with low electrode and electrolyte effective conductivities can only be effectively charged at a low current density for extended periods of time. ECs with high concentrations of impurity ions and redox species exhibit high self-discharge rates, which result in voltage decay after charging. Reduction of charging time by charging the EC fast, greatly reduced the rate of self-discharge compared with the slow charging process. The simulation showed that the typical electrode length scale over which the liquid potential drop occurs and electrode utilization can be used as a design parameter to optimize electrode thickness (effective

thickness) of the EC which should function within a specific current density range. This is also a guideline that can be used to determine the optimum electrodes thickness (100% electrodes utilization), optimum charging current density and optimum charging time for cells of a given voltage, electrode's thickness, and electrodes and electrolyte's effective conductivities. The energy density of the capacitor with specific electrodes and electrolyte effective conductivities was increased 2.125, 4.750 and 10.75 folds by reducing the electrode's thickness 1.33, 2.00, and 4.00 folds, respectively. The power density of the capacitor, with specific electrodes thickness, and given electrode and electrolyte effective conductivities charged at a specific current density, increased by a factor of 10, 100 and 1000, when the charging rate was increased 10, 100 and 1000, times respectively. The power density of the capacitor with specific electrodes thickness, and a given electrodes and electrolyte effective conductivities, also increased approximately eleven-fold when the electrode's thickness was reduced four-fold under a given charging conditions. The ragone plots generated for different electrode sizes via modeling and simulation, can be used to select optimum electrode dimensions to attain certain energy and power densities specifications. Theoretical expressions for performance parameters of different ECs were optimized by writing MATLAB scripts to solve them and also via the MATLAB R2014a optimization tool box. Performances of different kinds of ECs at given circumstances were compared through theoretical equations and simulation of various models, subject to the conditions of device components using optimal K_{BMopt} and K_{Eopt}, as well as the symmetric EDLC experimental data. The storable energy E_{ch}, maximum energy density ED_{max} and power density PD_{max} of symmetric and asymmetric EC using suitable electrode mass, operating potential range ratios and proper organic electrolyte (optimum K_{BMopt} and K_{Eopt}) were 562.78Wh, 382.42Wh/kg & 76.29W/kg and 1304.30Wh, 837.00Wh/kg & 167W/kg, respectively. Estimations of performance parameters were feasible and achievable once

details of electrodes mass ratio, operating potential range ratio and specific capacitance of electrolyte are known. Performances of asymmetric EC with suitable electrode mass and operating potential range ratios using aqueous electrolytes, and that with suitable electrode mass, operating potential range ratios and organic electrolyte with appropriate operating potential range and specific capacitance were 2.20 and 5.56 folds, respectively, greater than those of symmetric EDLC and asymmetric EC using the same aqueous electrolyte. This enhancement came together with reduction in cell mass and volume. Storable and deliverable energies of the asymmetric EC with suitable electrode mass and operating potential range ratios using proper organic electrolyte were also a factor of 12.9 greater than those of symmetric EDLCs using aqueous electrolyte reduction in cell mass and volume by a factor. Storable energy, energy density and power density of asymmetric EDLCs with suitable electrode mass and operating potential range ratios, using proper organic electrolyte, were a factor of 5.56 higher than those of similar symmetric EDLCs using aqueous electrolyte reduction in cell mass and volume by a factor 1.77. These results can obviously reduce the number of experiments needed to determine the optimum manufacturing state of ECs. They also demonstrated that introduction of an asymmetric electrode and organic electrolyte was very successful in improving performance of the EC with reduction in cell mass and volume. Introduction of an asymmetric EDLC with the same type of electrode, and suitable electrodes mass ratio, working potential range ratios and proper organic electrolyte, equally enhanced the performance of a conventional symmetric EDLC using aqueous electrolyte with reduction in cell mass and volume. These results can be a guideline for design, fabrication and operation of electrochemical capacitors with outstanding performance in terms of high storable energy, energy and power densities.

DEDICATION

This research work is dedicated to Almighty God, whose thoughts and plans are of good and not of evil, to give me an expected end. All I am and all I have were absolutely received from Him.

Also to my beloved wife, Calista Ndidiamaka Ike,the wonderful and peculiar children God gave us, my parents Mr and Mrs Fidelis .O. Ike, and to my brothers and sisters, for their inestimable support and being my source of strength and such a bundle of joy throughout the years of my study.

ACKNOWLEDGMENTS

Firstly, my profound gratitude goes to the Almighty God for His infinite grace, mercies and divine providence. An unidentified but real debt is warmly acknowledged to the Almighty God, the author of knowledge and understanding.

The timely and constructive comments, immerse supervision, motivation and valuable supports of my supervisors, Professor Sunny E. Iyuke, Professor Iakovos Sigalas and Professor Kenneth I. Ozoemena during the course of this research cannot be overemphasized. I inmensely appreciate such dedicated, clear and directional supervision.

The financial assistance of the National Research Foundation (NRF), Materials for Energy Research Group (MERG), the DST/NRF Centre of Excellence in Strong Materials (CoE-SM) and Financial Aid Office of the University of the Witwatersrand, South Africa, towards this research is hereby acknowledged.

My special appreciation goes to the management of Federal University of Technology Owerri, (FUTO) Nigeria in particular, and the Federal Republic of Nigeria at large, for their dedication and commitment in training their academic staff through Tertiary Education Trust Fund (TETfund) Academic Staff Training and Development (AST&D). Also to my big Boss Engr (Sir) Vita O. Abba, former Pro Chancellor of Federal University of Technology Owerri, (FUTO) Nigeria, for his contributions in my academic career and life at large.

Professor Alexander Quandt and Dr. Robert Warmbier of School of Physics, University of Witwatersrand, are greatly appreciated for their valuable contributions and scientific guidance to this work. My special thanks goes to Dr. Aderogba Adebayo of Department of Mathematics, Obafemi Awolowo University, Ile-Ife, Nigeria, who sacrificed immensely in writing Matlab scripts used in running computer programmes in the work.

I sincerely acknowledge the efforts and contributions of my mentors: Professor L. E. Aneke, Professor F.I. Ezema and Mr. F.C Ugwuanyi who immensely contributed academically, spiritually, materially and otherwise to the success of this work. Also to the entire Jesus Generation Ministry (JGM) and Deeper Life Campus Fellowship (DLCF) University of the Witwatersrand Chapter for their earnest prayers unto God for me.

I ever remain thankful and grateful to God Almighty for my lovely wife, Calista, for her wonderful supports, prayers, patience, sacrifices and forbearance; my mother, Mrs Caroline, and my siblings: Peter, Cyprain, Celestine and Jane for their encouragements throughout this period.

The contribution and support of colleague and research mate, Mrs Sharona Melchior is highly acknowledged. Also, each member of the Nanotechnology and Petroleum Research Group of the University of the Witwatersrand is also acknowledged for their in-depth and knowledgeable contribution through our weekly research meetings.

In conclusion, every glory and honour goes to the Most High God who linked up, in a special way, all that have been necessarily involved in the research work.

LIST OF PUBLICATIONS

1. **I.S. Ike,** I. Sigalas, and S. E. Iyuke, **"**Understanding Performance Limitation and Suppression of Leakage Current or Self-Discharge in Electrochemical Capacitors: A Review", *Phys. Chem. Chem. Phys.*, 2015, **18**, 661–680.

2. **I.S. Ike** and S. E. Iyuke, "*Mathematical Modeling and Simulation of Supercapacitors*" In **Nanomaterials in Advanced Batteries and Supercapacitors** (Edited by K.I.Ozoemena and S.W. Chen) Springer Publishing, New York, USA, 2016, Chapter 15 pp 515-562; DOI: 10.1007/978-3-319-26082-2; Online ISBN: 978-3-319-26082-2

3. **I.S. Ike**, I. Sigalas, and S. E. Iyuke, "The Effects of Self-Discharge on the Performance of Symmetric Electric Double Layer Capacitors and Active Electrolyte Enhanced Supercapacitors: Insights from Modeling and Simulation", *Journal of Elec Materi.* (2017) 46 (2) 1163-1189. doi:10.1007/s11664-016-5053-9.

4. **I.S. Ike**, I. Sigalas, and S. E. Iyuke, "The Effects of Self-Discharge on the Performance of Asymmetric/Hybrid Electrochemical Capacitors: Insights from Modeling and Simulation", under review with *Journal of Elec Materi.,* revised version based on reviewer's comments was submitted on May 16, 2017.

5. **I.S. Ike,** I. Sigalas, and S. E. Iyuke, "The Influences of Operating Conditions and Design Configurations on the Performance of Symmetric Electrochemical Capacitors"; *Phys. Chem. Chem. Phys.*, 18 (2016) 28626–28647.

6. **I.S. Ike,** I. Sigalas, and S. E. Iyuke, "Optimization of design parameters and operating conditions of electrochemical capacitors for high energy and power performances", *Journal of Elec Materi.* (2017) 46 (3) 1692-1713. doi:10.1007/s11664-016-5213-y.

7. **I.S. Ike,** I. Sigalas, and S. E. Iyuke, "Modelling and Optimization of Electrodes Utilization in Symmetric Electrochemical Capacitors for high Energy and Power", *Journal of Energy Storage* 12 (2017) 261–275.

TABLE OF CONTENTS

COVER PAGE.....i

DECLARATION.....ii

ABSTRACT.....iii

DEDICATION.....vii

ACKNOWLEDGMENTS.....viii

LIST OF PUBLICATIONS.....x

TABLE OF CONTENTS.....xi

LIST OF FIGURES.....xvii

LIST OF TABLES.....xxvi

LIST OF SYMBOLS.....xxviii

CHAPTER ONE.....1

1.0 Introduction.....1

1.1 Electric Double Layer Capacitors.....4

1.2 Pseudocapacitors.....6

1.3 Asymmetric/Hybrid Electrochemical Capacitors.....8

1.4 Materials of Electrochemical Capacitors.....9

1.4.1 Electrode Materials.....10

1.4.2 Layered Materials.....11

1.4.3 Electrolyte Materials.....13

1.5 Motivations of the Current Study.....14

1.6 Aims and Objectives of the Research.....17

1.7 Structure of the Thesis.....18

CHAPTER TWO.....21

2.0 Literature review.....21

2.1 Mathematical Modelling and Simulation of Supercapacitors.....21

2.2 Current status of electrochemical capacitors modelling and simulation.....25

2.2.1 Empirical models 25
2.2.2 Dissipation transmission line models 29
2.2.3 Continuum models (Poisson-Nernst-Planck Equations). 33
2.2.4 Atomistic models (Monte Carlos molecular dynamics) 35
2.2.5 Quantum models (Ab initio quantum chemistry and DFT) of electrochemical capacitors. 41
2.2.6 Simplified analytical models. 43
2.3 Energy and power density of electrochemical capacitors. 45
2.4 Heat production and heat modelling of electrochemical capacitors. 49
2.5 Modelling challenges of electrochemical capacitors. 52
2.6 Summary 54
2.7 Understanding Performance Limitation and Suppression of Leakage Current or Self-Discharge in Electrochemical Capacitors: A Review 56
2.8 Self-Discharge 57
2.9 Distinguishable mechanisms of self-discharge. 60
2.9.1. Self-discharge due to overcharged potentials of polarized electrodes. 62
2.9.2. Parasitic redox reaction of impurities like oxygen groups and metals in electrolyte and electrodes. 63
2.9.3. Possible short-circuits of the anode and cathode from improperly sealed bipolar electrodes (leakage current). 72
2.9.4. Non-uniformity of charge acceptance along the surface of electrode material pores (charge redistribution). 72
2.11 Progress made in EDLCs and pseudocapacitors self-discharge 76
2.12 Summary 77
CHAPTER THREE 79
3.0 Derivation of the Models 79
3.1 Homogeneous/symmetric electric double layer capacitors with electric double layer (EDL) electrodes. 79

3.1.1 For the negative electrode of electric double layer capacitors. 79

3.3.2 Self-discharge mechanisms in symmetric and asymmetric electrochemical capacitors. 89

3.1.3 For the separator 93

3.1.4 For the positive electrode of electric double layer capacitors. 94

3.2 Homogeneous/symmetric electrochemical capacitors with only composite electrodes. 95

3.2.1 The negative electrode of electrochemical capacitors with only composite electrodes. 96

3.2.2 The separator 105

3.2.3 The positive electrode of electrochemical capacitors with only composite electrodes. 105

3.3 Heterogeneous/asymmetric electrochemical capacitors with a negative EDLC electrode and positive composite electrode. 107

3.3.1 The negative electrode of electrochemical capacitor with EDLC electrode. 108

3.3.2 The separator 109

3.3.3 The positive electrode of electrochemical capacitors with composite electrode... 109

3.4 Homogeneous/symmetric electrochemical capacitors with only redox couple electrode. 111

3.4.1 The negative electrode of electrochemical capacitors with redox couple electrode. 111

3.4.2 The positive electrode of electrochemical capacitors with redox couple electrode. 114

3.5 Theoretical modelling for performance of electrochemical capacitors in terms of energy and power densities. 115

3.5.1 Symmetric electrochemical capacitor with aqueous electrolyte..... 116

3.5.2 Symmetric electrochemical capacitor with organic electrolyte..... 117

3.5.3 Asymmetric electrochemical capacitor with aqueous electrolyte 119

3.5.4 Asymmetric electrochemical capacitor with organic electrolyte. 121

3.5.5 Optimization of ECs design parameters and operating conditions for high energy and power performances. 123
CHAPTER FOUR 125
4.0 Solutions to the Models 125
4.1 Homogeneous/symmetric electric double layer capacitors (EDLCs) 125
4.2 Homogeneous/symmetric electrochemical capacitors without self-discharge. 126
4.3 The Separator 126
4.4 Homogeneous/Symmetric electrochemical capacitors with self-discharge. 130
4.5 Heterogeneous/Asymmetric electrochemical capacitor with negative EDLC electrode, positive faraday electrode and without self-discharges. 139
4.6 Heterogeneous/Asymmetric electrochemical capacitor with negative EDLC electrode, positive faraday electrode and with self-discharges 141
4.7 Heterogeneous/Asymmetric electrochemical capacitor with positive EDLC electrode, negative faraday electrode and without self-discharge. 144
4.8 Heterogeneous/Asymmetric electrochemical capacitor with positive EDLC electrode, negative faraday electrode and with self-discharge effects. 146
4.9 Homogeneous/Symmetric electrochemical capacitors with only faraday electrodes 148
4.10 Numerical solutions of the models 156
4.10.1 Numerical solutions of the models for EDLCs without self-discharge effects 156
4.10.2 Numerical solutions of the models for EDLCs with self-discharge effects. 158
4.10.3 Numerical solutions of the models with composite electrode and self-discharge effects 160
4.11 Optimization of ECs design parameters and operating conditions for high energy and power performances 166
4.12 Model Validation of the electrochemical capacitor 168
CHAPTER FIVE 174
5.0 Results and Discussions 174

5.1 The Effects of Self-Discharge on the Performance of Symmetric Electric Double Layer Capacitors and Active Electrolyte Enhanced Supercapacitors: Insights from Modelling and Simulation. 174
5.1.2 Discussions 175
5.2 The Effects of Self-Discharge on the Performance of Asymmetric/Hybrid Electrochemical Capacitors: Insights from Modeling and Simulation. 196
5.2.2 Discussions 197
5.3 The Influences of Operating Conditions and Design Configurations on the Performance of Symmetric Electrochemical Capacitors 216
5.3.2 Discussions 216
5.4 Optimization of design parameters and operating conditions of electrochemical capacitors for high energy and power performances 252
5.4.2 Discussions 253
CHAPTER SIX 278
6.0 Conclusions and Recommendations 278
6.1 Conclusions 278
6.1.1 The Effects of Self-Discharge on the Performance of Symmetric Electric Double Layer Capacitors and Active Electrolyte Enhanced Supercapacitors: Insights from Modelling and Simulation 279
6.1.2 The Effects of Self-Discharge on the Performance of Asymmetric/Hybrid Electrochemical Capacitors: Insights from Modeling and Simulation. 281
6.1.3 The Influences of Operating Conditions and Design Configurations on the Performance of Symmetric Electrochemical Capacitors 283
6.1.4 Optimization of electrochemical capacitors design parameters and operating conditions for high energy and power performances. 285
6.2 Contributions to knowledge 287
6.3 Recommendations 288
REFERENCES 290
Appendices 317

Appendix A 323
Homogeneous/symmetric electrochemical capacitors without self-discharge. 323
Appendix B 328
Homogeneous/Symmetric electrochemical capacitors with self-discharge. 328
Appendix C 334
Homogeneous/Symmetric electrochemical capacitors with only faraday electrodes 334
Appendix D 340
Numerical solutions of the models for EDLCs without self-discharge effects 340
Appendix E 345
Numerical solutions of the models for EDLCs with self-discharge effects 345
Appendix F 349
Numerical solutions of the models with composite electrode and self-discharge effects .. 349
Appendix G 360
MATLAB scripts for analytical numerical solutions of EDLCs models with and without self-discharge 360
MATLAB scripts for the numerical solutions of EDLCs models without self-discharge . 362
MATLAB scripts for the numerical solutions of EDLCs models with self-discharge 363

LIST OF FIGURES

Figure1.1: A diagrammatic representation of electric double layer capacitors (EDLCs) with the charge storage mechanism. 5
Figure1.2: A diagrammatic representation of pseudocapacitors with the charge storage mechanism. 7
Figure1.3: A diagrammatic representation of asymmetric or hybrid ECs with the charge storage mechanism. 8
Figure 2.1: Illustration of basic components and design of an EDLC. Arrows indicate the direction of movement for cations and anions [98]……..22

Figure 2.2**:** Proposed equivalent circuits of a double-layer capacitor at a constant current charging (a) and discharging (b) in the absence of parallel leakage phenomena and chemical disintegration of the solvent. K: electric switcher; R_{esr}: equivalent series resistance; I_{cell}: constant current for charging or discharging the capacitor; V_{cell}: capacitor cell voltage; C_{dl}: double-layer capacitance; V_{sc}: voltage across the C_{dl}; and i_{sc}: current used to charge or discharge respectively [22]. 26
Figure 2.3**:** Proposed equivalent circuits for a double-layer capacitor at a constant current charging (a) and discharging (b) in the presence of electrochemical decomposition of the solvent. K: electric switcher; R_{esr}: equivalent series resistance; R_{lk}: parallel leakage resistance; i_{lk}: parallel leakage current; I_{cell}: constant current for charging or discharging; V_{cell}: capacitor cell voltage; i_F: current of solvent electrochemical decomposition; C_{dl}: double-layer capacitance; i_{sc}: current used to charge or discharge the double-layer capacitance; V_F: electrode potential of the solvent electrochemical decomposition; and V_{sc} (=V_F): voltage across the double-layer capacitance, respectively [22]. 28
Figure 2.4: De Levie's transmission line equivalent circuit for an electrolyte filled conducting pore [105]. 29
Figure 2.5**:** (Colour online) Extension of circuit model outside pore [105]. 30
Figure 2.6**:** One dimensional pore [106]. 30
Figure 2.7: Half porous electrode model discretization [106]. 31
Figure 2.8**:** Equivalent circuit for capacitance and series resistance dependences as a function of frequency, voltage and temperature [102]. 32

Figure 2.9**:** Schematics of the electric double layer structure showing the arrangement of solvated ions near the electrode/electrolyte interface in the Stern layer and the diffuse layer. (a) Helmholtz model, (b) Gouy-Chapman model, and (c) Gouy-Chapman-Stern model [116]. 34
Figure 2.10**:** Schematic representations of a) the symmetric supercapacitor and b) the hybrid asymmetric supercapacitor with electrode dimensions not drawn to scale [89].....45
Figure 2.11: Schematic illustration on the self-discharge process (Note: ΔE-potential field;.58
Figure 2.12 Mechanism of charge discharge process for symmetric EDLC and energy storage mechanism for pseudocapacitor [191]. 59
Figure 2.13 Diagrammatic illustration of the electrode-electrolyte interface in electrochemical capacitors; (a) chemical reaction at electrode surface leads to loss of charge, (b) implementation of thin stopping membrane reduces rate of migration and improves energy stocking potential [220]. 65
Figure 2.14**:** Schematic illustration of the mechanism of charge and self-discharge of active electrolyte improved supercapacitor, AEESCs [244]. 70
Figure 2.15 Two master plans for preventing the defection of the mobile electrolyte among electrodes: (a) Utilizing ion-interchange layer separator; (b) Using a peculiar mobile electrolyte that is transformed into insoluble sorts on charge phenomenon [244]. 71
Figure 2.16 Schematic illustration of ion dispensation model for various charge periods: left, long charging; right, short charging [248]. 75
Figure 3.1: A symmetric electric double layer capacitor (EDLC) showing various functional layers on macroscale……79
Figure 3.2: A symmetric electrochemical capacitor cell with only composite electrodes showing various functional layers on macroscale 95
Figure 3.3: An asymmetric electrochemical capacitor with a negative EDL electrode and positive composite electrode showing various functional layers on macroscale.....108
Figure 3.4: A symmetric supercapacitor cell with only redox couple electrodes showing various functional layers on macroscale 111
Figure 5.1: Potential distribution profiles within the negative electrode of different electrode and electrolyte effective conductivities values α_1 and α_2 as a function of position after constant current charge process for (a) capacitors without self-discharge (b) capacitors with only EDLs instability self-discharge, and (c) capacitors with both side-reactions/redox reactions and EDLs instability self-discharge……179

Figure 5.2: Potential distribution profiles within the negative electrode of different electrode and electrolyte effective conductivities values α_1 and α_2 as a function of position after constant current discharge process for (a) capacitors without self-discharge (b) capacitors with only EDLs instability self-discharge, and (c) capacitors with both side-reactions/redox reactions and EDLs instability self-discharge.....180
Figure 5.3: Electrochemical capacitor voltage dependence on time during 18000s duration of constant current charge process for (a) capacitors without self-discharge, (b) capacitors with only EDLs instability self-discharge, and (c) capacitors with both side-reactions/redox reactions and EDLs instability self-discharge.....181
Figure 5.4: Electrochemical capacitor voltage dependence on time during 18000s duration of constant current discharge process for (a) capacitors without self-discharge, (b) capacitors with only EDLs instability self-discharge, and (c) capacitors with both side-reactions/redox reactions and EDLs instability self-discharge.....183
Figure 5.5: Electrochemical capacitor voltage dependence on time during 18000s duration of constant current charge process from 0V to 1.2V for (a) capacitors without self-discharge, (b) capacitors with only EDLs instability self-discharge, and (c) capacitors with both side-reactions/redox reactions and EDLs layers instability self-discharge. 184
Figure 5.6: Electrochemical capacitor voltage dependence on time during 180s duration of constant current charge process from 0V to 1.2V for (a) capacitors without self-discharge, (b) capacitors with only EDLs instability self-discharge, and (c) capacitors with both side-reactions/redox reactions and EDLs instability self-discharge. 185
Figure 5.7: Electrochemical capacitor voltage dependence on time during 18000s duration of constant current discharge process from 1.2V to 0V for (a) capacitors without self-discharge, (b) capacitors with only EDLs instability self-discharge, and (c) capacitors with both side-reactions/redox reactions and EDLs instability self-discharge. 186
Figure 5.8: Electrochemical capacitor voltage dependence on time during 180s duration of constant current discharge process from 1.2V to 0V for (a) capacitors without self-discharge, (b) capacitors with only EDLs instability self-discharge and (c) capacitors with both side-reactions/redox reactions and EDLs instability self-discharge. 187
Figure 5.9: The voltage $U_S(t)$ dependence on time for symmetric EDLCs with effective conductivities of 0.05S/cm during 18000s duration of constant current charge process from 0V to 1.2V for (a) capacitors without self-discharge, (b) capacitors with only EDLs instability

self-discharge, and (c) capacitors with both side-reactions/redox reactions and EDLs instability self-discharge. 188
Figure 5.10: The voltage $U_S(t)$ dependence on time for symmetric EDLCs with effective conductivities of 0.05S/cm during 180s duration of constant current charge process from 0V to 1.2V for (a) capacitors without self-discharge, (b) capacitors with only EDLs instability self-discharge, and (c) capacitors with both side-reactions/redox reactions and EDLs instability self-discharge. 190
Figure 5.11: Dependence of voltage $U_S(t)$ decay on time of storage for symmetric EDLC of different electrodes effective conductivities with (a) only EDLs instability self-discharge with $J_{VRM} = 1.25\text{x}10^{-3}$A/cm^2, (b) both side-reactions/redox reactions and the EDLs instability self-discharge with $J_{VRM} = 1.25\text{x}10^{-3}$A/cm^2 and $J_{VR1} = 3.2\text{x}10^{-3}$A/cm^2, (c) only EDLs instability self-discharge with $J_{VRM} = 4.0\text{x}10^{-4}$A/cm^2, and (d) both side-reactions or redox reactions and EDLs instability self-discharge with $J_{VRM} = 4.0\text{x}10^{-4}$A/cm^2 and $J_{VR1} = 3.2\text{x}10^{-3}$A/cm^2. 194
Figure 5.12: Dependence of voltage $U_S(t)$ decay on time of storage for symmetric EDLC with different electrodes effective conductivities and (a) only EDLs instability self-discharge with $J_{VR} = 4.0\text{x}10^{-5}$A/cm^2 and (b) both side-reactions/redox reactions and EDLs instability self-discharge with $J_{VR} = 4.0\text{x}10^{-5}$A/cm^2 and $J_{VR1} = 9.58\text{x}10^{-5}$A/cm^2.. 195
Figure 5.13: (a) Amount of charge moving from negative (cathode) electrode of asymmetric ECs into the solution over time due to redox reactions self-discharge using Equation 4.36; (b) potential change in negative electrode over time due to redox reactions self-discharge using Equation 4.52; and (c) the potential change over time due to both EDLs instability and redox reactions self-discharge. 198
Figure 5.14: The voltage dependence on time in ECs with different parameters charged for 18000s from 0.8V to 2.0V in (a) capacitors without self-discharge; (b) when devices with different parameters are discharged for 18000s from 2.0V to 0.8V in capacitors without self-discharge; (c) charging with self-discharge; and (d) when devices with different parameters are discharged for 18000s from 2.0V to 0.8V for capacitors with self-discharge. 200
Figure 5.15: The voltage dependence on time in ECs with different parameters charged for 1800s from 0.8V to 2.0V in (a) capacitors without self-discharge; (b) when devices with different parameters were discharged for 1800s from 2.0V to 0.8V in capacitors without self-discharge; (c) charging with self-discharge; and (d) when devices with different parameters were discharged for 1800s from 2.0V to 0.8V in capacitors with self-discharge. 202

Figure 5.16: The ECs voltage dependence on time when devices with different parameters were charged for 180s from 0.8V to 2.0V in (a) capacitors without self-discharge; (b) when devices with different parameters were discharged for 180s from 2.0V to 0.8V in capacitors without self-discharge; (c) charging with self-discharge; and (d) when devices with different parameters were discharged for 180s from 2.0V to 0.8V in capacitors with self-discharge..203
Figure 5.17: The ECs voltage dependence on time when devices with different parameters are charged for 18s from 0.8V to 2.0V in (a) capacitors without self-discharge; (b) when device with different parameters are discharged for 18s from 2.0V to 0.8V in capacitors without self-discharge; (c) charging with self-discharge; and (d) when devices with different parameters are discharged for 18s from 2.0V to 0.8V in capacitors with self-discharge.....204
Figure 5.18: The voltage decay over time in asymmetric electrochemical capacitors with different electrodes effective conductivities by both redox reactions and EDLs instability self-discharge after the device was charged from voltage of 0.8V to 2.0V at current density of (a) 0.00532A/cm^2 for 18000s charging time; (b) 0.0532A/cm^2 for 1800s charging time; (c) 0.532A/cm^2 for 180s charging time; and (d) 5.32A/cm^2 for 18s charging time.....206
Figure 5.19: The voltage decay over time in asymmetric electrochemical capacitors with electrodes effective conductivity of 0.05S/cm by both redox reactions and EDLs instability self-discharge after device are charged from voltage of 0.8V to 2.0V at current density of (a) 0.00532A/cm^2 for 18000s charging time; (b) 0.0532A/cm^2 for 1800s charging time; (c) 0.532A/cm^2 for 180s charging time; and (d) 5.32A/cm^2 for 18s charging time.....207
Figure 5.20: (a) The charging time of button asymmetric EC with 1 molL^{-1} Na_2SO_4 aqueous electrolyte solution charged at different current densities; (b) The discharging time of a button asymmetric EC with 1 molL^{-1} Na_2SO_4 aqueous electrolyte solution discharged at different current densities; (c) The charging time of a button asymmetric EC with 2 molL^{-1} KOH aqueous electrolyte solution charged at different current densities; (d) The discharging time of a button asymmetric EC with 2 molL^{-1} KOH aqueous electrolyte solution discharged at different current densities.....211
Figure 5.21: (a) Comparison of charging time of simulation with experiment in asymmetric EC with 1 molL^{-1} Na_2SO_4 aqueous electrolyte at different current densities; (b) Comparison of discharging time of simulation with experiment in asymmetric EC with 1 molL^{-1} Na_2SO_4 aqueous electrolyte at different current densities; (c) Comparison of charging time of simulation with experiment in asymmetric EC with 2 molL^{-1} KOH aqueous electrolyte at different current densities; (d) Comparison of discharging time of simulation with experiment in asymmetric EC with 2 molL^{-1} KOH aqueous electrolyte at different current densities.....212

Figure 5.22: The voltage decay due to self-discharge in capacitors with different electrodes effective conductivity α_1 under storage condition after charged to 2.0V for (a) devices with the following parameters (N=10^{20}cm^{-3},w_{sp}=0.1cm, J_{VR} =1.25x10^{-3}A/cm^2, C_{Ox} =3.0x10^{-4}mol/cm^3, D_{Ox} =1.8x10^{-5}cm^2/s and J_{VR1}=3.0x10^{-3}A/cm^2); and (b) devices with the following modified self-discharge parameters (N=10^{19}cm^{-3},wsp=0.1cm, J_{VR} =0.0004A/cm^2, C_{Ox} = 3.0x10^{-5}mol/cm^3, D_{Ox} = 1.8x10^{-6}cm^2/s and J_{VR1}=3.0x10^{-4}A/cm^2). 215
Figure 5.23: Potential distribution profiles within electrode of different electrode and electrolyte effective conductivities values α_1 and α_2 as a function of position after constant current charge process in capacitors (a) without self-discharge (b) with only EDLs instability self-discharge, and (c) with both side-reactions/redox reactions and EDLs instability self-discharge. 220
Figure 5.24: Solid-phase potential drop in capacitors of the same electrode thickness charged at various current densities and of electrode and electrolyte effective conductivities of (a) α_1 = 50S/cm and α_2 = 0.5S/cm; (b) α_1 = 5S/cm and α_2 = 0.05S/cm; liquid-phase potential drop in capacitors of the same electrode thickness charged at various current densities and of electrode and electrolyte effective conductivities of (c) α_1 = 50S/cm and α_2 = 0.5S/cm; and (d) α_1 = 5S/cm and α_2 = 0.05S/cm. 224
Figure 5.25: Solid-phase potential drop in capacitors of the same electrode thickness charged at various current densities and of electrode and electrolyte effective conductivity of (a) α_1 = 0.5S/cm and α_2 = 0.005S/cm; (b) α_1 = 0.05S/cm and α_2 = 0.0005S/cm; liquid-phase potential drop in capacitors of the same electrode thickness charged at various current densities and electrode and electrolyte effective conductivity of (c) α_1 = 0.5S/cm and α_2 = 0.005S/cm; and (d) α_1 = 0.05S/cm and α_2 = 0.0005S/cm. 227
Figure 5.26: Charging times of capacitors of the same electrode thickness and of electrode and electrolyte effective conductivity charged at various current densities with (a) α_1 =50S/cm and α_2 = 0.5S/cm; (b) α_1 =5S/cm and α_2 =0.05S/cm; (c) α_1 = 0.5S/cm and α_2 = 0.005S/cm; and (d) α_1 = 0.05S/cm and α_2 = 0.0005S/cm. 228
Figure 5.27: The voltage decay in symmetric ECs of different electrodes effective conductivities over time by both redox reactions and EDLs instability self-discharge after devices were charged from 0V to 1.2V at current density of (a) 0.00532A/cm^2 for 18000s

charging time; (b) 0.0532A/cm^2 for 1800s charging time; (c) 0.532A/cm^2 for 180scharging time; and (d) 5.32A/cm^2 for 18s charging time. 230
Figure 5.28: The length over which liquid potential drop occurs in electrodes $[w_e]$ of device of different effective conductivities at different current densities from (a) Simulations; (b) simulation, Kazaryan et al. and Sun et al. experiments; (c) simulation, Ma et al. 1- with 1 molL^{-1} Na_2SO_4 and Ma et al. 2- with 0.5 molL^{-1} Na_2SO_4 aqueous electrolytes; and (d) simulation, Kazaryan et al., Sun et al., Ma et al. 1- with 1 molL^{-1} Na_2SO_4 and Ma et al. 2- with 0.5 molL^{-1} Na_2SO_4. 232
Figure 5.29: Electrodes effective thickness in capacitor with a given electrodes thickness and different electrolyte effective conductivities, charged at different current densities: with effective conductivities (a) α_1 = 5S/cm and α_2 = 0.5S/cm; (b) α_1 = 5S/cm and α_2 = 0.05S/cm; (c) α_1 = 5S/cm and α_2 = 0.005S/cm; and (d) α_1 = 5S/cm and α_2 = 0.0005S/cm. 234
Figure 5.30: Electrodes utilization in capacitor with a given electrodes thickness and different electrolyte effective conductivities, charged at different current densities: with effective conductivities (a) α_1 = 5S/cm and α_2 = 0.5S/cm; (b) α_1 = 5S/cm and α_2 = 0.05S/cm; (c) α_1 = 5S/cm and α_2 = 0.005S/cm; and (d) α_1 = 5S/cm and α_2 = 0.0005S/cm. 235
Figure 5.31: Specified capacitance of various electrode widths at various current densities in Farad (a) per square centimetre (cm^2), and (b) per kilogram of electrochemical capacitor. .239
Figure 5.32: Variation of specific capacitance per kilogram of symmetric button capacitor with charging current density in device with $Mn_3(PO_4)_2$ composite electrodes and different aqueous electrolytes (a) 1 molL^{-1} Na_2SO_4, (b) 2 molL^{-1} KOH; and variation of specific energy of symmetric button capacitor with charging current density in device with aqueous electrolytes (c) 1 molL^{-1} Na_2SO_4, and (d) 2 molL^{-1} KOH. 241
Figure 5.33: Variation of specific power of symmetric button capacitor with charging current density in device with $Mn_3(PO_4)_2$ composite electrodes and different aqueous electrolytes (a) 1 molL^{-1} Na_2SO_4, (b) 2 molL^{-1} KOH; and ragone plot of symmetric button capacitor with aqueous electrolytes (c) 1 molL^{-1} Na_2SO_4, and (d) 2 molL^{-1} KOH. 242
Figure 5.34: (a) Variation of specific capacitance per kilogram of symmetric button capacitor with charging current density in device with nitrogen-doped rapeseed activated carbons (N-RCs) composite electrodes and 0.5 molL^{-1} Na_2SO_4 aqueous electrolytes; (b) variation of specific energy of symmetric button device 0.5 molL^{-1} Na_2SO_4 aqueous electrolytes; (c) variation of specific power of symmetric button device with 0.5 molL^{-1} Na_2SO_4 aqueous

electrolytes; and (d) ragone plot of symmetric button device with 0.5 molL^{-1} Na_2SO_4 aqueous electrolytes. 243
Figure 5.35: (a) Variation of specific capacitance per kilogram of symmetric button capacitor with charging current density in device with 1100CNF webs electrodes and 1 molL^{-1} Na_2SO_4 aqueous electrolytes; (b) variation of specific energy of symmetric button device with 1 molL^{-1} Na_2SO_4 aqueous electrolytes; (c) variation of specific power of symmetric button device with 1 molL^{-1} Na_2SO_4 aqueous electrolytes; and (d) ragone plot of symmetric button device with 1 molL^{-1} Na_2SO_4 aqueous electrolytes. 244
Figure 5.36: Energy densities of ECs with electrode and electrolyte effective conductivities $\alpha_1 = 50\text{S/cm}, \alpha_2 = 0.5\text{S/cm}$ and different electrode thicknesses charged at current density of (a) 0.00533A/cm^2 for 18000s, (b) 0.0533A/cm^2 for 1800s, (c) 0.533A/cm^2 for 180s, and (d) 5.33A/cm^2 for 18s. 246
Figure 5.37: Energy densities of ECs with electrode and electrolyte effective conductivities $\alpha_1 = 50\text{S/cm}, \alpha_2 = 0.5\text{S/cm}$ and different electrode thicknesses charged at current density of (a) 0.00533A/cm^2 for 18000s, (b) 0.0533A/cm^2 for 1800s, (c) 0.533A/cm^2 for 180s, and (d) 5.33A/cm^2 for 18s. 247
Figure 5.38: Ragone plots of electrochemical capacitors with different electrode thicknesses and electrodes and electrolyte effective conductivities $\alpha_1 = 50\text{S/cm}$, $\alpha_2 = 0.5\text{S/cm}$ charged at current density of (a) 0.00533A/cm^2 for 18000s, (b) 0.0533A/cm^2 for 1800s, (c) 0.533A/cm^2 for 180s, and (d) 5.33A/cm^2 for 18s. 250
Figure 5.39: Profile of value of the coefficient associated to battery-kind material, K_{BM} as a function of mass and operating potential window ratio factors of battery-kind electrode, k_1 and k_2 respectively for (a) 3-D side view plot of limits $0 < k_1 \le 1 \text{ and } 0 < k_2 \le 1$; (b) 3-D front view plot of limits $0 < k_1 \le 1 \text{ and } 0 < k_2 \le 1$;(c) 3-D side view plot of limits $0 < k_1 \le 0.5$ and $0 < k_2 \le 0.7$; and (d) 3-D front view plot of limits $0 < k_1 \le 0.5 \text{ and } 0 < k_2 \le 0.7$ 256
Figure 5.40: Profile of mass and operating potential window ratio factors of battery-kind electrode k_1 and k_2 respectively, for coefficient associated to battery-kind material $K_{BM} \ge 0.5$. 258
Figure 5.41: (a) Profile of stipulated requirement $K_E \ge 1.0$ as a function of k_3 and k_4 ratios; (b) 3-D front view profile of value of constant associated to electrolyte material K_E as a function

of k_3 and k_4 ratios; and (c) 3-D side view profile of value of constant associated to electrolyte material K_E as a function of k_3 and k_4 ratios. 263
Figure 5.42: (a) 3-D front view profile of value of constant associated to electrolyte material K_E as a function of k_3 and k_4 ratios for ranges of $0.3 \le k_3 < 1$ and $0.5 \le k_4 < 1$; and (b) 3-D side view profile of value of constant associated to electrolyte material K_E as a function of k_3 and k_4 ratios in range of $0.3 \le k_3 < 1$ and $0.5 \le k_4 < 1$.....266

LIST OF TABLES

Table 2.1: Chronology of research dedicated to self-discharge in electric double layer capacitors (EDLCs) and pseudocapacitors. 76

Table 5.1: The model parameters used for simulation of effects of self-discharge on the performance symmetric electric double layer capacitors and active electrolyte enhanced supercapacitors……...176

Table 5.2: Parameters of symmetric EDLCs without self-discharge, with only EDLs instability self-discharge, and with both side-reactions/redox reactions and EDLs instability self-discharge during charging and discharging processes. 190

Table 5.3: Parameters of symmetric EDLCs without self-discharge, with only EDLs instability self-discharge, and with both side-reactions/redox reactions and EDLs instability self-discharge during charging and discharging processes. 192

Table 5.4: Parameters of symmetric EDLCs without self-discharge, with only EDLs instability self-discharge, and with both side-reactions/redox reactions and EDLs instability self-discharge during charging and discharging processes. 193

Table 5.5: Parameters of asymmetric ECs in Case 1 without self-discharge; and Case 2 with self-discharge and N = 10^{20}cm^{-3} and J_{VRM} = 1.25x10^{-3}A/cm^2 during capacitors charging and discharging. 208

Table 5.6: Parameters of asymmetric ECs in Case 1, without self-discharge; and Case 2 with self-discharge and N = 10^{20}cm^{-3}, J_{VRM} = 1.25x10^{-3}A/cm^2, J_{VR1} = 9.58x10^{-4}A/cm^2, C_{Ox} = 3.0x10^{-4}mol/cm^3 and D_{Ox} = 1.8x10^{-5}cm^2/s during capacitors charging and discharging. 209

Table 5.7: Parameters of asymmetric ECs in Case 1, without self-discharge; and Case 2 with self-discharge N=10^{19}cm^{-3}, J_{VRM} = 4.0x10^{-4}A/cm^2, J_{VR1}=9.58x10^{-5}A/cm^2, C_{Ox} =3.0x10^{-5}mol/cm^3 and D_{Ox} = 1.8x10^{-6}cm^2/s, during capacitors charging and discharging. 213

Table 5.8: The model parameters used for simulation influences of operating conditions and design configurations on the performance of symmetric electrochemical capacitors 218

Table 5.9: ECs component scales for different applied current densities J_0, A/cm^2 and α_2 = 0.5S/cm 222

Table 5.10: ECs component scales for different applied current densities J_0, A/cm^2 and α_2 = 0.05S/cm 224

Table 5.11: ECs component scales for different applied current densities J_0, A/cm^2 and α_2 = 0.005S/cm 226
Table 5.12: ECs component scales for different applied current densities J_0, A/cm^2 and α_2 = 0.0005S/cm 229
Table 5.13: Comparison of expression for performance parameters of various electrochemical capacitors using aqueous and organic electrolytes, respectively 254
Table 5.14: Parameters of symmetric EDLC using aqueous electrolyte, asymmetric EDLC using aqueous electrolyte, and asymmetric EDLCs using organic electrolyte with voltage windows of 1.2V, 1.2V, and 2.4V & 4.0V, respectively, during charging and discharging processes in cases 1, 2, 3 and 4 259
Table 5.15: Parameters of asymmetric EDLC and asymmetric ECs using aqueous electrolytes and voltage windows of 1.2V during charging and discharging processes in cases 1, 2 and 3 261
Table 5.16: Parameters of asymmetric EDLC using aqueous electrolyte and asymmetric ECs using organic electrolytes and voltage windows of 1.2V and 2.4V & 2.4V, respectively, during charging and discharging processes in cases 1, 2 and 3 264
Table 5.17: Parameters of EDLC using aqueous electrolyte and asymmetric ECs using aqueous electrolytes and voltage windows of 1.2V and 3.0V & 3.0V, respectively, during charging and discharging processes in cases 1, 2 and 3 267
Table 5.18: Parameters of symmetric EDLC using aqueous electrolyte, asymmetric EC using aqueous electrolyte, and asymmetric ECs with self-discharge using organic electrolytes and voltage windows of 1.2V, 1.2V, 2.4V and 4.0V, respectively, during charging and discharging processes in cases 1, 2, 3 and 4. 269
Table 5.19: Parameters of asymmetric EDLC using aqueous electrolyte, asymmetric EDLC using organic electrolyte, asymmetric EC using aqueous electrolyte and asymmetric EC using organic electrolyte with voltage windows of 1.2V, 4.0V, 1.2V and 4.0V respectively, during charging and discharging processes in cases 1, 2, 3 and 4. 270
Table 5.20: Summary of performance parameters of various electrochemical capacitors using aqueous and organic electrolytes, respectively 272

LIST OF SYMBOLS

Electron's absolute charge	e
Rate of the charge's change when the ions are oxidized (reduced)	Z
Total concentration of the shuttle ions in the electrolyte, cm^{-3}	N
Surface rates of oxidation of ions, (cm^2/s)	s^+
Surface rates of reduction of ions, (cm^2/s)	s^-
Coefficients of diffusion of oxidized ions in separator filled with electrolyte, cm^2/s	D^+
Coefficients of diffusion of reduced ions in separator filled with electrolyte, cm^2/s	D^-
Capacitance, F	C
Volume specific capacitance, F/cm^2	C_V
Area of visible surface of electrodes, cm^2	A
Diffusivity of electrons (charge carriers) of the solid matrix of electrodes, cm^2/s	D_e
Diffusivity of holes (charge carriers) of the solid matrix of electrodes, cm^2/s	D_p
Diffusivity of the positive ions of electrolyte, cm^2/s	D_+
Diffusivity of the negative ions of electrolyte, cm^2/s	D_-
Values of the charges of the positive ions of the electrolyte, C	eZ^+
Values of the charges of the negative ions of the electrolyte, C	eZ^-
Number of electrons transferred in electrode reaction,	n
Surface density of current, mA/cm^2	J_0
Thicknesses of the negative electrode, cm	w_{ne}
Thicknesses of the positive electrode, cm	w_{pe}
Thicknesses of the separator electrode, cm	w_{sp}
Thicknesses of the capacitor , cm	w_C
Current densities in electrode, mA/cm^2	$J_1(x,t)$

Current densities in electrolyte, mA/cm^2	$J_2(x,t)$
Volume current of density of generation charge carriers in the capacitor, A/cm^3	$J_{VG}(x,t)$
Volume current of density of recombination charge carriers in the capacitor, A/cm^3	$J_{VR}(x,t)$
Time of charging, s	t_{ch}
Time of discharging, s	t_{dis}
Charging current, mA or A	I_{ch}
Discharging current, mA or A	I_{dis}
Self-discharge current, mA or A	$I_{selfdis}$
Columbic capacity of charging, C or Ah	Q_{ch}
Columbic capacity of discharging, C or Ah	Q_{dis}
Storable energy without account of ohmic losses,Wh	E_{Sch}
Deliverable energy without account of ohmic losses,Wh	E_{Sdis}
Residual energy after discharging, Wh	E_{Sadis}
Energy loss by polarization resistance during charging,Wh	E^{Rpolch}
Energy loss by polarization resistance during discharging,Wh	$E^{Rpoldis}$
Energy of the charged capacitor after a pause, Wh	$E_S{}^{apch}$
Energy of the discharged capacitor after a pause, Wh	$E_S{}^{apdis}$
Depolarization loss of energy during the charging, Wh	E^{dpolch}
Depolarization loss of energy during the discharging, Wh	$E^{dpoldis}$
Ohmic loss of energy during charging, Wh	E^{Rch}
Ohmic loss of energy during charging, Wh	E^{Rdis}
Potential storable energy, Wh	E_{ch}
Potential deliverable energy, Wh	E_{dis}
Total energy loss by self-discharge during charge and discharge, Wh	$E_{selfdis}$
Charge loss by self-discharge during charge and discharge, C or Ah	$Q_{selfdis}$

Residual columbic capacity after the discharge, C or Ah	QS_{adis}
Specific energy density of the symmetric electrochemical capacitor, Wh/kg	$ED_{max,sy}$
Specific power density of the symmetric electrochemical capacitor, kW/kg	$PD_{max,sy}$
Effective energy density of the symmetric electrochemical capacitor, Wh/kg	ED_{sy}^{eff}
Effective power density of the symmetric electrochemical capacitor, Wh/kg	PD_{sy}^{eff}
Effective charging current, mA or A	$I_{eff,ch}$
Effective discharging current, mA or A	$I_{eff,dis}$
Total energy loss by self-discharge during charge and discharge, Wh	$E_{selfdis}$
Specific energy density of the symmetric capacitor, Wh/kg	$ED_{max,asy}$
Specific effective energy density of the asymmetric capacitor, Wh/kg	$ED_{eff,asy}$
Specific power density of the asymmetric capacitor, kW/kg	$PD_{max,asy}$
Specific effective power density of the asymmetric capacitor, kW/kg	$PD_{eff,asy}$
Total energy loss of the capacitor, Wh	E_{Tloss}
Oxidized species,	Ox
Reduced species,	R
Metal such as iron, manganese, and titanium, etc.,	M
Redox active species,	P
Hydrogen ion	H^+
Initial concentration of reactant, mole/cm^3	C^0
Diffusion parameter that is determined by the initial voltage of a given device	m
Concentration of oxidized specie, mole/cm^3	$C_{Ox(x,t)}$
Total thickness of the separator and the anode, cm	l
Diffusion coefficient of the oxidized species, cm^2/s	D_{Ox}
Total current density that are lost due to self-discharge	$J_{VR1}(t)$

Potential decay due to self-discharge, V	$\varphi_D(t)$
Effective thickness of the electrical double-layer, cm	d
Faraday constant,	F
Molar mass of the metal oxide,	M
Mass of the capacitor, kg	m
Operating voltage window, V	V
Series resistance of all components/layers in the capacitor, Ω	R
Equivalent series resistance, Ω	R_{esr}
Constant current for charging or discharging the capacitor, A	I_{cell}
Capacitor cell voltage, V	V_{cell}
Double-layer capacitance, F	C_{dl}
Voltage across the C_{dl}, V	V_{sc}
Current used to charge or discharge, A	i_{sc}
Maximum cell voltage, V	V_{cell}^{max}
Voltage across the double layer capacitance at the end of charging, V	V_{SC}^{O}
Parallel leakage resistance, Ω	R_{lk}
Parallel leakage current, A	i_{lk}
Current of solvent electrochemical decomposition, A	i_F
Time, s	t
Position along a specific direction, cm	x
Electrode/electrolyte interface surface, cm^2/cm^3	a
Factor accounting for electrode roughness,	k_x
Coefficient that is dependent on applied technology,	K_v
Differential capacitance of an electrochemical capacitor, F	C_{diff}

Thickness of the electrode with EDL, cm	L_D
Thickness of the redox couple electrode, cm	L_R
Concentration, mol/cm^3	C
Coefficient of diffusivity, cm^2/s	D
Exchange current density, A/cm^2	i_0
Equilibrium potential of the capacitor, V	U_{eq}
Separator's thickness, cm	L_S
Cut-off time, s	t_C
Mass of the symmetric supercapacitor, kg	m_S
Mass of the asymmetric supercapacitor, kg	m_H
Heat generation rate, W/s	$\dot{q}$
Irreversible heat production rates, W/s	$\dot{q}_{irr}$
Reversible heat production rates, W/s	$\dot{q}_{rev}$
Heat production rate due to the effects from Joule heating, W/s	$\dot{q}_{E,j}$
Heat production rate due to the effects of ion diffusion, W/s	$\dot{q}_{E,d}$
Heat production rate due to the effects of steric, W/s	$\dot{q}_{E,s}$
Heat production rate due to effects mixing heat with concentration gradient,W/s	$\dot{q}_{S,c}$
Heat production rate due to the effects mixing heat with temperature gradient, W/s	$\dot{q}_{S,T}$
Capacitance of one capacitor-kind electrode with aqueous electrolyte, F	C_1
Storable energy of one capacitor-kind electrode with aqueous electrolyte, Wh	E_1
Specific energy density of a capacitor-kind electrode with aqueous electrolyte,Wh/kg	ED_1

Specific power density of a capacitor-kind electrode with aqueous electrolyte, W/kg PD_1

Charge stored in one capacitor-kind electrode material with aqueous electrolyte, Ah q_1

Electrode maximum working potential range of a capacitor-kind electrode with aqueous electrolyte, V ΔV_{max}

Mass of one capacitor-kind electrode, m^2 m_1

Maximum current for each electrode, A I_{max}

Capacitance of the whole symmetric capacitor with aqueous electrolyte, F C_s

Storable energy in the symmetric capacitor with aqueous electrolyte, Wh E_s

Specific energy density per unit mass of symmetric capacitor with aqueous electrolyte, Wh/kg ED_s

Specific power density per unit mass of symmetric capacitor using aqueous electrolyte, W/kg PD_s

Charge stored in the symmetric capacitor with aqueous electrolyte, Ah q_s

Mass of the symmetric capacitor, m^2 m_s

Capacitance of the whole asymmetric capacitor with aqueous electrolyte, F C_{as}

Storable energy in the symmetric capacitor with aqueous electrolyte, Wh E_{as}

Specific energy density per unit mass of asymmetric capacitor with aqueous electrolyte, Wh/kg ED_{as}

Specific power density per unit mass of asymmetric capacitor with aqueous electrolyte, W/kg PD_{as}

Charge stored in the asymmetric capacitor with aqueous electrolyte, Ah q_{as}

Mass of the asymmetric capacitor, kg m_{as}

Mass of the battery-type electrode, kg m_b

Mass of the capacitor-type electrode, kg m_c

Working potential range of battery-kind electrode with aqueous electrolyte, V ΔV_b

Working potential range of capacitor-kind electrode with aqueous electrolyte, V ΔV_c

Ratio of mass of battery-kind electrode to the total mass of battery-kind and the capacitor-kind electrodes k_1

Ratio of the operating potential range of battery-kind electrode to that of the capacitor-kind electrode k_2

Battery-kind material-associated coefficient that is dependent on k_1 and k_2 K_{BM}

Capacitance of one capacitor-kind electrode with organic electrolyte, F C_{o_1}

Storable energy of one capacitor-kind electrode with organic electrolyte, Wh E_{0_1}

Specific energy density per unit mass of one capacitor-kind electrode with organic electrolyte, Wh/kg ED_{o_1}

Specific power density per unit mass of one capacitor-kind electrode with organic electrolyte, W/kg PD_{0_1}

Charge stored in one capacitor-kind electrode material with organic electrolyte, Ah q_{0_1}

Electrode maximum working potential range one capacitor-kind electrode with organic electrolyte, V $\Delta V_{o_\max}$

Mass of a single capacitor-type electrode with organic electrolyte, kg m_{o_1}

Maximum current for each electrode with organic electrolyte. A $I_{o_\max}$

Capacitance of the whole asymmetric capacitor with organic electrolyte, F C_{o_as}

Storable energy in the symmetric capacitor with organic electrolyte, Wh E_{o_as}

Specific energy density per unit mass of asymmetric capacitor with organic electrolyte, Wh/kg ED_{o_as}

Specific power density per unit mass of asymmetric capacitor with organic electrolyte, W/kg PD_{o_as}

Charge stored in asymmetric capacitor with organic electrolyte, Ah q_{o_as}

Capacitor maximum working potential range in asymmetric capacitor with organic electrolyte, V $\Delta V_{o_\max}$

Mass of the asymmetric capacitor with organic electrolyte, kg m_{o_as}

Mass of the battery-type electrode with organic electrolyte, kg m_{o_b}

Mass of the capacitor-type electrode with organic electrolyte, kg m_{o_c}

Working potential range of the battery-type electrode in asymmetric capacitor with organic electrolyte, V ΔV_{o_b}

Working potential range of the capacitor-type electrode in asymmetric capacitor with organic electrolyte, V ΔV_{o_c}

Maximum current in the asymmetric capacitor with organic electrolyte, A $I_{o_\max}$

Electrolyte-related coefficient that is dependent on k_3 and k_4 K_E

Ratio of maximum operating potential range between aqueous and organic electrolytes k_3

Ratio of specific capacitance between capacitor-type electrodes in the aqueous and organic electrolyte k_4

Greek

Conductivity of the solid matrix of electrodes with DEL, S/cm σ_{ne}^{s}

Conductivity of the electrolyte in the pores of electrodes with DEL, S/cm σ_{ne}^{l}

Effective conductivity of the solid matrix of the electrode, S/cm α_1

Effective conductivity of the electrolyte, S/cm α_2

Effective mobility of the positive ions of the electrolyte, $cm^2/(V\ s)$ μ_+

Effective mobility of the negative ions of the electrolyte, $cm^2/(V\ s)$ μ_-

Effective mobility of electrons of the solid matrix of electrode, $cm^2/(V\ s)$ μ_n

Effective mobility of holes of the solid matrix of electrode, $cm^2/(V\ s)$	μ_p
Porosity of the electrode,	ε_0
Porosity of the separator,	ε_{sp}
Non-equilibrium concentrations of free electrons of the polarizable electrode, cm^{-3}	Δn
Non-equilibrium concentrations of positive ion of the electrolyte, cm^{-3}	Δn^+
Specific internal resistance, $\Omega\, cm^2$	ρ_{int}
Density of the negative/positive electrode, kg/cm^3	ρ_{ne}
Density of the electrolyte, kg/cm^3	ρ_e
Density of the separator, kg/cm^3	ρ_{sp}
Energy efficiency of the first charge–discharge cycle, %	η_{E1}
Energy efficiency of the stationary charge–discharge cycle, %	η_{E2}
Polarization loss of energy of charge–discharge cycle, %	δ_{ERpol}
Ohmic loss of energy of charge–discharge cycle, %	δ_{ER}
Depolarization loss of energy of charge–discharge cycle, %	δ_{Edpol}
Self-discharge loss of energy of charge–discharge cycle, %	$\delta_{Eselfdis}$
Total loss of energy during charge–discharge cycle, %	δ_{ET}
Potential in the solid matrix of the electrode, V	φ_1
Potential in the electrolyte, V	φ_2
Electrolyte potential at the interface of electrode/electrolyte, V	φ_{21}
Potentials of the negative electrodes, V	φ_{ne}

Potentials of the positive electrodes, V	φ_{pe}
Potentials of the negative electrodes before charging, V	φ_{ne}^{0+}
Potentials of the positive electrodes before charging, V	φ_{pe}^{0+}
Potentials of the negative electrodes before discharging, V	φ_{ne}^{0-}
Potentials of the positive electrodes before discharging, V	φ_{pe}^{0-}
Effective potentials before capacitors charge and discharge processes, V	φ_{ne}^{eff}
Overpotential in the double-layer electrode, V	η_D
Density of the electrodes with EDL, g/cm^3	ρ_D
Density of separator, g/cm^3	ρ_S
Density of the redox electrode, g/cm^3	ρ_R
Charge transfer coefficients of positive electrode	α_a
Charge transfer coefficients of negative electrodes	α_c
Overpotential of the redox couple electrode, V	η_R
Surface state of charge,	θ_s
Initial state of charge,	θ^0
State of charge,	θ
Conductivity of the electrode, $\Omega^{-1}cm^{-1}$	σ
Relative permittivity of the medium in the electrical double-layer,	ε_r
Permittivity of vacuum,	ε^0
Conductivity of the ions in electrolyte, $\Omega^{-1}cm^{-1}$	κ_s
Conductivity of the electrolyte, $\Omega^{-1}cm^{-1}$	κ
Bulk conductivity of the electrolyte, $\Omega^{-1}cm^{-1}$	κ_0

CHAPTER ONE

1.0 Introduction

Electrochemical Capacitors (ECs), also known as supercapacitors or ultracapacitors, has been the subject of great researches in recent years, owing to their potentials as electrical energy storage devices. ECs are typically classified into three categories based on their different energy storage mechanism: electric double layer capacitors (EDLCs), pseudocapacitors, and a hybrid type obtained by the combination of EDLC and pseudocapacitor. EDLCs store electric charges electrostatically through reversible adsorption of electrolytic ions onto active electrode materials. The electrode materials are electrochemically stable and have high accessible specific surface area to form the electric double layer at electrode/electrolyte interfaces accessible to ions present in the electrolyte [1–5]. The charge storage mechanism of EDLCs is physical without chemical reactions (redox reactions) in the electric double layers forming near the interface of electrode/electrolyte, thus, the process is highly reversible and the cycle life is essentially infinite [6].

Pseudocapacitors store energy through fast surface oxidation-reduction (redox) reactions as well as possible ion intercalation in the electrode [4,7–10]. Some ECs utilize fast reversible redox reactions at the surface of active materials. This describes exactly what is referred to as pseudo-capacitive performance, which performs higher than carbon materials employing solely double layer charge storage, giving an explanation for the great attention to these categories of systems. Consequently, pseudocapacitors usually supply higher energy density at the cost of shorter cycle lives and lower rates compared with the EDLCs [8,11]. Conway

[12] identified the following three kinds of pseudocapacitive mechanisms as a result of different physical processes and with different types of materials:

(1) Underpotential deposition which occurs when a monolayer formed by metal ions such as lead on the surface of a gold electrode [13] was adsorbed on the surfaces of a different metal under a potential higher than their redox potential.

(2) Redox pseudocapacitance which takes place when ions are adsorbed electrochemically on the surface of materials like RuO_2 with concurrent faradaic charge transfer occurring.

(3) Intercalation pseudocapacitance occurs when ions intercalate into layers created by redox-active materials with concomitant faradaic charge transfer taking place unaccompanied by any crystallographic phase change. Indistinguishable connections between potential and the extent of charges stored or released due to adsorption/desorption process at electrode/electrolyte interface [14] exist in these three kinds of mechanisms. Pseudo-capacitors, like batteries, often exhibit a lack of stability during cycling as a result of the presence of redox reactions.

Asymmetric or hybrid electrochemical capacitors, have appeared recently by merging pseudocapacitors and EDLCs [4,15–21]. In asymmetric/hybrid ECs, one carbon-based electrode stores charge physically in electric double layers whereas, the other electrode is redox-active and stores charge through reversible chemical reactions [4,15–21]. In asymmetric ECs, the pseudocapacitive electrode works as the energy source and the carbon-based electrode works as the power source [4,15–21]. The merits of ECs compared with other electrical energy storage devices are high power density, long cyclelife, high efficiency, and a wide range of operating temperatures, environmental friendliness, and safety. ECs also serve as a bridge for power/energy gap of conventional dielectric capacitors [22], and are

specifically suitable for applications that demands high power for a few seconds [4,12,23–25].

ECs are generally comprised electrodes (usually carbon coating on a current collector), separated by a non-conducting porous membrane, and plunged in electrolyte. The electrodes and separator are soaked or saturated with electrolyte solution, which allows movement of ionic current between electrodes while prohibiting electronic current from discharging the capacitor [26]. When the system is charged, anions of electrolyte are electrosorbed on a positively polarized electrode and cations on the negative one, giving rise to an electric double layer at each electrode. Separation of charge happens on partial or complete polar separation of positive and negative electric charges at the electrode–electrolyte interface, and thus generating what has been explained by Helmholtz as the double layer capacitance *C* [27–29]:

$$C = \frac{\varepsilon_0 \varepsilon_r A}{d} \qquad \text{or} \qquad \frac{C}{A} = \frac{\varepsilon_0 \varepsilon_r}{d} \tag{1.1}$$

where ε_r is the electrolyte dielectric constant, ε_0 is the dielectric constant of a vacuum, *d* is the double layer effective thickness (charge separation distance) and *A* is the electrode surface area. The amount of the energy stored in electrochemical capacitor, E is the directly proportional to its capacitance:

$$E = \frac{1}{2} C V^2 \tag{1.2}$$

The voltage during charge/discharge process of the capacitor is decided by equivalent series resistance. Generally, power P is the rate of spending energy and is usually given by:

$$P = I V = \frac{V^2}{4 \times ESR} \tag{1.3}$$

where I is applied current and V is applied voltage and ESR is equivalent series resistance (total resistance by capacitor's components to current flow) [6,22,30].

Ions in electrolyte solution diffuse across the separator into the pores of the electrode of opposite charge due to attraction forces of unlike charges in accordance with nature. The electrodes were designed and built in a manner to avert recombination of charge carriers, thus creating a double-layer of charge at each electrode. The electric double-layers, together with increased surface area and a reduction in gap between electrodes, permit EDLCs to acquire higher energy densities in comparison with the traditional capacitors [6,7,12].

In order to construct electrochemical capacitors with superior key parameters and optimal design for necessary high energy and power densities, high energy efficiency and long lifecycle, mathematical models and theoretical basis which emerge from fundamental principles of physics and electrochemistry for its design and optimization is inevitable. The models and theoretical basis are also to the subject to electrodes thickness, strong dependence of specific capacitance of electrodes on their potential, temperature distributions, mechanisms of self-discharge, type and value of electrodes material conductivity and conductivity of electrolyte in electrode pores. This will facilitate the design of ECs with desired properties, capable of replacing the batteries.

1.1 Electric Double Layer Capacitors

EDLCs store electrical energy and charge physically in the electric double layer forming at the interface between a high surface area activated carbon electrode and liquid electrolyte accessible to ions in electrolyte [1–5,12,27,31,32]. These kinds of electrochemical capacitors have drawn reasonable awareness in recent years due to their promises in commercial applications that demands high power density and long-term cycle stability, for example

electrical energy storage devices for high power applications such as hybrid electric vehicles and load-levelling [1–5,23,32]. These important features are warranted by the double-layer charging mechanism, which depend on physical ion adsorption/desorption in the Helmholtz layer of electrolyte as presented in Figure 1.1 below. It does not need slow-moving solid-state ion insertion/de-insertion reactions which also result in change in electrode volume and capacity reduction with cycling [33–35]. One of the major challenges in the field of electrochemical capacitors is to improve their restricted energy density as a sequel to electrostatic surface charging mechanism. Some recent findings concerning ion adsorption in microporous carbon with pores in nanometre range could assist in obtaining blueprint for the earnestly desired high energy density ECs. This justifies the reason for focusing today's EDLCs research mainly on improving their energy retention and performance and broadening temperature windows into the range that batteries cannot operate upon [7].

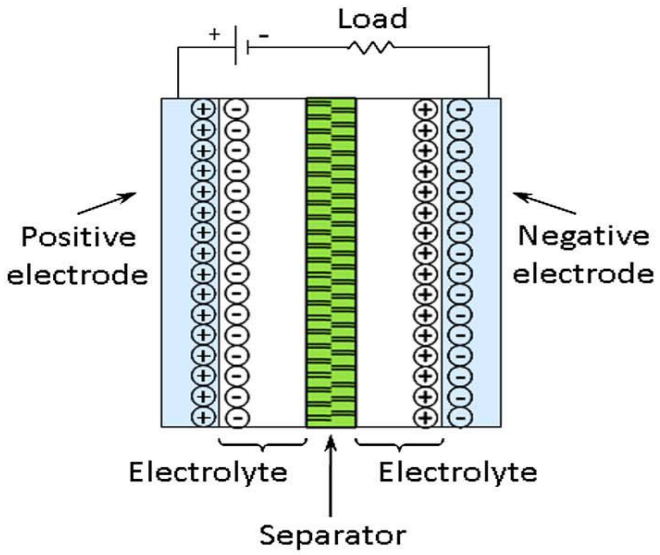

Figure1.1: A diagrammatic representation of electric double layer capacitors (EDLCs) with the charge storage mechanism [36].

EDLCs electrodes in reality are made of nanoporous or mesoporous carbons with a large surface area to increase capacitance and stored energy. The performance of EDLCs is

controlled by a combination of electrode material and morphology as well as electrolyte material. It also greatly relies on the choice of electrolyte made up of salt dissolved in solvent into its component ions. Besides, electrode materials pore size distribution equally has great influence on performance of EDLCs. It has been accepted that micropores of less than 2 nm subscribe significantly to emergence of an electric double layer [37–39], and that pores smaller than the ions normally do not contribute to double layer capacitance [4,40]. Moreover, porous electrodes must also be electrochemically accessible for ions. Thus, mesopores with a diameter within the 2 to 50 nm range are obligatory for fast dynamic charge due to the easier accessibility to ions [1,40–43]. The choice of electrolyte significantly affects the effective electrical resistance of ECs, and the two main factors that influence electrical conductivity of electrolytes are (1) the concentration of electrolyte and its capacity to separate into cations and anions working as free charge carriers and (2) the movability of the separated ions in electrolyte solution [44].

1.2 Pseudocapacitors

In order to increase the low energy density which is a crucial restriction to EDLCs technology, sizeable focus in exploring pseudocapacitive materials has emerged [45]. Pseudocapacitors require the movement of charges across the electrode-electrolyte interfaces and consequently the reduction and oxidation state of electrochemically active ions can equally be switched on the electrodes throughout redox reactions [46–48] as shown in Figure 1.2 below. The fast and reversible redox reactions related with pseudocapacitive-based materials, result in high specific capacitances and corresponding high energy densities, which are higher than convectional EDLCs by one order of magnitude [12,45]. It is highly advantageous to enhance the energy density of ECs to approach that of batteries, which could

authorize their application as main power sources [49,50]. Pseudocapacitance is formed by faradaic charge movement to or from species adsorbed at/in successful contact with an electrode surface or producing the electrode surface.

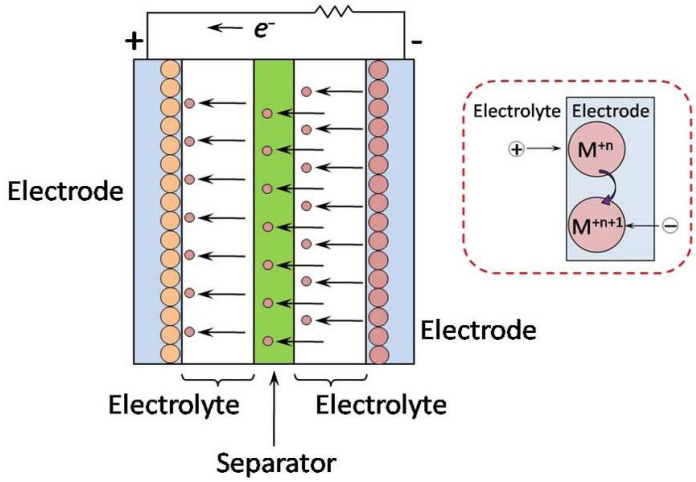

Figure1.2: A diagrammatic representation of pseudocapacitors with the charge storage mechanism [36].

Nevertheless, charge movement and build-up on an electrode surface form electrostatic stresses, which probably result in mechanical strain inside the electrode leading to a decrease in charge storage capacity. Pseudocapacitors are normally deprived of their capacity (fading) with repetitive charging and discharging much more rapidly compared with the EDLCs. High charge/discharge rates equally seem to create additional stress, resulting in smaller and ineffective device lifetime. Oxides and hydroxides pseudocapacitive materials like RuO_2, Co_3O_4, $Ni(OH)_2$, MnO_2, Fe_2O_3, and Fe_3O_4 are now explored for development of ECs with increased specific capacitances and high energy densities [51–55]. Three types of faradaic phenomena occur with pseudocapacitive electrodes: reversible adsorption such as adsorption of hydrogen on the surface of platinum or gold, redox reactions of transition metal oxides and reversible electrochemical doping–dedoping in conductive polymer electrodes [12].

1.3 Asymmetric/Hybrid Electrochemical Capacitors

Asymmetric/Hybrid electrochemical capacitors have appeared recently via a combination of pseudocapacitive electrodes and EDL electrodes as shown in Figure 1.3 [4,15,16,18–21,56–58]. These have been investigated largely to profit from both the merits of electrode materials in enhancing the overall capacitors performance [6,59,60]. In these hybrid ECs, electrical double-layer capacitance and faradaic capacitance mechanisms take place concurrently, but one presents a greater task compared with the other. The essential properties required in electrode materials to achieve a large capacitance in both mechanisms are large surface area, suitable pore-size distribution, and high conductivity. In asymmetric ECs, a carbon-type electrode which stores charges physically in electric double layers, plays the role of power source, while a redox-active electrode that stores charges via reversible chemical reactions serves as the energy source [4,15,16,18–21,56–58].

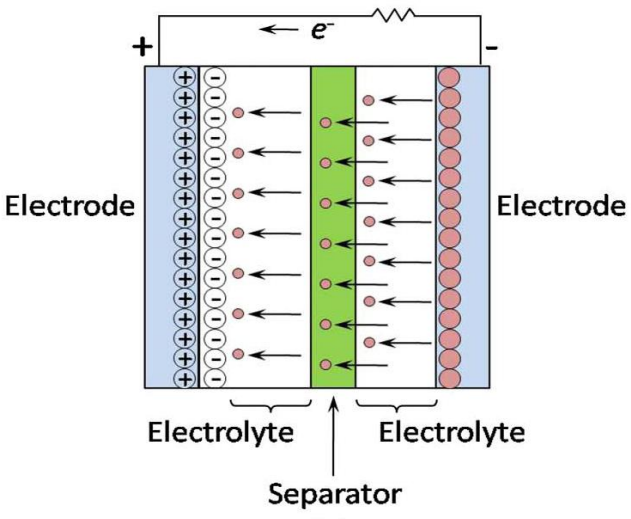

Figure1.3: A diagrammatic representation of asymmetric or hybrid ECs with the charge storage mechanism [36].

Two types of hybrids exist; the first one is the ‘‘hybrid electrode’’ whereby pseudocapacitive or faradic and non-faradic materials are integrated into a single electrode so as to utilize the

advantage of each charge storage mechanism [61], while the other one is the ‘‘hybrid device or hybrid combination’’ where a pseudocapacitive or faradic electrode and non-faradaic electrode one are used together in a single ECs [62]. These hybrid properties can prevail over the energy density restriction inherent in normal electrochemical capacitors, because they utilize both methods of a battery-type (Faradaic) electrode and an EDL-type (non-Faradaic) electrode, yielding larger working voltage and capacitance [6,63]. These structures are capable of doubling or tripling the energy density in comparison with that of normal ECs. Nevertheless, ion exchange rates at pseudocapacitive electrodes have to be increased to levels of EDL-type electrodes so as to equilibrate the two systems.

1.4 Materials of Electrochemical Capacitors

ECs fundamentally consist of two electrodes immersed into electrolyte and are isolated from electrical contact by a semipermeable membrane serving as separator. The separator is a non-electric conducting membrane that permits flow of charged ions but disallows electric contact. The electrodes and separator are impregnated with electrolyte solution which allows for movement of ionic current between electrodes while restricting electronic current from releasing charge and energy stored in the ECs [26]. The prpose of the separators is to prevent direct movement of electrons between the two electrodes, that is, it must be an electronic insulator, but also has to allow easier transmission of ions to complete the electric circuit. Current collectors conduct electrical current from the electrodes. A good separator is electrochemically stable, of high porosity, high thermal and chemical inertia [12]. Furthermore, the separator needs to be as thin as possible and relatively inexpensive in terms of cost since the separator is not active in capacitors [12]. The thinness of the separator is constrained by the following conditions: 1) electrical short circuit risk owing to free carbon

particles that will likely provide a contact between the electrodes [64]. 2) mechanical strength so as to permit the winding processes [12].

1.4.1 Electrode Materials

The overall performance of electrochemical capacitors is decided by both the electrode material and electrolyte used. Three basic classifications of electrode materials are used for ECs depending on the application of energy storage and needed capacitance ranges exists [25, 28, 47]: 1) Materials used in EDLCs are carbon aerogel, activated carbon, carbon fibres and carbon nanotubes; 2) Materials used in pseudocapacitors are transition metal oxides and conducting polymers; and 3) Materials used in hybrid ECs are carbon materials, metal oxides and conductive polymers. There is great focus on nanostructured materials that have larger surface area and enhanced capacitive performance features for ECs electrodes. Synthesis of these materials is now well acknowledged as the crucial factor through which high performance ECs could emerge.

Nanostructured materials have the potential to impact greatly on the performance of electrochemical energy storage devices because their smaller dimensions permit higher ion-diffusion/electron-transfer rates and consequently high power. These materials could potentially increase the diffusion rate of ions due to smaller transport distances within the particles, improved transportation of electrons, changing electrode potential by altering chemical potentials of ions and electrons for very small particles [28, 47]. This is also due to the constitution of increased extensive solid solutions for ions intercalation as merited, in comparison with micrometer-sized materials. Other types of materials frequently used for ECs electrodes are composite materials obtained by integrating two or more component materials.

1.4.2 Layered Materials

Layered nanomaterials can be seen naturally or synthesized in the laboratory in to suite certain applications. Some key layered materials occurring naturally includes graphite, graphene, clays and layered hydroxides (LDHs); while others have been synthesized through chemical combinations of some atomic species like boron nitride (BN), transition metal oxides (TMOs), LDHs, and transition metal dichalcogenides (TDMs) [65]. The most usual materials are three-dimensional and the atoms which make up their structures are arranged in regular, crystalline patterns, filling space like stacks of oranges. However, there is another category of materials where the atoms are arranged in flat layers and heaped on top of each other like sheets of paper in a stack. These layers were thought to be inseparable from each other until recently, when new techniques to separate out individual two-dimensional layers of material were developed. A customary path to production of layered nanomaterials is known as *exfoliation*. This is a process whereby individual layers in a bulk material are separated out either chemically, or through mechanical abrasion. This category of materials represents the largely unutilized source of two-dimensional (2D) systems with exotic electronic properties and high specific surface areas required for improved sensing, catalysis, and energy storage applications [66]. Other kinds of layered compounds like transition metal dichalcogenides (TMDs), transition metal oxides (TMOs), and other 2D compounds (BN, Bi_2Te_3, and Bi_2Se_3), LDHs have also been synthesized. Several hundreds of layered materials are now recognized in nature.

A large family of 2D materials known as MXenes are produced by exfoliation of the A-element from layered ternary carbides, such as Ti_3AlC_2 and other MAX phases [67] were

recently discovered [68,69]. The M is an early transition metal, A is an A group element and X is C or N. The MXenes produced to date, through Ti_3C_2 [68], Ti_2C, Ta_4C_3, $(Ti_{0.5}Nb_{0.5})_2C$, $(V_{0.5}Cr_{0.5})_3C_2$ and Ti_3CN [69] are, in many aspects graphene-like, forming piles of sheets and scrolls. They are equally good electrical conductors [68–72] and are predicted to have high elastic moduli [73]. Electrochemical intercalation of Li ions between the MXene sheets yields these solids promising materials for Li ion battery anodes and hybrid electrochemical capacitors [74–76]. However, there have been no reports of chemical intercalation or large-scale delamination of MXenes or any other transition metal carbides to date.

Layered Carbon Nanomaterials

Carbon is a very adaptable material which occurs naturally in different structural forms. It is the third most abundant element in the universe, after hydrogen and helium. The exceptional properties of carbon nanomaterials can be tracked down from the hybridization of carbon; electrons in the innermost shell of carbon atoms make up an electron 'core' adequately enclosed to allow the outer electrons to mix with other atoms to create a linear or one-dimensional (1D), plane or two-dimensional (2D) and tetrahedral or three-dimensional (3D) materials. Most common layered carbon materials are graphite and graphene. Graphite has a layered structure where atoms are arranged in a hexagonal pattern within each layer, with each atom having three neighbours.

Clay Materials

The term clay generally implies a natural earthy, fine-grained material which grows plasticity when mixed with water. The chemical structure of clay is a usually mixture of different metals like aluminium with materials such as silicon and high concentrations of oxygen.

1.4.3 Electrolyte Materials

The electrolyte, which is electrolyte salt and solvent, is one of the principal parts of ECs that gives the ionic conductivity and therefore make an easier charge compensation on each electrode in the capacitor. The electrolyte inside ECs not only performs a key function in EDL emergence in EDLCs and the reversible reduction-oxidation process for charge storage in pseudocapacitors, and it equally determines the EC's performance. The features of electrolyte that affects EDL capacitance and pseudocapacitance, energy/power densities and the ECs cycle-life are ion type and size; ion concentration and solvent; communication between ion and solvent; communication between electrolyte and electrode materials; and the potential range [39].

Different types of electrolytes have been developed and reported in literature, and are basically classified as either liquid electrolytes or solid/quasi-solid-state electrolytes. The liquid electrolytes are again categorized into aqueous electrolytes, organic electrolytes and ionic liquids (ILs), whereas solid or quasi-solid state electrolytes are widely grouped into organic electrolytes and inorganic electrolytes [77]. The perfect electrolyte that possesses all the features presented above is yet to be developed, for each one has its own merits and demerits. For instance, ECs with aqueous electrolytes have both high conductivity and capacitance with restricted working voltage range due to small decomposition voltage of aqueous electrolytes. Organic electrolytes and ILs can operate at higher voltages but have lower ionic conductivity, whereas solid-state electrolytes are free of the potential leakage problems associated with liquid electrolytes, but they equally have low conductivity [77].

Raising the ECs voltage is more effective with regard to energy density enhancement compared with increasing electrode capacitance because energy density is proportionate to the square of capacitor voltage. Furthermore, electrolytes/solutions play a critical function in setting up other crucial properties required in real-life use of ECs like power density, internal resistance, rate performance, operating temperature window, cycling lifetime, self-discharge rate and toxicity [78]. Thus, greater preference should be given to the development of novel electrolytes/solutions with wide potential windows, compared with that of novel electrode materials. The ECs operating voltage range is largely determined by the electrochemical stable potential window (ESPW) of the electrolytes when electrodes are stable within the working voltage range.

1.5 Motivations of the Current Study

In order to develop electrochemical capacitors capable of replacing batteries, worldwide research efforts are presently targeted at increasing the energy density by optimizing the pore size distribution of nano-porous carbon materials, as well as harnessing the use of non-aqueous electrolytes. In the breakthrough work of Gogotsi and co-workers [39], they synthesized carbide-derived carbon materials with unimodal micropores [77] smaller than 1 nm. They noticed that these carbide-derived carbon materials display an exceptional capacitance increase in acetonitrile organic electrolyte, compared with other carbon materials with pore sizes greater than 2 nm where capacitance is slightly enlarged as pore size increases. These results contradict the long-held idea that pores smaller than the size of solvated electrolyte ions are not involved in the energy storage process. This exceptional capacitance increase in subnanometer pores is ascribed to the desolvation of electrolyte ions

entering subnanometer pores [37,39] as substantiated by experimental study via ionic liquid electrolyte with no solvation shell within electrolyte ions [78].

Higher energy density could be achieved by increasing either the electrodes capacitance (by using high capacitance electrode materials) or the voltage window of electrolyte (via use of non-aqueous electrolytes with larger electrochemical window stability). It has been presented that to increase the voltage window to enhance the energy density is a more judicious approach, considering that energy density is proportional to voltage squared. In addition, there are few or no problems associated with an increase in the RC-time constant on growing capacitance to attain higher energy density [79].

Quantitative modelling has also been utilized to predict the theoretical restrictions of energy and power densities for electrochemical capacitors. Experimental and theoretical studies to determine the restricting factors that prohibit ECs from attaining their theoretical limit have also created novel insights in approaches to optimize capacitors design. While there has been consistent interest in developing enhanced electrode materials to increase energy densities, theoretical models suggested that it is the ion concentration and breakdown voltage of electrolyte that often limit the energy densities of ECs [80–82]. Furthermore, additional research suggested that the power densities of ECs can also be limited by electrolyte [83,84]. Thus, research results emphasize that the optimization of electrolyte is as important as that of the electrode in order to attain the energy and power densities closer to theoretical limits of electrochemical capacitors.

The characteristics of ECs has made it very competitive for applications in electric hybrid vehicles and digital communication devices such as mobile phones, digital cameras, electrical tools, pulse laser techniques and uninterruptible power supplies as well as energy storage in solar cells [7,31]. Unfortunately, some challenges such as low energy density, high cost, and

high self-discharge rate, have limited wider applications of ECs [85]. ECs are used when there is a high power demand, not only for power buffer and power saving units, but also for energy recovery [4,7,23–25]. Cordless tools like screwdrivers and electric cutters using ECs are already available in the market [23]. The transportation market will be a major target of ECs manufacturers in the coming years, including hybrid electric vehicles and metro trains which are already using the technology [85].

Mathematical modelling and simulation will be the key to success in designing tomorrow's high-energy and high-power devices. Varieties of models of symmetric and asymmetric electrochemical capacitors have been presented in the literature [86–97], but none was derived and solved subject to a particular mechanism or combination of distinct mechanisms of self-discharge. Mathematical theory that goes beyond equivalent circuits and couples charging to mechanics, energy dissipation, and uses physics and chemistry of solvents and ions in nanopores, electrode materials as well as the electron and ion transport in capacitors electrodes is inevitable. Notwithstanding numerous studies to enhance ECs performance, there are not many perspectives to comprehend theoretical aspects of calculation of energy density based on electrode electrochemically active material. Therefore, it is very difficult to predict the capacitors electrochemical performance, and so almost all studies, obtained the most excellent conditions for the utmost performance value using trial and error, which is neither effectual nor reliable. The big number of variables to be examined and the various competing processes involved, makes intuitive forecast very difficult, and experimental attitudes are normally time consuming and expensive. On the other hand, meticulous physical modelling and precise numerical models will make the design and optimization of electrode morphology easier and the recognition of the ideal electrolyte more structured and efficient. This research work is motivated by these knowledge gaps, and is therefore set to develop

from first the principles of physics and electrochemistry. This required mathematical models and theoretical basis for design and optimization of the desired high-energy density and power density, high energy efficiency and long lifecycle subject to more realistic assumptions.

1.6 Aims and Objectives of the Research

The main objectives of this research work are:

- To develop a mathematical description of mass transfer, energy transfer and charge conservation in symmetric and asymmetric electrochemical capacitors and parameters of processes which occur therein subject to physical, electrical, electrochemical and parameters of electrode materials, electrolyte, as well as the design of electrode, separator and entire ECs;
- To build a theoretical basis for calculations, control, and improvement of energy, capacity, power, cycle-life, charge-discharge cycle efficiency and energy retention of various types and designs of symmetric and asymmetric ECs with simultaneous accounts of physical, electrical, electrochemical properties of electrode materials and structures the design of electrodes and separator;
- To study the effects of self-discharge on the performance of ECs by incorporating a specific self-discharge mechanism or combination of different self-discharge mechanisms into ECs models during charging and discharging processes;
- To provide realistic alternatives to the time-consuming task of numerous experiments, by providing guidelines for the design and optimization methodology for ECs, with wide range of applications, using a modeling approach;

- To determine optimum electrode structural parameters and fabrication conditions, such as mass ratio, type, and electrochemical reaction of active material that will yield maximum ECs performance;
- To optimize ECs energy and power densities, cycle life, capacity, and the energy efficiency of charge–discharge cycles, subject to type and value of effective conductivity of electrodes and electrolyte, electrode thickness, porosity and specific capacitance, separator thickness and porosity and the values of ECs charge and discharge currents;
- To develop optimal process design parameters for electrochemical capacitors of different applications.

1.7 Structure of the Thesis

The structure of this thesis is as follows.

- **Chapter One** is the introductory chapter and contains: Research background and materials of electrochemical capacitors (ECs), motivation and justification of the study, research aims and objectives.
- **Chapter Two** provides an overview of fundamental concepts and existing models for electrochemical capacitors, current status of the modelling and simulation of electrochemical capacitors, energy and power density of ECs, EC heat production and heat modelling, and challenges in modelling electrochemical capacitors. Chapter Two also reviewed the basic concepts of energy losses in ECs, self-discharge and distinguishable mechanisms of self-discharge in electrochemical capacitors, energy dissipation during ECs self-discharge and progress made in EDLCs and pseudocapacitors self-discharge.

- **Chapter Three** presents the derivation of:

  (i) symmetric electric double layer capacitor (EDLC) model;

  (ii) model of symmetric electrochemical capacitors with only composite electrodes;

  (iii) model of symmetric ECs with only redox couple electrodes;

  (iv) model of an asymmetric ECs with capacitor-type electrode and composite electrode; and

  (v) models for optimization of performance-prospects assessment of various ECs in terms of energy and power densities.

- **Chapter Four** presents the analytical solution of:

  (i) symmetric electric double layer capacitor (EDLC) model without self-discharge;

  (ii) symmetric electric double layer capacitor (EDLC) model with self-discharge;

  (iii) asymmetric ECs using a capacitor-type electrode and a composite electrode without self-discharge, (iv) asymmetric ECs using a capacitor-type electrode and a composite electrode with self-discharge; and

  (v) symmetric ECs with only redox couple electrodes. Chapter Four also presents the numerical solutions of: (i) model for EDLCs without self-discharge, (ii) model for EDLCs with self-discharge, and (iii) model for asymmetric ECs using composite electrode with self-discharge.

- **Chapter Five** provides the results and discussions of:

  (i) effects of self-discharge on the performance of symmetric electric double layer capacitors (EDLCs) and active electrolyte enhanced supercapacitors (AEESs) from modelling and simulation;

  (ii) effects of self-discharge on the performance of asymmetric/hybrid electrochemical capacitors from modeling and simulation;

(iii) effects of operating conditions and design configurations on the performance of ECs; and

(iv) optimization of EC design parameters and operating conditions for high energy and power performances.

- **Chapter Six** finally provides a summary of the key findings of the present research, conclusions drawn from the results, contributions to knowledge and the recommendations for future work.

CHAPTER TWO

2.0 Literature review

The literature review was presented in two parts as follows: 1) mathematical modelling and simulation of supercapacitors; 2) understanding performance limitation and suppression of leakage current or self-discharge in electrochemical capacitors. These reviews have been published as stated in list of publications, and were presented in this thesis with permission from the publishers shown in appendices A1 and A2, respectively.

2.1 Mathematical Modelling and Simulation of Supercapacitors

Most part of this section has been published as a chapter in book by I.S. Ike and S. E. Iyuke, "Mathematical Modeling and Simulation of Supercapacitors" In "Nanomaterials in Advanced Batteries and Supercapacitors",: Nanostructure Science and Technology, 2016, pp 515-562; DOI: 10.1007/978-3-319-26082-2; Online ISBN: 978-3-319-26082-2. "Copyright notice and permission was obtained from Springer", and was presented in appendix A1.

The main performance parameters of capacitors are mass/area specific capacitance, energy and power density, rate capability and cycling stability [98]. It is desirable to reduce equivalent series resistance (R) and increase capacitance (C) and operating voltage window (V) in order to increase the device's energy and power densities. The maximum operating voltage window (V_m) attainable in ECs is solely dependent upon the type of electrolyte used,

and this voltage is limited by the thermodynamic stability of electrolyte. The maximum operating voltage window V_m for ECs using aqueous electrolyte is 1 V. A thin, high surface-area EDL with a high surface area of about 200m^2/g and very little charge separation (δ~10Å) [12] is a necessity for achieving larger double-layer capacitance. Figure 2.1 below depicts components of electrochemical capacitors. A good separator is electrochemically stable, of high porosity, high thermal and chemical inertia, and its thickness needs to be as thin as possible and relatively inexpensive. Although separator thinness is constrained by the electrical short circuit risk due to free carbon particles that will obviously provide a contact between electrodes [64]. The mechanical strength should also be high enough as to permit winding processes.

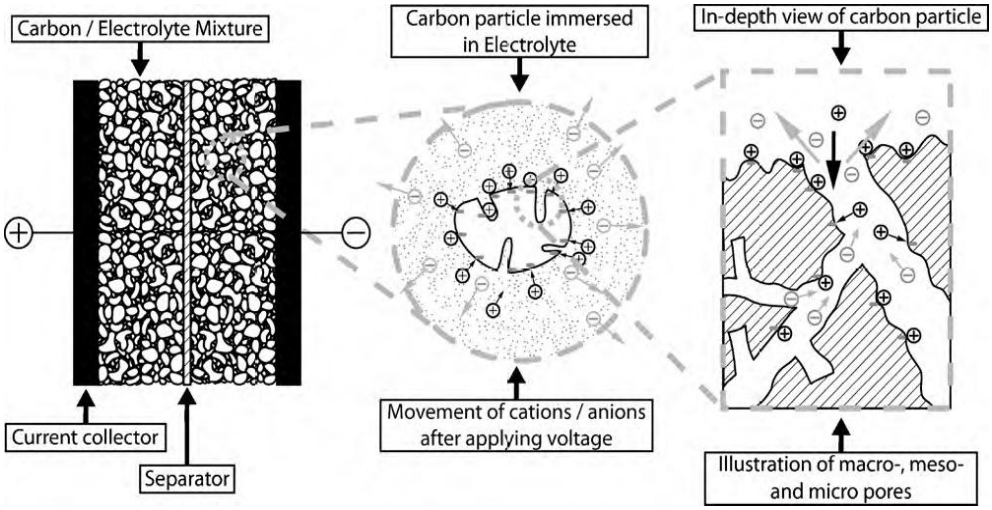

Figure 2.1: Illustration of basic components and design of an EDLC. Arrows indicate the direction of movement for cations and anions [99].

* "Reprinted from Electrochimica Acta , Vol 55, F. Favier, Julia Kowal, Dirk Uwe Sauer, Modelling the effects of charge redistribution during self-discharge of supercapacitors, 7516-7523, Copyright (2010), with permission from Elsevier ".

The electrode thickness and internal area, porosities and particle sizes of active material, and materials selected for electrolyte and electrode, are design elements that can be more accurately investigated with microstructural models, such as that described by Verbrugge and Liub [91]. Characteristics and parameters of processes occurring in ECs are closely interrelated and dependent on physical, electrical, electrochemical and crystallographic parameters of electrodes and electrolyte materials, and the design of its components and the capacitor as a whole. Therefore, modelling of capacitor for determination of its energy, capacity, and other operation characteristics, is inconceivable without a proper account of its component parameters. The majority of researchers do not consider the physical, electrical, and structural properties of electrode materials and other components while modelling and estimating the capacitor's parameters, hence the discrepancy between theoretical and experimental measurements of parameters of real-life capacitors [89]. Most of the existing models were developed on the assumption that an energy storage mechanism is solely by an electric double layer and overlooks side reactions at the boundary [100]. Even in models which accounted for these chemical side reactions [88,97,101], the reactions were oversimplified by not incorporating the temperature consideration into the models. Furthermore, the effect of pores and their different sizes has been not been handled qualitatively and no specific model has accounted for all necessary factors in a critical way. Thus, it is significant to recognise the setbacks in available models and then derived models based on first principles with a view to compensating for discrepancies in the modelling.

A model developed from a first principles view is able to forecast internal temperature and interfacial electric field in real life, so as to promote more realistic lifetime predictions. This also promote the process of designing ECs as compared to other electrical energy storage devices with the aim of maintaining a bus voltage around specific extents for arbitrary loading distributions, and to aid in development of porous structures that warrants quicker

rates of releasing stored charge and energy [3]. Available models for ECs and other energy storage devices are presently incapable of precisely predicting internal temperature rises inside the capacitor, interfacial field and temporal voltage reaction for arbitrary charge-discharge current distributions.

In this review, we considered progress made so far in the field of modelling and simulation of electrochemical capacitors by looking at two basic kinds of ECs and their hybrid capacitors. Their charge mechanisms were discussed with the aim of utilizing the most effective ways to obtain improved capacitor performance. The available models of ECs were reviewed and the merits and challenges of each kind discussed with the view to utilizing the relative advantages and compensate for disadvantages, in order to realize synergic and more realistic models which incorporate thermal models that account for temperature distribution inside a cylindrical and rectangular structured supercapacitor. The main objectives of this review are to develop mathematical descriptions of characteristics of symmetric and asymmetric ECs and parameters of processes therein, subject to physical, electrical, electrochemical and parameters of electrode materials, electrolyte and the design of components and the capacitor as a whole; to build a theoretical basis for calculations and improvement of parameters of various types and designs of symmetric and asymmetric ECs, with simultaneous accounts of the properties of electrode materials and structure parameters and separator; to provide an ideal alternative to the time-consuming task of conducting numerous experiments, by providing guidelines for design and optimization methodology for ECs with wide range of applications using a modelling approach ; to optimize the parameters of ECs subject to the type and value of the electrode's conductivity, porosity and specific capacitance, conductivity of electrolyte, separator thickness and porosity and values of charge and discharge currents of ECs.

2.2 Current status of electrochemical capacitors modelling and simulation.

Theoretical models for electrochemical capacitors begin with the original Helmholtz model to mean-field continuum models, surface curvature-based post-Helmholtz models and the recent atomistic simulations. Realistic models of ECs can be built using high stage of progress in classical and quantum molecular dynamics methods as well as parallel high performance computing. The categories of EC models have been suggested by authors/researchers: empirical, dissipative transmission line, continuum models (Poisson-Nernst-Planck equations), atomistic models (Monte Carlo, molecular dynamics), Quantum models (ab initio quantum chemistry and Density Functional Theory, DFT) and simplified analytical models. Each method has been developed to acheive various outcomes and, each displays various advantages and challenges.

2.2.1 Empirical models

This equivalent circuit model is frequently called a three-branch model and assumes that the long-term branch capacitance only accounts for differences in the charge for a maximum time of 30 minutes while the immediate branch depends on voltage. The earliest observed models which considered changes of capacitance over time were produced by Zubieta and Bonert [102]. Empirical models are better in estimating accurately an EC's electrical behavior than ordinary *RC* circuit and also it allows the users it to readily integrate the model into his/her system simulations. The empirical models could also be utilized in the characterization of self-discharge and/or leakage current parameters [103].

Ban et al [22] presented simple mathematical models incorporating voltage-independent parallel leakage processes and electrochemical decomposition to explain the behaviors of ECs during charging and discharging, in order to give a fundamental understanding of the behaviors of capacitors on operations through experimental validation. Experimental data were simulated to obtain the desired values of parameters such as specific capacitance and equivalent series resistance from which both energy and power densities can be calculated using the models. The simulated parameters value, considering both parallel leakage and solvent decomposition, could be used to predict the EC's self-discharge, shelf-life, performance/efficiency losses, as well as the limiting workable cell voltage. The models are therefore useful in evaluating and diagnosing supercapacitors, as well as a tool for understanding of the charging–discharging behavior of supercapacitors.

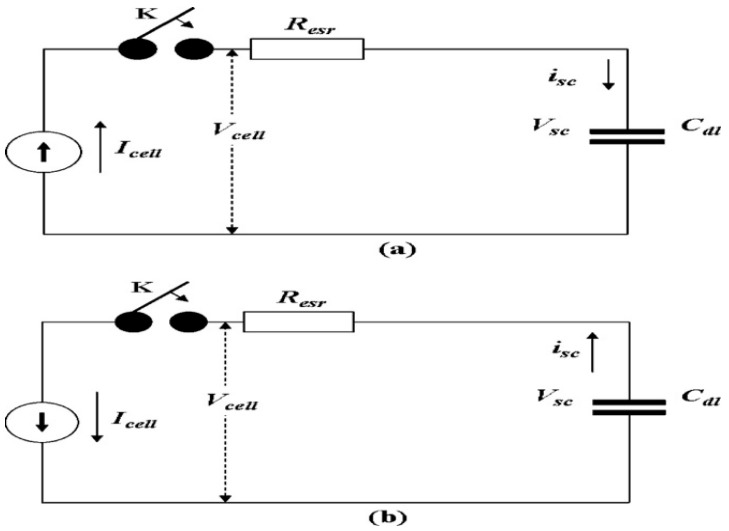

Figure 2.2**:** Proposed equivalent circuits of a double-layer capacitor at a constant current charging (a) and discharging (b) in the absence of parallel leakage phenomena and chemical disintegration of the solvent. K: electric switcher; R_{esr}: equivalent series resistance; I_{cell}: constant current for charging or discharging the capacitor; V_{cell}: capacitor cell voltage; C_{dl}: double-layer capacitance; V_{sc}: voltage across the C_{dl}; and i_{sc}: current used to charge or discharge respectively [22].

* "Reprinted from Electrochimica Acta , Vol. 90, Shuai Ban, Jiujun Zhang, Lei Zhang, Ken Tsay, Datong Song, Xinfu Zou, Charging and discharging electrochemical supercapacitors in the presence of both parallel leakage process and electrochemical decomposition of solvent , 542-549, Copyright (2013), with permission from Elsevier ".

The model could also be useful in obtaining the esential parameters of the capacitors, such as equivalent series resistance and capacitance based on recorded curves of charging–discharging. A schematic diagram of an electrical equivalent circuit of EDLCs during charging/discharging at a constant cell current in the absence of parallel leakage and solvents chemical disintegration is shown in Figure 2.2 below.

If capacitors are charged to a designed cell voltage of $V_{cell}^{\max}$, a discharge process at a constant current (I_{cell}) can be started immediately, as shown in Figure 2.2b. Figure 2.3 shows the schematic diagram of electrical equivalent circuit of EDLCs for constant current charging/discharging with involvement of parallel leakage phenomena and solvent chemical disintegration. The models developed by Shuai et al [22] could be used to explain charge and discharge characteristics of capacitors involving the voltage-independent parallel leakage process and solvent disintegration as suggested by its ability to reasonably fit experimental data. However, there is a slight mismatch/difference that might have originated from experimental trivial factors such as the effect of gaseous evolution, dissolution of current collectors, electrolyte crystallization in the separator, assembly quality, etc. at the discharge curves in particular.

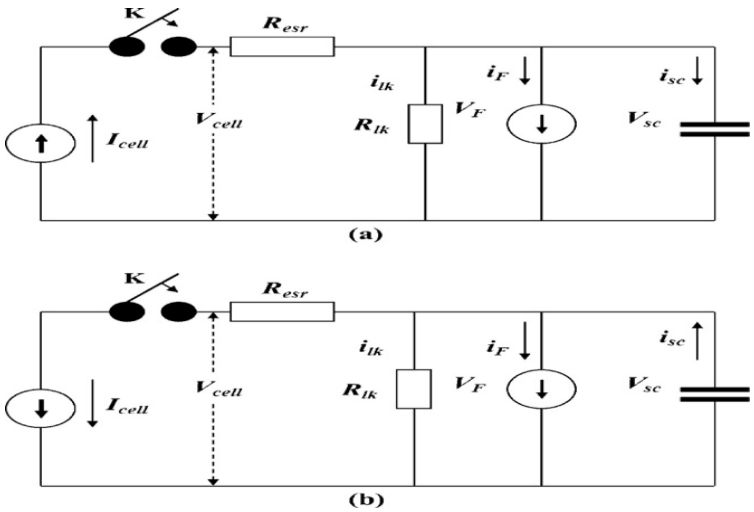

Figure 2.3**:** Proposed equivalent circuits for a double-layer capacitor at a constant current charging (a) and discharging (b) in the presence of electrochemical decomposition of the solvent. K: electric switcher; R_{esr}: equivalent series resistance; R_{lk}: parallel leakage resistance; i_{lk}: parallel leakage current; I_{cell}: constant current for charging or discharging; V_{cell}: capacitor cell voltage; i_F: current of solvent electrochemical decomposition; C_{dl}: double-layer capacitance; i_{sc}: current used to charge or discharge the double-layer capacitance; V_F: electrode potential of the solvent electrochemical decomposition; and V_{sc} (=V_F): voltage across the double-layer capacitance, respectively [22].

* "Reprinted from Electrochimica Acta , Vol. 90, Shuai Ban, Jiujun Zhang, Lei Zhang, Ken Tsay, Datong Song, Xinfu Zou, Charging and discharging electrochemical supercapacitors in the presence of both parallel leakage process and electrochemical decomposition of solvent , 542-549, Copyright (2013), with permission from Elsevier ".

The main setbacks of these models are their small quality for: conditions of operation which are quite different from those utilized in obtaining the parameters [104] and its inability to predict in extended time range when heat produced within the system alters the capacitors' electrical behaviors. Since these models were not derived from basic capacitor physics, they

are unable to estimate temperature growth within the system and can only be correct if temperature rise is negligible. On this understanding, it is unrealistic to utilize the models in the accurate prediction of a real life electrochemical capacitor.

2.2.2 Dissipation transmission line models

The pore structure of the electrodes mitigates ionic motions to regions situated deep into a pore and results in a nonlinear growth of terminal voltage. It is therefore beneficial to use models which explain movement and steady-state reaction of the electrolyte portion since its mass region is presented to first order by a simple resistor. The earliest porous electrode models that handled EDLC with a porous electrode's wall as a transmission line of shared electric double-layer capacitor and electrolyte resistance were developed by de Levie [105]. The effect of ion depletion on the charging rate of porous electrodes deserves further scrutiny for several reasons: 1) It will improve understanding of performance limits of double-layer capacitors as a function of device parameters. For instance, depletion can occur in both electrodes and separator, and tuning geometry may improve power and linearity. 2) Study of this phenomenon raises fundamental questions about the relationship between adsorption and transport of ions in nanoporous conductors and the influence of differing ion mobilities on these effects.

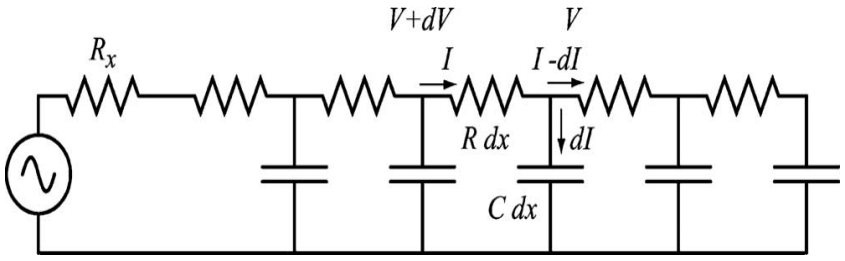

Figure 2.4: De Levie's transmission line equivalent circuit for an electrolyte filled conducting pore [106].

* Reprinted with permission from Journal of The Electrochem. Soc., 157 (8) A912-A918 (2010). Copyright 2010, The Electrochemical Society.

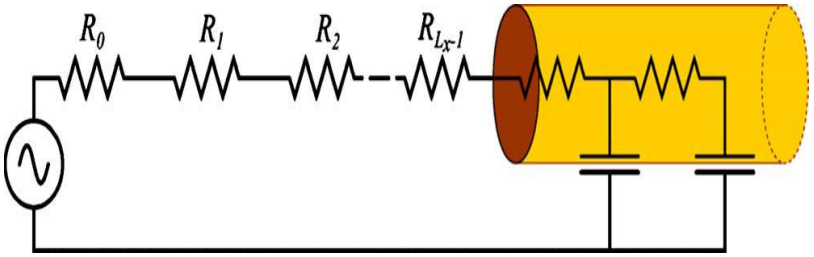

Figure 2.5**:** (Colour online) Extension of circuit model outside pore [106].

* Reprinted with permission from Journal of The Electrochem. Soc., 157 (8) A912-A918 (2010). Copyright 2010, The Electrochemical Society.

The de Levie model treats pore as a distributed *RC* circuit Figure 2.4 and states that voltage and current vary with respect to time *t* and position *x* along pores. De Levie assumed that concentration throughout the entire pore is constant, but the different solution environment outside of the pore must also be considered. The bulk solution between the pore entrance mark and the midpoint between the working and counter electrodes mark ought to be handled as a series of discrete resistors, with each resistance dependent on salt concentration at that specific position, so as to estimate voltage outside the pore as in Figure 2.5 above.

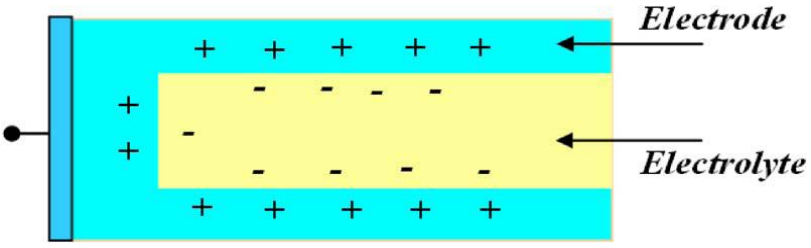

Figure 2.6**:** One dimensional pore [107].

© (2010) IEEE. Reprinted, with permission, from [N. Bertrand, J. Sabatier, O. Briat, J.-M. Vinassa, IEEE Trans. Ind. Electron. 57 (12) (2010) 3991].

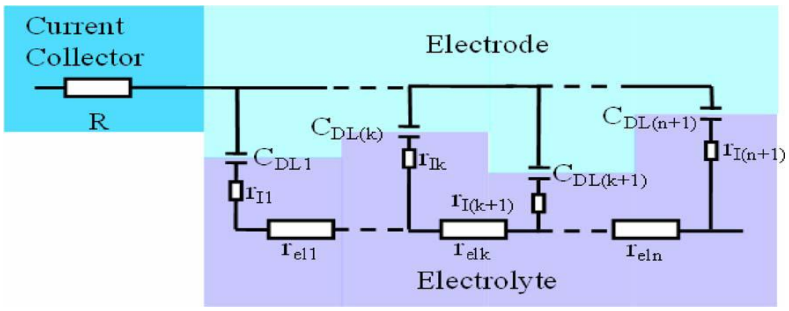

Figure 2.7: Half porous electrode model discretization [107].

© (2010) IEEE. Reprinted, with permission, from [N. Bertrand, J. Sabatier, O. Briat, J.-M. Vinassa, IEEE Trans. Ind. Electron. 57 (12) (2010) 3991].

The ruling expressions for ECs shown in this section, consider EDLCs with a rough portion of the electrode/electrolyte interface, and without voltage and temperature variations of the parameters. The capacitor is explained by a one-dimensional (1-D) pore as shown in Figure 2.6 above.This model has revealed that dependency of electrode conductivity on its operation is small, and as such the losses produced by the electrode's internal ohmic resistance are negligible. The 1-D discretization of former equations, in *n* layers, resulted to an electrical circuit. Wires and the separator effect, which was neglected in the past, has now been considered by *RS* resistance in series with the pore model, as shown in Figure 2.7.

The EDLC is a physical component which has a demanded capacitance, parasitic inductance as a result of the geometry, resistances owing to the internal resistances of electrons and ions and resistance due to current leakages between its electrodes. The equivalent series resistance ESR which is the summation of the series and parallel resistances R_s and R_p, respectively are

accountable for electrical losses that produce ECs heating. The main transmission-line model utilized in the description of the frequency characteristics of capacitance and series resistance, which ignored voltage and temperature variations subject to capacitance and series resistance has previously been developed by de Levie [105]. A simple model that accounts for extra linear variation of capacitance with tension has also been suggested by Zubieta et al. [102]. Dougal et al. [108] and Belhachemi et al. [109] have used comparable models whose capacitance consists of steady portion C_o and linear voltage variant one $C_V = K_V . U$, where K_v is a coefficient that is dependent on applied technology.

Conclusively, current and energy for a particular voltage are considerably more than the expectations from classical equations in the instance of steady capacitance. Values of capacitance and resistance vary with frequency spectrum and the performance can obviously be estimated with the Impedance Spectrum analyzer [110]. In order to consider the voltage, temperature and frequency reliabilities, a simple equivalent circuit was derived by Rafik et al (Figure 2.8) by combining De Levie frequency model and Zubieta voltage model and the inclusion of more functions to account for temperature dependence.

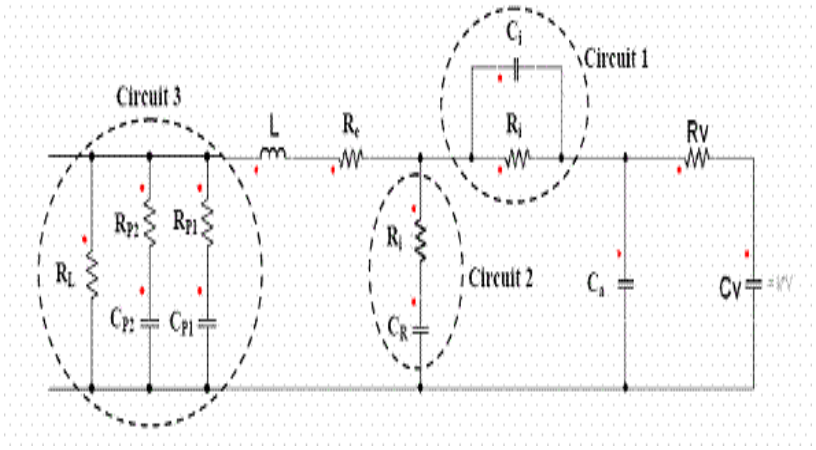

Figure 2.8**:** Equivalent circuit for capacitance and series resistance dependences as a function of frequency, voltage and temperature [103].

* "Reprinted from Journal of Power Sources, Vol. 165, Issue 2, Bor Yann Liaw, H. Gualous, R. Gallay, A. Crausaz, A. Berthon, Frequency, thermal and voltage supercapacitor

characterization and modelling, Pages 928-934, Copyright (2007), with permission from Elsevier ".

The series resistance consists of the electronic part, which is due to internal ohmic resistance in electrodes and the ionic part, which emerges from the mobility of ions in electrolyte. The major merit of the dissipative transmission line model is its capacity to produce acceptable access among pore structures and response time in the field of ECs. It also gives a first-order estimation of exponential growth/reduction in voltage level, while considering a steady current of charging and discharging cycle. It is built upon the physical structure of interface, instead of merely matching experimental measurements by integrating the passive circuit element. Nevertheless, this approach accounts for a small area of interfacial dynamics and is basically utilized in specific aims like the improvement of electrodes synthesis [111], the study of self-discharge characteristics [112], and the prediction of electrode surface impedance [113].

2.2.3 Continuum models (Poisson-Nernst-Planck Equations).

The very precise modeling method presently available utilized Poisson–Nernst–Planck (PNP) electrodiffusion theory to be the boundary of electrode and electrolyte, while physicochemical parameters became dependent on local surroundings rather than being constant, because the value of the electric field at the boundary is quite big. The PNP theory can estimate electrolyte properties correctly only if physicochemical parameters are independent of the local surroundings. Figure 2.9 represents the schematic model of EDL structures while considering an electrode that is positively charged for an instance. Helmholtz [114] initial proposal of an EDL model that consists of simple separation of

charges at the electrode/electrolyte interface like the convectional parallel capacitor in determining capacitance without considering the surface potential and the electrolyte concentration [115] is as represented in Figure 2.9a below. The Helmholtz model structure is like the structure of conventional capacitors using two planar electrodes separated by a dielectric.

Ions which are opposite to the sign of electrons on an electrode are distributed in the area of thickness higher than the Helmholtz layer (H), rather than being packed close at the electrode surface as demonstrated in Figure 2.9b. Chapman developed and solved the Poisson-Boltzmann equation steady-state manner in order to estimate electric potential in the diffuse region. This theory estimates wrongly huge ionic concentrations and the potentials of minute portions of 1V even with very dilute solutions. It can thereore hardly be utilized to model real ECs with the potential of 1V at the surface and an electrolyte concentration of 1 mol/L, since ions were taken as point charges, whereas their sizes are specific in real life [116].

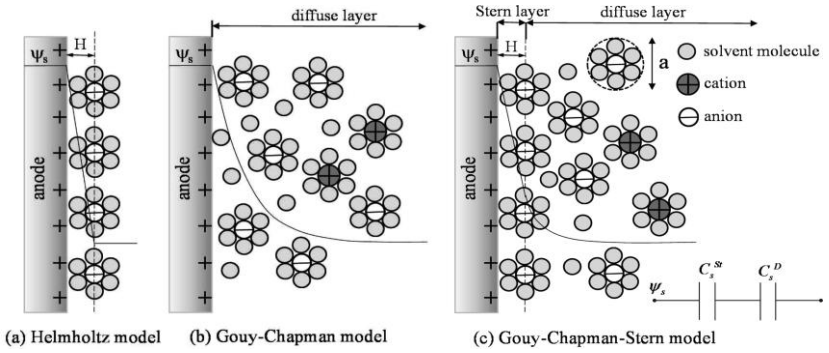

Figure 2.9**:** Schematics of the electric double layer structure showing the arrangement of solvated ions near the electrode/electrolyte interface in the Stern layer and the diffuse layer. (a) Helmholtz model, (b) Gouy-Chapman model, and (c) Gouy-Chapman-Stern model [117].

* "Reprinted (adapted) with permission from H. Wang, L. Pilon, J. Phys. Chem. C 115 (2011) 16711. Copyright (2011) American Chemical Society".

Stern in 1924 integrated the Helmholtz and Gouy-Chapman models to obtain the Gouy–Chapman–Stern EDL theory which was generally utilized in the evolution of EDLCs. This model clearly explained ion concentration in the stern and diffuse layer as clearly seen in Figure 2.9c. Grahame [118] modified the Stern's model by noting that ions adsorption at the surface of the electrode results in a double layer of different thicknesses in the Stern layer region [12]. This model derived by Stern and Grahame is known as the Stern model [119]. Wang and Pilon produced a three-dimensional (3D) model from continuum theory for characterizing EDLCs with organized electrode structures having meso-pores and critically considered 3-dimensional electrode morphology, definite size of ions, stern and diffuse region, and variations of electrolyte dielectric permittivity with local electric field [120]. Pairs of boundary conditions to estimate the Stern region, without characterizing it within electrolyte environment, was developed and utilized in estimating the electrode configuration of CP204-S15 mesoporous EDLC that was previously synthesized and described by Woo et al [120]. This created the possibility of simulating EDLCs with 3-dimensional organized electrode structures which correctly considered the stern and diffuse layers, the definite size of ions, and the variation of electrolyte permittivity on the local electric field [121].

2.2.4 Atomistic models (Monte Carlos molecular dynamics)

Molecular modelling is very significant for the optimal design of EDLCs. The notable merit of this method of modelling is it allows the estimation of processes that are not immediately apparent experimentally. For instance, the orientation of ions in electrolyte [122] and alteration of the electrode form as result of polarization [12] are essential conditions that affect electrode capacitance and are hardly determined from experiment. The interwoven

effect of these variables can be comprehensive and utilized in the design optimization of new EDLCs through exact simulations and physical modelling. Because of complex interactions among electrode and electrolyte properties, together with its effect on energy and power densities generally, active optimization of EDLCs design remains a serious concern. The electrolyte should be used simultaneously with specific pore geometries and sizes is an illustration of design considerations [116,118,119]. When ions have various kinetic sizes during charging and discharging, then models need to be derived for these specific electrolytes and the optimum size of pores in each electrode shall be different [120,121,123]. Electric conductivity of room temperature ionic-liquid electrolytes RTILs can be increased by introducing organic solvents while using optimal concentration of electrolyte [124,125] but another issue on optimization here becomes the influence of pore size on power density [126]. The energy density of EDLCs can be improved by using pores of a diameter that is approximately equal to the diameter of the ions [5,116]. Power density will be restricted by the high diffusion resistance created by small pores.

Molecular modelling will obviously enhance the comprehension of equilibrium and the dynamic processes taking place in an EDLC on atomic state, though its accuracy depends largely on the authenticity of the force fields applied, in explaining molecular behavoirs in the fluid phase and force fields of the electrode modelled. Monte Carlos (MC) simulation that relies on statistical mechanics via the significant choice of phase space of the molecular system and molecular dynamics (MD), are the most acceptable molecular simulation methods [107,127] MC simulation is restricted to estimation of equilibrium properties since it is based on statistical mechanics, while MD simulations evaluate Newton's equations of motion for several molecular systems, which properties are averaged over a short simulated time to estimate the system's properties. Another merit of MD simulations is its ability to estimate dynamic properties like diffusion of ions. Introducing electrode polarizability which

improves surface charge within the regions through induced charges which finally grows the field and capacitance [128], is cogent both for numerical variance generated between predicted results and correct representation of the basic physical aspect affecting capacitance and dynamics that occur in EDLCs. Erroneous small capacitance value, as compared with experimental results, will result if electrode polarization is ignored.

An important field of research in molecular modelling that has recently drawn more attention and which will guide in the characterization of novel EDLCs with improved energy density, is the simulation of surface functionalities and nano-surface tuning simultaneously with the optimum choice of RTIL electrolyte size. Simulations of RTILs at planar surfaces has revealed important understanding of the EDL structure and assisted in describing experimental differences noticed in differential capacitance, though this knowledge can not be utilized when designing EDLCs with high energy density because these types of electrodes have small surface areas and are not suitable. Porous electrodes are preferable for providing high surface areas, but are certainly controlled by several physics from a simulation perspective. The state of development of classical and quantum molecular dynamics and the use of parallel high performance calculations, permit the construction of realistic models of such systems. The consistent classical consideration of EDL at the boundary of metal and ionic liquid was performed in reference [129]. The molecular dynamics simulation of solid electrolytes with carbon nanotubes was carried out by Chaban et al [122]. This classic model makes it possible to satisfactorily describe the ionic subsystem of the electrolyte, but does not provide information on the electron subsystem of the material of the electron–hole conductor of the electrode.

Molecular dynamics (MD) simulation presents the most basic and modifiable method for analysing molecular behaviours and has been widely utilized in modelling electro-osmotic

flow [123–126,130,131], as well as treating higher charge densities which are of great significance in EDLCs [132–134]. However, computational cost makes this an unrealistic method of handling time and length scales which are obtainable in several applications. Calculating long-range Coulombic relationship and using boundary conditions creates challenges and an alternative approach is urgently required. Using results of quantum molecular dynamics calculations of Lankin et al. [135], estimates of the maximum specific capacity of an electric double layer on a defect-free graphite electrode surface has been estimated and the estimation correlated well with all existing experimental data.

Investigation of the density functional theory (DFT) investigation revealed a bell-shaped curve resulting from co-ion elimination and the introduction of a counter-ion without capacitance growth [136]. This observation in DFT computations is expected due to simplified RTIL ions in the constrained local model, as well as the chosen pore size. Huang et al. [137] presented exohedral an ECs model for spherical electrodes and cylindrical electrodes in order to explain the relative capacitance and size of either OLC or CNT. The origin of the curvature effect in EDL is yet to be fully been understood. Capacitance increases with decay in the size of electrodes as displayed by even theoretical models. Limited investigations have been done on the dependency of differential capacitance changes on potentials in ECs with OLC/CNT-based spherical electrodes and RTIL electrolytes, while attention has also been focused on proving that different C-V profiles were noticed in capacitors with planar electrodes [138–142].

Potentials of RTIL-based capacitors operating in large temperature windows enhance its applicability during strong conditions due to excellent thermal stability [137,143], and several research groups have utilized capacitor’s temperature dependence on capacitance. Some theoretical and experimental research showed that capacitance grows with temperature

[137,144], while some showed that capacitance decays with growth in temperature [145,146]. Others showed even a complex capacitance-temperature dependency. Lin et al. [147] demonstrated of recently that capacitance of ECs using OLC electrodes and RTIL electrolytes increases together with increases in temperature, while that of vertically aligned CNT electrodes with RTIL electrolytes react independent of temperature. MD simulations were utilized in modelling electrochemical capacitors with RTIL electrolyte and OLC/CNT electrodes to be dependent on temperature in order to obtain molecular understanding into temperature variations of capacitance [148,149].

A Monte Carlos investigation revealed that a change in position of counter-ions on a charged surface and packing of ions in particular, demonstrated the influence of EDL on temperature reliability near charged pore wall [150]. MD simulations, use several kinds of carbon electrodes to produce comprehensive molecular understandings of behaviour of RTIL-based ECs capacitance. The capacitance of capacitors with porous electrodes was shown to agree well with a particular form of RTILs, general features of pores and the applied potential. Most of the research forecast that capacitance decreases with increases in temperature or at least produces a complex behaviour between capacitance and temperature [143,146,150,151] as presented in MD simulations by Vatamanu et al. [146]. Monte Carlo simulations by Boda and Henderson [151] revealed a bell-shaped profile for capacitance-temperature relationships. Recent research with vertically aligned CNT electrodes and RTIL electrolytes showed that capacitance was almost invariant with temperature [147]. Thus, deeper studies are required in order to confirm concrete explanation of how temperature depends on capacitance as well as basic mechanisms that produce this process. Feng et al. [148] noticed that capacitance of EDL near the CNT electrode is almost independent of temperature within the range of 260K and 400 K, which agreed well with new research results by Lin et al. [147]; though they noted that capacitors' power, charge and discharge rates that severely rely on ion mobility

instead of packing cannot be evaluated from the obtained temperature reliance on capacitance.

Nano-pores have more charge storage capability compared with planar electrodes since the overall charge on the electrode is equilibrated by a single portion of ions not being overshadowed [152]. Optimal energy density is dependent on pore diameter and optimum pore diameter grows with voltage [153]. The electrode polarization which improves the surface charge through induced charges that lead to growth in the electric field strength and capacitance are crucial features that must be integrated into molecular models aimed at precisely matching its results with experimental results and exactly reflect real-life devices.

Comparatively, transport influences were modelled to a small level and opinions for utilizing these influences to improve EDLC performance were omitted. Since the modelling of ions transport effects has not be given due attention in the past, extensive research in molecular modelling should be broadened to place more emphasis on ionic transport, charge and discharge kinetics and to determine and enhance the efficiency of dense RTIL electrolytes in carbon electrodes of nano-pores. Again, simulations that can accurately estimate kinetics during different charge and discharge rates will certainly improve the optimization of energy and power densities. EDLC transport was derived to learn the effects of polarization relaxation, temperature, electrode shape, and ionic size only. Introducing organic solvent to RTILs electrolytes results in improved electrolyte function by increasing ionic conductivity and relative permittivity, and also reduces viscosity and ESR but responds with a decrease in density of ions that lowers capacitance. Simulations of very complex structures of electrodes like a 3-dimensional, hierarchical porous system that has not yet been accounted for, has to be introduced in molecular models so as to realize a high level of reality and to create a plarform to further enhance EDLC performance [154,155]. Similarly, pseudocapacitors and

hybrid capacitors with battery-type and EDLC electrodes are fields of research that are now drawing considerable attention, though realistic models for these capacitors are presently constrained to small MD simulations [156,157] and ab initio computations [158]. Developing active models in these directions will certainly be required for the accurate identification of situations and materials that could result in enormous advantages in EDLC performance.

2.2.5 Quantum models (Ab initio quantum chemistry and DFT) of electrochemical capacitors.

Recent research attention on ionic liquids appears justified, following unique simulations of behaviours such as electrolyte with small vapour pressure, all round functionalities and electrochemical potential range. Enormous efforts have been channelled into investigation of ionic liquid electrolyte capacitance changes with pore size in mini-nanometres region. Kornyshev and co-researchers [159] described unusual growth as image forces which exponentially block repulsion of similar-charged counter-ions within a small pore model of charged ions in a metallic slit pore. De-en and Jianzhong [136] addressed the issue of the microscopic attitude of the interface of electrode and electrolyte and capacitance dependence on pore size using classical density functional theory (c-DFT). De-en and Jianzhong discovered the enormous capability of the c-DFT approach in giving microscopic insights with little molecular coverage and calculation cost, and also the capability to handle a wider pore size window as compared with bigger ionic size scales.

Basic ideas and applications of c-DFT to electrolyte environments have recently been explained in some reviews [160,161]. They pointed out that the mathematical background of c-DFT is similar to well-known electronic DFT [162]. c-DFT for electrolytes expresses free

energy to be dependent upon the local densities of ions and solvent molecules instead of presenting the system energy to be dependent on the density of electrons. The simplicity of this theoretical model also enhances observation of the origin of the oscillation of capacitance in ionic liquid electrolyte and provides a full understanding of core parameters in a large range of environments. c-DFT suggests a small gap that causes the density profile of ions to interfere with EDLs between two charged surfaces, together with strong vibration-like profiles in the density of ions near a charged surface [163,164]. c-DFT is expected to be capable of estimating very complex forms of capacitance-potential curves with its charging processes and the changes in curvature shape with pore size, since the model for ionic liquid replicates real-life situations [165].

A total image of capacitance during transit into pore sizes from microscopic range to mesoscopic scales (>2 nm) is provided by c-DFT simulations, and capacitance virtually becomes independent of pore size, if pore size goes beyond a few nanometres. Modelling of EDLC behaviour in the past relied on dividing pore size frames into several sizes, such as below 1, 1-2, and 2-5 nm, etc. [77,166], which becomes irrelevant as it produces a steady change of structure and capacitance of EDL while pore size varies on c-DFT application. Absolute agreement with experimental results shows that c-DFT accounted for the most significant physics in the system. c-DFT research has not addressed the issues of the size of solvent molecules, solvent polarity, concentrations of ions, ionic charges, cations-anions size disparity and shape of electrode, which are important parameters that will improve comprehension of EDLCs with organic electrolyte [167,168]. It is important to consider the influence of these parameters while matching integral capacitance with differential capacitance [169]. The c-DFT method is the state-of-the-art method used by experimentalists to determine surface area and pore size distribution of real porous materials [170,171] and can handle modelling difficulties with how to confirm an estimation of interactions between

the structure and capacitance in real porous material and specific electrolyte. Consequently, c-DFT modelling can account for all phenomena of EDLCs charge storage, such as calculation of porosity, capacitance as well as charge and discharge kinetics. c-DFT is not yet able to account fully for complex porous electrodes and the estimation of perfect electrolyte and porous design to optimize energy and power densities of real-life EDLCs. A particular difficulty from a modelling view-point is the provision of the estimation of relationships between structure and capacitance in real porous material and specific electrolyte.

2.2.6 Simplified analytical models.

This kind of model is derived on the basis of the fundamentals of electrochemistry and physics of ECs. Algebraic and differential equations were utilized in characterizing the controlling properties of the chemical and physical processes (charged species transport and electrochemical reaction rate) of the system [88,101,107,127,172,173]. The ECs fall into two categories on basis of chemical and physical processes that accounts for total capacitance of the system: EDLC which stores charge electrostatically and pseudocapacitor which stores charge by fast and quick reversible chemical reaction. Several areas of ECs like the effect of side reactions [127], electrode pore structure [107,172], and estimation of specific energy and power [173] were investigated using these assumptions. Karthik et al. [89] developed a reduced models for EC analysed with scaling arguments, calibrated and validated with experimental data, without accounting for the equation of change of energy and heat generation, by assuming that temperature effect and side reactions are negligible and the system was assumed to be isothermal.

Major efforts related to EDLCs have been directed towards understanding the influence of electrode thickness and pore structure on energy density and device capacity. Efforts toward developing pseudocapacitors have mostly focused on creating different electrode materials with most emphasis given to metal oxides [4,89] and some effort goes toward the understanding of charge/discharge behaviour of these redox couple electrodes [12]. Devices in which two electrodes exhibit the same capacitive behaviour are known as symmetric capacitors [89]. If the capacitive behaviour of the two electrodes is different, the device is known as an asymmetric capacitor.

Analytical solutions for electrode voltage as a function of discharge current have been previously developed by Srinivasan and Weidner [87,88,90]. Discharge of a redox couple electrode is controlled by diffusion of a mobile ion through the film. The kinetic expression at this interface has been given previously presented [172,173] and was extended to hybrid asymmetric supercapacitors by John A et al. [90] as shown in Figure 2.10b. In the case of redox couple electrodes in hybrid asymmetric supercapacitors, the state of charge remains between approximately 0.4 and 0.6. The model for the redox couple electrode is generic, and could be applied to describe any electrode, as long as parameters such as initial ion concentration and diffusivity are known. Diffusivity values that were previously reported by experimental methods [109] were utilized while making the assumption that diffusivity is constant.

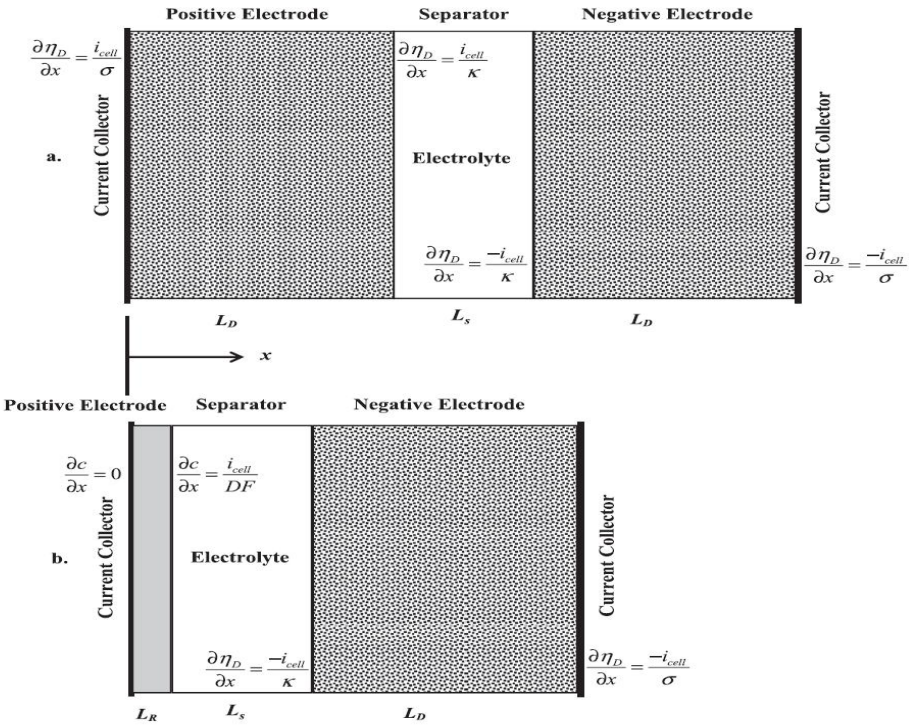

Figure 2.10**:** Schematic representations of a) the symmetric supercapacitor and b) the hybrid asymmetric supercapacitor with electrode dimensions not drawn to scale [90].

2.3 Energy and power density of electrochemical capacitors.

Different electrochemical energy storage devices can be compared using their respective energy and power densities and any advantage that hybrid asymmetric ECs (Figure 2.10a) possess over symmetric ECs (Figure 2.10b) can be demonstrated. The energy and power densities are dependent on the capacitor's mass. The mass of symmetric EC is given as the mass of each porous electrode, and electrolyte inside each electrode and inside the separator:

$$m_S = 2L_D A\rho_D + L_S A\rho_S + 2\varepsilon_0 L_D \rho_e + \varepsilon_S L_S \rho_e \qquad 2.1$$

where A is the capacitor cross-sectional area, ρ_D is the density of electrodes with EDL, L_S is the separator's thickness, ρ_S is the density of separator, ρ_e is the density of electrode, ε_0 is the

porosity of electrode and ε_S is the porosity of separator. The difference between the mass of the hybrid asymmetric EC and the symmetric EC is that the former only has one electrode with EDL, with a dense redox couple electrode as the positive electrode:

$$m_H = L_D A\rho_D + L_S A\rho_S + \varepsilon_0 L_D \rho_e + \varepsilon_S L_S \rho_e + L_R A\rho_R \quad 2.2$$

where ρ_R is the density of redox electrode.

The energy and power densities are calculated by integrating cell potential over cut-off time, or time required upon discharge for two electrode potentials to equal one another, which varies with discharge current density i_{cell} as given below:

$$E = \frac{i_{cell}}{m}\int_0^{t_C} V_{cell}\, dt \quad 2.3$$

$$P = \frac{i_{cell}}{mt}\int_0^{t_C} V_{cell}\, dt \quad 2.4$$

where V_{cell} is the cell potential, t_C is the cut-off time and m is the mass of either capacitor, representing either m_S or m_H. The moment the electrode parameters are known and the potential profile has been simulated, the dependency of the energy and power densities on the discharge rate could be determined. These models are generally applicable to any double-layer and redox couple electrode, so long as the properties of the materials are known.

The main advantage of the of this analytical model is its ability to describe electrical functioning of ECs using partial differential equations that explain~~s~~ the electrochemical and physical processes within the capacitor. This method is more flexible ~~to~~ in accommodating more parameters and sets of complementary equations and does not rely on empirical evidence to any great degree. However, this type of model makes it very difficult to estimate aging phenomena of battery and EC models which have the same analytical modelling approach as stated by Doyle et al. [173] in their article. This is basically because non-

homogeneity of electrolyte at the interface and integration of thermal variables were not considered when deriving the analytical model. Kazaryan et al. [89] developed models for calculations, control, and improvement of energy, capacity, power, and other parameters important for the safe and long operation of various types and designs of asymmetric electrochemical capacitors (heterogeneous) with simultaneous accounts of physical, electrical, electrochemical properties of electrode materials, designs, and spatial structures of electrodes and separator. They assumed that a negative electrode does not have self-discharge, and that the potential for a positive electrode being non-polarizable does not change during charging and discharging and so is constant along the coordinates of the positive electrode.

Jin et al. [174] developed a model for a simple planar EC, from where they showed that polarization density and electrolyte solution are absolutely critical and cannot be ignored in model derivation. Also, they noted that modelling of the surface contact area is of important concern since most of the charges are stored in such a small portion that its movement is dependent on several variables like electric and thermal fields, concentrations of species and impurities. Julian et al. [119] developed a three-dimensional model for ECs with cylindrical mesoporous electrodes to study the effects of the following: pore radius, electrolyte permittivity, porosity, ions effective diameter, and characteristics of electrolyte on diffuse layer capacitance. They proved that reduction of the ion effective diameter and radius of pores produced great growth in diffuse layer gravimetric capacitance. Ganesh and Sanjeev [175] derived from the first principles of ionic movement one-dimensional (1D) and two-dimensional (2D) models of an EC with no faradic reaction using isotropic transport properties to explain the recovery of potential during relaxation after discharge/charge and its dependence on current and concentration, as well as failure of the EC during charging at high currents and low concentrations of electrolyte.

Conductivity of the electrode during charging and discharging may change in wide a range, subject to specific capacitance parameters, type of conductivity, and electrophysical parameters of the electrode. The change has a considerable effect on both capacitance and other parameters of electrochemical capacitors. The parameter changes must be taken into considerations in order to obtain more precise results. Numerous nonlinear influences should be expected, both in the near-surface layers of walls and in wall pores, subject to the anisotropy of the electrode, as well as the different dimensions and forms of pores. The capacitances of the EDL from the side of the the electrolyte and to side of the electrode are serially connected with each other, and parameters of wall pores [176] perform a major role in changes in electrode total capacitance.

Kazaryan et al. [89] developed an analytical model of asymmetric ECs which made it possible to calculate energy, capacity, power parameters, energy efficiency of charge-discharge cycles of capacitors subject to the type and value of the conductivity of electrodes, conductivity of electrolyte, thickness and specific capacitance of electrodes, and values of capacitors charge and discharge currents. They also observed that growth of the volumetric specific capacitance of electrode produces growth in specific energy parameters of capacitors and growth of polarization and depolarization energy losses which manifest as heat. The major portion of energy losses resulted from polarization resistance of electrodes and electrolyte, while the remaining portion is due to depolarization of electrodes' potentials. They also noticed that the energy efficiency of charge-discharge cycles of ECs depends significantly on the conductivity of the electrode and electrolyte, thickness of the electrode, and the value of charge-discharge currents. An increase in conductivity of the electrode and electrolyte decreases nonlinearly the polarization and depolarization losses of energy during ECs charging and discharging.

2.4 Heat production and heat modelling of electrochemical capacitors.

Electrochemical capacitors are usually charged and discharged at a very high rate, which will obviously produce a great amount of heat within the capacitor. This condition of increased temperature will certainly increase capacitance and self-discharge, while equivalent series resistance (ESR) will be decaying [103,128,175,177,178]. ECs encounter "self-heating" which is promoted with growth in the electric field and temperature during charging and discharging. The activity of self-heating increases the temperature of the capacitor by enhancing non-reversible side reactions that reduce the electrolyte's ionic conductivity. This alone generates more heat over time and creates thermal runaway. During EDLC charging and discharging, the amount of electric charge is transformed to heat, and the heat production rate varies with the condition of operation, material of construction and capacitor's design [179]. Severe high temperatures result in the following: increased aging rate of capacitors [161–164,167–171,176,179–184], increased self-discharge rates [180–183], increased cell pressure, and possibly electrolyte evaporation [183]. The resistance of ECs increases and its capacitance decreases as it ages, which results increase in temperature and voltage in capacitors [184], which can cause voltage imbalance and unfavourable overvoltage of individual cells, when cells are serially connected [179,180]. Thermal modelling is very useful in estimating the temperature of operations, thermal functioning of new ECs and development of thermal management plans for existing EC designs.

The design and fabrication of modern day capacitors and their cooling plans greatly rely on the success of thermal simulation models. It is therefore essential to obtain mathematical descriptions of mechanisms that generate heat in the system. Estimation of the electrical

heating functioning of capacitors could be very challenging due to the very large series of processes like ionic and electronic transport, heat and mass diffusion, and the involvement of heterogeneous structures. Temperature distribution in supercapacitors depends on losses of power and energy within the devices. The relationship between the rate of heat generation during the continuous charge-discharge processes and temperature T (M, t) at a specific position in the EC, is mainly controlled by the heat diffusion expression as previously presented by Guillemet et al. [178]:

$$\nabla \cdot \left(-k(M) \cdot \nabla T(M,t)\right) + C_p \rho \frac{\partial T(M,t)}{\partial t} = \dot{q} \qquad 2.5$$

The heat generation rate $\dot{q}$ is caused by the following:

• Transportation of electrolyte ions that are in electrodes and separator, and transportation of electrons in current collectors and electrodes.

• Reversible and irreversible reactions at the electrode/electrolyte interface of porous structures.

• Thermal contact, electrical ohmic resistances of layers, and polarization and depolarization resistances.

Guillemet et al. [178] using their model performed thermal analysis on ECs, pointed out that the highest temperature is attained at the centre of the device as envisaged.

d'Entremont and Pilon [185] derived a physical model that describes the diffusion of electrons, heat production, and heat transport in EDLCs while charging and discharging. Their model is significant because it estimates spatial and temporal changes of various heat production rates and temperature within EDLCs from basic principles. It also considered irreversible Joule heating, as well as three reversible heat production rates coming from ion diffusion, steric effects, and changes in the entropy of mixing. The reversible heat production

rates are exothermic on capacitor charging, endothermic while discharging it, and localized in the electric double layers.

They developed the thermal model in order to understand the diffusion of electrons, heat production and heat transport in EDLCs at constant current charge and discharge cycles [185]. They achieved this by formulating irreversible Joule heating and reversible heat generation formula for EDLC, and were able to reproduce experimental data previously reported in literature thus providing some verification to their model. The energy equation developed by d'Entremont and Pilon [185] is expressed as equation 2.6 shown below:

$$\rho c_p \frac{\partial T}{\partial t} = \nabla . \left(k \nabla T \right) + \dot{q}_{irr} + \dot{q}_{rev} \qquad 2.6$$

where $\dot{q}_{irr}$ and $\dot{q}_{rev}$ are irreversible and reversible heat production rates; $\dot{q}_{irr} = \dot{q}_{E,j}$; and $\dot{q}_{rev} = \dot{q}_{E,d} + \dot{q}_{E,s} + \dot{q}_{S,c} + \dot{q}_{S,T}$. The heat production rates $\dot{q}_{E,j}, \dot{q}_{E,d}, \dot{q}_{E,s}$, $\dot{q}_{S,c}$ and $\dot{q}_{S,T}$ are the effects from Joule heating, ion diffusion, effects of steric, mixing heat with the concentration gradient and mixing heat with the temperature gradient respectively.

They noticed that the Joule heating term $\dot{q}_{E,j}$ is irreversible because the value remains positive while $\dot{q}_{E,d}$ and $\dot{q}_{E,s}$ account for reversible heat production since their value can be positive or negative. Movement of ions when charging capacitors is directed towards reducing electric potential energy to create EDLs and heat energy is released in the process. During the capacitor's discharging process, transportation of ions is controlled by diffusion and steric effects since EDLs are at rest and fluxes then move towards the increase in electric potential and heat energy is absorbed.

Heat energy is liberated when the potential energy of ions is reduced and there is effective contribution to the heat production rate because of chemical potential gradients, partial molar entropy and temperature. Heat is also liberated when solvent and/or ions molecules reduce

the entropy as predicted by Schiffer et al. [128]. Irreversible Joule heating alone will obviously result in linear temperature growth but further reversible heat production will cause the temperature profiles to oscillate, since reversible heat production is exothermic on charging and endothermic on discharging.

Furthermore, the increase in oscillation amplitude associated with ion diffusion was approximately twice that of either steric effects or heat of mixing with concentration gradient. The temperature evolution they predicted remarkably resembles the one noticed experimentally by Guillemet et al. [178] and Gualous et al. [186], which showed that the physical model pictured physical processes controlling heat functioning of EDLCs. Burheim et al. [187] observed from experimental results that smaller thermal conductivity of wet and dry electrodes using OLC materials largely showed that high effective pore volume is destructive to heat conduction, and must be taken into consideration when designing and fabricating electrodes from materials that have big pore volume or small packing density. Modelling internal temperature distribution of ECs on a very high cycle in a commercially sized unit showed that a temperature slope of many degrees is dependent on the internal ohmic resistance of the device with electrode materials expected to be wetted in long run.

2.5 Modelling challenges of electrochemical capacitors.

The simple charging and discharging operation of an EC requires comprehensive information on the impact of its geometry on the capacitor's functioning, the effects of electrons and ions on electric potential, and the effects of temperature and electric field on chemical reactions at the electrodes' surface. The process of modelling an ECs system

includes representation of a porous separator immersed in electrolyte, electrodes, interface of electrodes and electrolyte and contacts at the boundary of the electrode and current collector. Each stage/layer is required to be modelled separately, while handling pores of heterogeneous structure with different a interface and also the interface between the electrode and electrolyte. The kinetics within supercapacitors is mainly determined by temperature and electric field at the interface. It is always necessary to begin with a plane system and gradually increase the complexity of the model so as to describe and specify such a complex system.

Development of big signal models, which is on the assumption that temperature is constant is a significant route because it permits physics of the interface at steady temperature to be proved first at the starting stage. Effective optimization of EDLC is difficult, because of the complex interactions among electrodes and electrolyte features, and their effects on the entire energy and power performance of the capacitor. The effect of adsorption of ions to the electrode surface, kinetics of electrons, transport processes in solvated ions in pores of different geometries and sizes, and the electrolyte to be used with a pore of a given geometries and sizes are factors to be considered in the design of EDLCs. Prediction of surface tuning and its surface functionalization, along with the optimum choice of RTIL electrolyte subject to size, is a significant field of study for molecular modelling.Greater focus on this aspect might aid in the design of new EDLCs with improved energy densities. Predictions of RTILs with planar surfaces described the experimental difference in differential capacitance, but when designing EDLCs with improved performance, it is difficult to use, since porous electrodes are preferred due to their large surface area but are unfortunately controlled by greatly differing physics.

The process of thermal runway is the main factor that is not included in all available models of ECs. The methods of all existing models neglected this heating process and also, through

oversimplifications, restrained the incorporation of thermal variables. These models cannot be utilized to investigate the influence of capacitor design and the operation of heat production during constant-current charge and discharge cycles. It is therefore difficult to develop a plan to control heat generation for the electrical energy storage device which would keep the capacitor's functioning temperature constant and at a comfortable range. Models which modify the assumptions in available analytical models were built upon by designating electrolyte solutions using heat generations, charge redistribution, self-discharge, polarization and depolarization losses of energy, as well as taking due account of the key parameters of capacitor components and other factors in a rigorous manner. The model captures physical and electrochemical phenomena by considering charge conservation and energy, along with the relevant composite relations for EDL charging and faradic reaction. It has to do the same thing for all layers and groups within the device at macro and micro scales. However, charging and discharging of capacitors demands knowledge of the effect of capacitor geometry, contributions of electrons and ions to electric potential and chemical reactions subject to electric field and temperature.

2.6 Summary

Modelling and simulation remains the key to success in developing novel electrochemical capacitors with improved energy and power densities. Mathematical theory that moves beyond equivalent circuits to couple charging to mechanics, energy dissipation, and the use of physics and the chemistry of solvents and ions in nanoporous electrode materials, as well as electronic and ionic transports in ECs electrodes, is required. It is therefore necessary, subject to more realistic assumptions, to develop from the first principles of physics and electrochemistry, the required model and theoretical basis for the design, optimization and

fabrication of ECs of the desired energy and power densities, energy efficiency and long charge-discharge life. These models should be derived subject to: (i) electronic, atomic, and molecular polarization of solvent; (ii*)* deformation of external electron shells of ions and molecules of electrolyte in EDLC; (iii) changes of conductivity and density of electron levels on the electrode surface subject to potential; (iv) formation of the volume spatial charge in near-surface layers of the electrode matrix; and (v) strong electrode capacitance influence on potential so as to increase the accuracy of the theoretical calculations of parameters and an explanation of results from experiments for different capacitors in a wide range of operating voltages.

Results in literature generally show a basic relationship between EC components, but few existing models are currently able to take due account of EC parameters and other factors like internal temperature rise and interfacial electric field in a rigorous manner, hence the discrepancy between the results of theoretical and experimental measurements of parameters of real-life ECs. Investigation of temperature effects on performance of IL-based ECs with surface-curved electrodes performed by Guang Feng et al. [148] revealed that capacitance of ECs with CNT electrodes was almost invariant with temperature due to little variation in EDL structure. The capacitance of an OLC-based capacitor increases with temperature due to the reduction in EDL thickness with growth in temperature. This was exactly the same as new experimental results obtained by Lin et al. [147]. They also noted that actual capacitor performance in terms of power and charge/discharge rates, which heavily rely on the mobility of ions instead of ion packing, cannot be predicted from the capacitance behaviour with temperature. This is because of the introduction of polarization effects by metallic walls that could provide a complete understanding of the formation of the superionic state [139,146,175]. Moreover, lifetime expectancy and performance of EDLC decays irreversibly because of heat production via polarization and depolarization energy losses, the internal

ohmic resistance of electrodes and the resistance of ions in electrolyte. The self-heating processes increase the temperature of the capacitor and irreversibly catalyse side reactions which decay conductivity of ions in electrolyte, assuming all other factors are the same. These processes generate more heat which results in heat runaway with time.

The thermal model is crucial because it estimates spatial and temporal changes in various heat production rates and temperature within EDLCs fundamentally and accounts for irreversible Joule heating and the three reversible heat production rates resulting from ion diffusion, steric effects, and changes in entropy of mixing. Models incorporating the thermal model will therefore present the needed internal temperature distribution profile that will aid in designing electrode materials, predicting charging and discharging temperatures. It will also assist in the development of heat management/cooling plans for existing and new EDLC designs, as well as their conditions of operation. Equally, the integrated model will present the needed ECs temperature profile that could be utilized in the determination of optimum loading of the device, without compromising the amount of ions through irreversible chemical reactions or generation of gases in electrolyte. Models of electrochemical capacitors that integrate heat and electric fields subject to type and value of electrodes conductivity, conductivity of electrolyte, electrodes thickness, porosity and specific capacitance, separator thickness and porosity, values of charge and discharge currents as well as the effects of self-discharge were proposed in this review.

2.7 Understanding Performance Limitation and Suppression of Leakage Current or Self-Discharge in Electrochemical Capacitors: A Review

Reproduced from *Journal of Phys.Chem.Chem.Phys.,* 2016, 18, 661 with permission from the PCCP Owner Societies shown in appendix A2.

2.8 Self-Discharge

ECs like other energy storage devices, experiences self-discharge in the charged state owing to the thermodynamic driving force of higher free energy in the charged state, compared with the discharged state [12]. Self-discharge can be regarded as the volume of current density of spontaneous recombination of non-equilibrium charge carriers in ECs. The rates of spontaneous recombination of non-equilibrium charge carriers in electrode and electrolyte inside the electrode are also identical. The reduction in voltage when fully charged ECs are at rest (open circuit situation), produces a loss of power and energy densities due to the effects of self-discharge effect [12]. Figure 2.11 shows the schematic illustration of the self-discharge process in electrochemical capacitors.A degree of self-discharge in capacitor in a state of rest will obviously create undependability in the capacitor, especially when employed for critical purposes [4,189]. The self-discharge problem has since been identified and relatively large number of investigations were directed towards comprehension of its mechanism. For EDLCs whose electrodes are carbon materials, self-discharge behaviours could be affected by surface functionalities which contribute to the charge storage process by redox reactions on active materials. It has been reported that the degree of oxygen retention via physical adsorption or acidic functionalization on carbon surface might affect self-discharge rates in EDLCs [12,190]. A greater concentration of complexes on the electrodes surface would grow self-discharge rates, predicting that these complexes are the catalysing redox reactions in carbon materials [2,190,191].

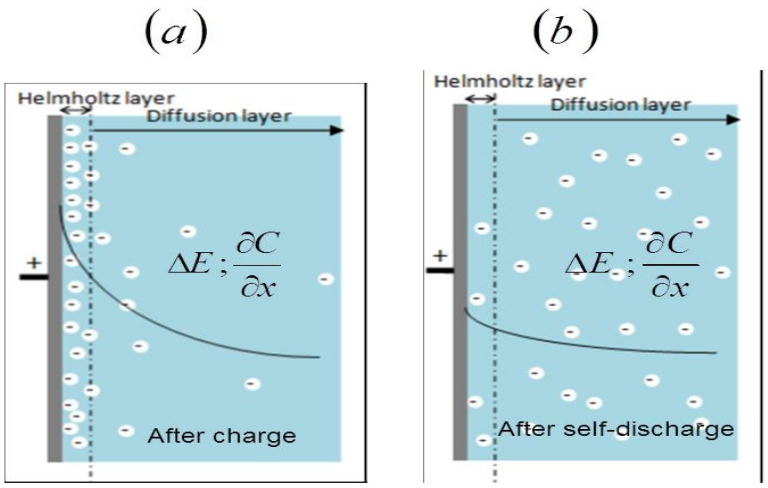

Figure 2.11: Schematic illustration on the self-discharge process (Note: ΔE-potential field; ∂c/∂x-concentration gradient of ions)

A large reduction in leakage current and self-discharge was noticed when functional groups on the electrodes surface were detached from the electrodes via an unorthodox thermal application in favourable conditions [2,190]. Typical pseudocapacitive electrode materials are transition metal oxides like ruthenium oxide (RuO_2), magnetite (Fe_3O_4), Nickel(II) oxide (NiO), and manganese (IV) oxide (MnO_2) and conducting redox polymers like polyanilines, polypyrroles, and polythiophenes, and the electrical energy storage processes in pseudocapacitors is illustrated in Figure 2.12 below. The major difference of EDLCs as compared with other types of ECs is that no chemical redox reaction is associated with the energy storage process and charges are stored only on the electrodes surface.

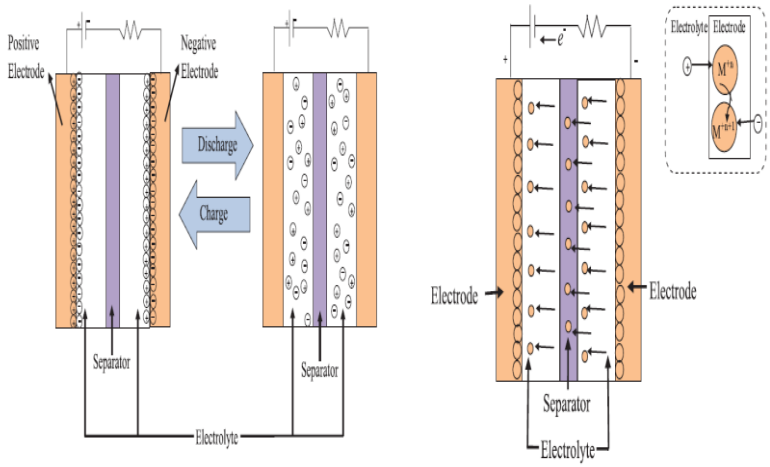

Figure 2.12 Mechanism of charge discharge process for symmetric EDLC and energy storage mechanism for pseudocapacitor [192].

* Reprinted with permission from *ECS J. Solid State Sci. Technol.*, 2013, **2**, M3101–M3119. Copyright 2013, The Electrochemical Society.

In comparison, fundamental self-discharge in pseudo-capacitive materials differs from carbon materials that display double-layer capacitance. This is because the charge transfer process in pseudo-capacitive materials is faradaic in nature as discussed earlier and involves various oxidation states which may correspond to different solid phases [193]. The reduction in potential of a completely charged pseudocapacitor over time is because of the diffusion-controlled process of self-discharge, which is fixed when a higher surface area conducting materials like graphite is available [194], thus creating a relaxed state of oxidation [12]. Increased active prismatic sites due to higher surface area were thought to be an agent that quickens the rate of self-discharge [195]. Another feasible approach to investigate self-discharge is to shift Nernst potentials for water decomposition. It was claimed that unwanted disintegration of electrolyte might take place on an electrode surface owing to the change of water decomposition potentials resulting from dissolved H_2 and O_2, which possibly

accelerates self-discharge of the entire capacitor when at rest. [95] The metallic impurity in electrolyte also significantly influences the self-discharge process [196–198]. Ions of Fe have been reported to show greater effect than other common metallic impurities on self-discharge rates, because of the shuttle effects of iron whereby Fe_2^+ ions are oxidised at anode and Fe_3^+ ions are reduced at the cathode [197].

Recently the influence of charge redistribution on the self-discharge outline of EDLCs with porous carbon electrodes has been investigated [99,112,199]. The use of high surface area activated carbon tends to form pores of different sizes, ranging from macro to micro level. Thus, electrode charging/discharging cannot proceed evenly along the pore wall due to voltage gradient, which appears to result in self-discharge in an open-circuit state. The challenge of utilizing ECs as an alternative power source to batteries lies in their poor energy retention due to their fast self-discharge rate [200–202]. It should be noted that, in an ideal situation, a polarizable electrode without any leakage in an ideal situation does not encounter self-discharge, since self-discharge will only occur as a result of faradaic electron-transfer processes at and below maximum potential obtained during charging or when electrodes are not properly sealed up and some leakages exist.

2.9 Distinguishable mechanisms of self-discharge.

Obtaining an understanding of ECs mechanism(s) of current leakage or self-discharge, and the subsequent derivation and solution of ECs models, subject to a particular mechanism or combination of distinct mechanisms of self-discharge, is the only solution to problems of ECs self-discharge. Although self-discharge rates are presented for new arrangements, there is no methodical investigation in literature considering the fundamental principles of loss of charge

over time. Reduction and elimination of inherent self-discharge and the energy loss rate is crucial to investigation of ECs, self-discharge since great capacitance is needed in implementations of electric vehicles or cross-breed electric vehicles. Conway et al. [193,203] suggested mathematical models which indicated that distribution of self-discharge relied on three likely procedures of self-discharge as a guide to finding out the ECs self-discharge mechanism, which has been a major challenge for capacitors applications. It should be emphasized that their model was derived for a single electrode and not for entire capacitor and so the self-discharge outline of electrodes in the entire device will most likely to be different.

An ECs known as Active Electrolyte Enhanced Supercapacitor (AEESC) has recently been presented by a number of research groups. In this type of ECs, the redox active types that produce great pseudocapacitance are disbanded in electrolyte, instead of being coated on the electrode's surface. Roldan et al., for instance introduced hydroquinone (HQ) into H_2SO_4 electrolyte of ECs using activated carbon or carbon nanotubes electrodes [204]. The electrode specific capacitance grew from almost 320 F g^{-1} in H_2SO_4 to 901 F g^{-1} in HQ/H_2SO_4 redox mobile electrolyte. The introduced HQ was oxidized into p-benzoquinone (BQ) near the anode [205] on charging, and p-benzoquinone BQ was reduced again to HQ on discharging the capacitor. Similarly, ferricyanide ($Fe(CN)_6^{4-}$), iodide (I^-), methylene blue and p-phenylenediamine are equally used as redox mobile electrolytes and they greatly improved the ECs performance [206–210]. However, earlier studies were basically concentrated on the enhancement of specific capacitance by instigating mobile electrolyte and influences of mobile electrolyte on ECs. The self-discharge phenomenon was completely ignored [211], whereas the self-discharge rate is the implication of the energy sustainability of the energy storage system. Capacitors with a large measure of self-discharge are of little/no real-life use, because of the fast loss of stored energy.

Unfortunately, most scientists have not presented self-discharge rates of their active electrolyte enhanced supercapacitors and utilising a few illustrations it was discovered that self-discharge of AEESCs were quicker compared with those of EDLCs [22]. Since a high self-discharge rate is an inherent attribute of AEESCs, ignoring it will certainly result to overestimating the viability of the capacitors. Situations arising in self-discharge processes, which ought to be identified in correlation to the option of an exploratory blueprint and a fundamental principle of explaining its outcomes are as follows: (1) Self-discharge due to overcharged potentials of polarized electrodes, (2) Parasitic redox reaction of impurities like oxygen groups and metals in electrolyte and electrodes, (3) Possible short-circuit of anode and cathode from improperly sealed bipolar electrodes, (4) Non-uniformity of charge acceptance along surface of electrode material pores.

2.9.1. Self-discharge due to overcharged potentials of polarized electrodes.

When electrodes are polarized to overvoltage, the disintegration of electrolyte start to generate gases [95]. If an ECs has been charged higher than its electrolyte disintegration potential capacity, self-discharge that correlates with an unconstrained reduction in overvoltage owing to extra-charging current, emerges from a steady release across the double-layer, until the overvoltage approaches zero. If cell voltage is too high, the electrochemical decomposition of the solvent may occur due to limited electrode material stability and/or the solvent's thermodynamic decomposition windows. The electrochemical decomposition of the solvent could produce gaseous products, leading to a pressure build-up inside the cell, thereby causing safety concerns and self-discharge [184,212–219]. Shuai et al. [22] introduced straightforward mathematical models to explain ECs charging and

discharging behaviors in the presence of electrochemical decomposition of solvent at constant cell current. They demonstrated from their models that it is better not to charge cells to the thermodynamic voltage of solvent decomposition for safe operation. They also pointed out that the build-up of product gasses such as O_2 and H_2 in a closed cell if, using aqueous electrolyte, may lead to mass transport limitations and also pressure build-up, which will have some impact on safety.

Electrolyte decomposition-motivated self-discharge mathematically presented by Pillay and Newman [85], showed that small concentrations of break-down O_2 and H_2 in EDLCs could move the Nernst potentials for water disintegration in a way that electrolyte disintegration may occur on the surface of the charged electrode and cause self-discharge when the charged capacitor is at rest. Ban et al [22] emphasized that for safe operation of the supercapacitor, it is better not to charge it to solvent thermodynamic decomposition voltage. They also noted that a build-up of product gasses such as O_2 and H_2 if using an aqueous electrolyte in a closed cell, may lead to mass transport limitations as well as pressure build-up, which will cause safety concerns, and self-discharge.

2.9.2. Parasitic redox reaction of impurities like oxygen groups and metals in electrolyte and electrodes.

Some species of ions in electrolyte are capable of being oxidized or reduced during reaction and, as a result, strengthen concentration of ionic species close to the electrode surfaces [12]. If ECs electrode materials and/or its electrolyte has adulterants which could be oxidized or reduced around a potential window, analogous to potential difference over capacitors during charging, the ECs then change to be reasonably non-polarizable. If the concentration of

adulterants available in the system is very low, redox self-discharge is referred to as diffusion-controlled. There is a 'shuttle' influence with 'red' and 'ox' types for redox adulterants; adulterants like Fe_2^+, Fe_3^+, O_2, and H_2O_2 exchanges, interchanges and disperses between the EC's anode and cathode. The metallic impurity in electrolyte also influences significantly the self-discharge process [196,197,220]. The presence of ions such as Fe, Mn, and Ti in electrodes of asymmetric ECs brings about the following: (*i*) an increase in leakage and/or self-discharge current, (*ii*) a decrease in discharge energy, storable energy, and coulombic efficiency, and (*iii*) a decrease in the overpotential progression of hydrogen and oxygen on negative and positive electrodes and capacitor operating voltage in general. During the long-time operation of the supercapacitor, the gradual transfer of impurities from carbon plates to the electrolyte and positive electrode will result in the destabilization of the EC's parameters and reduction of its cycle life.

Once the EC is charged, charges over the electric double layer should be conserved so as to store energy; electrons could move through the electric double layer and discharge stored charge via redox reactions on the electrode surfaces as presented in Figure 2.13a. The effect of these reactions is noticeable as leakage current that subsequently leads to self-discharge effects. Tevi et al [221] showed that an extremely-thin membrane of non-conducting substance could be used on the electrode surface to stop electron migration and decrease the escape of current in a bid to avert impending self-discharge as presented in Figure 2.13b.

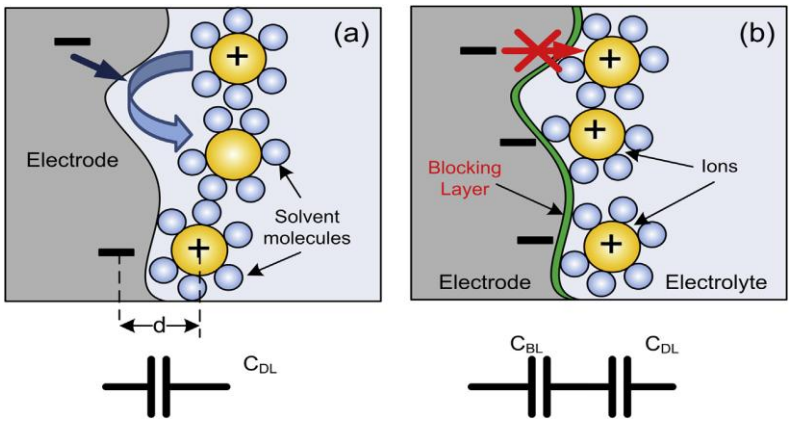

Figure 2.13 Diagrammatic illustration of the electrode-electrolyte interface in electrochemical capacitors; (a) chemical reaction at electrode surface leads to loss of charge, (b) implementation of thin stopping membrane reduces rate of migration and improves energy stocking potential [221].

* "Reprinted from J. Power Sources, Vol 241, T. Tevi, H. Yaghoubi, J. Wang and A. Takshi, Application of poly (p-phenylene oxide) as blocking layer to reduce self-discharge in supercapacitors, 589–596 , Copyright (2013), with permission from Elsevier ".

The basic cause of leakage current is faradic reactions at the electrode surface [193] and its value corresponds to the response measure. The measure of electron migration is dependent on the redox reaction decay potential E_0, and applied voltage, V over double membrane. The leakage current grows more rapidly along with growth in applied voltage since the faradic reaction rate is related largely to over-potential in the Tafel equation [222]. Tete et al. [221] through their experiments demonstrated that deposition of the blocking layer could be utilized in making more competent ECs for implementations that require higher charge storage retention time, since leakage current was reduced by 78%, while specific capacitance and energy density was also reduced by 56%.

The results of research by S. A. Kazaryan et al**.** [220], showed that in order to increase the accuracy of theoretical calculations and also provide for proper explanation of experimental results of energy parameters and self-discharge shuttle current in asymmetric ECs during their modelling, it is appropriate to note that oxidation and reduction of shuttle ions take place in the electrodes near surface layers. It also depends on the structure of the separator, temperature of electrolyte, and other parameters of the capacitor's components. Besides, theoretical calculations of the self-discharge shuttle current become more complicated because oxidation and reduction take place in the porous volume of electrodes. S. A. Kazaryan et al**.** [197] carried out research on the effect of shuttle self-discharge determined by manganese and titanium ions on energy parameters, and charging and discharging voltage of asymmetric ECs. They established that in shuttle self-discharge of ECs with electrolyte containing manganese and titanium, mostly MnO_4^-, Mn^{2+}, Ti^{3+} and TiO^{2+} ions, respectively were involved. They showed that in a stationary condition and at electrolyte's temperature T = constant, self-discharge current density J_{SDIS}, is expressed using a continuity equation by the following formula:

$$J_{SDIS} = \frac{eZN}{d\left(\frac{S_+ + S_-}{S_+ S_-} + \frac{D_+ + D_-}{D_+ D_-}\right)} \qquad 2.7$$

where e is electron's absolute charge, Z is rate of charge variation when ions are oxidized/reduced, N is the total concentration of shuttle ions in electrolyte, d is the thickness of separator, S_+ and S_- are surface rates of oxidation and reduction of ions, respectively, D_+ and D_- are coefficients of diffusion of oxidized and reduced ions respectively. Also, shuttle self-discharge current I_{SDIS} determined by iron ions Fe^{2+} and Fe^{3+} are expressed by:

$$I_{SDIS} = \frac{eN_{Fe}S}{d\left(\frac{S_{Fe^{3+}} + S_{Fe^{2+}}}{S_{Fe^{3+}} S_{Fe^{2+}}} + \frac{D_{Fe^{3+}} + D_{Fe^{2+}}}{D_{Fe^{3+}} D_{Fe^{2+}}}\right)} \qquad 2.8$$

where N_{Fe} is total concentration of iron ions Fe^{2+} and Fe^{3+} in electrolyte, S is surface area of separator, $S_{Fe^{3+}}$ is surface rate of oxidation of ions Fe^{2+}, $S_{Fe^{2+}}$ is surface rate of reduction of ions Fe^{3+}, $D_{Fe^{3+}}$ and $D_{Fe^{2+}}$ are coefficients of diffusion of Fe^{3+} and Fe^{2+} ions in separator filled with electrolyte. Again, quasi-maximum value of self-discharge current they obtained equation 2.9:

$$I_{SDIS} = \frac{eD}{2}\frac{SN_{Fe}}{d} \qquad 2.9$$

Faradaic charge transfer could be created by confined overcharging or adulterants [95]. If faradaic phenomenon is diffusion controlled, potential variations correspond to the square root of self-discharge time t [193]. Pseudo-capacitive faradaic reactions for capacitors using activated carbon electrodes were explained [223,224].

There are two fundamental types of self-discharge mechanisms in electric double-layer capacitors (EDLCs) [85,193,225–227]. One has the driving force of the anionic concentration gradient, $\partial c / \partial x$ (c is ionic concentration, varying with distance x from interface of electrode and electrolyte), and the other is driven by potential field, $\Delta U = V$ (V is voltage held by EDLCs). Self-discharge is a spontaneous process in which ions diffuse out of the double layer to reach its equilibrium of disorder [85,193,225,226] during which the voltage of ECs will decrease accordingly and energy stored in the double layer of packed ions will also dissipate. Chemical reactions barely exist in double layer charge structures, and so, the driving force for self-discharge will either be the concentration gradient, $\partial c / \partial x$ or the potential field, ΔU [85,225,226].

Zhang et al. [226] proposed and demonstrated the reliability of divided potential driving (DPD) model $V \propto V_f \exp\left(-\frac{t}{\tau_f}\right) + V_s \exp\left(-\frac{t}{\tau_s}\right)$ in fitting and characterizing this type of self-discharge, where the potential field is the dominating driving force for SWNT–$TEABF_4$ ECs self-discharge, and V_f and V_s are the first and second single potential-driving process (SPD), t is time, τ_f is potential-driving self-discharge of the first SPD process (electrolyte ions with slower self-discharge rate) and τ_f is potential-driving self-discharge of the second SPD process (electrolyte ions with faster self-discharge rate). The causes of DPD self-discharge model instead of single exponential decay $V \propto V \exp\left(\frac{-t}{\tau}\right)$ is still not clear but is predicted to be closely related to recognizable groups fastened to the SWNT surface, because heterogeneity on electrode surface chemistry would create two types of interactions between ions and electrode at the electrode/electrolyte interface.

Properties of carbon materials are greatly affected by chemisorbed oxygen in the form of various functional groups [228] and altering the quantities and species of attached functional groups, properties of carbon materials such as hydrophilicity [229] or electro-conductivity [230,231] can be manipulated. Thus, the performance of electrode materials in various areas such as electrocatalysts [232], gas adsorption [233], gas sensing [234,235], thermal sensing, composite strengthening [236–238], and electrochemical performance [239,240] can be effectively manipulated. They were able to gain insight into the triggering effects of the surface functional groups on DPD self-discharge performance and to tune self- discharge by means of surface chemistry modification by tracing SWNT ECs self-discharge performance with varied functional groups.

Zhang et al. [241] reported that self-discharge mechanisms of ECs built with single-walled carbon nanotubes (SWNTs) demonstrated the effects of surface chemistry on self- discharge by its interference in electrostatic interaction between electrolytic ions and the SWNT surface, and also explored the tunability of self-discharge. They also showed that divided potential driving process is the result of functional groups which create relatively weak bonding between ions and the charged electrode surface, making ionic diffusion out of Helmholtz layers much easier. Nohara et al. [12,242,243] investigated self-discharge characteristics of an EDLC constructed with polymer hydrogel electrolyte formulated from connected potassium poly (acrylate) (PAAK) and an aqueous solution of potassium hydroxide KOH. The possible side-reactions are predominantly as follows [12,244]: (i) shuttle effects by adulterants in carbon material or leftover oxygen (ii) hydrogen and oxygen advancement for aqueous solution (iii) decomposition of electrolyte constituent, etc,. These outcomes strongly predict that PAAK is linked to the prevention of side reactions like the shuttle effect by adulterants and micro-short circuit by fine carbon fibres. Shinyama et al. [243] showed from their experimental result that the self-discharge reaction is effectively prevented by confinement of redox shuttle substances like nitrogen-containing compounds in the sulfonated polyolefin (S-PO) separator until the concentration of redox shuttle substances becomes more than the confining strength of the S-PO separator.

The shuttle effects between the capacitor electrodes is the main explanation for fast self-discharge of active electrolyte enhanced supercapacitors (AEESCs), as designated by the investigation of a single electrode and also shown in Figure 2.18 below. The quicker self-discharge process in AEESCs is due to the migration of electrolysis products of active electrolyte which are soluble in electrolyte and diffuse from one electrode to another through the separator during charging/discharging. The AEESCs fast self-discharge due to the shuttle effect of ions are suppressed by using an ion-exchange membrane as a separator or choosing

a special active electrolyte, which is convertible into insoluble species during charge-discharge cycles.

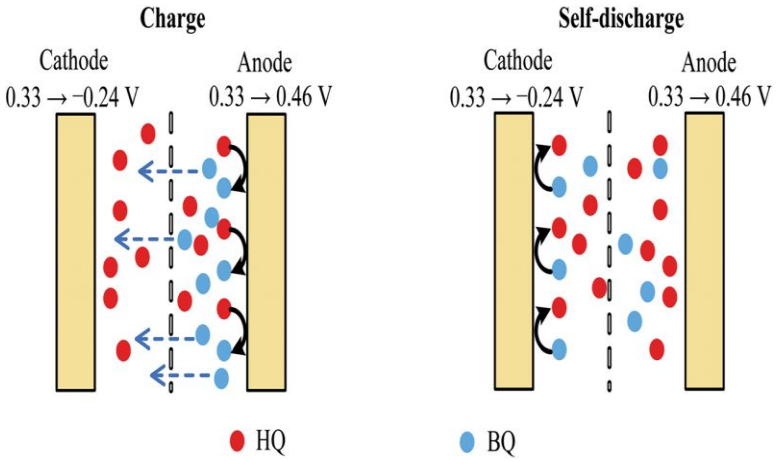

Figure 2.14**:** Schematic illustration of the mechanism of charge and self-discharge of active electrolyte improved supercapacitor, AEESCs [245].

*Reprinted with permission from [L. Chen, H. Bai, Z. Huang and L. Li, *Energy Env. Sci*, 2014, **7**, 1750–1759] - Published by The Royal Society of Chemistry.

Chen et al. [245], in attempt to stop defection of mobile electrolyte between two electrodes, originated two fundamental master plans: (1) utilization of an ion-exchange membrane separator which is capable of stopping defection of mobile electrolyte in ECs as shown in Figure 2.19a; and (2) utilization of a peculiar mobile electrolyte that is transformed to non-soluble species which are adsorbed onto electrode during electrochemical reaction (electrolysis) in the charge phenomenon as shown in Figure 2.19b. They confirmed from their experimental result that when Nafion® 117 membrane separators or $CuSO_4$ mobile electrolyte were used, self-discharge of AEESs was greatly reduced to the barest minimum. This result demonstrated that the EC fast self-discharge process can be successfully suppressed by applying an ion-exchange membrane separator or $CuSO_4$ mobile electrolyte. This gives insights to the modern day design of capacitors with great capacitance and high-ranking energy retention.

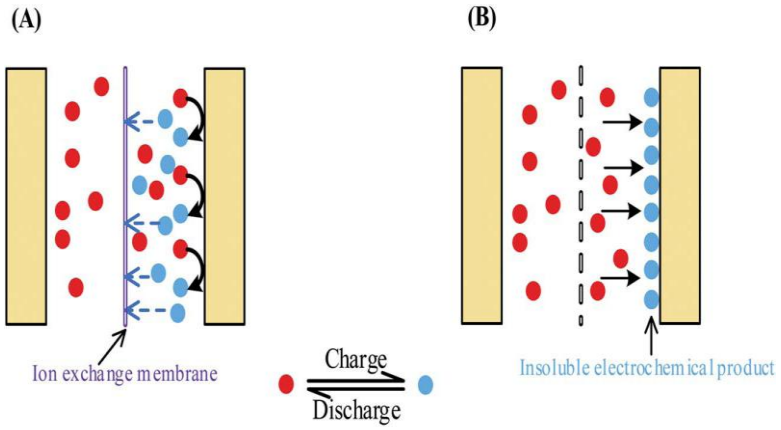

Figure 2.15 Two master plans for preventing the defection of the mobile electrolyte among electrodes: (a) Utilizing ion-interchange layer separator; (b) Using a peculiar mobile electrolyte that is transformed into insoluble sorts on charge phenomenon [245].

*Reprinted with permission from [L. Chen, H. Bai, Z. Huang and L. Li, *Energy Env. Sci*, 2014, **7**, 1750–1759] - Published by The Royal Society of Chemistry.

Wang et al. [246] reported hybrid ECs that utilizes both faradaic and capacitive energy storage in the same device using soluble redox species. They also showed that a polarizable electrode in a charged device retards diffusion of oppositely charged redox ions to mitigate self-discharge and also showed that the cell does not require an ion-exchange membrane separator for short time-scale energy storage. Recently, Chun et al. [247] reported on an aqueous redox-enhanced ECs with low self-discharge without an ion-discriminating separator due to adsorption of soluble redox couples in a charged state to the activated carbon electrode, as compared with devices that utilise inert electrolyte. They showed that the obtained low self-discharge is due to physical adhesion of oxidized species throughout the activated carbon surface to prevent cross diffusion, and also that negatively charged oxidation products are electrostatically kept in the double layer of a positively charged electrode.

2.9.3. Possible short-circuits of the anode and cathode from improperly sealed bipolar electrodes (leakage current).

ECs are potential energy storage devices due to their long life cycle and power density but are limited by high leakage current or self-discharge, which they exhibit in some real-life implementations [85]. The leakage is basically influenced by redox reactions at the electrode surface from where electrons move across the double layer. Tete et al. [221] have shown experimentally that a thin-blocking layer coating on the electrode's surface enhances energy retention ability by reducing current leakage, but compesates with a reduction in specific capacitance. Tevi and Takshi [248] developed a model that has straightforward quantum mechanical and electrochemical processes occurring throughout self-discharge activity to simulate the discharge outline and specific energy of ECs with blocking layers of different thicknesses. This model utilized basic physical and electrochemical representations of redox reactions at the electrode-electrolyte interface while examining the influence of the blocking layer on EC features. It was noticed that the model was able to describe outcomes from their earlier experiments [221]. It might possibly be employed as an instrument to predict electrochemical conducts of the blocking layer for specific width in existing EDLCs. Thus, this might play a role in choice of the optimum blocking layer material and width to minimize leakages for given applications.

2.9.4. Non-uniformity of charge acceptance along the surface of electrode material pores (charge redistribution).

This is a perceivable self-discharge over comparably small times, resulting from the interference of polarizing currents at porous-carbon electrodes due to non-uniformity of the

charge receipt down and within pores. Recent papers [99,199,249] explained a model of charge redistribution inceptively suggested by Conway et al. [193] in porous electrodes. The model illustrates that the 'memory' effect of charge redistribution, which is contrary to self-discharge, might result from voltage growth. EC voltage reduces during the charging process due to the charge redistribution phase and grows during discharging as a result of charge redistribution. The voltage changes of this EC are due to finite conductance of electrolyte at outer pores which leads to a voltage drop along the electrode thickness. Therefore, it takes charges much less time to move through the macro-pores at the electrode entrance than meso-pores and micro-pores, which are at electrode bottom. Due to this fact, superficial portions of pores are charged or discharged faster compared with the interior portion, and this produces ion concentration gradients in ECs.

Principally, if enough time is allowed after tye charging process, capacitance will evacuate charge from larger pores that are inceptively completely charged [250]. If EDLCs were charged and discharged to zero voltage, its voltage voluntarily regains itself at resting situations to a fragment of the inceptive voltage value [196,199,251]. The 'memory' and 'self-discharge' influences that are available after the EDLC charging and discharging process and with regards to energy acquired or released, cannot be comprehensively described. De Levie presented that charge/discharge phenomena do not occur with an equivalent time constant in every part of electrode material [105], because of restricted conductance of electrolyte that causes voltage decay along pores. However, when the capacitor is briefly charged, the majority of ions remain situated at the pore mouth, leading to a definite ion concentration gradient alongside the pores.

Experiments and modelling by Kaus et al. [99] clearly showed that most of the perceived reduction in voltage is not due to genuine self-discharge, because self-discharge is

authentically ascribed to the process in which charge bearers are consumed in side reactions and were not obtainable/accessible for discharge. Kaus et al. [99] noticed that very prolonged charging time results in a considerable decline in voltage of the capacitor in storage conditions, due to the redistribution effect which happens alongside pores, providing ions with sufficient time to move to extensive pore designs like meso- and micro-pores as was clearly shown in Figure 2.16 below. In fact, "self-discharge" should be employed very cautiously [249] as ECs voltage change while at rest and cannot be completely characterized by self-discharge. Self-discharge phenomena form only a portion of ECs voltage decays while at rest [99,249] unlike in battery technology, where self-discharge is the sole reason for open circuit voltage decay and charge loss. The EDLCs voltage increase and proportionally fast decay are basically due to charge redistribution phenomenon in pore formation and its interfaces [252]. Charge redistribution is a process in EDLCs where charge bearers are distributed or relaxed due to concentration slopes [99,107,249]. This differs from self-discharge whereby charge bearers are subject to side reactions and are consumed as in pseudocapacitors or asymmetric capacitors that employ metal oxides and conductive polymers.

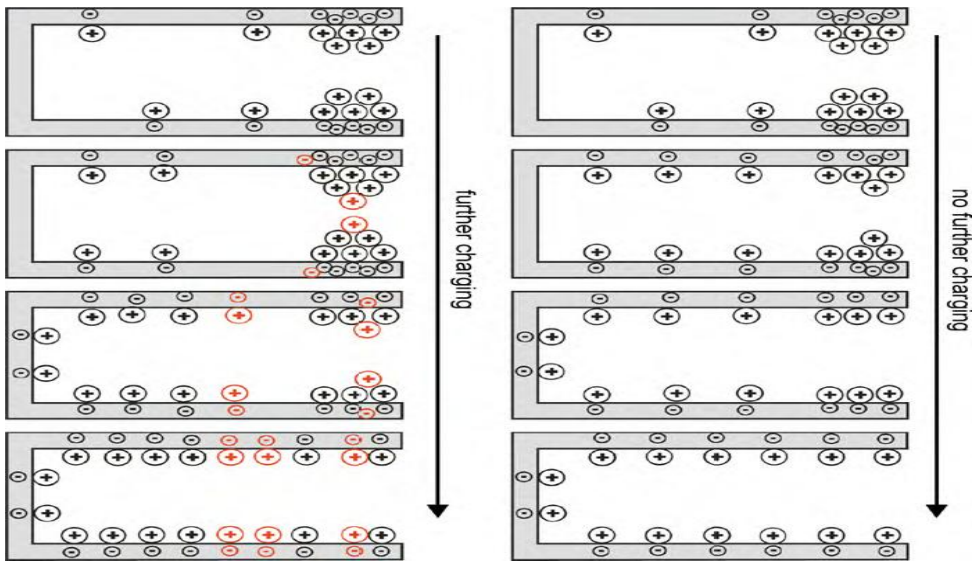

Figure 2.16 Schematic illustration of ion dispensation model for various charge periods: left, long charging; right, short charging [249].

* "Reprinted from *J. Power Sources*, Vol. 196, J. Kowal, E. Avaroglu, F. Chamekh, A. Šenfelds, T. Thien, D. Wijaya and D. U. Sauer, Detailed analysis of the self-discharge of supercapacitors , 573-579, Copyright (2011), with permission from Elsevier ".

The charge bearers are not consumed. They sink down into the pores [249]. ECs charge redistribution emerged from electrode pores, which are normally compact with large exterior areas at the interface of electrode and electrolyte. This improves the charge stored inside capacitors, which in turn create notable spreading and defection restrictions during charging and discharging [105,253]. In line with the physics of supercapacitors, the interface electrochemistry illustrates that RC web where resistors mainly show resistances to carbon molecules, ECs illustrate capacitances in electrodes and electrolyte [102] and can describe capacitors behaviours [254]. In addition to ECs physics [105,199,252,255], ECs equivalent circuit models can also be used to understand charge redistribution procedures.

In order to minimize model difficulty, straightforward equivalent circuit models that normally have a minimum of two RC branches to consider ECs charge redistribution have been proposed [99,104,254,256–259]. Available works on the charge redistribution of ECs, which concentrated solely on procedures of charge redistribution and voltage decay or gain throughout charge redistribution, were probed in [193,199,248,252], while those of low ionic mobility in supercapacitors micro-pores was suggested in [260]. Based on results by Kowal et al. [249], extreme carefulness is needed in order to use the term “self-discharge” more accurately. In earlier research articles, a mathematical model of an EC's self-discharge processes could be sufficiently represented by taking capacitor to be a capacitance C in parallel with steady leakage resistance R_P [206].

2.11 Progress made in EDLCs and pseudocapacitors self-discharge.

It is appropriate to use cleaner electrode materials and materials of other components in capacitors and also to make use of advanced technology in their manufacture, in order to reduce self-discharge. However, as the purity of activated carbon powders increases and new manufacturing technologies of capacitor components are employed, the overall cost grows and competitiveness declines. Most importantly, very low self-discharge or an outstanding energy retention potentiality could be obtained by modification of electrode/electrolyte design and several other approaches which are presented in Table 2.1.

Table 2.1: Chronology of research dedicated to self-discharge in electric double layer capacitors (EDLCs) and pseudocapacitors.

Researcher(s)	Year	Supercapacitor type	Self-discharge Mechanism	Approach used
S. Nohara et al. [242]	2006	Symmetric EDLCs	Leakage current due to shuttle reactions by adulterants and micro-short circuit by carbon fibres	Use of cross-linked potassium poly (acrylate) and high polymer content of polymer hydrogel electrolytes
SA Kazaryan et al [261], SA Kazaryan et al [197,220]	2007, 2007, 2008	Asymmetric supercapacitors	Shuttle effect due to impurities	Use of carbon powder (pure) with specific capacitance and design for carbon plate manufacture
K. Chiba et al [213]	2011	Symmetric EDLCs	Redox ions shuttle effect	Use of linear sulfones electrolyte systems: Ethyl isopropyl sulfone (EiPS) and Ethyl isobutyl sulfone (EiBS)
K. Chiba et al [262]	2011	Symmetric EDLCs	Redox ions shuttle effect	Introduction of methyl substituent into both the 4th and 5th positions for the 2, 3-butylene carbonate (2,3BC) electrolyte system
M. Kaus et al [99] and J. Kowal [249]	2010, 2011	Symmetric EDLCs	Redistribution of charge carriers into deeper micropores	By allowing enough charging and discharging time (between 2 hours and 5 days)
S. Ban et al [22]	2013	Symmetric EDLCs	Leakage process and electrochemical decomposition of solvent	The anode and cathode bipolar electrodes are properly sealed and the cells are not charged to a thermodynamic voltage of solvent decomposition.
T. Tevi et al [221]	2013	Symmetric EDLCs	Electron transfer and leakage current	Use of an ultra-thin layer of insulating material

F. Soavi et al. [263]	2014	An IL-based EDLCs	Current leakage and charge redistribution	Use of ILs with pure N-butyl-N-methyl-pyrrolidinium bis (trifluoromethanesulfonyl)imide ($PYR_{14}TFSI$) and N-methoxyethyl-N-methylpyrrolidinium bis(trifluoromethanesulfonyl)imide
Q. Zhang et al. [241]	2014	SWNT based symmetric EDLCs	Functional group-dependent self-discharge	Method of electrodes surface chemistry modification
B. Wang et al. [246]	2014	Hybrid Redox-supercapacitors	Diffusion of the oppositely charged ions	Use of soluble redox species (electrolytes) to mitigate self-discharge
L. Chen et al. [245]	2014	Asymmetric supercapacitors	Defection of the active electrolyte (shuttle effect)	Use of ion exchange membrane separator or $CuSO_4$ active electrolyte
T. Tevi and A. Takshi [248]	2015	Symmetric EDLC supercapacitors	Charge loss by Faradaic (redox) reactions at electrode surface.	Use of thin blocking layer that reduces kinetics of redox reactions
S. Chun et al [247]	2015	Redox EDLCs	Cross diffusion of oppositely charged ions	Use of soluble redox sorts that produce negatively charged oxidation products that are kept electrostatically in the double layer of positive electrode; and use of physical adhesion of oxidized sorts throughout activated carbon surface to prevent cross diffusion

2.12 Summary

The use of cleaner electrode materials and components from other capacitors, together with the use of advanced technology in their manufacture, will reduce self-discharge. Many impure shuttle ions penetrate into the crystal lattice of active materials during a capacitor's operation which decays capacity parameters, the life cycle of positive electrodes and entire capacitors, as well as creating increased leakage current/self-discharge current.

Modeling of complete self-discharge by an equivalent circuit produces acceptable simulation outcomes and permits assessment of self-discharge and losses in stored energy for various ECs. Short-circuiting between cathodes and anodes, due to improperly fastened bipolar electrode specifications, was seen as an insignificant origin of self-discharge. No single mechanisms of the self-discharge process can fully explain the practical processes of an EC's

self-discharge, especially with large capacitance. A hybridized procedure of ECs self-discharge is urgently needed. Tuning self-discharge rates of SWNT ECs is feasible via surface chemistry modification and is a significant step in the study of self-discharge in ECs which will benefit potential applications for energy storage.

The self-discharge process in ECs can also be effectively suppressed by utilizing an ion-interchange layer (ion-exchange membrane) separator or $CuSO_4$ mobile electrolyte that is convertible to an insoluble species by electrolysis during charging. This will help in an up-to-date blueprint of ECs with great capacitance and improved energy sustainability. It is appropriate to develop a new general theory of self-discharge for modern electrochemical capacitors, in order to progress technology for the manufacture of ECs of different kinds, create new ECs with optimal designs and improve energy capacity and operation parameters, subject to their different self-discharge mechanisms. It was proposed in this review that EC models should be developed and solved subject to combination of distinct mechanisms of self-discharge during charging, discharging and storage condition, in order to enhance the performance.

CHAPTER THREE

3.0 Derivation of the Models

3.1 Homogeneous/symmetric electric double layer capacitors with electric double layer (EDL) electrodes.

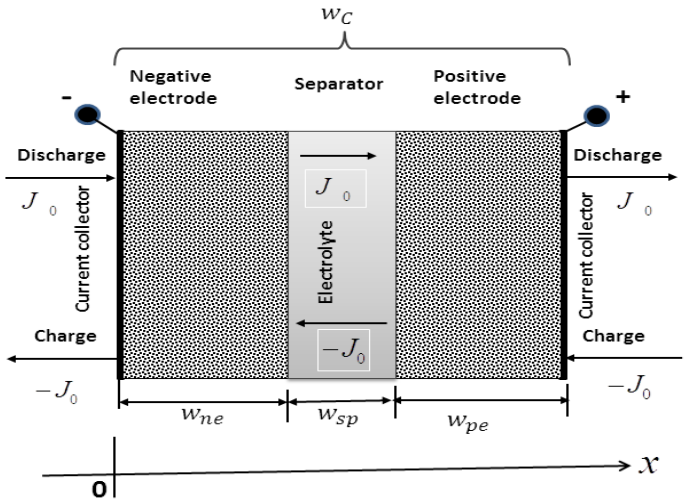

Figure 3.1: A symmetric electric double layer capacitor (EDLC) showing various functional layers on macroscale

3.1.1 For the negative electrode of electric double layer capacitors.

The following assumptions were made in order to simplify the model:

1) The rates of generation of charge carriers (charge generation) are much smaller than the rates of recombination of charge carriers (self-discharge);

2) The electrodes are carbon plate based on activated carbon powders with p-type conductivity,ie., it is electron conductivity;

3) The electrodes have self-discharge;

4) The concentrations of ions of electrolyte and conductivity of the electrode's pore do not vary during charging and discharging;

5) Capacitance depends very little on the value of potential;

6) The temperature is constant and uniform;

7) There were no ohmic (short-circuiting) leakage currents among cathodes and anodes in unsuitable secured bipolar electrodes;

8) Side-reactions or reactions of active redox species, several impurities and the instability of the electric double layers are responsible for self-discharge processes; and

9) All thermal influences were ignored.

Density changes of the electric charges $\phi_1(x,t)$ and $\phi_2(x,t)$ of an electrode during charging and discharging of electrochemical capacitors (ECs) are determined by equations of continuity given below [12,89]:

$$\frac{\partial \phi_1(x,t)}{\partial t} = div\, J_1(x,t) - G_1(x,t) + R_1(x,t) \qquad 3.1$$

$$\frac{\partial \phi_2(x,t)}{\partial t} = div\, J_2(x,t) + G_2(x,t) - R_2(x,t) \qquad 3.2$$

where $\phi_1(x,t)$ and $\phi_2(x,t)$ are charge densities of free carriers in the electrode and electrolyte, respectively; $J_1(x,t)$ and $J_2(x,t)$ are current densities in the electrode and electrolyte respectively; $G_1(x,t)$ and $R_1(x,t)$ are rates of generation and recombination of charge carriers in the electrodes respectively; $G_2(x,t)$ and $R_2(x,t)$ are rates of generation and recombination of charge carriers in electrolyte, respectively.

Rate of generation and recombination of charge carriers in the electrodes and electrolyte are respectively presented as:

$$G_1(x,t) = J_{VG1}(x,t) \quad 3.3$$

$$R_1(x,t) = J_{VR1}(x,t) \quad 3.4$$

$$G_2(x,t) = J_{VG2}(x,t) \quad 3.5$$

$$R_2(x,t) = J_{VR2}(x,t) \quad 3.6$$

where $J_{VG1}(x,t), J_{VR1}(x,t)$, and $J_{VG2}(x,t)$, $J_{VR2}(x,t)$ are current densities of generation and recombination of charge carriers in electrodes and electrolyte, respectively.

Electric charge in any point of the electrode with DEL should be compensated and is given as:

$$J_{VG1}(x,t) = J_{VG2}(x,t) = J_{VG}(x,t) \quad 3.7$$

$$J_{VR1}(x,t) = J_{VR2}(x,t) = J_{VR}(x,t) \quad 3.8$$

Case one.

When an electrode is polarizable and has electron conductivity in a solid matrix, the electric double layer (e/Z^+) consists of electrons (e) and positive ions (Z^+), and current densities $J_1(x,t)$ and $J_2(x,t)$ are determined by the formula given below:

$$J_1(x,t) = \sigma^s_{ne} E_1(x,t) - D_{e(p)} \nabla \phi_1(x,t) \quad 3.9$$

$$J_2(x,t) = \sigma^l_{ne} E_2(x,t) - D_+ \nabla \phi_2(x,t) \quad 3.10$$

where D_e and D_+ are diffusivity coefficients of main charge carriers of matrix and positive ions of EDL respectively; σ^s_{ne} and σ^l_{ne} are conductivity of electrode and electrolyte respectively; $E_1(x,t)$ and $E_2(x,t)$ are electric field intensity in electrode solid matrix and electrolyte, respectively.

Case two.

When an electrode is polarizable and has hole conductivity in a solid matrix, the EDL (e/Z^+) consists of electrons (e) and positive ions (Z^+), and current densities $J_1(x,t)$ and $J_2(x,t)$ are determined by the expression below:

$$J_1(x,t) = \sigma_{ne}^{s} E_1(x,t) - D_{p(e)} \nabla \phi_1(x,t) \quad 3.11$$

$$J_2(x,t) = \sigma_{ne}^{l} E_2(x,t) - D_{+} \nabla \phi_2(x,t) \quad 3.12$$

Recall that potentials $\varphi_1(x,t)$ and $\varphi_2(x,t)$ are related to $E_1(x,t)$ and $E_2(x,t)$by expressions given below:

$$E_1(x,t) = -\nabla \varphi_1(x,t) = -\frac{\partial \varphi_1(x,t)}{\partial x} \quad 3.13$$

$$E_2(x,t) = -\nabla \varphi_2(x,t) = -\frac{\partial \varphi_2(x,t)}{\partial x} \quad 3.14$$

where $\varphi_1(x,t)$ and $\varphi_2(x,t)$are potential (in relation to pzc) of solid matrix and electrolyte in the area of EDL. Examining the dependence of the parameters of EDLC whose solid matrix has electron or hole conductivity on polarizable electrodes potential, conductivity of solid matrix of electrode is represented as:

$$\sigma_{ne}^{s} = en_0\mu_n + ep_0\mu_p \quad 3.15$$

where n_0 and p_0 are equilibrium concentrations of free electrons and holes of the solid matrix (in the area of pore walls), respectively; μ_n and μ_p are effective mobilities of electrons and holes of the solid matrix, respectively, μ_n and μ_p are dependent on the porous structure and electrophysical properties of pore walls. Conductivity of liquid (electrolyte) in electrodes should also be represented as:

$$\sigma_{ne}^{l} = eZ^{+}n_0^{+}\mu_{+} + eZ^{-}n_0^{-}\mu_{-} \quad 3.16$$

where n_0^{+} and n_0^{-} are equilibrium concentrations of positive and negative ions of electrolyte in the pores of the electrode respectively; eZ^{+} and eZ^{-} are the amount of charges of positive

and negative ions, respectively; μ_+ and μ_- are effective mobilities of positive and negative ions, respectively. Conductivities in the electrode solid matrix pore walls and electrolyte in the pores of the electrode solid matrix are respectively determined by[89]:

$$\sigma_{ne}^{s} = e\mu_n(n_0 + \Delta n) + ep_0\mu_p \quad 3.17$$

$$\sigma_{ne}^{l} = eZ^+\mu_+ (n_0^+ + \Delta n^+) + eZ^- n_0^- \mu_- \quad 3.18$$

where Δn and Δn^+ are non-equilibrium concentrations of free electrons and positive ions in polarizable electrode pores.

The polarizable electrode is electrically neutral, not withstanding that the electric charge is accumulated in it during the capacitor's charging process. The electric neutrality is always retained in the elementary unit v_τ of the capacitor, i.e.

$$\int_{v_\tau} \iint [\phi_1(x,t) + \phi_2(x,t)] dv = 0 \quad 3.19$$

The capacitance of EDLC may be adequately characterized by the formula of capacitance of a capacitor with flat plates (C_{fc}):

$$C_{fc} = \frac{\varepsilon\, \varepsilon_0\, A}{d} \quad 3.20$$

where ε is the dielectric permittivity of the medium between the plates; ε_0 is the dielectric constant; A is surface area of the capacitor's plate, and *d* is distance between the plates.

It follows from equations 3.17, 3.18 and 3.19 above that density of non-equilibrium charges, potentials of polarizable electrode solid matrix and electrolyte are related by:

$$d\phi_1(x,t) = 2C_V\, d\varphi_1(x,t) \quad 3.21$$

$$d\phi_2(x,t) = 2C_V\, d\varphi_2(x,t) \quad 3.22$$

where C_V (F/cm^2) is specific (by area) capacitance of electrode; $\varphi_1(x,t)$ and $\varphi_2(x,t)$ are the potential (in relation to the pzc) of the negative electrode matrix and electrolyte in the area of EDL respectively.

It again follows from Equations 3.21 and 3.22 that $\Delta n\ (x,t)$, $\Delta p\ (x,t)$, $\Delta n^{+}(x,t)$, and $\Delta n^{-}\ (x,t)$ are related to each other by these expressions [89]:

$$\Delta n = -\frac{2\,C_V\ \varphi_1(x,t)}{e} \tag{3.23}$$

$$\Delta p = \frac{2\,C_V\ \varphi_2(x,t)}{e} \tag{3.24}$$

$$\Delta n^{+} = \frac{2\,C_V\ \varphi_2(x,t)}{(eZ^{+})} \tag{3.25}$$

$$\Delta n^{-} = -\frac{2\,C_V\ \varphi_1(x,t)}{(eZ^{-})} \tag{3.26}$$

Substituting the values of non-equilibrium charge carriers from Equations 3.23-3.26 into Equation 3.17 and 3.18 and considering Equations 3.13 and 3.14, we obtain expressions for conductivity of the polarizable electrode's solid matrix and electrolyte in electrode pores for the above-mentioned cases respectively:

Case one.

$$\sigma_{ne}^{s} = e\mu_n\left[n_0 - \frac{2\,C_V\ \varphi_1(x,t)}{e}\right] + ep_0\mu_p \tag{3.27}$$

$$\sigma_{ne}^{l} = eZ^{+}\mu_{+}\left[n_0^{+} + \frac{2\,C_V\ \varphi_2(x,t)}{(eZ^{+})}\right] + eZ^{-}n_0^{-}\mu_{-} \tag{3.28}$$

Case two.

$$\sigma_{ne}^{s} = e\mu_n n_0 + e\mu_p\left[p_0 + \frac{2\,C_V\ \varphi_1(x,t)}{e}\right] \tag{3.29}$$

$$\sigma_{ne}^{l} = eZ^{+}\mu_{+}\left[n_0^{+} + \frac{2\,C_V\ \varphi_2(x,t)}{(eZ^{+})}\right] + eZ^{-}n_0^{-}\mu_{-} \tag{3.30}$$

It was assumed that conductivity of the electrode matrix under consideration is electron (case one), and also that $G(x,t) = 0$. By substitution of appropriate expressions from equations 3.27, 3.28, 3.21, and 3.22 into Equations 3.9 and 3.10 in place of $\sigma_{ne}^{s}, \sigma_{ne}^{l}$, $d\phi_1(x,t)$ and $\phi_2(x,t)$, we obtain the expressions for $J_1(x,t)$ and $J_2(x,t)$ respectively:

$$J_1(x,t) = -\left\{ e\mu_n \left[n_0 - \frac{2\,C_V\,\varphi_1(x,t)}{e} \right] + ep_0\mu_p \right\} \frac{\partial \varphi_1(x,t)}{\partial x} - 2D_e C_V \frac{\partial \varphi_1(x,t)}{\partial x} \qquad 3.31$$

$$J_2(x,t) = -\left\{ eZ^+\mu_+ \left[n_0^+ + \frac{2\,C_V\,\varphi_2(x,t)}{(eZ^+)} \right] + eZ^-n_0^-\mu_- \right\} \frac{\partial \varphi_2(x,t)}{\partial x} - 2D_+ C_V \frac{\partial \varphi_2(x,t)}{\partial x}$$

3.32

The specific capacitance C_V at great deviations of capacitor electrode potential from potential of pzc becomes a function of potential in Equations 3.31 and 3.32, i.e, $C_V = C_V(\varphi)$. Although, results of research of capacitances of different types of electrochemical capacitors with EDL showed that at small deviations of electrodes potential, value of $C_V(\varphi)$ depends very little on value of potential. On substitution of Equations 3.31 and 3.32 into Equations 3.1 and 3.2 subject to Equations 3.21 and 3.22, and after necessary transformation, we obtain the given system of differential equations:

$$\frac{\partial \varphi_1(x,t)}{\partial t} = \frac{1}{2\,C_V(\varphi_{ne})} div\left\{ \left\{ e\mu_n \left[n - \frac{2\,C_V(\varphi_{ne})\,\varphi_1(x,t)}{e} + ep\mu_p + 2\,C_V(\varphi_{ne})D_e \right] \right\} \frac{\partial \varphi_1(x,t)}{\partial x} \right\}$$

$$+ \frac{J_{VR}(x,t)}{2\,C_V(\varphi_{ne})} \qquad 3.33$$

$$\frac{\partial \varphi_2(x,t)}{\partial t} = \frac{1}{2\,C_V(\varphi_{ne})} div\left\{ \left\{ eZ^+\mu_+ \left[n^+ + \frac{2\,C_V(\varphi_{ne})\,\varphi_2(x,t)}{e} \right] + eZ^-\mu_- n^- + 2\,C_V(\varphi_{ne})D_+ \right\} \right.$$

$$\left. \frac{\partial \varphi_2(x,t)}{\partial x} \right\} - \frac{J_{VR}(x,t)}{2\,C_V(\varphi_{ne})} \qquad 3.34$$

where $\varphi_{ne}(x,t)$ is specified as $\varphi_1(x,t) - \varphi_2(x,t)$.

Assuming that capacitance does not depend on capacitor electrode potential and that concentrations of charge carriers in pore walls and electrolyte of EDL respectively is greatly lower than the equilibrium concentrations, then capacitance is no longer a function of electrode potential.

$$n_0 >> \frac{2C_V\varphi_1(x,t)}{e} \quad 3.35$$

$$n^+ >> \frac{2C_V\varphi_2(x,t)}{eZ^+} \quad 3.36$$

Introduction of the notations:

$$\alpha_1 = \sigma_{ne}^s + 2D_eC_V \quad 3.37$$

$$\alpha_2 = \sigma_{ne}^l + 2D_+C_V \quad 3.38$$

where α_1 and α_2 are electrodes and electrolyte effective conductivities respectively. The electrolyte effective conductivity in electrodes (α_{2e}) and separator (α_{sp}) respectively is presented by Newman, [264] as:

$$\alpha_{2e} = \left(\sigma^l + 2D_+C_V\right)\varepsilon_e^{1.5} \quad (in\ electrodes) \quad 3.39$$

$$\alpha_{2sp} = \left(\sigma^l + 2D_+C_V\right)\varepsilon_{sp}^{1.5} \quad (in\ separator) \quad 3.40$$

where ε_e is porosity of electrodes , ε_{sp} is porosity of separator.

Recall that electronic current $J_1(x,t)$ and ionic current $J_2(x,t)$ are given by equations 3.41 and 3.42 respectively:

$$J_1(x,t) = -\alpha_1\nabla\varphi_1(x,t) \quad 3.41$$

$$J_2(x,t) = -\alpha_2\nabla\phi_2(x,t) \quad 3.42$$

The total current in the electrodes is the sum of the electronic current (J_1) and ionic current (J_2), and the entire current in the separator is carried by ions. For conservation of overall charge, we note that:

$$J_1 + J_2 \approx J_0 \quad 3.43$$

From equations 3.41 and 3.42, it can be written that the sum of electronic and ionic currents, potential drop in solid and liquid-phase, and in the separator where the entire current is by

ions with migration current as the dominating mechanism are:

$$-\alpha_1 \frac{\Delta\varphi_1(x,t)}{w_e} - \alpha_2 \frac{\Delta\varphi_2(x,t)}{w_e} \approx J_0 \quad 3.44$$

$$\Delta\varphi_1(x,t) \approx \frac{J_0 w_e}{\alpha_1} \quad 3.45$$

$$\Delta\varphi_2(x,t) \approx \frac{J_0 w_e}{\alpha_2} \quad 3.46$$

$$\Delta\varphi_{2s}(x,t) \approx \frac{J_0 w_{sp}}{\alpha_2} \quad 3.47$$

Conventionally, effective conductivity of electrodes is considerably larger than the effective conductivity of electrolyte in the electrochemical capacitors [93]. Thus the potential drop in the solid phase is considerably smaller than the potential drop in the liquid phase. The potential drop in the liquid phase of each electrode during charging or discharging can, at most, be equal to half of the entire cell voltage. It can then be written that:

$$\Delta\varphi_2(x,t) \approx \frac{V_{cell}}{2} \quad 3.48$$

The limit of potential drop and electrodes length [w_e] over which the liquid potential drop occurs are determined by the following expression:

$$[w_e] \approx \frac{\alpha_2 V_{cell}}{2J_0} = \frac{\alpha_2 V_{cell}}{2J_0} \quad 3.49$$

The typical length scale [w_e] over which the liquid-phase potential drop happens on electrodes, can be defined as the minimum value among electrode thickness w_e and electrode length [w_e] over which the liquid potential drop occurs:

$$[w_e] \approx \min\left(\frac{\alpha_2 V_{cell}}{2J_0}, w_e\right) = \min\left(\frac{\alpha_2 V_{cell}}{2J_0}, w_e\right) \quad 3.50$$

The ratio of electrode thickness w_e to length scale $[w_e]$ over which liquid phase potential drop occurs on electrodes, which is the determining factor for estimating the length scale in electrodes for the liquid phase potential drop is determined by:

$$\lambda \equiv \frac{w_e}{[w_e]} = \frac{2J_0 w_e}{\alpha_2 V_{cell}} \quad 3.51$$

Electrodes utilization u in the capacitor with electrolyte of specific effective conductivity α_2 and electrodes thickness w_e charged at a given current density J_0 is given as:

$$u = \frac{[w_e]}{w_e}.100\% = \frac{1}{\lambda}.100\% = \frac{\alpha_2 V_{cell}}{2J_0 w_e}.100\% \quad 3.52$$

Using the approximations and notations of Equations 3.35 & 3.36, and Equations 3.37 & 3.38 respectively, Equations 3.33 and 3.34 now becomes:

$$\frac{\partial \varphi_1(x,t)}{\partial t} = \frac{\alpha_1}{2C_V}\frac{\partial^2 \varphi_1(x,t)}{\partial x^2} + \frac{J_{VR}(x,t)}{2C_V} \quad 3.53$$

$$\frac{\partial \varphi_2(x,t)}{\partial t} = \frac{\alpha_2}{2C_V}\frac{\partial^2 \varphi_2(x,t)}{\partial x^2} - \frac{J_{VR}(x,t)}{2C_V} \quad 3.54$$

Multiplying Equation 3.53 by α_2 and Equation 3.54 by α_1, and subtracting Equation 3.54 from 3.53 term by term, one differential equation for potential $\varphi_{ne}(x,t)$ of negative electrode is obtained as below [89]:

$$\frac{\partial \varphi_{ne}(x,t)}{\partial t} = \beta^2 \frac{\partial^2 \varphi_{ne}(x,t)}{\partial x^2} + \frac{J_{VR}(x,t)}{C_V} \quad 3.55$$

$$\beta^2 = \frac{\alpha_1 \alpha_2}{C_V(\alpha_2 + \alpha_1)} \quad 3.56$$

$$J_{VR}(x,t) = J_{VR1}(x,t) = J_{VR2}(x,t) \quad 3.57$$

Equation 3.55 describes the variation of electrode potential with space and time, it is applicable to both Case one and Case two since the only difference is whether the conductivity is by electron or hole. The solution of Equation 3.55 subject to the specific or combination of different mechanisms of self-discharge makes it possible to investigate influence of mechanisms and parameters of self-discharge capacitor performance. It is therefore, possible to obtain the potential dependence of a polarizable negative electrode on its overall dimensions, physical, electrochemical, and capacitance parameters, at any point in time *t* during capacitor charge and discharge using the solution of differential Equation 3.55.

3.1.2 Self-discharge mechanisms in symmetric and asymmetric electrochemical capacitors.

It was assumed that the sources of self-discharge here are side-reactions, or reactions of active redox species and several impurities in electrodes, electrolytes, separator, current collectors of the device and various functional groups on CNTs electrodes. Side-reactions perform a largely dominant role in considering the mechanism of self-discharge. The side-reactions, or reactions of the active redox species, several impurities and the electric double layer's instability are responsible for the self-discharge processes.

The shuttle self-discharge current density of ECs has previously been given by Kazaryan et al [198] as:

$$J_{VRM} = \frac{eZN}{w_{sp}\left(\frac{s_+ + s_-}{s_+ s_-} + \frac{D_+ + D_-}{D_+ D_-}\right)} \qquad 3.58$$

where e is the electron's entire charge, Z is the rate of charge's change when ions are oxidized, N is the entire concentration of shuttle ions in electrolyte, (mol/cm^3), w_{sp} is the separator

thickness, s^+ is the surface rate of ionic oxidation, (cm^2/s), s^- is the surface rate of ionic reduction, (cm^2/s), D^+ is the diffusivity coefficient of oxidized ions in the separator's pores filled with electrolyte,(cm^2/s), D^- is the diffusivity coefficient of reduced ions in the separator's pores filled with electrolyte, (cm^2/s).

Some mechanisms of self-discharge in symmetric and asymmetric electrochemical capacitors are explained by the following equations:

Some mechanisms for reversible reactions into soluble components, one insoluble component and reversible redox active species into either soluble or insoluble species of self-discharge in symmetric and asymmetric ECs are explained by equations 3.59, 3.60 and 3.61 respectively:

$$Ox + n_e e^- \rightleftharpoons R \qquad 3.59$$

$$M^{n+} + n_e e^- \rightleftharpoons M \qquad 3.60$$

$$P \rightleftharpoons Q + n_e H^+ + n_e e^- \qquad 3.61$$

where Ox is the oxidized species, R is the reduced species, M is the metals such as iron, manganese, and titanium, etc., n_e is the number of electrons transferred per molecule of reactant, P is the redox active species, Q is the reduced species, H^+ is the hydrogen ion and e^- is the electrons.

The condition in which expression 3.59 is precisely followed is determined by obtaining the solution of Fick's second law (equation 3.62) [265,266] under initial condition that $C_{Ox}(x,t) = C_{Ox}(0,t) = C_{Oxi}$, and the boundary conditions that $C_{Ox}(x,t) = C_{Ox}(0,t) = C_{Oxi}$ and $C_{Ox}(x,t) = C_{Ox}(\infty,t) = C_{Ox}$:

$$\frac{\partial C_{Ox(x,t)}}{\partial t} = D_{Ox} \frac{\partial^2 C_{Ox(x,t)}}{\partial x^2} \qquad 3.62$$

where D_{Ox} is the diffusion coefficient of oxidized species Ox, (cm^2/s), C_{Ox} is the concentration

of reactant in oxidized form, (mole/cm^3), C_{Oxi} is the initial concentration of oxidized species Ox at the start of self-discharge, t is time, (s) and x is the distance from electrode surface, (cm).

The total charge Q is given by Faraday's law due to the fact that reactant reduction or oxidation progresses to completion throughout anodic or cathodic scan:

$$Q = nFVC^0 \tag{3.63}$$

where V is the volume of the solution, (cm^3), C^0 is the initial concentration of the reactant, (mole/cm^3). Equation 3.62 is solved and the oxidized species concentration and total charge $Q(t)$ and $C_{Ox(x,t)}$ moving to the solution from the negative electrode is respectively given as [265]:

$$C_{Ox(x,t)} = \frac{4C^0}{\pi}\sum_{m=1}^{\infty}\frac{1}{2m-1}\exp\left[\frac{-(2m-1)^2\pi^2 D_{Ox}t}{l^2}\right]\sin\frac{(2m-1)\pi\, x}{l} \tag{3.64}$$

$$Q(t) = nFVC_{Ox}\left\{1-\frac{8}{\pi^2}\sum_{m=1}^{\infty}\left(\frac{1}{2m-1}\right)^2\exp\left[\frac{-(2m-1)^2\pi^2 D_{Ox}t}{l^2}\right]\right\} \tag{3.65}$$

where m is the diffusion parameter which is evaluated by specific cell initial voltage, $C_{Ox(x,t)}$ is the oxidized species concentration, (mole/cm^3), A is electrode area, (cm^2), l is the entire thickness of the separator and anode, (cm), D_{Ox} is the oxidized species diffusion coefficient, (cm^2/s) , F is the Faraday constant and (C/mole), T is temperature, (^{0}K).

Applying the conditions and terms for which m >1 is negligibly small, Equation 3.65 becomes:

$$Q(t) = nFVC_{Ox}\left\{1-\frac{8}{\pi^2}\exp\left(\frac{-\pi^2 D_{Ox}t}{l^2}\right)\right\} \tag{3.66}$$

Thus the entire current density, liberated by the reversible redox reaction self-discharge due to the soluble products in solution $J_{VR1}(t)$ and potential decay by self-discharge $\varphi_D(t)$ is respectively given as:

$$J_{VR1}(t)=\frac{I(t)}{A}=\frac{\frac{dQ(t)}{dt}}{A}=\frac{\frac{8nFVD_{Ox}C_{Ox}}{l^2}\exp\left(\frac{-\pi^2 D_{Ox}t}{l^2}\right)}{A} \tag{3.67}$$

$$\varphi_D(t)=\frac{Q(t)}{C}=\frac{nFVC_{Ox}}{C}\left\{1-\frac{8}{\pi^2}\exp\left(\frac{-\pi^2 D_{Ox}t}{l^2}\right)\right\} \tag{3.68}$$

where C is the capacitance.

Since dissolved ions of impurities and redox species undergo diffusion and migration/shuttle processes, the overall self-discharge will be the summation of diffusion and migration/shuttle self-discharge current densities, which is shown in equation 3.58 and 3.67:

$$J_{VR}(x,t)=J_{VR}+J_{VR1}(t)=\frac{eZN}{w_{sp}\left(\frac{s_+ + s_-}{s_+ s_-}+\frac{D_+ + D_-}{D_+ D_-}\right)}+\frac{\frac{8nFVD_{Ox}C_{Ox}}{l^2}\exp\left(\frac{-\pi^2 D_{Ox}t}{l^2}\right)}{A} \tag{3.69}$$

The boundary conditions of this task during the capacitor discharge are as follows:

$$J_1(0,t)=-\alpha_1\frac{\partial\varphi_{ne}(x,t)}{\partial x}\Big|_{x=0}=J_0 \tag{3.70}$$

$$J_2(w,t)=\alpha_2\frac{\partial\varphi_{ne}(x,t)}{\partial t}\Big|_{x=w_{ne}}=J_0 \tag{3.71}$$

and the initial condition is as follows:

$$\varphi_{ne}(x,t)\big|_{t=0}=\varphi_{ne}^{0-} \tag{3.72}$$

The boundary conditions of this task during the capacitor charge are as follows:

$$J_1(0,t)=\alpha_1\frac{\partial\varphi_{ne}(x,t)}{\partial x}\Big|_{x=0}=J_0 \tag{3.73}$$

$$J_2(w,t)=-\alpha_2\frac{\partial\varphi_{ne}(x,t)}{\partial x}\Big|_{x=w_{ne}}=J_0 \tag{3.74}$$

and the initial condition is as follows:

$$\varphi_{ne}(x,t)\big|_{t=0} = \varphi_{ne}^{0+} \tag{3.75}$$

3.1.3 For the separator

Conductivity of the liquid matrix (electrolyte) in the separator should be represented as:

$$\sigma_{sp}^{l} = eZ^{+}n_0^{+}\mu_{+sp} + eZ^{-}n_0^{-}\mu_{-sp} \tag{3.76}$$

where n_0^+ and n_0^- are the equilibrium concentrations of positive and negative ions of electrolyte in the pores of separator respectively; eZ^+ and eZ^- are the values of the charges of the positive and negative ions of electrolyte respectively; μ_{+sp} and μ_{-sp} are effective mobilities of the positive and negative ions in the separator, respectively. The conductivity of electrolyte in the pores of the separator when the polarizable electrode is with p-type conductivity is determined, is by the given expression below:

$$\sigma_{sp}^{l} = eZ^{+}\mu_{+sp}\left(n_0^{+} + \Delta n^{+}\right) + eZ^{-}n_0^{-}\mu_{-sp} \tag{3.77}$$

where Δn^+ is the non-equilibrium concentration of the positive ion of electrolyte in the pores of the separator.Using Equations 3.10, 3.14, and 3.22 or 3.32, and the same approximation Equation 3.36 and notation Equation 3.40, it could still be shown that potential in the separator $\varphi_{sp}(x,t)$ is given as:

$$J_{2sp}(x,t) = -\alpha_{2sp}\frac{\partial\varphi_{sp}(x,t)}{\partial x} \tag{3.78}$$

$$\alpha_{2sp} = \sigma_{sp}^{l} + 2D_{+sp}C_V \tag{3.79}$$

3.1.4 For the positive electrode of electric double layer capacitors.

Case one.

When the electrode is polarizable and the solid matrix has electron conductivity, EDLS (p/Z^-) consists of electrons (p) and negative ions (Z^-), current densities $J_1(x,t)$ and $J_2(x,t)$ are determined by the formula given below:

$$J_2(x,t) = \sigma_{pe}^{l} E_2(x,t) - D_- \nabla \phi_2(x,t) \tag{3.80}$$

$$J_1(x,t) = \sigma_{pe}^{s} E_1(x,t) - D_{e(p)} \nabla \phi_1(x,t) \tag{3.81}$$

where D_- is the diffusivity coefficient of the negative non-equilibrium ion of electrolyte; σ_{pe}^{s} and σ_{pe}^{l} are conductivities of the electrode and electrolyte of the capacitor, respectively; $E_1(x,t)$ and $E_2(x,t)$ are the electric field intensities in the solid matrix and electrolyte of the electrode, respectively. Similarly, the model equation for potential $\varphi_{pe}(x,t)$ of the positive electrode is obtained as below:

$$\frac{\partial \varphi_{pe}(x,t)}{\partial t} = \beta^2 \frac{\partial^2 \varphi_{pe}(x,t)}{\partial x^2} + \frac{J_{VR}(x,t)}{C_V} \tag{3.82}$$

$$\beta^2 = \frac{\alpha_1 \alpha_2}{C_V(\alpha_2 + \alpha_1)} \tag{3.83}$$

It is therefore possible to obtain the dependence of the polarizable positive electrode on its overall dimensions, physical, electrochemical, and capacitance parameters at any point of time t during charging and discharging of the capacitor, using the solution of differential Equation 3.82. The boundary conditions of this task during discharging of the capacitor are as follows:

$$J_1(0,t) = -\alpha_1 \frac{\partial \varphi_{pe}(x,t)}{\partial x}\Big|_{x=0} = J_0 \tag{3.84}$$

$$J_2(w,t) = \alpha_2 \frac{\partial \varphi_{pe}(x,t)}{\partial t}\Big|_{x=w_{pe}} = J_0 \qquad 3.85$$

and the initial condition is:

$$\varphi_{pe}(x,t)\big|_{t=0} = \varphi_{pe}^{0-} \qquad 3.86$$

The boundary conditions of this task during capacitor charging are as follows:

$$J_1(0,t) = \alpha_1 \frac{\partial \varphi_{pe}(x,t)}{\partial x}\Big|_{x=0} = J_0 \qquad 3.87$$

$$J_2(w,t) = -\alpha_2 \frac{\partial \varphi_{pe}(x,t)}{\partial x}\Big|_{x=w_{pe}} = J_0 \qquad 3.88$$

and the initial condition is:

$$\varphi_{pe}(x,t)\big|_{t=0} = \varphi_{pe}^{0+} \qquad 3.89$$

3.2 Homogeneous/symmetric electrochemical capacitors with only composite electrodes.

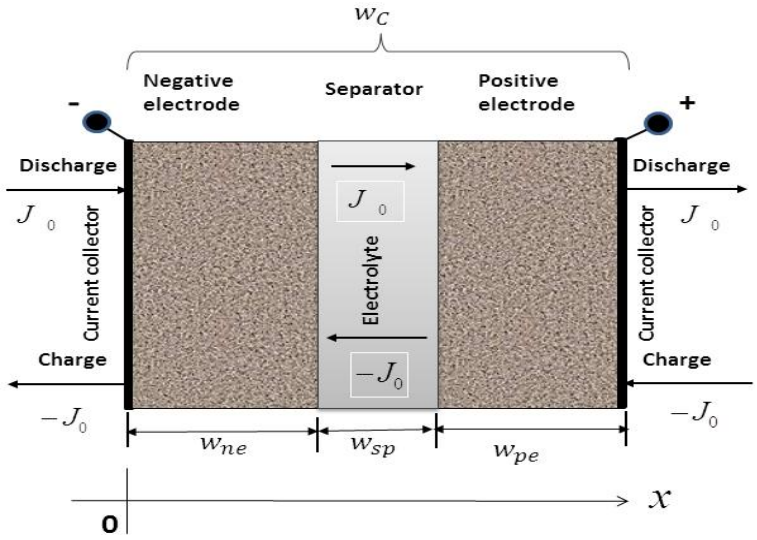

Figure 3.2: A symmetric electrochemical capacitor cell with only composite electrodes showing various functional layers on macroscale

3.2.1 The negative electrode of electrochemical capacitors with only composite electrodes.

The following assumptions were made in order to simplify the model:

1) The rates of generation of the charge carriers (charge generation) is very small compared with than rates of recombination of charge carriers (self-discharge);

2) The electrodes are the synergistic hybridization of the battery and capacitor components in single composites electrodes using active carbon material and metal oxides nanoparticles. This will increase the capacitance and conductivity of the electrodes;

3)The faradaic reaction occurs within positive and negative electrodes;

4) The electrodes have self-discharge;

5) The concentrations of the electrolyte ions and the conductivity of the electrodes change in a small range. The type of conductivity of the electrode's pore do not change during charging and discharging;

6) The capacitance depends very little on the value of potential;

7) Transport phenomena in the electrolyte phase are presumed to follow dilute solution theory [267] for binary electrolytes that have one-phase solvent;

8) The coefficient of diffusivity is taken to be independent of salt concentration;

9) Every other possible reaction and influence of temperature changes were ignored, that is, temperature is constant and uniform.

The changes of the electric charge densities $\phi_1(x,t)$ and $\phi_2(x,t)$ of the electrode during capacitor charging and discharging are determined by the given expression of continuity [12,89]:

$$\frac{\partial \phi_1(x,t)}{\partial t} = div\, J_1(x,t) - G_1(x,t) + R_1(x,t) \quad 3.90$$

$$\frac{\partial \phi_2(x,t)}{\partial t} = div\, J_2(x,t) - G_2(x,t) + R_2(x,t) \quad 3.91$$

where $\phi_1(x,t)$ and $\phi_2(x,t)$ are the charge densities of free carriers in the electrode solid matrix and electrolyte; $J_1(x,t)$ and $J_2(x,t)$ are the current densities in the electrode and electrolyte; $G_1(x,t)$ and $R_1(x,t)$ are the rates of generation and recombination of the charge carriers in the electrode; $G_2(x,t)$ and $R_2(x,t)$ are the rates of spontaneous generation and recombination of the charge carrier respectively.

Case one

When the electrode solid matrix has electron conductivity, the charge (e/Z^+) consists of electrons (e) and positive ions (Z^+), and current densities $J_1(x,t)$ and $J_2(x,t)$ are evaluated by the expressions given below:

$$J_1(x,t) = \sigma_{ne}^{s} E_1(x,t) - D_{e(p)} \nabla \phi_1(x,t) - M_1(x,t) - S_f J_{f1}(x,t) \quad 3.92$$

$$J_2(x,t) = \sigma_{ne}^{l} \left(E_2(x,t) + M_2(x,t) \right) + S_f J_{f2}(x,t) - D_{+} \nabla \phi_2(x,t) \quad 3.93$$

where D_e and D_+ are the diffusivity coefficients of the main charge carriers of the electrode and positive ions respectively; σ_{ne}^{s} and σ_{ne}^{l} are the conductivities of the electrode and electrolyte, respectively; $E_1(x,t)$ and $E_2(x,t)$ are the electric field intensity in the electrode solid matrix and electrolyte, respectively; $M_1(x,t)$ and $M_2(x,t)$ are the diffusion ionic current in the solid matrix and electrolyte, respectively; $J_{f1}(x,t)$ and $J_{f2}(x,t)$ are the faradaic transfer

current in the electrode solid matrix and electrolyte, respectively. The electric field intensity in the electrode solid matrix and electrolyte $E_1(x,t)$ and $E_2(x,t)$ are related to potentials $\varphi_1(x,t)$ and $\varphi_2(x,t)$ by the following expressions:

$$E_1(x,t) = -\nabla \varphi_1(x,t) = -\frac{\partial \varphi_1(x,t)}{\partial x} \quad 3.94$$

$$E_2(x,t) = -\nabla \varphi_2(x,t) = -\frac{\partial \varphi_2(x,t)}{\partial x} \quad 3.95$$

where $\varphi_1(x,t)$ and $\varphi_2(x,t)$ are the potential (in relation to pzc) of the electrode solid matrix and electrolyte, respectively. Considering the dependence of parameters of the electrochemical capacitors with the electrode whose solid matrix has electron or hole conductivity, conductivities of the electrode solid matrix and liquid (electrolyte) are represented respectively by the following expression:

$$\sigma_{ne}^{s} = en_0\mu_n + ep_0\mu_p \quad 3.96$$

$$\sigma_{ne}^{l} = eZ^{+}n_0^{+}\mu_{+} + eZ^{-}n_0^{-}\mu_{-} \quad 3.97$$

where n_0 and p_0 are the equilibrium concentrations of free electrons and holes of the electrode solid matrix; μ_n and μ_p are the effective mobilities of the electrons and the holes of the electrodes solid matrix, that depend on the parameters of the porous structure and the electrophysical properties of pore walls ; n_0^{+} and n_0^{-} are the equilibrium concentrations of positive and negative ions; eZ^{+} and eZ^{-} are values of the charges of positive and negative ions of electrolyte; μ_{+} and μ_{-} are the effective mobilities of positive and negative ions respectively.

If the electrode is assumed to have p-type conductivity, conductivities in the walls of the solid matrix pores and electrolyte are determined by the following expressions [89]:

$$\sigma_{ne}^{s} = e\mu_n\left(n_0 + \Delta n\right) + ep_0\mu_p \quad 3.98$$

$$\sigma_{ne}^{l} = eZ^{+}\mu_{+}\left(n_0^{+} + \Delta n^{+}\right) + eZ^{-}n_0^{-}\mu_{-} \quad 3.99$$

where Δn *and* Δn^{+} are the non-equilibrium concentrations of the free electrons in electrode and the positive ion of electrolyte, respectively. It follows that the density of non-equilibrium charges and the potentials of the electrode solid matrix and electrolyte are related by:

$$d\phi_1(x,t) = 2C_V\, d\varphi_1(x,t) \quad 3.100$$

$$d\phi_2(x,t) = 2C_V\, d\varphi_2(x,t) \quad 3.101$$

where C_V (F/cm^2) is the specific (by area) capacitance of the electrode; $\varphi_1(x,t)$ and $\varphi_2(x,t)$ are potential (in relation to the pzc) of the electrode matrix and electrolyte, respectively.

Again, it follows from Equations 3.100 and 3.101 that Δn (x,t), Δp (x,t), Δn^{+}(x,t), and Δn^{-} (x,t) are interrelated by the following expressions:

$$\Delta n = -\frac{2\,C_V\,\varphi_1(x,t)}{e} \quad 3.102$$

$$\Delta p = \frac{2\,C_V\,\varphi_2(x,t)}{e} \quad 3.103$$

$$\Delta n^{+} = \frac{2\,C_V\,\varphi_2(x,t)}{\left(eZ^{+}\right)} \quad 3.104$$

$$\Delta n^{-} = -\frac{2\,C_V\,\varphi_1(x,t)}{\left(eZ^{-}\right)} \quad 3.105$$

By substituting the values of the non-equilibrium charge carriers Equations 3.102-3.105 into Equations 3.98 and 3.99, we obtain expressions for conductivities of the electrode's solid matrix and electrolyte in its pores for the above-mentioned case:

Case one

$$\sigma_{ne}^{s} = e\mu_n\left[n_0 - \frac{2\,C_V\,\varphi_1(x,t)}{e}\right] + ep_0\mu_p \quad 3.106$$

$$\sigma_{ne}^{l} = eZ^{+}\mu_{+}\left[n_0^{+} + \frac{2\,C_V\,\varphi_2(x,t)}{\left(eZ^{+}\right)}\right] + eZ^{-}n_0^{-}\mu_{-} \quad 3.107$$

Case two

$$\sigma_{ne}^{s} = e\mu_n n_0 + e\mu_p \left[p_0 + \frac{2\, C_V\, \varphi_1(x,t)}{e} \right] \quad 3.108$$

$$\sigma_{ne}^{l} = eZ^{+}\mu_{+}\left[n_0^{+} + \frac{2\, C_V\, \varphi_2(x,t)}{(eZ^{+})} \right] + eZ^{-}n_0^{-}\mu_{-} \quad 3.109$$

The faradaic current transfer, $J_{f1}(x,t)$ and $J_{f2}(x,t)$ in the electrode solid matrix and electrolyte, respectively are given in form of the Butler-Volmer equation:

$$J_{f1}(x,t) = i_0 \{\exp[\alpha_a f\varphi_1(x,t) - \varphi_2(x,t) - U_1] - \exp[-\alpha_c f\varphi_1(x,t) - \varphi_2(x,t) - U_1]\} \quad 3.110$$

$$J_{f1}(x,t) = i_0 \{\exp[\alpha_a f\varphi_{ne}(x,t) - U_1] - \exp[-\alpha_c f\varphi_{ne}(x,t) - U_1]\} \quad 3.111$$

Also $J_{f2}(x,t)$ is given as:

$$J_{f2}(x,t) = i_0 \{\exp[\alpha_a f\varphi_{ne}(x,t) - U_1] - \exp[-\alpha_c f\varphi_{ne}(x,t) - U_1]\} \quad 3.112$$

where $\varphi_{ne}(x,t) = \varphi_1(x,t) - \varphi_2(x,t)$, and $J_{f1}(x,t) = J_{f2}(x,t) = J_f(x,t)$, i_0 is the exchange current density of the faradaic reaction, f is equal to $\frac{F}{RT}$, F is Faraday's constant, R is the universal gas constant, T is the absolute temperature, α_a and α_c are the anodic and cathodic transfer coefficients for the reactions respectively, and U_1 is the equilibrium potential of the faradaic reaction. U_1 is a function of the state of charge, which can be expressed by θ, the fraction of oxidized species in the electrode. The ionic diffusion current in the electrode solid matrix and electrolyte $M_1(x,t)$ and $M_2(x,t)$ are given by the expressions:

$$M_1(x,t) = \frac{\alpha_{ne}^{ls} RT}{F}\left(\frac{s_+}{n\nu_+} + \frac{t_+^0}{z_+\nu_+} \right) \frac{\partial^2 (\ln C_s)}{\partial x^2} \quad 3.113$$

$$M_2(x,t) = \frac{\alpha_{ne}^{l} RT}{F}\left(\frac{s_+}{n\nu_+} + \frac{t_+^0}{z_+\nu_+} \right) \frac{\partial^2 (\ln C_s)}{\partial x^2} \quad 3.114$$

where $M_1(x,t) = M_2(x,t) = M(x,t)$, $\sigma_{ne}^{ls} = \sigma_{ne}^{l}$ is the conductivity of electrolyte in the electrode, C_s is the electrolyte concentration, s_+ is the stoichiometric coefficient of cations in the electrode, t_+^0 is the cation transference number , ν_+ is the number of cations into which a mole of electrolyte salt dissociates, n is the number of electrons transferred in the electrode

reaction, and z_+ is the number of cations. When another variable, Q_f, the faradaic charge of the electrode is introduced, δ, the state of the charge in the faradaic reaction, θ, the fraction of oxidized species in the faradaic reaction and $J_f(x,t)$ are related by the following equations given below:

$$\theta(x,t) = \frac{Q_f - Q_{f,red}}{Q_{f,oxd} - Q_{f,red}} \quad 3.115$$

$$\delta = 0.5\theta(x,t) \quad 3.116$$

$$\frac{\partial Q_f}{\partial t} = S_f J_f(x,t) \quad 3.117$$

where $Q_{f,red}$ is the faradaic charge of the completely reduced electrode; S_f is the specific surface area for the faradaic redox reactions and $Q_{f,oxd}$ is the faradaic charge of a fully oxidized electrode. Equation 3.117 shows the rate of accumulation of the faradaic charge within the electrode to the faradaic transfer current. For the sake of simplicity, Equations 3.111, 3.115, and 3.117 are combined into a single equation given below:

$$\frac{\partial \theta(x,t)}{\partial t} = \frac{S_f i_0}{Q_{f,oxd} - Q_{f,red}} \{\exp[\alpha_a f \varphi_{ne}(x,t) - U_1] - \exp[-\alpha_c f \varphi_{ne}(x,t) - U_1]\} \quad 3.118$$

Again, in the concentrated solution theory field, salt mass balance results in equation 3.119:

$$\frac{\partial C_s(x,t)}{\partial t} = D_s \frac{\partial^2 C_s(x,t)}{\partial x^2} + \frac{S_d C_d (1 - t_+^0)}{2\varepsilon F} \frac{\partial \varphi_{ne}}{\partial t} + \frac{S_f (1 - t_+^0)}{2\varepsilon F} J_f(x,t) \quad 3.119$$

where ε and ε_s are the electrode and separator porosity respectively, S_d and C_d are the specific surface for EDL capacitance per unit of the electrode volume; (cm^2/cm^3) and EDL capacitance per area of the electrode, (F/cm^2).

Assuming that the conductivity of the electrode solid matrix under consideration is the electron-type (case one) and that $G(x,t) = 0$, substituting the appropriate expressions from Equations 3.106, 3.107, 3.94, 3.96, 3.101, 3.102, 3.111 and 3.113 into Equations 3.92 and 3.93 in place of $\sigma_{ne}^{ls}, \sigma_{ne}^{l}$, $d\phi_1(x,t)$ and $d\phi_2(x,t)$, we obtain the equations for $J_1(x,t)$ and $J_2(x,t)$ as shown:

$$J_1(x,t) = -\left\{ e\mu_n \left[n_0 - \frac{2\,C_V\,\varphi_1(x,t)}{e} \right] + ep_0\mu_p \right\} \frac{\partial \varphi_1(x,t)}{\partial x} - 2D_e C_V \frac{\partial \varphi_1(x,t)}{\partial x} - S_f i_0$$

$$\{\exp[\alpha_a f(\varphi_{ne}(x,t))] - \exp[-\alpha_c f(\varphi_{ne}(x,t))]\} - \frac{\sigma_{ne}^{ls} RT}{F} \left(\frac{s_+}{n\phi\nu_+} + \frac{t_+^0}{z_+\nu_+} \right) \frac{\partial^2 (\ln C_s(x,t))}{\partial x^2} \qquad 3.120$$

$$J_2(x,t) = -\left\{ eZ^+\mu_+ \left[n_0^+ + \frac{2\,C_V\,\varphi_2(x,t)}{(eZ^+)} \right] + eZ^-n_0^-\mu_- \right\} \frac{\partial \varphi_2(x,t)}{\partial x} - 2D_+ C_V \frac{\partial \varphi_2(x,t)}{\partial x} + S_f i_0$$

$$\{\exp[\alpha_a f(\varphi_{ne}(x,t))] - \exp[-\alpha_c f(\varphi_{ne}(x,t))]\} + \frac{\sigma_{ne}^{l} RT}{F} \left(\frac{s_+}{n\phi\nu_+} + \frac{t_+^0}{z_+\nu_+} \right) \frac{\partial^2 (\ln C_s(x,t))}{\partial x^2} \qquad 3.121$$

The specific capacitance C_V of electrodes at great deviations from the potential of pzc, becomes a function of potential, i.e., $C_V = C_V(\varphi)$ in Equations 3.120 and 3.121. Results of research of the capacitances of different types of EDLCs showed that the value of $C_V(\varphi)$ depends very little on the value of potential at small deviations of an electrode's potential.

When Equations 3.120 and 3.121 are substituted into Equations 3.90 and 3.91 subject to Equations 3.100 and 3.101, and after transformation, we get the differential equations:

$$\frac{\partial \varphi_1(x,t)}{\partial t} = \frac{1}{2\,C_V(\varphi_{ne})} div\left\{ \left\{ e\mu_n \left[n - \frac{2\,C_V(\varphi_{ne})\,\varphi_2(x,t)}{e} \right] + ep\mu_p + 2\,C_V(\varphi_{ne}) D_e \right\} \frac{\partial \varphi_1(x,t)}{\partial x} \right\}$$
$$- \frac{S_f i_0}{2C_V(\varphi_{ne})} \{\exp[\alpha_a f(\varphi_{ne}(x,t))] - \exp[-\alpha_c f(\varphi_{ne}(x,t))]\} + \frac{J_{VR}(x,t)}{2\,C_V(\varphi_{ne})} -$$
$$\frac{\sigma_{ne}^{ls} RT}{2C_V(\varphi_{ne}) F} \left(\frac{s_+}{n\nu_+} + \frac{t_+^0}{z_+\nu_+} \right) \frac{\partial^2 (\ln C_s(x,t))}{\partial x^2} \qquad 3.122$$

$$\frac{\partial \varphi_2(x,t)}{\partial t} = \frac{1}{2\,C_V(\varphi_{ne})} div\left\{ \left\{ eZ^+\mu_+ \left[n^+ + \frac{2\,C_V(\varphi_{ne})\,\varphi_2(x,t)}{eZ^+} \right] + eZ^-\mu_- n^- + 2\,C_V(\varphi_{ne}) D_+ \right\} \right.$$
$$\left. \frac{\partial \varphi_2(x,t)}{\partial x} \right\} + \frac{S_f i_0}{2C_V(\varphi_{ne})} \{\exp[\alpha_a f\varphi_{ne}(x,t) - U_1] - \exp[-\alpha_c f\varphi_{ne}(x,t) - U_1]\} - \frac{J_{VR}(x,t)}{2\,C_V(\varphi_{ne})} +$$

$$\frac{\sigma_{ne}^{l} RT}{2C_V(\varphi_{ne}) F} \left(\frac{s_+}{n\nu_+} + \frac{t_+^0}{z_+\nu_+} \right) \frac{\partial^2 (\ln C_s(x,t))}{\partial x^2} \qquad 3.123$$

where $\varphi_{ne}(x,t)$ is specified as $\varphi_1(x,t) - \varphi_2(x,t)$

On the assumption that capacitance does not depend on the potential of the electrochemical capacitor electrodes and concentrations of charge carriers in the walls of electrode pores and the electrolyte of EDLC is significantly lower than the equilibrium concentrations, that is,

$$n_0 >> \frac{2C_V\varphi_1(x,t)}{e} \tag{3.124}$$

$$n^+ >> \frac{2C_V\varphi_2(x,t)}{eZ^+} \tag{3.125}$$

Introducing the notations that

$$\alpha_1 = \sigma_{ne}^s + 2D_eC_V \tag{3.126}$$

$$\alpha_2 = \sigma_{ne}^l + 2D_+C_V \tag{3.127}$$

where α_1 and α_2 are the effective conductivities of the electrode and electrolyte respectively. Using Equations 3.124 & 3.125 and notations 3.126 & 3.127, Equations 3.122 and 3.123 becomes:

$$\frac{\partial\varphi_1(x,t)}{\partial t} = \frac{\alpha_1}{2C_V}\frac{\partial^2\varphi_1(x,t)}{\partial x^2} - \frac{S_f i_0}{2C_V}\{\exp[\alpha_a f\varphi_{ne}(x,t) - U_1] - \exp[-\alpha_c f\varphi_{ne}(x,t) - U_1]\}$$
$$-\frac{\sigma_{ne}^{ls}RT}{2C_VF}\left(\frac{s_+}{n\nu_+} + \frac{t_+^0}{z_+\nu_+}\right)\frac{\partial^2(\ln C_s(x,t))}{\partial x^2} + \frac{J_{VR}(x,t)}{2C_V} \tag{3.128}$$

$$\frac{\partial\varphi_2(x,t)}{\partial t} = \frac{\alpha_2}{2C_V}\frac{\partial^2\varphi_2(x,t)}{\partial x^2} + \frac{S_f i_0}{2C_V}\{\exp[\alpha_a f\varphi_{ne}(x,t) - U_1] - \exp[-\alpha_c f\varphi_{ne}(x,t) - U_1]\}$$
$$+\frac{\sigma_{ne}^{l}RT}{2C_VF}\left(\frac{s_+}{n\nu_+} + \frac{t_+^0}{z_+\nu_+}\right)\frac{\partial^2(\ln C_s(x,t))}{\partial x^2} - \frac{J_{VR}(x,t)}{2C_V} \tag{3.129}$$

Multiplying Equation 3.128 by α_2 and 3.129 by α_1, and subtracting Equation 3.129 from 3.128 term by term, one differential equation for the potential $\varphi_{ne}(x,t)$ of the electrode will be obtained, as shown below.

$$\frac{\partial \varphi_{ne}(x,t)}{\partial t} = \beta^2 \frac{\partial^2 \varphi_{ne}(x,t)}{\partial x^2} - \frac{S_f J_f(x,t)}{C_V} - \gamma \frac{\partial^2 (\ln C_s(x,t))}{\partial x^2} + \frac{J_{VR}(x,t)}{C_V} \quad 3.130$$

$$\beta^2 = \frac{\alpha_1 \alpha_2}{C_V(\alpha_2 + \alpha_1)} \quad 3.131$$

$$J_f(x,t) = i_0 \{\exp[\alpha_a f \varphi_{ne}(x,t) - U_1] - \exp[-\alpha_c f \varphi_{ne}(x,t) - U_1]\} \quad 3.132$$

$$\gamma = \frac{\sigma_{ne}^l RT}{C_V F}\left(\frac{s_+}{n\nu_+} + \frac{t_+^0}{z_+\nu_+}\right) \quad 3.133$$

Equation 3.130 is to be solved simultaneously with Equations 3.117 and 3.118 using the necessary boundary and initial conditions, and the solution(s) will be presented in chapter 4 which presents solution of the models.

$$\frac{\partial \theta(x,t)}{\partial t} = \frac{S_f i_0}{Q_{f,oxd} - Q_{f,red}} \{\exp[\alpha_a f \varphi_{ne}(x,t) - U_1] - \exp[-\alpha_c f \varphi_{ne}(x,t) - U_1]\} \quad 3.118$$

$$\frac{\partial C_s(x,t)}{\partial t} = D_s \frac{\partial^2 C_s(x,t)}{\partial x^2} + \frac{S_d C_d (1 - t_+^0)}{2\varepsilon F} \frac{\partial \varphi_{ne}(x,t)}{\partial t} + \frac{S_f (1 - t_+^0)}{2\varepsilon F} J_f(x,t) \quad 3.119$$

The boundary conditions of this task during the capacitor discharging are as follows:

$$J_1(0,t) = -\alpha_1 \frac{\partial \varphi_{ne}(x,t)}{\partial x}\Big|_{x=0} = J_0 \quad 3.134$$

$$\frac{\partial C_S(x,t)}{\partial x}\Big|_{x=0} = 0 \quad 3.135$$

$$J_2(w,t) = \alpha_2 \frac{\partial \varphi_{ne}(x,t)}{\partial t}\Big|_{x=w_{ne}} = J_0 \quad 3.136$$

$$\frac{\partial C_s(x,t)}{\partial x}\Big|_{x=w_{ne}} = \frac{(1 - t_+^0) J_0}{2\varepsilon_{sp} D_{ssp} F} \quad 3.137$$

and the initial condition are:

$$\varphi_{ne}(x,t)\big|_{t=0} = \varphi_{ne}^{0-} \quad 3.138$$

$$\theta(x,t)\big|_{t=0} = 1, \quad C_s(x,t)\big|_{t=0} = C_{s0} \quad 3.139$$

The boundary conditions of this task during the capacitor charging are:

$$J_1(0,t) = \alpha_1 \frac{\partial \varphi_{ne}(x,t)}{\partial x}\Big|_{x=0} = J_0 \qquad 3.140$$

$$\frac{\partial C_s(x,t)}{\partial x}\Big|_{x=0} = 0 \qquad 3.141$$

$$J_2(w,t) = -\alpha_2 \frac{\partial \varphi_{ne}(x,t)}{\partial x}\Big|_{x=w_{ne}} = J_0 \qquad 3.142$$

$$\left.\frac{\partial C_s(x,t)}{\partial x}\right|_{x=w_{ne}} = \frac{\left(1-t_+^0\right)J_0}{2\varepsilon_{sp}D_{ssp}F} \qquad 3.143$$

and the initial conditions are:

$$\varphi_{ne}(x,t)\big|_{t=0} = \varphi_{ne}^{0+} \qquad 3.144$$

$$\theta(x,t)\big|_{t=0} = 0\,, \quad C_s(x,t)\big|_{t=0} = C_{so} \qquad 3.145$$

3.2.2 The separator

Again, it could be shown that the potential in the separator $\varphi_{sp}(x,t)$ is given as:

$$J_{2sp}(x,t) = -\alpha_{2sp} \frac{\partial \varphi_{sp}(x,t)}{\partial x} \qquad 3.146$$

$$\alpha_{2sp} = \sigma_{sp}^{l} + 2D_{+sp}C_V \qquad 3.147$$

3.2.3 The positive electrode of electrochemical capacitors with only composite electrodes.

Because of the symmetrical feature of the two electrodes, expressions for the positive electrode with the necessary boundary and initial conditions could similarly be obtained as shown.

$$\frac{\partial \varphi_{pe}(x,t)}{\partial t} = \beta^2 \frac{\partial^2 \varphi_{pe}(x,t)}{\partial x^2} - \frac{S_f J_f(x,t)}{C_V} - \gamma \frac{\partial^2 (\ln C_s(x,t))}{\partial x^2} + \frac{J_{VR}(x,t)}{C_V} \quad 3.148$$

$$\beta^2 = \frac{\alpha_1 \alpha_2}{C_V(\alpha_2 + \alpha_1)} \quad 3.149$$

$$J_f(x,t) = i_0 \{\exp[\alpha_a f \varphi_{ne}(x,t) - U_1] - \exp[-\alpha_c f \varphi_{ne}(x,t) - U_1]\} \quad 3.150$$

$$\gamma = \frac{\sigma_{pe}^l RT}{C_V F}\left(\frac{s_+}{n\nu_+} + \frac{t_+^0}{z_+\nu_+}\right) \quad 3.151$$

Similarly, Equation 3.148 is to be solved simultaneously with Equations 3.152 and 3.153 using the boundary and initial conditions, and the solution(s) will be presented in chapter 4 which presents solution of the models.

$$\frac{\partial \theta(x,t)}{\partial t} = \frac{S_f i_0}{Q_{f,oxd} - Q_{f,red}} \{\exp[\alpha_a f \varphi_{ne}(x,t) - U_1] - \exp[-\alpha_c f \varphi_{ne}(x,t) - U_1]\} \quad 3.152$$

$$\frac{\partial C_s(x,t)}{\partial t} = D_s \frac{\partial^2 C_s(x,t)}{\partial x^2} + \frac{S_d C_d (1 - t_+^0)}{2\varepsilon F} \frac{\partial \varphi_{pe}(x,t)}{\partial t} + \frac{S_f (1 - t_+^0)}{2\varepsilon F} J_f(x,t) \quad 3.153$$

The boundary conditions of this task during the capacitor discharging are as follows:

$$J_1(0,t) = -\alpha_1 \frac{\partial \varphi_{pe}(x,t)}{\partial x}\Big|_{x=0} = J_0 \quad 3.154$$

$$\frac{\partial C_S(x,t)}{\partial x}\Big|_{x=0} = 0 \quad 3.155$$

$$J_2(w,t) = \alpha_2 \frac{\partial \varphi_{pe}(x,t)}{\partial t}\Big|_{x=w_{pe}} = J_0 \quad 3.156$$

$$\frac{\partial C_s(x,t)}{\partial x}\Big|_{x=w_{pe}} = \frac{(1 - t_+^0) J_0}{2\varepsilon_{sp} D_{ssp} F} \quad 3.157$$

and the initial conditions are:

$$\varphi_{pe}(x,t)\big|_{t=0} = \varphi_{pe}^{0-} \quad 3.158$$

$$\theta(x,t)\big|_{t=0}=1,\quad C_s(x,t)\big|_{t=0}=C_{so} \tag{3.159}$$

The boundary conditions of this task during the capacitor charging are as follows:

$$J_1(0,t)=\alpha_1\frac{\partial\varphi_{pe}(x,t)}{\partial x}\Big|_{x=0}=J_0 \tag{3.160}$$

$$\frac{\partial C_s(x,t)}{\partial x}\Big|_{x=0}=0 \tag{3.161}$$

$$J_2(w,t)=-\alpha_2\frac{\partial\varphi_{pe}(x,t)}{\partial x}\Big|_{x=w_{pe}}=J_0 \tag{3.162}$$

$$\frac{\partial C_s(x,t)}{\partial x}\Big|_{x=w_{pe}}=\frac{(1-t_+^0)J_0}{2\varepsilon_{sp}D_{ssp}F} \tag{3.163}$$

and the initial conditions are:

$$\varphi_{pe}(x,t)\big|_{t=0}=\varphi_{pe}^{0+} \tag{3.164}$$

$$\theta(x,t)\big|_{t=0}=1,\quad C_s(x,t)\big|_{t=0}=C_{so} \tag{3.165}$$

3.3 Heterogeneous/asymmetric electrochemical capacitors with a negative EDLC electrode and positive composite electrode.

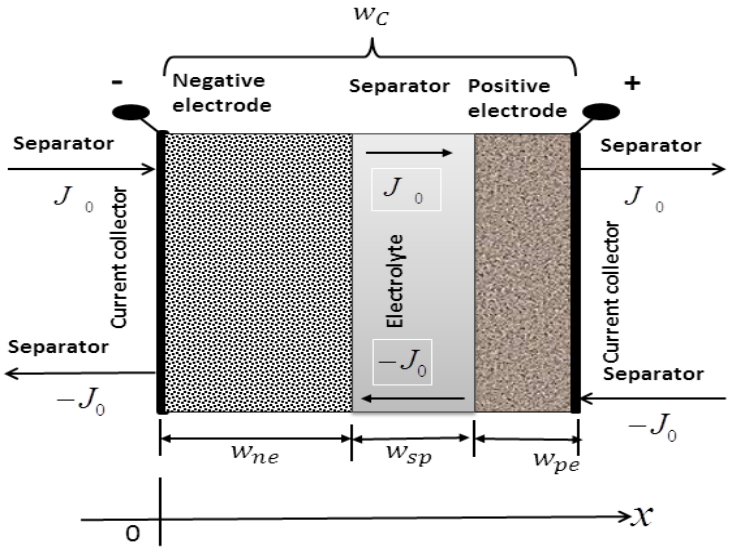

Figure 3.3: An asymmetric electrochemical capacitor with a negative EDL electrode and positive composite electrode showing various functional layers on macroscale

3.3.1 The negative electrode of electrochemical capacitor with EDLC electrode.

Because this electrode and its charge and discharge process is the same as in the symmetric EDLC, the model equation and the necessary boundary and initial conditions for the negative electrode are exactly the same.

$$\frac{\partial \varphi_{ne}(x,t)}{\partial t} = \beta^2 \frac{\partial^2 \varphi_{ne}(x,t)}{\partial x^2} + \frac{J_{VR}(x,t)}{C_V} \tag{3.166}$$

$$\beta^2 = \frac{\alpha_1 \alpha_2}{C_V(\alpha_2 + \alpha_1)} \tag{3.167}$$

$$J_{VR}(x,t) = J_{VR1}(x,t) = J_{VR2}(x,t) \tag{3.168}$$

The boundary conditions of this task during capacitor discharging are as follows:

$$J_1(0,t) = -\alpha_1 \frac{\partial \varphi_{ne}(x,t)}{\partial x}\Big|_{x=0} = J_0 \tag{3.169}$$

$$J_2(w,t) = \alpha_2 \frac{\partial \varphi_{ne}(x,t)}{\partial t}\Big|_{x=w_{ne}} = J_0 \tag{3.170}$$

and the initial condition is:

$$\varphi_{ne}(x,t)\big|_{t=0} = \varphi_{ne}^{0-} \tag{3.171}$$

The boundary conditions of this task during capacitor charging are:

$$J_1(0,t) = \alpha_1 \frac{\partial \varphi_{ne}(x,t)}{\partial x}\Big|_{x=0} = J_0 \tag{3.172}$$

$$J_2(w,t) = -\alpha_2 \frac{\partial \varphi_{ne}(x,t)}{\partial x}\Big|_{x=w_{ne}} = J_0 \tag{3.173}$$

and the initial condition is:

$$\varphi_{ne}(x,t)\big|_{t=0} = \varphi_{ne}^{0+} \tag{3.174}$$

3.3.2 The separator

Again it could also be shown that potential in the separator $\varphi_{sp}(x,t)$ is given as:

$$J_{2sp}(x,t) = -\alpha_{2sp}\frac{\partial\varphi_{sp}(x,t)}{\partial x} \tag{3.175}$$

$$\alpha_{2sp} = \sigma_{sp}^{l} + 2D_{+sp}C_V \tag{3.176}$$

3.3.3 The positive electrode of electrochemical capacitors with composite electrode.

It has been previously derived in an earlier section that expressions for the potential of the positive electrode of the electrochemical capacitors, with a composite electrode and the necessary boundary and initial conditions, are set for the positive electrode is as shown below:

$$\frac{\partial\varphi_{pe}(x,t)}{\partial t} = \beta^2\frac{\partial^2\varphi_{pe}(x,t)}{\partial x^2} - \frac{S_f J_f(x,t)}{C_V} - \gamma\frac{\partial^2(\ln C_s(x,t))}{\partial x^2} + \frac{J_{VR}(x,t)}{C_V} \tag{3.177}$$

$$\beta^2 = \frac{\alpha_1\alpha_2}{C_V(\alpha_2+\alpha_1)} \tag{3.178}$$

$$J_f(x,t) = i_0\left\{\exp\left[\alpha_a f\varphi_{pe}(x,t) - U_1\right] - \exp\left[-\alpha_c f\varphi_{pe}(x,t) - U_1\right]\right\} \tag{3.179}$$

$$\gamma = \frac{\sigma_{pe}^{l}RT}{C_V F}\left(\frac{s_+}{n\nu_+} + \frac{t_+^0}{z_+\nu_+}\right) \tag{3.180}$$

Equation 3.177 is to be solved simultaneously with Equations 3.181 and 3.182 using the boundary and initial conditions, and the solution(s) will be presented in chapter 4.

$$\frac{\partial\theta(x,t)}{\partial t}=\frac{S_f i_0}{Q_{f,oxd}-Q_{f,red}}\left\{\exp\left[\alpha_a f\varphi_{pe}(x,t)-U_1\right]-\exp\left[-\alpha_c f\varphi_{pe}(x,t)-U_1\right]\right\} \quad 3.181$$

$$\frac{\partial C_s(x,t)}{\partial t}=D_s\frac{\partial^2 C_s(x,t)}{\partial x^2}+\frac{S_d C_d\left(1-t_+^0\right)}{2\varepsilon F}\frac{\partial\varphi_{pe}(x,t)}{\partial t}+\frac{S_f\left(1-t_+^0\right)}{2\varepsilon F}J_f(x,t) \quad 3.182$$

where $C_V=S_d C_d$.

The boundary conditions of this task during capacitor discharging are as follows:

$$J_1(0,t)=-\alpha_1\frac{\partial\varphi_{pe}(x,t)}{\partial x}\Big|_{x=0}=J_0 \quad 3.183$$

and the initial condition are:

$$\frac{\partial C_S(x,t)}{\partial x}\Big|_{x=0}=0 \quad 3.184$$

$$J_2(w,t)=\alpha_2\frac{\partial\varphi_{pe}(x,t)}{\partial t}\Big|_{x=w_{pe}}=J_0 \quad 3.185$$

$$\frac{\partial C_s(x,t)}{\partial x}\Big|_{x=w_{pe}}=\frac{\left(1-t_+^0\right)J_0}{2\varepsilon_{sp}D_{ssp}F} \quad 3.186$$

$$\varphi_{pe}(x,t)\big|_{t=0}=\varphi_{pe}^{0-} \quad 3.187$$

$$\theta(x,t)\big|_{t=0}=1,\quad C_s(x,t)\big|_{t=0}=C_{s0} \quad 3.188$$

The boundary conditions of this task during capacitor charging are:

$$J_1(0,t)=\alpha_1\frac{\partial\varphi_{pe}(x,t)}{\partial x}\Big|_{x=0}=J_0 \quad 3.189$$

$$\frac{\partial C_s(x,t)}{\partial x}\Big|_{x=0}=0 \quad 3.190$$

$$J_2(w,t)=-\alpha_2\frac{\partial\varphi_{pe}(x,t)}{\partial x}\Big|_{x=w_{pe}}=J_0 \quad 3.191$$

$$J_2(w,t) = -\alpha_2 \left.\frac{\partial \varphi_{pe}(x,t)}{\partial x}\right|_{x=w_{pe}} = J_0 \qquad 3.192$$

$$\left.\frac{\partial C_s(x,t)}{\partial x}\right|_{x=w_{pe}} = \frac{\left(1-t_+^0\right)J_0}{2\varepsilon_{sp}D_{ssp}F} \qquad 3.193$$

and the initial condition are:

$$\varphi_{pe}(x,t)\big|_{t=0} = \varphi_{pe}^{0+} \qquad 3.194$$

$$\theta(x,t)\big|_{t=0} = 0\,, \quad C_s(x,t)\big|_{t=0} = C_{s0^+} \qquad 3.195$$

3.4 Homogeneous/symmetric electrochemical capacitors with only a redox couple electrode.

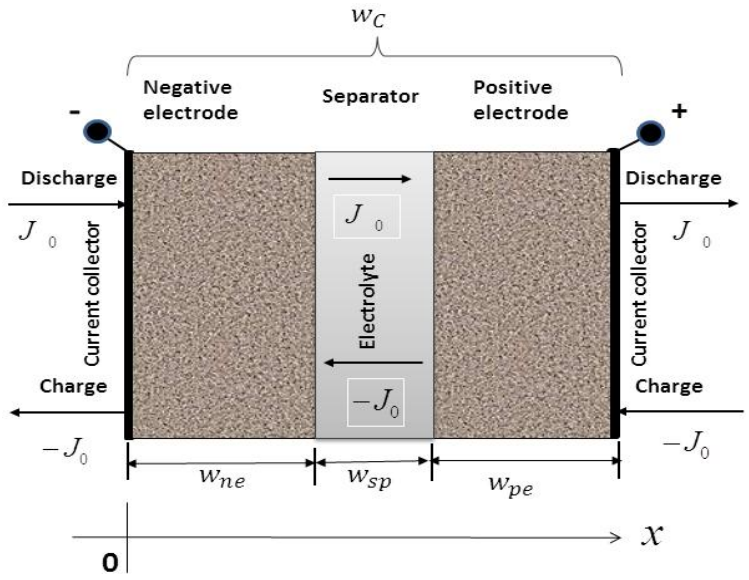

Figure 3.4: A symmetric supercapacitor cell with only redox couple electrodes showing various functional layers on macroscale

3.4.1 The negative electrode of electrochemical capacitors with redox couple electrode.

The following assumptions were made in order to simplify the model:

1) Physical properties such as the diffusion coefficients, transference number are not dependent on electrolyte concentration;

2) The exchange current density is not concentration dependent;

3) Isotropic materials properties are assumed because the experimental data are available, but those of nonisotropic are not yet available;

4) The double layer contributions is very small and negligible;

5) The faradaic reaction occurs within positive and negative electrodes;

6) The electrodes have self-discharge;

7) The concentrations of ions of electrolyte and the conductivity of the electrodes change in a small range. The type of conductivity of the electrode's pore does not change during charging and discharging;

8) Transport phenomena in electrolyte phase are taken, followed by dilute solution theory [267] consists of a binary electrolyte with one-phase solvent;

9) Charge storage through insertion/deinsertion inside the agglomerates is considered at microscale and adsorption/desorption is assumed to be negligible;

10) Every other possible reactions and influence of temperature changes were ignored, as temperature is constant and uniform.

In the context of concentrated solution theory [267], knowing that discharging in the redox couple electrode is controlled by diffusion of the mobile ion through the film [268], a mass balance on salt leads to the conclusion given below:

$$\frac{\partial C_s}{\partial t} = D_s \frac{\partial^2 C_s}{\partial x^2} + \frac{S_d C_d \left(1 - t_+^0\right)}{2\,\varepsilon\, F} \frac{\partial \varphi_{ne}}{\partial t} + \frac{S_f \left(1 - t_+^0\right) J_{Cell}}{2\,\varepsilon\, F} \qquad 3.196$$

The mobile ion diffusion into the redox couple electrode maintains the reaction at the film/separator interface, at $x = w_{ne}$. The kinetic expression was given previously [96,269] as:

$$J_{Cell} = i_0 \{\exp\left[\alpha_a f \varphi_{ne} - U_1\right] - \exp\left[-\alpha_c f \varphi_{ne} - U_1\right]\} \qquad 3.197$$

and is extended to the hybrid asymmetric electrochemical capacitor as:

$$J_{Cell} = i_0 \{\theta_s \exp\left[\alpha_a f \varphi_{ne} - U_1\right] - \left[1 - \theta_s\right] \exp\left[-\alpha_c f \varphi_{ne} - U_1\right]\} \qquad 3.198$$

where J_{Cell} is the cell current density, (A/cm^2), φ_{ne} is the potential of the negative electrode; i_0 is the exchange current density of the faradaic reaction; f is equal to $\frac{F}{RT}$, F is Faraday's constant; R is the universal gas constant; T is the absolute temperature; θ_s is the state of charge given by $\theta_s = C\left(1 - \theta^0\right)$; α_a and α_c are the anodic and cathodic transfer coefficients for the reactions respectively. U_1 is the equilibrium potential of the faradaic reaction and U_1 is dependent on the state of charge, which can be expressed by θ, the fraction of oxidized species in the electrode; ε is electrode porosity; S_d and C_d are the specific surface for EDL capacitance per unit of electrode volume, cm^2/cm^3 and EDL capacitance per area of electrode, (F/cm^2), and C_V is specific capacitance per area of electrode, (F/cm^2).

Assuming that effect of double layer charging in the electrode is negligible, Equation 3.196 will be expressed as:

$$\frac{\partial C_s}{\partial t} = D_s \frac{\partial^2 C_s}{\partial x^2} + \frac{S_f \left(1 - t_+^0\right) J_{Cell}}{2\,\varepsilon\, F} = D_s \frac{\partial^2 C_s}{\partial x^2} + \frac{J_{Cell}}{D_s \left(1 - \theta^0\right)} \qquad 3.199$$

The boundary conditions of this electrode during capacitor charging are as follows:

$$x = 0\,, \frac{\partial C_s}{\partial x} = 0 \tag{3.200}$$

$$x = w_{ne}\,, \quad \frac{\partial C_s}{\partial x} = \frac{J_{Cell}}{D_s\left(1-\theta^0\right)} \tag{3.201}$$

and the initial condition is:

$$At\ t = 0,\ C_{t=0} = C^0 \tag{3.202}$$

The boundary conditions of this electrode during capacitor discharging are:

$$x = 0\,, \frac{\partial C_s}{\partial x} = 0 \tag{3.203}$$

$$\frac{\partial C_s}{\partial x} = \frac{-J_{Cell}}{D_s\left(1-\theta^0\right)} \tag{3.204}$$

and the initial condition is given:

$$At\ t = 0,\ C_{t=0} = C^{0-} \tag{3.205}$$

The solution of equation 3. 199 will be presented in chapter 4 which presents solution of the models.

3.4.2 The positive electrode of electrochemical capacitors with redox couple electrode.

Similarly, a mass balance on salt in the positive redox couple electrode is expressed as:

$$\frac{\partial C_s}{\partial t} = D_s \frac{\partial^2 C_s}{\partial x^2} + \frac{S_f\left(1-t_+^0\right)J_{Cell}}{2\,\varepsilon\,F} = D_s \frac{\partial^2 C_s}{\partial x^2} + \frac{J_{Cell}}{D_s\left(1-\theta^0\right)} \tag{3.206}$$

Similarly, the boundary conditions of this positive electrode during capacitor charge are as follows:

$$x = 0\,, \frac{\partial C_s}{\partial x} = 0 \tag{3.207}$$

$$x = w_{pe}, \frac{\partial C_s}{\partial x} = \frac{J_{Cell}}{D_s\left(1-\theta^0\right)} \tag{3.208}$$

and the initial condition is given as:

$$At\ t = 0,\ C_{t=0} = C^0 \tag{3.209}$$

The boundary conditions of this positive electrode during capacitor discharging are as follows:

$$x = 0\,, \frac{\partial C_s}{\partial x} = 0 \tag{3.210}$$

$$x = w_{pe}, \frac{\partial C_s}{\partial x} = \frac{-J_{Cell}}{D_s\left(1-\theta^0\right)} \tag{3.211}$$

and the initial condition is given as:

$$At\ t = 0,\ C_{t=0} = C^{0-} \tag{3.212}$$

The solution of equation 3. 199 will be presented in chapter 4 which presents solution of the models.

3.5 Theoretical modelling for performance of electrochemical capacitors in terms of energy and power densities.

Choi and Park [270] recently presented theoretical expressions for the performance parameters of different types of electrochemical capacitors such as: a capacitor-type electrode system using aqueous electrolyte; a capacitor-type electrode system using organic electrolyte; symmetric capacitors; asymmetric capacitors using aqueous electrolyte; asymmetric capacitors using organic electrolyte; and a BatCap capcitor system.

Additional expressions for storable energy of a symmetric EDLC using organic electrolyte E_{o_s}, specific energy density of a symmetric EDLC using organic electrolyte ED_{o_s} and specific power density of a symmetric EDLC using organic electrolyte PD_{o_s} were derived in this section. This is to facilitate the comparison of the performance parameters of the symmetric EDLC using organic electrolyte, one capacitor-type electrode with organic electrolyte and one capacitor-type electrode with aqueous electrolyte. Storable energy, specific energy density and specific power density of an asymmetric EC using aqueous electrolyte presented by Choi and Park [270] were expanded and modified. Again, storable energy, specific energy density and specific power density of an asymmetric EC using organic electrolyte, were expanded and modified. The expansions and modifications are to facilitate the comparison of all these performance parameters for different types of electrochemical capacitors.

3.5.1 Symmetric electrochemical capacitor with aqueous electrolyte

Choi and Park [270] also presented storable energy in a symmetric capacitor of capacitor-type electrodes using aqueous electrolyte E_s, energy density per symmetric capacitor of capacitor-kind electrodes unit mass using aqueous electrolyte ED_s and power density per symmetric capacitor of capacitor-type electrodes unit mass using aqueous electrolyte PD_s respectively as:

$$E_s = \frac{1}{2} q_s \Delta V_{\max} = \frac{1}{2}\frac{1}{2} q_1 \Delta V_{\max} = \frac{1}{2} E_1 \tag{3.213}$$

$$ED_s = \frac{1}{2} \frac{q_s \Delta V_{\max}}{m_s} \frac{1}{3600s} = \frac{1}{2}\frac{1}{2} \frac{q_1 \Delta V_{\max}}{m_1} \frac{1}{3600s} = \frac{1}{2} ED_1 \tag{3.214}$$

$$PD_s = \frac{1}{2}\frac{q_s \Delta V_{\max}}{t\, m_s} = \frac{I_{\max}\Delta V_{\max}}{m_s} = PD_1 \qquad 3.215$$

where q_s is the amount of charge stored in a symmetric EC of capacitor-kind electrodes, using aqueous electrolyte, q_1 is the amount of charge stored in a single EC electrode using aqueous electrolyte. $\Delta V_{\max}$ is the capacitor's maximum working potential range using aqueous electrolyte; $m_s = \frac{m_1}{2} + \frac{m_1}{2} = m_1$ is the mass of the symmetric capacitor of capacitor-type electrodes using aqueous electrolyte; t is time of the charge or discharge process; $I_{\max}$ is the maximum current for each electrode. The maximum working potential range of the capacitor using aqueous electrolytes is lower than that of similar capacitors using organic electrolytes, while the conductivity is higher than that of those using organic electrolytes.

3.5.2 Symmetric electrochemical capacitor with organic electrolyte

The most straightforward EC is assembled employing two equal electrodes (symmetric) with equal mass, equal capacitance and basically the energy storage mechanism is via emergence of the electric double layer. Virtually all EDLCs fall into this category, because their energy storage mechanism is entirely electrostatic and current is not reliant on the potential. Thus, applied voltage to a symmetric EDLC, with a cathode and anode of the same mass, will equally break between positive and negative terminals, since the two electrodes have identical charge capacities. However, it is necessary to emphasize that this assertion is only justifiable for symmetric EDLC systems made of two equivalent electrodes [271,272]. In reality, capacitance distinctions exists between polarized electrodes of one capacitor [272], notwithstanding that they are constructed with the same material and of equal weight.

The storable energy of a symmetric EDLC using organic electrolyte E_{o_s}, energy density per unit mass of the symmetric EDLC using organic electrolyte ED_{o_s} and the power density per unit mass of the symmetric EDLC using organic electrolyte PD_{o_s} respectively were derived. This is to facilitate a comparison of the performance parameters of symmetric EDLCs using organic electrolyte, one capacitor-type electrode, with organic electrolyte and one capacitor-type electrode with aqueous electrolyte.

Since $\frac{q_{o_1}}{m_{o_1}\Delta V_{o_\max}} = k_4 \frac{q_1}{m_1 \Delta V_{\max}}$, $\Delta V_{o_\max}^2 = \frac{\Delta V_{\max}^2}{k_3^2}$ and $m_{o_1} = m_1$, we get that

$$\frac{q_{o_1}\Delta V_{o_\max}^2}{m_{o_1}\Delta V_{o_\max}} = k_4 \frac{q_1 \Delta V_{o_\max}^2}{m_1 \Delta V_{\max}} \Rightarrow \frac{q_{o_1}\Delta V_{o_\max}}{m_{o_1}} = \frac{k_4 q_1 \Delta V_{\max}}{m_1 k_3^2} \Rightarrow q_{o_1}\Delta V_{o_\max} = \frac{k_4}{k_3^2} q_1 \Delta V_{\max}$$

$$E_{o_s} = \frac{1}{2} q_{o_s} \Delta V_{o_\max} = \frac{1}{2}\frac{1}{2} q_{o_1} \Delta V_{o_\max} = \frac{1}{2}\frac{k_4}{k_3^2}\frac{1}{2} q_1 \Delta V_{\max}$$

But $K_E = \frac{k_4}{k_3^2}$ 3.216

$$= \frac{1}{2}\frac{1}{2} q_{o_1}\Delta V_{o_\max} = \frac{K_E}{2}\frac{1}{2} q_1 \Delta V_{\max}$$

$$E_{o_s} = \frac{1}{2}\frac{1}{2} q_{o_1}\Delta V_{o_\max} = \frac{K_E}{2}\frac{1}{2} q_1 \Delta V_{\max} = \frac{1}{2} E_{o_1} = \frac{K_E}{2} E_1 \quad 3.217$$

$$ED_{o_s} = \frac{1}{2}\frac{q_{o_s}\Delta V_{o_\max}}{m_{o_s}}\frac{1}{3600s} = \frac{1}{2}\frac{1}{2}\frac{q_{o_1}\Delta V_{o_\max}}{m_{o_1}}\frac{1}{3600s} = \frac{k_4}{2k_3^2}\frac{1}{2}\frac{q_1 \Delta V_{\max}}{m_1}\frac{1}{3600s}$$

$$ED_{o_s} = \frac{1}{2}\frac{1}{2}\frac{q_{o_1}\Delta V_{o_\max}}{m_{o_1}}\frac{1}{3600s} = \frac{K_E}{2}\frac{1}{2}\frac{q_1 \Delta V_{\max}}{m_1}\frac{1}{3600s} = \frac{1}{2} ED_{o_1} = \frac{K_E}{2} ED_1 \quad 3.218$$

$$PD_{o_s} = \frac{1}{2}\frac{q_{o_s}\Delta V_{o_\max}}{t\, m_{o_s}} = \frac{1}{2}\frac{1}{2}\frac{q_{o_1}\Delta V_{o_\max}}{t\, m_{o_1}} = \frac{k_4}{2k_3^2}\frac{1}{2}\frac{q_1 \Delta V_{\max}}{t\, m_1}$$

$$PD_{o_s} = \frac{1}{2}\frac{1}{2}\frac{q_{o_1}\Delta V_{o_\max}}{t\, m_{o_1}} = \frac{K_E}{2}\frac{1}{2}\frac{q_1 \Delta V_{\max}}{t\, m_1} = \frac{1}{2} PD_{o_1} = \frac{K_E}{2} PD_1 \quad 3.219$$

where q_{o_s} is the amount of charge stored in the symmetric EC of capacitor-type electrodes using organic electrolyte; $\Delta V_{\max}$ is the capacitor maximum working potential range using

organic electrolyte; $m_{o_s} = \frac{m_{o_1}}{2} + \frac{m_{o_1}}{2} = m_{o_1}$ is the mass of the symmetric capacitor of capacitor-type electrodes using organic electrolyte; t is the time of the charge or discharge process; $I_{\max}$ is the maximum current for each electrode; k_3 is the ratio of maximum operating potential range between aqueous and organic electrolytes; k_4 is the ratio of specific capacitance between capacitor-type electrodes in aqueous and organic electrolyte; K_E is a constant associated with electrolyte and is dependent on k_3 and k_4.

3.5.3 Asymmetric electrochemical capacitor with aqueous electrolyte

Mass balance is employed in this system so as to guarantee that the electrodes function in the most effective potential window to achieve the highest capacitor specific energy by enlarging its operating voltage. The calculation of theoretical specific capacitance of asymmetric-hybrid ECs from electrodes specific capacitances must be performed subject to the electrodes mass ratio [21]. The storable energy of asymmetric EC using aqueous electrolyte E_{as}, energy density per unit mass of asymmetric EC using aqueous electrolyte ED_{as} and power density per unit mass of asymmetric EC using aqueous electrolyte PD_{as} respectively were expanded and modified as shown below. The expansions and modifications are to facilitate comparison of all these performance parameters for asymmetric EC using aqueous electrolyte, symmetric EDLC using aqueous electrolyte and one capacitor-kind electrode with aqueous electrolyte.

$$E_{as} = q_{as}\Delta V_b + \frac{1}{2} q_{as}\Delta V_c = q_{as}\left(\Delta V_b + \frac{\Delta V_c}{2}\right)$$

Since $\Delta V_b = k_2.\Delta V_{\max}$, $\Delta V_c = \Delta V_{\max}.(1-k_2)$ and $m_{as} = \frac{m_c}{1-k_1}$

$$E_{as} = q_{as}\Delta V_{\max}\left(k_2 + \frac{(1+k_2)}{2}\right) = \frac{1}{2}q_{as}(1+k_2)\Delta V_{\max} = q_s(1-k_2^2)\Delta V_{\max} = \frac{1}{2}q_1(1-k_2^2)\Delta V_{\max}$$

But $K_{BM} = (1-k_1)(1-k_2^2)$ 3.220

$$= \frac{K_{BM}}{(1-k_1)}q_s\Delta V_{\max} = \frac{K_{BM}}{2(1-k_1)}q_1\Delta V_{\max}$$

$$E_{as} = \frac{K_{BM}}{(1-k_1)}q_s\Delta V_{\max} = \frac{K_{BM}}{2(1-k_1)}q_1\Delta V_{\max} = \frac{2K_{BM}}{(1-k_1)}E_s = \frac{K_{BM}}{(1-k_1)}E_1 \quad 3.221$$

$$ED_{as} = \frac{q_{as}}{m_{as}}\left(\Delta V_b + \frac{1}{2}\Delta V_c\right)\frac{1}{3600s} = (1-k_1)(1-k_2^2)\frac{q_s\Delta V_{\max}}{m_s}\frac{1}{3600s}$$

$$= (1-k_1)(1-k_2^2)\frac{q_s\Delta V_{\max}}{m_s}\frac{1}{3600s} = (1-k_1)(1-k_2^2)\frac{1}{2}\frac{q_1\Delta V_{\max}}{m_1}\frac{1}{3600s}$$

$$= K_{BM}\frac{q_s\Delta V_{\max}}{m_s}\frac{1}{3600s} = K_{BM}\frac{1}{2}\frac{q_1\Delta V_{\max}}{m_1}\frac{1}{3600s}$$

$$ED_{as} = K_{BM}\frac{q_s\Delta V_{\max}}{m_s}\frac{1}{3600s} = K_{BM}\frac{1}{2}\frac{q_1\Delta V_{\max}}{m_1}\frac{1}{3600s} = 2K_{BM}ED_s = K_{BM}ED_1 \quad 3.222$$

$$PD_{as} = \frac{q_{as}}{t\,m_{as}}\left(\Delta V_b + \frac{1}{2}\Delta V_c\right) = (1+k_2)\frac{1}{2}\frac{q_{as}\Delta V_{\max}}{t\,m_{as}} = (1-k_1)(1-k_2^2)\frac{q_s\Delta V_{\max}}{t\,m_s} = K_{BM}\frac{q_1\Delta V_{\max}}{2\,t\,m_1}$$

$$= 2(1-k_1)(1-k_2^2)\frac{I_{\max}\Delta V_{\max}}{m_s} = (1-k_1)(1-k_2^2)\frac{I_{\max}\Delta V_{\max}}{m_1}$$

$$= 2K_{BM}\frac{I_{\max}\Delta V_{\max}}{m_s} = K_{BM}\frac{I_{\max}\Delta V_{\max}}{m_1}$$

$$PD_{as} = 2K_{BM}\frac{I_{\max}\Delta V_{\max}}{m_s} = K_{BM}\frac{I_{\max}\Delta V_{\max}}{m_1} = 2K_{BM}PD_s = K_{BM}PD_1 \quad 3.223$$

where q_{as} is amount of charge stored in asymmetric EC with aqueous electrolyte, $\Delta V_{\max}$ is capacitor maximum working potential range in aqueous electrolyte, $m_{as} = m_b + m_c$ is mass of asymmetric capacitor using aqueous electrolyte, m_b is mass of battery-kind electrode, m_c is mass of capacitor-kind electrode, ΔV_b is working potential range of battery-kind electrode, ΔV_c is working potential range of capacitor-kind electrode, $I_{\max}$ is maximum current for each electrode, k_1 is ratio of mass of battery-kind electrode to total mass of battery-kind and capacitor-type electrodes, k_2 is ratio of operating potential range of

battery-kind electrode to that of capacitor maximum working potential range in aqueous electrolyte, K_{BM} is coefficient associated to battery-kind material and depends on k_1 and k_2. Note, that the maximum working potential range of capacitor using aqueous electrolytes is lower than that of similar capacitor using organic electrolytes, while the conductivity is higher than that of those using organic electrolytes.

3.5.4 Asymmetric electrochemical capacitor with organic electrolyte.

The storable energy of asymmetric EC using organic electrolyte E_{o_as}, energy density per unit mass of asymmetric EC using organic electrolyte ED_{o_as} and power density per unit mass of asymmetric EC using organic electrolyte PD_{o_as} respectively were expanded and modified as shown below. The expansions and modifications are to facilitate comparison of all these performance parameters for asymmetric EC using organic electrolyte, symmetric EDLC using organic electrolyte, one capacitor-kind electrode with organic electrolyte, symmetric EDLC using aqueous electrolyte, and one capacitor-kind electrode with aqueous electrolyte.

$$E_{o_as} = q_{o_as}\Delta V_{o_b} + \frac{1}{2}q_{o_as}\Delta V_{o_c} = \frac{1}{2}q_{o_as}(1+k_2)\Delta V_{o_\max} = q_{o_s}(1-k_2^2)\Delta V_{o_\max}$$
$$= \frac{1}{2}q_{o_as}(1+k_2)\Delta V_{o_\max} = q_{o_s}(1-k_2^2)\Delta V_{o_\max} = \frac{1}{2}q_{o_1}(1-k_2^2)\Delta V_{o_\max}$$
$$= q_{o_s}\frac{(1-k_2^2)}{(1-k_1)}\Delta V_{o_\max} = \frac{1}{2}q_{o_1}\frac{(1-k_2^2)}{(1-k_1)}\Delta V_{o_\max} = \frac{K_{BM}}{(1-k_1)}q_{o_s}\Delta V_{o_\max} = \frac{K_{BM}}{2(1-k_1)}q_{o_1}\Delta V_{o_\max}$$
$$= \frac{K_{BM}}{(1-k_1)}q_{o_s}\Delta V_{o_\max} = \frac{K_{BM}}{2(1-k_1)}q_{o_1}\Delta V_{o_\max} = \frac{K_{BM}K_E}{(1-k_1)}q_s\Delta V_{\max} = \frac{K_{BM}K_E}{2(1-k_1)}q_1\Delta V_{\max}$$

$$E_{o_as} = K_E E_{as} = \frac{2K_{BM}}{(1-k_1)}E_{o_s} = \frac{2K_EK_{BM}}{(1-k_1)}E_s = \frac{K_{BM}}{(1-k_1)}E_{o_1} = \frac{K_EK_{BM}}{(1-k_1)}E_1 \qquad 3.224$$

$$ED_{o_as} = \frac{q_{o_as}}{m_{o_as}}\left(\Delta V_{o_b} + \frac{1}{2}\Delta V_{o_c}\right)\frac{1}{3600s} = (1-k_1)(1-k_2^2)\frac{1}{2}\frac{q_{o_1}\Delta V_{o_\max}}{m_{o_1}}\frac{1}{3600s}$$

But $\frac{q_{o_1}}{m_{o_1}\Delta V_{o_\max}} = k_4 \frac{q_1}{m_1 \Delta V_{\max}}$, $\Delta V_{o_\max}^2 = \frac{\Delta V_{\max}^2}{k_3^2}$, $m_{o_1} = m_1$, $q_{o_1}\Delta V_{o_\max} = \frac{k_4}{k_3^2} q_1 \Delta V_{\max}$ and $q_{o_1} = 2q_{o_s}$

$$ED_{o_as} = (1-k_1)(1-k_2^2)\frac{1}{2}\frac{q_{o_1}\Delta V_{o_\max}}{m_{o_1}}\frac{1}{3600s} = \frac{k_4}{k_3^2}(1-k_1)(1-k_2^2)\frac{1}{2}\frac{q_1\Delta V_{\max}}{m_1}\frac{1}{3600s}$$

$$ED_{o_as} = K_{BM}\frac{q_{o_s}\Delta V_{o_\max}}{m_{o_s}}\frac{1}{3600s} = \frac{k_4}{k_3^2}K_{BM}\frac{q_s\Delta V_{\max}}{m_s}\frac{1}{3600s} = K_{BM}\frac{1}{2}\frac{q_{o_1}\Delta V_{o_\max}}{m_{o_1}}\frac{1}{3600s}$$

$$= \frac{k_4}{k_3^2}K_{BM}\frac{1}{2}\frac{q_1\Delta V_{\max}}{m_1}\frac{1}{3600s} \quad 3.225$$

$$ED_{o_as} = K_E ED_{as} = 2K_{BM}ED_{o_s} = 2K_E K_{BM}ED_s = K_{BM}ED_{o_1} = K_E K_{BM}ED_1 \quad 3.226$$

$$PD_{o_as} = \frac{q_{o_as}}{t\, m_{o_as}}\left(\Delta V_{o_b} + \frac{1}{2}\Delta V_{o_c}\right) = (1+k_2)\frac{1}{2}\frac{q_{o_as}\Delta V_{o_\max}}{t\, m_{o_as}} = (1-k_1)(1-k_2^2)\frac{q_{o_s}\Delta V_{o_\max}}{t\, m_{o_s}}$$

$$= K_{BM}\frac{q_{o_s}\Delta V_{o_\max}}{t\, m_{o_s}} = K_{BM}K_E\frac{q_s\Delta V_{\max}}{t\, m_s} = K_{BM}\frac{1}{2}\frac{q_{o_1}\Delta V_{o_\max}}{t\, m_{o_1}} = K_{BM}\frac{k_4}{k_3^2}\frac{q_1\Delta V_{\max}}{2t\, m_1}$$

$$= 2K_{BM}\frac{I_{o_\max}\Delta V_{o_\max}}{m_{o_s}} = 2K_E K_{BM}\frac{I_{\max}\Delta V_{\max}}{m_s} = K_{BM}\frac{I_{o_\max}\Delta V_{o_\max}}{m_{o_1}} = K_E K_{BM}\frac{I_{\max}\Delta V_{\max}}{m_1} \quad 3.227$$

$$PD_{o_as} = K_E PD_{as} = 2K_{BM}PD_{o_s} = 2K_E K_{BM}PD_s = K_{BM}PD_{o_1} = K_E K_{BM}PD_1 \quad 3.228$$

where q_{o_as} is amount of charge stored in asymmetric EC using organic electrolyte, $\Delta V_{o_\max}$ is the capacitor maximum working potential range in asymmetric EC using organic electrolyte, $m_{o_as} = m_{o_b} + m_{o_c}$ is mass of asymmetric capacitor using organic electrolyte, m_{o_b} is mass of battery-kind electrode using organic electrolyte, m_{o_c} is mass of capacitor-kind electrode using organic electrolyte, ΔV_{o_b} is working potential range of battery-kind electrode in asymmetric EC using organic electrolyte, ΔV_{o_c} is working potential range of capacitor-kind electrode in asymmetric EC using organic electrolyte, $I_{o_\max}$ is the maximum current in the asymmetric EC using organic electrolyte, k_3 is ratio of maximum operating potential range between aqueous and organic electrolytes, k_4 is the ratio of specific capacitance between

capacitor-kind electrodes in aqueous and organic electrolyte, K_E is a constant associated to electrolyte and depends on k_3 and k_4.

The summary of the relationships for parameters from theoretical equations for purpose of capacitors performance comparison is as follows:

$$E_{o_s} = K_E E_s = \frac{1}{2} E_{o_1} = \frac{K_E}{2} E_1 = 5.56E_s = 0.5E_{o_1} = 2.78E_1 \quad 3.229$$

$$ED_{o_s} = K_E ED_s = \frac{1}{2} ED_{o_1} = \frac{K_E}{2} ED_1 = 5.56ED_s = 0.5ED_{o_1} = 2.78ED_1 \quad 3.230$$

$$PD_{o_s} = K_E PD_s = \frac{1}{2} PD_{o_1} = \frac{K_E}{2} PD_1 = 5.56PD_s = 0.5PD_{o_1} = 2.78PD_1 \quad 3.231$$

$$E_{as} = \frac{2K_{BM}}{(1-k_1)} E_s = \frac{K_{BM}}{(1-k_1)} E_1 = 2.00E_s = 1.00E_1 \quad 3.232$$

$$ED_{as} = 2K_{BM} ED_s = K_{BM} ED_1 = 1.89ED_s = 0.95ED_1 \quad 3.233$$

$$PD_{as} = 2K_{BM} PD_s = K_{BM} PD_1 = 1.89PD_s = 0.95PD_1 \quad 3.234$$

$$E_{o_as} = K_E E_{as} = \frac{2K_{BM}}{(1-k_1)} E_{o_s} = \frac{2K_E K_{BM}}{(1-k_1)} E_s = \frac{K_{BM}}{(1-k_1)} E_{o_1} = \frac{K_E K_{BM}}{(1-k_1)} E_1$$
$$= 5.56E_{as} = 2.00E_{o_s} = 11.08E_s = 1.00E_{o_1} = 5.54E_1 \quad 3.235$$

$$ED_{o_as} = K_E ED_{as} = 2K_{BM} ED_{o_s} = 2K_E K_{BM} ED_s = K_{BM} ED_{o_1} = K_E K_{BM} ED_1$$
$$= 5.56ED_{as} = 1.89ED_{o_s} = 10.50ED_s = 0.95ED_{o_1} = 5.25ED_1 \quad 3.236$$

$$PD_{o_as} = K_E PD_{as} = 2K_{BM} PD_{o_s} = 2K_E K_{BM} PD_s = K_{BM} PD_{o_1} = K_E K_{BM} PD_1$$
$$= 5.56PD_{as} = 1.89PD_{o_s} = 10.50PD_s = 0.95PD_{o_1} = 5.25PD_1 \quad 3.237$$

3.5.5 Optimization of ECs design parameters and operating conditions for high energy and power performances.

In order to maximize storable energy, energy and power densities of electrochemical capacitors, we need to maximize the values of coefficient associated to battery-kind material in asymmetric ECs with aqueous electrolyte K_{BM} and constant associated to electrolyte in asymmetric ECs with organic electrolyte K_E subject to realistic constraints. These coefficients are given as equations 3.220 and 3.216, respectively. The constraint equations by Choi and Park were also modified as shown below, in order to capture realistic conditions and the limitations inherent in electrochemical energy storage systems. It is necessary to maximize the following coefficients subject to their respective constraints:

$$\text{Maximize } K_{BM} = (1-k_1)(1-k_2^2) \qquad 3.218$$

$$\text{Subject to: } \left.\begin{matrix} \delta_1 < \mathrm{k}_1 < 0.5 \\ \delta_2 < \mathrm{k}_2 < 0.7 \end{matrix}\right\} \qquad 3.238$$

where $\delta_1 = 0.05$ is the realistic minimum value of k_1 for EC systems as explained in [90] and $\delta_2 = 0.05$ the realistic minimum value of k_2 for EC systems as explained in [90].

$$\text{Maximize } K_E = \frac{k_4}{k_3^2} \qquad 3.213$$

$$\text{Subject to: } \left.\begin{matrix} \delta_3 \le \mathrm{k}_3 < 1 \\ 0 < \mathrm{k}_4 \le \delta_4 \end{matrix}\right\} \qquad 3.239$$

where $\delta_3 = 0.3$ is the realistic minimum value of k_3 for EC systems as explained in [270,273,274] and $\delta_4 = 0.5$ is the realistic maximum value of k_4 for EC systems as explained in [270,273,274].

The models developed above are validated in the next chapter with experimental data reported by the following research groups in literature: Kazaryan et al [89], Ma et al [275], Sun et al [276] and Zhao et al [277].

CHAPTER FOUR

4.0 Solutions to the Models

4.1 Homogeneous/symmetric electric double layer capacitors (EDLCs)

For the negative electrode of supercapacitors with an electric double layer electrode

$$\frac{\partial \varphi_{ne}(x,t)}{\partial t} = \beta^2 \frac{\partial^2 \varphi_{ne}(x,t)}{\partial x^2} + \frac{J_{VR}(x,t)}{C_V} \tag{4.1}$$

$$\beta^2 = \frac{\alpha_1 \alpha_2}{C_V(\alpha_2 + \alpha_1)} \tag{4.2}$$

The boundary conditions of this task during capacitor discharging are as follows:

$$J_1(0,t) = -\alpha_1 \frac{\partial \varphi_{ne}(x,t)}{\partial x}\Big|_{x=0} = J_0 \tag{4.3}$$

$$J_2(w,t) = \alpha_2 \frac{\partial \varphi_{ne}(x,t)}{\partial x}\Big|_{x=w_{ne}} = J_0 \tag{4.4}$$

and the initial condition are:

$$\varphi_{ne}(x,t_{=0}) = \varphi_{ne}^{0^-} - \frac{J_0\, x}{\alpha_1} + \frac{J_0(\alpha_1 + \alpha_2)x^2}{2w_{ne}\alpha_1\alpha_2}$$

$$\varphi_{ne}(x_{=0},t_{=0}) = \varphi_{ne}^{0^-} \tag{4.5}$$

The boundary conditions of this task during capacitor charging are:

$$J_1(0,t) = \alpha_1 \frac{\partial \varphi_{ne}(x,t)}{\partial x}\Big|_{x=0} = J_0 \tag{4.6}$$

$$J_2(w,t) = -\alpha_2 \frac{\partial \varphi_{ne}(x,t)}{\partial x}\Big|_{x=w_{ne}} = J_0 \tag{4.7}$$

and the initial conditions are:

$$\varphi_{ne}(x,t_{=0}) = \varphi_{ne}^{0^+} + \frac{J_0\, x}{\alpha_1} - \frac{J_0(\alpha_1+\alpha_2)\,x^2}{2w_{ne}\alpha_1\alpha_2}$$

$$\varphi_{ne}(x_{=0},t_{=0}) = \varphi_{ne}^{0^+} \qquad 4.8$$

This equation 4.1 can first be solved by assuming no self-discharge, ie, $\frac{J_{VR}(x,t)}{C_V} = 0$,to obtain:

$$\frac{\partial \varphi_{ne}(x,t)}{\partial t} = \beta^2 \frac{\partial^2 \varphi_{ne}(x,t)}{\partial x^2} \qquad 4.9$$

with inhomogeneous boundary conditions $\frac{\partial \varphi_{ne}}{\partial x}(0,t) = -\frac{J_0}{\alpha_1}, \frac{\partial \varphi_{ne}}{\partial x}(w_{ne},t) = \frac{J_0}{\alpha_2}$ and inhomogeneous initial conditions $\varphi_{ne}(t)\Big|_{t=0} = \varphi_{ne}^{0^+}$,which are the same as equtaions 4.3, 4.4 &4.5 and 4.6, 4.7 & 4.8 for capacitor's discharging and charging process, respectively.

4.2 Homogeneous/symmetric electrochemical capacitors without self-discharge.

For the homogeneous equation $\frac{\partial \varphi_{ne}}{\partial t} = \beta^2 \frac{\partial^2 \varphi_{ne}}{\partial x^2}$, with inhomogeneous boundary and initial conditions, it becomes $\frac{\partial \varphi_{ne}}{\partial t} - \beta^2 \frac{\partial^2 \varphi_{ne}}{\partial x^2} = 0$ 4.10

4.3 The Separator

$$J_{sp}(x,t) = -\alpha_{sp} \frac{\partial \varphi_{sp}(x,t)}{\partial x} \qquad 4.11$$

The boundary conditions of this task during capacitor's discharging are as follows:

$$\left.\begin{aligned} J_{sp}(0,t) &= -\alpha_{sp} \frac{\partial \varphi_{ne}(x,t)}{\partial x}\Big|_{x=0} = J_0 \\ J_{sp}(w,t) &= \alpha_{sp} \frac{\partial \varphi_{ne}(x,t)}{\partial x}\Big|_{x=w_{sp}} = J_0 \end{aligned}\right\} \qquad 4.12$$

Equation 4.10 was solved analytically subject to boundary and initial condition equations 4.3, 4.4 and 4.5 respectively as presented in appendix B, to obtain a solution for the negative electrode without self-discharge as equation 4.13:

$$\varphi_{ne}(x,t)=\varphi_{ne}^{0^{\pm}}\pm\frac{J_0}{w_{ne}C_V}\left\{t+C_V\left[\frac{(\alpha_2+\alpha_1)}{2\alpha_1\alpha_2}x^2-\frac{w_{ne}x}{\alpha_1}+\frac{w_{ne}^2(2\alpha_2-\alpha_1)}{6\alpha_1\alpha_2}-\frac{2w_{ne}^2}{\pi^2}\right.\right.$$
$$\left.\left.\sum_{n=1}^{\infty}\left(\frac{1}{\alpha_1}+\frac{(-1)^n}{\alpha_2}\right)\frac{\exp\left(\frac{\beta^2n^2\pi^2t}{w_{ne}^2}\right)}{n^2}Cos\left(\frac{n\pi x}{w_{ne}}\right)\right]\right\} \quad 4.13$$

$$\varphi_{ne}(x,t)=\varphi_{ne}^{pause}\pm\frac{J_0}{w_{ne}C_V}\left\{t+C_V\left[\frac{(\alpha_2+\alpha_1)}{2\alpha_1\alpha_2}x^2-\frac{w_{ne}x}{\alpha_1}-\frac{2w_{ne}^2}{\pi^2}\right.\right.$$
$$\left.\left.\sum_{n=1}^{\infty}\left(\frac{1}{\alpha_1}+\frac{(-1)^n}{\alpha_2}\right)\frac{\exp\left(\frac{\beta^2n^2\pi^2t}{w_{ne}^2}\right)}{n^2}Cos\left(\frac{n\pi x}{w_{ne}}\right)\right]\right\} \quad 4.14$$

$$where\ \ \varphi_{ne}^{pause}=\varphi_{ne}^{0^{\pm}}\pm\frac{J_0w_{ne}(2\alpha_2-\alpha_1)}{6\alpha_1\alpha_2}$$

Similarly, the positive electrode without self-discharge is expressed as:

$$\varphi_{pe}(x,t)=\varphi_{pe}^{0^{\pm}}\pm\frac{J_0}{w_{pe}C_V}\left\{t+C_V\left[\frac{(\alpha_2+\alpha_1)}{2\alpha_1\alpha_2}x^2-\frac{w_{pe}x}{\alpha_1}+\frac{w_{pe}^2(2\alpha_2-\alpha_1)}{6\alpha_1\alpha_2}-\frac{2w_{pe}^2}{\pi^2}\right.\right.$$
$$\left.\left.\sum_{n=1}^{\infty}\left(\frac{1}{\alpha_1}+\frac{(-1)^n}{\alpha_2}\right)\frac{\exp\left(\frac{\beta^2n^2\pi^2t}{w_{ne}^2}\right)}{n^2}Cos\left(\frac{n\pi x}{w_{pe}}\right)\right]\right\} \quad 4.15$$

$$\varphi_{pe}(x,t)=\varphi_{pe}^{pause}\pm\frac{J_0}{w_{ne}C_V}\left\{t+C_V\left[\frac{(\alpha_2+\alpha_1)}{2\alpha_1\alpha_2}x^2-\frac{w_{ne}x}{\alpha_1}-\frac{2w_{ne}^2}{\pi^2}\right.\right.$$
$$\left.\left.\sum_{n=1}^{\infty}\left(\frac{1}{\alpha_1}+\frac{(-1)^n}{\alpha_2}\right)\frac{\exp\left(\frac{\beta^2n^2\pi^2t}{w_{ne}^2}\right)}{n^2}Cos\left(\frac{n\pi x}{w_{ne}}\right)\right]\right\} \quad 4.16$$

Also, equation 4.11 was solved using the separation of variables subject to the boundary conditions equation 4.12 to obtain solution for potential in the separator as equation 4.17:

$$\frac{\partial \varphi_{sp}}{\partial x} = \frac{J_0}{\alpha_{sp}} \ , \Rightarrow \partial \varphi_{sp} = \int_0^l \frac{J_0}{\alpha_{sp}}\, dx$$

$$\varphi_{sp}\left(x,t\right) = \pm \frac{J_0}{\alpha_{sp}}\, x \qquad 4.17$$

The voltages $V\left(x,t\right)$ of the electrode without self-discharge as a function of its thickness and time of charging and discharging is given as [12]:

$$V\left(w_{ne},t\right) = -\ \frac{1}{2}\varphi_{ne}\left(w_{ne},t\right) - \ \frac{1}{2}\varphi_{ne}\left(0,t\right) \qquad 4.18$$

On substituting $x = w_{ne}$ *and* $x = 0$ into equation 4.13, equation 4.18 becomes:

$$V\left(w_{ne},t\right) = V_{0_{-}^{+}} \pm \frac{J_0}{w_{ne}C_V}\left\{t + \frac{C_V w_{ne}^2\left(\alpha_2+\alpha_1\right)}{2\,\alpha_2\alpha_1}\left[\frac{1}{6} - \frac{1}{\pi^2}\sum_{n=1}^{\infty}\frac{1}{n^2}\exp\left(\left(\frac{2n\pi}{w_{ne}}\right)^2\left(\frac{-\alpha_2\alpha_1 t}{C_V\left(\alpha_2+\alpha_1\right)}\right)\right)\right]\right\} \qquad 4.19$$

where $V_{0_{-}^{+}} = -\varphi_{ne}^{0_{-}^{+}}$ and the sign $\frac{J_0}{w_{ne}C_{ne}} < 0$ (“–“) represents the process of capacitors discharging and sign $\frac{J_0}{w_{ne}C_V} > 0$ (“+“) represents the process of the capacitors charging. When effective conductivities of both electrode and electrolyte are the same, that is $\alpha_1 = \alpha_2 = \alpha$, equation 4.19 is expressed as follows:

$$V\left(w_{ne},t\right) = V_{0_{-}^{+}} \pm \frac{J_0}{w_{ne}C_V}\left\{t + \frac{C_V w_{ne}^2}{\alpha}\left[\frac{1}{6} - \frac{1}{\pi^2}\sum_{n=1}^{\infty}\frac{1}{n^2}\exp\left(-\left(\frac{2\,n\,\pi}{w_{ne}}\right)^2\left[\frac{\alpha\, t}{2\,C_V}\right]\right)\right]\right\} \qquad 4.20$$

If we assume that during charging and discharging of the capacitor, the concentration of ions of electrolyte and the conductivity of electrodes change in a narrow range. The type of conductivity of the walls of the polarizable electrode pores does not change. The value of potential $\varphi\left(x,t\right)$ as a function of the capacitor’s position will be expressed as follows:

$$\varphi(x,t)=\varphi_{ne}^{0^+}\pm\frac{J_0}{w_{ne}C_V}\left\{t+C_V\left[\frac{(\alpha_2+\alpha_1)}{2\alpha_1\alpha_2}x^2-\frac{w_{ne}\,x}{\alpha_1}+\frac{w_{ne}^2(2\alpha_2-\alpha_1)}{6\alpha_1\alpha_2}-\frac{2\,w_{ne}^2}{\pi^2}\right.\right.$$

$$\left.\left.\left.\sum_{n=1}^{\infty}\left(\frac{1}{\alpha_1}+\frac{(-1)^n}{\alpha_2}\right)\frac{\exp\left(-\frac{\beta^2n^2\pi^2t}{w_{ne}^2}\right)}{n^2}Cos\left(\frac{n\pi x}{w_{ne}}\right)\right]\right\}\right\}\ at\ \ 0\ \le\ x\ \le\ w_{ne} \qquad 4.21a$$

$$\varphi(x,t)\ =\pm\frac{J_0}{\alpha_{sp}}x\Big\}\ at\ \ w_{ne}\le\ x\ \le\ w_{sp} \qquad 4.21b$$

$$\varphi(x,t)=\varphi_{pe}^{0^+}\pm\frac{J_0}{w_{pe}C_V}\left\{t+C_V\left[\frac{(\alpha_2+\alpha_1)}{2\alpha_1\alpha_2}x^2-\frac{w_{pe}\,x}{\alpha_1}+\frac{w_{pe}^2(2\alpha_2-\alpha_1)}{6\alpha_1\alpha_2}-\frac{2\,w_{pe}^2}{\pi^2}\right.\right.$$

$$\left.\left.\left.\sum_{n=1}^{\infty}\left(\frac{1}{\alpha_1}+\frac{(-1)^n}{\alpha_2}\right)\frac{\exp\left(-\frac{\beta^2n^2\pi^2t}{w_{ne}^2}\right)}{n^2}Cos\left(\frac{n\pi x}{w_{pe}}\right)\right]\right\}\right\}\ at\ \ w_{sp}\le\ x\ \le\ w_{pe} \qquad 4.21c$$

Electromotive force (voltage of device) of capacitors, U_S is determined as [89]:

$$U_S(w_{ne},w_{sp},w_{pe},\beta,C_V,t)=\varphi_{pe}(0,\ t)-\varphi_{ne}(0,\ t) \qquad 4.22$$

It should be noted that real-life positive electrodes in symmetric supercapacitors are polarized during their charge and discharge in a wide ranges of potentials [12,89,270]. As a result, we note that the potential of negative and positive electrodes changes during charging and discharging, but depends on the coordinates in the range of $w_{sp}\le x\le w_{pe}$. From Equations 4.19 we obtain the analytical expression for the voltage of the capacitor without self-discharge during charging and discharging by constant current as:

$$U_S(w_{ne},t)=U_{S0}\pm\frac{J_0}{C_Vw_{ne}}\left\{t+C_Vw_{ne}^2\left[\frac{2\alpha_2-\alpha_1}{6\alpha_1\alpha_2}-\frac{2}{\pi^2}\sum_{n=1}^{\infty}\left(\frac{1}{\alpha_1}+\frac{(-1)^n}{\alpha_2}\right)\frac{\exp\left(-\left(\frac{n\pi\beta}{w_{ne}}\right)^2t\right)}{n^2}\right]\right\} \qquad 4.23$$

where $U_{S0} = \varphi_{pe}^{0^+_-} - \varphi_{ne}^{0^+_-}$ is the capacitor voltage at t = 0; and the sign $\frac{J_0}{w_{ne}C_V} < 0$ (“–“) represents the process of the capacitor discharging and sign $\frac{J_0}{w_{ne}C_V} > 0$ (“+“) represents the process of the capacitor charging and $w_{ne} = w_{pe}$. The supercapacitor has specific internal resistance $\rho_{\text{int}}\left(\Omega\, cm^2\right)$, which is determined by the resistances of the current collector of electrodes and the separator (which was not taken into account during calculations), and of the electrodes. Specific internal resistance was not included in equations for electrodes potential and voltage, because it was considered during derivation of expression for electrodes potential voltage. It was only included in the equation for capacitor's voltage since the entire cell contains current collectors and separator. Therefore, supercapacitor voltage during charging and discharging is expressed as:

$$U_S\left(w_{ne},t\right) = U_{S0} \pm J_0\rho_{\text{int}}\frac{J_0}{C_V w_{ne}}\left\{t + C_V w_{ne}^2\frac{2\alpha_2 - \alpha_1}{6\alpha_1\alpha_2} - \right.$$

$$\left.\frac{2}{\pi^2}\left[\sum_{n=1}^{\infty}\left(\frac{1}{\alpha_1} + \frac{(-1)^n}{\alpha_2}\right)\frac{\exp\left(\frac{-n\pi\beta}{w_{ne}}\right)^2 t}{n^2}\right]\right\} \qquad 4.24$$

4.4 Homogeneous/Symmetric electrochemical capacitors with self-discharge.

For the negative electrode of supercapacitors with only an electric double layer electrode (EDLs) self-discharge

For the inhomogeneous equation $\frac{\partial \varphi_{ne}(x,t)}{\partial t} = \beta^2 \frac{\partial^2 \varphi_{ne}(x,t)}{\partial x^2} + \frac{J_{VR}(x,t)}{C_V}$ having self-discharge with inhomogeneous boundary conditions $\frac{\partial \varphi_{ne}}{\partial x}(0,t) = -\frac{J_0}{\alpha_1}, \frac{\partial \varphi_{ne}}{\partial x}(w_{ne},t) = \frac{J_0}{\alpha_2}$ and the inhomogeneous initial condition $\varphi_{ne}(t)\Big|_{t=0} = \varphi_{ne}^{0^+}$, the inhomogeneous equation becomes:

$$\frac{\partial \varphi_{ne}(x,t)}{\partial t} - \beta^2 \frac{\partial^2 \varphi_{ne}(x,t)}{\partial x^2} = \frac{J_{VR}(x,t)}{C_V} \tag{4.25}$$

Equation 4.25 was solved analytically using the boundary and initial condition equations 4.3, 4.4 and 4.5 respectively as shown in appendix C, to obtain the solution for the negative electrode with only the electric double layer (EDL) instability self-discharge as equation 4.26:

$$\varphi_{ne}(x,t) = \varphi_{ne}^{0^+} \pm \frac{J_0}{w_{ne} C_V} \left\{ t + C_V \left[\frac{(\alpha_2 + \alpha_1)}{2\alpha_1\alpha_2} x^2 - \frac{w_{ne}\, x}{\alpha_1} + \frac{w_{ne}^2 (2\alpha_2 - \alpha_1)}{6\alpha_1\alpha_2} - \frac{2\, w_{ne}^2}{\pi^2} \right.\right.$$
$$\left.\left. \sum_{n=1}^{\infty} \left(\frac{1}{\alpha_1} + \frac{(-1)^n}{\alpha_2} \right) \frac{\exp\left(-\frac{\beta^2 n^2 \pi^2 t}{w_{ne}^2} \right)}{n^2} Cos\left(\frac{n\pi x}{w_{ne}} \right) \right] \right\} - \frac{J_{VR}}{C_V} \left\{ t + \frac{2\, C_V w_{ne}^2}{\pi^3} \sum_{n=1}^{\infty} \frac{(-1)^n (\alpha_2 + \alpha_1)}{\alpha_1\alpha_2} \right.$$
$$\left. \left(\frac{1 - \exp\left(-\frac{\beta^2 n^2 \pi^2}{w_{ne}^2} (t - t_0) \right)}{n^3} \right) Cos\left(\frac{n\pi x}{w_{ne}} \right) \right\} \tag{4.26}$$

$$\varphi_{ne}(x,t) = \varphi_{ne}^{pause} \pm \frac{J_0}{w_{ne} C_V} \left\{ t + C_V \left[\frac{(\alpha_2 + \alpha_1)}{2\alpha_1\alpha_2} x^2 - \frac{w_{ne}\, x}{\alpha_1} - \frac{2\, w_{ne}^2}{\pi^2} \right.\right.$$
$$\left.\left. \sum_{n=1}^{\infty} \left(\frac{1}{\alpha_1} + \frac{(-1)^n}{\alpha_2} \right) \frac{\exp\left(-\frac{\beta^2 n^2 \pi^2 t}{w_{ne}^2} \right)}{n^2} Cos\left(\frac{n\pi x}{w_{ne}} \right) \right] \right\} - \frac{J_{VR}}{C_V} \left\{ t + \frac{2\, C_V w_{ne}^2}{\pi^3} \sum_{n=1}^{\infty} \frac{(-1)^n (\alpha_2 + \alpha_1)}{\alpha_1\alpha_2} \right.$$

$$\left.\left(\frac{1-\exp\left(-\frac{\beta^2 n^2\pi^2}{w_{ne}^2}\left(t-t_0\right)\right)}{n^3}\right)Cos\left(\frac{n\pi x}{w_{ne}}\right)\right\} \qquad 4.27$$

where $\varphi_{ne}^{pause}=\varphi_{ne}^{0^+_-}\pm\frac{J_0 w_{ne}\left(2\alpha_2-\alpha_1\right)}{6\alpha_1\alpha_2}$ and the sign $\frac{J_0}{w_{ne}C_V}<0$ ("–") represents the charging process of the capacitor and sign $\frac{J_0}{w_{ne}C_V}>0$ ("+") represents discharging process of the capacitor discharging. Similarly, the positive electrode with only the electric double layer (EDL) instability, self-discharge is given as:

$$\varphi_{pe}(x,t)=\varphi_{pe}^{0^+_-}\pm\frac{J_0}{w_{pe}C_V}\left\{t+C_V\left[\frac{\left(\alpha_2+\alpha_1\right)}{2\alpha_1\alpha_2}x^2-\frac{w_{pe}\,x}{\alpha_1}+\frac{w_{pe}^2\left(2\alpha_2-\alpha_1\right)}{6\alpha_1\alpha_2}-\frac{2\,w_{pe}^2}{\pi^2}\right.\right.$$

$$\left.\left.\sum_{n=1}^{\infty}\left(\frac{1}{\alpha_1}+\frac{(-1)^n}{\alpha_2}\right)\frac{\exp\left(-\frac{\beta^2 n^2\pi^2 t}{w_{pe}^2}\right)}{n^2}Cos\left(\frac{n\pi x}{w_{pe}}\right)\right]\right\}-\frac{J_{VR}}{C_V}\left\{t+\frac{2\,C_V w_{pe}^2}{\pi^3}\sum_{n=1}^{\infty}\frac{(-1)^n\left(\alpha_2+\alpha_1\right)}{\alpha_1\alpha_2}\right.$$

$$\left.\left(\frac{1-\exp\left(-\frac{\beta^2 n^2\pi^2}{w_{pe}^2}\left(t-t_0\right)\right)}{n^3}\right)Cos\left(\frac{n\pi x}{w_{pe}}\right)\right\} \qquad 4.28$$

$$\varphi_{pe}(x,t)=\varphi_{pe}^{pause}\pm\frac{J_0}{w_{pe}C_V}\left\{t+C_V\left[\frac{\left(\alpha_2+\alpha_1\right)}{2\alpha_1\alpha_2}x^2-\frac{w_{pe}\,x}{\alpha_1}-\frac{2\,w_{pe}^2}{\pi^2}\right.\right.$$

$$\left.\left.\sum_{n=1}^{\infty}\left(\frac{1}{\alpha_1}+\frac{(-1)^n}{\alpha_2}\right)\frac{\exp\left(-\frac{\beta^2 n^2\pi^2 t}{w_{pe}^2}\right)}{n^2}Cos\left(\frac{n\pi x}{w_{pe}}\right)\right]\right\}-\frac{J_{VR}}{C_V}\left\{t+\frac{2\,C_V w_{pe}^2}{\pi^3}\sum_{n=1}^{\infty}\frac{(-1)^n\left(\alpha_2+\alpha_1\right)}{\alpha_1\alpha_2}\right.$$

$$\left.\left(\frac{1-\exp\left(-\frac{\beta^2 n^2\pi^2}{w_{pe}^2}\left(t-t_0\right)\right)}{n^3}\right)Cos\left(\frac{n\pi x}{w_{pe}}\right)\right\} \qquad 4.29$$

where the sign $\frac{J_0}{w_{pe}C_V} < 0$ ("–") represents the charging process of the capacitor and sign $\frac{J_0}{w_{pe}C_V} > 0$ ("+") represents the discharging process of the capacitor. On substituting $x = w_{ne}$ and $x = 0$ into equation 4.26, equation 4.18, the voltage $V(x,t)$ of the electrode with only the electric double layer (EDL) instability self-discharge as a function of its thickness and time of charging and discharging is given as:

$$V(w_{ne},t) = V_{0_-^+} \pm \frac{J_0}{w_{ne}C_V}\left\{t + \frac{C_V w_{ne}^2(\alpha_2+\alpha_1)}{2\,\alpha_2\alpha_1}\left[\frac{1}{6} - \frac{1}{\pi^2}\sum_{n=1}^{\infty}\frac{1}{n^2}\exp\left(\left(\frac{-2\,n\,\pi}{w_{ne}}\right)^2\left(\frac{\alpha_2\alpha_1 t}{C_V(\alpha_2+\alpha_1)}\right)t\right)\right]\right\}$$

$$-\frac{J_{VR}}{C_V}\left\{t + \frac{1}{\pi^3}\sum_{n=1}^{\infty}\frac{C_V w_{ne}^2}{n^3}\left[\frac{(\alpha_2+\alpha_1)}{\alpha_1\alpha_2}\left(1-\exp\left(-\frac{2\,n\,\pi\,\beta}{w_{ne}}\right)^2 t\right)\right]\right\} \qquad 4.30$$

where $V_{0_-^+} = -\varphi_{ne}^{0_-^+}$, the sign $\frac{J_0}{w_{ne}C_V} < 0$ ("–") represents the discharging process of the capacitor and sign $\frac{J_0}{w_{ne}C_V} > 0$ ("+") represents the charging process of capacitor. When effective conductivities of the electrode and electrolyte are the same, that is, $\alpha_1 = \alpha_2 = \alpha$, equation 4.30 becomes:

$$V(w_{ne},t) = V_{0_-^+} \pm \frac{J_0}{w_{ne}C_V}\left\{t + \frac{C_V w_{ne}^2}{\alpha}\left[\frac{1}{6} - \frac{1}{\pi^2}\sum_{n=1}^{\infty}\frac{1}{n^2}\,\ell^{-\left(\frac{2\,n\,\pi}{w_{ne}}\right)^2\left[\frac{\alpha\,t}{2\,C_V}\right]}\right]\right\}$$

$$-\frac{J_{VR}}{C_V}\left\{t + \frac{1}{\pi^3}\sum_{n=1}^{\infty}\frac{C_V w_{ne}^2}{n^3}\left[\frac{2}{\alpha}\left(1-\ell^{-\left(\frac{2\,n\,\pi}{w_{ne}}\right)^2\left[\frac{\alpha\,t}{2\,C_V}\right]}\right)\right]\right\} \qquad 4.31$$

If we assume that during charging and discharging of the capacitor, the concentration of ions of electrolyte and conductivity of the positive and negative electrodes change in a narrow range, and the type of conductivity of the walls of the polarizable electrode pores does not

change, the value of potential $\varphi(x,t)$ as a function of the capacitor's position is expressed as follows:

$$\varphi(x,t)=\varphi_{ne}^{0^+}\pm\frac{J_0}{w_{ne}C_V}\left\{t+C_V\left[\frac{(\alpha_2+\alpha_1)}{2\alpha_1\alpha_2}x^2-\frac{w_{ne}\,x}{\alpha_1}+\frac{w_{ne}^2(2\alpha_2-\alpha_1)}{6\alpha_1\alpha_2}-\frac{2\,w_{ne}^2}{\pi^2}\right.\right.$$

$$\left.\left.\sum_{n=1}^{\infty}\left(\frac{1}{\alpha_1}+\frac{(-1)^n}{\alpha_2}\right)\frac{\exp\left(-\frac{\beta^2n^2\pi^2t}{w_{ne}^2}\right)}{n^2}Cos\left(\frac{n\pi x}{w_{ne}}\right)\right]\right\}-\frac{J_{VR}}{C_V}\left\{t+\frac{2\,C_Vw_{ne}^2}{\pi^3}\right.$$

$$\left.\left.\sum_{n=1}^{\infty}\frac{(-1)^n(\alpha_2+\alpha_1)}{\alpha_1\alpha_2}\left(\frac{1-\exp\left(-\frac{\beta^2n^2\pi^2}{w_{ne}^2}(t-t_0)\right)}{n^3}\right)Cos\left(\frac{n\pi x}{w_{ne}}\right)\right\}\right\}\ at\ \ 0\ \le\ x\ \le\ w_{ne} \qquad 4.32a$$

$$\varphi(x,t)=\ \pm\frac{J_0}{\alpha_{sp}}x\Big\}\ at\ \ w_{ne}\le\ x\ \le w_{sp} \qquad 4.32b$$

$$\varphi(x,t)=\varphi_{pe}^{0^+}\pm\frac{J_0}{w_{pe}C_V}\left\{t+C_V\left[\frac{(\alpha_2+\alpha_1)}{2\alpha_1\alpha_2}x^2-\frac{w_{pe}\,x}{\alpha_1}+\frac{w_{pe}^2(2\alpha_2-\alpha_1)}{6\alpha_1\alpha_2}-\frac{2\,w_{pe}^2}{\pi^2}\right.\right.$$

$$\left.\left.\sum_{n=1}^{\infty}\left(\frac{1}{\alpha_1}+\frac{(-1)^n}{\alpha_2}\right)\frac{\exp\left(-\frac{\beta^2n^2\pi^2t}{w_{pe}^2}\right)}{n^2}Cos\left(\frac{n\pi x}{w_{pe}}\right)\right]\right\}-\frac{J_{VR}}{C_V}\left\{t+\frac{2\,C_Vw_{pe}^2}{\pi^3}\right.$$

$$\left.\left.\sum_{n=1}^{\infty}\frac{(-1)^n(\alpha_2+\alpha_1)}{\alpha_1\alpha_2}\left(\frac{1-\exp\left(-\frac{\beta^2n^2\pi^2}{w_{pe}^2}(t-t_0)\right)}{n^3}\right)Cos\left(\frac{n\pi x}{w_{pe}}\right)\right\}\right\}at\ w_{sp}\le x\le w_{pe} \qquad 4.32c$$

where $\varphi_{ne}^{0^+}$ and $\varphi_{ne}^{0^-}$ are the potentials of the negative electrode of the supercapacitor before charging and discharging; $\varphi_{pe}^{0^+}$ and $\varphi_{pe}^{0^-}$ are the potentials of the negative electrode of the supercapacitor before charging and discharging; ρ_{sp} and α_{sp} are the specific electric resistance and effective conductivity of the separator and w_{ne}, w_{sp} and w_{pe} are the thickness of the

negative electrode, separator and positive electrode, respectively. The sign $\frac{J_0}{w_{pe}C_V} < 0$ and $\frac{J_0}{w_{ne}C_V} < 0$ ("–") represents charging process of the capacitor and sign $\frac{J_0}{w_{pe}C_V} > 0$ and $\frac{J_0}{w_{ne}C_V} > 0$ ("+") represents discharging process of the capacitor. It should be noted that real-life positive electrodes in symmetric capacitors, during their charge and discharge, are polarized in a wide range of potentials [12,89,270]. Therefore, the potential of both the negative and positive electrodes change during charging and discharging, but this depends on the coordinates in the range of $w_{sp} \le x \le w_{pe}$.

The electromotive force (voltage of device) of supercapacitors is determined as [89]:

$$U_S\left(w_{ne}, w_{sp}, \beta, C_V, t\right) = \varphi_{pe}\left(w_{pe},\ t\right) - \varphi_{ne}\left(0,\ t\right) \tag{4.33}$$

From Equations 4.32 we obtain an analytical expression for the emf of supercapacitors with self-discharges during charging and discharging by constant current. This is given as:

$$U_S\left(w_{ne},t\right) = U_{S0} \pm \frac{J_0}{C_V w_{ne}} \left\{ t + C_V w_{ne}^2 \left[\frac{2\alpha_2 - \alpha_1}{6\alpha_1\alpha_2} - \frac{2}{\pi^2} \sum_{n=1}^{\infty} \left(\frac{1}{\alpha_1} + \frac{(-1)^n}{\alpha_2} \right) \frac{\exp\left(-\left(\frac{\beta n \pi}{w_{ne}} \right)^2 t \right)}{n^2} \right] \right\}$$

$$- \frac{J_{VR}}{C_V} \left\{ t + \frac{2C_V w_{ne}^2}{\pi^3} \sum_{n=1}^{\infty} \frac{(-1)^n (\alpha_2 + \alpha_1)}{\alpha_1\alpha_2} \left(\frac{1 - \exp\left(-\left(\frac{\beta n \pi}{w_{ne}} \right)^2 t \right)}{n^3} \right) \right\} \tag{4.34}$$

where $U_{S0} = \varphi_{pe}^{0_-^+} - \varphi_{ne}^{0_-^+}$ is the capacitor's voltage at t = 0; and the sign $\frac{J_0}{w_{ne}C_V} < 0$ ("–") represents the discharging of the capacitor and sign $\frac{J_0}{w_{ne}C_V} > 0$ ("+") represents the charging

of the supercapacitor and $w_{ne} = w_{pe}$. Because the supercapacitor has specific internal resistance $\rho_{\text{int}}\ \left(\Omega\, cm^2\right)$, which is determined by the resistances of the current collectors of the negative and positive electrodes and resistance of the separator (which was not taken into account during calculations), the supercapacitor voltage during charging and discharging is expressed as:

$$U_S\left(w_{ne},t\right) = U_{S0} \pm J_0\rho_{\text{int}} \pm \frac{J_0}{C_V w_{ne}}\left\{t + C_V w_{ne}^2\left[\frac{2\alpha_2-\alpha_1}{6\alpha_1\alpha_2} - \frac{2}{\pi^2}\sum_{n=1}^{\infty}\left(\frac{1}{\alpha_1}+\frac{(-1)^n}{\alpha_2}\right)\frac{\exp\left(\frac{-\beta n\pi}{w_{ne}}\right)^2 t}{n^2}\right]\right\}$$

$$-\frac{J_{VR}}{C_V}\left\{t + \frac{2C_V w_{ne}^2}{\pi^3}\sum_{n=1}^{\infty}\frac{(-1)^n(\alpha_2+\alpha_1)}{\alpha_1\alpha_2}\left(\frac{1-\exp\left(-\left(\frac{\beta n\pi}{w_{ne}}\right)^2 t\right)}{n^3}\right)\right\} \qquad 4.35$$

For electrochemical capacitors with both reversible redox reactions of redox species and electric double layer (EDLs) instability self-discharges

Recall that self-discharge potential decay is $\varphi_D(t) = \frac{nFVC_{Ox}}{C}\left\{1 - \frac{8}{\pi^2}\exp\left(\frac{-\pi^2 D_{Ox} t}{l^2}\right)\right\}$ 3.68

If both the reversible redox reactions and the electric double layer (EDLs) instability self-discharge are present, equation 3.68 in chapter three was subtracted from equation 4.27 to obtain the expression for negative electrode as:

$$\varphi_{ne}\left(x,t\right) = \varphi_{ne}^{pause} \pm \frac{J_0}{w_{ne}C_V}\left\{t + C_V\left[\frac{(\alpha_2+\alpha_1)}{2\alpha_1\alpha_2}x^2 - \frac{w_{ne}\,x}{\alpha_1} - \frac{2\,w_{ne}^2}{\pi^2}\right.\right.$$

$$\sum_{n=1}^{\infty}\left(\frac{1}{\alpha_1}+\frac{(-1)^n}{\alpha_2}\right)\frac{\exp\left(-\frac{\beta^2 n^2\pi^2 t}{w_{ne}^2}\right)}{n^2}Cos\left(\frac{n\pi x}{w_{ne}}\right)\Bigg]\Bigg\}-\frac{J_{VR}}{C_V}\Bigg\{t+\frac{2w_{ne}^2}{\pi^3}\sum_{n=1}^{\infty}\frac{(-1)^n(\alpha_2+\alpha_1)}{\alpha_1\alpha_2}$$

$$\left(\frac{1-\exp\left(-\frac{\beta^2 n^2\pi^2}{w_{ne}^2}(t-t_0)\right)}{n^3}\right)Cos\left(\frac{n\pi x}{w_{ne}}\right)-\frac{nFVC_{Ox}}{C}\left\{1-\frac{8}{\pi^2}\exp\left(\frac{-\pi^2 D_{Ox}t}{l^2}\right)\right\} \quad 4.36$$

where $\frac{nFVC_{Ox}}{C}\left\{1-\frac{8}{\pi^2}\exp\left(\frac{-\pi^2 D_{Ox}t}{l^2}\right)\right\}$ is potential decay $\varphi_D(t)$ due to reversible redox reactions self-discharge. Similarly, voltage $V(x,t)$ of the electrode with both the reversible redox reactions and the electric double layer (EDL) instability self-discharges as a function of its thickness and time of charging and discharging is given as:

$$V(w_{ne},t)=V_{0_-^+}\pm\frac{J_0}{w_{ne}C_V}\left\{t+\frac{C_V w_{ne}^2(\alpha_2+\alpha_1)}{2\,\alpha_2\alpha_1}\left[\frac{1}{6}-\frac{1}{\pi^2}\sum_{n=1}^{\infty}\frac{1}{n^2}\exp\left(\left(\frac{-2n\pi}{w_{ne}}\right)^2\left(\frac{\alpha_2\alpha_1 t}{C_V(\alpha_2+\alpha_1)}\right)t\right)\right]\right\}$$

$$-\frac{J_{VR}}{C_V}\left\{t+\frac{2C_V w_{ne}^2}{\pi^3}\sum_{n=1}^{\infty}\frac{(-1)^n(\alpha_2+\alpha_1)}{\alpha_1\alpha_2}\left(\frac{1-\exp\left(\frac{-\beta n\pi}{w_{ne}}\right)^2 t}{n^3}\right)\right\}-\frac{nFVC_{Ox}}{C}$$

$$\left\{1-\frac{8}{\pi^2}\exp\left(\frac{-\pi^2 D_{Ox}t}{l^2}\right)\right\} \quad 4.37$$

where $V_{0_-^+}=-\varphi_{ne}^{0_-^+}$, the sign $\frac{J_0}{w_{ne}C_V}<0$ (sign "–") represents the discharging of the capacitor and sign $\frac{J_0}{w_{ne}C_V}>0$ (sign "+") represents charging of the capacitor. Also, when effective conductivities of electrodes and electrolyte are the same, that is $\alpha_1=\alpha_2=\alpha$, equation 4.37 becomes:

$$V\left(w_{ne},t\right)=V_{0^{+}_{-}}\pm\frac{J_0}{w_{ne}C_V}\left\{t+\frac{C_V w_{ne}^2}{\alpha}\left[\frac{1}{6}-\frac{1}{\pi^2}\sum_{n=1}^{\infty}\frac{1}{n^2}\exp\left(-\left(\frac{2\,n\,\pi}{w_{ne}}\right)^2\left[\frac{\alpha\,t}{2\,C_V}\right]\right)\right]\right\}-\frac{J_{VR}}{C_V}$$

$$\left\{t+\frac{1}{\pi^3}\sum_{n=1}^{\infty}\frac{C_V w_{ne}^2}{n^3}\left[\frac{2}{\alpha}\left(1-\exp\left(\left(\frac{-2\,n\,\pi}{w_{ne}}\right)^2\frac{\alpha\,t}{2\,C_V}\right)\right)\right]\right\}-\frac{nFVC_{Ox}}{C}\left\{1-\frac{8}{\pi^2}\exp\left(\frac{-\pi^2 D_{Ox}t}{l^2}\right)\right\} \quad 4.38$$

From Equations 4.35 we obtain an analytical expression for the voltage of the supercapacitor with both the reversible redox reactions and the electric double layer (EDL) instability self-discharge during constant current charging and discharging. This is given as:

$$U_S\left(w_{ne},t\right)=U_{S0}\pm\frac{J_0}{C_V w_{ne}}\left\{t+C_V w_{ne}^2\left[\frac{2\alpha_2-\alpha_1}{6\alpha_1\alpha_2}-\frac{2}{\pi^2}\sum_{n=1}^{\infty}\left(\frac{1}{\alpha_1}+\frac{(-1)^n}{\alpha_2}\right)\frac{\exp\left(-\left(\frac{\beta n\pi}{w_{ne}}\right)^2 t\right)}{n^2}\right]\right\}$$

$$-\frac{J_{VR}}{C_V}\left\{t+\frac{2C_V w_{ne}^2}{\pi^3}\sum_{n=1}^{\infty}\frac{(-1)^n(\alpha_2+\alpha_1)}{\alpha_1\alpha_2}\left(\frac{1-\exp\left(\frac{-\beta n\pi}{w_{ne}}\right)^2 t}{n^3}\right)\right\}-\frac{nFVC_{Ox}}{C}$$

$$\left\{1-\frac{8}{\pi^2}\exp\left(\frac{-\pi^2 D_{Ox}t}{l^2}\right)\right\} \quad 4.39$$

where $U_{S0}=\varphi_{pe}^{0^{+}_{-}}-\varphi_{ne}^{0^{+}_{-}}$ is the voltage of the capacitors at t = 0; and sign $\frac{J_0}{w_{ne}C_V}<0$ (sign "–") represents discharging of the capacitor and sign $\frac{J_0}{w_{ne}C_V}>0$ (sign "+") represents charging of the capacitor charging and $w_{ne}=w_{pe}$.

Specific internal resistance was not included in equations for the electrodes potential and voltage, because it was considered during derivation of the expression for electrodes potential voltage. The voltage of capacitors with both reversible redox reactions and electric double layer (EDL) instability self-discharge, while considering specific internal resistance

$\rho_{\text{int}}\left(\Omega\, cm^2\right)$ of electrodes current collectors and resistance of separator during charging and discharging is expressed as:

$$U_S(w_{ne},t)=U_{S0}\pm J_0\rho_{\text{int}}\pm\frac{J_0}{C_V w_{ne}}\left\{t+C_V w_{ne}^2\left[\frac{2\alpha_2-\alpha_1}{6\alpha_1\alpha_2}-\frac{2}{\pi^2}\sum_{n=1}^{\infty}\left(\frac{1}{\alpha_1}+\frac{(-1)^n}{\alpha_2}\right)\frac{\exp\left(\frac{-\beta n\pi}{w_{ne}}\right)^2 t}{n^2}\right]\right.$$

$$\left.-\frac{J_{VR}}{C_V}\left\{t+\frac{2C_V w_{ne}^2}{\pi^3}\sum_{n=1}^{\infty}\frac{(-1)^n(\alpha_2+\alpha_1)}{\alpha_1\alpha_2}\left(\frac{1-\exp\left(\left(\frac{-\beta n\pi}{w_{ne}}\right)^2 t\right)}{n^3}\right)\right\}\right.$$

$$-\frac{nFVC_{Ox}}{C}\left\{1-\frac{8}{\pi^2}\exp\left(\frac{-\pi^2 D_{Ox}t}{l^2}\right)\right\} \qquad 4.40$$

4.5 Heterogeneous/Asymmetric electrochemical capacitor with negative EDLC electrode, positive faraday electrode and without self-discharges.

The voltages $V(x,t)$ of the electrode without self-discharge as a function of its thickness and the time of charging and discharging is given as [3]:

$$V(w_{ne},t)=-\frac{1}{2}\varphi_{ne}(w_{ne},t)-\frac{1}{2}\varphi_{ne}(0,t) \qquad 4.18$$

On substituting $x=w_{ne}$ *and* $x=0$ into equation 4.13, equation 4.18 becomes:

$$V(w_{ne},t)=V_{0^+_-}\pm\frac{J_0}{w_{ne}C_V}\left\{t+\frac{C_V w_{ne}^2(\alpha_2+\alpha_1)}{2\,\alpha_2\alpha_1}\left[\frac{1}{6}-\frac{1}{\pi^2}\sum_{n=1}^{\infty}\frac{1}{n^2}\exp\left(\left(\frac{-2n\pi}{w_{ne}}\right)^2\frac{\alpha_2\alpha_1\, t}{C_V(\alpha_2+\alpha_1)}\right)\right]\right\} \qquad 4.41$$

where $V_{0^+_-} = -\varphi_{ne}^{0^+_-}$, the sign $\frac{J_0}{w_{ne}C_{ne}} < 0$ (sign "–") represents discharging of the capacitors and sign $\frac{J_0}{w_{ne}C_V} > 0$ (sign "+") represents charging of the capacitors charging. When the effective conductivities of the electrode and electrolyte are the same, that is, $\alpha_1 = \alpha_2 = \alpha$, equation 4.41 is expressed as follows:

$$V(w_{ne},t) = V_{0^+_-} \pm \frac{J_0}{w_{ne}C_V}\left\{t + \frac{C_V w_{ne}^2}{\alpha}\left[\frac{1}{6} - \frac{1}{\pi^2}\sum_{n=1}^{\infty}\frac{1}{n^2}\exp\left(\left(\frac{-2n\pi}{w_{ne}}\right)^2\frac{\alpha\, t}{2C_V}\right)\right]\right\} \quad 4.42$$

For the redox couple electrode in the asymmetric supercapacitor system, the potential remains constant during charging/discharging of the system due to redox reaction on the surface of the redox couple electrode following the Nernst equation [12,89,270]. Hence, we assume that the potential of the positive electrode does not change during charging and discharging, but depends on the coordinates in range of $w_{sp} \le x \le w_{pe}$.

The electromotive force (voltage of device) of supercapacitors, U_S is determined as [89]:

$$U_S(w_{ne}, w_{sp}, \beta, C_V, t) = \varphi_{pe}(w_{pe},\ t) - \varphi_{ne}(0,\ t) \quad 4.43$$

From Equations 4.21 we obtain an analytical expression for the voltage of the supercapacitor without self-discharge during constant current charging and discharging as:

$$U_S(w_{ne},t) = U_{S0} \pm \frac{J_0}{C_V w_{ne}}\left\{t + C_V w_{ne}^2\left[\frac{(2\alpha_2 - \alpha_1)}{6\alpha_1\alpha_2} - \frac{2}{\pi^2}\sum_{n=1}^{\infty}\left(\frac{1}{\alpha_1} + \frac{(-1)^n}{\alpha_2}\right)\frac{\exp\left(\frac{-n\pi\beta}{w_{ne}}\right)^2 t}{n^2}\right]\right\} \quad 4.44$$

where $U_{S0} = \varphi_{pe}^{0^+_-} - \varphi_{ne}^{0^+_-}$ is the voltage of the capacitor at *t = 0;* and the sign $\frac{J_0}{w_{ne}C_V} < 0$ ("–") represents discharging of the capacitor and sign $\frac{J_0}{w_{ne}C_V} > 0$ ("+") represents charging of the capacitor.

Specific internal resistance $\rho_{\text{int}}\left(\Omega\, cm^2\right)$ was not included in the equations for the potential and voltage of the electrodes, because this was considered during derivation of expression for the electrode's potential voltage. Since the entire supercapacitor contains current collectors and the separator whose internal resistances were not considered in the model's derivation, the cell's voltage during charging and discharging is expressed as:

$$U_S\left(w_{ne},t\right)=U_{S0}\pm J_0\rho_{\text{int}}\pm\frac{J_0}{C_V w_{ne}}\left\{t+C_V w_{ne}^2\left[\frac{\left(2\alpha_2-\alpha_1\right)}{6\alpha_1\alpha_2}-\frac{2}{\pi^2}\sum_{n=1}^{\infty}\left(\frac{1}{\alpha_1}+\frac{\left(-1\right)^n}{\alpha_2}\right)\right.\right.$$

$$\left.\left.\frac{\exp\left(\frac{-n\pi\beta}{w_{ne}}\right)^2 t}{n^2}\right]\right\} \qquad 4.45$$

4.6 Heterogeneous/Asymmetric electrochemical capacitor with negative EDLC electrode, positive faraday electrode and with self-discharges

The voltages $V\left(x,t\right)$ of the electrode with only an electric double layer (EDL) instability self-discharge as a function of its thickness and time of charging and discharging is given as [12]:

$$V\left(w_{ne},t\right)=-\frac{1}{2}\varphi_{ne}\left(w_{ne},t\right)-\frac{1}{2}\varphi_{ne}\left(0,t\right) \qquad 4.18$$

On substituting $x=w_{ne}\ and\ x=0$ into equation 4.21, equation 4.73 becomes:

$$V\left(w_{ne},t\right)=V_{0_-^+}\pm\frac{J_0}{w_{ne}C_V}\left\{t+\frac{C_V w_{ne}^2\left(\alpha_2+\alpha_1\right)}{2\,\alpha_2\alpha_1}\left[\frac{1}{6}-\frac{1}{\pi^2}\sum_{n=1}^{\infty}\frac{1}{n^2}\exp\left(\left(\frac{-2n\pi}{w_{ne}}\right)^2\frac{\alpha_2\alpha_1\, t}{C_V\left(\alpha_2+\alpha_1\right)}\right)\right]\right\}$$

$$-\frac{J_{VR}}{C_V}\left\{t+\frac{1}{\pi^3}\sum_{n=1}^{\infty}\frac{C_V w_{ne}^2}{n^3}\left[\frac{\left(\alpha_2+\alpha_1\right)}{\alpha_1\alpha_2}\left(1-\exp\left(\frac{-2n\pi\beta}{w_{ne}}\right)^2 t\right)\right]\right\} \qquad 4.46$$

where $V_{0_-^+} = -\varphi_{ne}^{0_-^+}$, the sign $\frac{J_0}{w_{ne}C_{ne}} < 0$ ("–") represents the discharging process of the capacitor and sign $\frac{J_0}{w_{ne}C_V} > 0$ ("+") represents the charging process of the capacitor. When the effective conductivities of the electrodes and electrolyte are the same, that is, $\alpha_1 = \alpha_2 = \alpha$, equation 4.46 becomes:

$$V\left(w_{ne},t\right) = V_{0_-^+} \pm \frac{J_0}{w_{ne}C_V}\left\{t + \frac{C_V w_{ne}^2}{\alpha}\left[\frac{1}{6} - \frac{1}{\pi^2}\sum_{n=1}^{\infty}\frac{1}{n^2}\exp\left(\left(\frac{-2\,n\,\pi}{w_{ne}}\right)^2\left[\frac{\alpha\,t}{2\,C_V}\right]\right)\right]\right\}$$
$$-\frac{J_{VR}}{C_V}\left\{t + \frac{1}{\pi^3}\sum_{n=1}^{\infty}\frac{C_V w_{ne}^2}{n^3}\left[\frac{2}{\alpha}\left(1 - \exp\left(\left(\frac{-2\,n\,\pi}{w_{ne}}\right)^2\left[\frac{\alpha\,t}{2\,C_V}\right]\right)\right)\right]\right\} \quad 4.47$$

For the redox couple electrode in an asymmetric supercapacitor system, the potential remains constant during charging/discharging of the system due to redox reaction on the surface of the redox couple electrode following the Nernst equation [12,89,270]. It is therefore assume that the potential of the positive electrode does not change during charging and discharging and does not depend on coordinates in the range of $w_{sp} \le x \le w_{pe}$.

The electromotive force (voltage of device) of the supercapacitor, U_S is determined as [89]:

$$U_S\left(w_{ne}, w_{sp}, w_{pe}, \beta, C_V, t\right) = \varphi_{pe}\left(w_{pe},\ t\right) - \varphi_{ne}\left(0,\ t\right) \quad 4.48$$

From Equation 4.32 we obtain the analytical expression for the voltage of the supercapacitor with only an electric double layer (EDL) instability self-discharge during constant current charging and discharging. This is given as:

$$U_S\left(w_{ne},t\right) = U_{S0} \pm \frac{J_0}{w_{ne}C_V}\left\{t + C_V w_{ne}^2\left[\frac{\left(2\alpha_2 - \alpha_1\right)}{6\alpha_1\alpha_2} - \frac{2}{\pi^2}\sum_{n=1}^{\infty}\left(\frac{1}{\alpha_1} + \frac{\left(-1\right)^n}{\alpha_2}\right)\frac{\exp\left(\left(\frac{-\beta n\pi}{w_{ne}}\right)^2 t\right)}{n^2}\right]\right\}$$

$$-\frac{J_{VR}}{C_V}\left\{t+\frac{2C_V w_{ne}^2}{\pi^3}\sum_{n=1}^{\infty}\left[\frac{(-1)^n(\alpha_2+\alpha_1)}{\alpha_1\alpha_2}\left(\frac{1-\exp\left(-\left(\frac{\beta n\pi}{w_{ne}}\right)^2 t\right)}{n^3}\right)\right]\right\} \qquad 4.49$$

where $U_{S0}=\varphi_{pe}^{0^+}-\varphi_{ne}^{0^+}$ is the voltage of the capacitor at *t = 0;* and the sign $\frac{J_0}{w_{ne}C_V}<0$ ("–") represents discharging process of capacitor and sign $\frac{J_0}{w_{ne}C_V}>0$ ("+") represents the charging process of the capacitor.

Specific internal resistance $\rho_{\text{int}}\left(\Omega\, cm^2\right)$ was not included in the equations for the potential and voltage of electrodes, because this was considered during derivation of the expression for the electrode's potential voltage. Since the entire supercapacitor contains current collectors and a separator whose internal resistances were not considered in models derivation, the cell's voltage during charging and discharging is expressed as:

$$U_S(w_e,t)=U_{S0}\pm J_0\rho_{\text{int}}\pm\frac{J_0}{w_{ne}C_V}\left\{t+C_V w_{ne}^2\left[\frac{(2\alpha_2-\alpha_1)}{6\alpha_1\alpha_2}-\frac{2}{\pi^2}\sum_{n=1}^{\infty}\left(\frac{1}{\alpha_1}+\frac{(-1)^n}{\alpha_2}\right)\frac{\exp\left(\frac{-\beta n\pi}{w_{ne}}\right)^2 t}{n^2}\right]\right\}$$

$$-\frac{J_{VR}}{C_V}\left\{t+\frac{2C_V w_{ne}^2}{\pi^3}\sum_{n=1}^{\infty}\left[\frac{(-1)^n(\alpha_2+\alpha_1)}{\alpha_1\alpha_2}\left(\frac{1-\exp\left(\left(\frac{-\beta n\pi}{w_{ne}}\right)^2 t\right)}{n^3}\right)\right]\right\} \qquad 4.50$$

Similarly, 4.49 and 4.50 for capacitors with both reversible redox reactions and the electric double layer (EDL) instability is given as:

$$U_S(w_{ne},t)=U_{S0}\pm\frac{J_0}{C_V w_{ne}}\left\{t+C_V w_{ne}^2\left[\frac{2\alpha_2-\alpha_1}{6\alpha_1\alpha_2}-\frac{2}{\pi^2}\sum_{n=1}^{\infty}\left(\frac{1}{\alpha_1}+\frac{(-1)^n}{\alpha_2}\right)\frac{\exp\left(\left(\frac{-\beta n\pi}{w_{ne}}\right)^2 t\right)}{n^2}\right]\right\}-\frac{J_{VR}}{C_V}$$

$$\left\{t+\frac{2C_V w_{ne}^2}{\pi^3}\sum_{n=1}^{\infty}\frac{(-1)^n(\alpha_2+\alpha_1)}{\alpha_1\alpha_2}\left(\frac{1-\exp\left(\frac{-\beta n\pi}{w_{ne}}\right)^2 t}{n^3}\right)\right\}-\frac{nFVC_{Ox}}{C}\left\{1-\frac{8}{\pi^2}\exp\left(\frac{-\pi^2 D_{Ox}t}{l^2}\right)\right\} \quad 4.51$$

The expression to describe how the cell voltage decays with time by self-discharge processes during asymmetric charging of the capacitor is given as:

$$U_S(t)=U_S-\frac{J_{VR}}{C_V}\left\{t+\frac{2C_V w_{ne}^2}{\pi^3}\frac{(-1)(\alpha_2+\alpha_1)}{\alpha_1\alpha_2}\left(1-\exp\left(\left(\frac{-\beta\pi}{w_{ne}}\right)^2 t\right)\right)\right\}-$$

$$\frac{nFAVC_{Ox}}{C}\left\{1-\frac{8}{\pi^2}\exp\left(\frac{-\pi^2 D_{Ox}t}{l^2}\right)\right\} \quad 4.52$$

where U_S is the cell upper voltage for the fully charged state without self-discharge.

$$U_S(w_{ne},t)=U_{S0}\pm J_0\rho_{\text{int}}\pm\frac{J_0}{C_V w_{ne}}\left\{t+C_V w_{ne}^2\left[\frac{2\alpha_2-\alpha_1}{6\alpha_1\alpha_2}-\frac{2}{\pi^2}\sum_{n=1}^{\infty}\left(\frac{1}{\alpha_1}+\frac{(-1)^n}{\alpha_2}\right)\frac{\exp\left(\frac{-\beta n\pi}{w_{ne}}\right)^2 t}{n^2}\right]\right\}$$

$$-\frac{J_{VR}}{C_V}\left\{t+\frac{2C_V w_{ne}^2}{\pi^3}\sum_{n=1}^{\infty}\frac{(-1)^n(\alpha_2+\alpha_1)}{\alpha_1\alpha_2}\left(\frac{1-\exp\left(\frac{-\beta n\pi}{w_{ne}}\right)^2 t}{n^3}\right)\right\}$$

$$-\frac{nFVC_{Ox}}{tC_V}\left\{1-\frac{8}{\pi^2}\exp\left(\frac{-\pi^2 D_{Ox}t}{l^2}\right)\right\} \quad 4.53$$

4.7 Heterogeneous/Asymmetric electrochemical capacitor with positive EDLC electrode, negative faraday electrode and without self-discharge.

For a redox couple electrode in an asymmetric supercapacitor system, potential remains constant during charging/discharging of the system due to redox reaction on the surface of the redox couple electrode following the Nernst equation [12,89,270].

The electromotive force (voltage of device) of supercapacitors is determined as [89]:

$$U_S\left(w_{ne}, w_{sp}, w_{pe}, \beta, C_V, t\right) = \varphi_{pe}\left(w_{pe},\ t\right) - \varphi_{ne}\left(0,\ t\right) \tag{4.54}$$

From Equations 4.21 we obtain analytical expression for the the voltage of supercapacitor without self-discharge during constant current charging and discharging. This is given by:

$$U_S\left(w_{pe}, t\right) = U_{S0} \pm \frac{J_0}{C_V w_{Pe}}\left\{ t + C_V w_{Pe}^2 \left[\frac{\left(2\alpha_2 - \alpha_1\right)}{6\alpha_1\alpha_2} - \frac{2}{\pi^2}\sum_{n=1}^{\infty}\left(\frac{1}{\alpha_1} + \frac{(-1)^n}{\alpha_2} \right) \frac{\exp\left(\frac{-n\pi\beta}{w_{Pe}} \right)^2 t}{n^2} \right] \right\} \tag{4.55}$$

where $U_{S0} = \varphi_{pe}^{0^+_-} - \varphi_{ne}$ is the voltage of the capacitor at *t = 0;* and the sign $\frac{J_0}{w_{pe}C_V} < 0$ ("–") represents the process of capacitor discharging and sign $\frac{J_0}{w_{pe}C_V} > 0$ ("+") represents the process of the capacitor charging.

Because the supercapacitor has specific internal resistance $\rho_{\text{int}}\ \left(\Omega\, cm^2\right)$, which is determined by the resistances of the current collectors of negative and positive electrodes, and the resistance of the separator (which was not taken into account during calculations), the supercapacitor voltage during charging and discharging is expressed by:

$$U_S\left(w_{ne}, t\right) = U_{S0} \pm J_0\rho_{\text{int}} \pm \frac{J_0}{C_V w_{ne}}\left\{ t + C_V w_{ne}^2 \left[\frac{\left(2\alpha_2 - \alpha_1\right)}{6\alpha_1\alpha_2} - \frac{2}{\pi^2}\sum_{n=1}^{\infty}\left(\frac{1}{\alpha_1} + \frac{(-1)^n}{\alpha_2} \right) \frac{\exp\left(\frac{-n\pi\beta}{w_{ne}} \right)^2 t}{n^2} \right] \right\} \tag{4.56}$$

4.8 Heterogeneous/Asymmetric electrochemical capacitor with positive EDLC electrode, negative faraday electrode and with self-discharge effects.

For the redox couple electrode in an asymmetric supercapacitor system, potential remains constant during charging/discharging of the system due to the redox reaction on the surface of the redox couple electrode following the Nernst equation [12,89,270].

The electromotive force (voltage of device) of supercapacitors, U_S is determined as [89]:

$$U_S\left(w_{ne}, w_{sp}, w_{pe}, \beta, C_V, t\right) = \varphi_{pe}\left(0\,,\ t\right) - \varphi_{ne}\left(w_{ne}\,,\ t\right) \tag{4.54}$$

From Equations 4.54 we obtain the analytical expression for voltage of the supercapacitor with only the EDL's self-discharge during constant current charging and discharging given as:

$$U_S\left(w_{pe},t\right) = U_{S0} \pm \frac{J_0}{w_{pe}C_V}\left\{t + C_V w_{pe}^2\left[\frac{\left(2\alpha_2-\alpha_1\right)}{6\alpha_1\alpha_2} - \frac{2}{\pi^2}\sum_{n=1}^{\infty}\left(\frac{1}{\alpha_1}+\frac{\left(-1\right)^n}{\alpha_2}\right)\frac{\exp\left(\left(\frac{-\beta n\pi}{w_{pe}}\right)^2 t\right)}{n^2}\right]\right\}$$

$$-\frac{J_{VR}}{C_V}\left\{t + \frac{2C_V w_{pe}^2}{\pi^3}\sum_{n=1}^{\infty}\left[\frac{\left(-1\right)^n\left(\alpha_2+\alpha_1\right)}{\alpha_1\alpha_2}\left(\frac{1-\exp\left(\left(\frac{-\beta n\pi}{w_{pe}}\right)^2 t\right)}{n^3}\right)\right]\right\} \tag{4.57}$$

where $U_{S0} = \varphi_{pe}^{0^+_-} - \varphi_{ne}$ is the voltage of the capacitor at *t = 0;* and the sign $\frac{J_0}{w_{pe}C_V} < 0$ ("–") represents the process of the capacitor discharging and sign $\frac{J_0}{w_{pe}C_V} > 0$ ("+") represents the

process of the capacitor charging. Because the supercapacitor has specific internal resistance $\rho_{\text{int}}\left(\Omega\, cm^2\right)$, which is determined by the resistances of the current collectors of negative and positive electrodes, and the resistance of the separator (which was not taken into account during calculations), the supercapacitor voltage during charging and discharging is expressed by:

$$U_S\left(w_{pe},t\right)=U_{S0}\pm J_0\rho_{\text{int}}\pm\frac{J_0}{w_{pe}C_V}\left\{t+C_V w_{pe}^2\left[\frac{\left(2\alpha_2-\alpha_1\right)}{6\alpha_1\alpha_2}-\frac{2}{\pi^2}\sum_{n=1}^{\infty}\left(\frac{1}{\alpha_1}+\frac{\left(-1\right)^n}{\alpha_2}\right)\frac{\exp\left(\frac{-\beta n\pi}{w_{pe}}\right)^2 t}{n^2}\right]\right\}$$

$$-\frac{J_{VR}}{C_V}\left\{t+\frac{2C_V w_{pe}^2}{\pi^3}\sum_{n=1}^{\infty}\left[\frac{\left(-1\right)^n\left(\alpha_2+\alpha_1\right)}{\alpha_1\alpha_2}\left(\frac{1-\exp\left(\frac{-\beta n\pi}{w_{pe}}\right)^2 t}{n^3}\right)\right]\right\} \qquad 4.58$$

Similarly, 4.57 and 4.58 for capacitors with both reversible redox reactions and an electric double layer (EDL) instability self-discharge becomes:

$$U_S\left(w_{ne},t\right)=U_{S0}\pm\frac{J_0}{C_V w_{ne}}\left\{t+C_V w_{ne}^2\left[\frac{2\alpha_2-\alpha_1}{6\alpha_1\alpha_2}-\frac{2}{\pi^2}\sum_{n=1}^{\infty}\left(\frac{1}{\alpha_1}+\frac{\left(-1\right)^n}{\alpha_2}\right)\frac{\exp\left(-\frac{\beta n\pi}{w_{ne}}\right)^2 t}{n^2}\right]\right\}-\frac{J_{VR}}{C_V}$$

$$\left\{t+\frac{2C_V w_{ne}^2}{\pi^3}\sum_{n=1}^{\infty}\frac{\left(-1\right)^n\left(\alpha_2+\alpha_1\right)}{\alpha_1\alpha_2}\left(\frac{1-\exp\left(\frac{-\beta n\pi}{w_{ne}}\right)^2 t}{n^3}\right)\right\}-\frac{nFVC_{Ox}}{C}\left\{1-\frac{8}{\pi^2}\exp\left(\frac{-\pi^2 D_{Ox}t}{l^2}\right)\right\} \qquad 4.59$$

$$U_S(w_{ne},t)=U_{S0}\pm J_0\rho_{\text{int}}\pm\frac{J_0}{w_{ne}}\left\{C_V t+w_{ne}^2\left[\frac{2\alpha_2-\alpha_1}{6\alpha_1\alpha_2}-\frac{2}{\pi^2}\sum_{n=1}^{\infty}\left(\frac{1}{\alpha_1}+\frac{(-1)^n}{\alpha_2}\right)\frac{\exp\left(\frac{-\beta n\pi}{w_{ne}}\right)^2 t}{n^2}\right]\right\}-\frac{J_{VR}}{C_V}$$

$$\left\{t+\frac{2C_V w_{ne}^2}{\pi^3}\sum_{n=1}^{\infty}\frac{(-1)^n(\alpha_2+\alpha_1)}{\alpha_1\alpha_2}\left(\frac{1-\exp\left(\frac{-\beta n\pi}{w_{ne}}\right)^2 t}{n^3}\right)\right\}-\frac{nFVC_{Ox}}{C}\left\{1-\frac{8}{\pi^2}\exp\left(\frac{-\pi^2 D_{Ox}t}{l^2}\right)\right\} \quad 4.60$$

4.9 Homogeneous/Symmetric electrochemical capacitors with only faraday electrodes

For the negative electrode of supercapacitors with redox couple electrode

$$\frac{\partial C_s}{\partial t}=D_s\frac{\partial^2 C_s}{\partial x^2}+\frac{J_{Cell}}{D_s\left(1-\theta^0\right)} \quad 4.61$$

The boundary conditions of the negative electrode during capacitor charging are as follows:

$$x=0,\frac{\partial C_s}{\partial x}=0 \quad 4.62$$

$$x=w_{ne},\ \frac{\partial C_s}{\partial x}=\frac{J_{Cell}}{D_s\left(1-\theta^0\right)} \quad 4.63$$

and the initial condition is given as follows:

$$At\ t=0,\ C_{t=0}=C^0 \quad 4.64$$

The boundary conditions of the negative electrode during capacitor discharging are as follows:

$$x=0,\frac{\partial C_s}{\partial x}=0 \quad 4.65$$

$$x=w_{ne},\ \frac{\partial C_s}{\partial x}=-\frac{J_{Cell}}{D_s\left(1-\theta^0\right)} \quad 4.66$$

and the initial condition is given as:

$$At\ t=0,\ C_{t=0}=C^{0-} \tag{4.67}$$

Equation 4.61 was solved analytically, subject to boundary and initial condition equations 4.62, 4.63 and 4.64 respectively as presented in appendix D, to obtain the solution for the negative electrode without self-discharge as equation 4.68:

$$C_s(x,t)=C^0+\frac{J_{Cell}\ t}{D_s(1-\theta^0)}-\frac{J_{Cell}\ t}{D_s(1-\theta^0)w_{ne}}+$$

$$\sum_{n=1}^{\infty}\left(\left(\frac{2w_{ne}C^0(-1)^n}{\pi^2n^2}-\frac{2w_{ne}^3(-1)^nJ_{Cell}}{D_s(1-\theta^0)D_sn^4\pi^4}\right)\exp\left(-\frac{D_sn^2\pi^2}{w_{ne}^2}(t-t_0)\right)+\frac{2w_{ne}^3(-1)^nJ_{Cell}}{D_s(1-\theta^0)D_sn^4\pi^4}\right)Cos\left(\frac{n\pi x}{w_{ne}}\right)$$

$$C_s(x,t)=C^0+\frac{J_{Cell}}{D_s(1-\theta^0)}\left\{\left(1-\frac{1}{w_{ne}}\right)t+\frac{2w_{ne}^3}{\pi^2}\right.$$

$$\left.\sum_{n=1}^{\infty}\left(\left(\frac{D_s(1-\theta^0)}{J_{Cell}}\frac{C^0(-1)^n}{w_{ne}^2n^2}-\frac{(-1)^n}{D_sn^4\pi^2}\right)\exp\left(-\frac{D_sn^2\pi^2}{w_{ne}^2}(t-t_0)\right)+\frac{(-1)^n}{D_sn^4\pi^2}\right)Cos\left(\frac{n\pi x}{w_{ne}}\right)\right\} \tag{4.68}$$

The time needed for the electrochemical capacitor to be fully charged or discharged t_{scale} is obtained by expressions previously derived by Samosundaram et al [93] as:

$$\left[t_{scale}\right]\approx\left.\begin{array}{ll}\dfrac{w_{ne,pe}C_V(U_{Sch}-U_{Sdis})}{J_0}\approx\dfrac{w_{ne,pe}A_dC_d}{z_+}\left(\dfrac{dq_+}{dq}\right)\dfrac{V_{cell}}{J_0}, & \lambda\le 1\\ \dfrac{\alpha_2C_V(U_{Sch}-U_{Sdis})^2}{2J_0^2}\approx\dfrac{\alpha_2A_dC_d}{2}\left(\dfrac{dq_+}{dq}\right)\dfrac{V_{cell}^2}{J_0^2}\quad , & \lambda>1\end{array}\right\} \tag{4.69}$$

$$\text{where } \lambda\equiv\frac{w_{ne,pe}}{\left[w_{ne,pe}\right]}=\frac{2J_0w_{ne,pe}}{\alpha_2(U_{Sch}-U_{Sdis})}=\frac{2J_0w_{ne,pe}}{\alpha_2V_{cell}} \tag{4.70}$$

Note that the potential drop in the solid and liquid-phase and in the separator, where the entire current is ionic and which is dominated by migration current is respectively given by:

$$-\alpha_1\frac{\Delta\varphi_1(x,t)}{w_e}-\alpha_2\frac{\Delta\varphi_2(x,t)}{w_e}\approx J_0 \tag{3.38}$$

$$\Delta\varphi_1(x,t) \approx \frac{J_0 w_e}{\alpha_1} \tag{3.39}$$

$$\Delta\varphi_2(x,t) \approx \frac{J_0 w_e}{\alpha_2} \tag{3.40}$$

$$\Delta\varphi_{2s}(x,t) \approx \frac{J_0 w_{sp}}{\alpha_2} \tag{3.41}$$

The potential drop in the solid phase is considerably smaller than the potential drop in the liquid phase and this potential drop in the liquid phase of each electrode during charging or discharging can at most equal to approximately half of the entire cell voltage. This is given as:

$$\Delta\varphi_2(x,t) \approx \frac{V_{cell}}{2} \tag{3.42}$$

The limit to the potential drop and the length of the electrode [w_e] over which the liquid potential drop occurs, are determined by the following expression:

$$[w_e] \approx \frac{\alpha_2 V_{cell}}{2J_0} = \frac{\alpha_2 V_{cell}}{2J_0} \tag{3.43}$$

The typical length scale [w_e] over which the liquid-phase potential drop happens on the electrodes can be defined as the minimum value of the electrode thickness w_e and the length of the electrode [w_e] over which the liquid potential drop occurs:

$$[w_e] \approx \min\left(\frac{\alpha_2 V_{cell}}{2J_0}, w_e\right) = \min\left(\frac{\alpha_2 V_{cell}}{2J_0}, w_e\right) \tag{3.44}$$

Electrodes utilization u in capacitor with electrolyte of specific effective conductivity α_2 and electrodes thickness w_e charged at a given current density J_0 is given as:

$$u = \frac{[w_e]}{w_e}.100\% = \frac{1}{\lambda}.100\% = \frac{\alpha_2 V_{cell}}{2J_0 w_e}.100\% \tag{3.46}$$

The ratio of electrodes thickness w_e to length scale [w_e] over which liquid phase potential drop occurs on electrodes, which is determining factor for estimating the length scale in electrodes for liquid phase potential drop is determined by:

$$\lambda \equiv \frac{w_e}{[w_e]} = \frac{2J_0 w_e}{\alpha_2 V_{cell}} \quad 4.70$$

The maximum stored energy ($E_{\max}$), the maximum electric charge stored in $Q_{\max}$ and the energy required for the symmetric electrochemical capacitor to be charged (without accounting for the ohmic internal resistance losses) to the voltage value of upper operating emf E_{Sch} in the emf operating range of U_{Sch} *and* U_{Sdis} are respectively given as follows:

$$E_{\max} = \frac{C\left(U_{Sch}^2 - U_{Sdis}^2\right)}{2} \quad 4.71$$

$$E_{Sch} = \frac{C\left(U_{Sch}^2 - U_{Sdis}^2\right)}{2} \quad 4.72$$

$$Q_{\max} = C\left(U_{Sch} - U_{Sdis}\right) \quad 4.73$$

where C is the capacitance of the electrochemical capacitor ,U_{Sch} is the cell voltage at the charged state and U_{Sdis} is the voltage at the discharged state. Because capacitors have internal ohmic resistance, a portion of the stored energy, known as the ohmic loss of energy, $\left(E_{ch}^R\right)$ is dissipated during capacitor charging.

The value of the ohmic loss of energy E_{ch}^R during constant current $\left(I_{ch}\right)$charging is calculated by the following formula:

$$\left(E_{ch}^R\right) = I_{ch}^2 \; R \; t_{ch} \quad 4.74$$

where *R* is the internal ohmic resistance.

A portion of energy E_{Sch} called effective energy $\left(E_{Sch}^{eff}\right)$ was stored in the capacitor, while another portion, known as the loss of energy in polarization resistance (E_{ch}^{Rpol}), was dissipated

at the polarization resistance of the capacitor. The value of energy dissipated at the polarization resistance of capacitor E_{ch}^{Rpol} is determined by the expression:

$$E_{ch}^{Rpol} = E_{Sch} - E_{Sch}^{eff} \tag{4.75}$$

Some of the stored energy, known as depolarization loss of energy $\left(E_{ch}^{dpol}\right)$, changes into heat during the depolarization of charged capacitors, and the capacitor's energy after depolarization is $\left(E_{Sch}^{ap}\right)$. The value of the energy loss due to depolarization is determined by the following expression:

$$E_{ch}^{dpol} = E_{Sch}^{eff} - E_{Sch}^{ap} \tag{4.76}$$

The value of aggregate energy $\left(E_{ch}\right)$ during symmetric capacitor charging is therefore given by the following expression:

$$E_{ch} = E_{Sch} + E_{ch}^{R} = E_{ch}^{Rpol} + E_{ch}^{dpol} + E_{Sch}^{ap} + E_{ch}^{R} \tag{4.77}$$

For symmetric discharging of ECs, the calculation of delivered energy $\left(E_{Sdic}\right)$ during the discharging of capacitors, (without accounting for ohmic internal resistance losses), is obtained from the following expression:

$$E_{Sdis} = \frac{C\left(U_{Sbdis}^{2} - U_{Sedis}^{2}\right)}{2} \tag{4.78}$$

where U_{Sbdis} and U_{Sedis} are the cell voltage before and at end of the discharging process. The residual electric charge $\left(Q_{Sadis}\right)$, which is retained in capacitors after discharging, also depends on the values of the discharge current and effective conductivities of the electrodes and electrolytes, and is determined by the expression given below:

$$Q_{Sadis} = C\left(U_{Sdis}^{ap} - U_{Slor}\right) = Q_{ch} - Q_{dis} \tag{4.79}$$

where U_{Slor} is the supercapacitor's lower operating voltage value, and

$$U_{Sdis}^{ap} = \frac{Q_{Sadis}}{C} + U_{Slor} \tag{4.80}$$

The residual energy stored in capacitors after discharging, (E_{Sadis}) is determined by the following expression

$$E_{Sadis} = \frac{C\left(U_{Sedis}^2 - U_{Slor}^2\right)}{2} \quad 4.81$$

A portion of residual energy E_{Sadis} was lost during redistribution of the electric charge of the double electric layer along the thickness of the polarizable electrode after discharging and energy E_{dis}^{ap} was retained in the capacitor and is calculated by the formula given below

$$E_{dis}^{ap} = \frac{C\left(U_{Sdis}^{ap\ 2} - U_{Slor}^2\right)}{2} \quad 4.82$$

A portion of stored energy in the capacitor $\left(E_{dis}^{Rpol}\right)$ was dissipated at internal polarization resistance during discharging and is determined by the following formula

$$E_{dis}^{Rpol} = E_{Sch}^{ap} - E_{Sdis} - E_{Sadis} \quad 4.83$$

Again, a portion of the energy $\left(E_{dis}^{dpol}\right)$ is dissipated at polarization resistance during potential depolarization of the electrode after capacitor discharging and is determined by the expression given below:

$$E_{dis}^{dpol} = E_{Sadis} - E_{dis}^{ap} \quad 4.84$$

When the capacitor is being discharged by constant current I_{dis}, a portion of energy E_{dis}^{R} dissipated at the internal resistance and is determined by the following formula:

$$E_{dis}^{R} = I_{dis}^2\ R\ t_{dis} \quad 4.85$$

The value of energy released to the load (E_{dis}) during discharging of the symmetric capacitor is therefore determined by the formula:

$$E_{dis} = E_{Sdis} - E_{dis}^{R} = E_{Sch}^{ap} - E_{dis}^{dpol} - E_{dis}^{ap} - E_{dis}^{Rpol} - E_{dis}^{R} \quad 4.86$$

During charging and discharging of the capacitor, energy losses occur which are determined by the following: polarization resistance $\left(E_{ch}^{Rpol}, E_{dis}^{Rpol}\right)$; ohmic resistance $\left(E_{ch}^{R}, E_{dis}^{R}\right)$; and depolarization of the polarizable electrode $\left(E_{ch}^{dpol}, E_{dis}^{dpol}\right)$ after capacitor charging.

The mass of the symmetric EDLC is the mass of each porous electrode, separator, and electrolyte inside each electrode and separator, and is determined by:

$$M_{sy} = 2w_{ne}A\rho_{ne} + w_{sp}A\rho_{sp} + 2\varepsilon_0 w_{ne}\rho_e + \varepsilon_{sp}w_{sp}\rho_e \quad 4.87$$

where A is the cross-sectional area of the capacitor, w_{ne} is the thickness of the negative/positive electrode, ρ_{ne} is the density of the negative/positive electrode, w_{sp} is the thickness of the separator, ρ_{sp} is the density of the separator, ε_0 is porosity of the negative/positive electrode ρ_e is the density of electrolyte, and ε_{sp} is the porosity of the separator.

The energy density ED_{sy} and power density PD_{sy} of the symmetric EDLC are dependent on the mass of the capacitor and are given by the following expressions:

$$ED_{sy} = \frac{E_{ch}}{M_{sy}} \quad 4.88$$

$$PD_{sy} = \frac{E_{ch}}{M_{sy}\, t_{ch}} \quad 4.89$$

Similarly, the effective energy density ED_{sy}^{eff} and the effective power density PD_{sy}^{eff} of the symmetric EDLC are respectively given by:

$$ED_{sy}^{eff} = \frac{E_{Sch}}{M_{sy}} \quad 4.90$$

$$PD_{sy}^{eff} = \frac{E_{Sch}}{M_{sy}\, t_{ch}} \quad 4.91$$

The aggregate polarization loss of energy δ_{ERpol} during charging and discharging is determined by the following formula

$$\delta_{ERpol} = \frac{E_{ch}^{Rpol} + E_{dis}^{Rpol}}{E_{ch}} 100\% \quad 4.92$$

The aggregate depolarization loss of energy δ_{Edpol} and the aggregate ohmic loss of energy δ_{ER} during charge and discharge of the capacitor are respectively determined by the expressions

$$\delta_{Edpol} = \frac{E_{ch}^{dpol} + E_{dis}^{dpol}}{E_{ch}} 100\% \quad 4.93$$

$$\delta_{ER} = \frac{E_{ch}^{R} + E_{dis}^{R}}{E_{ch}} 100\% \quad 4.94$$

$$\delta_{Selfdis} = \frac{E_{selfdis1} + E_{selfdis2}}{E_{ch}} 100\% \quad 4.95$$

where $E_{selfdis1}$ and $E_{selfdis2}$ is the total energy loss by self-discharge during charging and discharging respectively.

Taking into consideration the fact that during capacitor charging, energy (E_{ch}) is spent and energy delivered to the load during discharging is (E_{dis}), the energy efficiency of the first charge–discharge cycle can be determined by the formula given below:

$$\eta_{E1} = \frac{E_{dis}}{E_{ch}} 100\% \quad 4.96$$

A new parameter of energy efficiency of the charge–discharge cycle (η_{E2}) which takes account of energy E_{dis}^{ap} that is retained in the capacitor after discharging and a pause is introduced, shows that a portion of the energy stored during the capacitor charge is retained in the capacitor during discharging.

The energy efficiency of second charge–discharge cycle of η_{E2} is determined by the expression:

$$\eta_{E2} = \frac{E_{dis} + E_{dis}^{ap}}{E_{ch}} 100\% \quad 4.97$$

4.10 Numerical solutions of the models

4.10.1 Numerical solutions of the models for EDLCs without self-discharge effects

Finite difference scheme for Crank-Nicolson Method

$$\frac{\partial\varphi(x,t)}{\partial t}=\frac{\varphi_i^{n+1}-\varphi_i^n}{\Delta t} \tag{4.98}$$

$$\frac{\partial^2\varphi(x,t)}{\partial x^2}=\frac{1}{2}\frac{\left(\varphi_{i+1}^{n+1}-2\varphi_i^{n+1}+\varphi_{i-1}^{n+1}\right)+\left(\varphi_{i+1}^{n}-2\varphi_i^{n}+\varphi_{i-1}^{n}\right)}{(\Delta x)^2} \tag{4.99}$$

The boundary conditions are:

$$\frac{\partial\varphi(x=0,t)}{\partial x}=\frac{\varphi_{i+1}^{n+1}-\varphi_{i-1}^{n}}{2\Delta x},\Rightarrow\frac{\varphi_{i+1}^{n+1}-\varphi_{i-1}^{n}}{2\Delta x}=\frac{-J_0}{\alpha_1},\Rightarrow\frac{\varphi_2^{n+1}-\varphi_0^{n}}{2\Delta x}=\frac{J_0}{\alpha_1}\ at\quad i=1 \tag{4.100}$$

$$\frac{\partial\varphi(x=w,t)}{\partial x}=\frac{\varphi_{i+1}^{n+1}-\varphi_{i-1}^{n}}{2\Delta x},\Rightarrow\frac{\varphi_{i+1}^{n+1}-\varphi_{i-1}^{n}}{2\Delta x}=\frac{J_0}{\alpha_2},\Rightarrow\frac{\varphi_{nx+1}^{n+1}-\varphi_{nx-1}^{n}}{2\Delta x}=-\frac{J_0}{\alpha_2}\ at\quad i=nx \tag{4.101}$$

Substitute equations 4.98 and 4.99 into equation 4.1 while assuming self-discharge to be zero ($\frac{J_{VR}(x,t)}{C_V}=0$), we obtain:

$$\frac{\varphi_i^{n+1}-\varphi_i^n}{\Delta t}=\frac{\beta^2}{2}\left[\frac{\left(\varphi_{i+1}^{n+1}-2\varphi_i^{n+1}+\varphi_{i-1}^{n+1}\right)+\left(\varphi_{i+1}^{n}-2\varphi_i^{n}+\varphi_{i-1}^{n}\right)}{(\Delta x)^2}\right] \tag{4.102}$$

Equation 4.102 was solved subject to the boundary conditions equations 4.100 and 4.101 as presented in Appendix E to obtain equation 4.103:

$$A_i^{n+1}\varphi_i^{n+1}=a_i^n-a_i^{n+1}+A_i^n\varphi_i^n \tag{4.103}$$

Equation 4.103 is written in matrix form as equation 4.98:

$$\begin{bmatrix} 2+2r & 0 & 0 & \bullet & 0 & 0 & 0 \\ -r & 2+2r & -r & \bullet & 0 & 0 & 0 \\ 0 & -r & 2+2r & \bullet & 0 & 0 & 0 \\ \bullet & \bullet & \bullet & \bullet & \bullet & \bullet & \bullet \\ 0 & 0 & 0 & \bullet & 2+2r & -r & 0 \\ 0 & 0 & 0 & \bullet & -r & 2+2r & -r \\ 0 & 0 & 0 & \bullet & 0 & -2r & 2+2r \end{bmatrix} \begin{bmatrix} \varphi_1^{n+1} \\ \varphi_2^{n+1} \\ \varphi_3^{n+1} \\ \bullet \\ \varphi_{nx-2}^{n+1} \\ \varphi_{nx-1}^{n+1} \\ \varphi_{nx}^{n+1} \end{bmatrix} =$$

$$\begin{bmatrix} 2-2r & 0 & 0 & \bullet & 0 & 0 & 0 \\ r & 2-2r & r & \bullet & 0 & 0 & 0 \\ 0 & r & 2-2r & \bullet & 0 & 0 & 0 \\ \bullet & \bullet & \bullet & \bullet & \bullet & \bullet & \bullet \\ 0 & 0 & 0 & \bullet & 2-2r & r & 0 \\ 0 & 0 & 0 & \bullet & r & 2-2r & r \\ 0 & 0 & 0 & \bullet & 0 & 2r & 2-2r \end{bmatrix} \begin{bmatrix} \varphi_1^{n} \\ \varphi_2^{n} \\ \varphi_3^{n} \\ \bullet \\ \varphi_{nx-2}^{n} \\ \varphi_{nx-1}^{n} \\ \varphi_{nx}^{n} \end{bmatrix} + \begin{bmatrix} 2r\left(\varphi_0^{n+1} + \varphi_0^{n} + j\right) \\ 0 \\ 0 \\ \bullet \\ 0 \\ 0 \\ 2rk \end{bmatrix} \qquad 4.104$$

and finally $\varphi_i^{n+1} = \left(A_i^{n+1}\right)^{-1}\left(a_i^n - a_i^{n+1} + A_i^n \varphi_i^n\right)$ 4.105

The matrix inversion is very time consuming and computationally inefficient. The matrix A_i^{n+1} is tridiagonal and can be decomposed into the product of the two other matrices such that A=LU, and the matrix form is equation 4.106:

$$\begin{bmatrix} 2+2r & 0 & 0 & \bullet & 0 & 0 & 0 \\ -r & 2+2r & -r & \bullet & 0 & 0 & 0 \\ 0 & -r & 2+2r & \bullet & 0 & 0 & 0 \\ \bullet & \bullet & \bullet & \bullet & \bullet & \bullet & \bullet \\ 0 & 0 & 0 & \bullet & 2+2r & -r & 0 \\ 0 & 0 & 0 & \bullet & -r & 2+2r & -r \\ 0 & 0 & 0 & \bullet & 0 & -2r & 2+2r \end{bmatrix} = \begin{bmatrix} 1 & 0 & 0 & 0 & 0 & 0 & 0 \\ l_2 & 1 & 0 & 0 & 0 & 0 & 0 \\ 0 & l_3 & 1 & \bullet & 0 & 0 & 0 \\ 0 & 0 & l_4 & \bullet & 0 & 0 & 0 \\ 0 & 0 & 0 & \bullet & 1 & 0 & 0 \\ 0 & 0 & 0 & 0 & l_{nx-2} & 1 & 0 \\ 0 & 0 & 0 & 0 & 0 & l_{nx-1} & 1 \end{bmatrix}$$

$$\begin{bmatrix} d_1 & p_1 & 0 & 0 & 0 & 0 & 0 \\ 0 & d_2 & p_2 & 0 & 0 & 0 & 0 \\ 0 & 0 & d_3 & \bullet & 0 & 0 & 0 \\ 0 & 0 & 0 & \bullet & p_{nx-4} & 0 & 0 \\ 0 & 0 & 0 & \bullet & d_{nx-2} & p_{nx-3} & 0 \\ 0 & 0 & 0 & 0 & 0 & d_{nx-1} & p_{nx-2} \\ 0 & 0 & 0 & 0 & 0 & 0 & d_{nx} \end{bmatrix} \qquad 4.106$$

where $d_1=2+2r$, $l_n d_{n-1}=p_{n-1}=-r$ and $d_n=2+2r-l_n p^{n-1}$ for $2 \le n \le nx-1$.

Note that we work from n=1 to n= nx sequentially.

Let $A_i^{n+1}\varphi_i^{n+1} = A\varphi \; and \; a_i^n - a_i^{n+1} + A_i^n\varphi_i^n = q, then \; A\varphi = q$, $LU\varphi = q$, $Lw = q$, $U\varphi = w$

Step one gives:

w_1=q_1 and $w_n = q_n - l_n w_{n-1} \quad for \quad 2 \le n \le n_{x-1}$.

Step two involves working backwards from n=nx-2 to n=1:

$$\varphi_{nx-1} = \frac{w_{nx-1}}{d_{nx-1}} \quad and \quad \varphi_n = \frac{w_n - p_n\varphi_{n+1}}{d_n} \quad for \quad n_{x-2} \ge 2 \ge 1$$

4.10.2 Numerical solutions of the models for EDLCs with self-discharge effects.

Substitute equations 4.92 and 4.93 into equation 4.1, is obtained with the self-discharge term:

$$\frac{\varphi_i^{n+1} - \varphi_i^n}{\Delta t} = \frac{\beta^2}{2}\left[\frac{\left(\varphi_{i+1}^{n+1} - 2\varphi_i^{n+1} + \varphi_{i-1}^{n+1}\right) + \left(\varphi_{i+1}^n - 2\varphi_i^n + \varphi_{i-1}^n\right)}{(\Delta x)^2}\right] + \frac{J_{VRi}^n}{C_V} \qquad 4.107$$

Equation 4.107 was solved subject to the boundary conditions equations 4.100 and 4.101 as presented in Appendix F to obtain equation 4.108:

$$A_i^{n+1}\varphi_i^{n+1} = a_i^n - a_i^{n+1} + A_i^n\varphi_i^n + bJ_{VRi}^n \qquad 4.108$$

Equation 4.108 is written in matrix form as equation 4.109:

$$\begin{bmatrix} 2+2r & 0 & 0 & \bullet & 0 & 0 & 0 \\ -r & 2+2r & -r & \bullet & 0 & 0 & 0 \\ 0 & -r & 2+2r & \bullet & 0 & 0 & 0 \\ \bullet & \bullet & \bullet & \bullet & \bullet & \bullet & \bullet \\ 0 & 0 & 0 & \bullet & 2+2r & -r & 0 \\ 0 & 0 & 0 & \bullet & -r & 2+2r & -r \\ 0 & 0 & 0 & \bullet & 0 & -2r & 2+2r \end{bmatrix} \begin{bmatrix} \varphi_1^{n+1} \\ \varphi_2^{n+1} \\ \varphi_3^{n+1} \\ \bullet \\ \varphi_{nx-2}^{n+1} \\ \varphi_{nx-1}^{n+1} \\ \varphi_{nx}^{n+1} \end{bmatrix} =$$

$$\begin{bmatrix} 2-2r & 0 & 0 & \bullet & 0 & 0 & 0 \\ r & 2-2r & r & \bullet & 0 & 0 & 0 \\ 0 & r & 2-2r & \bullet & 0 & 0 & 0 \\ \bullet & \bullet & \bullet & \bullet & \bullet & \bullet & \bullet \\ 0 & 0 & 0 & \bullet & 2-2r & r & 0 \\ 0 & 0 & 0 & \bullet & r & 2-2r & r \\ 0 & 0 & 0 & \bullet & 0 & 2r & 2-2r \end{bmatrix} \begin{bmatrix} \varphi_1^n \\ \varphi_2^n \\ \varphi_3^n \\ \bullet \\ \varphi_{nx-2}^n \\ \varphi_{nx-1}^n \\ \varphi_{nx}^n \end{bmatrix} + \begin{bmatrix} 2r\left(\varphi_0^{n+1} + \varphi_0^n + j\right) \\ 0 \\ 0 \\ \bullet \\ 0 \\ 0 \\ 2rk \end{bmatrix} + \text{b}$$

$$\begin{bmatrix} J_{VR0}^n \\ J_{VR1}^n \\ \bullet \\ \bullet \\ \bullet \\ J_{VRnx-1}^n \\ J_{VRnx}^n \end{bmatrix} \qquad 4.109$$

and finally $\varphi_i^{n+1} = \left(A_i^{n+1}\right)^{-1}\left(a_i^n - a_i^{n+1} + A_i^n \varphi_i^n + bJ_{VRi}^n\right)$ 4.110

Again, the matrix inversion is very time consuming and computationally inefficient. The matrix A_i^{n+1} is tridiagonal and can be decomposed into the product of the two other matrices such that A=LU, and the matrix form is equation 4.111:

$$\begin{bmatrix} 2+2r & 0 & 0 & \bullet & 0 & 0 & 0 \\ -r & 2+2r & -r & \bullet & 0 & 0 & 0 \\ 0 & -r & 2+2r & \bullet & 0 & 0 & 0 \\ \bullet & \bullet & \bullet & \bullet & \bullet & \bullet & \bullet \\ 0 & 0 & 0 & \bullet & 2+2r & -r & 0 \\ 0 & 0 & 0 & \bullet & -r & 2+2r & -r \\ 0 & 0 & 0 & \bullet & 0 & -2r & 2+2r \end{bmatrix} = \begin{bmatrix} 1 & 0 & 0 & 0 & 0 & 0 & 0 \\ l_2 & 1 & 0 & 0 & 0 & 0 & 0 \\ 0 & l_3 & 1 & \bullet & 0 & 0 & 0 \\ 0 & 0 & l_4 & \bullet & 0 & 0 & 0 \\ 0 & 0 & 0 & \bullet & 1 & 0 & 0 \\ 0 & 0 & 0 & 0 & l_{nx-2} & 1 & 0 \\ 0 & 0 & 0 & 0 & 0 & l_{nx-1} & 1 \end{bmatrix}$$

$$\begin{bmatrix} d_1 & p_1 & 0 & 0 & 0 & 0 & 0 \\ 0 & d_2 & p_2 & 0 & 0 & 0 & 0 \\ 0 & 0 & d_3 & \bullet & 0 & 0 & 0 \\ 0 & 0 & 0 & \bullet & p_{nx-4} & 0 & 0 \\ 0 & 0 & 0 & \bullet & d_{nx-2} & p_{nx-3} & 0 \\ 0 & 0 & 0 & 0 & 0 & d_{nx-1} & p_{nx-2} \\ 0 & 0 & 0 & 0 & 0 & 0 & d_{nx} \end{bmatrix} \qquad 4.111$$

where $d_1 = 2+2r$, $l_n d_{n-1} = p_{n-1} = -r$ and $d_n = 2+2r-l_n p_{n-1}$ *for* $2 \le n \le nx-1$.

Note that we work from $n = 1 \; to \; n = nx$ sequentially.

Let $A_i^{n+1}\varphi_i^{n+1} = A\varphi \; and \; a_i^n - a_i^{n+1} + A_i^n\varphi_i^n = q, then \; A\varphi = q$, $LU\varphi = q$, $Lw = q$, $U\varphi = w$

Step one gives:

w_1=q_1 and $w_n = q_n - l_n w_{n-1} \quad for \quad 2 \le n \le n_{x-1}$.

Step two involves working backwards from $n = nx - 2 \; to \; n = 1$:

$$\varphi_{nx-1} = \frac{w_{nx-1}}{d_{nx-1}} \quad and \quad \varphi_n = \frac{w_n - p_n\varphi_{n+1}}{d_n} \quad for \quad n_{x-2} \ge 2 \ge 1$$

4.10.3 Numerical solutions of the models with composite electrode and self-discharge effects.

$$\frac{\partial\varphi_{ne}(x,t)}{\partial t} = \beta^2 \frac{\partial^2\varphi_{ne}(x,t)}{\partial x^2} - \frac{S_f J_f(x,t)}{C_V} - \gamma\frac{\partial^2(\ln C(x,t))}{\partial x^2} + \frac{J_{VR}(x,t)}{C_V} \qquad 4.112$$

$$\beta^2 = \frac{\alpha_1\alpha_2}{C_V(\alpha_2 + \alpha_1)} \qquad 4.113$$

$$\gamma = \frac{\sigma_{ne}^l RT}{C_V F}\left(\frac{s_+}{nv_+} + \frac{t_+^0}{z_+v_+}\right) \qquad 4.114$$

$$J_f(x,t) = i_0\{\exp[\alpha_a f\varphi_{ne}(x,t) - U_1] - \exp[-\alpha_c f\varphi_{ne}(x,t) - U_1]\} \qquad 4.115$$

$$J_{VR}(x,t) = J_{VR} + J_{VR1}(t) = \frac{eZN}{w_{sp}\left(\frac{s_+ + s_-}{s_+s_-} + \frac{D_+ + D_-}{D_+D_-}\right)} + \frac{\frac{8nFVD_{Ox}C_{Ox}}{l^2}\exp\left(\frac{-\pi^2 D_{Ox}t}{l^2}\right)}{A} \qquad 4.116$$

$$J_{VR} = \frac{eZN}{w_{sp}\left(\frac{s_+ + s_-}{s_+s_-} + \frac{D_+ + D_-}{D_+D_-}\right)} \qquad 4.117$$

$$J_{VR1}(t)=\frac{\frac{8nFVD_{Ox}C_{Ox}}{l^2}\exp\left(\frac{-\pi^2 D_{Ox}t}{l^2}\right)}{A} \tag{4.118}$$

$$\frac{\partial\theta(x,t)}{\partial t}=\frac{S_f J_f}{Q_{f,oxd}-Q_{f,red}} \tag{4.119}$$

$$where\ f=\frac{F}{RT}$$

$$\frac{\partial C_s(x,t)}{\partial t}=D_s\frac{\partial^2 C_s(x,t)}{\partial x^2}+\frac{S_d C_d\left(1-t_+^0\right)}{2\varepsilon F}\frac{\partial\varphi_{ne}(x,t)}{\partial t}+\frac{S_f\left(1-t_+^0\right)}{2\varepsilon F}J_f(x,t) \tag{4.120}$$

The boundary conditions of this task during the capacitor discharge are as follows:

$$J_1(0,t)=-\alpha_1\frac{\partial\varphi_{ne}(x,t)}{\partial x}\Big|_{x=0}=J_0 \tag{4.121}$$

$$J_2(w,t)=\alpha_2\frac{\partial\varphi_{ne}(x,t)}{\partial x}\Big|_{x=w_{ne}}=J_0 \tag{4.122}$$

$$\frac{\partial C(x,t)}{\partial x}\Big|_{x=0}=0 \tag{4.123}$$

$$\frac{\partial C(x,t)}{\partial x}\Big|_{x=w}=\frac{\left(1-t_+^0\right)J_0}{2\varepsilon_{sp}D_{sp}F} \tag{4.124}$$

and the initial conditions are:

$$\varphi_{ne}(x,t_{=0})=\varphi_{ne}^{0^-}-\frac{J_0\,x}{\alpha_1}+\frac{J_0(\alpha_1+\alpha_2)x^2}{2w_{ne}\alpha_1\alpha_2}$$

$$\varphi_{ne}(x_{=0},t_{=0})=\varphi_{ne}^{0^-} \tag{4.125}$$

$$\theta(x.t=0)=1,\quad C(x,t=0)=C_{so^-}+\frac{\left(1-t_0^+\right)J_0}{2\varepsilon_{sp}D_{ssp}F}\frac{1\,x^2}{2w_{ne}}$$

$$C(x_{=0},t_{=0})=C_{so^-} \tag{4.126}$$

Finite difference scheme for the Crank-Nicolson Method

$$\frac{\partial\varphi(x,t)}{\partial t}=\frac{\varphi_i^{n+1}-\varphi_i^n}{\Delta t} \tag{4.127}$$

$$\frac{\partial^2\varphi(x,t)}{\partial x^2}=\frac{1}{2}\frac{\left(\varphi_{i+1}^{n+1}-2\varphi_i^{n+1}+\varphi_{i-1}^{n+1}\right)+\left(\varphi_{i+1}^{n}-2\varphi_i^{n}+\varphi_{i-1}^{n}\right)}{(\Delta x)^2} \tag{4.128}$$

$$\frac{\partial^2\ln C(x,t)}{\partial x^2}=\frac{1}{2}\frac{\left(\ln C_{i+1}^{n+1}-2\ln C_i^{n+1}+\ln C_{i-1}^{n+1}\right)+\left(\ln C_{i+1}^{n}-2\ln C_i^{n}+\ln C_{i-1}^{n}\right)}{(\Delta x)^2} \tag{4.129}$$

$$\varphi(x,t)=\frac{1}{2}\left(\varphi_{i+1}^{n}+\varphi_{i}^{n}\right) \tag{4.130}$$

$$\frac{\partial\theta(x,t)}{\partial t}=\frac{\theta_{i}^{n+1}-\theta_{i}^{n}}{\Delta t} \tag{4.131}$$

$$\frac{\partial C(x,t)}{\partial t}=\frac{C_{i}^{n+1}-C_{i}^{n}}{\Delta t} \tag{4.132}$$

$$\frac{\partial^{2}C(x,t)}{\partial x^{2}}=\frac{1}{2}\frac{\left(C_{i+1}^{n+1}-2C_{i}^{n+1}+C_{i-1}^{n+1}\right)+\left(C_{i+1}^{n}-2C_{i}^{n}+C_{i-1}^{n}\right)}{(\Delta x)^{2}} \tag{4.133}$$

The boundary conditions equations 4.121, 4.122, 4.123 and 4.124 are

$$\frac{\partial\varphi(x=0,t)}{\partial x}=\frac{\varphi_{i+1}^{n+1}-\varphi_{i-1}^{n}}{2\Delta x},\Rightarrow\frac{\varphi_{i+1}^{n+1}-\varphi_{i-1}^{n}}{2\Delta x}=\frac{-J_{0}}{\alpha_{1}},\Rightarrow\frac{\varphi_{2}^{n+1}-\varphi_{0}^{n}}{2\Delta x}=\frac{-J_{0}}{\alpha_{1}}\ at\quad i=1 \tag{4.134}$$

$$\frac{\partial\varphi(x=w,t)}{\partial x}=\frac{\varphi_{i+1}^{n+1}-\varphi_{i-1}^{n}}{2\Delta x},\Rightarrow\frac{\varphi_{i+1}^{n+1}-\varphi_{i-1}^{n}}{2\Delta x}=\frac{J_{0}}{\alpha_{2}},\Rightarrow\frac{\varphi_{nx+1}^{n+1}-\varphi_{nx-1}^{n}}{2\Delta x}=\frac{J_{0}}{\alpha_{2}}\ at\quad i=nx \tag{4.135}$$

$$\frac{\partial C(x=0,t)}{\partial x}=\frac{C_{i+1}^{n+1}-C_{i-1}^{n}}{2\Delta x},\Rightarrow\frac{C_{i+1}^{n+1}-C_{i-1}^{n}}{2\Delta x}=0,\Rightarrow\frac{C_{2}^{n+1}-C_{0}^{n}}{2\Delta x}=0\ at\quad i=1 \tag{4.136}$$

$$\frac{\partial C(x=w,t)}{\partial x}=\frac{C_{i+1}^{n+1}-C_{i-1}^{n}}{2\Delta x},\Rightarrow\frac{C_{i+1}^{n+1}-C_{i-1}^{n}}{2\Delta x}=\frac{\left(1-t_{+}^{0}\right)J_{0}}{2\varepsilon_{sp}D_{sp}F},\Rightarrow\frac{C_{nx+1}^{n+1}-C_{nx-1}^{n}}{2\Delta x}=\frac{\left(1-t_{+}^{0}\right)J_{0}}{2\varepsilon_{sp}D_{sp}F} \tag{4.137}$$

$at\quad i=nx$

Substitute equations 4.127, 4.128 and 4.129 into 4.111; equation 4.131 into 4.119; and equations 4.127, 4.132 and 4.133 into 4.130 respectively to obtain:

$$\frac{\varphi_{i}^{n+1}-\varphi_{i}^{n}}{\Delta t}=\frac{\beta^{2}}{2}\left[\frac{\left(\varphi_{i+1}^{n+1}-2\varphi_{i}^{n+1}+\varphi_{i-1}^{n+1}\right)+\left(\varphi_{i+1}^{n}-2\varphi_{i}^{n}+\varphi_{i-1}^{n}\right)}{(\Delta x)^{2}}\right]-\frac{S_{f}J_{f\,i}^{n}}{C_{V}}-$$

$$\frac{\gamma}{2}\left[\frac{\left(\ln C_{i+1}^{n+1}-2\ln C_{i}^{n+1}+\ln C_{i-1}^{n+1}\right)+\left(\ln C_{i+1}^{n}-2\ln C_{i}^{n}+\ln C_{i-1}^{n}\right)}{(\Delta x)^{2}}\right]+\frac{J_{VRi}^{n}}{C_{V}} \tag{4.138}$$

$$\frac{\theta_{i}^{n+1}-\theta_{i}^{n}}{\Delta t}=b\,J_{f\,i}^{n} \tag{4.139}$$

$$\frac{C_{i}^{n+1}-C_{i}^{n}}{\Delta t}=\frac{D}{2}\left[\frac{\left(C_{i+1}^{n+1}-2C_{i}^{n+1}+C_{i-1}^{n+1}\right)+\left(C_{i+1}^{n}-2C_{i}^{n}+C_{i-1}^{n}\right)}{(\Delta x)^{2}}\right]+\frac{d\left(\varphi_{i}^{n+1}-\varphi_{i}^{n}\right)}{\Delta t}+eJ_{f\,i}^{n} \tag{4.140}$$

$$where\quad z=\frac{S_{f}}{Q_{f,oxd}-Q_{f,red}},\ d=\frac{S_{d}C_{d}\left(1-t_{+}^{0}\right)}{2\varepsilon F},\ and\quad e=\frac{S_{f}\left(1-t_{+}^{0}\right)}{2\varepsilon F}$$

Equation 4.138, 4.139 and 4.140 were solved, subject to the boundary condition equations 4.93, 4.94, 4.96 and 4.97 as presented in Appendix G, to obtain equations 4.141 and 4.142 respectively:

$$A_i^{n+1}\varphi_i^{n+1} = B_i^n\varphi_i^n + b_i^n + H_i^n \ln C_i^n + h_i^n - G_i^{n+1}\ln C_i^{n+1} - g_i^{n+1} - a_i^{n+1} - u\,J_{f\,i}^n + s\,J_{VR\,i}^n \qquad 4.141$$

$$Q_i^{n+1}C_i^{n+1} = V_i^n C_i^n + v_i^n - q_i^{n+1} - d\,\varphi_i^{n+1} - d\,\varphi_i^n + e\,J_{f\,i}^n \qquad 4.142$$

Equations 4.141 and 4.142 are written in matrix form as equations 4.143 and 4.144 respectively:

$$\begin{bmatrix} 2+2r & 0 & 0 & \bullet & 0 & 0 & 0 \\ -r & 2+2r & -r & \bullet & 0 & 0 & 0 \\ 0 & -r & 2+2r & \bullet & 0 & 0 & 0 \\ \bullet & \bullet & \bullet & \bullet & \bullet & \bullet & \bullet \\ 0 & 0 & 0 & \bullet & 2+2r & -r & 0 \\ 0 & 0 & 0 & \bullet & -r & 2+2r & -r \\ 0 & 0 & 0 & \bullet & 0 & -2r & 2+2r \end{bmatrix} \begin{bmatrix} \varphi_1^{n+1} \\ \varphi_2^{n+1} \\ \varphi_3^{n+1} \\ \bullet \\ \varphi_{nx-2}^{n+1} \\ \varphi_{nx-1}^{n+1} \\ \varphi_{nx}^{n+1} \end{bmatrix} =$$

$$\begin{bmatrix} 2-2r & 0 & 0 & \bullet & 0 & 0 & 0 \\ r & 2-2r & r & \bullet & 0 & 0 & 0 \\ 0 & r & 2-2r & \bullet & 0 & 0 & 0 \\ \bullet & \bullet & \bullet & \bullet & \bullet & \bullet & \bullet \\ 0 & 0 & 0 & \bullet & 2-2r & r & 0 \\ 0 & 0 & 0 & \bullet & r & 2-2r & r \\ 0 & 0 & 0 & \bullet & 0 & 2r & 2-2r \end{bmatrix} \begin{bmatrix} \varphi_1^n \\ \varphi_2^n \\ \varphi_3^n \\ \bullet \\ \varphi_{nx-2}^n \\ \varphi_{nx-1}^n \\ \varphi_{nx}^n \end{bmatrix} + \begin{bmatrix} 2r\left(\varphi_0^{n+1} + \varphi_0^n + j\right) \\ 0 \\ 0 \\ \bullet \\ 0 \\ 0 \\ 2rk \end{bmatrix} +$$

$$\begin{bmatrix} 2m & 0 & 0 & \bullet & 0 & 0 & 0 \\ -m & 2m & -m & \bullet & 0 & 0 & 0 \\ 0 & -m & 2m & \bullet & 0 & 0 & 0 \\ \bullet & \bullet & \bullet & \bullet & \bullet & \bullet & \bullet \\ 0 & 0 & 0 & \bullet & 2m & -m & 0 \\ 0 & 0 & 0 & \bullet & -m & 2m & -m \\ 0 & 0 & 0 & \bullet & 0 & -2m & 2m \end{bmatrix} \begin{bmatrix} \ln C_1^n \\ \ln C_2^n \\ \ln C_3^n \\ \bullet \\ \ln C_{nx-2}^n \\ \ln C_{nx-1}^n \\ \ln C_{nx}^n \end{bmatrix} -$$

$$\begin{bmatrix} -2m & 0 & 0 & \bullet & 0 & 0 & 0 \\ m & -2m & m & \bullet & 0 & 0 & 0 \\ 0 & m & -2m & \bullet & 0 & 0 & 0 \\ \bullet & \bullet & \bullet & \bullet & \bullet & \bullet & \bullet \\ 0 & 0 & 0 & \bullet & -2m & m & 0 \\ 0 & 0 & 0 & \bullet & m & -2m & m \\ 0 & 0 & 0 & \bullet & 0 & 2m & -2m \end{bmatrix} \begin{bmatrix} \ln C_1^{n+1} \\ \ln C_2^{n+1} \\ \ln C_3^{n+1} \\ \bullet \\ \ln C_{nx-2}^{n+1} \\ \ln C_{nx-1}^{n+1} \\ \ln C_{nx}^{n+1} \end{bmatrix} + \begin{bmatrix} -2r\left(\ln C_0^{n+1} + \ln C_0^n - j\right) \\ 0 \\ 0 \\ \bullet \\ 0 \\ 0 \\ 2rk \end{bmatrix}$$

$$-u \begin{bmatrix} J_{f0}^n \\ J_{f1}^n \\ \bullet \\ \bullet \\ \bullet \\ J_{f\,nx-1}^n \\ J_{f\,nx}^n \end{bmatrix} + s \begin{bmatrix} J_{VR0}^n \\ J_{VR1}^n \\ \bullet \\ \bullet \\ \bullet \\ J_{VRnx-1}^n \\ J_{VRnx}^n \end{bmatrix} \qquad 4.143$$

$$\begin{bmatrix} 2+2\eta & 0 & 0 & \bullet & 0 & 0 & 0 \\ -\eta & 2+2\eta & -\eta & \bullet & 0 & 0 & 0 \\ 0 & -\eta & 2+2\eta & \bullet & 0 & 0 & 0 \\ \bullet & \bullet & \bullet & \bullet & \bullet & \bullet & \bullet \\ 0 & 0 & 0 & \bullet & 2+2\eta & -\eta & 0 \\ 0 & 0 & 0 & \bullet & -\eta & 2+2\eta & -\eta \\ 0 & 0 & 0 & \bullet & 0 & -2\eta & 2+2\eta \end{bmatrix} \begin{bmatrix} C_1^{n+1} \\ C_2^{n+1} \\ C_3^{n+1} \\ \bullet \\ C_{nx-2}^{n+1} \\ C_{nx-1}^{n+1} \\ C_{nx}^{n+1} \end{bmatrix} =$$

$$\begin{bmatrix} 2-2\eta & 0 & 0 & \bullet & 0 & 0 & 0 \\ \eta & 2-2\eta & \eta & \bullet & 0 & 0 & 0 \\ 0 & \eta & 2-2\eta & \bullet & 0 & 0 & 0 \\ \bullet & \bullet & \bullet & \bullet & \bullet & \bullet & \bullet \\ 0 & 0 & 0 & \bullet & 2-2\eta & \eta & 0 \\ 0 & 0 & 0 & \bullet & \eta & 2-2\eta & \eta \\ 0 & 0 & 0 & \bullet & 0 & -2\eta & 2+2\eta \end{bmatrix} \begin{bmatrix} C_1^n \\ C_2^n \\ C_3^n \\ \bullet \\ C_{nx-2}^n \\ C_{nx-1}^n \\ C_{nx}^n \end{bmatrix} + \begin{bmatrix} 2r\left(C_0^{n+1} + C_0^n + j\right) \\ 0 \\ 0 \\ \bullet \\ 0 \\ 0 \\ 2rk \end{bmatrix}$$

$$-d \begin{bmatrix} \varphi_0^n \\ \varphi_1^n \\ \varphi_2^1 \\ \bullet \\ \varphi_{nx}^n \\ \varphi_{nx}^n \\ \varphi_{nx}^n \end{bmatrix} - d \begin{bmatrix} \varphi_0^{n+1} \\ \varphi_1^{n+1} \\ \varphi_1^{n+1} \\ \bullet \\ \varphi_{nx-1}^{n+1} \\ \varphi_{nx}^{n+1} \end{bmatrix} + e \begin{bmatrix} J_{f0}^n \\ J_{f1}^n \\ \bullet \\ \bullet \\ \bullet \\ J_{f\,nx-1}^n \\ J_{f\,nx}^n \end{bmatrix} \qquad 4.144$$

And finally:

$$\varphi_i^{n+1} = \left(A_i^{n+1}\right)^{-1}\left(B_i^n \varphi_i^n + b_i^n + H_i^n \ln C_i^n + h_i^n - G_i^{n+1} \ln C_i^{n+1} - g_i^{n+1} - a_i^{n+1} - u\, J_{f\,i}^n + s\, J_{VR\,i}^n\right) \quad 4.145$$

$$C_i^{n+1} = \left(Q_i^{n+1}\right)^{-1}\left(V_i^n C_i^n + v_i^n - q_i^{n+1} - d\, \varphi_i^{n+1} - d\, \varphi_i^n + e\, J_{f\,i}^n\right) \quad 4.146$$

Further, equation 4.139 is given as:

$$\theta_i^{n+1} = \theta_i^n + z\Delta t\, J_{f\,i}^n \quad 4.147$$

However, the matrix inversion is very time consuming and computationally inefficient. The matrices A_i^{n+1} and Q_i^{n+1} are tridiagonal and can be decomposed into the product of the two other matrices such that A=LU. There the matrices A_i^{n+1} and Q_i^{n+1} are now written as equations 4.148 and 4.149 respectively:

$$\begin{bmatrix} 2+2r & 0 & 0 & \bullet & 0 & 0 & 0 \\ -r & 2+2r & -r & \bullet & 0 & 0 & 0 \\ 0 & -r & 2+2r & \bullet & 0 & 0 & 0 \\ \bullet & \bullet & \bullet & \bullet & \bullet & \bullet & \bullet \\ 0 & 0 & 0 & \bullet & 2+2r & -r & 0 \\ 0 & 0 & 0 & \bullet & -r & 2+2r & -r \\ 0 & 0 & 0 & \bullet & 0 & -2r & 2+2r \end{bmatrix} = \begin{bmatrix} 1 & 0 & 0 & 0 & 0 & 0 & 0 \\ l_2 & 1 & 0 & 0 & 0 & 0 & 0 \\ 0 & l_3 & 1 & \bullet & 0 & 0 & 0 \\ 0 & 0 & l_4 & \bullet & 0 & 0 & 0 \\ 0 & 0 & 0 & \bullet & 1 & 0 & 0 \\ 0 & 0 & 0 & 0 & l_{nx-2} & 1 & 0 \\ 0 & 0 & 0 & 0 & 0 & l_{nx-1} & 1 \end{bmatrix}$$

$$\begin{bmatrix} d_1 & p_1 & 0 & 0 & 0 & 0 & 0 \\ 0 & d_2 & p_2 & 0 & 0 & 0 & 0 \\ 0 & 0 & d_3 & \bullet & 0 & 0 & 0 \\ 0 & 0 & 0 & \bullet & p_{nx-4} & 0 & 0 \\ 0 & 0 & 0 & \bullet & d_{nx-2} & p_{nx-3} & 0 \\ 0 & 0 & 0 & 0 & 0 & d_{nx-1} & p_{nx-2} \\ 0 & 0 & 0 & 0 & 0 & 0 & d_{nx} \end{bmatrix} \quad 4.148$$

$$\begin{bmatrix} 2+2\eta & 0 & 0 & \bullet & 0 & 0 & 0 \\ -\eta & 2+2\eta & -\eta & \bullet & 0 & 0 & 0 \\ 0 & -\eta & 2+2\eta & \bullet & 0 & 0 & 0 \\ \bullet & \bullet & \bullet & \bullet & \bullet & \bullet & \bullet \\ 0 & 0 & 0 & \bullet & 2+2\eta & -\eta & 0 \\ 0 & 0 & 0 & \bullet & -\eta & 2+2\eta & -\eta \\ 0 & 0 & 0 & \bullet & 0 & -2\eta & 2+2\eta \end{bmatrix} = \begin{bmatrix} 1 & 0 & 0 & 0 & 0 & 0 & 0 \\ l_2 & 1 & 0 & 0 & 0 & 0 & 0 \\ 0 & l_3 & 1 & \bullet & 0 & 0 & 0 \\ 0 & 0 & l_4 & \bullet & 0 & 0 & 0 \\ 0 & 0 & 0 & \bullet & 1 & 0 & 0 \\ 0 & 0 & 0 & 0 & l_{nx-2} & 1 & 0 \\ 0 & 0 & 0 & 0 & 0 & l_{nx-1} & 1 \end{bmatrix}$$

$$\begin{bmatrix} d_1 & p_1 & 0 & 0 & 0 & 0 & 0 \\ 0 & d_2 & p_2 & 0 & 0 & 0 & 0 \\ 0 & 0 & d_3 & \bullet & 0 & 0 & 0 \\ 0 & 0 & 0 & \bullet & p_{nx-4} & 0 & 0 \\ 0 & 0 & 0 & \bullet & d_{nx-2} & p_{nx-3} & 0 \\ 0 & 0 & 0 & 0 & 0 & d_{nx-1} & p_{nx-2} \\ 0 & 0 & 0 & 0 & 0 & 0 & d_{nx} \end{bmatrix} \qquad 4.149$$

For equation 4.148, $d_1 = 2 + 2r$, $l_n d_{n-1} = p_{n-1} = -r$ and $d_n = 2 + 2r - l_n p_{n-1}$ *for* $2 \le n \le nx - 1$,

and for equation 4.149, $d_1 = 2 + 2\eta$, $l_n d_{n-1} = p_{n-1} = -\eta$ and

$d_n = 2 + 2\eta - l_n p_{n-1}$ *for* $2 \le n \le nx - 1$.

Note that we work from $n = 1$ *to* $n = nx$ sequentially. Let

$A_i^{n+1}\varphi_i^{n+1} = A\varphi$ *and* $B_i^n\varphi_i^n + b_i^n + H_i^n \ln C_i^n + h_i^n - G_i^{n+1} \ln C_i^{n+1} - g_i^{n+1} - a_i^{n+1} - uJ_{fi}^n + sJ_{VRi}^n = q$,
then $A\varphi = q$, $LU\varphi = q$, $Lw = q$, $U\varphi = w$ *for equation* 4.148

Also, let

$A_i^{n+1}\varphi_i^{n+1} = A\varphi$ *and* $V_i^n C_i^n + v_i^n - q_i^{n+1} - d\varphi_i^{n+1} - d\varphi_i^n + uJ_{fi}^n = q$, *then* $A\varphi = q$, $LU\varphi = q$,
$Lw = q$, $U\varphi = w$ *for equation* 4.149

Step one gives:

$w_1 = q_1$ and $w_n = q_n - l_n w_{n-1}$ *for* $2 \le n \le n_{x-1}$.

Step two requires working backwards from $n = nx - 2$ *to* $n = 1$:

$$\varphi_{nx-1} = \frac{w_{nx-1}}{d_{nx-1}} \text{ and } \varphi_n = \frac{w_n - p_n\varphi_{n+1}}{d_n} \text{ for } n_{x-2} \ge 2 \ge 1$$

4.11 Optimization of ECs design parameters and operating conditions for high energy and power performances

In order to maximize storable energy, energy and power densities of electrochemical capacitors, we need to maximize the values of the coefficient associated to battery-type material in asymmetric ECs with the aqueous electrolyte K_{BM} and the constant associated to the electrolyte in asymmetric ECs with the organic electrolyte K_E subject to realistic constraints. These coefficients are given as equations 3.214 and 3.210 respectively. The constraint equations by Choi and Park were also modified as presented below, in order to capture realistic conditions and limitations inherent in electrochemical energy storage systems. The following coefficients should be maximized, subject to their respective constraints:

$$\text{Maximize } K_{BM} = (1-k_1)(1-k_2^2) \qquad 3.214$$

$$\text{Subject to: } \left.\begin{matrix} \delta_1 < \mathrm{k}_1 < 0.5 \\ \delta_2 < \mathrm{k}_2 < 0.7 \end{matrix}\right\} \qquad 3.232$$

where $\delta_1 = 0.05$ is realistic minimum value of k_1 for EC systems as explained in [90] and $\delta_2 = 0.05$ realistic minimum value of k_2 for EC systems as explained in [90].

$$\text{Maximize } K_E = \frac{k_4}{k_3^2} \qquad 3.210$$

$$\text{Subject to: } \left.\begin{matrix} \delta_3 \le \mathrm{k}_3 < 1 \\ 0 < \mathrm{k}_4 \le \delta_4 \end{matrix}\right\} \qquad 3.233$$

where $\delta_3 = 0.3$ is the realistic minimum value of k_3 for EC systems as explained in [270,273,274] and $\delta_4 = 0.5$ is the realistic maximum value of k_4 for EC systems as explained in [270,273,274].

Equations 3.210 and 3.214 were solved subject to constraint equations 3.232 and 3.233 respectively by writing MATLAB scripts to optimize the objective functions K_{BM} and K_E shown in Appendix H4 - H6 and using the MATLAB R2014a optimization tool box.

Optimum value of parameters $k_1, k_2, k_3, k_4, K_{BM}$ and K_E together with experimental data in Table 5.1 were used to solve and simulate the symmetric EDLC model given by equation 3.49 under different conditions, subject to the boundary and initial condition equations 3.64, 3.65 and 3.66, respectively, using the MATLAB scripts shown in Appendix H4 - H6. The optimal values of parameters $k_1, k_2, k_3, k_4, K_{BM}$ and K_E were used to solve and simulate asymmetric EDLC and asymmetric EC models given by equations 3.124, 3.112 and 3.113 under different conditions subject to boundary and initial condition equations 3.128, 3.129, 3.130, 3.131 and 3.132 & 3.133, respectively, using MATLAB scripts shown in Appendix H4 - H6. Optimal parameters $k_1, k_2, k_3, k_4, K_{BM}$ and K_E were used to compute the performance parameters of different types of EC models under different conditions for performance comparison purposes. Finally, optimum values of $k_1, k_2, k_3, k_4, K_{BM}$ and K_E were also substituted into performance parameter equations 3.223–3.231 in order to compare the results from these equations with those computed from simulation of different types of capacitor models. The results of the various performance parameters from simulations were compared with the resultant performance parameter equations to ascertain the extent of their agreement.

4.12 Model Validation of the electrochemical capacitor

The experimental results of two symmetric button electrochemical capacitors with composite electrodes $Mn_3(PO_4)_2//Mn_3(PO_4)_2$ using aqueous 1molL^{-1} Na_2SO_4 electrolyte and aqueous 2molL^{-1} KOH electrolyte [275] are used to validate the symmetric models. Also, symmetric electrochemical capacitors with nitrogen-doped rapeseed activated carbons (N-RCs) composite electrodes and 1100CNFs webs electrodes with aqueous 0.5molL^{-1} and 1mol L^{-1}

Na_2SO_4 electrolyte respectively [276] and [277] are used to validate the symmetric models. Similarly, experimental results of two button asymmetric electrochemical capacitors with composite and activated carbon electrodes $Mn_3(PO_4)_2$//AC using aqueous 1molL^{-1} Na_2SO_4 electrolyte and aqueous 2molL^{-1} KOH electrolyte [275] are used to validate the asymmetric models. These capacitors are charged and discharged at different current densities, and the performance parameters measured at the various current densities. The material synthesis, electrodes preparation and supercapacitors fabrication were detailed in literature Ma et al [275], Sun et al [276] and [277], which are briefly explained below.

The experimental data were obtained by testing symmetric and asymmetric cells. In the works of Ma et al [275], the electrodes contained a mixture of 80wt% of manganese phosphate $Mn_2(PO_4)_2$, 7.5wt% of acetylene black, 7.5wt% of graphite, and 5wt% of polytetrafluoroethylene (PTFE), pasted onto a nickel foam current collector. For the asymmetric button device, $Mn_2(PO_4)_2$ and activated carbon served as electrodes, and for the symmetric button device, $Mn_2(PO_4)_2$ were used as electrodes. Each electrode contained 85wt% of active material, 10wt% of acetylene black and 5wt% of PTFE on a nickel form current collector. The separator (glass micro-fiber filter paper) was in between the two electrodes soaked in either 1molL^{-1} aqueous Na_2SO_4 solution or 2molL^{-1}aqueous KOH solution [275].

In the work of Sun et al [276], the electrodes contained a mixture of 80wt% of nitrogen-doped rapeseed residues activated carbons (N-RC2),10wt% of carbon black and 10wt% of polyvinylidene fluoride (PVDF), coated on a 1.0cm^2 nickel foam current collector. For the symmetric button device, N-RC2 were used as the electrodes. The N-RC2 electrode fitted with a separator (thin polypropylene film) and 0.5molL^{-1} aqueous Na_2SO_4 solution electrolyte, were symmetrically assembled into the electrode/separator/electrode construction (sandwich-kind devices) [276]. In the work of Zhao et al [277], the CNFs were prepared in

the form of self-sustaining webs by thermal conversion of electrospun polyacrylonitrile (PAN) nanofibers in NH_3 atmosphere via stabilization and carbonization in a convectional tube furnance. The CNFs webs, glass fiber papers and Ni foils were cut into pieces of 1x2cm size and used as the electrodes, separator, and current collectors respectively. The CNFs webs were directly pasted on the glass fiber papers soaked in $1molL^{-1}$ aqueous Na_2SO_4 solution electrolyte, and were sandwiched between the pieces of Ni foils and the edges were sealed with polytetrafluoroethene [277].

The experimental results of the two button symmetric device fabricated with $Mn_2(PO_4)_2$// $Mn_2(PO_4)_2$ electrodes [275], presented in Tables 4.1 and 4.2, will be used alongside models to determine the level of agreement between models and experiments. Again, experimental data of the button symmetric device, fabricated with N-RC2//N-RC2 electrodes [276] presented in Tables 4.3, will be used to determine the level of agreement between models and experiments. Also, experimental data of the symmetric device, fabricated with CNFs //CNFs electrodes [277] presented in Tables 4.4, will be used to determine the level of agreement between models and experiments. Similar results of two coin asymmetric devices of different electrodes thickness, fabricated with $Mn_3(PO_4)_2$//AC electrodes, presented in Tables 4.5 and 4.6, will also be employed alongside models to see the extent of their agreement. Note that input data of these experiments, such as charging and discharging times, electrodes and electrolyte effective conductivities, cell voltage, cell mass and electrodes thickness, were used to calculate the performance parameters (specific capacitance, energy density and power density) from the models.

Table 4.1:Experimental results of the performance parameters of the symmetric capacitor with $Mn_3(PO_4)_2$ composite electrodes and aqueous 1molL^{-1} Na_2SO_4 electrolyte and voltage of 1.6V [275]

Symmetric cell with $Mn_3(PO_4)_2$//$Mn_3(PO_4)_2$ electrodes and aqueous 1molL^{-1} Na_2SO_4 electrolyte charged and cell voltage of 1.6V					
Current density (A/g)	Charging time (s)	Discharging time (s)	Specific capacitance (F/kg)	Energy density (Wh/kg)	Power density (W/kg)
0.50	200.0	175.0	53700	19.09	392.78
1.00	100.0	80.0	53100	18.88	790.33
2.00	50.0	37.5	52600	18.70	1602.86
3.00	30.0	25.0	52000	18.49	2465.19
4.00	25.0	20.0	51400	18.28	3193.80
5.00	20.0	15.0	50800	18.06	3989.20
10.00	15.0	10.0	47700	16.96	8033.68

Reproduced in part from *RSC Adv., 2016,6, 40077- 40085* with permission of The Royal Society of Chemistry, which was presented in appendix A3.

Table 4.2: Experimental results of performance parameters of a symmetric capacitor with $Mn_3(PO_4)_2$ composite electrodes and aqueous 2molL^{-1} KOH electrolyte and voltage of 1.6V [275]

Symmetric cell with $Mn_3(PO_4)_2$//$Mn_3(PO_4)_2$ electrodes and aqueous 2molL^{-1} KOH electrolyte charged and cell voltage of 1.6V					
Current density (A/g)	Charging time (s)	Discharging time (s)	Specific capacitance (F/kg)	Energy density (Wh/kg)	Power density (W/kg)
0.50	175.0	155.0	48400	17.21	399.72
1.00	95.0	50.0	47700	16.96	803.37
2.00	45.0	15.0	47100	16.75	1603.41
3.00	30.0	10.0	46500	16.53	2400.00
4.00	20.0	7.5	45900	16.32	3193.04
5.00	10.0	5.5	45200	16.07	3990.07
10.00	5.0	5.0	42700	15.18	8037.63

Reproduced in part from *RSC Adv., 2016,6, 40077- 40085* with permission of The Royal Society of Chemistry, which was presented in appendix A3.

Table 4.3: Experimental results of performance parameters of a symmetric capacitor with nitrogen-doped rapeseed activated carbons (N-RCs) composite electrode and aqueous 0.5molL^{-1} Na_2SO_4 electrolyte and voltage of 1.8V [276]

Symmetric cell with N-RC2//N-RC2 electrodes and aqueous 0.5molL^{-1} Na_2SO_4 electrolyte charged and cell voltage of 1.8V					
Current density (A/g)	Charging time (s)	Discharging time (s)	Specific capacitance (F/kg)	Energy density (Wh/kg)	Power density (W/kg)
0.25	200.0	150.0	62500	13.55	399.80
0.50	100.0	50.0	56250	10.88	790.33
1.00	50.0	25.0	55000	9.70	1380.86
2.00	20.0	7.5	53750	8.49	2230.19
3.00	15.0	5.0	52500	7.28	3031.86
5.00	5.0	3.0	51250	6.46	4240.20
8.00	2.5	2.0	50700	5.69	6401.00

Table 4.4: Experimental results of performance parameters of a symmetric capacitor with 1100CNF webs electrodes and aqueous 1molL^{-1} Na_2SO_4 electrolyte and voltage of 1.8V [277]

Symmetric cell with 1100CNF web//1100CNF web electrodes and aqueous 1molL^{-1} Na_2SO_4 electrolyte charged and cell voltage of 1.8V					
Current density (A/g)	Charging time (s)	Discharging time (s)	Specific capacitance (F/kg)	Energy density (Wh/kg)	Power density (W/kg)
0.5	400.0	230.0	64666.7	29.1	450.0
1.0	125.0	75.0	55555.6	25.0	1000.0
2.0	50.0	45.0	51555.6	23.2	2000.0
4.0	30.0	14.0	48000.0	21.6	3700.0
8.0	10.0	10.0	43111.1	19.4	7200.0

Table 4.5: Experimental results of performance parameters of an asymmetric capacitor with $Mn_3(PO_4)_2$ composite electrode, AC electrode and aqueous 1molL^{-1} Na_2SO_4 electrolyte and voltage of 1.6V [275]

Asymmetric cell with $Mn_3(PO_4)_2$//AC electrode with $Mn_3(PO_4)_2$, aqueous 2molL^{-1} Na_2SO_4 electrolyte and cell voltage of 1.6V					
Current density	Charging time (s)	Discharging time (s)	Specific capacitanc	Energy density	Power density

(A/g)			e (F/kg)	(Wh/kg)	(W/kg)
0.50	200.0	120.0	46800	16.64	399.36
1.00	100.0	45.0	46200	16.42	798.81
2.00	62.5	32.5	45600	16.21	1598.79
3.00	50.0	15.0	55000	16.00	2400.00
4.00	37.5	12.5	44300	15.75	3194.37
5.00	25.5	12.5	43700	15.54	3996.00
10.00	10.0	10.0	41800	14.86	7984.48

Reproduced in part from *RSC Adv., 2016,6, 40077- 40085* with permission of The Royal Society of Chemistry, which was presented in appendix A3.

Table 4.6: Experimental results of performance parameters of an asymmetric capacitor with $Mn_3(PO_4)_2$ composite electrode, AC electrode and aqueous 2molL^{-1} KOH electrolyte and voltage of 1.6V [275]

Asymmetric cell with $Mn_3(PO_4)_2$//AC electrodes with $Mn_3(PO_4)_2$, aqueous 2molL^{-1} KOH electrolyte and cell voltage of 1.6V					
Current density (A/g)	Charging time (s)	Discharging time (s)	Specific capacitance (F/kg)	Energy density (Wh/kg)	Power density (W/kg)
0.50	175.0	125.0	41900	14.89	400.03
1.00	75.0	55.0	41200	14.65	800.24
2.00	35.0	25.0	40600	14.43	1599.02
3.00	25.0	22.0	39900	14.19	2397.75
4.00	20.0	10.0	39300	13.97	3204.07
5.00	12.5	7.5	38600	13.72	3984.50
10.00	2.5	2.5	37100	13.19	8048.81

Reproduced in part from *RSC Adv., 2016,6, 40077- 40085* with permission of The Royal Society of Chemistry, which was presented in appendix A3.

CHAPTER FIVE

5.0 Results and Discussions

Results were discussed here in four parts, namely: the effects of self-discharge on the performance of symmetric electric double layer capacitors and active electrolyte enhanced supercapacitors; the effects of self-discharge on the performance of asymmetric/hybrid electrochemical capacitors; the effects of operating conditions and design configurations on the performance of electrochemical capacitors; and the optimization of design parameters and operating conditions of electrochemical capacitors for high performance. Three of these parts from have been published as stated in the list of publications, and were presented in this thesis with permission from the publishers shown in appendices A4, A5 and A6, respectively.

5.1.1 The Effects of Self-Discharge on the Performance of Symmetric Electric Double Layer Capacitors and Active Electrolyte Enhanced Supercapacitors: Insights from Modelling and Simulation.

In order to either simplify the models, or to facilitate a solution of the models, all the existing models of EDLCs were built on the assumption that either the electrodes or the capacitor do not have self-discharge. All existing models equally fail toexhibit significant responsibility of current in presenting the mechanism of self-discharge. Whereas numerous models for symmetric ECs have been developed, to the best of my knowledge, there has not been a general model that incorporated self-discharge and solved, subjects to self-discharge. The purpose of this section is to discuss the effects of self-discharge on the performance of symmetric EDLCs and AEECS by incorporating self-discharge into the models during the

charging and discharging processes. It was presumed that the coefficient of diffusivity in the solid and solution phases, and the transport number are not dependent on electrolyte concentration. It was also assumed that sources of self-discharge here are side-reactions or reactions of active redox species and several impurities in the electrodes, electrolytes, separator, current collectors of the device and various functional groups on CNTs electrodes. Side-reactions perform a very dominant role in considering the mechanism of self-discharge. The side-reactions or reactions of the active redox species, several impurities and instability of the electric double layers, are responsible for self-discharge processes. This will provide a platform on which to study the effect of each self-discharge parameter and how they could be adjusted to improve the performance of EDLCs and active electrolyte enhanced supercapacitors (AEESCs).

5.1.2 Discussions

The experimental data used in simulations were based on the works of Kazaryan and co-worker [89], Staser and Weidner [90] and [265] as presented in Table 5.1 . Reasonable values were assumed for unavailable parameters based on literature. The symmetric device discharged to 0.00V was charged by constant current to upper voltage of 1.20V for the charging duration (t_{ch}) of 5hrs. Thereafter it was discharged by constant current from 1.20V to lower voltage of 0.00V for the discharge duration (t_{dis}) of 5hrs. The electrode effective conductivity α_1 was varied in the simulation as follows: 0.0005, 0.0010, 0.0050, and 0.0500S/cm, while the following charging conditions were also considered 0.0053A/cm^2 for 18000s, 0.0533A/cm^2 for 1800s, 0.5330A/cm^2 for 180s and 5.3300A/cm^2 for 18s. Selection of the charging conditions is based on the fact that low current density needs longer time, while high current density needs shorter time. The first current density was multiplied by

factor of 10, 100 and 1000 while charging time was divided by the same factor to get the second, third and fourth conditions, respectively. The potential difference of negative and positive electrodes under is 0.60V and – 0.60V respectively, hence their potential before and after charging was assumed to be 0.00V & 0.00V and 0.60V & – 0.60V, respectively.

The three cases examined here are as follows:

(1) Device without self-discharge, $J_{VR}(x,t)$=0;

(2) Device with only electric double layers (EDLs) instability self-discharge, $J_{VR}(x,t)=J_{VR}$;and

(3) Device with both EDLs instability and the side-reactions or redox reactions of active redox species self-discharges, $J_{VR}(x,t)= J_{VR}+J_{VR1}(t)$.

Simulation and computation of the performance parameters of the EDLC without self-discharge, with only the EDL's instability self-discharge, and with both side-reactions/redox reactions and the EDL's instability self-discharge during charging and discharging, were performed. The simulation and computation of the performance parameters of EDLCs with self-discharge during charging and discharging were also performed, with tuned key self-discharge parameters. The purpose of calculation of these parameters is to clearly reveal the effects of self-discharge on the performance of devices with self-discharge.

Table 5.1: The model parameters used for simulation of the effects of self-discharge on the performance of symmetric electric double layer capacitors and active electrolyte enhanced supercapacitors

Parameters	**Units**	**Separator**	**Positive electrode**	**Negative electrode**
Applied current density, J_0	A/cm^2	–	0.00533 [89]	–
Capacitance per unit volume, C_v	F/cm^3	–	400 [89]	400 [89]

Electrode thickness, w_e	cm	–	0.2 [89]	0.2 [89]
Electrode visible surface area, A	cm^2	–	6290 [89]	6290 [89]
Electrode effective conductivity, α_1	S/cm	–	0.0005- 0.05 [89]	0.0005-0.05 [89]
Electrolyte effective conductivity, α_2	S/cm	–	0.05 [89]	0.05 [89]
Separator's thickness, w_{sp}	cm	0.05 [89]	–	–
Electrode density, ρ_e	g/cm^3		1.0 [90]	1.0 [90]
Electrolyte density, ρ_l	g/cm^3		1.25 [90]	1.25 [90]
Separator density, ρ_{sp}	g/cm^3		0.95 [90]	–
Electrode porosity, ε_e	–	–	0.25 [90]	0.25 [90]
Separator porosity, ε_{sp}	–	0.70 [90]	–	–
Specific internal ohmic resistance, ρ_{int}	Ωcm^2	–	9 [89]	9 [89]
Oxidized species concentration, C_{Ox}	$mole/cm^3$	–	0.0003 [265]	–
Oxidized species diffusivity, D_{Ox}	cm^2/s	–	0.000018 [265]	–
Thickness of separator and anode, l	cm	0.25 [265]	–	–
Volume of reduced species, V	cm^3	–	0.1 [265]	–
Number electrons transferred, n	–	–	2	–
Ideal gas constant, R	J/mole K,	–	8.31447	–
Faraday constant, F	coul/equiv		96487	–
Absolute temperature, T	^0K	–	298	–
Electrode potential before charging, $\varphi_e^{0^+}$	V	–	0 [assumed]	0 [assumed]
Electrode potential before discharge $\varphi_e^{0^-}$	V	–	0.6 [assumed]	-0.6 [assumed]
Charge and discharge time, t	S	–	18000	–
Pi, π	–	–	22/7	–

The potential profiles in Figure 5.1 shows that the surface layer of electrodes are charged more efficiently, compared with the central part as expected, and are more noticeable in capacitors with low electrode and electrolyte effective conductivities. This was due to the fact

that in devices of low electrode and electrolyte effective conductivities, there was great resistance to ionic charge movement through various electrode pores, thereby creating high potential during charging time, but the potential decays after a long pause, when ions move deep inside smaller pores. In the case without self-discharge, the electrode was charged to designed potential as shown in Figure 5.1a, compared with only the EDL's instability self-discharge, where the electrode was charged to potential slightly below target potential as seen in Figure 5.1b.

In the case with both side-reactions/redox reactions and the EDL's instability self-discharge, the electrode was charged to a potential much below the target potential as presented in Figure 5.1c. For example, the electrode of the capacitor with electrode and electrolyte effective conductivity $\alpha_1 = \alpha_2 =$ 0.05S/cm was charged to – 0.60V, – 0.55V and – 0.40V in the case without self-discharge, with only the EDL's instability self-discharge and with both side-reactions/redox reactions and the EDLs instability self-discharge respectively, as shown in Figure 5.1.

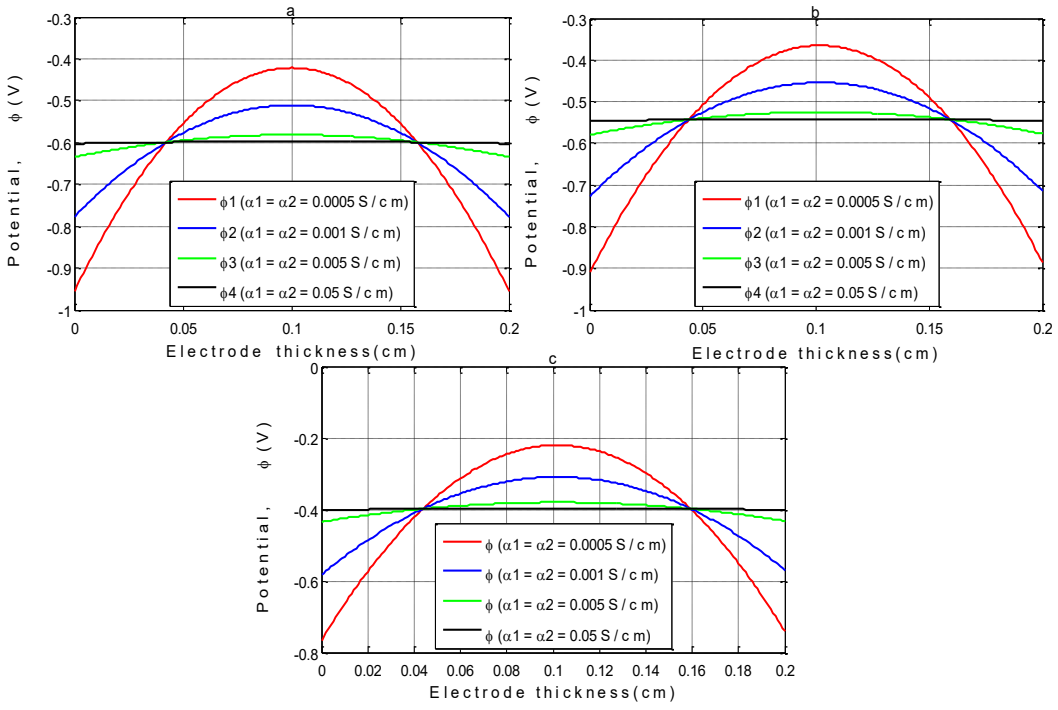

Figure 5.1: Potential distribution profiles within the negative electrode of different electrode and electrolyte effective conductivities values α_1 and α_2 as a function of position after constant current charging process for (a) capacitors without self-discharge (b) capacitors with only the EDL's instability self-discharge, and (c) capacitors with both side-reactions/redox reactions and the EDL's instability self-discharge.

Similarly, potential profiles of an electrode of different electrode and electrolyte effective conductivities at the end of constant current discharging process of capacitors without self-discharge, with only the EDLs instability self-discharge and with both side-reactions/redox reactions and the EDLs layers instability self-discharge follow the same pattern as shown in Figure 5.2. The electrode of capacitors without self-discharge, with only the EDLs instability self-discharge and with both side-reactions/redox reactions and EDLs instability self-discharge was discharged to 0.00V, 0.05V and 0.20V respectively in the device with $\alpha_1 = \alpha_2 =$ 0.05S/cm as shown in Figures 5.2a, 5.2b and 5.2c respectively.

The effects of charge redistribution was present in both charging and discharging processes in the three cases under consideration, but were more noticeable in capacitors with low electrode and electrolyte effective conductivities. For instance, the voltage of the capacitor with $\alpha_1 = \alpha_2 =$ 0.05S/cm, at the end of the charging process, was 1.55V, 1.50V and 1.35V in the device without self-discharge, with only the EDL's instability self-discharge and with both side-reactions/redox reactions and the EDL's instability self-discharge respectively, but decreased to 1.20V after a long pause. Similarly, voltage of the same capacitor at the end of the discharging process was – 0.35V,–0.30V and – 0.15V in the device without self-discharge, with only the EDL's instability self-discharge and with both side-reactions/redox reactions and the EDL's instability self-discharge respectively, but increased to 0.00V after a long pause.

In the three conditions considered, there was levelling of the charge (potential decay) along the electrode's thickness after the capacitor charging process and another levelling of the charge (potential growth) along the electrodes thickness after the capacitor discharging process. The levelling processes resulted in energy loss and gain, which is dependent on the parameter and mode of charging and discharging of the electrodes, in line with results in literature [89,278,279].

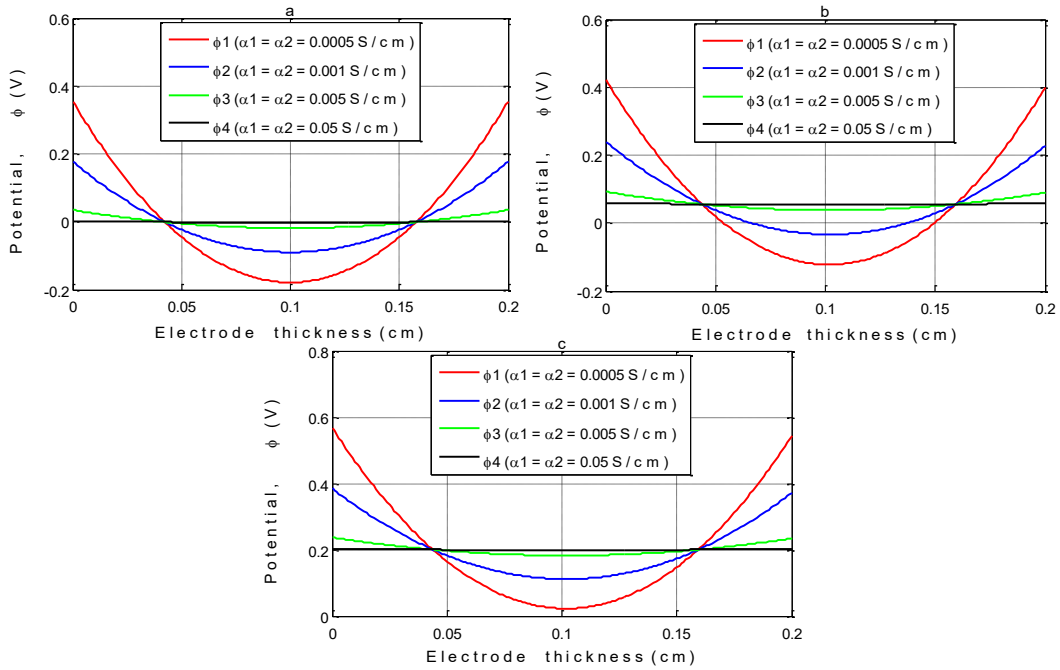

Figure 5.2: Potential distribution profiles within the negative electrode of different electrode and electrolyte effective conductivities values α_1 and α_2 as a function of position after constant current discharging process for (a) capacitors without self-discharge (b) capacitors with only EDLs instability self-discharge, and (c) capacitors with both side-reactions/redox reactions and EDLs instability self-discharge.

Figure 5.3 depicts EC voltage dependence on time during the constant current charging process in a device without self-discharge, with only the EDLs layers instability self-discharge and capacitors with both the side-reactions/redox reactions and EDL's instability self-discharge. The voltage of devices with low electrode and electrolyte effective

conductivities were charged from 0.00V to values higher than the target upper voltage of 1.20V and then reduced to 1.20V after a long pause, because of high charge redistribution in the capacitor's electrodes. Charge redistribution was negligible in capacitors with high electrode and electrolyte effective conductivities, since their voltage did not reduce, but remained approximately the same after a long pause. The voltage of the capacitor electrode and electrolyte effective conductivity $\alpha_1 = \alpha_2 =$ 0.05S/cm at the end of the charging process was 1.20V, 1.15V and 1.00V in the capacitor without self-discharge, with only the EDL's instability self-discharge and capacitors with both side-reactions/redox reactions and EDL's instability self-discharge respectively, as shown in Figure 5.3. A voltage drop of 0.05V and 0.20V were experienced in capacitors as a result of only the EDL's instability self-discharge and both side-reactions/redox reactions and the EDL's instability as seen in Figure 5.3b and 5.3c, respectively.

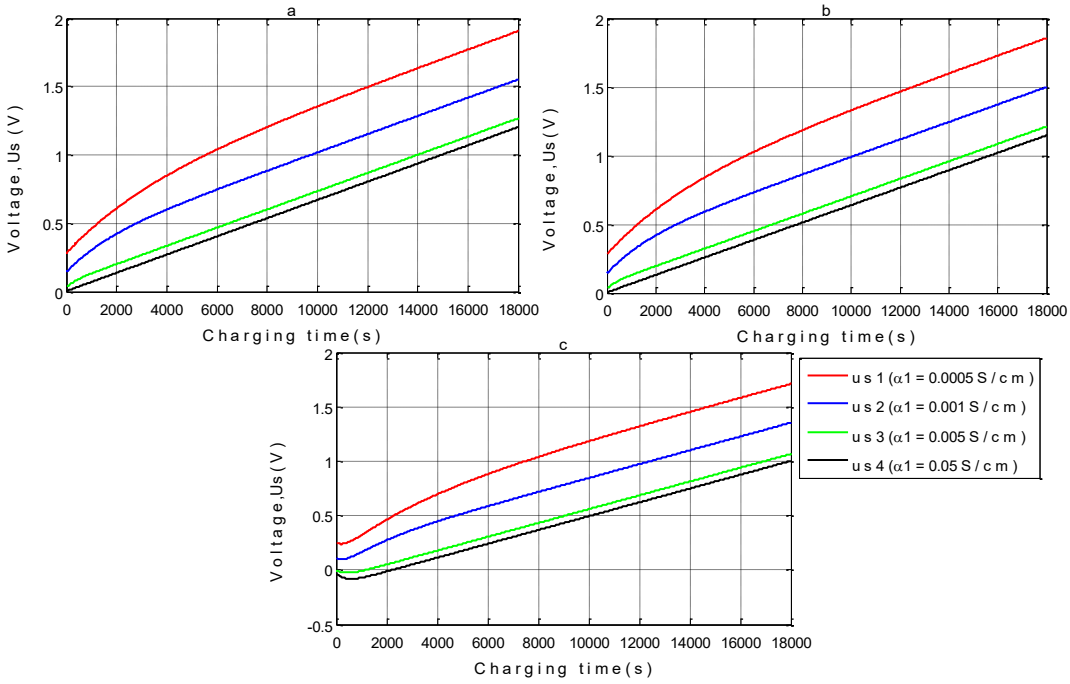

Figure 5.3: Electrochemical capacitor voltage dependence on time during 18000s duration of constant current charging process for (a) capacitors without self-discharge, (b) capacitors

with only the EDL's instability self-discharge, and (c) capacitors with both side-reactions/redox reactions and the EDL's instability self-discharge.

In the same way, devices with low electrode and electrolyte effective conductivities were discharged to values below the target lower voltage of 0.0V and then increased to 0.0V after long pause, because of high charge redistribution in the capacitor's electrodes as shown in Figure 5.4. The voltage of the capacitor of $\alpha_1 = \alpha_2 =$ 0.05S/cm at the end of the discharge process was 0.00V, – 0.05V and – 0.20V in the capacitor without self-discharge, with only the EDL's instability self-discharge and both side-reactions/redox reactions and the EDL's instability self-discharge respectively, as shown in Figure 5.4. The same capacitor with only the EDL's instability self-discharge was entirely discharged to the target lower voltage within 17000s against 18000s, while that with both side-reactions/redox reactions and the EDL's instability self-discharge was within 15000s because of self-discharge as shown in Figures 5.4b and 5.4c.

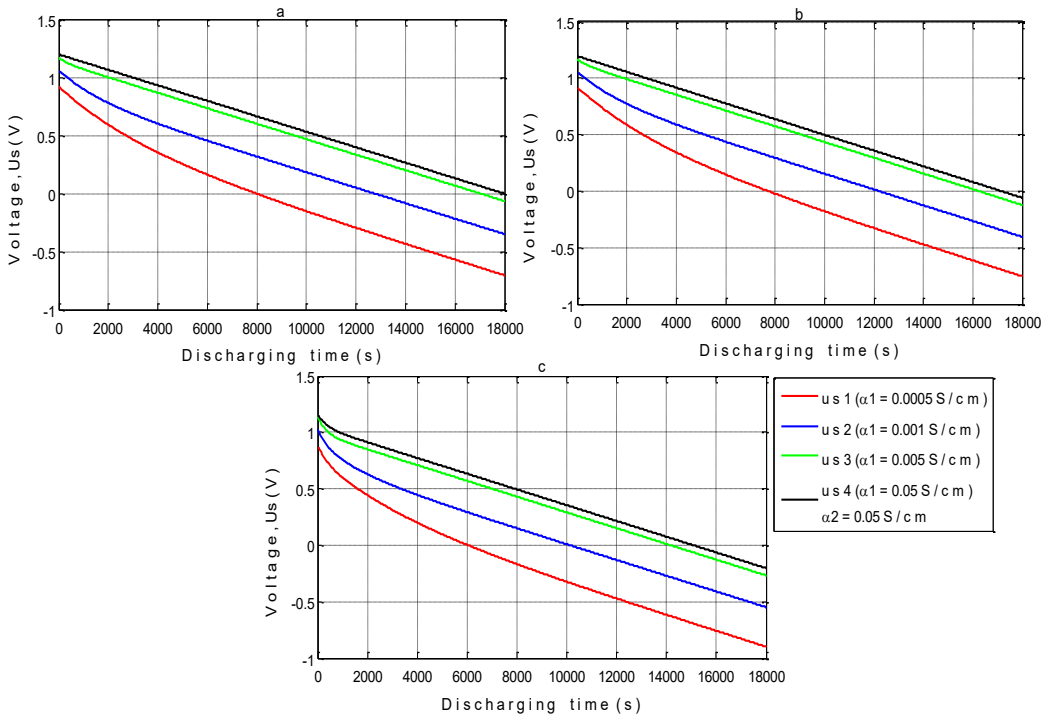

Figure 5.4: Electrochemical capacitor voltage dependence on time during 18000s duration of constant current discharging process for (a) capacitors without self-discharge, (b) capacitors with only the EDL's instability self-discharge, and (c) capacitors with both side-reactions/redox reactions and the EDL's instability self-discharge.

Figure 5.5 present the profiles of voltage dependence on time for constant current charging of capacitors with different electrode and electrolyte effective conductivities from 0.00V to 1.20V. It follows from Figure 5.5 that the capacitor's voltage profiles during charging and discharging were nonlinearly dependent on time, and this nonlinearity dependence on time reduced as the effective conductivity of the electrodes was increased. The device without self-discharge was charged from 0.00V to target voltage of 1.20V within target charging time, as shown in Figure 5.5a; whereas the device with only the EDL's instability self-discharge was charged from 0.00V to 1.15V, which was less than the target voltage within the target time as seen in Figure 5.5b. The capacitor with both side-reactions/redox reactions and the EDL's instability self-discharge was charged from 0.00V to 1.00V, which was also less than the target voltage of 1.20V within the target time as seen in Figure 5.5c.

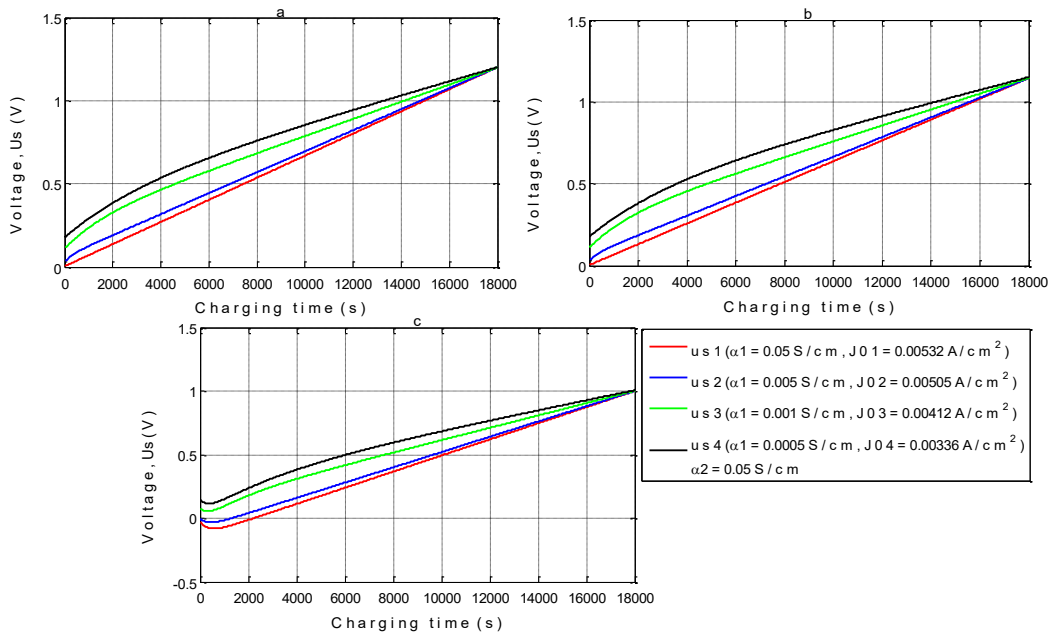

Figure 5.5: Electrochemical capacitor voltage dependence on time during 18000s duration of constant current charging process from 0.0V to 1.2V for (a) capacitors without self-discharge, (b) capacitors with only the EDL's instability self-discharge, and (c) capacitors with both side-reactions/redox reactions and the EDL's layers instability self-discharge.

It follows from Figure 5.6 that an increase in charging current density and a reduction in charging time reduced voltage drop in capacitors with self-discharge, provided that the effective conductivities are high enough to permit easy movements of charges through electrodes at such a high rate. Capacitors with only the EDL's instability self-discharge were charged fast from 0.00V to 1.18V within the target time as seen in Figure 5.6b. Also, capacitors with both side-reactions/redox reactions and EDL's instability self-discharge were charged fast from 0.00V to 1.10V within the target time as shown in Figure 5.6c.

It is important to note that when capacitors were charged and discharged fast, energy loss by self-discharge was reduced to the barest minimum as long as electrodes and electrolyte effective conductivity were high enough and concentrations of impurities were not increased in the course of enhancing electrode and electrolyte effective conductivity, as shown in Figures 5.6b & 5.6c and 5.8b & 5.8c. The fast charging process reduced the voltage drop in the capacitor with only the EDL's instability self-discharge and those with both side-reactions/redox reactions and the EDL's instability self-discharge from 0.05V to 0.02V and 0.20V to 0.10V respectively.

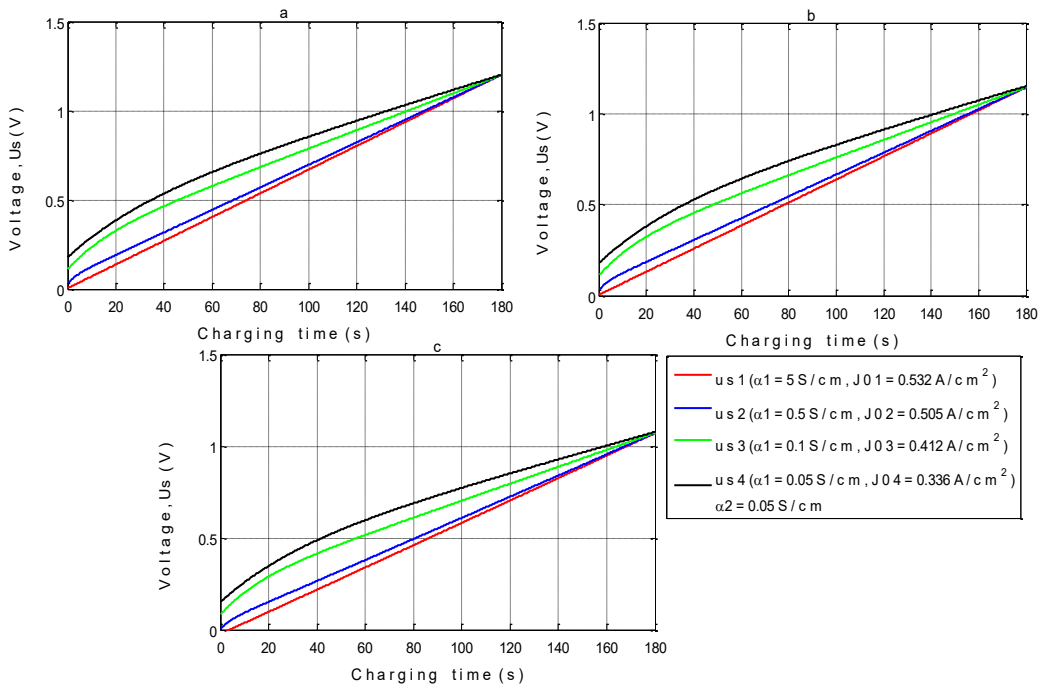

Figure 5.6: Electrochemical capacitor voltage dependence on time during 180s duration of constant current charging process from 0.0V to 1.2V for (a) capacitors without self-discharge, (b) capacitors with the only EDL's instability self-discharge, and (c) capacitors with both side-reactions/redox reactions and the EDL's instability self-discharge.

The device without self-discharge was discharged from 1.2V to the target lower voltage of 0.0V within the target discharging time (18000s) as shown in Figure 8a; while those with only the EDL's instability self-discharge were discharged from 1.2V to 0.0V within 17000s, quite before the target discharging time as shown in Figure 5.7b. capacitors with both side-reactions/redox reactions and instability self-discharge were also discharged from 1.2V to 0.0V within 15000s, well before the target time as seen in Figure 5.7c. This fast discharging reduced the voltage drop in capacitors with only the EDL's instability self-discharge and those with both side-reactions/redox reactions and the EDL's instability self-discharge as shown in Figures 5.8b and 5.8c respectively.

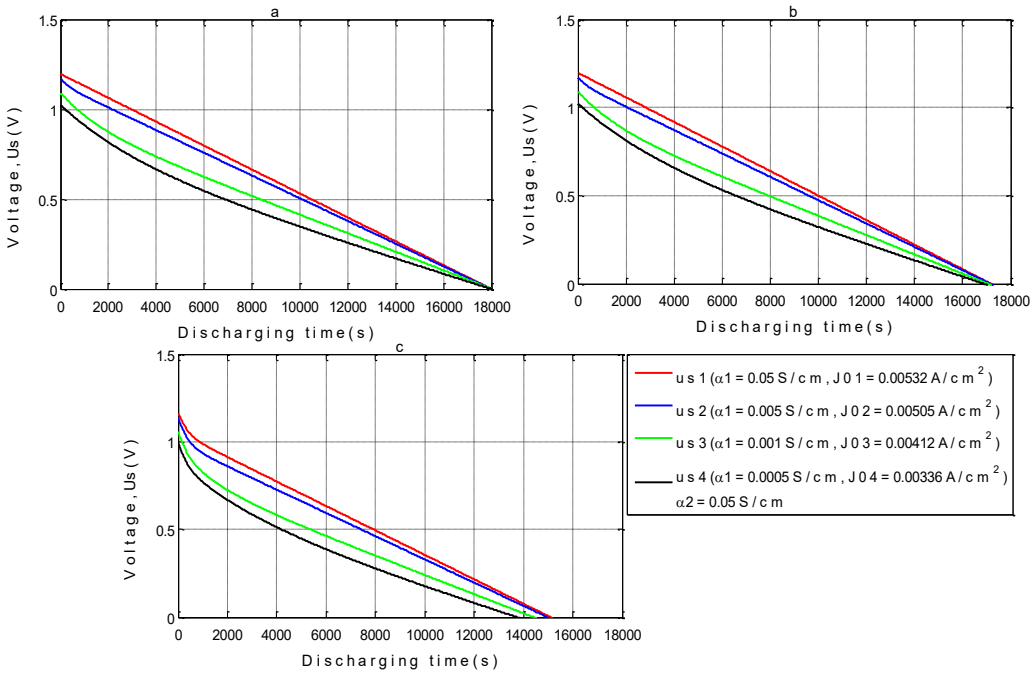

Figure 5.7: Electrochemical capacitor voltage dependence on time during 18000s duration of constant current discharging process from 1.2V to 0.0V for (a) capacitors without self-discharge, (b) capacitors with only the EDL's instability self-discharge, and (c) capacitors with both side-reactions/redox reactions and the EDL's instability self-discharge.

In comparison, it took capacitors with self-discharge more than the target charging time to be fully charged as seen in Figures 5.5b, 5.5c, 5.6b and 5.6c, while devices without self-discharge were completely charged within the target charging time as presented in Figures 5.5a and 5.6a. Also, it took fully charged capacitors with self-discharge a shorter time than the target discharging time to be completely discharged by self-discharge, as was evident in Figures 5.7b, 5.7c, 5.8b and 5.8c.

Figure 5.9 shows that at the end of 18000s constant current charging of the capacitor of $\alpha_1 = \alpha_2 =$ 0.05S/cm without self-discharge, the voltage was 1.2000V as seen in Figure 5.9a. The voltage of a similar capacitor, with only the EDL's instability self-discharge charged under the same conditions, was 1.1490V at the end of the charging process as shown in Figure 5.9b. The voltage of a similar capacitor with both side-reactions/redox reactions and

the EDL's instability self-discharge was 1.0700V under the same charging conditions as depicted in Figure 5.9b. It follows from Figure 5.10 that whereas the voltage of a device of

$\alpha_1 =$ 0.05S/cm and $\alpha_2 =$0.05S/cm without self-discharge at the end of the 180s constant current charging process was 1.2000V as seen in Figure 5.10a, that of similar device with only the EDL's instability self-discharge, charged under the same conditions was 1.1996V at the end of the charging process as shown in Figure 5.10b.

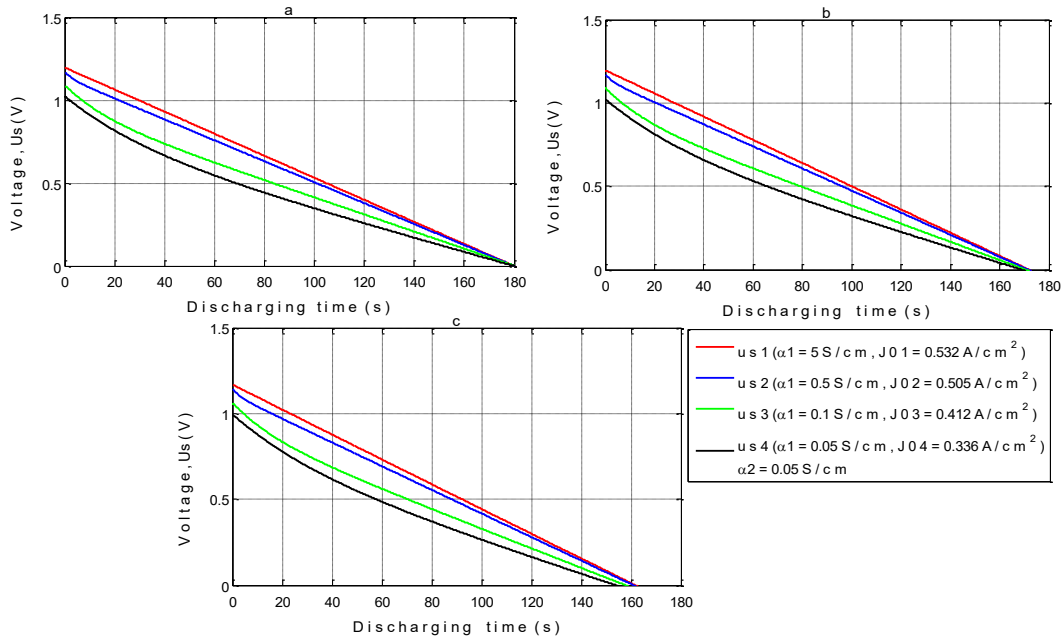

Figure 5.8: Electrochemical capacitor voltage dependence on time during 180s duration of constant current discharging process from 1.2V to 0.0V for (a) capacitors without self-discharge, (b) capacitors with only the EDL's instability self-discharge and (c) capacitors with both side-reactions/redox reactions and the EDL's instability self-discharge.

Also, the voltage of a similar capacitor with both side-reactions/redox reactions and the EDL's instability self-discharge was 1.1525V under the same charging conditions as depicted in Figure 5.10b. This shows that when capacitors with self-discharge were charged fast, by increasing applied current density and reducing charging time without any increase in concentrations of impurities, 0.0505V and 0.0825V respectively were conserved by charging

the capacitors with self-discharge fast (180s) as presented in Figures 5.10b and 5.10c. Both capacitors with and without self-discharge liberate some portion of their storable energy as polarization resistance energies E_{ch}^{Rpol} and E_{dis}^{Rpol} during device charging and discharging. Also, they all liberate some portion of their storable energy as depolarization energies E_{ch}^{dpol} and E_{dis}^{dpol} during capacitors charging and discharging respectively.

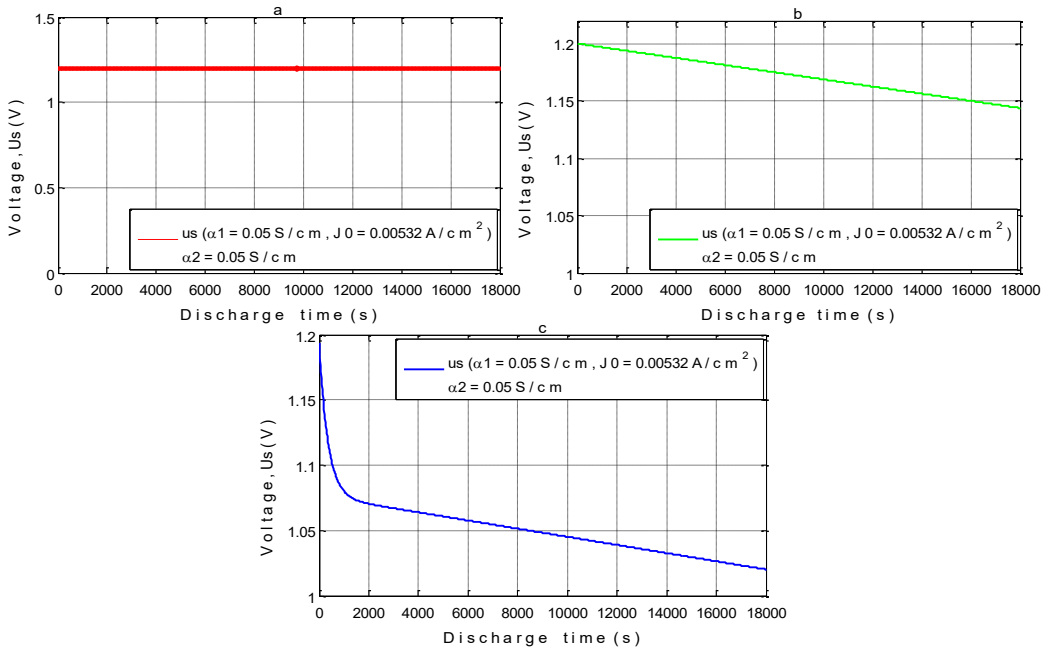

Figure 5.9: The voltage $U_S(t)$ dependence on time for symmetric EDLCs with effective conductivities of 0.05S/cm during 18000s duration of constant current charging process from 0.0V to 1.2V for (a) capacitors without self-discharge, (b) capacitors with only EDL's instability self-discharge, and (c) capacitors with both side-reactions/redox reactions and EDL's instability self-discharge.

These energies are considerably dependent on the effective conductivity of the electrodes and electrolyte conductivity α_1 and α_2, and are more evident in capacitors of low electrodes and electrolyte effective conductivities. Again, ohmic resistance energies E_{ch}^{R} and E_{dis}^{R} are released due to internal ohmic resistance during capacitor charging and discharging.

Equations 4.72, 4.78, 4.75 – 4.76, 4.83 – 4.84, 4.88 – 4.89, and 4.95 – 4.97 were used to calculate performance parameters of the devices in the cases presented in Tables 5.2 – 5.4. It follows from Table 5.2 that total energy loss by polarization resistance, depolarization and internal ohmic resistance in the capacitor without self-discharge during charging and discharging was 17.21Wh; and 24.72Wh and 55.06Wh in similar a capacitor with only the EDL's instability self-discharges and both side-reactions/redox reactions and the EDL's instability self-discharges respectively. Energy loss by only the EDL's instability self-discharge and both side-reactions/redox reactions and the EDL's instability self-discharge during charging and discharging, amounted to 9.73Wh and 28.38Wh respectively, as presented in Table 5.2.

Storable energy in the device with only the EDL's instability self-discharge and both side-reactions/redox reactions and the EDL's instability self-discharge, was 96.50Wh and 70.24Wh respectively, as compared with 101.20Wh in a similar device without self-discharge. Also, deliverable energy in the two capacitors with self-discharge was 90.86Wh and 50.56Wh respectively, while in a similar device without self-discharge it was 100.10Wh. Capacitors with self-discharge lost portions of energy by self-discharge during charging and discharging. In the first and second charge–discharge cycles η_{E1} and η_{E2}, the energy efficiencies of the three capacitors were 84.24% & 84.25%, 72.33% & 72.34% and 38.13% & 38.14% in device without self-discharge, with only the EDL's instability self-discharge, and with both side-reactions/redox reactions and the EDL's instability self-discharge respectively.

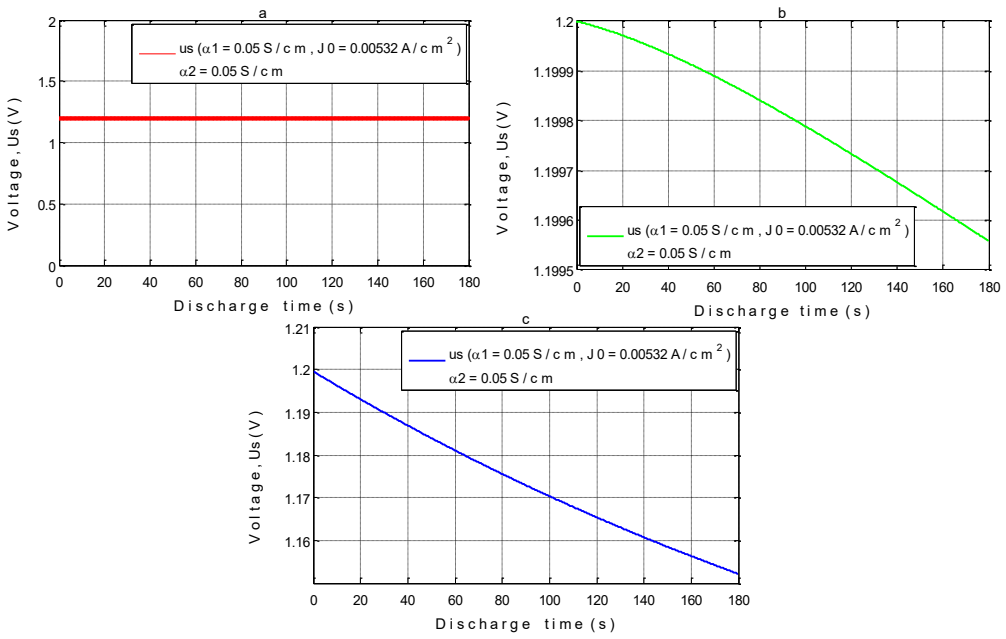

Figure 5.10: The voltage $U_S(t)$ dependence on time for symmetric EDLCs with effective conductivities of 0.05S/cm during 180s duration of constant current charging process from 0V to 1.2V for (a) capacitors without self-discharge, (b) capacitors with only the EDL's instability self-discharge, and (c) capacitors with both side-reactions/redox reactions and the EDL's instability self-discharge.

Side-reactions/redox reactions self-discharges in the device with a high concentration of redox species, contributed the majority of self-discharge in symmetric EDLCs and AEESs as presented in case 3 of Table 5.2. When products of redox reactions are insoluble in electrolyte solution, they adsorbed onto electrodes which resulted in the suppression of self-discharge and enhanced device capacitance, as presented and explained in the work of Chen et al and Ike et al [245,280]. It follows from equations 3.52 and 3.62 that reduction of the concentration of impurities ions and redox species and the increase in the separator thickness, reduced the current densities of only the EDL's instability self-discharge and both side-reactions/redox reactions and the EDL's instability self-discharge J_{VR} and J_{VR1} to $4.0\text{x}10^{-4}$A/cm^2 and $9.58\text{x}10^{-5}$A/cm^2 respectively.

Table 5.2: Parameters of symmetric EDLCs without self-discharge, with only the EDL's instability self-discharge, and with both side-reactions/redox reactions and the EDL's instability self-discharge during charging and discharging processes.

S/N	Parameter	Unit	α_2 = 0.05 S/cm					
			Case 1:Without Self-discharge and w_{sp} = 0.05cm		Case 2: N = 10^{20}cm^{-3}, w_{sp} = 0.05cm , and J_{VR} =1.25x10^{-3}A/cm^2		Case 3: N =10^{20}cm^{-3}, w_{sp} = 0.05cm, J_{VR} = 1.25x10^{-3}A/cm^2 and D_{Ox} =1.8x10^{-5}cm^2/s, C_{Ox} =3.0x10^{-4} mole/cm^3, J_{VR1} = 9.58x10^{-4}A/cm^2	
			α_1		α_1		α_1	
			0.0005	**0.0500**	**0.0005**	**0.0500**	**0.0005**	**0.0500**
1	E_{Sch}	Wh	87.240	101.20	82.210	96.500	66.786	70.242
2	E_{Sdis}	Wh	45.110	100.10	39.392	90.862	17.447	50.557
3	$I_{selfdis}$	A	0.0000	0.0000	0.7862	0.7862	2.8092	2.8092
4	$Q_{selfdis}$	Ah	0.0000	0.0000	13.967	15.743	54.428	66.987
5	$E_{selfdis}$	Wh	0.0000	0.0000	13.879	9.7336	34.497	28.377
6	$_{ERpol}$	Wh	26.140	1.0840	29.479	4.8039	21.025	1.1184
7	$_{ER}$	Wh	4.4820	16.050	4.4812	16.047	4.4812	16.047
8	$_{Edpol}$	Wh	4.1410	0.0820	2.4701	0.1327	28.170	15.517
9	E_{Tloss}	Wh	34.750	17.210	42.309	24.717	70.173	55.058
10	ED_{sy}	Wh/kg	30.992	35.957	29.204	34.282	23.726	24.953
11	PD_{sy}	W/kg	6.1829	7.1734	5.8263	6.8393	4.7333	4.9782
12	$\delta_{Eselfdis}$	%	0.0000	0.0000	14.879	8.5707	36.403	27.386
13	δ_{ET}	%	38.430	15.776	45.934	21.047	74.493	52.930
14	η_{E1}	%	54.600	84.241	34.416	72.334	6.8300	38.130
15	η_{E2}	%	54.620	84.245	38.763	72.340	7.2474	38.144

Tuning the key self-discharge parameters as in Table 5.3 reduced the energy loss in the capacitor with only the EDL's instability self-discharge and both side-reactions or redox reactions and the EDL's instability self-discharge during charging and discharging to 3.02Wh and 5.60Wh respectively. The tuning effect reduced self-discharge and increased storable energy in the two capacitors, with self-discharge to 98.22Wh and 95.84Wh respectively, while deliverable energy was equally increased to 97.06Wh and 92.37Wh respectively as shown in Table 5.3. The first and second charge–discharge cycle energy efficiency of the capacitor with only the EDL's instability self-discharge and both side-reactions/redox

reactions and the EDL's instability self-discharge increased to 81.48% & 82.01% and 77.00% & 77.53% respectively as shown in Table 5.3.

Table 5.3: Parameters of symmetric EDLCs without self-discharge, with only the EDL's instability self-discharge, and with both side-reactions/redox reactions and the EDL's instability self-discharge during charging and discharging processes.

S/N	Parameter	Unit	α_2 = 0.05 S/cm					
			Case 1:Without Self-discharge and w_{sp} = 0.1cm		Case 2: N= $10^{19}cm^{-3}$, w_{sp} = 0.1cm , and J_{VR} =4.0x10^{-4}A/cm^2		Case 3: N =$10^{19}cm^{-3}$, w_{sp} = 0.1cm, J_{VR} =4.0x10^{-4}A/cm^2 and D_{Ox} =1.8x$10^{-6}cm^2$/s, C_{Ox} = 3.0x10^{-5} mole/cm^3, J_{VR1} = 9.58x10^{-5}A/cm^2	
			α_1		α_1		α_1	
			0.0005	**0.0500**	**0.0005**	**0.0500**	**0.0005**	**0.0500**
1	E_{Sch}	Wh	87.240	101.20	85.820	98.224	84.286	95.842
2	E_{Sdis}	Wh	45.110	100.10	43.354	97.059	40.651	92.365
3	$I_{selfdis}$	A	0.0000	0.0000	0.5032	0.5032	0.9058	0.9058
4	$Q_{selfdis}$	Ah	0.0000	0.0000	4.4696	5.0378	8.4960	9.0643
5	$E_{selfdis}$	Wh	0.0000	0.0000	4.6672	3.0250	8.5410	5.6005
6	$_{ERpol}$	Wh	26.140	1.0840	10.068	1.0840	9.1089	0.1500
7	$_{ER}$	Wh	4.4820	16.050	4.4812	16.047	4.4812	16.047
8	$_{Edpol}$	Wh	4.1410	0.0820	16.537	0.1487	16.325	2.5296
9	E_{Tloss}	Wh	34.750	17.210	35.753	19.633	43.876	24.327
10	ED_{sy}	Wh/kg	30.992	35.957	27.562	31.545	27.068	30.780
11	PD_{sy}	W/kg	6.1829	7.1734	5.4986	6.2933	5.4003	6.1407
12	$\delta_{Eselfdis}$	%	0.0000	0.0000	5.0902	2.7686	9.2304	5.1263
13	δ_{ET}	%	38.430	15.776	38.993	17.969	41.560	22.267
14	η_{E1}	%	54.600	84.241	43.708	81.479	38.770	77.003
15	η_{E2}	%	54.620	84.245	58.826	82.014	54.658	77.530

Further tuning of these key self-discharge parameters as shown in in Table 5.4, reduced energy loss in the device with only the EDL's instability self-discharge and both side-reactions/redox reactions and EDLs instability self-discharge further to 0.94Wh and 1.11Wh respectively. Storable energy in these two capacitors with self-discharge was further improved to 100.89Wh and 99.52Wh respectively, compared with 101.20Wh in the device without self-discharge, as presented in Table 5.4. The first and second charge–discharge cycle energy efficiency of the capacitor with only the EDL's instability self-discharge and

both side-reactions/redox reactions and the EDL's instability self-discharge improved to 83.98% & 84.22% and 80.54% & 81.56% respectively. Figures 5.11 and 5.12 depict voltage decay on the storage time of the symmetric EDLC with different electrodes effective conductivities and different self-discharge processes. The time to entirely discharge the fully charged capacitor on storage by different self-discharge processes, greatly depends on the key self-discharge parameters.

Table 5.4: Parameters of symmetric EDLCs without self-discharge, with only the EDL's instability self-discharge, and with both side-reactions/redox reactions and the EDL's instability self-discharge during charging and discharging processes.

S/N	Parameter	Unit	α_2 = 0.05 S/cm					
			Case 1:Without Self-discharge and w_{sp} = 0.1cm		Case 2: N = 10^{18}cm^{-3}, w_{sp} = 0.1cm , and J_{VR} = 4.0x10^{-5}A/cm^2		Case 3: N = 10^{20}cm^{-3}, w_{sp} = 0.1cm, J_{VR} = 4.0x10^{-5}A/cm^{2}and D_{Ox} =1.8x10^{-6}cm^2/s, C_{Ox} = 3.0x10^{-5} mole/cm^3, J_{VR1} = 9.58x10^{-5}A/cm^2	
			α_1		α_1		α_1	
			0.0005	**0.0500**	**0.0005**	**0.0500**	**0.0005**	**0.0500**
1	E_{Sch}	Wh	87.240	101.20	87.150	100.89	85.820	99.520
2	E_{Sdis}	Wh	45.110	100.10	45.067	99.746	42.310	95.990
3	$I_{selfdis}$	A	0.0000	0.0000	0.0504	0.0504	0.4530	0.4530
4	$Q_{selfdis}$	Ah	0.0000	0.0000	0.4470	0.5038	4.4734	4.5300
5	$E_{selfdis}$	Wh	0.0000	0.0000	2.4694	0.9439	4.4300	1.1067
6	$_{ERpol}$	Wh	26.140	1.0840	9.7421	2.6039	8.8120	2.7950
7	$_{ER}$	Wh	4.4820	16.050	4.4812	16.047	4.4812	16.050
8	$_{Edpol}$	Wh	4.1410	0.0820	3.0961	0.5286	20.245	2.6540
9	E_{Tloss}	Wh	34.750	17.210	17.789	16.720	37.968	17.020
10	ED_{sy}	Wh/kg	30.992	35.957	28.053	32.401	27.560	35.090
11	PD_{sy}	W/kg	6.1829	7.1734	5.5966	6.4641	5.4983	7.0003
12	$\delta_{Eselfdis}$	%	0.0000	0.0000	0.5169	0.2807	4.8315	2.5380
13	δ_{ET}	%	38.430	15.776	19.587	15.363	41.409	20.538
14	η_{E1}	%	54.600	84.241	47.995	83.980	42.835	80.540
15	η_{E2}	%	54.620	84.245	61.474	84.224	56.673	81.560

It follows from Figures 5.11a, 5.11c and 5.11a that the fully charged symmetric EDLC with the electrode's effective conductivity α_1 =0.05 S/cm and only the EDL's instability self-discharge under conditions presented in case 2 of Tables 5.2, 5.3 and 5.4, took 14.0 days,

136.6 days and 137.7 days respectively, to be completely discharged by self-discharge. Voltage of the fully charged symmetric EDLC of α_1=0.05S/cm with both side-reactions/redox reactions and the EDL's instability self-discharge under conditions in case 4 of Table 5.2 decayed sharply to approximately 1.05V within 27.7h of storage (1.2days) as shown in Figure 5.11b.

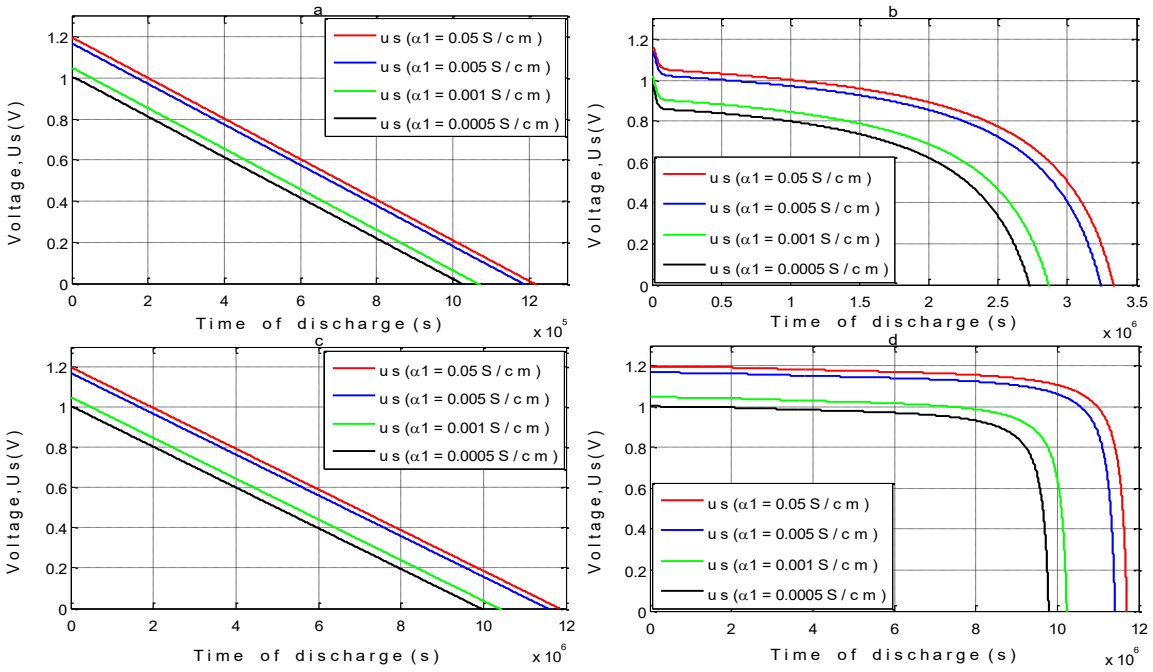

Figure 5.11: Dependence of voltage $U_S(t)$ decay on time of storage for symmetric EDLC of different electrodes effective conductivities with (a) only the EDL's instability self-discharge with J_{VRM} =1.25x10^{-3}A/cm^2, (b) both side-reactions/redox reactions and the EDL's instability self-discharge with J_{VRM} =1.25x10^{-3}A/cm^2 and J_{VR1}=9.58x10^{-4}A/cm^2, (c) only the EDL's instability self-discharge with J_{VRM} = 4.0x10^{-4}A/cm^2, and (d) both side-reactions or redox reactions and the EDL's instability self-discharge with J_{VRM} = 4.0x10^{-4}A/cm^2 and J_{VR1} =9.58x10^{-5}A/cm^2.

After this quick decay, the voltage remained fairly constant for several days before subsequent slow decay. It took this capacitor under storage conditions 38.8 days to be completely discharged by self-discharge alone as pictured in Figure 5.11b. It follows from Figures 5.11d and 5.12b that the voltage of a fully charged symmetric EDLC with α_1 = 0.05S/cm and both side-reactions/redox reactions and the EDL's instability self-discharge, but with tuned key self-discharge, remained almost constant at 1.2V for 92.6 days and 925.9 days respectively, before decaying. It took this capacitor 135.4 days and 1365.7 days respectively to be entirely discharged by self-discharge as shown in Figures 5.12a and 5.12b. Incorporation of self-discharge in the capacitor's models created an avenue for a more accurate estimation of the energy parameters during charging, discharging and on storage.

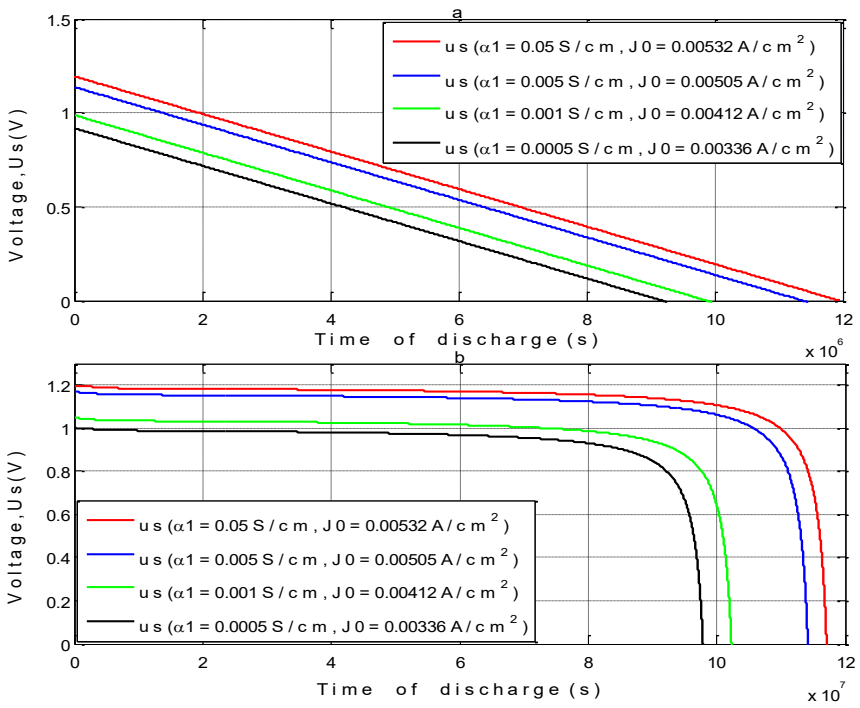

Figure 5.12: Dependence of voltage $U_S(t)$ decay on time of storage for symmetric EDLC with different electrodes effective conductivities and (a) only the EDL's instability self-discharge with J_{VR} = 4.0x10^{-5}A/cm^2 and (b) both side-reactions/redox reactions and the EDL's instability self-discharge with J_{VR} = 4.0x10^{-5}A/cm^2 and J_{VR1} = 9.58x10^{-5}A/cm^2.

The above results and analysis showed that self-discharge has a significant role in the stability of ECs' parameters during charging and discharging, and the method of charging and discharging is important in getting optimal energy parameters. This model with self-discharge could be used to explain self-discharge experimental results available in references [197,198,245]. It can also be used to study the effects of each self-discharge parameter on the capacitor's overall performance and how the key-parameters can be tuned to improve device performance. The model presented a more realistic estimate of the potential drop and energy loss in ECs, since it considered, in addition to energy loss by polarization and depolarization resistance, both side-reactions/reactions of active redox species and the electric double layers instability self-discharge during charging and discharging processes.

5.2 The Effects of Self-Discharge on the Performance of Asymmetric/Hybrid Electrochemical Capacitors: Insights from Modeling and Simulation.

In order to bridge the gap between theoretical and practical understanding of this subject, we incorporated the self-discharge term into asymmetric ECs mass transfer and charge conservation equations for capacitors during charging and discharging, by assuming that self-discharge was not zero. Our ultimate motivation was to develop a platform to study self-discharge effects in asymmetric ECs via modelling and simulation, by incorporating self-discharge into the model equation while charging and discharging. This will enhance evaluation of the effects of self-discharge and its key parameters on the overall performance of ECs. The effects of varios kinds of self-discharge can be studied by incorporating a combination of various expressions for self-discharge mechanisms obtainable in asymmetric ECs. We assumed that side-reactions or reactions of active redox species and several impurities and electric double layers (EDLs) instability are responsible for self-discharge

processes, and ignored the existence of ohmic leakage currents among cathode and anode. The EDL's instability self-discharge can be caused by the presence of functional groups or impurities in electrode materials, shuttling of electrolyte impurities among electrodes, charge redistribution and attractive force from opposite ions in the electrolyte phase.

5.2.2 Discussions

The data operated upon are based on the experiment variables of Kazaryan et al. [89] and Staser et al. [90]. As presented in Table 5.1 a sensible figure were presumed, based on literature for unavailable parameters.The EC discharged to 0.8V is charged by constant current to an upper voltage of 2.0V for the charging duration (t_{ch}) of 5 hours. Thereafter it is discharged by a constant current from 2.0V to a lower voltage of 0.8V for the discharging duration (t_{dis}) of 5 hours. We carried out simulations on the asymmetric electrochemical capacitor's self-discharge parameter with the device design described in Table 5.1. Electrode effective conductivity α_1 was varied in the simulation as follows: 0.0005, 0.0010, 0.0050, and 0.0500S/cm, while the following charging conditions were also considered 0.00533A/cm^2 for 18000s, 0.05330A/cm^2 for 1800s, 0.53300A/cm^2 for 180s and 5.33000A/cm^2 for 18s. The choice of the charging conditions is based on the fact that low current density needs longer time, while high current density needs shorter time. The first current density was multiplied by a factor of 10, 100 and 1000 while charging time was divided by the same factor to get the second, third and fourth conditions, respectively.

In order to validate the model accuracy, experimental results of two button asymmetric electrochemical capacitors $Mn_3(PO_4)_2$//AC composite electrodes using aqueous 1molL^{-1} Na_2SO_4 electrolyte and aqueous 2molL^{-1} KOH electrolyte [275] were used to validate the

asymmetric models. The devices were charged and discharged at different current densities and times (different rates), in order to confirm the effects of the charging and discharging rate on the device's self-discharge rate. Plots of the voltage of the button device against charging and discharging time were used to verify the validity of the models. The fabricated button devices were charged from 0.0V to 1.6V, and thereafter discharged from 1.6V to 0.0V.

The presence of redox species or impurities in the electrodes or electrolyte will produce oxidized molecules at a positive electrode (anode) during the capacitor charging process. These oxidized molecules will spread across the separator and get to the negative electrode surface where they are readily reduced, because cathode potential falls by way of charging EDLs as presented in equations 3.53, 3.54 and 3.55. The quantity of charge leaving the negative electrode into solution grows exponentially as shown in Figure 5.13a, generated from equation 3.61.

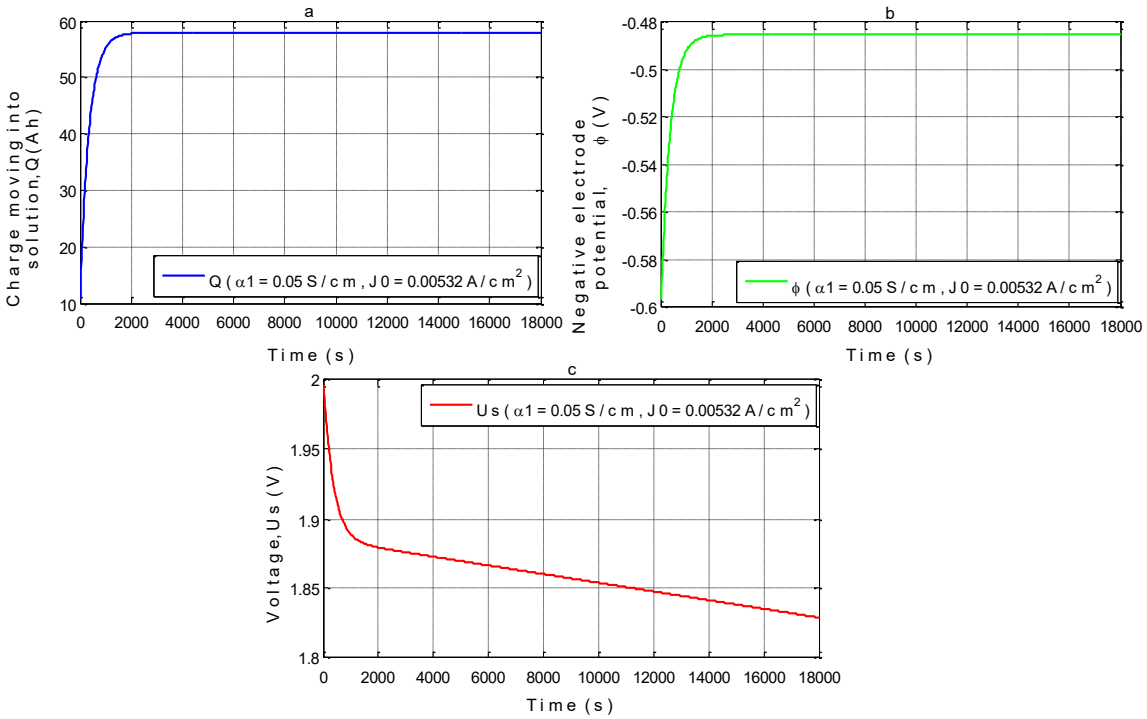

Figure 5.13: (a) Amount of charge moving from negative (cathode) electrode of asymmetric ECs into the solution over time due to redox reactions self-discharge using Equation 4.36; (b)

potential change in negative electrode over time due to redox reactions self-discharge using Equation 4.52; and (c) the potential change over time due to both the EDL's instability and redox reactions self-discharge.

It follows from equations 4.36 and 4.39 that the device negative electrode potential and voltage reduced exponentially over time, due to migrations of redox species or impurities in electrolyte as shown in Figures 5.13b and 2c.

It was noticed that the concentration of oxidized molecules and the entire thickness of the separator and positive electrode substantially affects the rate of shuttle self-discharge. Equations 4.51 and 4.52 show that the voltage of the asymmetric cell decays exponentially by self-discharge during charging as evident in Figure 5.13d.

This decay was very sharp at the initial phase of the self-discharge process (within the first 10min (600s)), when the concentration of redox species or/and shuttle impurities was high and thereafter became linear throughout the remaining charging duration as shown in Figure 5.13d. It was noted the that concentration of redox species or/and shuttle impurities and the entire thickness of the device separator and anode greatly determine the rate of self-discharge.

During the device charging, redox species/impurities in electrodes or electrolyte undergo galvanostatic electrolysis to produce oxidized molecules on the surface of the positive electrode (anode). These oxidized molecules migrate through the separator to the surface of the negative electrode (cathode). These oxidized species are readily reduced at the cathode surface, where they increase the negative electrodes' operating potential window above the electrochemical range of the solvent, thereby speeding up the self-discharge process. Thus, migration of the redox species/impurities and electrochemical products were, to greater

extent, the causes of self-discharge in asymmetric ECs. This clearly shows that efficiency of the capacitor's charging and its voltage is significantly dependent on the self-discharge rate in the device. Asymmetric capacitors with high electrodes and electrolyte effective conductivity ($\alpha_1 = \alpha_2 = 0.05$S/cm) without self-discharge were charged to the target upper voltage (2.0V) within the stipulated charging time, whereas similar capacitors with self-discharge were charged to a voltage below the target upper voltage (1.8V) within stipulated charging time due to self-discharge, as shown in Figures 5.14a and 5.14c respectively. ECs with low electrodes and electrolyte effective conductivity ($\alpha_1 = \alpha_2 = 0.0005$S/cm) without self-discharge were charged 2.0V within the target charging time, while similar capacitors with self-discharge were charged to 1.8 V within the same time, as seen in Figures 5.14a and 5.14c respectively. The voltage profiles of the device with high electrode and electrolyte effective conductivities increased linearly during charging, as compared with the nonlinear increase in the device with low electrodes and electrolyte effective conductivities.

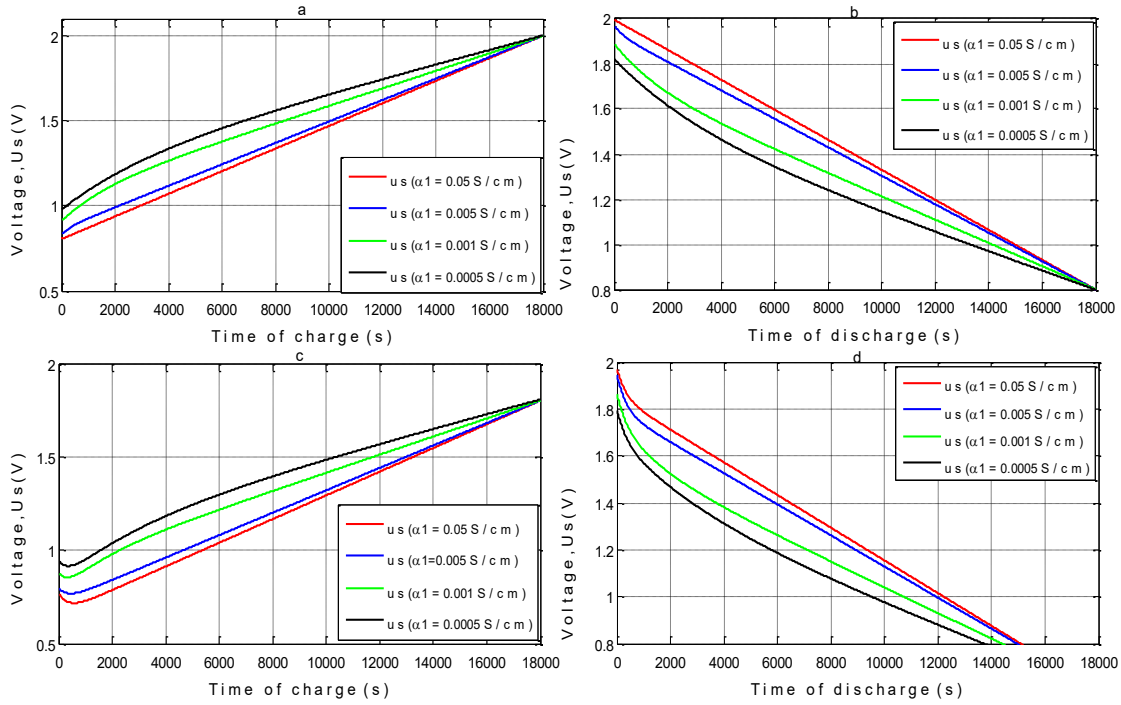

Figure 5.14: The voltage dependence on time in ECs with different parameters charged for 18000s from 0.8V to 2.0V in (a) capacitors without self-discharge; (b) when devices with

different parameters are discharged for 18000s from 2.0V to 0.8V in capacitors without self-discharge; (c) charging with self-discharge; and (d) when devices with different parameters are discharged for 18000s from 2.0V to 0.8V for capacitors with self-discharge.

This clearly showed that the charging efficiency of the capacitor, its voltage and time is greatly dependent on the electrodes and electrolyte effective conductivities α_1 and α_2. Similar ECs with self-discharge were not charged to target voltage within the target charging time (18000s) due to self-discharge and additional time is needed to achieve that.

Similarly, capacitors without self-discharge were discharged to 0.8V within the stipulated discharging time; whereas similar capacitors with self-discharge were discharged to 0.8V in a shorter time (15000s) than the target due to self-discharge loss, as evident in Figures 5.14b and 5.14d respectively.

In order to study the effects of the charging and discharging rate on the self-discharge process, ECs were charged and discharged faster for 30min (1800s), 3min (180s) and 0.3min (18s) by multiplying the effective conductivities and applied current densities by a factor of 10, 100, and 1000 respectively. The charging condition in ECs with electrodes and electrolyte effective conductivities of 0.5S/cm, 5S/cm and 50S/cm was applied at a current density of 0.0532A/cm^3 for 1800s, 0.53200A/cm^3 for 180s and 5.32000A/cm^3 for 18s respectively. When the EC with self-discharge was charged at a current density of 0.05320 A/cm^3 for 1800s, the device voltage at the end of the charging process was 1.88V due to self-discharge as shown in Figure 5.15c, compared with 1.80V when charged at 0.00532A/cm^3 for 5hrs (18000s) as seen in Figure 5.14c. The voltage of similar capacitors without self-discharges when charged for 30min (1800s) at the rate of 0.05320A/cm^3 was 2.0V as shown in Figure 5.15a.

In the same manner, when the EC with self-discharge was discharged at a current density of 0.0532A/cm^3 to 0.8V, it took it 1580s due to self-discharge as shown in Figure 5.15d, compared with 15000s discharge duration for rate of 0.00532A/cm^3 as seen in Figure 5.14d. A similar capacitor without self-discharge, discharged its voltage to 0.8V within the target discharge time (30min (1800s)) at the same rate as shown in Figure 5.15b.

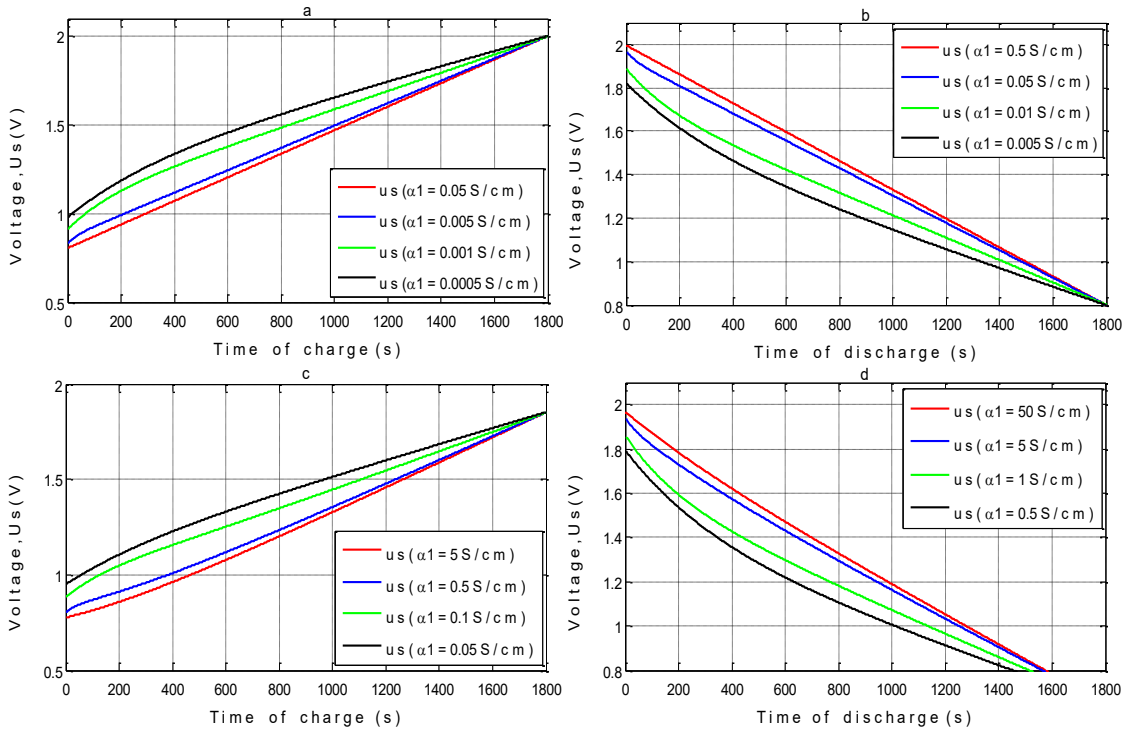

Figure 5.15: The voltage dependence on time in ECs with different parameters charged for 1800s from 0.8V to 2.0V in (a) capacitors without self-discharge; (b) when devices with different parameters were discharged for 1800s from 2.0V to 0.8V in capacitors without self-discharge; (c) charging with self-discharge; and (d) when devices with different parameters were discharged for 1800s from 2.0V to 0.8V in capacitors with self-discharge.

When the EC with self-discharge was charged at a current density of 0.5320A/cm^3 for 3min (180s), the voltage at end of the charging process was 1.95V due to self-discharge as seen in Figure 5.16c, in comparison with 1.88V in a similar device charged at 0.0532A/cm^3 for 30min (1800s) as seen in Figure 5.15c. Again, the similar device without self-discharge

effects was charged to 2.0V at the end of 3min (180s) charging as shown in Figure 5.16a. When the capacitor with self-discharge was discharged 0.8V at the rate of 0.5320A/cm^3, it took it 170s to discharge its voltage as seen in Figure 5.16d, compared with 180s it took the similar device without self-discharge at the same rate as shown in Figure 5.16b. It took a similar capacitor with self-discharge 1580s to be discharged to the target lower voltage at a rate of 0.0532A/cm^3 as depicted in Figure 5.15d. These results clearly showed that charging capacitors fast with higher current density and less time reduced the self-discharge rate and the consequent voltage losses.

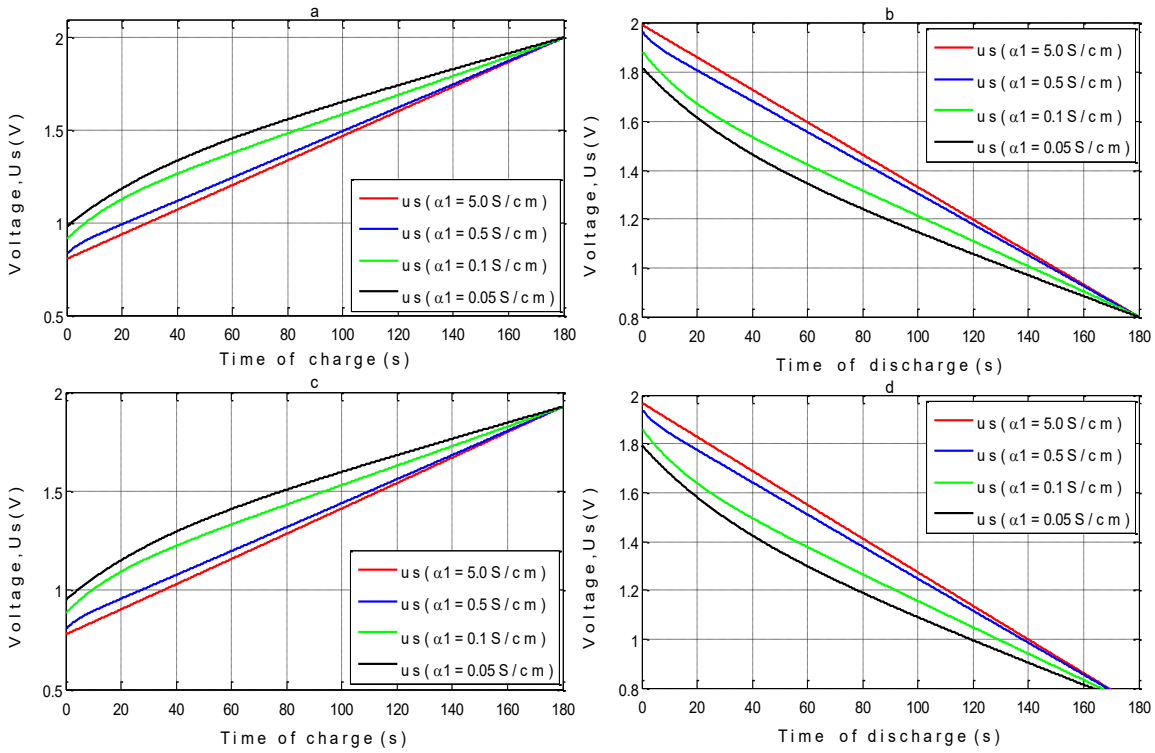

Figure 5.16: The ECs voltage dependence on time when devices with different parameters were charged for 180s from 0.8V to 2.0V in (a) capacitors without self-discharge; (b) when devices with different parameters were discharged for 180s from 2.0V to 0.8V in capacitors without self-discharge; (c) charging with self-discharge; and (d) when devices with different parameters were discharged for 180s from 2.0V to 0.8V in capacitors with self-discharge.

A further increase in the capacitor's charging rate to a current density of 5.3200A/cm^2 for 0.3min (18s), improved the voltage at the end of the charging duration to 1.9950V as presented in Figures 5.17b, compared with 1.95V when charged at a rate of 0.5320A/cm^2 for 3 min (18s) as in Figures 5b. Similar capacitors without self-discharge were charged to 2.0V at the same rate as shown in Figure 5.17a. Similar capacitors with self-discharge were completely discharged to 0.8V at the same rate within 17.6s as depicted in Figure 5.17d, compared to the 18s it took similar capacitors without self-discharge at the same rate as seen in Figure 5.17b.

Fast charging of ECs with self-discharge at current densities of 0.0532A/cm^2 for 1800s, 0.5320A/cm^2 for 180s and 5.3200A/cm^2 for 18s, reduced the voltage drop from 0.200V to 0.120V, 0.120V to 0.050V and 0.050V to 0.005V respectively. Figure 5.18 depicts the voltage decay in asymmetric ECs with different electrodes effective conductivities over time due to both redox reactions and the EDL's instability self-discharge during the charging process at different charging conditions.

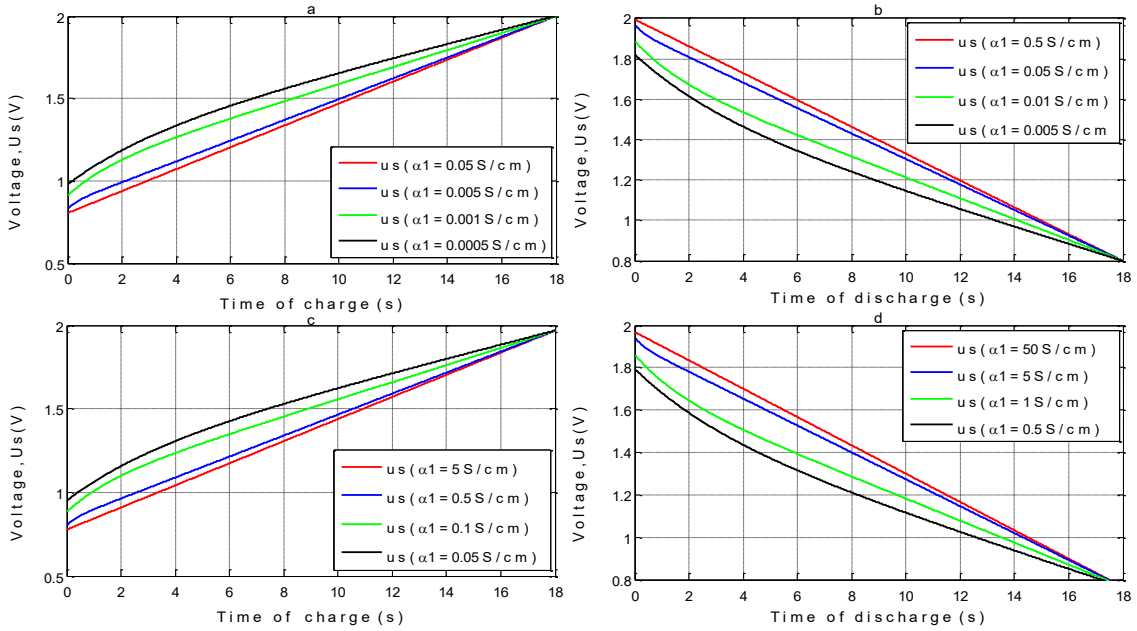

Figure 5.17: The ECs voltage dependence on time when devices with different parameters are charged for 18s from 0.8V to 2.0V in (a) capacitors without self-discharge; (b) when device

with different parameters are discharged for 18s from 2.0V to 0.8V in capacitors without self-discharge; (c) charging with self-discharge; and (d) when devices with different parameters are discharged for 18s from 2.0V to 0.8V in capacitors with self-discharge.

It follows from Figures 5.18a and 5.18b that the voltage drop at the initial stage of the charging processes (600s and 60s respectively) was very sharp for charging rates of 0.0053A/cm^2 for 18000s and 0.0532A/cm^2 for 1800s. This is because redox products have enough time to migrate from one electrode to another, thereby increasing the self-discharge rate. For a charging condition of 0.5320A/cm^2 for 180s, the voltage drop was very small within the first 6s and thereafter the voltage became approximately constant throughout the remaining time as shown in Figure 5.18c. When the capacitors were charged at a current density of 5.3200A/cm^2 for 18s, the voltage drops were so insignificant that their profiles remained constant throughout the duration as presented in Figure 5.18d.

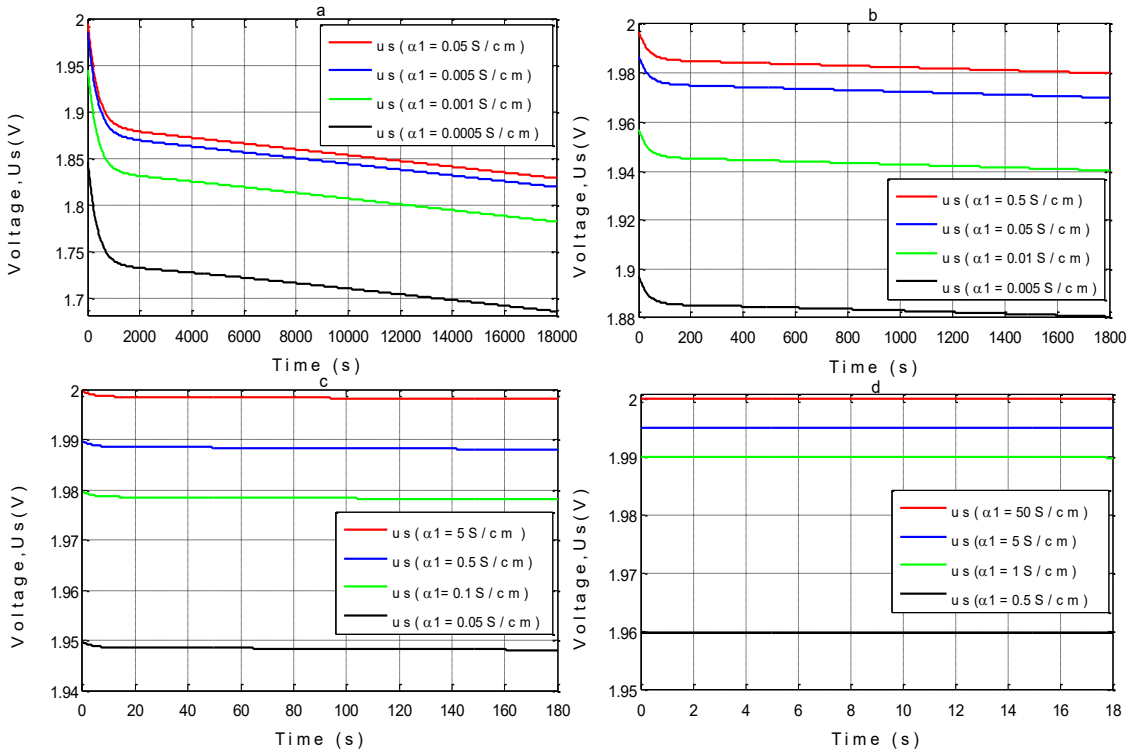

Figure 5.18: The voltage decay over time in asymmetric electrochemical capacitors with different electrodes effective conductivities by both redox reactions and EDLs instability self-discharge after the device was charged from voltage of 0.8V to 2.0V at current density of (a) 0.0053A/cm^2 for 18000s charging time; (b) 0.0532A/cm^2 for 1800s charging time; (c) 0.5320A/cm^2 for 180s charging time; and (d) 5.3200A/cm^2 for 18s charging time.

Figure 5.19 shows voltage decay of asymmetric ECs with the same electrodes effective conductivity over time, by both redox reactions and the EDL's instability self-discharge during the device's charging process to 2.0V at different charging conditions. When the capacitor with electrodes effective conductivity of 0.05S/cm was charged at a current density of 0.0053A/cm^2 for 18000s, 0.0532A/cm^2 for 1800s, 0.5320A/cm^2 for 180s and 5.3200A/cm^2 for 18s, its voltage dropped from 2.000V to 1.800V, 2.000V to 1.980V, 2.000V to 1.998V and 2.000V to 1.9998V respectively, as seen in Figures 5.19a, 5.19b, 5.19c and 5.19d. Actual voltage drops by self-discharge during charging at the four different conditions were 0.200V, 0.020V, 0.002V and 0.0002V respectively. It was clearly seen from Figure 5.19 and the above discussion that the capacitors' voltage drop for conditions in Figure 5.19c and 5.19d were negligible.

It follows from Table 5.5 that the energy loss in the asymmetric EC with electrode effective conductivity of α_1= 0.0500S/cm and 0.0005S/cm by only the EDL's instability self-discharge during the charging and discharging processes, was 21.99Wh and 22.49Wh respectively. Energy loss by EDLs instability self-discharge reduced along with an increase in the capacitors' electrode effective conductivity α_1. Total energy loss E_{Tloss} in the EC with self-discharge was 44.49Wh and 86.41Wh in the device with α_1=0.0500S/cm and 0.0005S/cm respectively, compared with 22.51Wh and 63.99Wh in a similar EC without self-discharge.

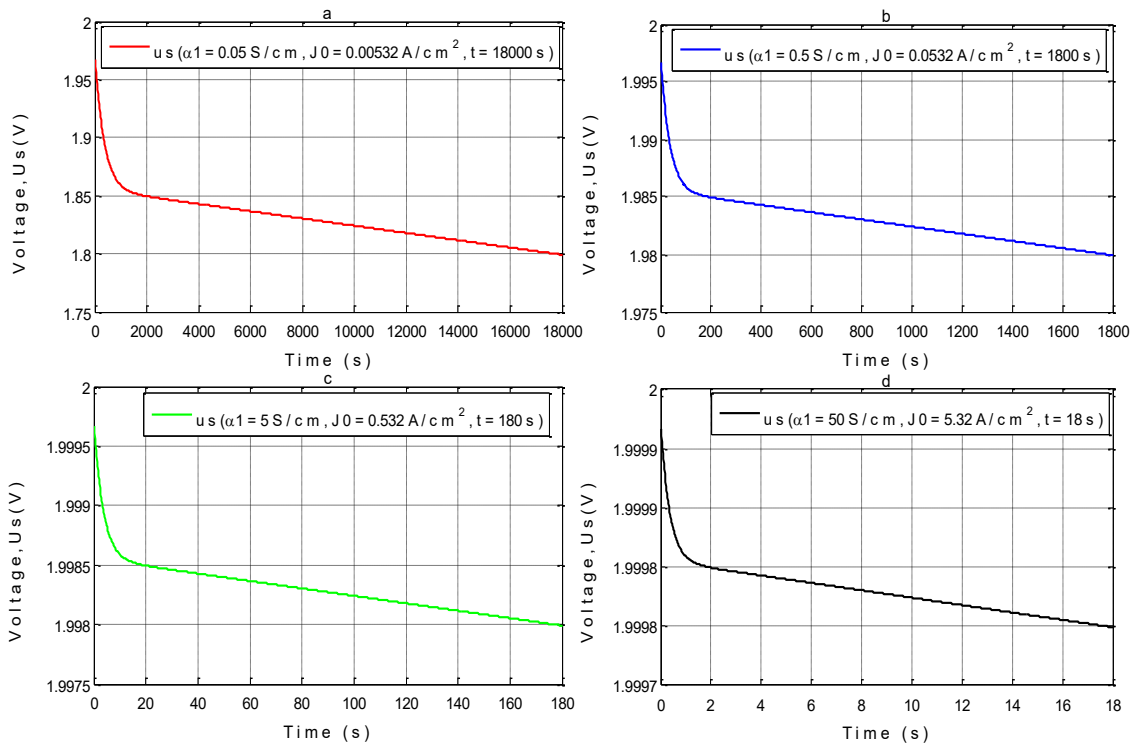

Figure 5.19: The voltage decay over time in asymmetric electrochemical capacitors with electrodes effective conductivity of 0.05S/cm by both redox reactions and the EDL's instability self-discharge after the devices are charged from voltage of 0.8V to 2.0V at a current density of (a) 0.0053A/cm^2 for 18000s charging time; (b) 0.0532A/cm^2 for 1800s charging time; (c) 0.5320A/cm^2 for 180s charging time; and (d) 5.3200A/cm^2 for 18s charging time.

Storable energy of the EC with self-discharge was 225.38Wh, 218.63Wh, 185.83Wh and 156.99Wh, while deliverable energy was 217.77Wh, 189.09Wh, 116.74Wh and 63.56Wh. Storable energy of similar a EC without self-discharge was 234.58Wh and 166.00Wh, whereas deliverable energy was 233.15Wh and 71.72Wh. The first and second charge–discharge cycle efficiencies η_{E1} and η_{E2} of the EC with α_1=0.0500S/cm and 0.0005S/cm and only the EDL's instability self-discharge during charging and discharging were 84.98% &

85.11% and 26.74% & 49.51%, respectively; and 90.72% & 90.82% and 41.13% & 62.65% respectively in similar a EC without self-discharge as presented in Table 5.5

Table 5.5: Parameters of asymmetric ECs in Case 1 without self-discharge; and Case 2 with self-discharge and N = 10^{20}cm^{-3} and J_{VRM} = 1.25x10^{-3}A/cm^2 during capacitors charging and discharging.

S/N	Parameter	Unit	α_2= 0.05S/cm			
			Case 1: Without Self-discharge and w_{sp}=0.1cm		Case 2: N=10^{20}cm^{-3}, w_{sp}=0.1cm and J_{VR} =1.25x10^{-3}A/cm^2	
			α_1 (S/cm)		α_1 (S/cm)	
			0.0005	**0.0500**	**0.0005**	**0.0500**
1	E_{Sch}	Wh	165.99	234.58	156.99	225.38
2	E_{Sdis}	Wh	71.724	233.15	63.562	217.77
3	$I_{selfdis}$	A	0.0000	0.0000	0.7862	0.7862
4	$E_{selfdis}$	Wh	0.0000	0.0000	22.485	21.990
5	E_{Tloss}	Wh	63.991	22.506	86.414	44.485
6	ED_{asy}	Wh/kg	74.666	107.56	62.523	91.531
7	PD_{asy}	W/kg	14.933	21.512	12.505	18.306
8	M_{asy}	kg	2.5791	2.5791	2.5791	2.5791
9	η_{E1}	%	41.131	90.723	26.744	84.980
10	η_{E2}	%	62.653	90.823	49.514	85.106

It follows from Table 5.6 that the energy loss in the asymmetric EC with α_1= 0.0500S/cm and 0.0005S/cm by both the EDL's instability and redox reaction self-discharge during charging and discharging was 59.53Wh and 87.88Wh respectively. Total energy loss by self-discharge in the EC with α_1=0.0500S/cm and 0.0005S/cm was 63.61Wh and 126.45Wh respectively, compared with 22.51Wh and 63.99Wh in similar a EC without self-discharge as seen in Table 5.6. Storable energy of the EC with self-discharge was 214.48Wh and 147.17Wh in device with α_1= 0.0500S/cm and 0.0005S/cm respectively; whereas deliverable energy was

209.37Wh and 61.27Wh respectively. The first and second charge–discharge cycle efficiencies η_{E1} and η_{E2} of asymmetric ECs with α_1=0.0500S/cm and 0.0005S/cm and both EDL's instability and redox reaction self-discharges was 79.57% & 82.03% and 18.05% & 31.95% respectively; compared with 90.72% & 90.82% and 41.13%, 62.65% respectively in similar ECs without self-discharge as seen in Table 5.6. Storable and deliverable energies were lower because of the high rate of self-discharge due to migration of soluble redox reaction products from one electrode to another.

Table 5.6: Parameters of asymmetric ECs in Case 1, without self-discharge; and Case 2 with self-discharge and N = 10^{20}cm^{-3}, J_{VRM} = 1.25x10^{-3}A/cm^2, J_{VR1} = 9.58x10^{-4}A/cm^2, C_{Ox} = 3.0x10^{-4}mol/cm^3 and D_{Ox} = 1.8x10^{-5}cm^2/s during capacitors charging and discharging.

S/N	Parameter	Unit	α_2 = 0.05S/cm			
			Case 1: Without Self-discharge and w_{sp}=0.1cm		Case 2: N=10^{20}cm^{-3}, w_{sp}= 0.1cm and J_{VR} = 1.25x10^{-3}A/cm^2 and J_{VR1}= 9.58x10^{-4}A/cm^2, C_{Ox} = 3.0x10^{-4}mol/cm^3 and D_{Ox} =1.8x10^{-5} cm^2/s	
			α_1 (S/cm)		α_1 (S/cm)	
			0.0005	**0.0500**	**0.0005**	**0.0500**
1	E_{Sch}	Wh	165.99	234.58	147.17	214.48
2	E_{Sdis}	Wh	71.724	233.15	61.265	209.36
3	$I_{selfdis}$	A	0.0000	0.0000	5.6186	5.6186
4	$E_{selfdis}$	Wh	0.0000	0.0000	87.875	59.533
5	E_{Tloss}	Wh	63.991	22.506	126.45	63.608
6	ED_{asy}	Wh/kg	74.666	107.56	58.716	87.303
7	PD_{asy}	W/kg	14.933	21.512	11.743	17.461
8	M_{asy}	kg	2.5791	2.5791	2.5791	2.5791
9	η_{E1}	%	41.131	90.723	18.047	79.574
10	η_{E2}	%	62.653	90.823	31.945	82.026

Figure 5.21 presents the charging and discharging times of Ma et al [275] asymmetric device with $Mn_3(PO_4)_2$//AC electrodes using 1 $molL^{-1}$ Na_2SO_4 and 2$molL^{-1}$ KOH aqueous electrolyte at different current densities. It follows from Figure 5.20 that the charging and discharging time of the device reduced as the applied current density was increased. It was shown that when the device with 1 $molL^{-1}$ Na_2SO_4 aqueous electrolyte was charged and discharged at a current density of 0.5A/g, the time it took it to be charged to 1.6V and thereafter discharged to 0V was 200s and 120s respectively, as shown in Figures 5.20a and 5.20b. The device was discharged faster and the difference in the values of charging and discharging times (80s) was due to self-discharge, since the values of charging and discharging current density were the same.

When the same device was charged and discharged at a current density of 10.0A/g, it took the device 10.5s and 10.0s to be charged to 1.6V and discharged to 0.0V respectively. The difference in charging and discharging times due to self-discharge was reduced to 0.5s, because the self-discharge rate reduced as a result of the increased charging and discharging rate.

Similarly, when the device with 2 $molL^{-1}$ KOH aqueous electrolytes was charged and discharged at a current density of 0.5A/g, it took it 175s and 125s to be charged to 1.6V and discharged to 0.0V respectively, as shown in Figure 5.20c and 5.20d. The difference in charging and discharging times due to self-discharge was 50s. When it was also charged and discharged at current density of 10.0A/g, it took it 2.5s and 2.0s to be charged to 1.6V and discharged to 0.0V respectively. The difference in the charging and discharging times due to self-discharge reduced to 0.5s. This also showed that charging and discharging ECs faster reduced the self-discharge rate significantly.

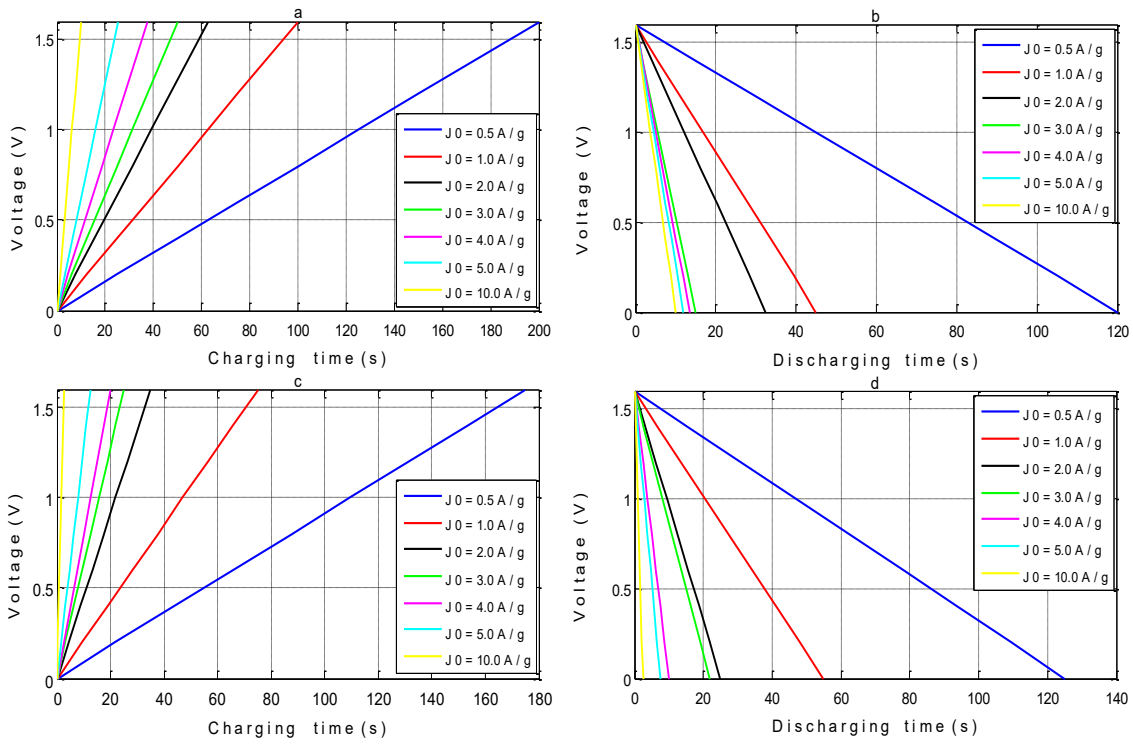

Figure 5.20: (a) The charging time of a button asymmetric EC with 1 molL^{-1} Na_2SO_4 aqueous electrolyte solution charged at different current densities; (b) The discharging time of a button asymmetric EC with 1 molL^{-1} Na_2SO_4 aqueous electrolyte solution discharged at different current densities; (c) The charging time of a button asymmetric EC with 2 molL^{-1} KOH aqueous electrolyte solution charged at different current densities; (d) The discharging time of a button asymmetric EC with 2 molL^{-1} KOH aqueous electrolyte solution discharged at different current densities. [The straight lines in Figure 5.20 does not necessarily mean that voltage is directly proportional to charging or discharging time].

Figure 5.21 presents the comparison of charging and discharging times of the simulation with the experiment of Ma et al [275] for asymmetric ECs with $Mn_3(PO_4)_2$//AC electrodes using 1 molL^{-1} Na_2SO_4 and 2molL^{-1} KOH aqueous electrolyte at different current densities. It was seen that the charging and discharging time from simulation and Ma et al experiments agreed to a large extent as depicted in Figure 5.21.

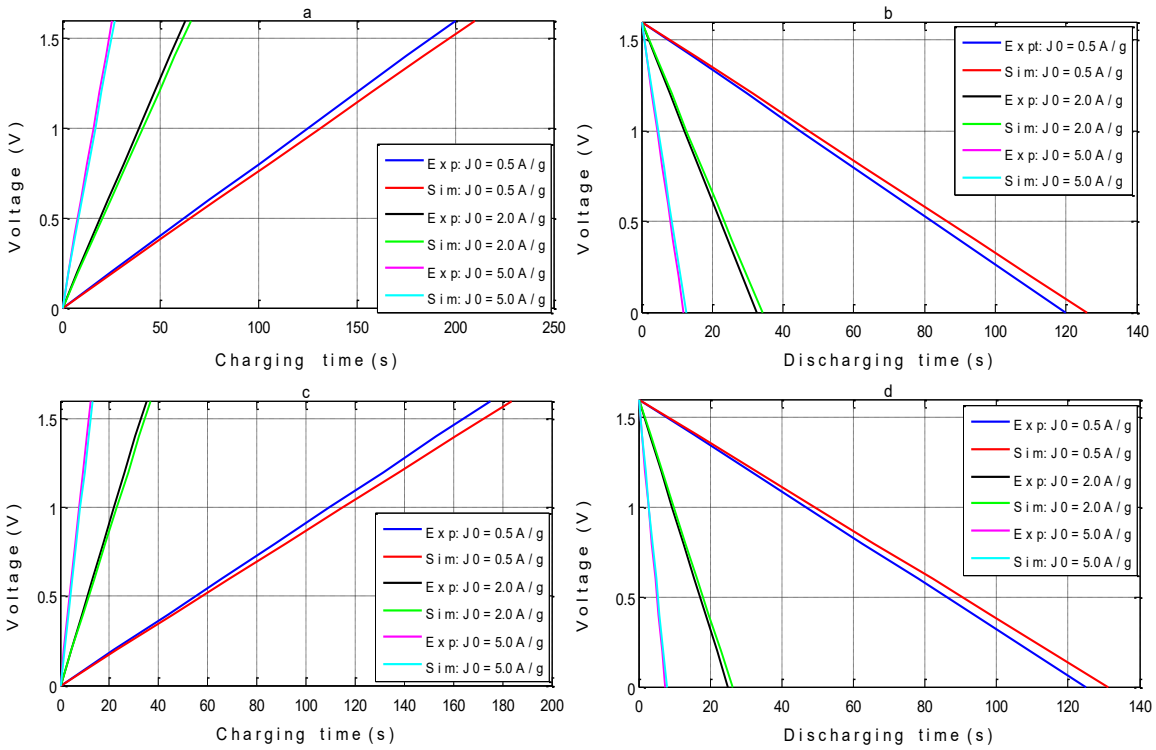

Figure 5.21: (a) Comparison of charging time of simulation with experiment in asymmetric EC with 1 molL^{-1} Na_2SO_4 aqueous electrolyte at different current densities; (b) Comparison of discharging time of simulation with experiment in asymmetric EC with 1 molL^{-1} Na_2SO_4 aqueous electrolyte at different current densities; (c) Comparison of charging time of simulation with experiment in asymmetric EC with 2 molL^{-1} KOH aqueous electrolyte at different current densities; (d) Comparison of discharging time of simulation with experiment in asymmetric EC with 2 molL^{-1} KOH aqueous electrolyte at different current densities densities. [The straight lines in Figure 5.21 does not necessarily mean that voltage is directly proportional to charging or discharging time].

In order to study the effects of some self-discharge parameters on the self-discharge rate, the concentration of functional groups in electrodes or impurities ions in electrolyte was reduced, which resulted in a reduction of the EDL's self-discharge current density. Reduction in the concentration of the redox species and redox species coefficient of diffusivity also resulted in a reduction of redox reaction self-discharge current density. It follows from Table 5.7 that

tuning the self-discharge parameters enhanced the performance and efficiency of ECs by reducing charge and energy losses due to self-discharge during charging/discharging. The tuning operation enhanced EC storable energy to 245.09Wh and 168.96Wh in device with α_1 =0.0500S/cm and 0.0005S/cm respectively, whereas deliverable energy was 244.02Wh, and 74.67Wh respectively as presented in Table 5.7. Energy loss in the capacitor by the self-discharge process during charging and discharging was reduced to 7.43Wh and 18.26Wh respectively, while the total energy loss was reduced to 23.94Wh and 68.70Wh respectively.

The first and second charge–discharge cycle energy efficiencies η_{E1} and η_{E2} of devices with electrodes effective conductivity α_1 = 0.0500S/cm and 0.0005S/cm and self-discharge, were enhanced to 90.46% & 90.80% and 40.79% & 62.05% respectively; compared with 90.72% & 90.82% and 41.13% & 62.65% in similar capacitors without self-discharge as seen in Table 5.7. Storable and deliverable energies of the capacitors with tuned self-discharge parameters and insoluble redox reaction products were higher than those of similar capacitors without self-discharge. This is because redox reaction products are insoluble and adsorbed onto the cathode, thereby increasing the energy capacity of the device as evident in Table 5.7. Thus, reduction of shuttle impurity concentration and use of redox-active species that produces insoluble products suppresses the rate of self-discharge.

Table 5.7: Parameters of asymmetric ECs in Case 1, without self-discharge; and Case 2 with self-dischargeN =10^{19}cm^{-3}, J_{VRM} = 4.0x10^{-4}A/cm^2, J_{VR1}=9.58x10^{-5}A/cm^2, C_{Ox} =3.0x10^{-5}mol/cm^3 and D_{Ox} = 1.8x10^{-6}cm^2/s, during capacitors charging and discharging.

S/N	Paramete	Unit	α_2 = 0.05S/cm

	r		Case 1: Without Self-discharge and w_{sp}= 0.1cm		Case 2: N=10^{19}cm^{-3} , w_{sp} = 0.1cm, J_{VR} = 4.0x10^{-4}A/cm^2, J_{VR1}=9.58x10^{-5}A/cm^2, C_{Ox} = 3.0x10^{-5}mol/cm^3 and D_{Ox} = 1.8x10^{-6}cm^2/s	
			α_1 (S/cm)		α_1 (S/cm)	
			0.0005	**0.0500**	**0.0005**	**0.0500**
1	E_{Sch}	Wh	165.99	234.58	168.96	245.09
2	E_{Sdis}	Wh	71.724	233.15	74.670	244.02
3	$I_{selfdis}$	A	0.0000	0.0000	0.9078	0.9078
4	$E_{selfdis}$	Wh	0.0000	0.0000	18.263	7.4290
5	E_{Tloss}	Wh	63.991	22.506	68.702	23.939
6	ED_{asy}	Wh/kg	74.666	107.56	80.287	113.75
7	PD_{asy}	W/kg	14.933	21.512	18.057	26.551
8	M_{asy}	kg	2.5791	2.5791	2.5791	2.5791
9	η_{E1}	%	41.131	90.723	40.792	90.458
10	η_{E2}	%	62.653	90.823	62.054	90.789

The voltage decay of fully charged ECs under storage conditions with different electrode effective conductivity and both the EDL's instability and redox reactions self-discharge, follows the profile shown in Figure 5.22. It took completely charged capacitors with different α_1 under storage and the self-discharge parameters presented in case 2 of Table 5.6, 38.7 days, 38.0 days, 34.3 days and 31.3 days respectively, to be entirely discharged to 0.8V by self-discharge as shown in Figure 5.22a. Also, it took completely charged similar capacitors with different α_1 under storage and tuned self-discharge parameters as in case 2 of Table 5.7, 135.4 days, 133.1 days, 121.2 days and 112.8 days respectively to be fully discharged to 0.8V by self-discharge as seen in Figure 5.22b. It was noted that the key self-discharge parameters to be tuned to enhance the performance and efficiency of ECs are the concentration of the electrode's functional groups or impurity ions in electrolyte, concentration of oxidized species, and the total thickness of the separator and positive electrode.

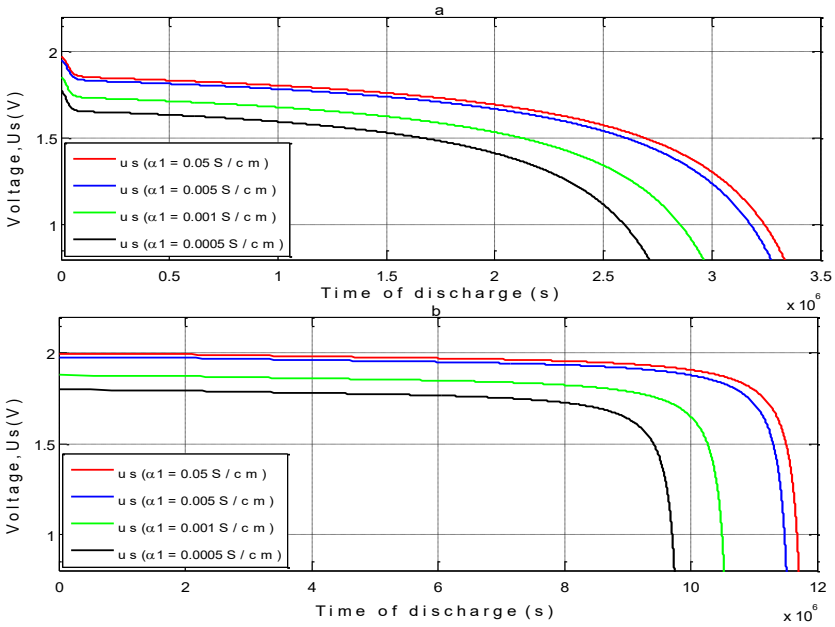

Figure 5.22: The voltage decay due to self-discharge in capacitors with different electrodes effective conductivity α_1 under storage condition after charged to 2.0V for (a) devices with parameters(N=10^{20}cm^{-3},w_{sp}=0.1cm, J_{VR} =1.25x10^{-3}A/cm^2, C_{Ox} =3.0x10^{-4}mol/cm^3, D_{Ox} = 1.8x10^{-5}cm^2/s and J_{VR1}=9.58x10^{-4}A/cm^2); and (b) devices with modified self-discharge parameters (N=10^{19}cm^{-3},wsp=0.1cm, J_{VR} =0.0004A/cm^2, C_{Ox} = 3.0x10^{-5}mol/cm^3, D_{Ox} = 1.8x10^{-6}cm^2/s and J_{VR1}=9.58x10^{-5}A/cm^2).

Tuning the self-discharge key parameters enhanced the energy retention capability of ECs with electrode effective conductivity α_1 =0.0500, 0.0050, 0.0010 and 0.0005S/cm from 38.7 days, 38.0 days, 34.3 days and 31.3 days to 135.4 days, 133.1 days 121.2 days and 112.8 days respectively. It was also noticed that quick charging and discharging of capacitors significantly reduced the self-discharge rate and energy loss during the operation as shown in Figures 5.15, 5.16, 5.17 and 5.18, compared with slow charging and discharging as seen in Figure 5.14.

5.3 The Influences of Operating Conditions and Design Configurations on the Performance of Symmetric Electrochemical Capacitors

This section discusses the effects of different charging current densities, charging times, electrode and electrolyte effective conductivities, and structural parameters such as the thickness of electrodes, porosity, separator thickness and porosity on the performance of symmetric ECs. Mathematical representation of mass transfer and charge conservation equations of electrochemical capacitors during charging and discharging, based on the work of Kazaryan et al. [89] were derived and used to perform this task. It was assumed that side-reactions or reactions of active redox species and several impurities and the electric double layers' (EDLs') instability are responsible for self-discharge. The EDLs' instability self-discharge is due to the presence of functional groups or impurity ions in the electrode materials, shuttling of electrolyte impurities among electrodes, charge redistribution and attractive force from opposite ions in the electrolyte phase. A couple of numerical experiments were performed using MATLAB R2014a, in order to examine the influences of various operating conditions and design configurations on EC capacitance, energy density and power density. The simulation results obtained could be employed to optimize the design of ECs for practical applications.

5.3.2 Discussions

In order to validate the model accuracy, simulation curves of the length over which the liquid potential drop occurs in electrodes $[w_e]$ were compared with those of experimental data reported by Ma et al. [275] and Sun et al. [276], as well as those of Kazaryan et al.

[89] data. All developed models were also validated with experimental data reported by following research groups in literature: Kazaryan et al. [89], Ma et al. [275], Sun et al. [276] and Zhao et al. [277]. The experimental data of two symmetric button electrochemical capacitors $Mn_3(PO_4)_2//Mn_3(PO_4)_2$ composite electrodes using aqueous $1molL^{-1}$ Na_2SO_4 electrolyte and aqueous $2molL^{-1}$ KOH electrolyte [275] was used to validate symmetric models. Also, experimental data of a symmetric capacitor with nitrogen-doped rapeseed activated carbons (N-RCs) composite electrodes and 1100CNFs webs electrodes with aqueous $0.5molL^{-1}$ and $1mol\ L^{-1}$ Na_2SO_4 electrolyte respectively [276] and [277] was used to validate the symmetric models. The performance parameters to be measured and determined at various current densities are charging time, discharging time, specific capacitance, energy density and power density. Plots of specific capacitance and specific energy and the specific power of fabricated symmetric button devices reported by Ma et al. [275], Sun et al. [276] and Zhao et al .[277] were also used to verify the validity of the models. The fabricated button devices were charged from 0.0V to 1.6V and 1.0V, and thereafter discharged from 1.6V and 1.8V to 0.0V, respectively.

In the simulation, the EC was charged from its lower voltage of 0.0V to the upper voltage of 1.2V. The porous electrode theory that does not consider the electrode's diverse microstructure like morphology, pore forms, pore dimensions, and the pore linkages for a One-Dimensional model was used. The data operated upon were based on experiment variables of Kazaryan et al.[89] and Staser et al.[90] presented in Table 5.8 and sensible figures were assigned, based on literature, to the parameters which are unavailable. The EC discharged to 0.0V and was charged by constant current to the upper voltage of 1.2V for the charging period (t_{ch}) of 5h. Thereafter it was discharged by a constant current to the lower voltage of 0.0V for a discharging period (t_{dis}) of 5h. The mass transfer and charge conservation equations of each capacitor's component during the charging and discharging

processes were considered, and the current collector's resistance were ignored due to their high conductivity.

Table 5.8: The model parameters used for simulation influences of operating conditions and design configurations on the performance of symmetric electrochemical capacitors

Parameters name	**Parameter's symbol**	**Units**	**Positive electrode**	**Negative electrode**
Applied current density	J_0	A/cm^2	0.00533 [89]	–
Capacitance per unit volume	C_v	F/cm^3	400 [89]	400 [89]
Electrode thickness	w_e	cm	0.2 [89]	0.2 [89]
Electrode visible surface area	A	cm^2	6290 [89]	6290 [89]
Electrode effective conductivity	α_1	S/cm	50 [assumed]	50 [assumed]
Electrolyte effective conductivity	α_2	S/cm	0.5 [89]	0.5 [89]
Separator's thickness	w_{sp}	cm	0.05 [89]]	–
Electrode density	ρ_e	g/cm^3	1.0 [90]	1.0 [90]
Electrolyte density	ρ_l	g/cm^3	1.25 [90]	1.25 [90]
Separator density	ρ_{sp}	g/cm^3	0.95 [90]	–
Electrode porosity	ε_e	–	0.25 [90]	0.25 [90]
Separator porosity	ε_{sp}	–	0.70 [90]	–
specific internal ohmic resistance	ρ_{int}	Ωcm^2	9 [assumed]	9 [assumed]

Generally, solid-phase conductivity is reasonably greater than liquid-phase conductivity in electrochemical capacitor. Thus, the solid-phase potential drop is considerably lower than that of the liquid-phase during the capacitor's charging or discharging. The electrodes of the device are similar in terms of composition since it is a symmetric EC. The total current in the electrodes is a total of electronic current J_1 and ionic current J_2, whereas the entire current in the separator is ionic. The total current at the electrode/separator interface is purely by ions, whereas total current at the interface of the current collector/electrode is purely by electrons.

In the subsequent sections, modelling and simulation was used to present the effects of using different design variables/configurations and operating conditions like charging rate and time, electrodes and electrolyte effective conductivities, electrode thickness, electrode porosity and separator porosity on the performance of the EC during charging and discharging. Furthermore, the EC's performance was presented on ragone plots for several design variables and operating conditions. These plots could be used to obtain optimum design parameters and operating conditions for realistic application, because every utilization has a definite energy and power density that match exactly with an area on the ragone graph.

5.3.1.1 Effects of concentration of impurity ions and active redox species in capacitor's components

Side-reactions or reactions of active redox species and several impurities in the electrodes, electrolytes, separator, current collectors and various functional groups on CNTs electrodes are sources of the ECs self-discharge processes. Also, migration of impurity ions or redox species from one electrode to other and the instability of the electric double layers are responsible for self-discharge processes, but side-reactions perform a dominant role in the EC's self-discharge processes. If the concentration of impurity ions and redox species in the device is high, the rate of self-discharge will be high and cell potential and voltage will decay due to self-discharge as presented in Figure 5.23. High concentrations of impurity ions and redox species in the device leads to a high rate of self-discharge caused by diffusion of ions in the EDLs, migration/shuttling of products of redox reactions from one electrode to another and consumption of negative charges on the cathode. It follows from Figure 5.23 that the capacitor of electrode and electrolyte effective conductivities of $\alpha_1 = \alpha_2 =$ 0.05S/cm without self-discharge, was charged to a potential of

– 0.6V as in Figure 5.23a, while a similar device with only EDL's instability self-discharge and both side-reactions/redox reactions and EDL's instability were charged to a potential of – 0.55V and – 0.40V as seen in Figures 5.23b and 5.23c, respectively.

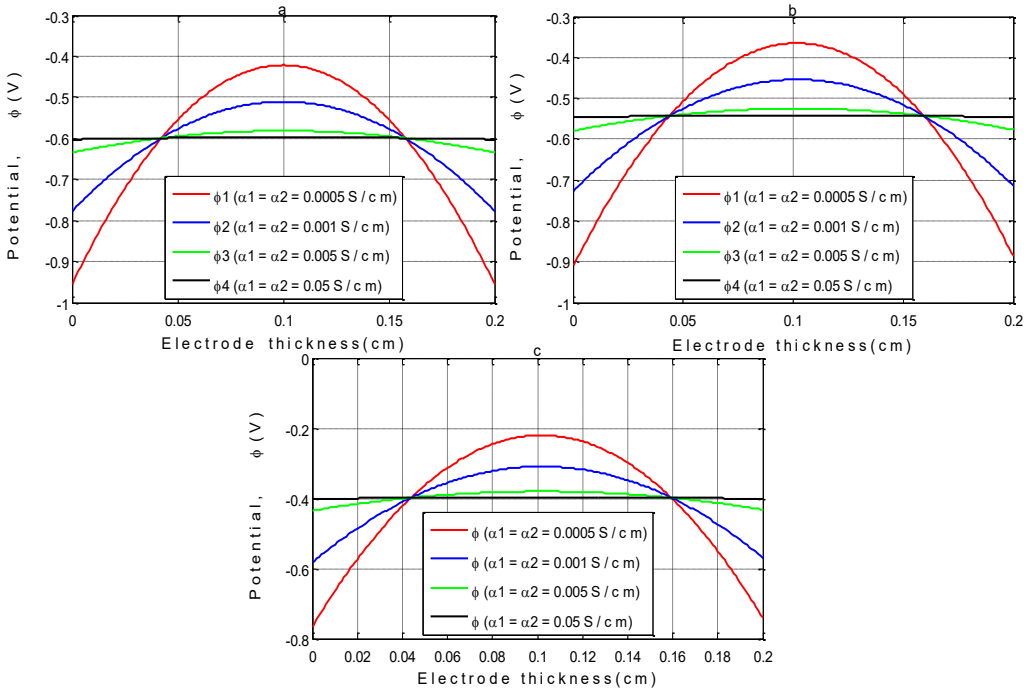

Figure 5.23: Potential distribution profiles within electrode of different electrode and electrolyte effective conductivities values α_1 and α_2 as function of position after constant current charging of capacitors (a) without self-discharge (b) with only EDLs instability self-discharge, and (c) with both side-reactions/redox reactions and EDLs instability self-discharge.

5.3.1.2 Effects of charging current density and charging time (charging rate)

In order to carry out a more accurate comparison of the parameters of ECs with various charging rates, charging current densities and charging times are selected so as to make

sure that the multiplying factor of current density is equal to the division factor of charging time. This is significant since the increase in the EC's charging current density and reduction in charging duration results in a change of the device voltage operating range and energy parameters. The rate of the change is related to electrode parameters and the value of the capacitor's applied current density. For instance, the charging condition with capacitor electrode's effective conductivity of α_1=50S/cm, electrolyte effective conductivity of α_2=0.05S/cm, and 0.2cm electrode thickness can be increased from 0.00533A/cm^2 for 18000s by multiplying the current density and dividing the charging time by a factor of 10, 100 and 1000, respectively. This results in the following charging conditions: 0.0533A/cm^2 for 1800s, 0.533A/cm^2 for 180s and 5.33A/cm^2 for 5.062s as shown in Table 5.9.

Generally, potential drop in the solid-phase is significantly lower than that in the liquid-phase, because solid-phase conductivity is significantly larger than liquid-phase conductivity in electrochemical capacitors. At high charging or discharging rates, charging/reaction occurs much faster close to the electrode/separator interface and the remaining portion of the electrode is not utilized due to the small time scale. Thus, the length over which the liquid potential drop happens ($[w_e]$) is not the entire electrode thickness, but a width determined by the applied current density. The length corresponds to the degree of electrode utilization at a given applied current density. This length can be employed as design parameter to optimize electrodes thickness in capacitors designed to function under specific current ranges. The length $[w_e]$ decreases along with increases in the current density for specific electrode and electrolyte effective conductivities and

electrode thickness as presented in Tables 5.9–5.12. This is also clearly seen in equation 4.120.

Table 5.9: ECs component scales for different applied current densities J_0, A/cm^2 and α_2 = 0.5S/cm

Parameters and its Expressions	α_1 **=50S/cm,** α_2 **=0.5S/cm,** w_e **=0.2cm,** V_{cell} **=1.2V and** w_{sp} **=0.05cm**			
	Current Density, J_0 **(A/cm^2)**			
	0.00533	**0.05330**	**0.53300**	**5.33000**
$[w_e]=\frac{\alpha_2 V_{cell}}{2J_0}$ (cm)	$5.629\text{x}10^{1}$	$5.629\text{x}10^{0}$	$5.629\text{x}10^{-1}$	$5.629\text{x}10^{-2}$
$[w]=\min\left(\frac{\alpha_2 V_{cell}}{2J_0}, w_e\right)$ (cm)	$2.000\text{x}10^{-1}$	$2.000\text{x}10^{-1}$	$2.000\text{x}10^{-1}$	$5.629\text{x}10^{-2}$
$\Delta\varphi_1(x,t)=\frac{J_0[w]}{\alpha_1}$ (V)	$2.132\text{x}10^{-5}$	$2.132\text{x}10^{-4}$	$2.132\text{x}10^{-3}$	$6.000\text{x}10^{-3}$
$\Delta\varphi_2(x,t)=\frac{J_0[w]}{\alpha_2}$ (V)	$2.132\text{x}10^{-3}$	$2.132\text{x}10^{-2}$	$2.132\text{x}10^{-1}$	$6.000\text{x}10^{-1}$
$\Delta\varphi_{2sp}(x,t)=\frac{J_0 w_{sp}}{\alpha_2}$ (V)	$5.330\text{x}10^{-4}$	$5.330\text{x}10^{-3}$	$5.330\text{x}10^{-2}$	$5.330\text{x}10^{-1}$
$\lambda=\frac{2J_0[w]}{\alpha_2 V_{cell}}$	$3.553\text{x}10^{-3}$	$3.553\text{x}10^{-2}$	$3.553\text{x}10^{-1}$	$1.000\text{x}10^{0}$
$[t_{scale}]=\frac{[w]A_d C_d V_{cell}}{J_0}$ (s)	$1.801\text{x}10^{4}$	$1.801\text{x}10^{3}$	$1.801\text{x}10^{2}$	$5.062\text{x}10^{0}$

The charging rate is estimated as the amount of applied charging current per unit of area and time (A/cm^{2}s), and this shows the speed with which capacitors are charged or discharged. The charging or discharging time (time scale) of electrochemical capacitors decreases along with an increase in applied current density as presented in Tables 5.9–5.12. For example, the charging time of a similar capacitor with electrodes effective conductivity of α_1=50S/cm, electrolyte effective conductivity of α_2=0.05S/cm, and 0.2cm electrode thickness using four different current densities (J_0=5.33x10^{-3}A/cm^2, 5.33x10^{-2}A/cm^2, 0.533A/cm^2 and 5.33A/cm^2) are 18011.3s, 1801.100s, 180.100s and 5.062s

respectively as shown in Table 5.9. The applied current density to effectively charge a capacitor is largely dependent upon electrodes and electrolyte effective conductivities as well as electrodes thickness. This is supported by equations 4.116 and 4.117.

Figure 5.24 depicts the solid and liquid-phase potential drops in capacitors of the same electrode thickness charged at various current densities and electrode and electrolyte effective conductivities. Since solid and liquid-phase potential drops varies with three variables (applied current density, electrodes thickness and effective conductivity) according to equations 4.116 and 4.117, potential drops in the device, charged at different applied current density, were presented in terms of the electrode effective conductivity, electrolyte effective conductivity and electrode thickness. The potential drop value for each applied current density at every point along the electrode thickness was equally shown in Figure 5.24. For example, when a capacitor with electrodes and electrolyte effective conductivities α_1=50S/cm and α_2=0.5S/cm was charged at four different current densities (J_0= 5.33x10^{-3}A/cm^2, 5.33x10^{-2}A/cm^2, 0.533A/cm^2 and 5.330A/cm^2), solid and liquid-phase potential drops were 2.132 x10^{-5}V, 2.132 x10^{-4}V, 2.132 x10^{-3}V & 6.0 x10^{-3}V and 2.132 x10^{-3}V, 2.132 x10^{-2}V, 0.2132V & 0.600V respectively as presented in Table 5.9 and Figures 5.24a and 5.24c respectively. The liquid-phase potential drops when the device was charged at a current density of 0.533A/cm^2 and 5.330A/cm^2 were both half of cell voltage (0.600V). The plot of current density of 0.533A/cm^2 was not shown in Figures 5.24b and 5.24d, because its value was equal to that of 5.33A/cm^2. Similarly, the liquid-phase potential drop in the device with α_2=0.005S/cm charged at the four current densities was 0.020V, 0.600V, 0.600V and 0.600V, respectively as presented in Table 5.10. Again, The liquid-phase potential drop in the capacitor with α_2=0.005S/cm was 0.200V and

0.600V in the first and last three densities respectively, as shown in Table 5.11, and was 0.600V in all the four current densities as presented in Table 5.12.

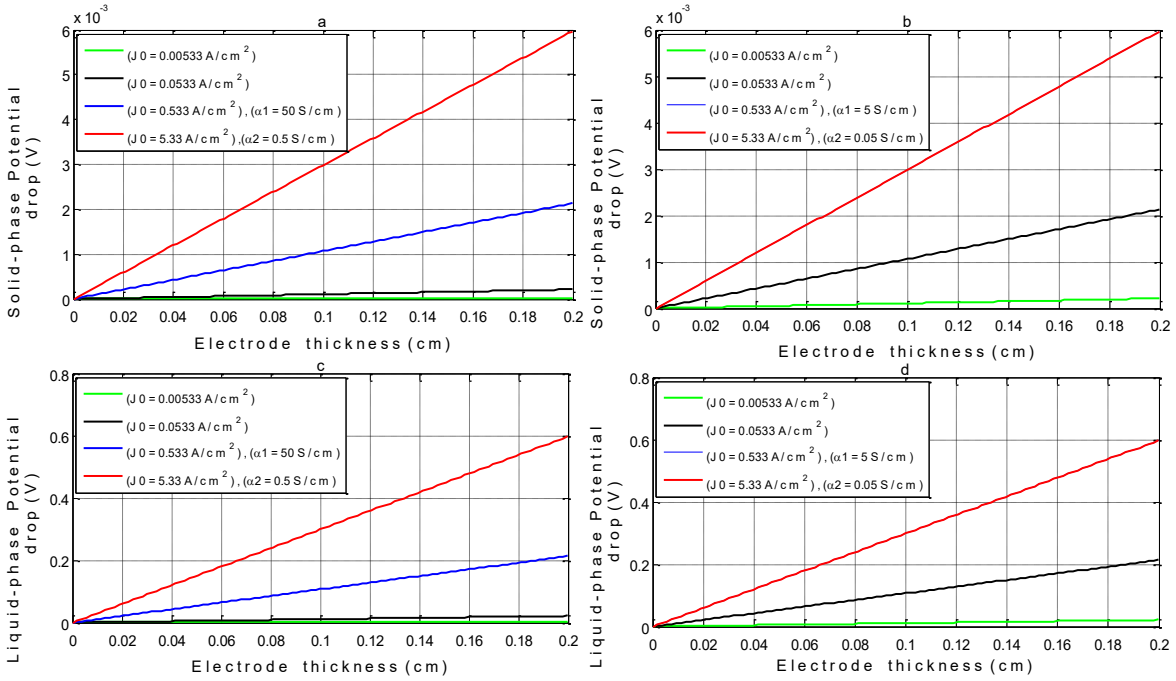

Figure 5.24: Solid-phase potential drop in capacitors of the same electrode thickness charged at various current densities and of electrode and electrolyte effective conductivities of (a) α_1 = 50S/cm and α_2 = 0.50S/cm; (b) α_1 = 5S/cm and α_2 = 0.05S/cm; liquid-phase potential drop in capacitors of the same electrode thickness charged at various current densities and of electrode and electrolyte effective conductivities of (c) α_1 = 50S/cm and α_2 = 0.50S/cm; and (d) α_1 = 5S/cm and α_2 = 0.05S/cm.

Table 5.10: ECs component scales for different applied current densities J_0, A/cm^2 and α_2 = 0.05S/cm

Parameters and its Expressions	**α_1 =5S/cm, α_2 =0.05S/cm, w_e =0.2cm, V_{cell} =1.2V and w_{sp} =0.05cm**			
	Current Density, J_0 (A/cm^2)			
	0.00533	**0.05330**	**0.53300**	**5.33000**
$[w_e] = \frac{\alpha_2 V_{cell}}{2J_0}$ (cm)	5.629x10^{0}	5.629x10^{-1}	5.629x10^{-2}	5.629x10^{-3}

$[w]=\min\left(\frac{\alpha_2 V_{cell}}{2J_0}, w_e\right)$ (cm)	$2.000\text{x}10^{-1}$	$2.000\text{x}10^{-1}$	$5.629\text{x}10^{-2}$	$5.629\text{x}10^{-3}$
$\Delta\varphi_1(x,t)=\frac{J_0[w]}{\alpha_1}$ (V)	$2.132\text{x}10^{-4}$	$2.132\text{x}10^{-3}$	$6.000\text{x}10^{-3}$	$6.000\text{x}10^{-3}$
$\Delta\varphi_2(x,t)=\frac{J_0[w]}{\alpha_2}$ (V)	$2.132\text{x}10^{-2}$	$2.132\text{x}10^{-1}$	$6.000\text{x}10^{-1}$	$6.000\text{x}10^{-1}$
$\Delta\varphi_{2sp}(x,t)=\frac{J_0 w_{sp}}{\alpha_2}$ (V)	$5.330\text{x}10^{-3}$	$5.330\text{x}10^{-2}$	$5.330\text{x}10^{-1}$	$5.330\text{x}10^{0}$
$\lambda=\frac{2J_0[w]}{\alpha_2 V_{cell}}$	$3.553\text{x}10^{-2}$	$3.553\text{x}10^{-1}$	$1.000\text{x}10^{-1}$	$1.000\text{x}10^{0}$
$[t_{scale}]=\frac{[w]A_d C_d V_{cell}}{J_0}$ (s)	$1.801\text{x}10^{4}$	$1.801\text{x}10^{3}$	$5.069\text{x}10^{1}$	$5.069\text{x}10^{-1}$

Similarly, the solid-phase potential drop in the capacitor with electrodes and electrolyte effective conductivity α_1 =0.500S/cm and α_2 =0.005S/cm when charged at the four current densities was 2.132 x10^{-3}V, 6.0 x10^{-3}V, 6.0 x10^{-3}V and 6.0 x10^{-3}V, respectively as shown in Figures 5.25a and 5.25c. The plots of the capacitor charged at current densities with 0.0533A/cm^2 and 0.5330A/cm^2 were not shown in Figure 5.25a and 5.25c because their values were the same as that of 5.330A/cm^2. It was seen that the liquid-phase potential drop in the capacitor with electrolyte effective conductivity of α_2 =0.005S/cm, when charged at the four current densities were all high. The liquid-phase potential drop at a current density of 5.33x10^{-3}A/cm^2 was 0.200V, while the liquid-phase potential drop at the other current density was half of the cell voltage (0.600V). Again, the solid-phase potential drop in the capacitor with electrodes and electrolyte effective conductivity of α_1 = 0.0500S/cm and α_2 = 0.0005S/cm, when charged at the four current densities was 6.0 x10^{-3}V, while that in the liquid-phase was 0.600V as presented in Table 5.12 and Figures 5.25b and 5.25d.

Also, plots of the capacitor charged at a current density of 0.0053A/cm^2, 0.0533A/cm^2 and 0.5330A/cm^2 were not shown in Figure 5.25b and 5.25d, because they coincided with that

of 5.3300A/cm^2. The liquid-phase potential drops when the device was charged at the four current densities were all equal to half of the device voltage (0.600V).

Table 5.11: ECs component scales for different applied current densities J_0, A/cm^2 and α_2 = 0.005S/cm

Parameters and its expressions	α_1 **=0.5S/cm,** α_2 **=0.005S/cm,** w_e **=0.2cm,** V_{cell} **=1.2V and** w_{sp} **=0.05cm**			
	Current Density, J_0 **(A/cm^2)**			
	0.00533	**0.05330**	**0.53300**	**5.33000**
$[w_e] = \frac{\alpha_2 V_{cell}}{2J_0}$ (cm)	5.629x10^{-1}	5.629x10^{-2}	5.629x10^{-3}	5.629x10^{-4}
$[w] = \min\left(\frac{\alpha_2 V_{cell}}{2J_0}, w_e\right)$ (cm)	2.000x10^{-1}	5.629x10^{-2}	5.629x10^{-3}	5.629x10^{-4}
$\Delta\varphi_1(x,t) = \frac{J_0[w]}{\alpha_1}$ (V)	2.132x10^{-3}	6.000x10^{-3}	6.000x10^{-3}	6.000x10^{-3}
$\Delta\varphi_2(x,t) = \frac{J_0[w]}{\alpha_2}$ (V)	2.132x10^{-1}	6.000x10^{-1}	6.000x10^{-1}	6.000x10^{-1}
$\Delta\varphi_{2sp}(x,t) = \frac{J_0 w_{sp}}{\alpha_2}$ (V)	5.330x10^{-2}	5.330x10^{-1}	5.330x10^{0}	5.330x10^{1}
$\lambda = \frac{2J_0[w]}{\alpha_2 V_{cell}}$	3.553x10^{-1}	1.000x10^{-1}	1.000x10^{0}	1.000x10^{0}
$[t_{scale}] = \frac{[w]A_d C_d V_{cell}}{J_0}$ (s)	1.801x10^{4}	5.069x10^{2}	5.069x10^{0}	5.069x10^{-2}

This shows that it was not effective and realistic to charge the capacitor with electrolyte effective conductivity of α_2 = 0.0005S/cm at the four current densities examined, since the liquid-phase potential drop was up to half of the cell voltage. Also, it was not effective to charge the capacitor with electrolyte effective conductivity of α_2 = 0.0050S/cm at current densities of 5.33x10^{-2}A/cm^2, 0.533A/cm^2 and 5.330A/cm^2 because the liquid-phase potential drop was also half of the device voltage. Again, it was ineffective for the capacitor with electrolyte effective conductivity of α_2=0.0500S/cm to be charged at current densities of 0.5330A/cm^2 and 5.3300A/cm^2. It was also unrealistic for the device

with electrolyte effective conductivity of α_2 =0.5000S/cm to be charged at a current density of 5.3300A/cm^2, because the liquid-phase potential drop in the device was half of the cell voltage.

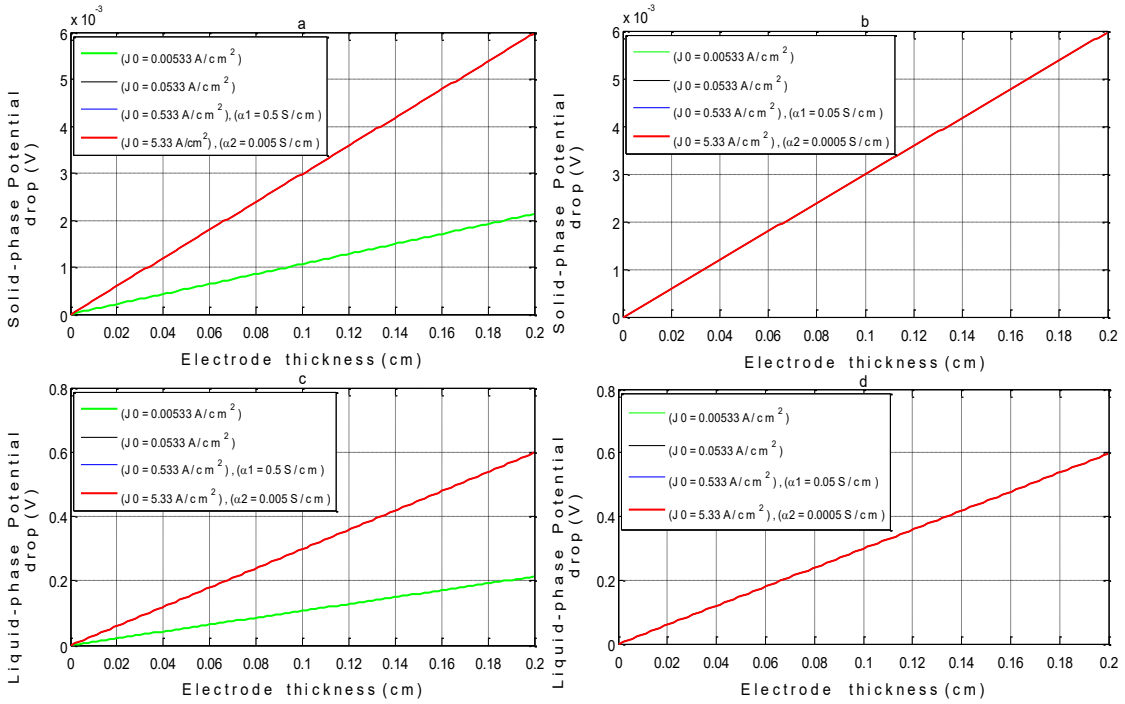

Figure 5.25: Solid-phase potential drop in capacitors of the same electrode thickness charged at various current densities and of electrode and electrolyte effective conductivity of (a) α_1 = 0.5000S/cm and α_2 = 0.0050S/cm; (b) α_1 = 0.0500S/cm and α_2 = 0.0005S/cm; liquid-phase potential drop in capacitors of the same electrode thickness charged at various current densities and electrode and electrolyte effective conductivity of (c) α_1 = 0.5000S/cm and α_2 = 0.0050S/cm; and (d) α_1 = 0.0500S/cm and α_2 = 0.0005S/cm.

The effective charging time of the capacitor with electrodes and electrolyte effective conductivities α_1 = 50S/cm and α_2 = 0.50S/cm, at current densities of 5.33x10^{-3}A/cm^2, 5.33x10^{-2}A/cm^2, 0.533A/cm^2 and 5.33A/cm^2 are 1.801x10^{4}s, 1.801x10^{3}s, 1.801x10^{2}s and 5.062s, respectively as presented in Table 5.9 and Figure 5.26a. Also, the effective charging time of the capacitor with electrodes and electrolyte effective conductivities α_1

=5.00S/cm and α_2 = 0.05S/cm, at the same current densities are 1.801x10^{4}s, 1.801x10^{3}s, 50.6900s and 0.5069s, respectively as presented in Table 5.10 and Figure 5.26b.

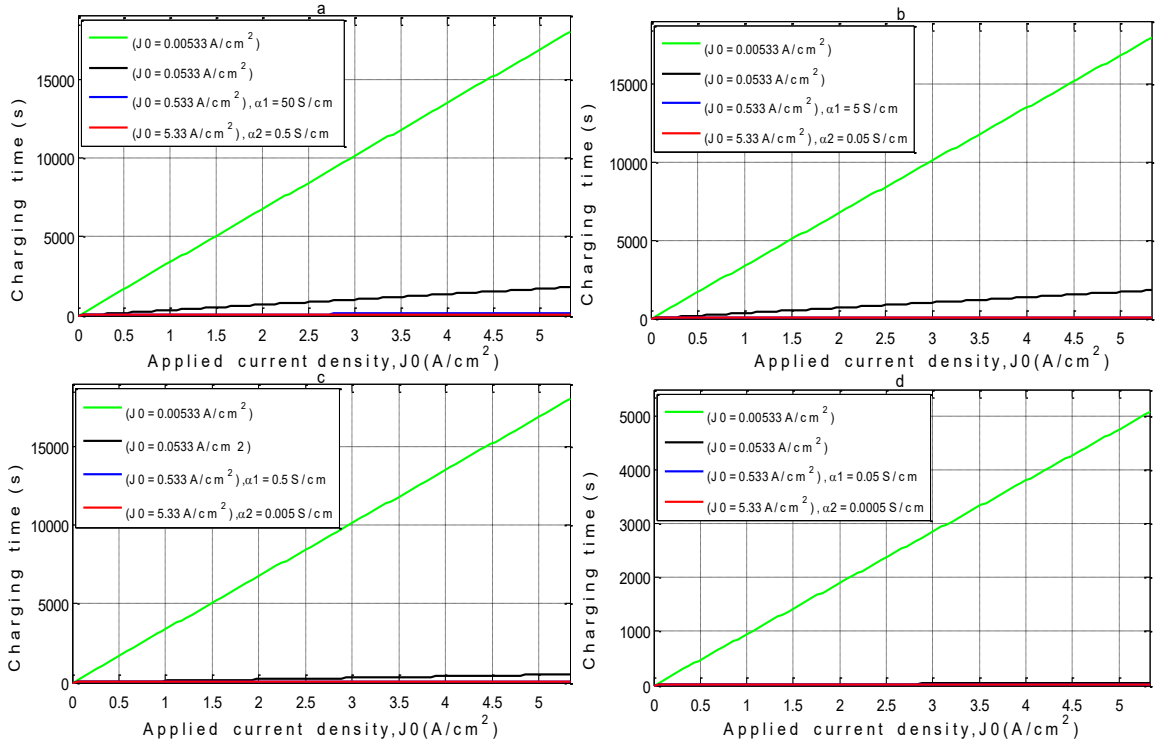

Figure 5.26: Charging times of capacitors of the same electrode thickness and of electrode and electrolyte effective conductivity charged at various current densities with (a) α_1 =50S/cm and α_2 = 0.500S/cm; (b) α_1 =5S/cm and α_2 =0.050S/cm; (c) α_1 = 0.500S/cm and α_2 = 0.005S/cm; and (d) α_1 = 0.050S/cm and α_2 = 0.0005S/cm.

Again, the effective charging time of the capacitor with electrodes and electrolyte effective conductivities α_1 =0.500S/cm and α_2 =0.005S/cm, charged at the same current densities was 1.801x10^{4}s, 5.069x10^{2}s, 5.069s and 0.05069s, respectively as presented in Table 5.11 and Figure 5.26c. The effective charging time of the capacitor with electrodes and electrolyte effective conductivities α_1 =0.050S/cm and α_2 =0.0005S/cm, charged at the same current densities was 5.069x10^{3}s, 50.69s, 0.507s and 5.069x10^{-3}s, respectively as presented in Table 5.12 and Figure 5.26d. It follows from these results and equation 4.113, that the

capacitor's charging time reduced with an increase in applied current density because higher current density means a higher charging rate.

Table 5.12: ECs component scales for different applied current densities J_0, A/cm^2 and α_2 = 0.0005S/cm

Parameters and its expressions	**α_1 =0.05S/cm, α_2 =0.0005S/cm, w_e =0.2cm, V_{cell} =1.2V and w_{sp} =0.05cm**			
	Current Density, J_0 (A/cm^2)			
	0.00533	**0.05330**	**0.53300**	**5.33000**
$[w_e]=\frac{\alpha_2 V_{cell}}{2J_0}$ (cm)	5.629 x10^{-2}	5.629 x10^{-3}	5.629 x10^{-4}	5.629 x10^{-5}
$[w]=\min\left(\frac{\alpha_2 V_{cell}}{2J_0}, w_e\right)$ (cm)	5.629 x10^{-2}	5.629x10^{-3}	5.629 x10^{-4}	5.629 x10^{-5}
$\Delta\varphi_1(x,t)=\frac{J_0[w]}{\alpha_1}$ (V)	6.000 x10^{-3}	6.000x10^{-3}	6.000 x10^{-3}	6.000 x10^{-3}
$\Delta\varphi_2(x,t)=\frac{J_0[w]}{\alpha_2}$ (V)	6.000 x10^{-1}	6.000 x10^{-1}	6.000 x10^{-1}	6.000 x10^{-1}
$\Delta\varphi_{2sp}(x,t)=\frac{J_0 w_{sp}}{\alpha_2}$ (V)	5.330 x10^{-1}	5.330 x10^{0}	5.330 x10^{1}	5.330 x10^{2}
$\lambda=\frac{2J_0[w]}{\alpha_2 V_{cell}}$	1.000 x10^{0}	1.000 x10^{0}	1.000 x10^{0}	1.000 x10^{0}
$[t_{scale}]=\frac{[w]A_d C_d V_{cell}}{J_0}$ (s)	5.069 x10^{3}	5.069 x10^{1}	5.069 x10^{-1}	5.069 x10^{-3}

Figure 5.27 depicts the voltage decay in the asymmetric EC of the effective conductivities of different electrodes over time, due to both redox reactions and the EDL's instability self-discharge, when charged from 0.00V to 1.20V at different charging conditions. It follows from Figures 5.27a and 5.27b that the voltage drop at the initial stage of self-discharge (600s and 60s respectively) was very sharp for charging conditions of 0.0053A/cm^2 for 18000s and 0.0532A/cm^2 for 1800s. This was because redox products have enough time to migrate from one electrode to the other, where they consume negative charges and diffuse into EDLs, and increase the self-discharge rate there. When the

capacitor was charged at 0.5320A/cm^2 for 180s, the voltage drop was very small at the first 6s and thereafter the voltage became approximately constant throughout the remaining period as seen in Figure 5.27c. When the capacitors were charged at an applied current density of 5.3200A/cm^2 for 18s, voltage drops were so insignificant that their profiles remained constant throughout the duration as shown in Figure 5.27d. Reduction of charging time by charging the EC fast with a high current density greatly reduced the rate of self-discharge during charging, compared with slow charging with low current density.

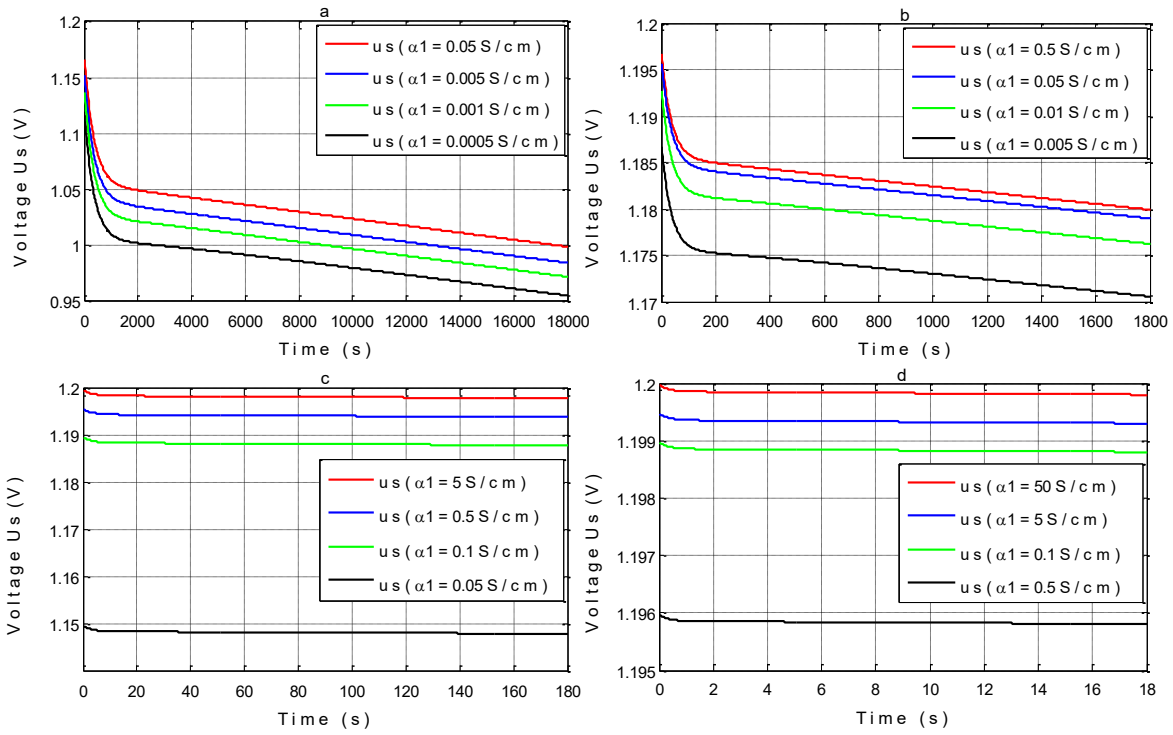

Figure 5.27: The voltage decay in symmetric ECs of different electrodes effective conductivities over time due to both redox reactions and EDLs instability self-discharge after devices were charged from 0V to 1.2V at current density of (a) 0.0053A/cm^2 for 18000s charging time; (b) 0.0532A/cm^2 for 1800s charging time; (c) 0.5320A/cm^2 for 180scharging time; and (d) 5.3200A/cm^2 for 18s charging time.

5.3.1.3 Effects of electrodes and electrolyte effective conductivities

In order to study the effect of various effective conductivities of the electrode and electrolyte on the EC's performance, solid and liquid-phase potential drops and the length over which liquid potential drop occurs in electrodes $[w_e]$ under given operating conditions, were considered in devices of different effective conductivities. The value of current density that should be used to successfully charge an EC is largely determined by the effective conductivities of the electrode and electrolyte, as well as the electrode's thickness. In fact, the applied current density to effectively charge an EC is mainly determined by the effective conductivities of electrolyte and electrodes thickness, because electrode conductivity is usually very high compared with electrolyte conductivity in ECs.

Figures 5.28 depicts the length over which the liquid potential drop occurs in electrodes $[w_e]$ of devices of different effective conductivities and different current densities. It follows from Figure 5.28 that the length over which the liquid potential drop occurs in a capacitor with given electrode and electrolyte effective conductivities charged at different current densities, decreased along with the increase in current density. It follows from Figure 5.28a that the capacitor with an electrodes thickness of 0.200cm and electrolyte effective conductivity of 0.500S/cm and 0.050S/cm, should not be charged with current density greater than 1.500A/cm^2 and 0.150A/cm^2 respectively, because this will result in a high liquid-phase potential drop. For a given current density to be effective in charging a capacitor of a given thickness and electrolyte effective conductivity, the length over which the liquid potential drop occurs in electrodes $[w_e]$ must be equal to, or more than the electrode's thickness.

Figures 5.28b shows the length over which the liquid potential drop occurs in electrodes $[w_e]$ in simulation of the study of the experiments of Kazaryan et al. and Sun et al. with electrolyte's effective conductivity of 0.060S/cm, 0.050S/cm and 0.051S/cm, respectively. It follows from Figure 5.28b that the effective current density for the capacitor is less than or equal to 0.150A/cm^2, less than or equal to 0.180A/cm^2 and less than or equal to 0.250A/cm^2, respectively. Figure 5.28b shows that the mean relative error between the lengths over which the liquid potential drop occurs in electrodes determined from simulation of the model, Kazaryan et al. and Sun et al. experimental data, was equal to 1.8% and 2% (highest relative error was 4% and 6% respectively).

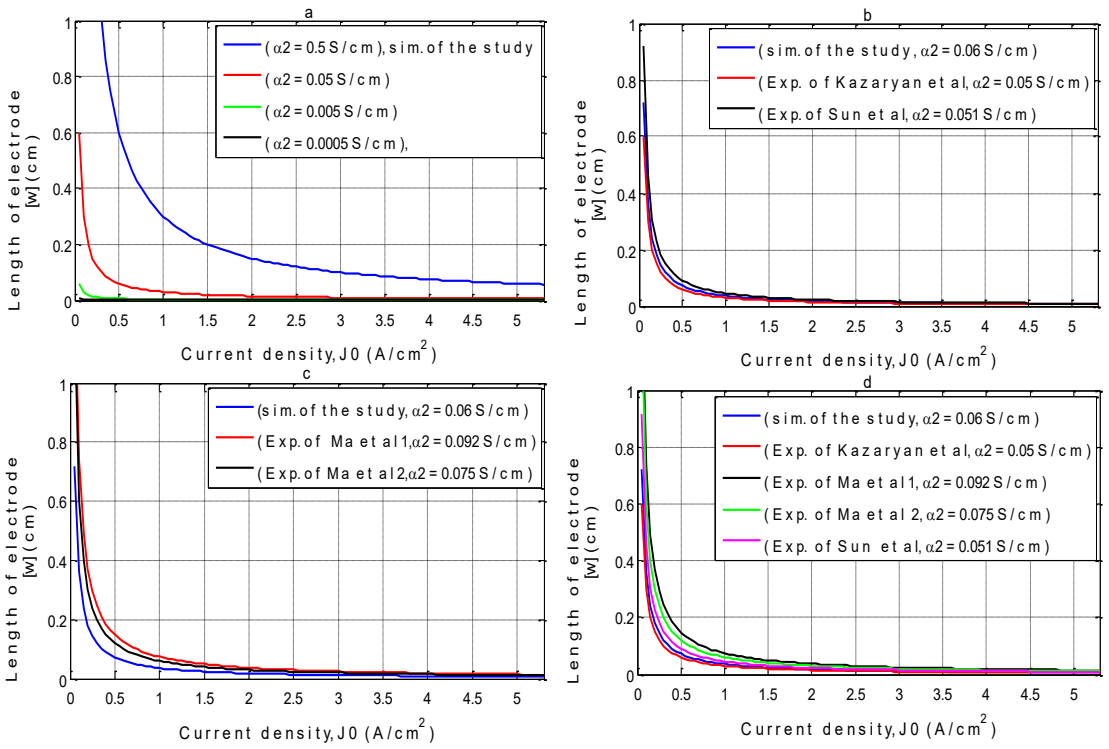

Figure 5.28: The length over which liquid potential drop occurs in electrodes $[w_e]$ of device of different effective conductivities at different current densities from (a) Simulation in this study; (b) simulation in this study, and experimental data from Kazaryan et al and Sun et al (c) simulation in this study, and experimental data from Ma et al 1- with 1 molL^{-1} Na_2SO_4 and Ma et al 2- with 0.5 molL^{-1} Na_2SO_4 aqueous electrolytes; and (d) simulation in this

study, and experimental data from Kazaryan et al, Sun et al, Ma et al 1- with 1 $molL^{-1}$ Na_2SO_4 and Ma et al 2- with 0.5 $molL^{-1}$ Na_2SO_4.

The mean relative error between the lengths over which the liquid potential drop occurs in electrodes, is determined from simulation of the model, Ma et al. 1 and Ma et al. 2 Experimental data was equal to 2% and 3% (highest relative error was 6% or 7%) as shown in Figure 5.28c. Comparison of the lengths over which the liquid potential drop occurs in electrodes was determined from simulation of the model, Kazaryan et al., Ma et al. 1, Ma et al. 2 and Sun et al. Experimental data were also presented in Figure 5.28d.

Figures 5.29 depicts the effective thickness of electrodes in a capacitor of different electrolyte effective conductivities charged at different current densities. Figure 5.29 shows that the effective thickness of electrodes in a capacitor with the electrolyte's effective conductivity of 0.5S/cm, decrease as applied current density increases. For example, the effective thickness of electrodes in the capacitor with electrolyte's effective conductivity of 0.500S/cm, when charged at a current density of 1.000A/cm^2, 1.500A/cm^2, 2.000A/cm^2, 3.000A/cm^2, and 6.000A/cm^2 was 0.300cm, 0.200cm, 0.150cm, 0.100cm and 0.050cm respectively, as pictured in Figure 5.29a. In addition, the effective thickness of electrodes in the capacitor with electrolyte's effective conductivity of 0.050S/cm, when charged at a current density of 1.000A/cm^2, 1.500A/cm^2, 2.000A/cm^2, 3.000A/cm^2, and 6.000A/cm^2 was 0.030cm, 0.020cm, 0.015cm 0.010cm and 0.005cm, respectively as shown in Figure 5.29b. The effective thickness of the electrodes in the capacitor with electrolyte's effective conductivity of 0.005S/cm and 0.005S/cm, charged at the same current density was 0.003cm, 0.002cm, 0.0015cm 0.0010cm & 0.0005cm and 0.0003cm, 0.0002cm, 0.00015cm 0.0001cm and 0.00005cm, respectively as pictured in Figure 5.29c and 5.29d. The power density (rate of charging and discharging) of the device with the electrolyte's effective conductivity of 0.5000S/cm and electrodes thickness of 0.200cm,

expected to be charged at a current density of 1.500A/cm^2, can be increased by reducing the electrode's thickness to 0.150cm, 0.100cm and 0.050cm, and increasing the applied current density to 2.000A/cm^2, 3.000A/cm^2 and 6.000A/cm^2 respectively. Every charging current density of the capacitor, with electrolyte of a given effective conductivity, has a corresponding optimum electrode thickness (effective thickness) that results in 100% electrodes utilization with little or no potential drop in the liquid phase.

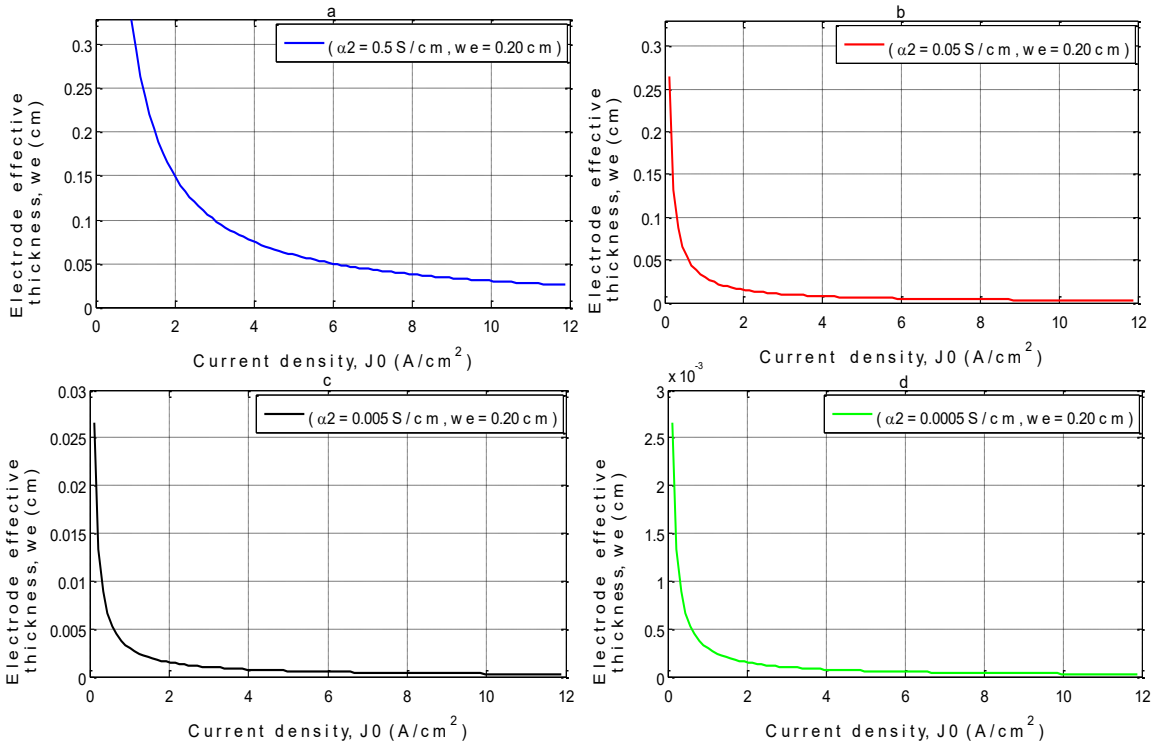

Figure 5.29: Electrodes effective thickness in capacitor with a given electrodes thickness and different electrolyte effective conductivities, charged at different current densities: with effective conductivities (a) $\alpha_1 =$ 5S/cm and $\alpha_2 =$ 0.500S/cm; (b) $\alpha_1 =$ 5S/cm and $\alpha_2 =$ 0.050S/cm; (c) $\alpha_1 =$ 5S/cm and $\alpha_2 =$ 0.005S/cm; and (d) $\alpha_1 =$ 5S/cm and $\alpha_2 =$ 0.0005S/cm.

Figure 5.30 depicts the utilization of electrodes in capacitors with the same electrode thickness and different electrolyte effective conductivities charged at different current densities. Figure 5.30a shows that the electrode's utilization in capacitors of 0.200cm

electrode thickness and electrolyte of effective conductivity of 0.5S/cm, are greater than or equal to 100% when charged at a current density range of 0.000A/cm^2 – 1.500A/cm^2. When the device was charged at a current density of 1.500A/cm^2, the electrode's utilization was 100% as shown in Figure 5.30a. When the capacitor with 0.200cm electrodes thickness and electrolyte of effective conductivity of 0.050S/cm was charged at a current density range of 0.000A/cm^2 – 0.200A/cm^2, the electrode's utilization was greater than or equal to 100% as pictured in Figure 5.30b.

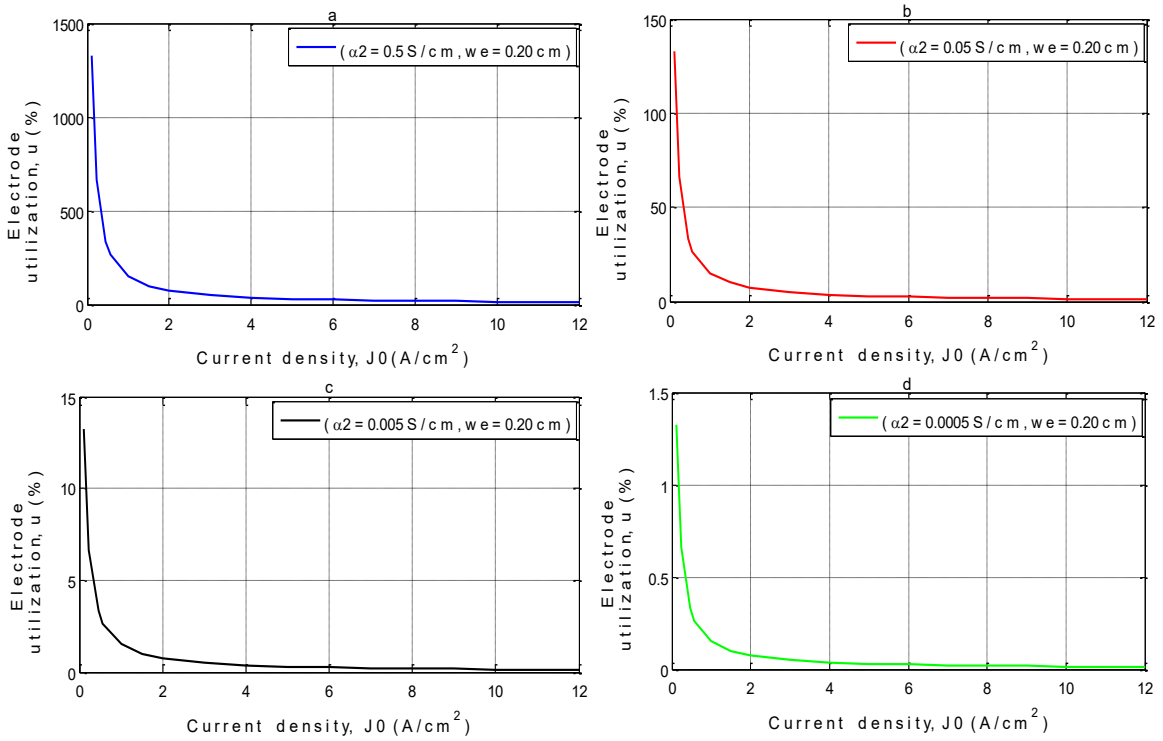

Figure 5.30: Electrodes utilization in capacitor with a given electrodes thickness and different electrolyte effective conductivities, charged at different current densities: with effective conductivities (a) α_1 = 5S/cm and α_2 = 0.500S/cm; (b) α_1 = 5S/cm and α_2 = 0.050S/cm; (c) α_1 = 5S/cm and α_2 = 0.005S/cm; and (d) α_1 = 5S/cm and α_2 = 0.0005S/cm.

When the capacitor's electrolyte effective conductivities are 0.0050S/cm and 0.0005S/cm, the electrodes' utilization were greater than or equal to 1% and 0.100% respectively, when

charged at a current density range of 0.00A/cm^2 – 1.500A/cm^2 as shown in Figures 5.30c and 5.30d. Figure 5.30 shows that the electrode's utilization in the device with electrolyte of specific effective conductivity, the electrode's thickness decreases' along with an increase in the applied current density.

In order to increase the power density (rate of charging and discharging per mass) of the capacitor without compromising energy density, effective conductivities of electrodes and electrolyte must be high enough, and high current density, with corresponding effective thickness of electrodes, must be selected. Since electrode conductivity is usually quite high in ECs [93,281,282], the solid-phase potential drop is mostly very small and negligible[93]. For instance, when the EC with α_1 = 50S/cm and α_2 = 0.500S/cm was charged at high current density of 5.330A/cm^2, the potential drop in the solid-phase was 0.006V, while that in the liquid-phase was 0.600V as presented in Table 5.9. The solid-phase potential drop in the device with electrodes and electrolyte effective conductivities α_1 = 5S/cm & α_2 = 0.050S/cm, α_1 = 0.500S/cm & α_2 = 0.005S/cm and α_1 =0.050S/cm & α_2 =0.0005S/cm, charged at a current density of 5.330A/cm^2 was 0.006V as presented in Tables 5.10–5.12; whereas the liquid-phase potential drop was 0.600V as shown in Tables 5.10–5.12.

It was clearly shown in Figure 5.24 and Table 5.9 that when the capacitor with electrolyte effective conductivity of 0.500S/cm was charged at high current density like 5.330A/cm^2, the length over which the liquid potential drop occurs ($[w_e]$) was smaller than the electrode's thickness and the liquid-phase potential drop became up to half of the cell voltage (0.600V). This implied that it was ineffective to charge such a device at 5.330A/cm^2 for the expected charging duration, since half of the cell voltage would be lost. On the same note, it was not effective to charge the capacitor with electrolyte of effective

conductivity of 0.050S/cm at current densities of 0.533A/cm^2 and 5.330A/cm^2 for the expected charging duration. This is because the length over which the liquid potential drop occurs ($[w_e]$) is smaller than the electrode's thickness and potential drops are half of the cell voltage. For the same reasons, it was ineffective to charge the capacitor with electrolyte of effective conductivity of 0.005S/cm at current densities of 0.0533A/cm^2, 0.5330A/cm^2 and 5.3300A/cm^2 for the expected charging duration.

When the device with electrolyte of effective conductivity of 0.0005S/cm was charged at current densities of 0.0053A/cm^2, 0.0533A/cm^2, 0.5330A/cm^2 and 5.3300A/cm^2, the lengths over which the liquid potential drop occurs ($[w_e]$) are very small compared with the electrode's thickness, and the potential drops were half of the cell voltage as seen in Table 5.12 and Figure 5.25d. Thus, the device with electrolyte of low effective conductivity (0.0005S/cm) cannot be charged effectively at these four current densities for the expected duration, because the electrode's utilization was extremely low. It can be seen from the above discussions that the speed at which ECs can effectively be charged/discharged is greatly dependent on the effective conductivities of electrode and electrolyte.

Plots in Figures 5.28, 5.29 and 5.30 could be used to select electrode dimensions to achieve at least 100% electrode utilization with minimum or no potential drop in the EC at a specific current density and effective conductivities. When a device with thicker electrodes was charged at a high current density, the length $[w_e]$ became considerably smaller than the electrode's thickness, and resulted in device inefficiencies due to high potential drops. The potential drops and inefficiencies were most notable when the device with thicker electrodes and electrolyte of low effective conductivity was charged at a high current density.

5.3.1.4 Effects of electrode thickness

The thickness of the positive and negative electrodes of the symmetric EC under investigation is 0.200cm as presented in Table 5.8 [89]. In order to effectively examine the effects of various electrode thicknesses on the EC's performance, capacitance per kg or cm^2, the energy and power density of the capacitor with different electrode thicknesses from 0.050cm to 0.200cm were simulated. All other design variables of the model are kept constant. The capacitance per square centimetre of the symmetric EC increased linearly together with the increase in the electrode thickness as clearly shown in Figure 5.31a. This is because the EC with a thicker electrode of similar accessible porosity, holds greater electrolytes in its pores and has the ability to store more charges during the charging process. Thus, ECs with thicker electrodes have larger specific capacitance. Moreover, increase in the electrode's thickness results in steeper growth in capacitance per cm^2 at low applied current densities. The capacitance per kilogram of ECs grows almost parabolically as electrode width becomes thicker as presented in Figure 5.31b, provided that the thickness did not exceed the electrode's effective thickness determined by the length $[w_e]$. For example, specific capacitance per kilogram of the capacitors with electrode thickness of 0.200cm, 0.150cm, 0.100cm and 0.050cm was 1.7876×10^5F/kg, 1.7265×10^5F/kg, 1.6161×10^5F/kg and 1.3558×10^5F/kg, respectively.

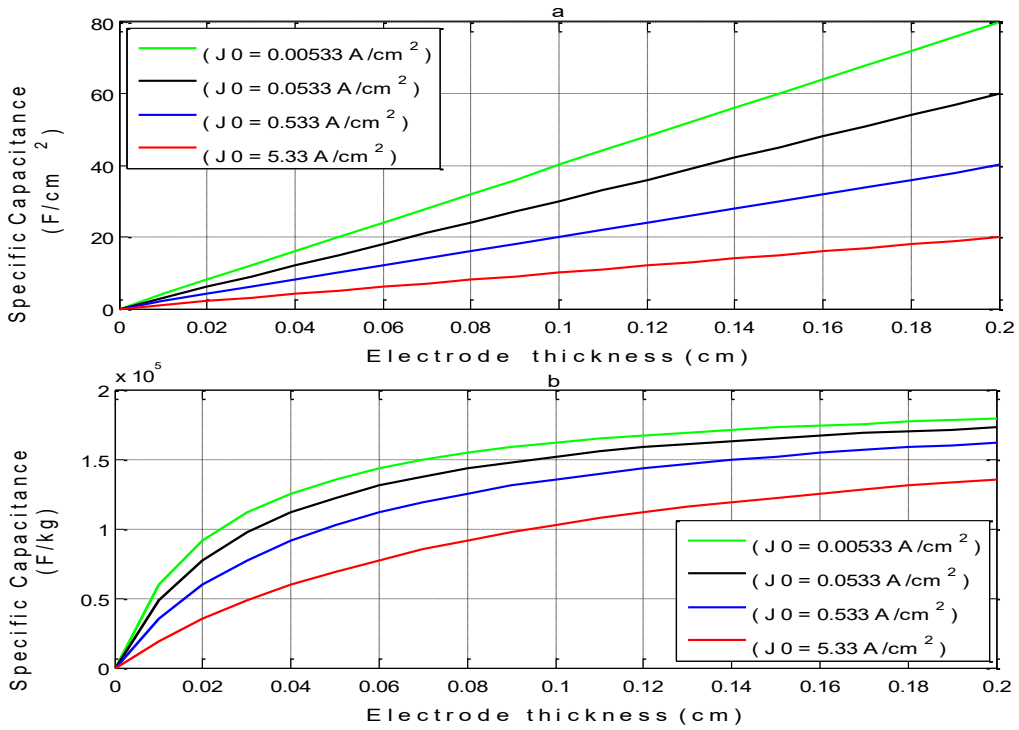

Figure 5.31: Specified capacitance of various electrode widths at various current densities in Farad (a) per square centimetre (cm^2), and (b) per kilogram of electrochemical capacitor.

Capacitance per kilogram of ECs decays almost parabolically with increase in the electrode's thickness, when the electrode width goes beyond its effective thickness. Specific capacitance per kilogram of the device with 0.200cm, 0.150cm and 0.100cm electrode thickness was 1.319 times, 1.273 times and 1.192 times that of the device with an electrode thickness of 0.050cm. The increase in specific capacitance per kilogram with electrode thickness was higher at low current density than high current density. The lower rate at high current density was caused by fast charging rates that occur near the electrode/separator interface, leaving the remaining part of the electrode unutilized. Figures 5.31a and 5.31b shows that specific capacitance of the device with a given electrode thickness, reduced as applied current density increased.

Figure 5.32 presents the variation of specific capacitance per kilogram and the specific energy of the symmetric device using two different aqueous electrolyte solutions with applied current density for simulation of the study and experiment of Ma et al. [275]. Specific capacitance per kilogram of the device with 1 $molL^{-1}$ Na_2SO_4 and 2 $molL^{-1}$ KOH aqueous electrolytes was highest when charged at low current density, but decreased along with increase in the current density as pictured in Figures 5.32a and 5.32c respectively. The specific energy of the symmetric device with 1 $molL^{-1}$ Na_2SO_4 and 2 $molL^{-1}$ KOH aqueous electrolytes was also highest when charged at a low current density, and decreased as current density was increased as shown in Figures 5.32b and 5.32d respectively. Specific capacitance and specific energy of the symmetric device with 1 $molL^{-1}$ Na_2SO_4 aqueous electrolyte were higher than those of the device with 2 $molL^{-1}$ KOH aqueous electrolytes, because effective conductivity of 1 $molL^{-1}$ Na_2SO_4 aqueous electrolyte (0.092S/cm) is higher than that of 2 $molL^{-1}$ KOH aqueous electrolyte (0.075S/cm).

Similarly, Figure 5.33 presents the variation of specific power and the ragone plot of the symmetric device with two different aqueous electrolytes solutions, with applied current density for the simulation of the model and experiment Ma et al. [275]. It was clearly shown in Figures 10b and 10d respectively, that the specific power of the symmetric device with 1 $molL^{-1}$ Na_2SO_4 and 2 $molL^{-1}$ KOH aqueous electrolytes was also lowest when charged at low current density, and increased as current density was increased. Figure 5.32 and 5.33 shows that mean relative error between specific capacitance of a button device from the simulation of model and experimental data of Ma et al. [275] in the cells was equal to 2.3% (highest relative error was 6%). The difference between simulation and experiment was related to both experimental and modelling assumptions. In the experiments, the mass of the two electrodes were taken as the mass of the device, but the mass of electrodes, together with the mass of the separator and electrolyte were included in the simulation.

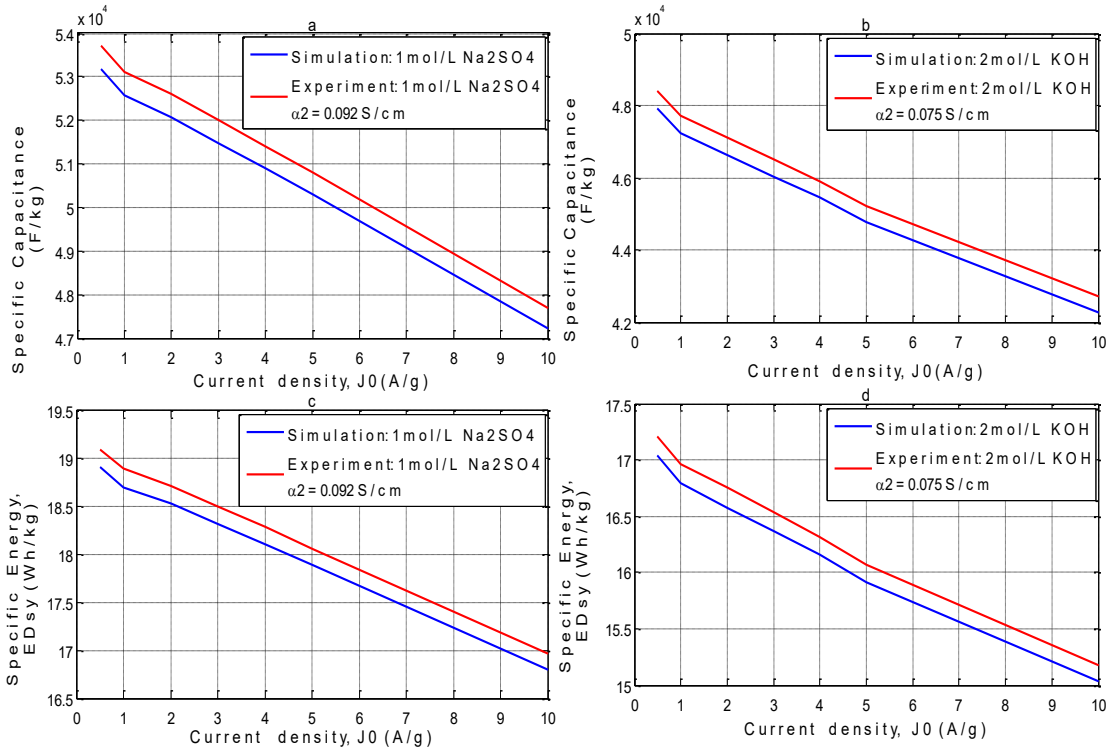

Figure 5.32: Variation of specific capacitance per kilogram of symmetric button capacitor with charging current density in device with $Mn_3(PO_4)_2$ composite electrodes and different aqueous electrolytes (a) 1 $molL^{-1}$ Na_2SO_4, (b) 2 $molL^{-1}$ KOH; and variation of specific energy of symmetric button capacitor with charging current density in device with aqueous electrolytes (c) 1 $molL^{-1}$ Na_2SO_4, and (d) 2 $molL^{-1}$ KOH.

Again, the porous electrode theory used in the present study did not account for the heterogeneous microstructure of electrodes like morphology, pore size, and pore connections. Also, the 1-D model employed will cause a slight deviation of the experiment from the modelling. Comparison of the specific capacitance and specific energy density of the device verified the validity of the models.

Figure 5.34 presents the variation of specific capacitance per kilogram, specific energy, specific power and the ragone plot of the symmetric device using aqueous electrolytes solution with applied current density for the simulation and experiment of Sun et al. [276]. The specific capacitance per kilogram and specific energy of the device with 1 $molL^{-1}$

Na_2SO_4 aqueous electrolyte were highest when charged at a low current density, and decreased with the increase in the charging current density as depicted in Figures 5.34a and 5.34b respectively.

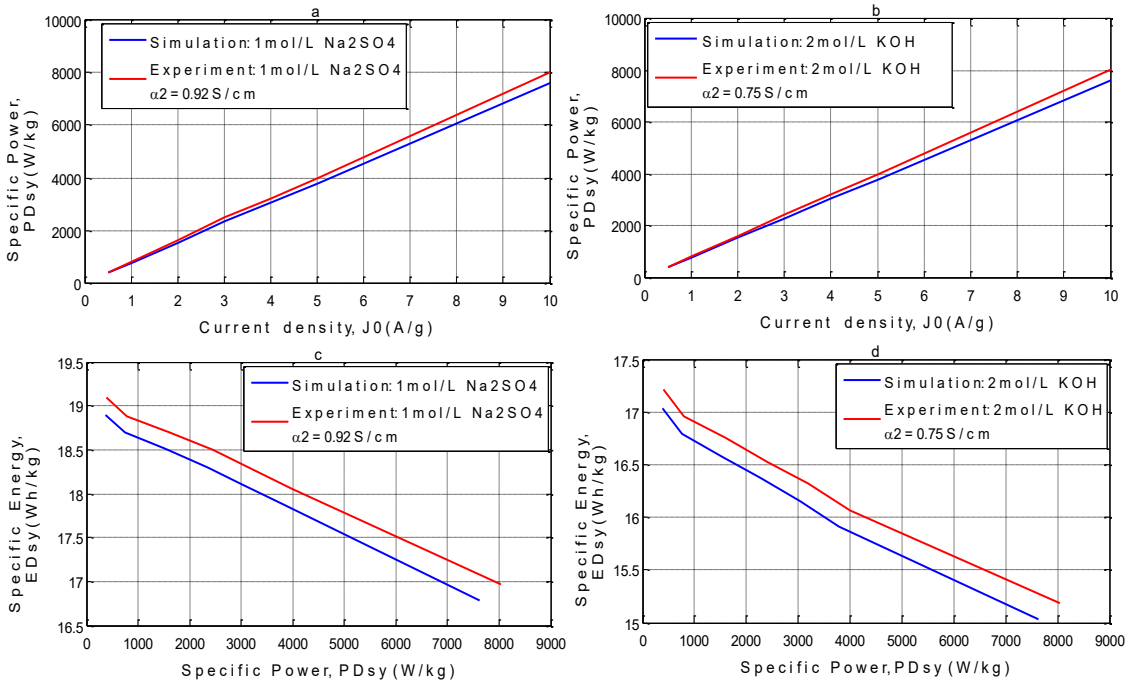

Figure 5.33: Variation of specific power of symmetric button capacitor with charging current density in device with $Mn_3(PO_4)_2$ composite electrodes and different aqueous electrolytes (a) 1 $molL^{-1}$ Na_2SO_4, (b) 2 $molL^{-1}$ KOH; and ragone plot of symmetric button capacitor with aqueous electrolytes (c) 1 $molL^{-1}$ Na_2SO_4, and (d) 2 $molL^{-1}$ KOH.

Conversely, the specific power of the symmetric device was lowest when charged at a low current density, but decreased as the charging current density was increased as shown in Figure 5.34c. It was clearly seen in Figure 5.34d that the device has the lowest specific power at the highest specific energy, and increased as specific energy decayed until it attained the highest value at the lowest specific energy.

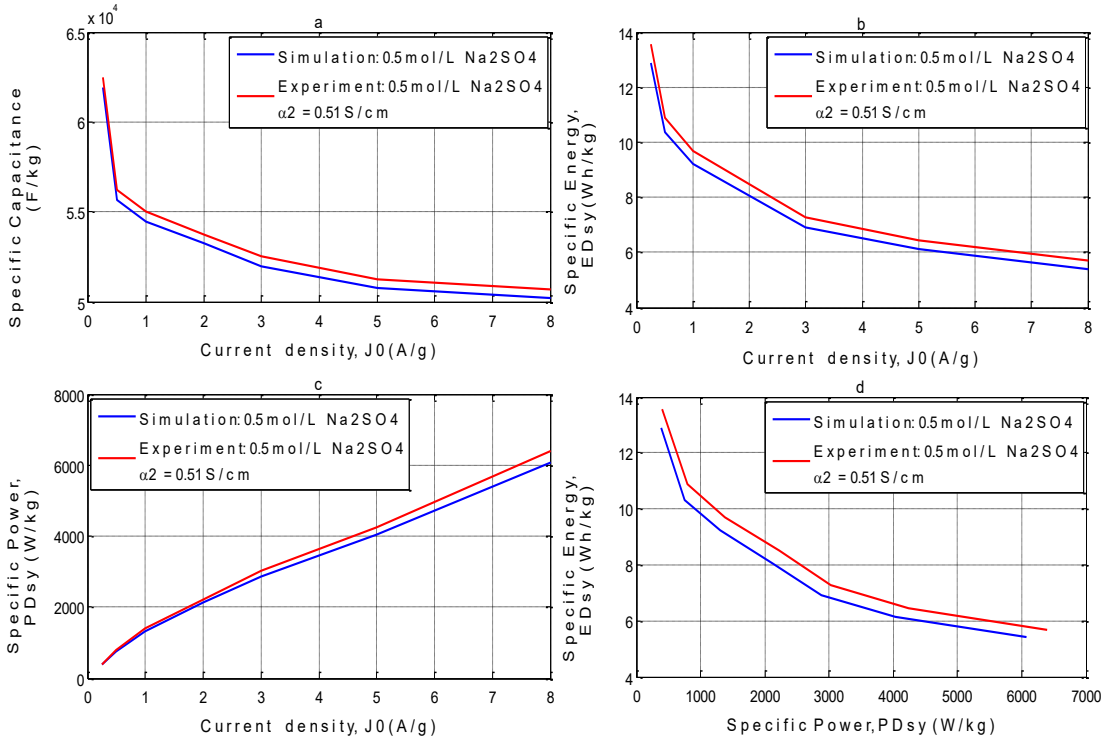

Figure 5.34: (a) Variation of specific capacitance per kilogram of symmetric button capacitor with charging current density in device with nitrogen-doped rapeseed activated carbons (N-RCs) composite electrodes and 0.5 molL^{-1} Na_2SO_4 aqueous electrolytes; (b) variation of specific energy of symmetric button device 0.5 molL^{-1} Na_2SO_4 aqueous electrolytes; (c) variation of specific power of symmetric button device with 0.5 molL^{-1} Na_2SO_4 aqueous electrolytes; and (d) ragone plot of symmetric button device with 0.5 molL^{-1} Na_2SO_4 aqueous electrolytes.

Figure 5.35 presents the variation of specific capacitance per kilogram, specific energy, specific power and the ragone plot of the symmetric device using aqueous electrolytes solution with applied current density for simulation of the model and experiment of Zhao et al. [277]. The specific capacitance per kilogram and specific energy of the device with 1 molL^{-1} Na_2SO_4 aqueous electrolyte decayed from the highest values at low current density to the lowest values at high charging current density as shown in Figures 5.35a and 5.35b respectively. However, the specific power of the symmetric device increased from the lowest

value at a low current density to the highest value at a high charging current density as shown in Figures 5.35c. The device's specific power was lowest at the highest specific energy, and increased to the highest value at the lowest specific energy as seen in (the ragone plot) Figure 5.35d. It is obvious from the discussions and Figures 5.33, 5.34, 5.35 and 5.36 that the high effectivity conductivity of the electrolytes yielded high specific energy and power.

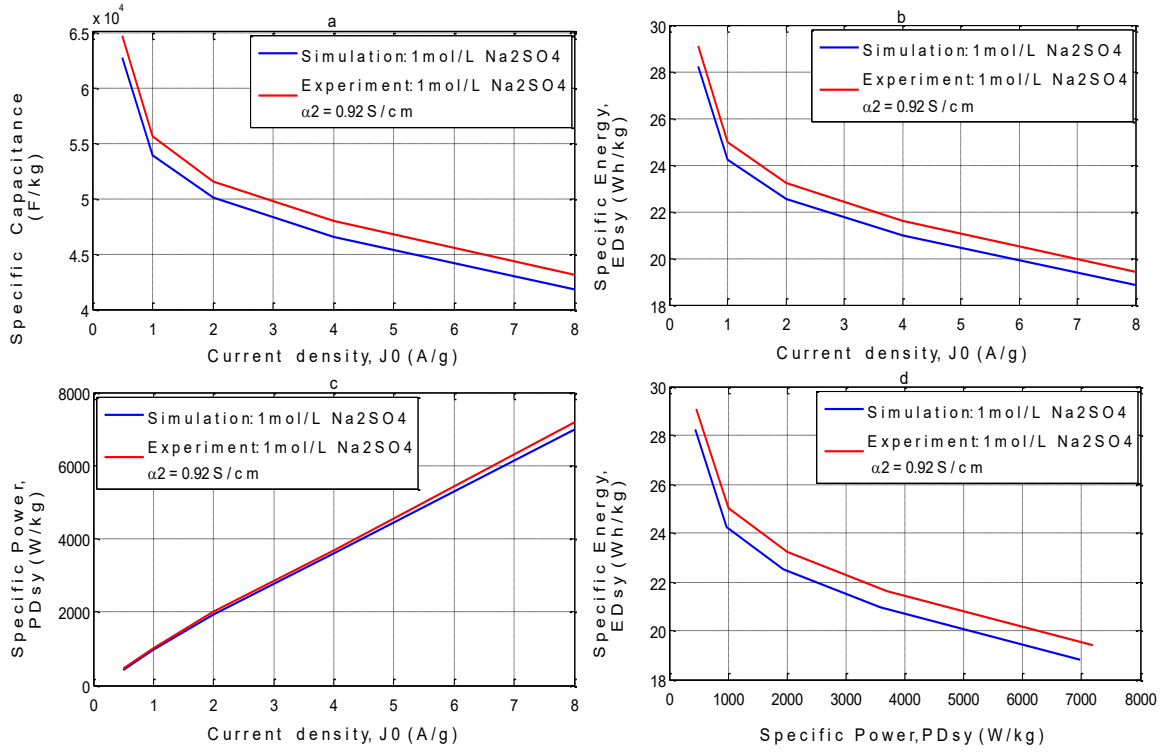

Figure 5.35: (a) Variation of specific capacitance per kilogram of symmetric button capacitor with charging current density in device with 1100CNF webs electrodes and 1 molL^{-1} Na_2SO_4 aqueous electrolytes; (b) variation of specific energy of symmetric button device with 1 molL^{-1} Na_2SO_4 aqueous electrolytes; (c) variation of specific power of symmetric button device with 1 molL^{-1} Na_2SO_4 aqueous electrolytes; and (d) ragone plot of symmetric button device with 1 molL^{-1} Na_2SO_4 aqueous electrolytes.

The mass of the EC grows as the electrode's width become thicker. For instance, the mass of the capacitor with electrode thickness of 0.050cm, 0.100cm, 0.150cm and 0.200cm was

0.928kg, 1.616kg, 1.186kg and 2.815kg respectively. The mass of the device with electrodes thickness of 0.200cm, 0.150cm and 0.100cm was 3.034 times, 2.356 times and 1.678 times that of the device with 0.050cm electrodes thickness; whereas the specific capacitance per kilogram of the device with 0.200cm, 0.150cm and 0.100cm electrodes thickness was 1.319 times, 1.273 times and 1.192 times that of 0.050cm electrode thickness. At low current densities, using thicker electrodes resulted in larger capacitance per kilogram of ECs, but thinner electrodes will have more specific energy when charged for the same period of time. This is because thicker electrodes have more electrochemical accessible pores to store charges, and need more time to fill the entire pores in the electrodes. Electric charge will enter smaller pores at lower rate and require more time to fill all the electrochemical accessible pores, while charging time was enough for all the electrochemical accessible pores in the thinner electrodes to be completely filled. Also, the mass ratio of the device with the thickest electrodes to one with the thinnest electrodes was 2.3 times larger than the specific capacitance per kilogram ratio of the device with the thickest to one with the thinnest electrodes. Energy density is described as energy per unit capacitor mass and unit time.

It follows from Figure 5.36 that when capacitors of the same electrode and electrolyte effective conductivities with different electrodes thickness were charged at different current densities, their energy densities were the same in different charging conditions, provided that effective conductivity of the electrode and electrolyte were very high. For instance, when the device with 0.05cm electrodes thickness and effective conductivities $\alpha_1 = 50$S/cm and $\alpha_2 =$ 0.50S/cm was charged at current densities of 0.0053A/cm^2 for 18000s, 0.0533 A/cm^2 for 1800s, 0.5330 A/cm^2 for 180s, and 5.3300 A/cm^2 for 18s, energy density was 430Wh/kg in the four charging conditions presented in Figures 5.36a – 5.36d. Similarly, the energy density

of the device with electrodes thickness of 0.100cm, 0.150cm and 0.200cm charged at the four charging conditions was 190Wh/kg, 85Wh/kg and 40Wh/kg respectively.

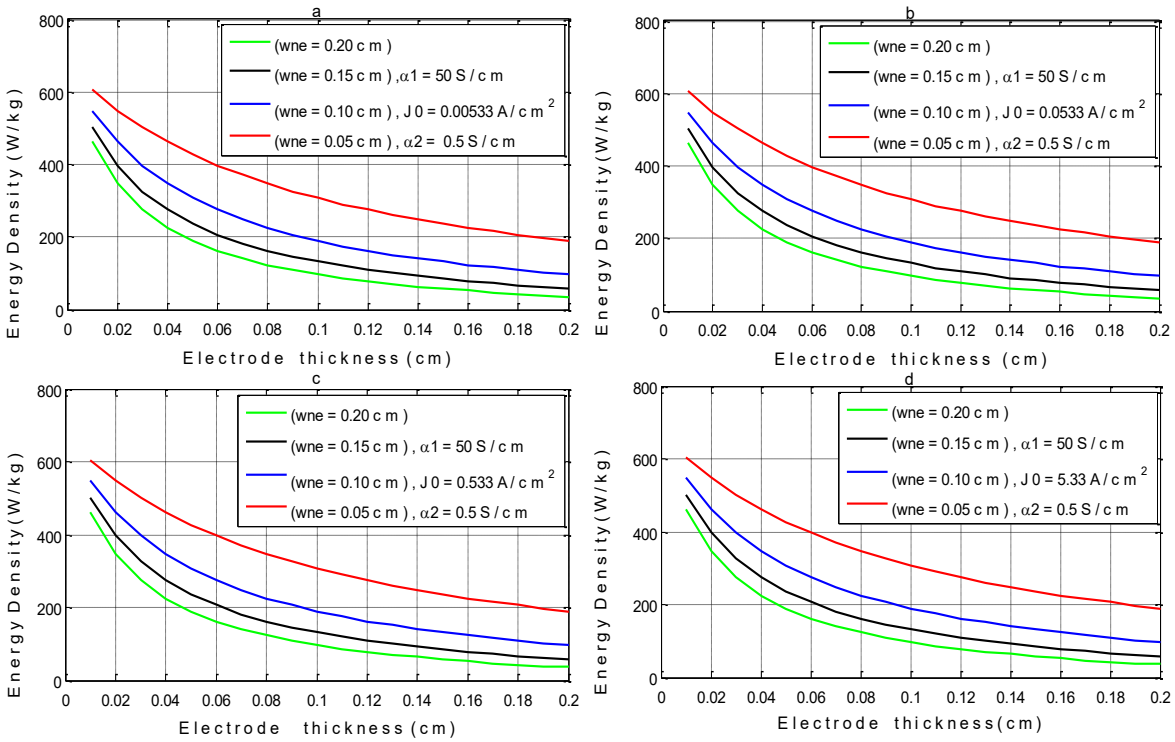

Figure 5.36: Energy densities of ECs with electrode and electrolyte effective conductivities $\alpha_1 = 50\text{S/cm}, \alpha_2 = 0.50\text{S/cm}$ and different electrode thicknesses charged at current density of (a) 0.0053A/cm^2 for 18000s, (b) 0.0533A/cm^2 for 1800s, (c) 0.5330A/cm^2 for 180s, and (d) 5.3300A/cm^2 for 18s.

It is clear from Figure 5.36 and the discussions above, that energy density of the capacitor decreases with the increase in electrodes thickness in all the charging conditions examined. In addition, the energy density of the capacitor with effective conductivities $\alpha_1 = 50\text{S/cm}$ and $\alpha_2 = 0.50\text{S/cm}$ charged at a current density of 0.0053A/cm^2 for 18000s, increased from 40Wh/kg to 430Wh/kg when the electrode thickness was reduced from 0.200cm to 0.050cm. When the charging condition of the device, specific electrode thickness and effective conductivities was changed as presented in Figure 5.36, the energy density remained the

same. The power densities of the electrochemical capacitor with the same effective conductivity and different electrode thicknesses, charged at different current densities are depicted in Figure 5.37.

Power densities of capacitors charged at a specific current density increased as the electrodes' thickness was reduced. The power density of the capacitor also increased as the applied current density was increased. When the current densities of the EC with the same electrode and electrolyte effective conductivities and different electrode thicknesses were increased and charging times also reduced by the same factor as discussed earlier, the power densities were also increased by the same factor as presented in Figure 5.37.

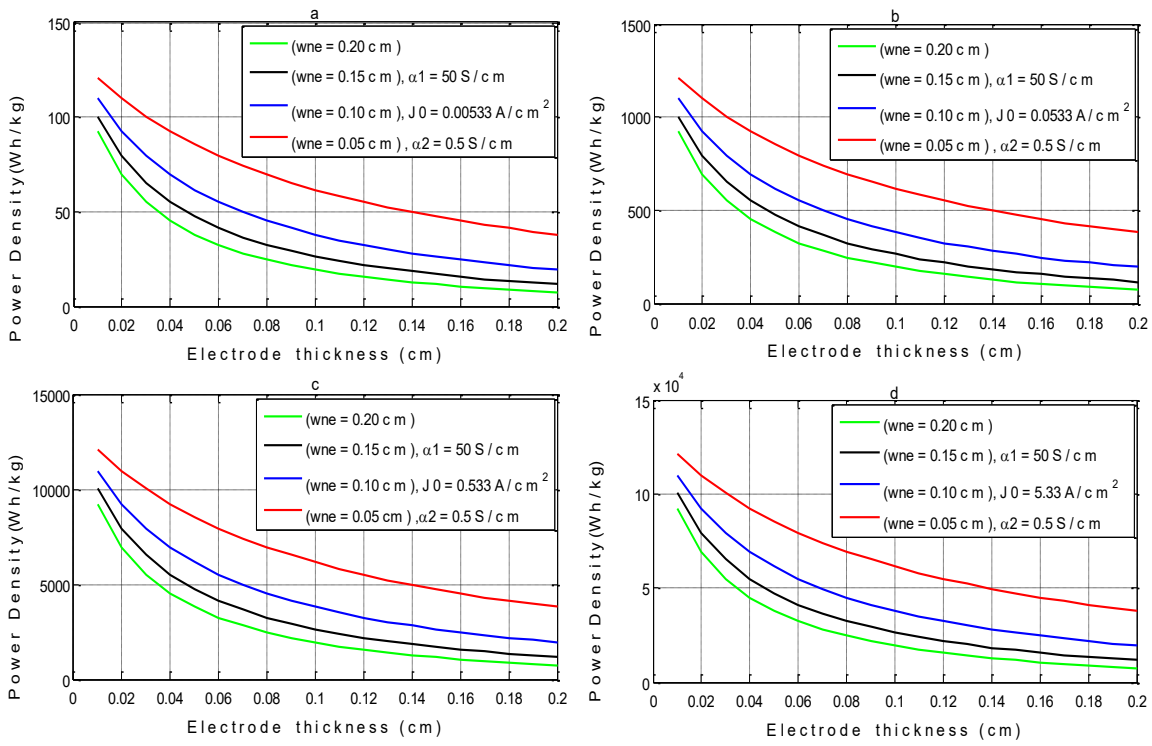

Figure 5.37: Energy densities of ECs with electrode and electrolyte effective conductivities $\alpha_1 = 50\text{S/cm}, \alpha_2 = 0.50\text{S/cm}$ and different electrode thicknesses charged at current density of (a) 0.0053A/cm^2 for 18000s, (b) 0.0533A/cm^2 for 1800s, (c) 0.5330A/cm^2 for 180s, and (d) 5.3300A/cm^2 for 18s.

For example, the power density of the capacitor with the electrode's thickness of 0.2cm and effective conductivities $\alpha_1 = 50$S/cm and $\alpha_2 = 0.50$S/cm, charged at 0.0053A/cm^2 for 18000s, was increased from 8W/kg to 85.5W/kg by reduction of the electrode's thickness from 0.200cm to 0.050cm as depicted in Figure 5.37a.

Similarly, when the charging rate of the device with an electrodes thickness of 0.200cm was changed from 0.0053A/cm^2 for 18000s to 0.0533A/cm^2 for 1800s, the power density was increased from 8W/kg to 80W/kg and from 80W/kg to 855W/kg when the electrodes thickness was reduced from 0.200cm to 0.050cm respectively as seen in Figure 5.37b. In the same manner, when the capacitor charging rate was changed from 0.0533 A/cm^2 to 0.5330 A/cm^2 and 5.3300A/cm^2, the power density was increased from 80W/kg to 800W/kg and 800W/kg to 8,000W/kg, respectively.

Power density was also increased from 800W/kg to 8,550W/kg and 8,000W/kg to 85,500W/kg by making the electrodes thinner from 0.200cm to 0.050cm as shown in Figures 5.37c and 5.37d. The power densities of the capacitor with different electrode thicknesses and the same effective conductivities $\alpha_1 = 50$S/cm and $\alpha_2 = 0.50$S/cm, charged at 0.0053A/cm^2 for 18000s were increased by a factor of 10, 100 and 1000 when the charging rate was increased to 0.0533A/cm^2, 0.5330A/cm^2 and 5.3300A/cm^2 respectively as presented in Figures 5.37a – 5.37d.

It was clearly shown in Figures 5.32, 5.33 and 5.34 that in the device with given electrodes thickness and effective conductivities of the electrodes and electrolyte, that whereas specific capacitance and specific energy are decreased, along with an increase in current density, specific power was increased. This is because the increase in the current density without a corresponding increase and decrease in the effective conductivities and electrodes thickness, results in underutilization of electrodes, increased inefficiencies due to non-uniform charging

and potential drops in cell. Therefore, it is very important to determine and employ optimum current density to charge/discharge the capacitor with a given electrodes thickness and effective conductivities of electrodes and electrolyte in order to achieve optimal performance.

The ragone plots in Figure 5.38 presents the effects of charging different capacitors of the same electrode and electrolyte effective conductivity and different electrodes thickness at different conditions, by using higher current densities as explained earlier. It was shown from the plots that the power densities of devices in conditions described in Figures 5.38b, 5.38c and 5.38d were ten-fold, a hundred-fold and a thousand fold respectively, of those in the condition shown in Figure 5.34a. For example, when the EC of effective conductivities α_1 = 50S/cm and $\alpha_2 = 0.500$S/cm and electrodes thickness of 0.050cm was charged at 0.0053A/cm^2, 0.0533A/cm^2, 0.5330A/cm^2 and 5.3300A/cm^2, the power density that corresponded to the energy density of 400Wh/kg was 36W/kg, 360W/kg, 3,600W/kg and 38,000W/kg respectively as seen in Figures 5.38a – 5.38d.

The last three power densities were 10-fold, 100-fold and 1000-fold of first one respectively. Similarly, power densities that correspond to energy density of 300Wh/kg in the first charging condition in a similar EC with electrode thickness of 0.050cm, 0.100cm, 0.150cm and 0.200cm was 63W/kg, 29W/kg, 18W/kg and 13W/kg, respectively as shown in Figure 5.38a. Also, power densities that correspond to the energy density of 300Wh/kg in the second charging condition of the device were 630W/kg, 290W/kg, 180W/kg and 130W/kg respectively, as shown in Figure 5.38b. The power densities of the capacitor in the third charging condition presented in Figure 5.38c was 6,300W/kg, 2,900W/kg, 1,800W/kg and 1,300W/kg respectively, while that in the fourth charging condition shown in Figure 5.38d was 63,000W/kg, 29,000W/kg, 18,000W/kg and 13,000W/kg respectively. The ragone plots of devices with diverse electrode thicknesses portrayed in Figure 5.38 can be used to select

electrode dimensions to achieve a given energy and power density specifications. Use of thicker electrodes resulted in higher capacitance per kilogram and higher capacitor~~'s~~ mass as well. Therefore, the overall effect of thicker electrodes obviously results in lower energy and power densities as shown in Figures 5.36, 5.37 and 5.38 respectively, since energy and power density are defined as energy and power per capacitor mass and unit time.

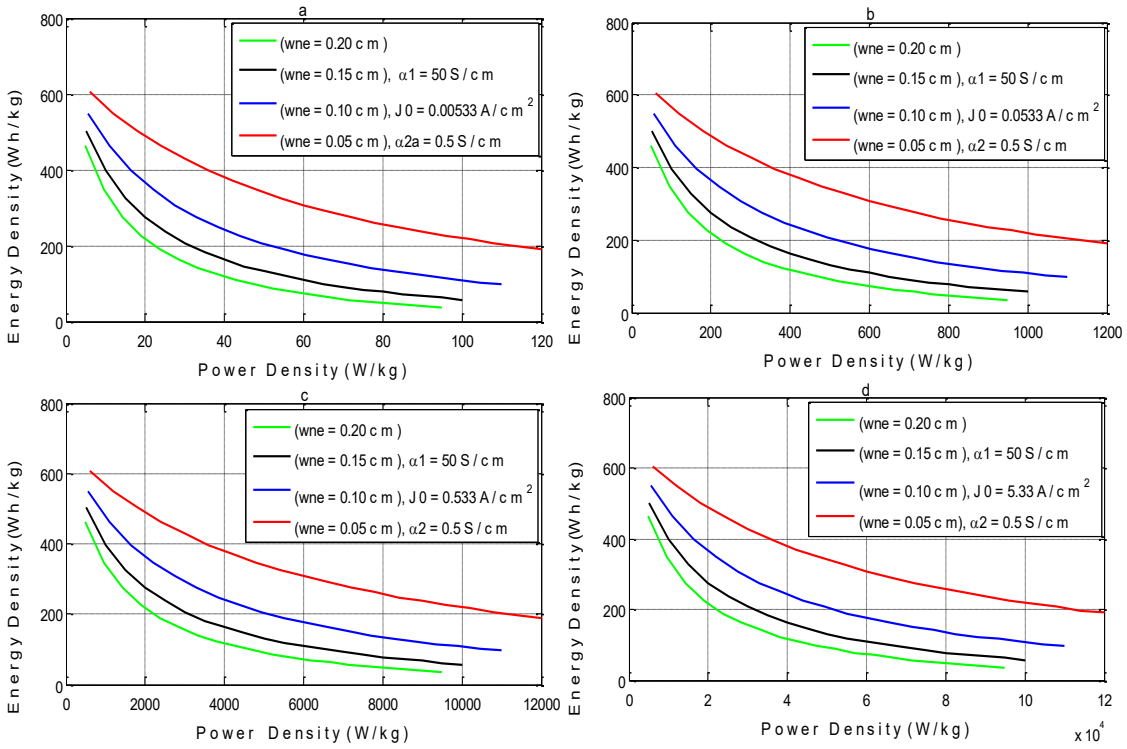

Figure 5.38: Ragone plots of electrochemical capacitors with different electrode thicknesses and electrodes and electrolyte effective conductivities $\alpha_1 = 50$S/cm, $\alpha_2 = 0.50$S/cm charged at current density of (a) 0.0053A/cm^2 for 18000s, (b) 0.0533A/cm^2 for 1800s, (c) 0.5330A/cm^2 for 180s, and (d) 5.3300A/cm^2 for 18s.

Moreover, energy loss due to polarization and depolarization resistance to electrode potential during the charging process decreased with reduction in the electrode's thickness, together with an increase in electrodes and electrolyte effective conductivities. It was also supported by the fact that specific capacitance per kilogram of the device with the thickest electrodes

was 1.319 times that with thinnest electrodes, while the mass of the device with the thickest electrodes was 3.034 times that with thinnest electrodes.

For electrodes and electrolyte materials of specific effective conductivities and given cell voltage, electrodes optimum thickness (effective thickness), charging current density and charging time for optimum specific capacitance, specific energy and specific power were easily obtained from equations 3.44 and 3.46, as well as Figures 5.29 and 5.30. For example, the capacitor with 0.200cm electrode thickness and electrolyte of 0.500S/cm effective conductivity has optimum electrodes thickness of 0.200cm (100% electrodes utilization) and optimum charging current density of 1.500A/cm^2, as pictured in Figures 5.29a and 5.30a respectively. Thus, equations 3.44 and 3.46 can be used to determine optimum electrodes thickness, optimum charging current density and optimum charging time for the cell of given voltage, electrodes thickness, electrodes and electrolyte's effective conductivities.

5.3.1.4 Effects of electrodes and separator porosities

The impact of using various electrode porosities on the symmetric EC's performance was examined in this section. Porosity in this context is described as a fraction of the pores volume over the entire volume. The porosity of the capacitor's electrode under study is 0.25 as contained in data source [89]. It was assumed that porosity increased at the same rate as the electrochemical accessible surface area is increased. This assumption was based on the fact that the electrode interfacial electrochemical accessible area is a linear function of porosity. It follows from equations 3.33 and 3.34 that electrolyte effective conductivity inside the electrode and separator are respectively dependent upon the electrode and

separator porosities. Electrolyte effective conductivity inside the electrode and separator increases along with the increase in porosity.

Specific capacitance increased with the increase in electrodes porosity for all current densities, because the EC with the electrode of larger electrochemical accessible porosity has more accessible pores to store energy, hence larger capacitance. For instance, capacitance per kilogram and per unit area was 1.25 times and 2.00 times respectively, larger when the accessible porosity of electrodes was doubled from 0.25 to 0.50 respectively. For all current densities considered, capacitance per kilogram increased approximately parabolically with the increase in electrode accessible porosity, which increased with the increase in electrodes thickness. Capacitance per unit area increased linearly with the increase in electrode accessible porosity. The effective mass of the electrode reduced with the increase in electrodes accessible porosity, and more electrolytes were accommodated since more accessible pores were available. Thus, the EC with higher electrodes and separator porosities has a smaller mass compared with a similar device of lower accessible porosities.

5.4 Optimization of design parameters and operating conditions of electrochemical capacitors for high energy and power performances

In this section, the theoretical and computational features of the different electrochemical capacitors were presented through computation of storable energy, specific energy density and specific power density. Theoretical expressions for these parameters were optimized, subject to their appropriate constraint equations, which captured the realistic conditions and limitations inherent in various electrochemical energy storage systems via the MATLAB R2014a optimization tool box and writing MATLAB scripts to solve the

optimization. The performance of the different kinds of ECs at given circumstances were compared through theoretical equations and simulation of various models from the data of our symmetric EDLC, subject to the conditions of the device components using optimal coefficient associated to battery-type material K_{BMopt} and constant associated to electrolyte material K_{Eopt}. The variation of the electrochemical device performance with electrode and electrolyte manufacturing conditions, like electrode mass ratio, type, reaction of active material, electrolyte potential operating range and specific capacitance was effectively demonstrated from the theory and simulation of various models.

5.4.2 Discussions

In order to verify the validity of the optimum parameters obtained from optimization via the MATLAB R2014a optimization tool box, the ECs storable and deliverable energies, specific energy and power were computed using the optimum parameters and our derived symmetric EDLC model. The EDLC was charged from its lower voltage of 0.000V to the upper voltage of 1.200V. The data employed were based on the experiment variables of Kazaryan et al. [89] and Staser et al. [90] as presented in Table 5.1 and reasonable figures were assigned, based on literature, to parameters that are unavailable. The capacitor discharged to 0.000V was charged by constant current to an upper voltage of 1.200V for a charging duration (t_{ch}) of 5 hours. It was thereafter discharged by constant current to a lower voltage of 0.000V for the discharging duration (t_{dis}) of 5hours. The mass transfer and charge conservation equations for each capacitor's component during the charging and discharging processes were considered and the current collector's resistance was ignored due to its high conductivity.

Although expressions for storable energy, energy density and power density of symmetric EDLC represented by equations 3.211, 3.212 and 3.213 do not contain parameters k_1 and k_2 , the mode of operations of the symmetric EDLC shows that the ratio of mass of one electrode to the mass of the two electrodes defined here as k_1 is 0.500, while the ratio of the working potential range of one electrode to the maximum working potential range of the the device defined here as k_2 is also 0.500. Thus, k_1 and k_2 values were presented in case 1 of Tables 5.14 – 5.20 as 0.500 for comparison purpose, but were not used in the calculation of parameters in the tables. In cases 2, 3 and 4 of Table 5.14, EDLCs were operated as asymmetric devices by using the same type of material with different masses as positive and negative electrodes causing the voltage applied to the cell to split unevenly between both terminals. Therefore, they were considered like the asymmetric EC with k_1, k_2, k_3 and k_4 parameters as presented in Table 5.14. In case 2 of Tables 5.15, 5.16 and 5.17, it was assumed that the potential of the positive electrode changes very little or undergoes galvanostatic electrolysis $(\Delta V_b \cong 0)$ during charging and discharging as presented in [89,90,245]. The ratio of working potential range to cell maximum working potential then becomes negligible $(k_2 \cong 0)$.

Table 5.13 presents the comparison of expression for the performance parameters of various electrochemical capacitors, using aqueous and organic electrolytes, respectively and operated under different conditions.

Table 5.13: Comparison of expression for performance parameters of various electrochemical capacitors using aqueous and organic electrolytes, respectively

S/N	Electrochemical capacitor systems	Expression for performance parameters		
		Storable energy (Wh)	Energy density (Wh/kg)	Power density (W/kg)

1	Single electrode with aqueous electrolyte	$E_1 = \frac{1}{2} q_1 \Delta V_{\max}$	$ED_1 = 1.\frac{1}{2}.q_1 \Delta V_{\max}$	$PD_1 = \frac{I_{\max} \Delta V_{\max}}{m_1}$
2	Symmetric EDLC with aqueous electrolyte	$E_S = \frac{1}{2}.\frac{1}{2} q_1 \Delta V_{\max} = \frac{1}{2} E_1$	$ED_S = \frac{1}{2}.\frac{1}{2}\frac{q_1 \Delta V_{\max}}{m_1} = \frac{1}{2} ED_1$	$PD_S = \frac{I_{\max} \Delta V_{\max}}{m_s} = PD_1$
3	Asymmetric EDLC with aqueous electrolyte	$E_{as} = \frac{(1-k_1)(1-k_2^2)}{2(1-k_1)} q_1 \Delta V_{\max} = \frac{(1-k_1)(1-k_2^2)}{(1-k_1)} E_1$	$ED_{as} = (1-k_1)(1-k_2^2).\frac{1}{2}.\frac{q_1 \Delta V_{\max}}{m_1} = (1-k_1)(1-k_2^2).ED_1$	$PD_{as} = (1-k_1)(1-k_2^2).\frac{I_{\max} \Delta V_{\max}}{m_1} = (1-k_1)(1-k_2^2).PD_1$
4	Asymmetric capacitor with aqueous electrolyte	$E_{as} = \frac{(1-k_1)(1-k_2^2)}{2(1-k_1)} q_1 \Delta V_{\max} = \frac{(1-k_1)(1-k_2^2)}{(1-k_1)} E_1$	$ED_{as} = (1-k_1)(1-k_2^2).\frac{1}{2}.\frac{q_1 \Delta V_{\max}}{m_1} = (1-k_1)(1-k_2^2).ED_1$	$PD_{as} = (1-k_1)(1-k_2^2).\frac{I_{\max} \Delta V_{\max}}{m_1} = (1-k_1)(1-k_2^2).PD_1$
5	Single electrode with organic electrolyte	$E_{o_1} = \frac{1}{2} q_{o_1} \Delta V_{o_\max}$	$ED_{o_1} = 1.\frac{1}{2}\frac{q_{o_1} \Delta V_{o_\max}}{m_{o_1}}$	$PD_{o_1} = \frac{I_{o_\max} \Delta V_{o_\max}}{m_{o_1}}$
6	Symmetric EDLC with organic electrolyte	$E_{o_s} = \frac{1}{2}.\frac{1}{2} q_{o_1} \Delta V_{o_\max} = \frac{1}{2}.E_{o_1} = \frac{k_4}{k_3^2}.\frac{1}{2} E_1$	$ED_{o_s} = \frac{1}{2}\frac{1}{2}\frac{q_{o_1} \Delta V_{o_\max}}{m_{o_1}} = \frac{1}{2} ED_{o_1} = \frac{k_4}{k_3^2}.\frac{1}{2} ED_1$	$PD_{o_s} = \frac{1}{2} PD_{o_1} = \frac{k_4}{k_3^2}.\frac{1}{2} PD_1$
7	Asymmetric EDLC with organic electrolyte	$E_{o_as} = \frac{(1-k_1)(1-k_2^2)}{(1-k_1)}.E_{o_1} = \frac{k_4}{k_3^2}.\frac{(1-k_1)(1-k_2^2)}{(1-k_1)}.E_1$	$ED_{o_as} = (1-k_1)(1-k_2^2).ED_{o_1} = \frac{k_4}{k_3^2}.(1-k_1)(1-k_2^2).ED_1$	$PD_{o_as} = (1-k_1)(1-k_2^2).PD_{o_1} = \frac{k_4}{k_3^2}.(1-k_1)(1-k_2^2).PD_1$
8	Asymmetric capacitor with organic electrolyte	$E_{o_as} = \frac{(1-k_1)(1-k_2^2)}{(1-k_1)}.E_{o_1} = \frac{k_4}{k_3^2}.\frac{(1-k_1)(1-k_2^2)}{(1-k_1)}.E_1$	$ED_{o_as} = (1-k_1)(1-k_2^2).ED_{o_1} = \frac{k_4}{k_3^2}.(1-k_1)(1-k_2^2).ED_1$	$PD_{o_as} = (1-k_1)(1-k_2^2).PD_{o_1} = \frac{k_4}{k_3^2}.(1-k_1)(1-k_2^2).PD_1$

Figure 5.39 depicts the profile of coefficient associated to battery-type material, K_{BM} as a function of mass and operating potential window ratios of a battery-type electrode, k_1 and k_2 respectively. It follows from Figure 5.39a and 5.39b that the value of the coefficient associated with battery-type material, K_{BM} increases as k_1 and k_2 is reduced from 1.000 to

0.000 and become highest at $k_1 = k_2 = 0$. It was shown in Figures 5.39a and 5.39b that the value of K_{BM} was 0.500 when $k_1 = 0.500$ and $k_2 = 0.700$, and was lower than 0.500 when the value of $k_1 > 0.500$ and $k_2 > 0.700$. Figure 5.39c and 5.39d shows the portion of the plot for which the value of K_{BM} is equal to and higher than 0.500, it was presented that when value of $k_1 \leq 0.500$ and $k_2 \leq 0.700$, value of was $K_{BM} \geq 0.500$.

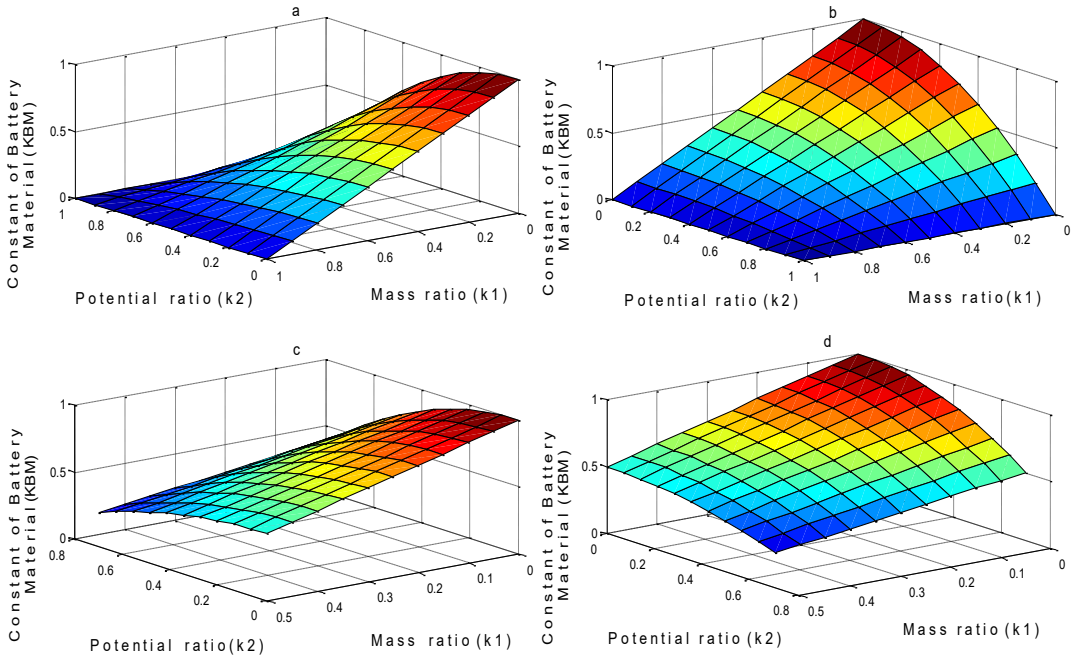

Figure 5.39: Profile of value of coefficient associated to battery-kind material, K_{BM} as functions of mass and operating potential window ratio factors of battery-kind electrode, k_1 and k_2 respectively for (a) 3-D side view plot of limits $0 < k_1 \leq 1$ and $0 < k_2 \leq 1$; (b) 3-D front view plot of limits $0 < k_1 \leq 1$ and $0 < k_2 \leq 1$;(c) 3-D side view plot of limits $0 < k_1 \leq 0.5$ and $0 < k_2 \leq 0.7$; and (d) 3-D front view plot of limits $0 < k_1 \leq 0.5$ and $0 < k_2 \leq 0.7$

It follows from Table 5.14 that symmetric EDLCs built with electrodes of the same mass and the same charge capacity have applied voltage shared evenly among electrodes as presented in case 1. The symmetric EDLC can be operated as asymmetric ECs by employing capacitor-type electrodes with different mass [19,21,283]. This can also be

achieved by using equal capacitor-type electrodes with different charge capacities due to the different adsorption strengths of ions in each electrode [84] or due to different cations and ions sizes and charges contained in the electrolyte [284]. Asymmetric ECs that emanated from using capacitor-type electrodes with different mass were presented in cases 2 and 4 of Table 5.14.The maximum energy and power densities $ED_{\max}$ and $PD_{\max}$ of the symmetric EDLC of 1.2V using aqueous electrolyte were enhanced from 38.81Wh/kg and 7.74W/kg to 68.78Wh/kg and 13.72W/kg respectively, by using electrode mass and operating potential window ratios $k_1 = 0.050$ and $k_2 = 0.080$ as shown in case 2 of Table 5.14; while storable and deliverable energies remained unchanged (101.22Wh and 100.91Wh).

Storable and deliverable energies E_{ch} and E_{dis} of the symmetric EDLC were enhanced from 101.22Wh and 100.91Wh to 201.22Wh and 200.69Wh respectively by using organic electrolyte of twice the operating potential range and half the specific capacitance of aqueous electrolyte respectively, as shown in case 3 of Table 5.14. Similarly, maximum energy and power densities of the device ED_{max} and PD_{max}, were improved to 74.57Wh/kg and 14.88W/kg, respectively.

The plane for the coefficient associated to battery-type material$K_{BM} \geq 0.500$ shown in Figure 5.40 is to facilitate comparison of the energy densities of symmetric and asymmetric capacitors ED_s and ED_{as}. It follows from equation 3.211 that k_1 has a more dominating influence on the value of K_{BM} than k_2 because k_2 is squared in the expression for K_{BM}. The value of K_{BM} for asymmetric capacitors must be higher than 0.500 for storable energy and the energy density ED_{as} must be higher than that of symmetric capacitors using the same aqueous electrolyte. It follows from Figure 5.40 that the mass of the battery-type electrode k_1 must be less than 0.5 and the operating potential window of the battery-type

electrode k_2 must be less than 0.707 ($\sqrt{0.5}$) of the entire potential operating window of asymmetric capacitors with aqueous electrolyte for value of K_{BM} must be higher than 0.500.

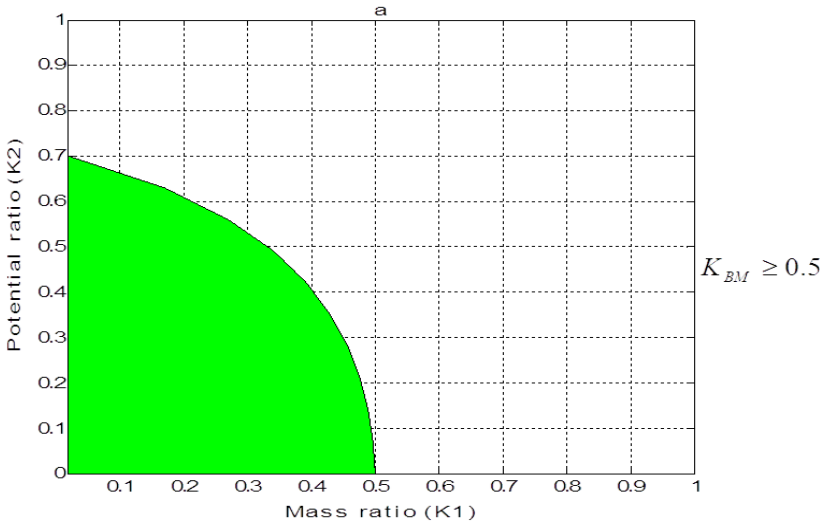

Figure 5.40: Profile of mass and operating potential window ratio factors of battery-kind electrode k_1 and k_2 respectively, for coefficient associated to battery-kind material $K_{BM} \geq 0.5$.

The first and second charge–discharge cycle efficiency η_{E1} and η_{E2} of the symmetric capacitor were enhanced from 84.24% and 84.25% to 91.80% and 91.81% respectively, as seen in case 3 of Table 5.14. When the symmetric EDLC consists of electrode mass and operating potential window ratios $k_1 =$ 0.050 and $k_2 =$ 0.080, together with organic electrolyte of twice the operating potential range and half the specific capacitance of aqueous electrolyte respectively, its storable and deliverable energies E_{ch} and E_{dis} of the symmetric EDLC were enhanced to 335.33Wh and 334.48Wh respectively. Also, the maximum energy and maximum power densities of the device ED_{max} and PD_{max}, were improved to 216.18Wh/kg and 211.12W/kg, respectively, as presented in case 4 of Table 5.14.

The asymmetric EDLC with electrodes of different mass, but with suitable mass and operating potential range ratios using aqueous electrolyte has 1.800 times the energy and power densities of a convectional symmetric EDLC using the same aqueous electrolyte, as seen in case 2 of Table 5.14. When the symmetric EDLC consists of electrodes of the same mass and capacity with organic electrolyte of twice the operating potential range and half the specific capacitance of aqueous electrolyte respectively, its storable and deliverable energies are twice those of a similar device using aqueous electrolyte. The device's energy and power densities are 1.9 times those of a similar device using aqueous electrolyte, as seen in case 3 Table 5.14. The asymmetric EDLC that consists of electrodes with suitable mass and operating potential range ratios, together with organic electrolyte of twice the operating potential range and half the specific capacitance of aqueous electrolyte has 3.300 times the storable and deliverable energies of a convectional symmetric EDLC using aqueous electrolyte. The energy and power densities of the asymmetric EDLC are 5.560 times those of the convectional symmetric EDLC using aqueous electrolyte as seen in case 4 Table 5.14.

Table 5.14: Parameters of symmetric EDLC using aqueous electrolyte, asymmetric EDLC using aqueous electrolyte, and asymmetric EDLCs using organic electrolyte with voltage windows of 1.200V, 1.200V, and 2.400V & 4.000V, respectively, during charging and discharging processes in cases 1, 2, 3 and 4

S/N	Parameter	Unit	α_1= 0.05S/cm and α_2 = 0.05S/cm			
			Case 1	Case 2	Case 3	Case 4
			Symmetric EDLC with $k_1 = 0.50,\ k_2 = 0.50,\ \Delta V_{max} = 1.2V$	Asymmetric EDLC with $k_1 = 0.05,\ k_2 = 0.08,\ \Delta V_{max} = 1.2V$	Asymmetric EDLC with $k_1 = 0.5,\ k_2 = 0.5,\ k_3 = 0.5,\ k_4 = 0.5,\ \Delta V_{max} = 2.4V$	Asymmetric EDLC with $k_1 = 0.05,\ k_2 = 0.08,\ k_3 = 0.3, k_4 = 0.5,\ \Delta V_{max} = 4.0V$
1	E_{ch}	Wh	101.22	101.22	201.22	562.78

2	E_{dis}	Wh	100.91	100.91	200.69	560.06
3	ED_{max}	Wh/kg	38.810	68.781	74.566	382.42
4	ED_{eff}	Wh/kg	35.957	63.725	71.713	354.31
5	PD_{max}	W/kg	7.7425	13.722	14.876	76.294
6	PD_{eff}	W/kg	7.1734	12.713	14.307	70.684
7	η_{E1}	%	84.241	84.241	91.794	97.500
8	η_{E2}	%	84.251	84.251	91.795	97.603
9	$M_{ele,pe}$	kg	1.2580	0.0315	1.2580	0.0315
10	$M_{ele,ne}$	kg	1.2580	1.2580	1.2580	1.2580
11	M_{Cell}	kg	2.8149	1.5883	2.8149	1.5883

Table 5.15 presents the parameters of symmetric EDLCs and asymmetric ECs of 1.2V voltage using aqueous electrolytes during the charging and discharging processes. Two different asymmetric ECs using a capacitor-type negative electrode and positive battery-type electrode with mass and operating potential range ratios $k_1 = 0.500$ & $k_2 = 0.000$ and $k_1 = 0.050$ & $k_2 = 0.080$ respectively, were examined as presented in Table 5.15. It follows from case 2 of Table 5.15 that storable and deliverable energies of an asymmetric EC with the same voltage and k_1 value were 234.58Wh and 233.15Wh, respectively, compared with 101.22Wh and 100.91Wh respectively in the symmetric EDLC. The maximum energy and power densities ED_{max} and PD_{max} of an asymmetric EC with the same voltage and k_1 were enhanced to 87.11Wh/kg and 17.42W/kg respectively, compared with 38.81Wh/kg and 7.74W/kg respectively in the symmetric EDLC. The first and second charge–discharge cycle efficiency of the asymmetric EC η_{E1} and η_{E2} in case 2 of Table 4 was enhanced to 90.72% and 90.82% respectively. Similarly, when the optimum value of the battery-type mass and operating potential range ratios $k_{1opt} = 0.050$ and $k_{2opt} = 0.080$ were used as presented in case 3 of Table 5.15. Maximum energy and power densities ED_{max} and PD_{max} of the asymmetric EC were improved to 150.54Wh/kg and 30.11W/kg respectively. The

capacitor storable energy, deliverable energy and first and second charge–discharge cycle efficiency remained the same as shown in cases 2 and 3 of Table 5.15.

The asymmetric EC assembled and operated as described in case 3 of Table 4, enhanced the energy and power densities ED_{max} and PD_{max} to 3.900 times those of the symmetric EDLC. It was noticed that changes in the value of the coefficient associated to battery-type material K_{BM} changed only the energy and power densities, while storable energy, deliverable energy and efficiency remained unchanged as shown in cases 2 and 3 of Table 5.15. The improvement in energy and power densities at the specific value of the constant associated with electrolyte material K_E was due to the improved value of coefficient K_{BM} The asymmetric EC with the battery-type electrode with suitable mass and operating potential range ratios using aqueous electrolyte (K_{BM} =0.94), stored and delivered 2.320 times the energies of a similar symmetric EDLC using the same electrolyte. The energy and power densities of this device were a factor of 3.900 greater than those of a similar symmetric EDLC using the same aqueous electrolyte.

Table 5.15: Parameters of asymmetric EDLC and asymmetric ECs using aqueous electrolytes and voltage windows of 1.200V during charging and discharging processes in cases 1, 2 and 3

S/N	Parameter	Unit	α_1= 0.05S/cm and α_2 = 0.05S/cm		
			Case 1	Case 2	Case 3
			Asymmetric EDLC with $k_1 = 0.05$, $k_2 = 0.08$, $\Delta V_{max} = 1.2V$	Asymmetric EC with $k_1 = 0.50$, $k_2 = 0$, $\Delta V_{max} = 1.2V$	Asymmetric EC with $k_{1opt} = 0.05$, $k_{2opt} = 0.08$, $\Delta V_{max} = 1.2V$
1	E_{ch}	Wh	101.22	234.58	234.58
2	E_{dis}	Wh	100.91	233.15	233.15
3	ED_{max}	Wh/kg	68.781	87.111	150.54
4	ED_{eff}	Wh/kg	63.725	83.317	143.98
5	PD_{max}	W/kg	13.722	17.422	30.108

6	PD_{eff}	W/kg	12.713	16.663	28.797
7	η_{E1}	%	84.241	90.723	90.723
8	η_{E2}	%	84.251	90.823	90.823
9	$M_{ele,pe}$	Kg	0.0315	1.2586	0.0723
10	$M_{ele,ne}$	Kg	1.2580	1.2580	1.2580
11	M_{Cell}	Kg	1.5883	2.8155	1.6292

It follows from equation 3.196 that organic electrolyte can only enhance the energy density of ECs when the value of constant associated to electrolyte material K_E is higher than 1 in comparison with aqueous electrolyte. Figure 5.41a presents the area of stipulated requirement for the constant associated to electrolyte material to be greater than or equal to 1($K_E \geq 1.0$) as functions of k_3 and k_4 ratios. It was shown in Figure 5.41a, 5.41b and 5.41c that the value of the constant associated to electrolyte material K_E is lowest (1.000) when the ratio of the maximum operating potential window among aqueous and organic electrolytes k_3 and the ratio of specific capacitance of the capacitor-type electrode in organic electrolytes to that in aqueous k_4 are equal to 1, that is when $k_3 = k_4 = 1.000$. The constant associated to electrolyte material K_E increases along with the reduction in k_3 and k_4 It follows from Figure 5.41b and 5.41c that the value of K_E when $k_3 = 0.100$ and $k_4 = 0.100$ is 10, and 5 when $k_3 = 0.200$ and $k_4 = 0.200$.

Apart from maximization of the coefficient associated to electrode material K_{BM} via the optimal values of k_1 and k_2, performance of the asymmetric EC can also be enhanced by using organic electrolyte with the maximum constant associated to electrolyte material K_E through the maximum values of k_3 and k_4. The asymmetric EC with the battery-type electrode mass ratio $k_1 = 0.500$, the operating potential range ratio $k_2 \cong 0$, the maximum operating potential window ratio among aqueous and organic electrolytes $k_3 = 0.500$, and

the specific capacitance ratio of the capacitor-type electrode in aqueous and organic electrolytes $k_4 = 0.500$, were assembled as presented in case 2 of Table 5.16. It was noticed that the asymmetric EC of 2.400V and the same k_1 improved storable and deliverable energies to 467.99Wh and 467.98Wh respectively, as presented on case 2 of Table 5.16, whereas the maximum energy and power densities were improved to 170.01Wh/kg and 34.0W/kg respectively. The first and second charge–discharge cycle efficiency of the asymmetric EC e η_{E1} and η_{E2} presented in case 2 of Table 5.16, was 95.54% and 95.60%, respectively. Storable and deliverable energies of the asymmetric EC of 2.400V and the same k_1 using organic electrolyte were improved to 4.620 times those of the asymmetric EDLC using aqueous electrolyte, while the maximum energy and power densities were improved to 4.38 times those of the asymmetric EDLC using aqueous electrolyte. Similarly, the maximum energy and power densities of the asymmetric device described in case 4 of Table 5.16 were enhanced to 293.80Wh/kg and 58.76W/kg, respectively.

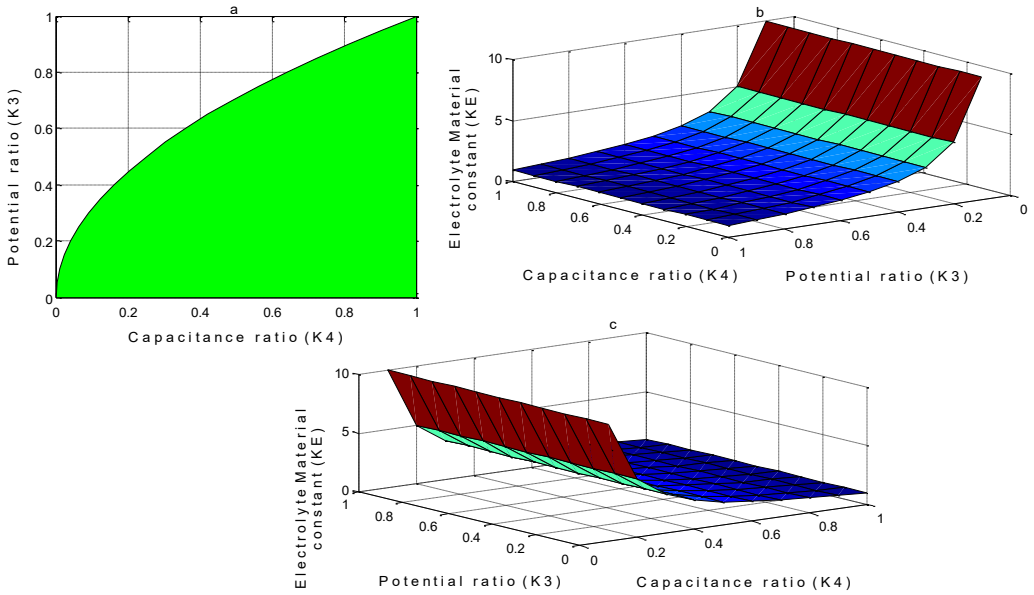

Figure 5.41: (a) Profile of stipulated requirement $K_E \geq 1.0$ as function of k_3 and k_4 ratios; (b) 3-D front view profile of value of constant associated to electrolyte material K_E as a

function of k_3 and k_4 ratios; and (c) 3-D side view profile of value of constant associated to electrolyte material K_E as a function of k_3 and k_4 ratios.

Energy and power densities enhancement in the capacitor in case 4 of Table 5 was a factor of 7.600 greater than those of the convectional symmetric EDLC using aqueous electrolyte. It was observed in Tables 5.15–5.17 that when the constant associated to electrolyte material K_E was varied, energy density, power density, storable energy and deliverable energy were changed, but variations in the coefficient associated to the battery-type material K_{BM} resulted in changes in only the energy and power densities. When the value of K_E was constant and K_{BM} was increased as described in cases 3 of Table 5.16, only energy and power densities were enhanced. An increase in the value of the constant associated to electrolyte material K_E improved all performance parameters: efficiency, storable energy, deliverable energy, energy density and power density.

Table 5.16: Parameters of asymmetric EDLC using aqueous electrolyte and asymmetric ECs using organic electrolytes and voltage windows of 1.200V and 2.400V & 2.400V, respectively, during charging and discharging processes in cases 1, 2 and 3

S/N	Parameter	Unit	α_1= 0.05S/cm and α_2 = 0.05S/cm		
			Case 1	Case 2	Case 3
			Asymmetric EDLC with $k_1 = 0.05$, $k_2 = 0.08$, $\Delta V_{max} = 1.2V$	Asymmetric EC with $k_1 = 0.50$, $k_2 = 0, k_3 = 0.5$, $k_{4opt} = 0.5$, $\Delta V_{max} = 2.4V$	Asymmetric EC with $k_{1opt} = 0.05$, $k_{2opt} = 0.08$, $k_3 = 0.5$, $k_{4opt} = 0.5$, $\Delta V_{max} = 2.4V$
1	E_{ch}	Wh	101.22	467.99	467.99
2	E_{dis}	Wh	100.91	467.98	467.98
3	ED_{max}	Wh/kg	68.781	170.01	293.80
4	ED_{eff}	Wh/kg	63.725	166.21	287.24
5	PD_{max}	W/kg	13.722	34.002	58.760
6	PD_{eff}	W/kg	12.713	33.243	57.449
7	η_{E1}	%	84.241	95.545	95.545

8	η_{E2}	%	84.251	95.601	95.601
9	$M_{ele,pe}$	kg	0.0315	1.2586	0.0723
10	$M_{ele,ne}$	Kg	1.2580	1.2580	1.2580
11	M_{Cell}	Kg	1.5883	2.8155	1.6292

The ratio of the maximum operating potential window among aqueous and organic electrolytes k_3 and the specific capacitance ratio of the capacitor-type electrode in aqueous and organic electrolytes k_4 in the asymmetric device using Li-ion salts containing organic solvent are approximately 0.300 and 0.500, respectively ($k_3 \cong 0.3$ and $k_4 \cong 0.5$ for Li^+ ion). The implication is that the operating potential window of organic electrolyte consisting of li-ion salt is almost 3.330 times that of aqueous electrolyte, while the specific capacitance of the capacitor-type electrode in aqueous electrolytes is more than twice that of organic electrolytes. Figure 5.42 depicts the profile of the constant associated to electrolyte material K_E as functions of k_3 and k_4 ratios for ranges of $0.3 \le k_3 < 1$ and $0 < k_4 \le 0.5$. It was shown in Figures 5.42a and 5.42b that the maximum value of the constant associated to electrolyte material K_E was 5.56 when $k_3 = 0.3$ and $k_4 = 0.5$, and minimum (1.0) when $k_3 = 1.0$ and $k_4 = 1.0$.

Two different asymmetric ECs were assembled and operated with different k_3, k_4, k_1 and k_2 as described in cases 2 and 3 of Table 5.17. In these cases, it was assumed that the operating potential range of organic electrolyte was two and half folds (2.500 folds) that of aqueous electrolyte, while the specific capacitance of electrodes in organic electrolyte was two-fifth folds (0.400 times) that in aqueous electrolyte. Thus, the value of k_3 and k_4 were given as 0.400, in these two cases. When the asymmetric EC was assembled and operated as explained in case 2 using organic electrolyte, storable and deliverable energies were improved to 584.67Wh and 584.58Wh, respectively. Also, maximum energy and power

densities were improved to 191.92Wh/kg and 38.38W/kg, respectively. Storable and deliverable energies were enhanced by a factor of 5.780 compared with those of the asymmetric EDLC of the same k_1 using aqueous electrolyte, while the maximum energy and power densities were enhanced by a factor of 2.790 compared with those of the asymmetric EDLC of the same k_1 using aqueous electrolyte.

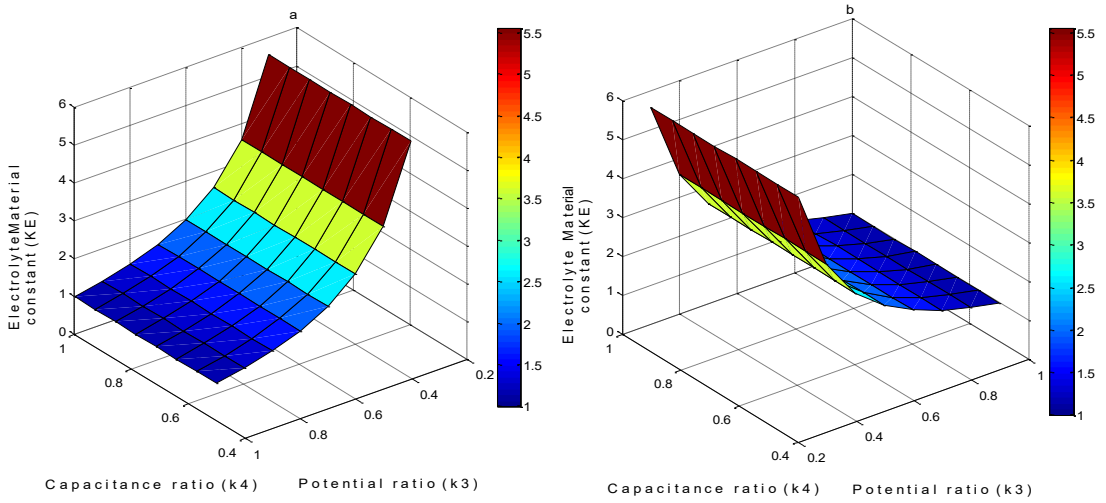

Figure 5.42: (a) 3-D front view profile of value of constant associated to electrolyte material K_E as function of k_3 and k_4 ratios for ranges of $0.3 \le k_3 < 1$ and $0.5 \le k_4 < 1$; and (b) 3-D side view profile of value of constant associated to electrolyte material K_E as function of k_3 and k_4 ratios in range of $0.3 \le k_3 < 1$ and $0.5 \le k_4 < 1$.

First and second charge–discharge cycle efficiency η_{E1} and η_{E2} of the asymmetric EC was equally improved to 96.40% and 96.43% respectively. In the same manner, energy and power densities of the asymmetric EC assembled and operated with a maximum value of K_{BMopt} = 0.94 (at k_{1opt}=0.050 and k_{2opt}=0.080) as described in case 3 of Table 5.17 using organic electrolyte were improved to 365.43Wh/kg and 73.09W/kg, respectively. Energy and power densities improvement in the asymmetric EC were a factor of 5.300 greater than those of the asymmetric EDLC using aqueous electrolyte.

Using organic electrolyte with a higher operating potential range is one of the appropriate approaches to improve the EC's storable energy, energy density and power density, and several studies on the application of organic electrolyte in combination with asymmetric configuration have been conducted [247,285–287]. The asymmetric EC with a battery-type electrode of suitable mass and operating potential range, organic electrolyte with a two-fold operating potential range of aqueous electrolyte and half of the electrode specific capacitance in aqueous electrolyte, stored approximately 2.000 times the energy of the asymmetric EC using aqueous electrolyte as shown in case 3 of Table 5.16.

Table 5.17: Parameters of EDLC using aqueous electrolyte and asymmetric ECs using aqueous electrolytes and voltage windows of 1.200V and 3.000V & 3.000V, respectively, during charging and discharging processes in cases 1, 2 and 3

S/N	Parameter	Unit	α_1= 0.05S/cm and α_2 = 0.05S/cm		
			Case 1	Case 2	Case 3
			Asymmetric EDLC with $k_1 = 0.05$, $k_2 = 0.08$, $\Delta V_{max} = 1.2V$	Asymmetric EC with $k_1 = 0.50$, $k_2 = 0$, $k_3 = 0.4$, $k_4 = 0.4$, $\Delta V_{max} = 3.0V$	Asymmetric EC with $k_{1opt} = 0.05$, $k_{2opt} = 0.08$, $k_3 = 0.4$, $k_4 = 0.4$, $\Delta V_{max} = 3.0V$
1	E_{ch}	Wh	101.22	584.68	584.68
2	E_{dis}	Wh	100.91	584.58	584.58
3	ED_{max}	Wh/kg	68.781	191.92	365.43
4	ED_{eff}	Wh/kg	63.725	188.50	358.87
5	PD_{max}	W/kg	13.722	38.383	73.086
6	PD_{eff}	W/kg	12.713	37.700	71.774
7	η_{E1}	%	84.241	96.402	96.402
8	η_{E2}	%	84.251	96.431	96.431
9	$M_{ele,pe}$	kg	0.0315	1.2586	0.0723
10	$M_{ele,ne}$	kg	1.2580	1.2580	1.2580
11	M_{Cell}	kg	1.5883	2.8155	1.6292

The energy and power densities of the asymmetric EC with a proper mass and operating potential range are also approximately 2.000 times those of similar asymmetric EC using

aqueous electrolyte as presented in case 3 of Table 5.16. Storable energy of the asymmetric EC with suitable mass and operating potential range, organic electrolyte with 2.500 times the operating potential range of aqueous electrolyte and two-fifths of electrode specific capacitance in aqueous electrolyte was approximately 2.500 times that of a similar asymmetric EC using an aqueous electrolyte as presented in case 3 of Table 5.17. The maximum energy and power densities of the device were a factor of 2.430 greater than (as seen in case 3 of Table 5.17) those of a similar asymmetric EC using aqueous electrolyte shown in case 3 of Table 5.15.

When self-discharge was incorporated into the asymmetric EC with suitable a electrode mass and operating potential range ratios using aqueous electrolyte (K_{BMopt}), it stored and delivered 214.48Wh and 209.36Wh, (case 2 of Table 5.18) respectively, compared with 96.50Wh and 90.86Wh stored and delivered respectively by the symmetric EDLC with self-discharge as presented in case 1 of Table 5.18. Storable and deliverable energy losses as self-discharge in the asymmetric EC with self-discharge are 20.10Wh and 23.79Wh, respectively. The asymmetric EC with a maximum coefficient associated to battery-type material K_{BMopt} = 0.94, organic electrolyte of twice the operating potential range of aqueous electrolyte, half the electrode specific capacitance in aqueous electrolyte and self-discharge, stored and delivered 428.96Wh and 418.72Wh respectively, as presented in Table 5.18. Its storable and deliverable energies are twice those of a similar asymmetric EC with self-discharge using aqueous electrolyte; whereas the energy and power densities are 1.950 folds (280.51Wh/kg and 56.10W/kg) those of a similar asymmetric EC with self-discharge using aqueous electrolyte.

When the asymmetric EC with self-discharge used suitable electrode with a maximum coefficient associated to battery-type material and a maximum constant associated to

electrolyte material (K_{BMopt} and K_{Eopt}), it stored and delivered 5.560 times (1192.50Wh and 1164.00Wh) the energies of similar asymmetric devices using aqueous electrolyte. Similarly, its energy and power densities are also 5.560 times (799.97Wh/kg and 159.97W/kg) those of a similar asymmetric capacitor using aqueous electrolyte as seen in Table 5.18. In comparison, the difference in the value of parameters in Tables 5.18 and 5.19 were due to self-discharge inherent in the device presented in Table 5.18. For instance, maximum storable energy and energy density in the device without self-discharge (case 4 of Table 5.19) was 1304.26Wh and 837.00Wh/kg respectively, while those of the device with self-discharge (case 4 of Table 5.18) was 1192.50Wh and 799.97Wh/kg, respectively.

Table 5.18: Parameters of symmetric EDLC using aqueous electrolyte, asymmetric EC using aqueous electrolyte, and asymmetric ECs with self-discharge using organic electrolytes and voltage windows of 1.200V, 1.200V, 2.400V and 4.000V, respectively, during charging and discharging processes in cases 1, 2, 3 and 4.

S/N	Parameter	Unit	α_1= 0.05S/cm and α_2 = 0.05S/cm			
			Case 1	Case 2	Case 3	Case 4
			Symmetric EDLC with k_1 = 0.50, k_2 = 0.50, ΔV_{max} = 1.2V, with only EDLs instability self-discharge	Asymmetric EC with k_{1opt} = 0.05, k_{2opt} = 0.08, ΔV_{max} = 1.2V with EDLs instability & redox reactions	Asymmetric EC with k_{1opt} = 0.05, k_{2opt} = 0.08, k_3 = 0.5, k_4 = 0.5 ΔV_{max} = 2.4V with EDLs instability & redox reactions	Asymmetric EC with k_{1opt} = 0.05, k_{2opt} = 0.08, k_{3opt} = 0.3, k_{4opt} = 0.5, ΔV_{max} = 4.0V with EDLs instability & redox reactions
1	E_{ch}	Wh	96.502	214.48	428.96	1192.5
2	E_{dis}	Wh	90.862	209.36	418.72	1164.0
3	ED_{max}	Wh/kg	38.605	143.88	280.51	799.97
4	ED_{eff}	Wh/kg	35.282	116.43	227.03	647.35
5	PD_{max}	W/kg	7.7016	28.771	56.10	159.97
6	PD_{eff}	W/kg	6.8393	23.285	45.405	129.46
7	η_{E1}	%	75.596	67.218	74.794	78.426
8	η_{E2}	%	75.601	75.500	82.471	86.158

9	$M_{ele,pe}$	kg	1.2580	0.0723	0.0723	0.0723
10	$M_{ele,ne}$	kg	1.2580	1.2580	1.2580	1.2580
11	M_{Cell}	kg	2.8149	1.6292	1.6292	1.6292

The maximum coefficient associated to battery-kind material K_{BMopt} is 0.940, while that associated to electrolyte material K_{Eopt} is 5.560. The asymmetric EC with proper mass and operating potential range, organic electrolyte of 3.330 times the operating potential range of aqueous electrolyte and half the electrode specific capacitance in aqueous electrolyte (K_{BMopt} and K_{Eopt}) stored 5.560 time the energy (case 3 of Table 5.19) of a similar asymmetric EC using aqueous electrolyte as shown in case 4 of Table 5.19. Energy and power densities in this configuration were also a factor of 5.560 greater than those of a similar asymmetric EC using aqueous electrolyte as seen in Table 5.19. Storable and deliverable energies of this asymmetric device was 1304.26Wh and 1296.31Wh, respectively, while energy and power densities were as high as 837.00Wh/kg and 167.40W/kg, respectively as presented in Table 5.19.

Table 5.19: Parameters of asymmetric EDLC using aqueous electrolyte, asymmetric EDLC using organic electrolyte, asymmetric EC using aqueous electrolyte and asymmetric EC using organic electrolyte with voltage windows of 1.200V, 4.000V, 1.200V and 4.000V respectively, during charging and discharging processes in cases 1, 2, 3 and 4.

S/N	Parameter	Unit	α_1= 0.05S/cm and α_2 = 0.05S/cm			
			Case 1	Case 2	Case 3	Case 4
			Asymmetric EDLC with k_{1opt} = 0.05, k_{2opt} = 0.08, ΔV_{max} = 1.2V	Asymmetric EDLC with k_{1opt} = 0.05, k_{2opt} = 0.08, k_{3opt} = 0.3, k_{4opt} = 0.5, ΔV_{max} = 4.0V	Asymmetric EC with k_{1opt} = 0.05, k_{2opt} = 0.08, and ΔV_{max} = 1.2V	Asymmetric EC with k_{1opt} = 0.05, k_{2opt} = 0.08, k_{3opt} = 0.3, k_{4opt} = 0.5, ΔV_{max} = 4.0V
1	E_{asch}	Wh	101.22	562.78	234.58	1304.3
2	E_{asdis}	Wh	100.91	560.06	233.15	1296.3

3	ED_{max}	Wh/kg	68.781	382.42	150.54	837.00
4	ED_{eff}	Wh/kg	63.725	354.31	143.98	800.53
5	PD_{max}	W/kg	13.722	76.294	30.108	167.40
6	PD_{eff}	W/kg	12.713	70.684	28.797	160.11
7	η_{E1}	%	84.241	97.500	90.723	97.505
8	η_{E2}	%	84.251	97.603	90.823	97.631
9	$M_{ele,pe}$	kg	0.0315	0.0315	0.0723	0.0723
10	$M_{ele,ne}$	kg	1.2580	1.2580	1.2580	1.2580
11	M_{Cell}	kg	1.5883	1.5883	1.6292	1.6292

A summary of the performance parameters of various electrochemical capacitors using aqueous and organic electrolytes were presented in Table 5.20. It is obvious from Table 5.20 that the energy and power densities of the asymmetric EDLC using aqueous electrolyte were a factor of 1.800 higher than those of the symmetric EDLC using aqueous electrolyte, while storable energies are the same with a reduction in the device mass and volume by a factor of 1.770. Also, energy and power densities of the asymmetric EDLC using organic electrolyte were a factor of 1.800 greater than those of the symmetric EDLC using organic electrolyte, while storable energies are the same with reduction in device mass and volume by a factor of 1.770. Storable energy of asymmetric EC with aqueous electrolyte was a factor of 2.320 greater than that of the asymmetric EDLC using aqueous electrolyte with an increase in device mass and volume by a factor of 1.030, whereas energy and power densities of the asymmetric EC with aqueous electrolyte were a factor of 2.200 higher than those of the asymmetric EDLC with aqueous electrolyte. Also, energy and power densities of the asymmetric EC with organic electrolyte were a factor of 2.200 greater than those of the symmetric EDLC with organic electrolyte, whereas its storable energy of the asymmetric EC with organic electrolyte was a factor of 2.320 greater than that of the asymmetric EDLC using organic electrolyte with reduction in device mass and volume by a factor of 1.770.

Energy and power densities of the asymmetric EC with aqueous electrolyte were 3.880 times those of the symmetric EDLC using aqueous electrolyte with a reduction in the device mass and volume by a factor of 1.770, whereas storable energy of the asymmetric EC with aqueous electrolyte was 2.320 times that of the symmetric EDLC with aqueous electrolyte. Similarly, energy and power densities of the asymmetric EC with organic electrolyte were 3.880 times those of the symmetric EDLC with organic electrolyte, whereas its storable energy of the asymmetric EC with organic electrolyte was 2.320 times that of the symmetric EDLC with organic electrolyte. Storable energy, energy density and power density of the symmetric EDLC using organic electrolyte were a factor of 5.560 greater than those of the symmetric EDLC using aqueous electrolyte with the same device mass and volume. Storable energy, energy density and power density of the asymmetric EDLC using organic electrolyte were a factor of 5.560 greater than those of the asymmetric EDLC using aqueous electrolyte with the same cell mass and volume. Again, storable energy, energy density and power density of the asymmetric EC using organic electrolyte were a factor of 5.560 higher than those of the asymmetric EC using aqueous electrolyte with the same cell mass and volume.

In addition, storable energy of the asymmetric EC with organic electrolyte was a factor of 12.900 greater than that of the symmetric EDLC with aqueous electrolyte with a reduction in cell mass and volume by a factor of 1.730, while energy and power densities of the asymmetric EC with organic electrolyte were a factor of 21.60 greater than that of the symmetric EDLC with aqueous electrolyte.

Table 5.20: Summary of performance parameters of various electrochemical capacitors using aqueous and organic electrolytes, respectively

S/	Electrochemical capacitor systems	Performance parameters

N		Storable energy (Wh)	Energy density (Wh/kg)	Power density (W/kg)
1	Symmetric EDLC with aqueous electrolyte, $k_1 = 0.5, k_2 = 0.5$ and 1.2V	$E_S = 101.22$	$ED_S = 38.81$	$PD_S = 7.743$
2	Asymmetric EDLC with aqueous electrolyte, $k_1 = 0.05$, $k_2 = 0.08$, and 1.2V	$E_{as} = 101.22$	$ED_{as} = 68.78$	$PD_{as} = 13.72$
3	Asymmetric EC with aqueous electrolyte, $k_1 = 0.05, k_2 = 0.08$, and 1.2V	$E_{as} = 234.58$	$ED_{as} = 150.54$	$PD_{as} = 30.11$
4	Symmetric EDLC with organic electrolyte, $k_1 = 0.5, k_2 = 0.5$, $k_3 = 0.3$, $k_4 = 0.5$ and 4.0V	$E_{o_s} = 562.78$	$ED_{o_s} = 215.78$	$PD_{o_s} = 43.05$
5	Asymmetric EDLC with organic electrolyte, $k_1 = 0.05, k_2 = 0.08$, $k_3 = 0.3$, $k_4 = 0.5$ and 4.0V	$E_{o_as} = 562.78$	$ED_{o_as} = 382.42$	$PD_{o_as} = 76.68$
6	Asymmetric EC with organic electrolyte, $k_1 = 0.05, k_2 = 0.08$, $k_3 = 0.3$, $k_4 = 0.5$ and 4.0V	$E_{o_as} = 1304.30$	$ED_{o_as} = 837.0$	$PD_{o_as} = 167.40$

The summary of the relationships for parameters from simulations for purpose of capacitors performance comparison is as follows:

$$E_{o_s} = 5.56\, E_s \quad (5.1)$$

$$ED_{o_s} = 5.56\, ED_s \quad (5.2)$$

$$PD_{o_s} = 5.56\, PD_s \quad (5.3)$$

$$E_{as} = 2.3\, E_s = E_{as} = 0.42\, E_{o_s} \quad (5.4)$$

$$ED_{as} = 2.2\, ED_s = ED_{as} = 0.39\, ED_{o_s} \quad (5.5)$$

$$PD_{as} = 2.2\, PD_s = PD_{as} = 0.39\, PD_{o_s} \quad (5.6)$$

$$E_{o_as} = 12.9\, E_s = 5.56\, E_{as} = 2.31\, E_{o_s} \quad (5.7)$$

$$ED_{o_as} = 21.6\, ED_s = 5.56\, ED_{as} = 2.20\, ED_{o_s} \quad (5.8)$$

$$PD_{o_as} = 21.6\, PD_s = 5.56\, PD_{as} = 2.20\, PD_{o_s} \quad (5.9)$$

The summary of the relationships for parameters from theoretical equations for purpose of capacitors performance comparison is as follows:

$$E_{o_s} = K_E E_s = \frac{1}{2} E_{o_1} = \frac{K_E}{2} E_1 = 5.56E_s = 0.5E_{o_1} = 2.78E_1 \quad 3.212$$

$$ED_{o_s} = K_E ED_s = \frac{1}{2} ED_{o_1} = \frac{K_E}{2} ED_1 = 5.56ED_s = 0.5ED_{o_1} = 2.78ED_1 \quad 3.213$$

$$PD_{o_s} = K_E PD_s = \frac{1}{2} PD_{o_1} = \frac{K_E}{2} PD_1 = 5.56PD_s = 0.5PD_{o_1} = 2.78PD_1 \quad 3.214$$

$$E_{as} = \frac{2K_{BM}}{(1-k_1)} E_s = \frac{K_{BM}}{(1-k_1)} E_1 = 2.00E_s = 1.00E_1 \quad 3.215$$

$$ED_{as} = 2K_{BM} ED_s = K_{BM} ED_1 = 1.89ED_s = 0.95ED_1 \quad 3.216$$

$$PD_{as} = 2K_{BM} PD_s = K_{BM} PD_1 = 1.89PD_s = 0.95PD_1 \quad 3.217$$

$$E_{o_as} = K_E E_{as} = \frac{2K_{BM}}{(1-k_1)} E_{o_s} = \frac{2K_E K_{BM}}{(1-k_1)} E_s = \frac{K_{BM}}{(1-k_1)} E_{o_1} = \frac{K_E K_{BM}}{(1-k_1)} E_1$$
$$= 5.56E_{as} = 2.00E_{o_s} = 11.08E_s = 1.00E_{o_1} = 5.54E_1 \quad 3.218$$

$$ED_{o_as} = K_E ED_{as} = 2K_{BM} ED_{o_s} = 2K_E K_{BM} ED_s = K_{BM} ED_{o_1} = K_E K_{BM} ED_1$$
$$= 5.56ED_{as} = 1.89ED_{o_s} = 10.50ED_s = 0.95ED_{o_1} = 5.25ED_1 \quad 3.219$$

$$PD_{o_as} = K_E PD_{as} = 2K_{BM} PD_{o_s} = 2K_E K_{BM} PD_s = K_{BM} PD_{o_1} = K_E K_{BM} PD_1$$
$$= 5.56PD_{as} = 1.89PD_{o_s} = 10.50PD_s = 0.95PD_{o_1} = 5.25PD_1 \quad 3.220$$

It was clearly seen from equations 3.211, 3.212 and 3.213 that storable energy E_{o_s}, energy density ED_{o_s} and power density PD_{o_s} of the symmetric EC using organic electrolyte were a factor of 5.560 greater than (E_{o_s} =5.56 E_s , ED_{o_s} =5.56 ED_s and PD_{o_s} =5.56 PD_s) those of the similar symmetric EC using aqueous electrolyte. It was also obvious from equations 3.218, 3.219 and 3.220 that storable energy E_{as}, energy density ED_{as} and power density PD_{as} of the asymmetric EC using aqueous electrolyte were factors of 0.360, 0.340 and 0.340 respectively, less than (E_{as} = 0.360 E_{o_s} , ED_{as} =0.340 ED_{o_s} and PD_{as} =0.340 PD_{o_s}) those of the symmetric EC using organic electrolyte. Storable energy E_{as}, energy density ED_{as} and power density PD_{as} of the asymmetric EC using aqueous electrolyte were factors of 2.000, 1.890 and 1.890, respectively, greater than (E_{as} =2.000

E_s, ED_{as} =1.890 ED_s and PD_{as} =1.890 PD_s) those of the symmetric EC using aqueous electrolyte.

Equations 3.218, 3.219 and 3.220 show that storable energy E_{o_as}, energy density ED_{o_as} and power density PD_{o_as} of the asymmetric EC using organic electrolyte were 5.560 times (E_{o_as} = 5.560 E_{as}, ED_{o_as} = 5.560 ED_{as} and PD_{o_as} = 5.560 PD_{as}) those of the asymmetric EC using aqueous electrolyte; and were also 2.000, 1.890 and 1.890 times respectively those of the symmetric EC using organic electrolyte. Storable energy E_{o_as}, energy density ED_{o_as} and power density PD_{o_as} of the asymmetric EC using organic electrolyte were equally factors of 11.080, 10.500 and 10.500 respectively, higher than those of the symmetric EC using aqueous electrolyte.

Results from the simulation showed that storable energy, specific energy density and specific power density of the asymmetric EC using aqueous electrolyte were respectively a factor of 2.300, 2.200 and 2.200 higher than those of the symmetric EC using the same electrolyte. It again shows that storable energy, energy density and power density of the asymmetric EC using aqueous electrolyte was respectively a factor of 0.420, 0.390 and 0.390 less than those of the symmetric EC using organic electrolyte. Storable energy, energy density and power density of the symmetric EC using organic electrolyte were a factor of 5.560 higher than those of the similar symmetric EC using aqueous electrolyte. Storable energy, energy density and power density of the asymmetric EC using organic electrolyte were a factor of 5.560 greater than those of a similar asymmetric EC using aqueous electrolyte. Storable energy, energy density and power density of the asymmetric EC using aqueous electrolyte were respectively factors of 2.320, 2.200 and 2.200 higher than those of the asymmetric EDLC using aqueous electrolyte. Again, storable energy,

energy density and power density of the asymmetric EC using organic electrolyte were respectively factors of 2.320, 2.200 and 2.200 higher than those of the asymmetric EDLC using organic electrolyte. Also, storable energy, energy density and power density of asymmetric EC using organic electrolyte were factors of 12.90, 21.60 and 21.60 respectively, greater than those of the symmetric EC using aqueous electrolyte. The simulation results were summarised in equations 5.1–5.9 and presented in Table 5.19. The results from the simulation agreed reasonably with results from theoretical equations. ~~and~~ A slight difference observed was due to different densities for the capacitor-type and battery-type electrodes in simulations, while the same density was used in theoretical equations. The degree of agreement between the simulation results using data from our symmetric EDLC model (equation 4.1) presented in case 1 of Tables 3 and 5.18 and those from the proposed procedure and methodology is reliable.

The analysis and discussions above comprehensibly revealed that the asymmetric EC has superior electrochemical performance compared with the symmetric capacitor using the same aqueous electrolyte. The asymmetric EC with suitable electrode mass and operating potential range ratios is able to store and deliver twice as much energy than those of the symmetric EDLC and, in addition, have more than twice the energy and power densities of the symmetric EDLC using the same aqueous electrolyte. It was also very clear that assemblage of he asymmetric EC configuration, together with organic electrolyte, has superior capacity to enhance the performance of electrochemical devices, in line with earlier reports by several researchers [285,288].

The asymmetric EC, with the proper electrode mass and operating potential range ratios, together with the use of organic electrolyte of appropriate operating potential range and electrode specific capacitance has over five-times the storable energy, deliverable energy, energy density and power density of the similar asymmetric EC using aqueous electrolyte.

The superior performances of the asymmetric EC are in terms of storable and deliverable energies, energy and power densities as well as charge–discharge cycle efficiency, as presented in Table 5.19. A symmetric EDLC using the same type of electrode with different mass, and with suitable mass and operating potentials range ratios, also has superior capacity to store more energy than conventional symmetric EDLC using the same aqueous electrolyte as seen in Table 5.14.

CHAPTER SIX

6.0 Conclusions and Recommendations

6.1 Conclusions

Conclusions were presented in four parts namely: the effects of self-discharge on performance of symmetric electric double layer capacitors and active electrolyte enhanced supercapacitors; the effects of self-discharge on performance of asymmetric/hybrid electrochemical capacitors; the effects of operating conditions and design configurations on performance of electrochemical capacitors; and the optimization of design parameters and operating conditions of electrochemical capacitors for high performance.

Theoretical basis and models for calculations, control, and improvement of performance of various types and designs of the symmetric and asymmetric ECs with simultaneous account of physical, electrical, electrochemical properties of electrode materials and structures design of the electrodes and the separator were developed. The effects of self-discharge, operating conditions and design configurations on performance of different types of ECs during charging, discharging and on storage condition was discovered from modeling. Guideline to determine optimal process design parameters for maximum performances of electrochemical capacitors of different applications, subject to type and value of electrodes, electrolyte and separator's properties, as well as values of applied current densities were developed using a modeling approach.

6.1.1 The Effects of Self-Discharge on the Performance of Symmetric Electric Double Layer Capacitors and Active Electrolyte Enhanced Supercapacitors: Insights from Modelling and Simulation

The effects of self-discharge on the performance of symmetric EDLCs have been studied through inclusion of self-discharge, via a combination of different self-discharge mechanisms, into capacitors' mass transfer and charge conservation equations during charging and discharging. The contributions of each key self-discharge parameter on capacitor performance and how they could be tuned to improve device performance, can be easily studied using the model. First and second charge–discharge cycle energy efficiency η_{E1} and η_{E2} of similar capacitors without self-discharge was 84.24% and 84.25%, while that of a device with self-discharge was less. Thus, energy efficiency of EDLCs without self-discharge was higher than that of similar EDLCs with self-discharges.

Side-reactions or redox reactions self-discharge contributed the majority of self-discharge in symmetric EDLCs and AEESs when the concentration of redox species that produces soluble products during the charging process are high. The quick self-discharge process was caused by the migration of soluble products of redox reactions from one electrode to another through the separator during the charging/discharging process. Tuning key self-discharge parameters reduced energy loss by self-discharges from 28.38Wh to 1.12Wh in a device with both side-reactions/redox reactions and EDLs instability self-discharge. Storable energy was improved from 70.24Wh to 99.52Wh in the capacitor with self-discharge, compared with 101.20Wh in the device without self-discharge. Similarly, first and second charge–discharge cycle energy efficiencies η_{E1} and η_{E2} of the capacitor with both side-reactions/redox reactions and EDLs

instability self-discharge improved from 38.13% and 38.14% to 80.54% and 81.56% respectively .

It was noticed that capacitors with self-discharge took a longer time to be charged to target voltage than those without self-discharge, while fully charged capacitors with self-discharge discharged all stored energy faster than those without self-discharge. This is because earlier stored charges are lost by self-discharge during the charging process, while the fully charged device loses part of the stored charge by self-discharge. The effects of self-discharge during capacitor storage was negligible since it took a fully charged capacitor, in all conditions studied, a minimum of 14.0 days to be entirely discharged by self-discharge, hence self-discharge in the storage condition can be ignored.

From the above results, ignoring self-discharge in symmetric EDLCs models amounts to over-rating the capacitor's performance. It was discovered that key self-discharge parameters needed to be tuned to suppress the self-discharge rate, are the concentration of shuttle impurities, concentration of redox species, and thickness of the separator. It was noticed that the EDLs instability self-discharges, which is predominant in EDLCs, are caused by functional groups or impurities in electrode materials, shuttling of electrolyte impurities among electrodes, charge redistribution and attractive force from opposite ions in the electrolyte phase. In AEESs, both EDLs instability and side-reactions, or reactions self-discharge, were present in reasonable measures, but that of the redox reactions contributed the majority, due to migration of redox reaction soluble products from one electrode to another. In summary, it was observed that the effects of self-discharge are to large to be ignored in EC models. Models with self-discharge presented a more realistic estimate of potential drop and energy loss during operations.

6.1.2 The Effects of Self-Discharge on the Performance of Asymmetric/Hybrid Electrochemical Capacitors: Insights from Modeling and Simulation.

The effects of self-discharge were incorporated into the asymmetric ECs model during charging and discharging using an applicable specific self-discharge mechanism and a combination of different self-discharge mechanisms. The effects of self-discharge on the performance of asymmetric ECs were studied via simulations of the model which emerged. The first and second charge–discharge cycle energy efficiency η_{E1} and η_{E2} of the device with electrodes effective conductivity α_1=0.05S/cm and both EDLs instability and redox reactions self-discharge was 79.57% and 82.03% respectively, compared with 90.72% and 90.82% in a similar capacitor without self-discharge. Energy loss in the asymmetric EC with electrodes and electrolyte effective conductivity $\alpha_1 = \alpha_2$ =0.05S/cm and both EDLs' instability and redox reactions self-discharge during charging and discharging was 59.53Wh.

Key self-discharge parameters to be tuned in order to suppress the self-discharge rate in the asymmetric devices are concentration of impurity ions, concentration of impurity oxidized species and total thickness of the separator and positive electrode. Moreover, energy efficiencies η_{E1} and η_{E2} of the device with both EDLs' instability and redox reactions self-discharge, and tuned self-discharge parameters, was enhanced to 90.46% and 90.79% respectively. The energy loss of both EDLs instability and redox reactions self-discharge in the device with tuned key self-discharge parameters was 7.43Wh. The capacitor with both EDLs' instability and redox reactions, self-discharge using untuned self-discharge parameters with soluble redox reactions products and using tuned self-discharge parameters with insoluble redox reactions products, stored 214.48Wh and 245.33Wh energy respectively, compared with 234.58Wh stored in similar capacitors without self-discharge. These

capacitors also delivered 209.36Wh and 244.02Wh energies respectively during the discharging process, in comparison with 233.15Wh delivered by a similar capacitor without self-discharge. Storable and deliverable energies of capacitors with tuned self-discharge parameters and insoluble redox reaction products were higher than those of similar capacitors without self-discharge. Thus, the reduction of shuttle impurity concentration, and the use of redox-active species that produces insoluble products, suppresses the rate of self-discharge. The modification of key self-discharge parameters improved the asymmetric EC's energy efficiency, storable energy and deliverable energy.

It was noticed that when the asymmetric EC was charged and discharged at speed, the rate of self-discharge reduced greatly, compared with slow charging and discharging processes because there was not enough time for shuttle self-discharge and charge redistribution to occur when charged quickly. Incorporation of self-discharge into the asymmetric ECs model, created a platform to examine the effects of self-discharge parameters during charging and discharging with a view to improving performance. In asymmetric capacitors, side-reactions or reactions of active redox species self-discharge contributed the majority of self-discharge, compared with that of EDLs instability, because soluble products of redox reaction shuttles from one electrode to another. The asymmetric ECs performance is obviously over-rated when self-discharge was completely neglected in the models. The charging time of asymmetric EC's significantly depends on the self-discharge rate, which decays its voltage and energy, increases charging time and causes deterioration in the device. Models that incorporate self-discharge give a more practical evaluation of potential decay and energy dissipation during self-discharge.

6.1.3 The Influences of Operating Conditions and Design Configurations on the Performance of Symmetric Electrochemical Capacitors

Mathematical models were used to determine the effects of different charging current densities, charging times, electrode and electrolyte effective conductivities, electrode thickness, and electrode porosities on the symmetric EC's performance parameters ~~like~~ such as capacitance, energy density and power density. Successful charging of the EC using current density is greatly dependent on the device's electrodes and electrolyte effective conductivities, as well as the thickness of electrodes. Also, In addition, the speed with which the EC can be effectively charged is dependent on the charging current density, effective conductivity of electrodes and electrolyte as well as the electrode's thickness. For ECs to be charged very fast, they must have thin electrodes and high electrode and electrolyte effective conductivities to permit effective charging without potential drops at such a rate. Therefore, ECs of low electrode and electrolyte effective conductivities cannot be charged effectively at high current density, because potential drops becomes as high as half of cell's voltage at such a rate. Conversely, ECs with thin electrodes and high electrode and electrolyte effective conductivities are effectively charged at a high current density in a time range of a few to micro seconds and will have high power densities. The typical length scale $[w_e]$ over which the liquid potential drop occurs, can be used as a design parameter to optimize the electrode's thickness (effective thickness) for ECs designed to function under given current density spans.

ECs with a high concentration of impurity ions or redox species exhibit~~s~~ a high self-discharge rate, and charging ECs fast greatly reduced the self-discharge rate, compared with slow charging, provided that the electrode's and electrolyte's effective conductivities are high

enough. Electrodes utilization u can also be used to determine the optimum thickness/effective thickness of the electrodes, optimum current density and charging time in a cell of specific voltage and effective conductivities of electrodes and electrolyte. This guideline can be used to determine optimum electrodes thickness (100% electrodes utilization), optimum charging current density and optimum charging time for a cell of given voltage, electrodes thickness, electrodes and electrolyte's effective conductivities. It is therefore recommended that for a device with given electrodes and electrolyte effective conductivities expected to be charged at a certain current density, the electrode's thickness must be equivalent to the electrode's effective thickness (100% electrodes utilization) at the given current density, in order to avoid deadweight that reduces specific energy and power. Also, it is very important to use the optimum current density to charge/discharge the capacitor with a given electrodes thickness and effective conductivities of electrodes and electrolyte, in order to avoid underutilization of the electrodes, increased inefficiencies and potential drops, and achieve high energy and power densities.

Energy density of a capacitor with given electrodes and electrolyte effective conductivities was increased in 2.13, 4.75 and 10.75 by reducing the electrode's thickness in 1.33, 2.00, and 4.00 respectively. The power density of the capacitor with specific electrodes thickness and very high electrodes and electrolyte effective conductivities ($\alpha_1 = 50$S/cm and $\alpha_2 = 0.50$S/cm) charged at a specific current density was increased by a factor of 10, 100, 1000 without compromising energy density by increasing and reducing the current density and charging time by the same amount. The effective mass of the electrodes reduces as accessible pores are increased; thus, the EC with higher electrodes and separator porosities has a smaller mass than a similar device with lower accessible porosities. The Ragone plots of electrochemical capacitors with diverse electrode thicknesses and different electrode and electrolyte effective conductivities, charged at different current densities for

different times can be used to select electrode dimensions to achieve a given energy and power density specifications.

6.1.4 Optimization of electrochemical capacitors design parameters and operating conditions for high energy and power performances.

Modified theoretical expressions for different electrochemical capacitors facilitated comprehensive comparison of the performance parameters of various capacitors categorized in terms of electrolyte type and electrodes symmetry. The maximum value of the coefficient associated to battery-type material K_{BMopt} was 0.94 at k_{1opt} = 0.05 & k_{2opt} = 0.08, while the constant associated to electrolyte material K_{Eopt} was 5.56 at k_{3opt} = 0.30 & k_{4opt} = 0.50. Estimations of storable energy E_{ch}, deliverable energy E_{dis}, maximum energy density ED_{max} and maximum power density PD_{max} were feasible and achievable once details of the electrode's mass ratio, operating potential range ratio and electrode specific capacitance in the electrolyte of the device were known.

The asymmetric EC with suitable electrode mass and operating potential range ratios has over twice the storable energy, deliverable energy, energy density and power density of the symmetric EDLC using the same aqueous electrolyte with a reduction in cell mass and volume by a factor of 1.73. In addition, storable energy, deliverable energy, energy density and power density of the asymmetric EC with proper electrode mass and operating potential range ratios, together with organic electrolyte of an appropriate operating potential range and specific capacitance were a factor of 5.56 higher than those of a similar asymmetric EC using aqueous electrolyte with a reduction in cell mass and volume by a

factor of 1.73. Storable energy and deliverable energies of the asymmetric EC with a suitable electrode mass and operating potential range ratios, together with proper organic electrolyte were a factor of 12.90 greater than those of the symmetric EDLC using aqueous electrolyte, while its energy and power densities were a factor of 21.60 greater than those of the symmetric EDLC using aqueous electrolyte with a reduction in cell mass and volume by a factor of 1.73. The asymmetric EDLC with a suitable electrode mass and operating potential range ratios using proper organic electrolyte has more than five-times (5.56) the performance parameters of a similar symmetric EDLC using aqueous electrolyte with a reduction in cell mass and volume by a factor of 1.73. Also, the asymmetric EC with a suitable electrode mass and operating potential range ratios using proper organic electrolyte has more than twice (2.20) the performance parameters of the symmetric EDLC using organic electrolyte with a reduction in cell mass and volume by a factor of 1.73.

Optimal design requirements for an asymmetric EC using aqueous electrolytes are: the mass ratio of a battery-type electrode to the mass of two electrodes in aqueous electrolyte should be 1:19; the ratio of the working potential range of a battery-type electrode to maximum working potential of the device with aqueous electrolyte ought to be 1:12. Optimal design requirements for an asymmetric EC using organic electrolytes in addition to mass and working potential range ratio are: the ratio of maximum working range of aqueous electrolyte to that of organic electrolyte should be 1:3.33; and the ratio of specific capacitance of capacitor-type electrodes in aqueous electrolyte to that of capacitor-type electrodes in organic electrolyte should be 1:2.

These results obviously reduce the number of experiments needed to determine the optimum manufacturing state of an electrochemical energy storage device. These analyses and simulations intelligibly demonstrated that the institution of asymmetric electrodes and organic electrodes was very successful in improving the ECs' performance with a

reduction in cell mass and volume. The introduction of asymmetric EDLCs with the same type of electrode, but suitable electrodes mass and working potential range ratios, and proper organic electrolyte, enhanced the performance of conventional symmetric EDLCs using aqueous electrolyte with a reduction in cell mass and volume. These results could be a good guideline for the design and fabrication of ECs with outstanding performance in terms of storable energy, energy density and power density.

6.2 Contributions to knowledge

The following are areas of contribution to knowledge from this study:

- Incorporation of self-discharge into the electrochemical capacitor's model created a platform to study the effects of key self-discharge parameters and determine the minimum allowable concentration of impurities and redox species in a device's components for optimal performance.
- Models with self-discharge also created an approach to reduce the number of experiments required to determine the minimum impurity or redox species concentration and the optimum total thickness of the separator and anode.
- A guideline that can be used to determine optimum design configurations and operating conditions for optimal performance of electrochemical capacitors was created, using typical length scale $[w]$ over which the liquid potential drop occurs, effective electrodes thickness and electrodes utilization .
- The necessity to determine and employ the optimum current density to charge/discharge a capacitor with a given electrode thickness and effective conductivities of electrodes and electrolyte in order to avoid the underutilization of

electrodes increased inefficiencies and potential drops, and achieve high energy and power densities was shown.

- ❖ The generated ragone plots of ECs with different electrode thicknesses and electrode and electrolyte effective conductivities charged at different current densities for different times, can be used to select electrode dimensions to attain specific energy and power density specifications.
- ❖ The research created an avenue to reduce the number of experiments needed to determine the optimum electrode mass and operating potential range ratios, together with proper organic electrolyte for optimal performance of electrochemical energy storage devices.
- ❖ The study presented guidelines and requirements for the design and fabrication of electrochemical capacitors of outstanding performance in terms of high energy and power densities with a reduction in device mass and volume.

6.3 Recommendations

Based on the contributions of this study, time constraints and the necessity to investigate beyond the set aims and objectives of this research, the following recommendations were made:

1) The models should be extended to incorporate the heat generation term, in order to facilitate estimation of the temperature of operations, thermal functioning of new devices and the development of thermal management plans for existing ECs designs.
2) Symmetric electric double layer capacitors that operate as asymmetric capacitors using the optimum electrodes mass and potential range ratio should be fabricated and their

performance examined to ascertain the degree of improvement, compared with convectional EDLCs.

3) An asymmetric capacitors with the optimum battery-type mass ratio, potential range ratio, maximum potential range of aqueous electrolyte to organic electrolyte, and ratio of capacitance of capacitor-kind electrode in aqueous electrolyte to organic electrolyte should be fabricated and characterized to confirm its level of superiority. This could be implemented by fabricating the device using the optimum mass and potential ratios and organic electrolyte determined in this research.

REFERENCES

[1] E. Frackowiak, Carbon materials for supercapacitor application, Phys. Chem. Chem. Phys. 9 (2007) 1774–1785. doi:10.1039/B618139M.

[2] A.G. Pandolfo, A.F. Hollenkamp, Carbon properties and their role in supercapacitors, J. Power Sources. 157 (2006) 11–27. doi:10.1016/j.jpowsour.2006.02.065.

[3] D. Pech, M. Brunet, H. Durou, P. Huang, V. Mochalin, Y. Gogotsi, P.-L. Taberna, P. Simon, Ultrahigh-power micrometre-sized supercapacitors based on onion-like carbon, Nat. Nanotechnol. 5 (2010) 651–654. doi:10.1038/nnano.2010.162.

[4] P. Simon, Y. Gogotsi, Materials for electrochemical capacitors, Nat. Mater. 7 (2008) 845–854. doi:10.1038/nmat2297.

[5] L.L. Zhang, X.S. Zhao, Carbon-based materials as supercapacitor electrodes, Chem. Soc. Rev. 38 (2009) 2520–2531. doi:10.1039/B813846J.

[6] A. Burke, Ultracapacitors: why, how, and where is the technology, J. Power Sources. 91 (2000) 37–50. doi:10.1016/S0378-7753(00)00485-7.

[7] R. Kötz, M. Carlen, Principles and applications of electrochemical capacitors, Electrochimica Acta. 45 (2000) 2483–2498. doi:10.1016/S0013-4686(00)00354-6.

[8] Y. Zhang, H. Feng, X. Wu, L. Wang, A. Zhang, T. Xia, H. Dong, X. Li, L. Zhang, Progress of electrochemical capacitor electrode materials: A review, Int. J. Hydrog. Energy. 34 (2009) 4889–4899. doi:10.1016/j.ijhydene.2009.04.005.

[9] J.W. Kim, V. Augustyn, B. Dunn, The Effect of Crystallinity on the Rapid Pseudocapacitive Response of Nb2O5, Adv. Energy Mater. 2 (2012) 141–148. doi:10.1002/aenm.201100494.

[10] V. Augustyn, J. Come, M.A. Lowe, J.W. Kim, P.-L. Taberna, S.H. Tolbert, H.D. Abruña, P. Simon, B. Dunn, High-rate electrochemical energy storage through Li+ intercalation pseudocapacitance, Nat. Mater. 12 (2013) 518–522. doi:10.1038/nmat3601.

[11] B.E. Conway, V. Birss, J. Wojtowicz, The role and utilization of pseudocapacitance for energy storage by supercapacitors, J. Power Sources. 66 (1997) 1–14. doi:10.1016/S0378-7753(96)02474-3.

[12] B.E. Conway, Electrochemical supercapacitors: scientific fundamentals and technological applications, Kluwer Academic/Plenum, New York; London, 1999.

[13] E. Herrero, L.J. Buller, H.D. Abruña, Underpotential Deposition at Single Crystal Surfaces of Au, Pt, Ag and Other Materials, Chem. Rev. 101 (2001) 1897–1930. doi:10.1021/cr9600363.

[14] B.E. Conway, Two-dimensional and quasi-two-dimensional isotherms for Li intercalation and upd processes at surfaces, Electrochimica Acta. 38 (1993) 1249–1258. doi:10.1016/0013-4686(93)80055-5.

[15] D.B. Jeffrey W. Long, Asymmetric electrochemical capacitors—Stretching the limits of aqueous electrolytes, MRS Bull. 36 (2011) 513–522. doi:10.1557/mrs.2011.137.

[16] Y.-P. Lin, N.-L. Wu, Characterization of MnFe2O4/LiMn2O4 aqueous asymmetric supercapacitor, J. Power Sources. 196 (2011) 851–854. doi:10.1016/j.jpowsour.2010.07.066.

[17] F. Wang, S. Xiao, Y. Hou, C. Hu, L. Liu, Y. Wu, Electrode materials for aqueous asymmetric supercapacitors, RSC Adv. 3 (2013) 13059–13084. doi:10.1039/C3RA23466E.

[18] Y.-G. Wang, Z.-D. Wang, Y.-Y. Xia, An asymmetric supercapacitor using RuO2/TiO2 nanotube composite and activated carbon electrodes, Electrochimica Acta. 50 (2005) 5641–5646. doi:10.1016/j.electacta.2005.03.042.

[19] V. Khomenko, E. Raymundo-Piñero, F. Béguin, Optimisation of an asymmetric manganese oxide/activated carbon capacitor working at 2 V in aqueous medium, J. Power Sources. 153 (2006) 183–190. doi:10.1016/j.jpowsour.2005.03.210.

[20] L. Demarconnay, E. Raymundo-Piñero, F. Béguin, Adjustment of electrodes potential window in an asymmetric carbon/MnO2 supercapacitor, J. Power Sources. 196 (2011) 580–586. doi:10.1016/j.jpowsour.2010.06.013.

[21] T. Brousse, P.-L. Taberna, O. Crosnier, R. Dugas, P. Guillemet, Y. Scudeller, Y. Zhou, F. Favier, D. Bélanger, P. Simon, Long-term cycling behavior of asymmetric activated carbon/MnO2 aqueous electrochemical supercapacitor, J. Power Sources. 173 (2007) 633–641. doi:10.1016/j.jpowsour.2007.04.074.

[22] S. Ban, J. Zhang, L. Zhang, K. Tsay, D. Song, X. Zou, Charging and discharging electrochemical supercapacitors in the presence of both parallel leakage process and electrochemical decomposition of solvent, Electrochimica Acta. 90 (2013) 542–549. doi:10.1016/j.electacta.2012.12.056.

[23] Miller, J. R, Burke, A. F, Electrochemical Capacitors: Challenges and Opportunities for Real-World Applications., Electrochem. Soc. Interface. 17 (2008) 53–57.

[24] N.-L. Wu, Nanocrystalline oxide supercapacitors, Mater. Chem. Phys. 75 (2002) 6–11. doi:10.1016/S0254-0584(02)00022-6.

[25] Simon, P, Burke, A. F, Nanostructured Carbons: Double-Layer Capacitance and More., Electrochem. Soc. Interface. 17 (2008) 38–43.

[26] M.D. Stoller, S. Park, Y. Zhu, J. An, R.S. Ruoff, Graphene-Based Ultracapacitors, Nano Lett. 8 (2008) 3498–3502. doi:10.1021/nl802558y.

[27] F. Beguin, E. Frackowiak, Supercapacitors: Materials, Systems and Applications, John Wiley & Sons, 2013.

[28] J. Huang, B.G. Sumpter, V. Meunier, A Universal Model for Nanoporous Carbon Supercapacitors Applicable to Diverse Pore Regimes, Carbon Materials, and Electrolytes, Chem. – Eur. J. 14 (2008) 6614–6626. doi:10.1002/chem.200800639.

[29] J. Huang, B.G. Sumpter, V. Meunier, Theoretical Model for Nanoporous Carbon Supercapacitors, Angew. Chem. 120 (2008) 530–534. doi:10.1002/ange.200703864.

[30] A. Chu, P. Braatz, Comparison of commercial supercapacitors and high-power lithium-ion batteries for power-assist applications in hybrid electric vehicles: I. Initial characterization, J. Power Sources. 112 (2002) 236–246. doi:10.1016/S0378-7753(02)00364-6.

[31] F. Beguin, E. Frackowiak, Carbons for Electrochemical Energy Storage and Conversion Systems, CRC Press, 2009.

[32] J.R. Miller, P. Simon, Electrochemical Capacitors for Energy Management, Science. 321 (2008) 651–652. doi:10.1126/science.1158736.

[33] W. van Schalkwijk, B. Scrosati, Advances in Lithium Ion Batteries Introduction, in: W.A. van Schalkwijk, B. Scrosati (Eds.), Adv. Lithium-Ion Batter., Springer US, 2002: pp. 1–5. doi:10.1007/0-306-47508-1_1.

[34] Huggins, Robert A, Advanced Batteries, Springer US, Boston, MA, 2009. http://link.springer.com/10.1007/978-0-387-76424-5 (accessed November 17, 2015).

[35] Reddy, T. Linden, Linden's Handbook of Batteries, 4th Edition, 4 edition, McGraw-Hill Education, New York, 2010.

[36] I.S. Ike, S. Iyuke, Mathematical Modeling and Simulation of Supercapacitors, in: Nanomater. Adv. Batter. Supercapacitors, Springer International Publishing Switzerland 2016, New York, USA, 2016: pp. 515–562. 10.1007/978-3-319-26082-2.

[37] J. Chmiola, G. Yushin, Y. Gogotsi, C. Portet, P. Simon, P.L. Taberna, Anomalous Increase in Carbon Capacitance at Pore Sizes Less Than 1 Nanometer, Science. 313 (2006) 1760–1763. doi:10.1126/science.1132195.

[38] J. Chmiola, G. Yushin, R. Dash, Y. Gogotsi, Effect of pore size and surface area of carbide derived carbons on specific capacitance, J. Power Sources. 158 (2006) 765–772. doi:10.1016/j.jpowsour.2005.09.008.

[39] J. Chmiola, C. Largeot, P.-L. Taberna, P. Simon, Y. Gogotsi, Desolvation of Ions in Subnanometer Pores and Its Effect on Capacitance and Double-Layer Theory, Angew. Chem. Int. Ed. 47 (2008) 3392–3395. doi:10.1002/anie.200704894.

[40] E. Frackowiak, F. Béguin, Carbon materials for the electrochemical storage of energy in capacitors, Carbon. 39 (2001) 937–950. doi:10.1016/S0008-6223(00)00183-4.

[41] G. Gryglewicz, J. Machnikowski, E. Lorenc-Grabowska, G. Lota, E. Frackowiak, Effect of pore size distribution of coal-based activated carbons on double layer capacitance, Electrochimica Acta. 50 (2005) 1197–1206. doi:10.1016/j.electacta.2004.07.045.

[42] C. Vix-Guterl, E. Frackowiak, K. Jurewicz, M. Friebe, J. Parmentier, F. Béguin, Electrochemical energy storage in ordered porous carbon materials, Carbon. 43 (2005) 1293–1302. doi:10.1016/j.carbon.2004.12.028.

[43] A.B. Fuertes, G. Lota, T.A. Centeno, E. Frackowiak, Templated mesoporous carbons for supercapacitor application, Electrochimica Acta. 50 (2005) 2799–2805. doi:10.1016/j.electacta.2004.11.027.

[44] L. Pilon, H. Wang, A. d'Entremont, Recent Advances in Continuum Modeling of Interfacial and Transport Phenomena in Electric Double Layer Capacitors, J. Electrochem. Soc. 162 (2015) A5158–A5178. doi:10.1149/2.0211505jes.

[45] V. Augustyn, P. Simon, B. Dunn, Pseudocapacitive oxide materials for high-rate electrochemical energy storage, Energy Environ. Sci. 7 (2014) 1597–1614. doi:10.1039/C3EE44164D.

[46] K. Chen, Y.D. Noh, S. Lin, S. Komarneni, D. Xue, Crystallization of MnO2 by Microwave-Hydrothermal Synthesis and Its Applications for Supercapacitors and Lithium-Ion Batteries, Mater. Focus. 2 (2013) 86–91. doi:10.1166/mat.2013.1056.

[47] Y. Zhang, C. Sun, D. Xue, Manganese Oxides Prepared with Various Alcohols and Their Application in Supercapacitors, Energy Environ. Focus. 1 (2012) 131–136. doi:10.1166/eef.2012.1018.

[48] K. Chen, Y.D. Noh, S. Lin, S. Komarneni, D. Xue, Crystallization of MnO2 for Lithium-Ion Battery and Supercapacitor, Mater. Focus. 2 (2013) 195–200. doi:10.1166/mat.2013.1074.

[49] X. Chen, K. Chen, H. Wang, D. Xue, Functionality of Fe(NO3)3 salts as both positive and negative pseudocapacitor electrodes in alkaline aqueous electrolyte, Electrochimica Acta. 147 (2014) 216–224. doi:10.1016/j.electacta.2014.08.132.

[50] X. Chen, K. Chen, H. Wang, S. Song, D. Xue, Crystallization of Fe3+ in an alkaline aqueous pseudocapacitor system, CrystEngComm. 16 (2014) 6707–6715. doi:10.1039/C4CE00660G.

[51] K. Chen, Y. Dong Noh, W. Huang, J. Ma, S. Komarneni, D. Xue, Microwave-hydrothermal synthesis of Fe-based materials for lithium-ion batteries and supercapacitors, Ceram. Int. 40 (2014) 2877–2884. doi:10.1016/j.ceramint.2013.10.024.

[52] K. Chen, Y.D. Noh, R.R. Patel, W. Huang, J. Ma, K. Li, S. Komarneni, D. Xue, Microwave- or conventional–hydrothermal synthesis of Co-based materials for electrochemical energy storage, Ceram. Int. 40 (2014) 8183–8188. doi:10.1016/j.ceramint.2014.01.014.

[53] K. Chen, S. Song, D. Xue, An ionic aqueous pseudocapacitor system: electroactive ions in both a salt electrode and redox electrolyte, RSC Adv. 4 (2014) 23338–23343. doi:10.1039/C4RA03037K.

[54] S. Lin, K. Li, K. Chen, D. Xue, MnO2 as a Supercapacitor Electrode via Grinding Redox Reactions, Mater. Focus. 2 (2013) 53–57. doi:10.1166/mat.2013.1050.

[55] Y. Zhang, C. Sun, D. Xue, A Simple Self-Template Strategy to Synthesize ε-MnO2 and Its Application in Supercapacitors, Mater. Focus. 1 (2012) 245–251. doi:10.1166/mat.2012.1038.

[56] F. Wang, S. Xiao, Y. Hou, C. Hu, L. Liu, Y. Wu, Electrode materials for aqueous asymmetric supercapacitors, RSC Adv. 3 (2013) 13059–13084. doi:10.1039/C3RA23466E.

[57] L.-J. Xie, J.-F. Wu, C.-M. Chen, C.-M. Zhang, L. Wan, J.-L. Wang, Q.-Q. Kong, C.-X. Lv, K.-X. Li, G.-H. Sun, A novel asymmetric supercapacitor with an activated carbon cathode and a reduced graphene oxide–cobalt oxide nanocomposite anode, J. Power Sources. 242 (2013) 148–156. doi:10.1016/j.jpowsour.2013.05.081.

[58] K. Naoi, W. Naoi, S. Aoyagi, J. Miyamoto, T. Kamino, New Generation "Nanohybrid Supercapacitor," Acc. Chem. Res. 46 (2013) 1075–1083. doi:10.1021/ar200308h.

[59] M.C. Kisacikoglu, M. Uzunoglu, M.S. Alam, Load sharing using fuzzy logic control in a fuel cell/ultracapacitor hybrid vehicle, Int. J. Hydrog. Energy. 34 (2009) 1497–1507. doi:10.1016/j.ijhydene.2008.11.035.

[60] S.-B. Ma, K.-W. Nam, W.-S. Yoon, X.-Q. Yang, K.-Y. Ahn, K.-H. Oh, K.-B. Kim, A novel concept of hybrid capacitor based on manganese oxide materials, Electrochem. Commun. 9 (2007) 2807–2811. doi:10.1016/j.elecom.2007.09.015.

[61] A. Fedorková, A. Nacher-Alejos, P. Gómez-Romero, R. Oriňáková, D. Kaniansky, Structural and electrochemical studies of PPy/PEG-LiFePO4 cathode material for Li-ion batteries, Electrochimica Acta. 55 (2010) 943–947. doi:10.1016/j.electacta.2009.09.060.

[62] D.P. Dubal, G.S. Gund, C.D. Lokhande, R. Holze, Controlled Growth of CoSx Nanostrip Arrays (CoSx-NSA) on Nickel Foam for Asymmetric Supercapacitors, Energy Technol. 2 (2014) 401–408. doi:10.1002/ente.201300193.

[63] I. Plitz, A. DuPasquier, F. Badway, J. Gural, N. Pereira, A. Gmitter, G.G. Amatucci, The design of alternative nonaqueous high power chemistries, Appl. Phys. A. 82 (2005) 615–626. doi:10.1007/s00339-005-3420-0.

[64] Richner, R.P., Entwicklung neuartig gebundener Kohlenstoff- materiaien fur electrische Dop-pelschichtkondensatorelektronden, Swiss Federal Institute of Technology Zurich, 2001.

[65] Yaya, A, AgyeiI-Tuffour, b, Dodoo-Arhin, D, Nyankson, E, Annan, E, Konadu, D. S, Sinayobye, E, Baryeh, E . A, Ewels, C. P, Layered Nanomaterials-A Review, GJDT Vol 1 2 201232 -41 Glob. J. Eng. Des. Technol. 1 (2012) 32–41.

[66] J.N. Coleman, M. Lotya, A. O'Neill, S.D. Bergin, P.J. King, U. Khan, K. Young, A. Gaucher, S. De, R.J. Smith, I.V. Shvets, S.K. Arora, G. Stanton, H.-Y. Kim, K. Lee, G.T. Kim, G.S. Duesberg, T. Hallam, J.J. Boland, J.J. Wang, J.F. Donegan, J.C. Grunlan, G. Moriarty, A. Shmeliov, R.J. Nicholls, J.M. Perkins, E.M. Grieveson, K. Theuwissen, D.W. McComb, P.D. Nellist, V. Nicolosi, Two-Dimensional Nanosheets Produced by Liquid Exfoliation of Layered Materials, Science. 331 (2011) 568–571. doi:10.1126/science.1194975.

[67] M.W. Barsoum, The MN+1AXN phases: A new class of solids, Prog. Solid State Chem. 28 (2000) 201–281. doi:10.1016/S0079-6786(00)00006-6.

[68] M. Naguib, M. Kurtoglu, V. Presser, J. Lu, J. Niu, M. Heon, L. Hultman, Y. Gogotsi, M.W. Barsoum, Two-Dimensional Nanocrystals Produced by Exfoliation of Ti3AlC2, Adv. Mater. 23 (2011) 4248–4253. doi:10.1002/adma.201102306.

[69] M. Naguib, O. Mashtalir, J. Carle, V. Presser, J. Lu, L. Hultman, Y. Gogotsi, M.W. Barsoum, Two-dimensional transition metal carbides, ACS Nano. 6 (2012) 1322–1331. doi:10.1021/nn204153h.

[70] L.M. Viculis, J.J. Mack, R.B. Kaner, A chemical route to carbon nanoscrolls, Science. 299 (2003) 1361. doi:10.1126/science.1078842.

[71] M.V. Savoskin, V.N. Mochalin, A.P. Yaroshenko, N.I. Lazareva, T.E. Konstantinova, I.V. Barsukov, I.G. Prokofiev, Carbon nanoscrolls produced from acceptor-type graphite intercalation compounds, Carbon. 45 (2007) 2797–2800. doi:10.1016/j.carbon.2007.09.031.

[72] A.N. Enyashin, A.L. Ivanovskii, Atomic structure, comparative stability and electronic properties of hydroxylated Ti2C and Ti3C2 nanotubes, Comput. Theor. Chem. 989 (2012) 27–32. doi:10.1016/j.comptc.2012.02.034.

[73] M. Kurtoglu, M. Naguib, Y. Gogotsi, M.W. Barsoum, First principles study of two-dimensional early transition metal carbides, MRS Commun. 2 (n.d.) 133–137. doi:10.1557/mrc.2012.25.

[74] Tang Qing, Zhen Zhou,, Panwen Shen, Are MXenes Promising Anode Materials for Li Ion Batteries? Computational Studies on Electronic Properties and Li Storage Capability of Ti3C2 and Ti3C2X2 (X = F, OH) Monolayer, J Am Chem Soc 2012 134 40 Pp 16909–16916. 134 (2012) 16909–16916. doi:10.1021/ja308463r.

[75] M. Naguib, J. Come, B. Dyatkin, V. Presser, P.-L. Taberna, P. Simon, M.W. Barsoum, Y. Gogotsi, MXene: a promising transition metal carbide anode for lithium-ion batteries, Electrochem. Commun. 16 (2012) 61–64. doi:10.1016/j.elecom.2012.01.002.

[76] J. Come, M. Naguib, P. Rozier, M.W. Barsoum, Y. Gogotsi, P.-L. Taberna, M. Morcrette, P. Simon, A Non-Aqueous Asymmetric Cell with a Ti2C-Based Two-Dimensional Negative Electrode, J. Electrochem. Soc. 159 (2012) A1368–A1373. doi:10.1149/2.003208jes.

[77] J. Huang, B.G. Sumpter, V. Meunier, Theoretical Model for Nanoporous Carbon Supercapacitors, Angew. Chem. Int. Ed. 47 (2008) 520–524. doi:10.1002/anie.200703864.

[78] C. Largeot, C. Portet, J. Chmiola, P.-L. Taberna, Y. Gogotsi, P. Simon, Relation between the Ion Size and Pore Size for an Electric Double-Layer Capacitor, J. Am. Chem. Soc. 130 (2008) 2730–2731. doi:10.1021/ja7106178.

[79] W.G. Pell, B.E. Conway, Voltammetry at a de Levie brush electrode as a model for electrochemical supercapacitor behaviour, J. Electroanal. Chem. 500 (2001) 121–133. doi:10.1016/S0022-0728(00)00423-X.

[80] J.P. Zheng, The Limitations of Energy Density of Battery/Double-Layer Capacitor Asymmetric Cells, J. Electrochem. Soc. 150 (2003) A484–A492. doi:10.1149/1.1559067.

[81] J.P. Zheng, Theoretical Energy Density for Electrochemical Capacitors with Intercalation Electrodes, J. Electrochem. Soc. 152 (2005) A1864–A1869. doi:10.1149/1.1997152.

[82] J.P. Zheng, J. Huang, T.R. Jow, The Limitations of Energy Density for Electrochemical Capacitors, J. Electrochem. Soc. 144 (1997) 2026–2031. doi:10.1149/1.1837738.

[83] W.G. Pell, B.E. Conway, Analysis of power limitations at porous supercapacitor electrodes under cyclic voltammetry modulation and dc charge, J. Power Sources. 96 (2001) 57–67. doi:10.1016/S0378-7753(00)00682-0.

[84] B.E. Conway, W.G. Pell, Double-layer and pseudocapacitance types of electrochemical capacitors and their applications to the development of hybrid devices, J. Solid State Electrochem. 7 (2003) 637–644. doi:10.1007/s10008-003-0395-7.

[85] B.W. Ricketts, C. Ton-That, Self-discharge of carbon-based supercapacitors with organic electrolytes, J. Power Sources. 89 (2000) 64–69. doi:10.1016/S0378-7753(00)00387-6.

[86] C. Lin, J.A. Ritter, B.N. Popov, R.E. White, A Mathematical Model of an Electrochemical Capacitor with Double-Layer and Faradaic Processes, J. Electrochem. Soc. 146 (1999) 3168–3175. doi:10.1149/1.1392450.

[87] V. Srinivasan, J.W. Weidner, Mathematical Modeling of Electrochemical Capacitors, J. Electrochem. Soc. 146 (1999) 1650–1658. doi:10.1149/1.1391821.

[88] C. Lin, B.N. Popov, H.J. Ploehn, Modeling the Effects of Electrode Composition and Pore Structure on the Performance of Electrochemical Capacitors, J. Electrochem. Soc. 149 (2002) A167–A175. doi:10.1149/1.1431575.

[89] S.A. Kazaryan, S.N. Razumov, S.V. Litvinenko, G.G. Kharisov, V.I. Kogan, Mathematical Model of Heterogeneous Electrochemical Capacitors and Calculation of Their Parameters, J. Electrochem. Soc. 153 (2006) A1655–A1671. doi:10.1149/1.2212057.

[90] J.A. Staser, J.W. Weidner, Mathematical Modeling of Hybrid Asymmetric Electrochemical Capacitors, J. Electrochem. Soc. 161 (2014) E3267–E3275. doi:10.1149/2.031408jes.

[91] M.W. Verbrugge, P. Liu, Microstructural Analysis and Mathematical Modeling of Electric Double-Layer Supercapacitors, J. Electrochem. Soc. 152 (2005) D79–D87. doi:10.1149/1.1878052.

[92] V. Srinivasan, J.W. Weidner, R.E. White, Mathematical models of the nickel hydroxide active material, J. Solid State Electrochem. 4 (2000) 367–382. doi:10.1007/s100080000107.

[93] K. Somasundaram, E. Birgersson, A.S. Mujumdar, Analysis of a Model for an Electrochemical Capacitor, J. Electrochem. Soc. 158 (2011) A1220–A1230. doi:10.1149/2.062111jes.

[94] G. Sikha, R.E. White, B.N. Popov, A Mathematical Model for a Lithium-Ion Battery/Electrochemical Capacitor Hybrid System, J. Electrochem. Soc. 152 (2005) A1682–A1693. doi:10.1149/1.1940749.

[95] B. Pillay, J. Newman, The Influence of Side Reactions on the Performance of Electrochemical Double-Layer Capacitors, J. Electrochem. Soc. 143 (1996) 1806–1814. doi:10.1149/1.1836908.

[96] D. Fan, R.E. White, Mathematical Modeling of a Nickel-Cadmium Battery Effects of Intercalation and Oxygen Reactions, J. Electrochem. Soc. 138 (1991) 2952–2960. doi:10.1149/1.2085347.

[97] H. Kim, B.N. Popov, A Mathematical Model of Oxide/Carbon Composite Electrode for Supercapacitors, J. Electrochem. Soc. 150 (2003) A1153–A1160. doi:10.1149/1.1593039.

[98] M.D. Stoller, R.S. Ruoff, Best practice methods for determining an electrode material's performance for ultracapacitors, Energy Environ. Sci. 3 (2010) 1294–1301. doi:10.1039/C0EE00074D.

[99] M. Kaus, J. Kowal, D.U. Sauer, Modelling the effects of charge redistribution during self-discharge of supercapacitors, Electrochimica Acta. 55 (2010) 7516–7523. doi:10.1016/j.electacta.2010.01.002.

[100] S. Vazquez, S.M. Lukic, E. Galvan, L.G. Franquelo, J.M. Carrasco, Energy Storage Systems for Transport and Grid Applications, IEEE Trans. Ind. Electron. 57 (2010) 3881–3895. doi:10.1109/TIE.2010.2076414.

[101] S. Devan, V.R. Subramanian, R.E. White, Analytical Solution for the Impedance of a Porous Electrode, J. Electrochem. Soc. 151 (2004) A905–A913. doi:10.1149/1.1739218.

[102] L. Zubieta, R. Bonert, Characterization of double-layer capacitors for power electronics applications, IEEE Trans. Ind. Appl. 36 (2000) 199–205. doi:10.1109/28.821816.

[103] F. Rafik, H. Gualous, R. Gallay, A. Crausaz, A. Berthon, Frequency, thermal and voltage supercapacitor characterization and modeling, J. Power Sources. 165 (2007) 928–934. doi:10.1016/j.jpowsour.2006.12.021.

[104] Y. Diab, P. Venet, H. Gualous, G. Rojat, Self-Discharge Characterization and Modeling of Electrochemical Capacitor Used for Power Electronics Applications, IEEE Trans. Power Electron. 24 (2009) 510–517. doi:10.1109/TPEL.2008.2007116.

[105] R. de Levie, On porous electrodes in electrolyte solutions: I. Capacitance effects, Electrochimica Acta. 8 (1963) 751–780. doi:10.1016/0013-4686(63)80042-0.

[106] D.B. Robinson, C.-A.M. Wu, B.W. Jacobs, Effect of Salt Depletion on Charging Dynamics in Nanoporous Electrodes, J. Electrochem. Soc. 157 (2010) A912–A918. doi:10.1149/1.3416905.

[107] N. Bertrand, J. Sabatier, O. Briat, J.-M. Vinassa, Embedded fractional nonlinear supercapacitor model and its parametric estimation method, IEEE Trans. Ind. Electron. 57 (2010) 3991–4000. doi:10.1109/TIE.2010.2076307.

[108] R.A. Dougal, L. Gao, S. Liu, Ultracapacitor model with automatic order selection and capacity scaling for dynamic system simulation, J. Power Sources. 126 (2004) 250–257. doi:10.1016/j.jpowsour.2003.08.031.

[109] F. Belhachemi, S. Rael, B. Davat, A physical based model of power electric double-layer supercapacitors, in: Conf. Rec. 2000 IEEE Ind. Appl. Conf. 2000, 2000: pp. 3069–3076 vol.5. doi:10.1109/IAS.2000.882604.

[110] P. Kurzweil, H.-J. Fischle, A new monitoring method for electrochemical aggregates by impedance spectroscopy, J. Power Sources. 127 (2004) 331–340. doi:10.1016/j.jpowsour.2003.09.030.

[111] D.B. Robinson, Optimization of power and energy densities in supercapacitors, J. Power Sources. 195 (2010) 3748–3756. doi:10.1016/j.jpowsour.2009.12.004.

[112] J. Black, H.A. Andreas, Prediction of the self-discharge profile of an electrochemical capacitor electrode in the presence of both activation-controlled discharge and charge redistribution, J. Power Sources. 195 (2010) 929–935. doi:10.1016/j.jpowsour.2009.08.040.

[113] El Brouji, E. H., Briat,O., Vinassa, J. M., Bertrand, N., Woirgard, E., Impact of calendar life and cycling ageing on supercapacitor performance., IEEE Trans Veh Technol. 58 (2009) 3917–3929.

[114] Hunter, R. J, Foundations of Colloid Science, Clarendon, Oxford, Clarendon, Oxford, 1987.

[115] G. Gouy, Sur la constitution de la charge electrique a la surface d'un electrolyte, J Phys Fr. 9 (1910).

[116] Masliyah, J . H., Bhattacharjee, S., Electrokinetic and Colloid Transport Phenomena, John Wiley & Sons, Hoboken, NJ, 2006.

[117] H. Wang, L. Pilon, Accurate Simulations of Electric Double Layer Capacitance of Ultramicroelectrodes, J. Phys. Chem. C. 115 (2011) 16711–16719. doi:10.1021/jp204498e.

[118] D.C. Grahame, The Electrical Double Layer and the Theory of Electrocapillarity., Chem. Rev. 41 (1947) 441–501. doi:10.1021/cr60130a002.

[119] J. Varghese, H. Wang, L. Pilon, Simulating Electric Double Layer Capacitance of Mesoporous Electrodes with Cylindrical Pores, J. Electrochem. Soc. 158 (2011) A1106–A1114. doi:10.1149/1.3622342.

[120] S.-W. Woo, K. Dokko, H. Nakano, K. Kanamura, Preparation of three dimensionally ordered macroporous carbon with mesoporous walls for electric double-layer capacitors, J. Mater. Chem. 18 (2008) 1674–1680. doi:10.1039/B717996K.

[121] H. Wang, L. Pilon, Mesoscale modeling of electric double layer capacitors with three-dimensional ordered structures, J. Power Sources. 221 (2013) 252–260. doi:10.1016/j.jpowsour.2012.08.002.

[122] V.V. Chaban, O.N. Kalugin, Structure and dynamics in methanol and its lithium ion solution confined by carbon nanotubes, J. Mol. Liq. 145 (2009) 145–151. doi:10.1016/j.molliq.2008.06.003.

[123] J.B. Freund, Electro-osmosis in a nanometer-scale channel studied by atomistic simulation, J. Chem. Phys. 116 (2002) 2194–2200. doi:10.1063/1.1431543.

[124] R. Qiao, N.R. Aluru, Ion concentrations and velocity profiles in nanochannel electroosmotic flows, J. Chem. Phys. 118 (2003) 4692–4701.

[125] A.P. Thompson, Nonequilibrium molecular dynamics simulation of electro-osmotic flow in a charged nanopore, J. Chem. Phys. 119 (2003) 7503–7511. doi:10.1063/1.1609194.

[126] R. Qiao, N.R. Aluru, Charge Inversion and Flow Reversal in a Nanochannel Electro-osmotic Flow, Phys. Rev. Lett. 92 (2004) 198301. doi:10.1103/PhysRevLett.92.198301.

[127] A.M. Johnson, J. Newman, Desalting by Means of Porous Carbon Electrodes, J. Electrochem. Soc. 118 (1971) 510–517. doi:10.1149/1.2408094.

[128] J. Schiffer, D. Linzen, D.U. Sauer, Heat generation in double layer capacitors, J. Power Sources. 160 (2006) 765–772. doi:10.1016/j.jpowsour.2005.12.070.

[129] S.A. Kislenko, I.S. Samoylov, R.H. Amirov, Molecular dynamics simulation of the electrochemical interface between a graphite surface and the ionic liquid [BMIM][PF6], Phys. Chem. Chem. Phys. 11 (2009) 5584–5590. doi:10.1039/B823189C.

[130] D. Kim, E. Darve, Molecular dynamics simulation of electro-osmotic flows in rough wall nanochannels, Phys. Rev. E. 73 (2006) 051203. doi:10.1103/PhysRevE.73.051203.

[131] P. Wu, R. Qiao, Physical origins of apparently enhanced viscosity of interfacial fluids in electrokinetic transport, Phys. Fluids 1994-Present. 23 (2011) 072005. doi:10.1063/1.3614534.

[132] S.T. Cui, H.D. Cochran, Molecular dynamics simulation of interfacial electrolyte behaviors in nanoscale cylindrical pores, J. Chem. Phys. 117 (2002) 5850–5854. doi:10.1063/1.1501585.

[133] G. Feng, R. Qiao, J. Huang, B.G. Sumpter, V. Meunier, Ion Distribution in Electrified Micropores and Its Role in the Anomalous Enhancement of Capacitance, ACS Nano. 4 (2010) 2382–2390. doi:10.1021/nn100126w.

[134] M.C.F. Wander, K.L. Shuford, Molecular Dynamics Study of Interfacial Confinement Effects of Aqueous NaCl Brines in Nanoporous Carbon, J. Phys. Chem. C. 114 (2010) 20539–20546. doi:10.1021/jp104972e.

[135] A.V. Lankin, G.E. Norman, V.V. Stegailov, Atomistic simulation of the interaction of an electrolyte with graphite nanostructures in perspective supercapacitors, High Temp. 48 (2010) 837–845. doi:10.1134/S0018151X10060106.

[136] D. Jiang, J. Wu, Microscopic Insights into the Electrochemical Behavior of Nonaqueous Electrolytes in Electric Double-Layer Capacitors, J. Phys. Chem. Lett. 4 (2013) 1260–1267. doi:10.1021/jz4002967.

[137] F. Silva, C. Gomes, M. Figueiredo, R. Costa, A. Martins, C.M. Pereira, The electrical double layer at the [BMIM][PF6] ionic liquid/electrode interface – Effect of

temperature on the differential capacitance, J. Electroanal. Chem. 622 (2008) 153–160. doi:10.1016/j.jelechem.2008.05.014.

[138] A.A. Kornyshev, Double-Layer in Ionic Liquids: Paradigm Change?, J. Phys. Chem. B. 111 (2007) 5545–5557. doi:10.1021/jp067857o.

[139] V. Lockett, M. Horne, R. Sedev, T. Rodopoulos, J. Ralston, Differential capacitance of the double layer at the electrode/ionic liquids interface, Phys. Chem. Chem. Phys. 12 (2010) 12499–12512. doi:10.1039/C0CP00170H.

[140] S. Baldelli, Surface Structure at the Ionic Liquid−Electrified Metal Interface, Acc. Chem. Res. 41 (2008) 421–431. doi:10.1021/ar700185h.

[141] M. Trulsson, J. Algotsson, J. Forsman, C.E. Woodward, Differential Capacitance of Room Temperature Ionic Liquids: The Role of Dispersion Forces, J. Phys. Chem. Lett. 1 (2010) 1191–1195. doi:10.1021/jz900412t.

[142] G. Feng, J.S. Zhang, R. Qiao, Microstructure and Capacitance of the Electrical Double Layers at the Interface of Ionic Liquids and Planar Electrodes, J. Phys. Chem. C. 113 (2009) 4549–4559. doi:10.1021/jp809900w.

[143] M. Holovko, V. Kapko, D. Henderson, D. Boda, On the influence of ionic association on the capacitance of an electrical double layer, Chem. Phys. Lett. 341 (2001) 363–368. doi:10.1016/S0009-2614(01)00505-X.

[144] V. Lockett, R. Sedev, J. Ralston, M. Horne, T. Rodopoulos, Differential Capacitance of the Electrical Double Layer in Imidazolium-Based Ionic Liquids: Influence of Potential, Cation Size, and Temperature, J. Phys. Chem. C. 112 (2008) 7486–7495. doi:10.1021/jp7100732.

[145] M.T. Alam, M.M. Islam, T. Okajima, T. Ohsaka, Measurements of Differential Capacitance at Mercury/Room-Temperature Ionic Liquids Interfaces, J. Phys. Chem. C. 111 (2007) 18326–18333. doi:10.1021/jp075808l.

[146] J. Vatamanu, O. Borodin, G.D. Smith, Molecular Insights into the Potential and Temperature Dependences of the Differential Capacitance of a Room-Temperature Ionic Liquid at Graphite Electrodes, J. Am. Chem. Soc. 132 (2010) 14825–14833. doi:10.1021/ja104273r.

[147] R. Lin, P.-L. Taberna, S. Fantini, V. Presser, C.R. Pérez, F. Malbosc, N.L. Rupesinghe, K.B.K. Teo, Y. Gogotsi, P. Simon, Capacitive Energy Storage from −50 to 100 °C Using an Ionic Liquid Electrolyte, J. Phys. Chem. Lett. 2 (2011) 2396–2401. doi:10.1021/jz201065t.

[148] G. Feng, S. Li, J.S. Atchison, V. Presser, P.T. Cummings, Molecular Insights into Carbon Nanotube Supercapacitors: Capacitance Independent of Voltage and Temperature, J. Phys. Chem. C. 117 (2013) 9178–9186. doi:10.1021/jp403547k.

[149] S. Li, G. Feng, P.F. Fulvio, P. Hillesheim C., C. Liao, S. Dai, P.T. Cummings, Molecular Dynamics Simulation Study of the Capacitive Performance of a Binary Mixture of Ionic Liquids near an Onion-like Carbon Electrode, J. Phys. Chem. Lett. 3 (2012) 2465–2469. doi:10.1021/jz3009387.

[150] D. Boda, D. Henderson, K.-Y. Chan, Monte Carlo study of the capacitance of the double layer in a model molten salt, J. Chem. Phys. 110 (1999) 5346–5350. doi:10.1063/1.478429.

[151] D. Boda, D. Henderson, The capacitance of the solvent primitive model double layer at low effective temperatures, J. Chem. Phys. 112 (2000) 8934–8938. doi:10.1063/1.481507.

[152] C. Merlet, B. Rotenberg, P.A. Madden, P.-L. Taberna, P. Simon, Y. Gogotsi, M. Salanne, On the molecular origin of supercapacitance in nanoporous carbon electrodes, Nat. Mater. 11 (2012) 306–310. doi:10.1038/nmat3260.

[153] S. Kondrat, C.R. Pérez, V. Presser, Y. Gogotsi, A.A. Kornyshev, Effect of pore size and its dispersity on the energy storage in nanoporous supercapacitors, Energy Environ. Sci. 5 (2012) 6474. doi:10.1039/c2ee03092f.

[154] G. Feng, J. Huang, B.G. Sumpter, V. Meunier, R. Qiao, A “counter-charge layer in generalized solvents” framework for electrical double layers in neat and hybrid ionic liquid electrolytes, Phys. Chem. Chem. Phys. 13 (2011) 14723. doi:10.1039/c1cp21428d.

[155] E. Frackowiak, G. Lota, J. Pernak, Room-temperature phosphonium ionic liquids for supercapacitor application, Appl. Phys. Lett. 86 (2005) 164104. doi:10.1063/1.1906320.

[156] L. Xing, J. Vatamanu, O. Borodin, G.D. Smith, D. Bedrov, Electrode/Electrolyte Interface in Sulfolane-Based Electrolytes for Li Ion Batteries: A Molecular Dynamics Simulation Study, J. Phys. Chem. C. 116 (2012) 23871–23881. doi:10.1021/jp3054179.

[157] J. Vatamanu, O. Borodin, G.D. Smith, Molecular Dynamics Simulation Studies of the Structure of a Mixed Carbonate/LiPF6 Electrolyte near Graphite Surface as a Function of Electrode Potential, J. Phys. Chem. C. 116 (2012) 1114–1121. doi:10.1021/jp2101539.

[158] V. Ozoliņš, F. Zhou, M. Asta, Ruthenia-Based Electrochemical Supercapacitors: Insights from First-Principles Calculations, Acc. Chem. Res. 46 (2013) 1084–1093. doi:10.1021/ar3002987.

[159] S. Kondrat, A. Kornyshev, Superionic state in double-layer capacitors with nanoporous electrodes, J. Phys. Condens. Matter. 23 (2011) 022201. doi:10.1088/0953-8984/23/2/022201.

[160] J. Wu, Density functional theory for chemical engineering: From capillarity to soft materials, AIChE J. 52 (2006) 1169–1193. doi:10.1002/aic.10713.

[161] J. Wu, Z. Li, Density-Functional Theory for Complex Fluids, Annu. Rev. Phys. Chem. 58 (2007) 85–112. doi:10.1146/annurev.physchem.58.032806.104650.

[162] P. Hohenberg, W. Kohn, Inhomogeneous Electron Gas, Phys. Rev. 136 (1964) B864–B871. doi:10.1103/PhysRev.136.B864.

[163] D. Jiang, D. Meng, J. Wu, Density functional theory for differential capacitance of planar electric double layers in ionic liquids, Chem. Phys. Lett. 504 (2011) 153–158. doi:10.1016/j.cplett.2011.01.072.

[164] J. Wu, T. Jiang, D. Jiang, Z. Jin, D. Henderson, A classical density functional theory for interfacial layering of ionic liquids, Soft Matter. 7 (2011) 11222–11231. doi:10.1039/C1SM06089A.

[165] L. Xing, J. Vatamanu, O. Borodin, D. Bedrov, On the atomistic nature of capacitance enhancement generated by ionic liquid electrolyte confined in subnanometer pores, J. Phys. Chem. Lett. 4 (2013) 132–140. doi:10.1021/jz301782f.

[166] J. Huang, B.G. Sumpter, V. Meunier, A Universal Model for Nanoporous Carbon Supercapacitors Applicable to Diverse Pore Regimes, Carbon Materials, and Electrolytes, Chem. – Eur. J. 14 (2008) 6614–6626. doi:10.1002/chem.200800639.

[167] G. Feng, D. Jiang, P.T. Cummings, Curvature Effect on the Capacitance of Electric Double Layers at Ionic Liquid/Onion-Like Carbon Interfaces, J. Chem. Theory Comput. 8 (2012) 1058–1063. doi:10.1021/ct200914j.

[168] P.T.M. Nguyen, C. Fan, D.D. Do, D. Nicholson, On the Cavitation-Like Pore Blocking in Ink-Bottle Pore: Evolution of Hysteresis Loop with Neck Size, J. Phys. Chem. C. 117 (2013) 5475–5484. doi:10.1021/jp4002912.

[169] O. Pizio, S. Sokołowski, Z. Sokołowska, Electric double layer capacitance of restricted primitive model for an ionic fluid in slit-like nanopores: A density functional approach, J. Chem. Phys. 137 (2012) 234705. doi:10.1063/1.4771919.

[170] P.I. Ravikovitch, A.V. Neimark, Density Functional Theory Model of Adsorption on Amorphous and Microporous Silica Materials, Langmuir. 22 (2006) 11171–11179. doi:10.1021/la0616146.

[171] G.Y. Gor, M. Thommes, K.A. Cychosz, A.V. Neimark, Quenched solid density functional theory method for characterization of mesoporous carbons by nitrogen adsorption, Carbon. 50 (2012) 1583–1590. doi:10.1016/j.carbon.2011.11.037.

[172] D. Dunn, J. Newman, Predictions of Specific Energies and Specific Powers of Double-Layer Capacitors Using a Simplified Model, J. Electrochem. Soc. 147 (2000) 820–830. doi:10.1149/1.1393278.

[173] M. Doyle, T.F. Fuller, J. Newman, Modeling of Galvanostatic Charge and Discharge of the Lithium/Polymer/Insertion Cell, J. Electrochem. Soc. 140 (1993) 1526–1533. doi:10.1149/1.2221597.

[174] J.H. Chang, F.P. Dawson, K.K. Lian, A First Principles Approach to Develop a Dynamic Model of Electrochemical Capacitors, IEEE Trans. Power Electron. 26 (2011) 3472–3480. doi:10.1109/TPEL.2011.2161096.

[175] H. Gualous, D. Bouquain, A. Berthon, J.M. Kauffmann, Experimental study of supercapacitor serial resistance and capacitance variations with temperature, J. Power Sources. 123 (2003) 86–93. doi:10.1016/S0378-7753(03)00527-5.

[176] Conway, B. E, Niu , J, Pell, W.G, Seminar on Double Layer Capacitor and Hybrid Energy Storage Devices, in: Proc. 13th Int. Semin. Double Layer Capacit. Hybrid Energy Storage Devices, Florida, 2003.

[177] R. Kötz, M. Hahn, R. Gallay, Temperature behavior and impedance fundamentals of supercapacitors, J. Power Sources. 154 (2006) 550–555. doi:10.1016/j.jpowsour.2005.10.048.

[178] P. Guillemet, Y. Scudeller, T. Brousse, Multi-level reduced-order thermal modeling of electrochemical capacitors, J. Power Sources. 157 (2006) 630–640. doi:10.1016/j.jpowsour.2005.07.072.

[179] W. Henson, Optimal battery/ultracapacitor storage combination, J. Power Sources. 179 (2008) 417–423. doi:10.1016/j.jpowsour.2007.12.083.

[180] M.B. Camara, H. Gualous, F. Gustin, A. Berthon, B. Dakyo, DC/DC Converter Design for Supercapacitor and Battery Power Management in Hybrid Vehicle Applications #x2014;Polynomial Control Strategy, IEEE Trans. Ind. Electron. 57 (2010) 587–597. doi:10.1109/TIE.2009.2025283.

[181] W. Greenwell, A. Vahidi, Predictive Control of Voltage and Current in a Fuel Cell #x2013;Ultracapacitor Hybrid, IEEE Trans. Ind. Electron. 57 (2010) 1954–1963. doi:10.1109/TIE.2009.2031663.

[182] A. Payman, S. Pierfederici, F. Meibody-Tabar, Energy Management in a Fuel Cell/Supercapacitor Multisource/Multiload Electrical Hybrid System, IEEE Trans. Power Electron. 24 (2009) 2681–2691. doi:10.1109/TPEL.2009.2028426.

[183] S. Lemofouet, A. Rufer, A Hybrid Energy Storage System Based on Compressed Air and Supercapacitors With Maximum Efficiency Point Tracking (MEPT), IEEE Trans. Ind. Electron. 53 (2006) 1105–1115. doi:10.1109/TIE.2006.878323.

[184] P. Kurzweil, M. Chwistek, Electrochemical stability of organic electrolytes in supercapacitors: Spectroscopy and gas analysis of decomposition products, J. Power Sources. 176 (2008) 555–567. doi:10.1016/j.jpowsour.2007.08.070.

[185] A. d'Entremont, L. Pilon, First-principles thermal modeling of electric double layer capacitors under constant-current cycling, J. Power Sources. 246 (2014) 887–898. doi:10.1016/j.jpowsour.2013.08.024.

[186] H. Gualous, H. Louahlia, R. Gallay, Supercapacitor characterization and thermal modelling with reversible and irreversible heat effect, IEEE Trans. Power Electron. 26 (2011) 3402–3409. doi:10.1109/TPEL.2011.2145422.

[187] O.S. Burheim, M. Aslan, J.S. Atchison, V. Presser, Thermal conductivity and temperature profiles in carbon electrodes for supercapacitors, J. Power Sources. 246 (2014) 160–166. doi:10.1016/j.jpowsour.2013.06.164.

[188] S. Kondrat, N. Georgi, M.V. Fedorov, A.A. Kornyshev, A superionic state in nano-porous double-layer capacitors: insights from Monte Carlo simulations, Phys. Chem. Chem. Phys. 13 (2011) 11359–11366. doi:10.1039/C1CP20798A.

[189] H. Zhang, G. Cao, Y. Yang, Carbon nanotube arrays and their composites for electrochemical capacitors and lithium-ion batteries, Energy Environ. Sci. 2 (2009) 932–943. doi:10.1039/B906812K.

[190] A. Yoshida, I. Tanahashi, A. Nishino, Effect of concentration of surface acidic functional groups on electric double-layer properties of activated carbon fibers, Carbon. 28 (1990) 611–615. doi:10.1016/0008-6223(90)90062-4.

[191] T. Morimoto, K. Hiratsuka, Y. Sanada, K. Kurihara, Electric double-layer capacitor using organic electrolyte, J. Power Sources. 60 (1996) 239–247. doi:10.1016/S0378-7753(96)80017-6.

[192] N.S.A. Manaf, M.S.A. Bistamam, M.A. Azam, Development of High Performance Electrochemical Capacitor: A Systematic Review of Electrode Fabrication Technique Based on Different Carbon Materials, ECS J. Solid State Sci. Technol. 2 (2013) M3101–M3119. doi:10.1149/2.014310jss.

[193] B.E. Conway, W.G. Pell, T.-C. Liu, Diagnostic analyses for mechanisms of self-discharge of electrochemical capacitors and batteries, J. Power Sources. 65 (1997) 53–59. doi:10.1016/S0378-7753(97)02468-3.

[194] C.-T. Hsieh, H. Teng, Influence of oxygen treatment on electric double-layer capacitance of activated carbon fabrics, Carbon. 40 (2002) 667–674. doi:10.1016/S0008-6223(01)00182-8.

[195] E. Skipworth, S.W. Donne, Role of graphite in self-discharge of nickel(III) oxyhydroxide, J. Power Sources. 174 (2007) 186–190. doi:10.1016/j.jpowsour.2007.07.078.

[196] H.A. Andreas, K. Lussier, A.M. Oickle, Effect of Fe-contamination on rate of self-discharge in carbon-based aqueous electrochemical capacitors, J. Power Sources. 187 (2009) 275–283. doi:10.1016/j.jpowsour.2008.10.096.

[197] S.A. Kazaryan, S.V. Litvinenko, G.G. Kharisov, Self-Discharge of Heterogeneous Electrochemical Supercapacitor of PbO2 | H2SO4 | C Related to Manganese and Titanium Ions, J. Electrochem. Soc. 155 (2008) A464–A473. doi:10.1149/1.2904456.

[198] S.A. Kazaryan, G.G. Kharisov, S.V. Litvinenko, V.I. Kogan, Self-Discharge Related to Iron Ions and its Effect on the Parameters of HES PbO2 | H2SO4 | C Systems, J. Electrochem. Soc. 154 (2007) A751–A759. doi:10.1149/1.2742335.

[199] J. Black, H.A. Andreas, Effects of charge redistribution on self-discharge of electrochemical capacitors, Electrochimica Acta. 54 (2009) 3568–3574. doi:10.1016/j.electacta.2009.01.019.

[200] L. Demarconnay, E. Raymundo-Piñero, F. Béguin, A symmetric carbon/carbon supercapacitor operating at 1.6 V by using a neutral aqueous solution, Electrochem. Commun. 12 (2010) 1275–1278. doi:10.1016/j.elecom.2010.06.036.

[201] C. Zhang, D. Long, B. Xing, W. Qiao, R. Zhang, L. Zhan, X. Liang, L. Ling, The superior electrochemical performance of oxygen-rich activated carbons prepared from bituminous coal, Electrochem. Commun. 10 (2008) 1809–1811. doi:10.1016/j.elecom.2008.09.019.

[202] L. Diederich, E. Barborini, P. Piseri, A. Podesta, P. Milani, A. Schneuwly, R. Gallay, Supercapacitors based on nanostructured carbon electrodes grown by cluster-beam deposition, Appl. Phys. Lett. 75 (1999) 2662–2664. doi:10.1063/1.125111.

[203] J. Niu, W.G. Pell, B.E. Conway, Requirements for performance characterization of C double-layer supercapacitors: Applications to a high specific-area C-cloth material, J. Power Sources. 156 (2006) 725–740. doi:10.1016/j.jpowsour.2005.06.002.

[204] S. Roldán, C. Blanco, M. Granda, R. Menéndez, R. Santamaría, Towards a Further Generation of High-Energy Carbon-Based Capacitors by Using Redox-Active Electrolytes, Angew. Chem. Int. Ed. 50 (2011) 1699–1701. doi:10.1002/anie.201006811.

[205] S. Roldán, M. Granda, R. Menéndez, R. Santamaría, C. Blanco, Mechanisms of Energy Storage in Carbon-Based Supercapacitors Modified with a Quinoid Redox-Active Electrolyte, J. Phys. Chem. C. 115 (2011) 17606–17611. doi:10.1021/jp205100v.

[206] S. Roldán, M. Granda, R. Menéndez, R. Santamaría, C. Blanco, Supercapacitor modified with methylene blue as redox active electrolyte, Electrochimica Acta. 83 (2012) 241–246. doi:10.1016/j.electacta.2012.08.026.

[207] J. Cong, X. Yang, L. Kloo, L. Sun, Iodine/iodide-free redox shuttles for liquid electrolyte-based dye-sensitized solar cells, Energy Environ. Sci. 5 (2012) 9180–9194. doi:10.1039/C2EE22095D.

[208] W. Chen, R.B. Rakhi, H.N. Alshareef, Capacitance enhancement of polyaniline coated curved-graphene supercapacitors in a redox-active electrolyte, Nanoscale. 5 (2013) 4134–4138. doi:10.1039/C3NR00773A.

[209] H. Yu, L. Fan, J. Wu, Y. Lin, M. Huang, J. Lin, Z. Lan, Redox-active alkaline electrolyte for carbon-based supercapacitor with pseudocapacitive performance and excellent cyclability, RSC Adv. 2 (2012) 6736–6740. doi:10.1039/C2RA20503C.

[210] H. Yu, J. Wu, L. Fan, Y. Lin, S. Chen, Y. Chen, J. Wang, M. Huang, J. Lin, Z. Lan, Y. Huang, Application of a novel redox-active electrolyte in MnO2-based supercapacitors, Sci. China Chem. 55 (2012) 1319–1324. doi:10.1007/s11426-012-4673-z.

[211] M. Tachibana, T. Ohishi, Y. Tsukada, A. Kitajima, H. Yamagishi, M. Murakami, Supercapacitor Using an Electrolyte Charge Storage System, Electrochemistry. 79 (2011) 882–886. doi:10.5796/electrochemistry.79.882.

[212] H. Yang, Y. Zhang, Self-discharge analysis and characterization of supercapacitors for environmentally powered wireless sensor network applications, J. Power Sources. 196 (2011) 8866–8873. doi:10.1016/j.jpowsour.2011.06.042.

[213] K. Chiba, T. Ueda, Y. Yamaguchi, Y. Oki, F. Shimodate, K. Naoi, Electrolyte Systems for High Withstand Voltage and Durability I. Linear Sulfones for Electric Double-Layer Capacitors, J. Electrochem. Soc. 158 (2011) A872–A882. doi:10.1149/1.3593001.

[214] C. Peng, S. Zhang, X. Zhou, G.Z. Chen, Unequalisation of electrode capacitances for enhanced energy capacity in asymmetrical supercapacitors, Energy Environ. Sci. 3 (2010) 1499–1502. doi:10.1039/C0EE00228C.

[215] A.M. Bittner, M. Zhu, Y. Yang, H.F. Waibel, M. Konuma, U. Starke, C.J. Weber, Ageing of electrochemical double layer capacitors, J. Power Sources. 203 (2012) 262–273. doi:10.1016/j.jpowsour.2011.10.083.

[216] I. Nicotera, G.D. McLachlan, G.D. Bennett, I. Plitz, F. Badway, G.G. Amatucci, S.G. Greenbaum, Solid-State NMR Characterization of Electrolyte Breakdown Products in Nonaqueous Asymmetric Hybrid Supercapacitors, Electrochem. Solid-State Lett. 10 (2007) A5–A8. doi:10.1149/1.2372225.

[217] T. Abdallah, D. Lemordant, B. Claude-Montigny, Are room temperature ionic liquids able to improve the safety of supercapacitors organic electrolytes without degrading the performances?, J. Power Sources. 201 (2012) 353–359. doi:10.1016/j.jpowsour.2011.10.115.

[218] R. Kötz, M. Hahn, P. Ruch, R. Gallay, Comparison of pressure evolution in supercapacitor devices using different aprotic solvents, Electrochem. Commun. 10 (2008) 359–362. doi:10.1016/j.elecom.2007.12.016.

[219] S. Ishimoto, Y. Asakawa, M. Shinya, K. Naoi, Degradation Responses of Activated-Carbon-Based EDLCs for Higher Voltage Operation and Their Factors, J. Electrochem. Soc. 156 (2009) A563–A571. doi:10.1149/1.3126423.

[220] S.A. Kazaryan, G.G. Kharisov, S.V. Litvinenko, V.I. Kogan, Erratum: Self-Discharge Related to Iron Ions and Its Effect on the Parameters of HES PbO2 | H2SO4 | C Systems [J. Electrochem. Soc. , 154 , A751 (2007)], J. Electrochem. Soc. 154 (2007) S18–S18. doi:10.1149/1.2775570.

[221] T. Tevi, H. Yaghoubi, J. Wang, A. Takshi, Application of poly (p-phenylene oxide) as blocking layer to reduce self-discharge in supercapacitors, J. Power Sources. 241 (2013) 589–596. doi:10.1016/j.jpowsour.2013.04.150.

[222] A. J. Bard, L. R. Faulkner, Electrochemical methods. Fundamentals and applications, 2nd ed., John Wiley & Sons, INC, John Wiley, New York, 2001. https://www.academia.edu/7035501/Allen_J._Bard_-_Electrochemical_methods._Fundamentals_and_applications (accessed April 24, 2015).

[223] B.E. Conway, Transition from "Supercapacitor" to "Battery" Behavior in Electrochemical Energy Storage, J. Electrochem. Soc. 138 (1991) 1539–1548. doi:10.1149/1.2085829.

[224] S. Sarangapani, B.V. Tilak, C.-P. Chen, Materials for Electrochemical Capacitors Theoretical and Experimental Constraints, J. Electrochem. Soc. 143 (1996) 3791–3799. doi:10.1149/1.1837291.

[225] Q. Zhang, J. Rong, D. Ma, B. Wei, The governing self-discharge processes in activated carbon fabric-based supercapacitors with different organic electrolytes, Energy Environ. Sci. 4 (2011) 2152–2159. doi:10.1039/C0EE00773K.

[226] Q. Zhang, J. Rong, B. Wei, A divided potential driving self-discharge process for single-walled carbon nanotube based supercapacitors, RSC Adv. 1 (2011) 989–994. doi:10.1039/C1RA00318F.

[227] P.J. Hall, M. Mirzaeian, S.I. Fletcher, F.B. Sillars, A.J.R. Rennie, G.O. Shitta-Bey, G. Wilson, A. Cruden, R. Carter, Energy storage in electrochemical capacitors: designing functional materials to improve performance, Energy Environ. Sci. 3 (2010) 1238–1251. doi:10.1039/C0EE00004C.

[228] S. Kundu, Y. Wang, W. Xia, M. Muhler, Thermal Stability and Reducibility of Oxygen-Containing Functional Groups on Multiwalled Carbon Nanotube Surfaces: A Quantitative High-Resolution XPS and TPD/TPR Study, J. Phys. Chem. C. 112 (2008) 16869–16878. doi:10.1021/jp804413a.

[229] H. Zhu, B. Wei, Direct fabrication of single-walled carbon nanotube macro-films on flexible substrates, Chem. Commun. (2007) 3042–3044. doi:10.1039/B702523H.

[230] Y. Si, E.T. Samulski, Synthesis of Water Soluble Graphene, Nano Lett. 8 (2008) 1679–1682. doi:10.1021/nl080604h.

[231] K. Jiang, A. Eitan, L.S. Schadler, P.M. Ajayan, R.W. Siegel, N. Grobert, M. Mayne, M. Reyes-Reyes, H. Terrones, M. Terrones, Selective Attachment of Gold Nanoparticles to Nitrogen-Doped Carbon Nanotubes, Nano Lett. 3 (2003) 275–277. doi:10.1021/nl025914t.

[232] Y. Li, W. Zhou, H. Wang, L. Xie, Y. Liang, F. Wei, J.-C. Idrobo, S.J. Pennycook, H. Dai, An oxygen reduction electrocatalyst based on carbon nanotube-graphene complexes, Nat. Nanotechnol. 7 (2012) 394–400. doi:10.1038/nnano.2012.72.

[233] A. Cao, H. Zhu, X. Zhang, X. Li, D. Ruan, C. Xu, B. Wei, J. Liang, D. Wu, Hydrogen storage of dense-aligned carbon nanotubes, Chem. Phys. Lett. 342 (2001) 510–514. doi:10.1016/S0009-2614(01)00619-4.

[234] J.A. Robinson, E.S. Snow, Ş.C. Bădescu, T.L. Reinecke, F.K. Perkins, Role of Defects in Single-Walled Carbon Nanotube Chemical Sensors, Nano Lett. 6 (2006) 1747–1751. doi:10.1021/nl0612289.

[235] A. Modi, N. Koratkar, E. Lass, B. Wei, P.M. Ajayan, Miniaturized gas ionization sensors using carbon nanotubes, Nature. 424 (2003) 171–174. doi:10.1038/nature01777.

[236] S. Stankovich, D.A. Dikin, G.H.B. Dommett, K.M. Kohlhaas, E.J. Zimney, E.A. Stach, R.D. Piner, S.T. Nguyen, R.S. Ruoff, Graphene-based composite materials, Nature. 442 (2006) 282–286. doi:10.1038/nature04969.

[237] G. Viswanathan, N. Chakrapani, H. Yang, B. Wei, H. Chung, K. Cho, C.Y. Ryu, P.M. Ajayan, Single-Step in Situ Synthesis of Polymer-Grafted Single-Wall Nanotube Composites, J. Am. Chem. Soc. 125 (2003) 9258–9259. doi:10.1021/ja0354418.

[238] J. Zhu, J. Kim, H. Peng, J.L. Margrave, V.N. Khabashesku, E.V. Barrera, Improving the Dispersion and Integration of Single-Walled Carbon Nanotubes in Epoxy Composites through Functionalization, Nano Lett. 3 (2003) 1107–1113. doi:10.1021/nl0342489.

[239] H.R. Byon, B.M. Gallant, S.W. Lee, Y. Shao-Horn, Role of Oxygen Functional Groups in Carbon Nanotube/Graphene Freestanding Electrodes for High Performance Lithium Batteries, Adv. Funct. Mater. 23 (2013) 1037–1045. doi:10.1002/adfm.201200697.

[240] J.-S. Ye, X. Liu, H.F. Cui, W.-D. Zhang, F.-S. Sheu, T.M. Lim, Electrochemical oxidation of multi-walled carbon nanotubes and its application to electrochemical double layer capacitors, Electrochem. Commun. 7 (2005) 249–255. doi:10.1016/j.elecom.2005.01.008.

[241] Q. Zhang, C. Cai, J. Qin, B. Wei, Tunable self-discharge process of carbon nanotube based supercapacitors, Nano Energy. 4 (2014) 14–22. doi:10.1016/j.nanoen.2013.12.005.

[242] S. Nohara, H. Wada, N Furukawa, H. Inoue, C. Iwakura, Self-discharge characteristics of an electric double-layer capacitor with polymer hydrogel electrolyte, Res. Chem. Intermed. 32 (2006) 491–496.

[243] K. Shinyama, H. Nakamura, I. Yonezu, S. Matsuta, R. Maeda, Y. Harada, T. Nohma, Effect of separators on the self-discharge reaction in nickel–metal hydride batteries, Res Chem Intermed. 32 (2006) 447–452.

[244] M. Ishikawa, M. Morita, M. Ihara, Y. Matsuda, Electric Double-Layer Capacitor Composed of Activated Carbon Fiber Cloth Electrodes and Solid Polymer Electrolytes Containing Alkylammonium Salts, J. Electrochem. Soc. 141 (1994) 1730–1734. doi:10.1149/1.2054995.

[245] L. Chen, H. Bai, Z. Huang, L. Li, Mechanism investigation and suppression of self-discharge in active electrolyte enhanced supercapacitors, Energy Env. Sci. 7 (2014) 1750–1759. doi:10.1039/C4EE00002A.

[246] B. Wang, J.A. Maciá-Agulló, D.G. Prendiville, X. Zheng, D. Liu, Y. Zhang, S.W. Boettcher, X. Ji, G.D. Stucky, A Hybrid Redox-Supercapacitor System with Anionic Catholyte and Cationic Anolyte, J. Electrochem. Soc. 161 (2014) A1090–A1093. doi:10.1149/2.058406jes.

[247] S.-E. Chun, B. Evanko, X. Wang, D. Vonlanthen, X. Ji, G.D. Stucky, S.W. Boettcher, Design of aqueous redox-enhanced electrochemical capacitors with high specific energies and slow self-discharge, Nat. Commun. 6 (2015) 7818. doi:10.1038/ncomms8818.

[248] T. Tevi, A. Takshi, Modeling and simulation study of the self-discharge in supercapacitors in presence of a blocking layer, J. Power Sources. 273 (2015) 857–862. doi:10.1016/j.jpowsour.2014.09.133.

[249] J. Kowal, E. Avaroglu, F. Chamekh, A. Šenfelds, T. Thien, D. Wijaya, D.U. Sauer, Detailed analysis of the self-discharge of supercapacitors, J. Power Sources. 196 (2011) 573–579. doi:10.1016/j.jpowsour.2009.12.028.

[250] J.W. Graydon, M. Panjehshahi, D.W. Kirk, Charge redistribution and ionic mobility in the micropores of supercapacitors, J. Power Sources. 245 (2014) 822–829. doi:10.1016/j.jpowsour.2013.07.036.

[251] S. Yamazaki, A. Takegawa, Y. Kaneko, J. Kadokawa, M. Yamagata, M. Ishikawa, Performance of Electric Double-Layer Capacitor with Acidic Cellulose–Chitin Hybrid Gel Electrolyte, J. Electrochem. Soc. 157 (2010) A203–A208. doi:10.1149/1.3270498.

[252] W.G. Pell, B.E. Conway, W.A. Adams, J. de Oliveira, Electrochemical efficiency in multiple discharge/recharge cycling of supercapacitors in hybrid EV applications, J. Power Sources. 80 (1999) 134–141. doi:10.1016/S0378-7753(98)00257-2.

[253] H. Yang, Y. Zhang, A study of supercapacitor charge redistribution for applications in environmentally powered wireless sensor nodes, J. Power Sources. 273 (2015) 223–236. doi:10.1016/j.jpowsour.2014.09.061.

[254] J.-S. Lai, S. Levy, M.F. Rose, High energy density double-layer capacitors for energy storage applications, IEEE Aerosp. Electron. Syst. Mag. 7 (1992) 14–19. doi:10.1109/62.143193.

[255] M. Yaniv, A. Soffer, The Transient Behavior of an Ideally Polarized Porous Carbon Electrode at Constant Charging Current, J. Electrochem. Soc. 123 (1976) 506–511. doi:10.1149/1.2132864.

[256] H. Yang, Y. Zhang, Self-discharge analysis and characterization of supercapacitors for environmentally powered wireless sensor network applications, J. Power Sources. 196 (2011) 8866–8873. doi:10.1016/j.jpowsour.2011.06.042.

[257] N. Devillers, S. Jemei, M.-C. Péra, D. Bienaimé, F. Gustin, Review of characterization methods for supercapacitor modelling, J. Power Sources. 246 (2014) 596–608. doi:10.1016/j.jpowsour.2013.07.116.

[258] S. Buller, E. Karden, D. Kok, R.W. De Doncker, Modeling the dynamic behavior of supercapacitors using impedance spectroscopy, IEEE Trans. Ind. Appl. 38 (2002) 1622–1626. doi:10.1109/TIA.2002.804762.

[259] R. Faranda, A new parameters identification procedure for simplified double layer capacitor two-branch model, Electr. Power Syst. Res. 80 (2010) 363–371. doi:10.1016/j.epsr.2009.10.024.

[260] T. Liu, W.G. Pell, B.E. Conway, Self-discharge and potential recovery phenomena at thermally and electrochemically prepared RuO2 supercapacitor electrodes, Electrochimica Acta. 42 (1997) 3541–3552. doi:10.1016/S0013-4686(97)81190-5.

[261] S.A. Kazaryan, V.I. Kogan, S.V. Litvinenko, G.G. Kharisov, V.I. Shumovsky, Specific features and characteristics of PbO2|H2SO4|C electrochemical capacitors of Universal Supercapacitors LLC, in: 2007.

[262] K. Chiba, T. Ueda, Y. Yamaguchi, Y. Oki, F. Saiki, K. Naoi, Electrolyte Systems for High Withstand Voltage and Durability II. Alkylated Cyclic Carbonates for Electric Double-Layer Capacitors, J. Electrochem. Soc. 158 (2011) A1320–A1327. doi:10.1149/2.038112jes.

[263] F. Soavi, C. Arbizzani, M. Mastragostino, Leakage currents and self-discharge of ionic liquid-based supercapacitors, J. Appl. Electrochem. 44 (2013) 491–496. doi:10.1007/s10800-013-0647-x.

[264] Newman, J . S, Thomas-Alyea, K. E., Electrochemical Systems, 3rd Edition, 3 edition, Wiley-Interscience, Hoboken, N.J, 2004.

[265] A.T. Hubbard, D.G. Peters, Electrochemistry in Thin Layers of Solution, C R C Crit. Rev. Anal. Chem. 3 (1973) 201–242. doi:10.1080/10408347308542661.

[266] A.P. Fickett, Electrochemical systems, John S. Newman, Prentice-Hall, Inc., Englewood Cliffs, New Jersey (1973). 432 pages, AIChE J. 19 (1973) 879–879. doi:10.1002/aic.690190440.

[267] Newman, J.S., Electrochemical Systems by Newman, John S.: Prentice Hall 9780132487580 Hardcover, 2nd Edition - Floridia Libri, 2nd Edition, Prentice Hall, Englewood Cliffs, NJ, 1991. http://www.abebooks.com/Electrochemical-Systems-Newman-John-S-Prentice/12704196326/bd (accessed November 27, 2015).

[268] Z. Mao, R.E. White, The Self-Discharge of the NiOOH / Ni (OH) 2 Electrode Constant Potential Study, J. Electrochem. Soc. 139 (1992) 1282–1289. doi:10.1149/1.2069397.

[269] Z. Mao, P.D. Vidts, R.E. White, J. Newman, Theoretical Analysis of the Discharge Performance of a NiOOH / H 2 Cell, J. Electrochem. Soc. 141 (1994) 54–64. doi:10.1149/1.2054710.

[270] H.S. Choi, C.R. Park, Theoretical guidelines to designing high performance energy storage device based on hybridization of lithium-ion battery and supercapacitor, J. Power Sources. 259 (2014) 1–14. doi:10.1016/j.jpowsour.2014.02.001.

[271] D. Qu, H. Shi, Studies of activated carbons used in double-layer capacitors, J. Power Sources. 74 (1998) 99–107. doi:10.1016/S0378-7753(98)00038-X.

[272] W.G. Pell, B.E. Conway, Peculiarities and requirements of asymmetric capacitor devices based on combination of capacitor and battery-type electrodes, J. Power Sources. 136 (2004) 334–345. doi:10.1016/j.jpowsour.2004.03.021.

[273] C. Zhong, Y. Deng, W. Hu, J. Qiao, L. Zhang, J. Zhang, A review of electrolyte materials and compositions for electrochemical supercapacitors, Chem. Soc. Rev. 44 (2015) 7484–7539. doi:10.1039/C5CS00303B.

[274] H. Gao, K. Lian, Proton-conducting polymer electrolytes and their applications in solid supercapacitors: a review, RSC Adv. 4 (2014) 33091–33113. doi:10.1039/C4RA05151C.

[275] X.-J. Ma, W.-B. Zhang, L.-B. Kong, Y.-C. Luo, L. Kang, Electrochemical performance in alkaline and neutral electrolytes of a manganese phosphate material possessing a broad potential window, RSC Adv. 6 (2016) 40077–40085. doi:10.1039/C6RA02217K.

[276] K. Sun, Zheng Xiaoping, Zhu Yanrong, Zheng Yanping, Ma Mingguang, Zhao Guohu, Ma Guofu, Nitrogen-doped Porous Carbon Derived from Rapeseed residues for High-performance Supercapacitors, Int. J. Electrochem. Sci. (2016) 4743–4754. doi:10.20964/2016.06.22.

[277] L. Zhao, Y. Qiu, J. Yu, X. Deng, C. Dai, X. Bai, Carbon nanofibers with radially grown graphene sheets derived from electrospinning for aqueous supercapacitors with high working voltage and energy density, Nanoscale. 5 (2013) 4902. doi:10.1039/c3nr33927k.

[278] R. de Levie, On porous electrodes in electrolyte solutions, Electrochimica Acta. 8 (1963) 751–780. doi:10.1016/0013-4686(63)80042-0.

[279] R. de Levie, On porous electrodes in electrolyte solutions—IV, Electrochimica Acta. 9 (1964) 1231–1245. doi:10.1016/0013-4686(64)85015-5.

[280] I.S. Ike, S. Iyuke, I. Sigalas, Understanding Performance Limitation and Suppression of Leakage Current or Self-Discharge in Electrochemical Capacitors: A Review, Phys. Chem. Chem. Phys. (2015). doi:10.1039/C5CP05459A.

[281] M.-Q. Zhao, C.E. Ren, Z. Ling, M.R. Lukatskaya, C. Zhang, K.L. Van Aken, M.W. Barsoum, Y. Gogotsi, Flexible MXene/Carbon Nanotube Composite Paper with High Volumetric Capacitance, Adv. Mater. 27 (2015) 339–345. doi:10.1002/adma.201404140.

[282] Z. Ling, C.E. Ren, M.-Q. Zhao, J. Yang, J.M. Giammarco, J. Qiu, M.W. Barsoum, Y. Gogotsi, Flexible and conductive MXene films and nanocomposites with high capacitance, Proc. Natl. Acad. Sci. 111 (2014) 16676–16681. doi:10.1073/pnas.1414215111.

[283] E. Frackowiak, V. Khomenko, K. Jurewicz, K. Lota, F. Béguin, Supercapacitors based on conducting polymers/nanotubes composites, J. Power Sources. 153 (2006) 413–418. doi:10.1016/j.jpowsour.2005.05.030.

[284] V. Ruiz, C. Blanco, R. Santamaría, J.M. Juárez-Galán, A. Sepúlveda-Escribano, F. Rodríguez-Reinoso, Carbon molecular sieves as model active electrode materials in supercapacitors, Microporous Mesoporous Mater. 110 (2008) 431–435. doi:10.1016/j.micromeso.2007.06.027.

[285] V. Khomenko, E. Raymundo-Piñero, F. Béguin, High-energy density graphite/AC capacitor in organic electrolyte, J. Power Sources. 177 (2008) 643–651. doi:10.1016/j.jpowsour.2007.11.101.

[286] T. Brousse, R. Marchand, P.-L. Taberna, P. Simon, TiO2 (B)/activated carbon non-aqueous hybrid system for energy storage, J. Power Sources. 158 (2006) 571–577. doi:10.1016/j.jpowsour.2005.09.020.

[287] Z. Chen, V. Augustyn, J. Wen, Y. Zhang, M. Shen, B. Dunn, Y. Lu, High-Performance Supercapacitors Based on Intertwined CNT/V2O5 Nanowire Nanocomposites, Adv. Mater. 23 (2011) 791–795. doi:10.1002/adma.201003658.

[288] D. Cericola, R. Kötz, Hybridization of rechargeable batteries and electrochemical capacitors: Principles and limits, Electrochimica Acta. 72 (2012) 1–17. doi:10.1016/j.electacta.2012.03.151.

[289] M. S Gockenbach, Partial Differential Equations: Analytical and Numerical Methods, Siam Society for Industrial and Applied Mathematics, Philadelphia, Houghton,Philadelphia., 2002. https://www.scribd.com/doc/237723937/Mark-S-Gockenbach-Partial-Differential-Equation (accessed August 31, 2015).

[290] N.S. Koshlyakov, M.M. Smirnov, E.B. Gliner, Differential Equations of Mathematical Physics, First English Edition edition, North-Holland, 1964.

Appendices

Appendix A

Appendix A1: Permission to republish the book chapter titled " Mathematical Modeling and Simulation of Supercapacitors".

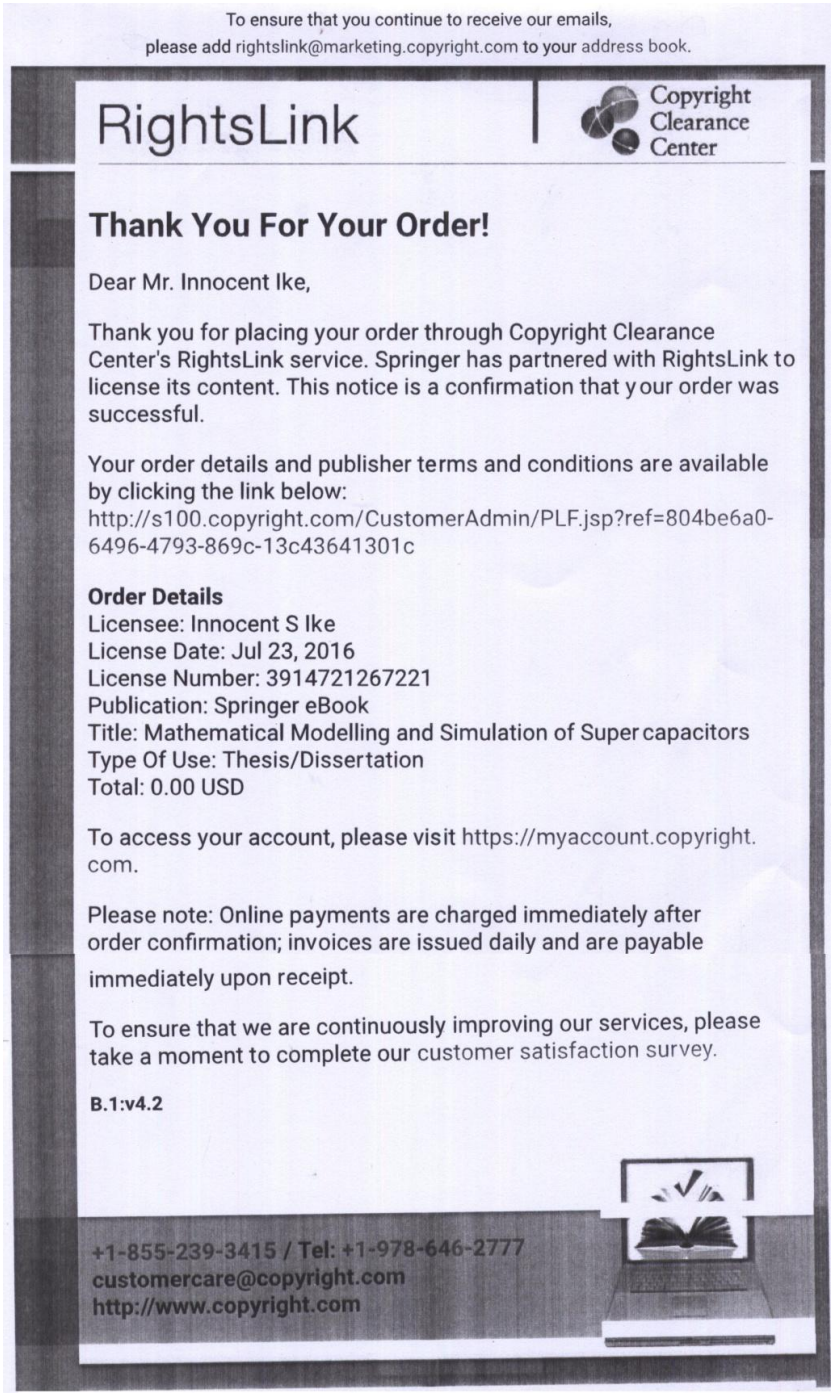

To ensure that you continue to receive our emails,
please add rightslink@marketing.copyright.com to your address book.

RightsLink | Copyright Clearance Center

Thank You For Your Order!

Dear Mr. Innocent Ike,

Thank you for placing your order through Copyright Clearance Center's RightsLink service. Springer has partnered with RightsLink to license its content. This notice is a confirmation that your order was successful.

Your order details and publisher terms and conditions are available by clicking the link below:
http://s100.copyright.com/CustomerAdmin/PLF.jsp?ref=804be6a0-6496-4793-869c-13c43641301c

Order Details
Licensee: Innocent S Ike
License Date: Jul 23, 2016
License Number: 3914721267221
Publication: Springer eBook
Title: Mathematical Modelling and Simulation of Supercapacitors
Type Of Use: Thesis/Dissertation
Total: 0.00 USD

To access your account, please visit https://myaccount.copyright.com.

Please note: Online payments are charged immediately after order confirmation; invoices are issued daily and are payable immediately upon receipt.

To ensure that we are continuously improving our services, please take a moment to complete our customer satisfaction survey.

B.1:v4.2

+1-855-239-3415 / Tel: +1-978-646-2777
customercare@copyright.com
http://www.copyright.com

Appendix A2: Permission to republish the "Understanding Performance Limitation and Suppression of Leakage Current or Self-Discharge in Electrochemical Capacitors: A Review".

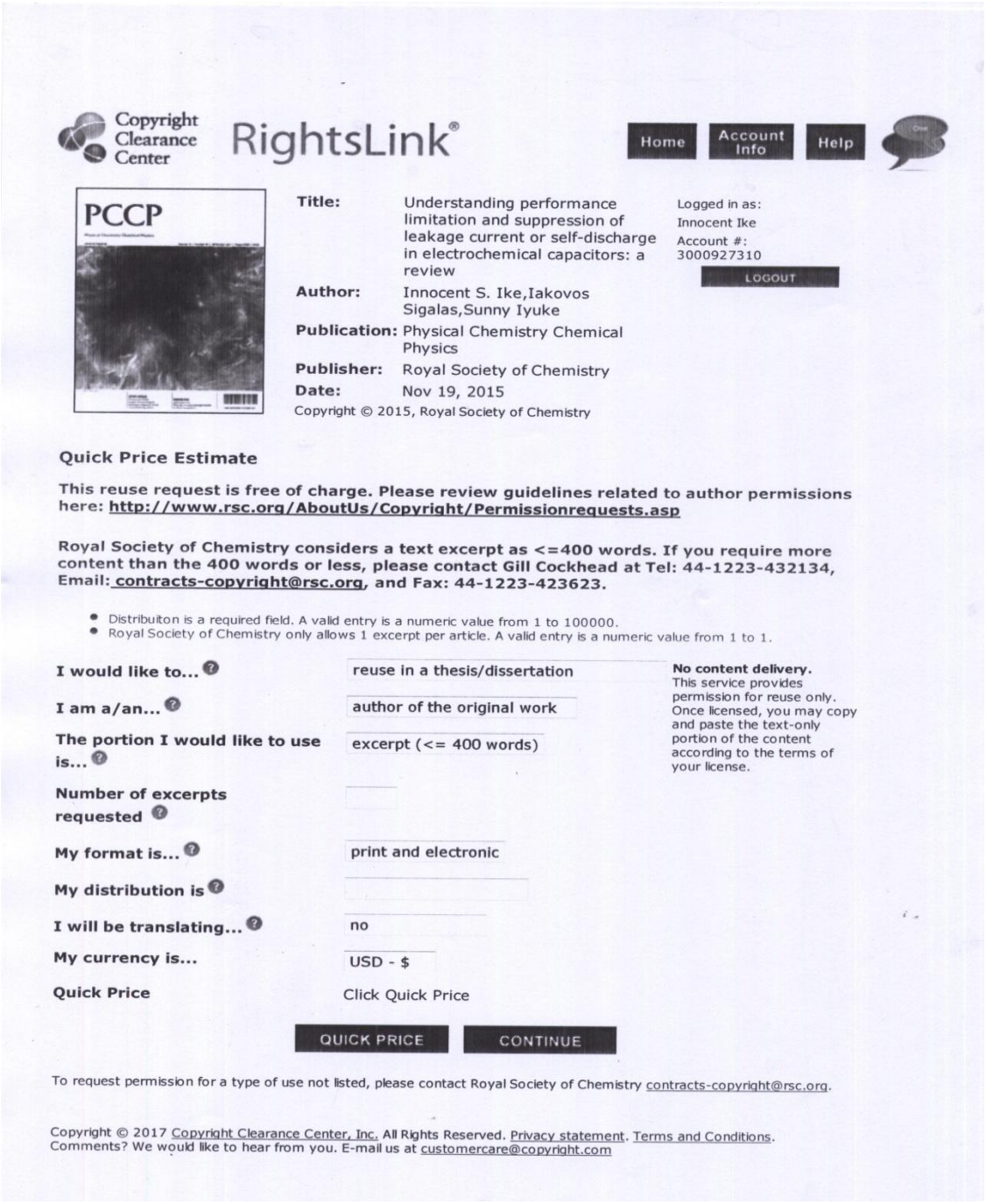

Copyright Clearance Center RightsLink®

Home | Account Info | Help

Title: Understanding performance limitation and suppression of leakage current or self-discharge in electrochemical capacitors: a review

Author: Innocent S. Ike,Iakovos Sigalas,Sunny Iyuke

Publication: Physical Chemistry Chemical Physics

Publisher: Royal Society of Chemistry

Date: Nov 19, 2015

Copyright © 2015, Royal Society of Chemistry

Logged in as:
Innocent Ike
Account #:
3000927310
LOGOUT

Quick Price Estimate

This reuse request is free of charge. Please review guidelines related to author permissions here: http://www.rsc.org/AboutUs/Copyright/Permissionrequests.asp

Royal Society of Chemistry considers a text excerpt as <=400 words. If you require more content than the 400 words or less, please contact Gill Cockhead at Tel: 44-1223-432134, Email: contracts-copyright@rsc.org, and Fax: 44-1223-423623.

- Distribuiton is a required field. A valid entry is a numeric value from 1 to 100000.
- Royal Society of Chemistry only allows 1 excerpt per article. A valid entry is a numeric value from 1 to 1.

I would like to...	reuse in a thesis/dissertation
I am a/an...	author of the original work
The portion I would like to use is...	excerpt (<= 400 words)
Number of excerpts requested	
My format is...	print and electronic
My distribution is	
I will be translating...	no
My currency is...	USD - $
Quick Price	Click Quick Price

No content delivery. This service provides permission for reuse only. Once licensed, you may copy and paste the text-only portion of the content according to the terms of your license.

QUICK PRICE CONTINUE

To request permission for a type of use not listed, please contact Royal Society of Chemistry contracts-copyright@rsc.org.

Copyright © 2017 Copyright Clearance Center, Inc. All Rights Reserved. Privacy statement. Terms and Conditions.
Comments? We would like to hear from you. E-mail us at customercare@copyright.com

Appendix A3: permission to republish Tables in the artcle titled " Electrochemical performance in alkaline and neutral electrolytes of a manganese phosphate material possessing a broad potential window".

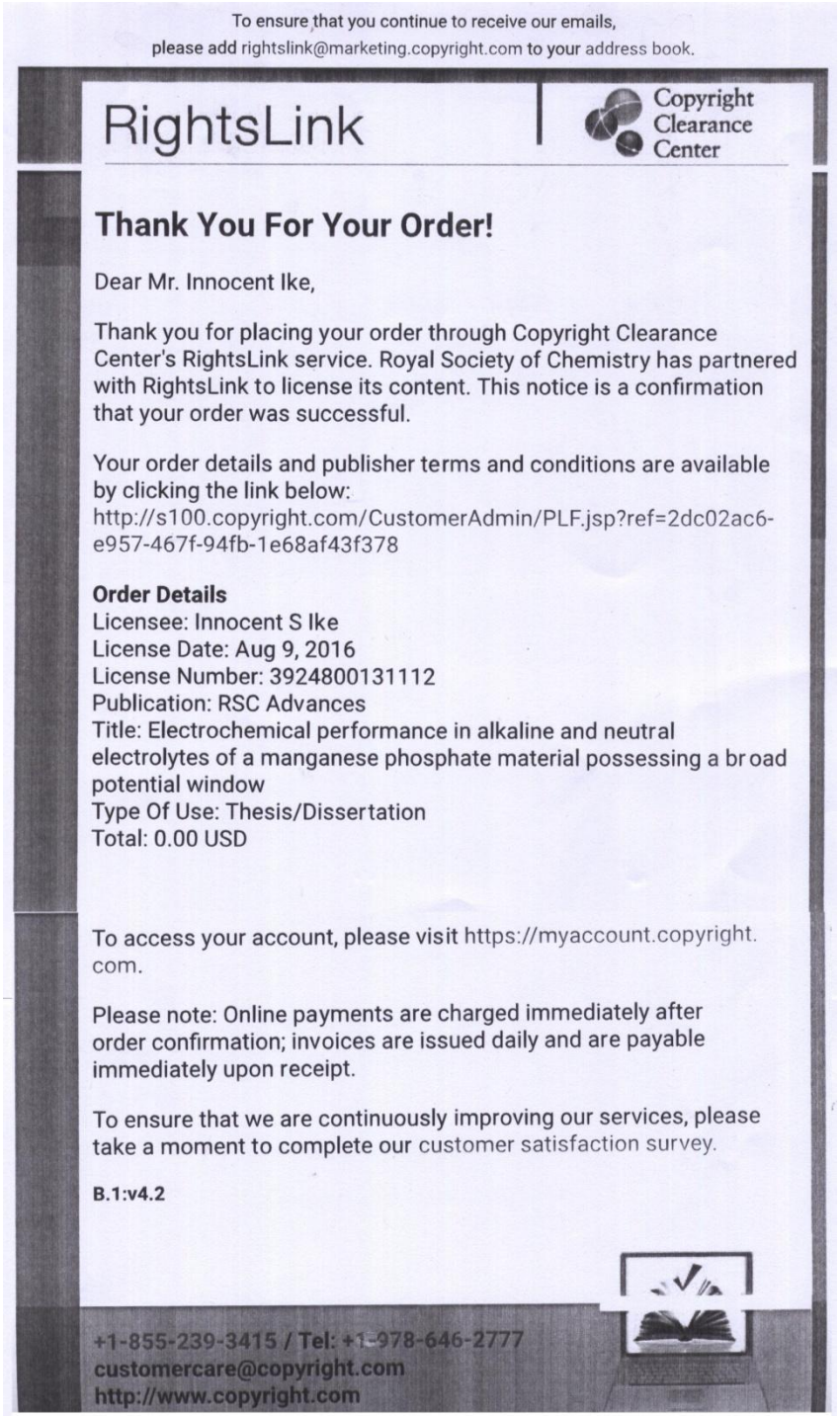

To ensure that you continue to receive our emails,
please add rightslink@marketing.copyright.com to your address book.

RightsLink | Copyright Clearance Center

Thank You For Your Order!

Dear Mr. Innocent Ike,

Thank you for placing your order through Copyright Clearance Center's RightsLink service. Royal Society of Chemistry has partnered with RightsLink to license its content. This notice is a confirmation that your order was successful.

Your order details and publisher terms and conditions are available by clicking the link below:
http://s100.copyright.com/CustomerAdmin/PLF.jsp?ref=2dc02ac6-e957-467f-94fb-1e68af43f378

Order Details
Licensee: Innocent S Ike
License Date: Aug 9, 2016
License Number: 3924800131112
Publication: RSC Advances
Title: Electrochemical performance in alkaline and neutral electrolytes of a manganese phosphate material possessing a br oad potential window
Type Of Use: Thesis/Dissertation
Total: 0.00 USD

To access your account, please visit https://myaccount.copyright.com.

Please note: Online payments are charged immediately after order confirmation; invoices are issued daily and are payable immediately upon receipt.

To ensure that we are continuously improving our services, please take a moment to complete our customer satisfaction survey.

B.1:v4.2

+1-855-239-3415 / Tel: +1-978-646-2777
customercare@copyright.com
http://www.copyright.com

Appendix A4: Permission to republish "The Effects of Self-Discharge on the Performance of Symmetric Electric Double Layer Capacitors and Active Electrolyte Enhanced Supercapacitors".

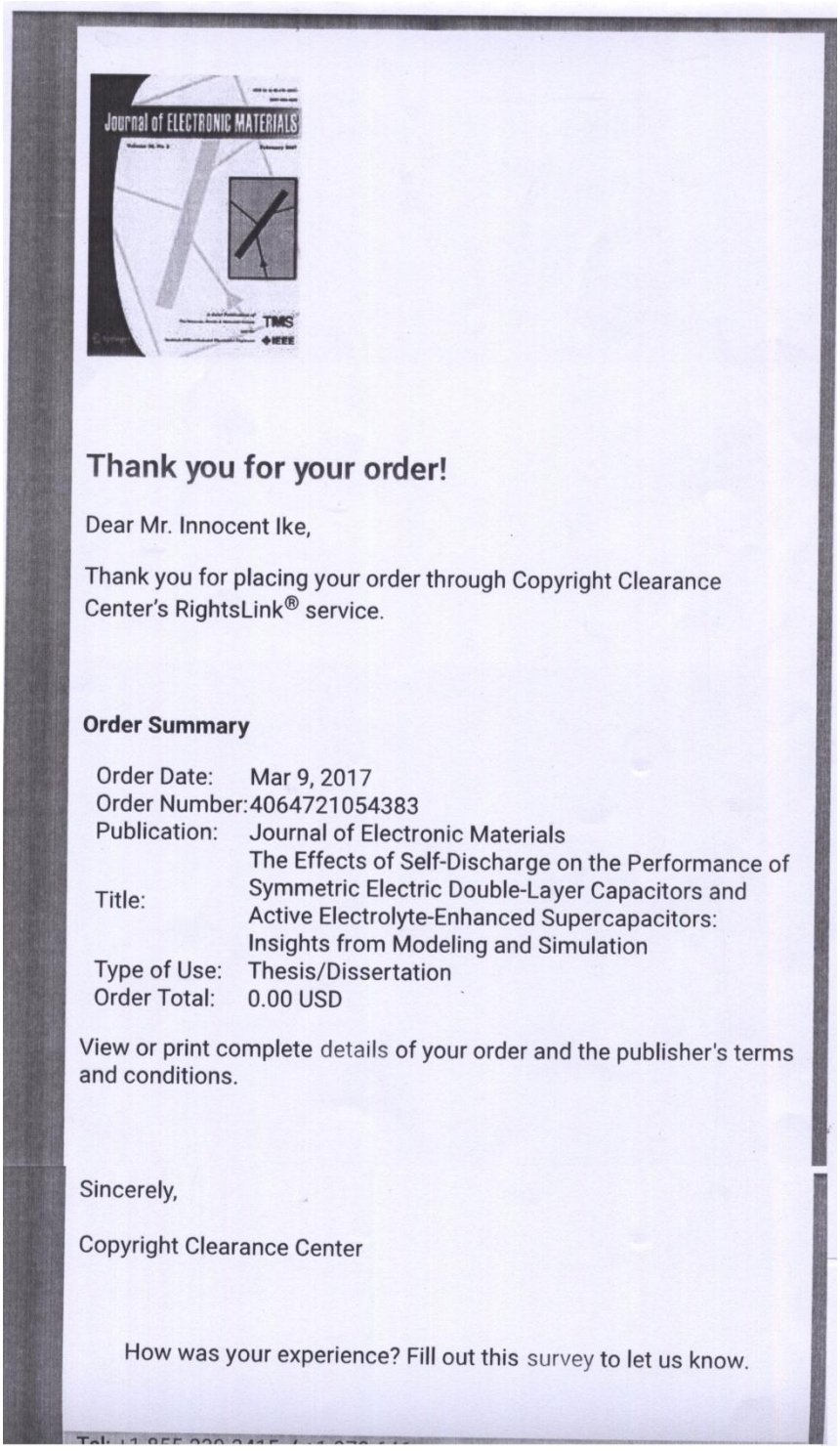

Appendix A5: Permission to republish " The Influences of Operating Conditions and Design Configurations on the Performance of Symmetric Electrochemical Capacitors".

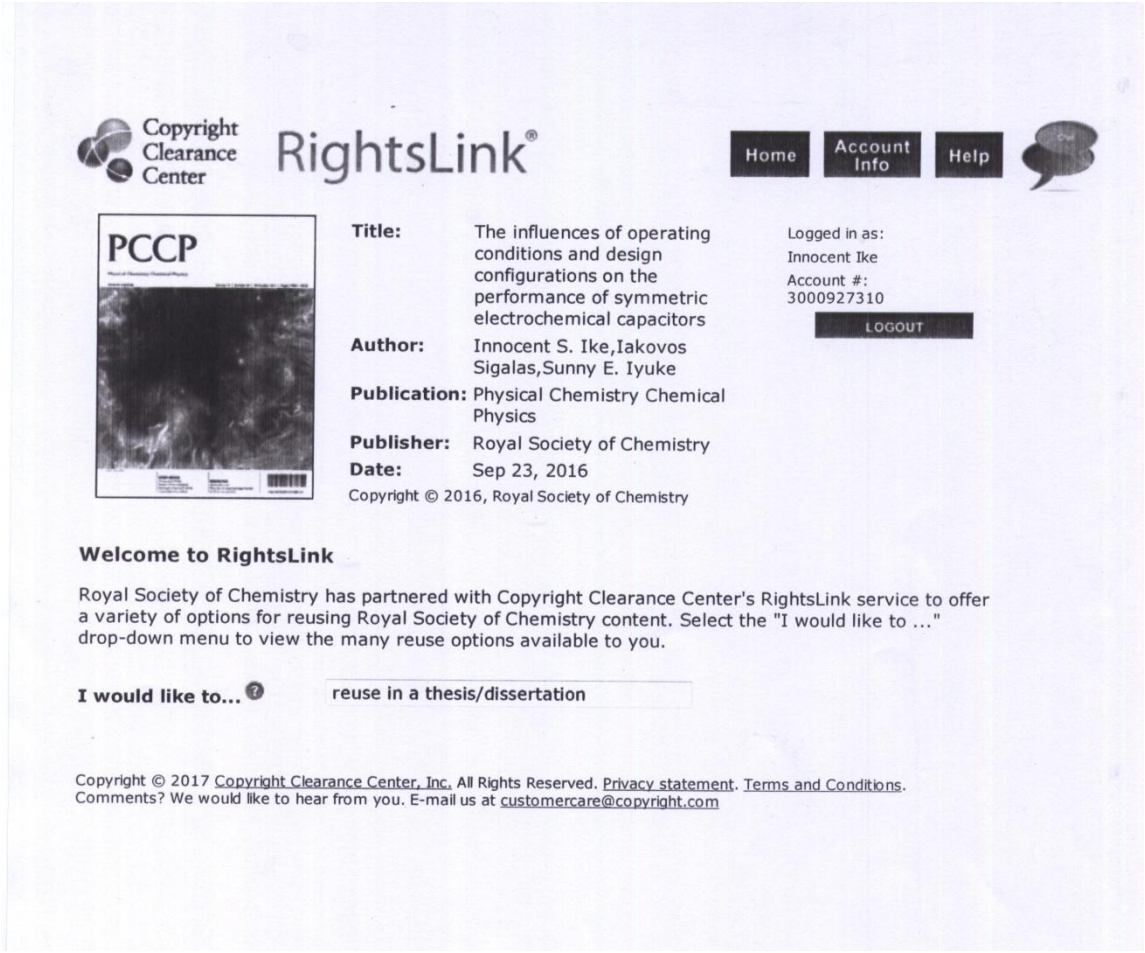

Copyright Clearance Center RightsLink®

Home | Account Info | Help

Title: The influences of operating conditions and design configurations on the performance of symmetric electrochemical capacitors

Author: Innocent S. Ike,Iakovos Sigalas,Sunny E. Iyuke

Publication: Physical Chemistry Chemical Physics

Publisher: Royal Society of Chemistry

Date: Sep 23, 2016

Copyright © 2016, Royal Society of Chemistry

Logged in as:
Innocent Ike
Account #:
3000927310

LOGOUT

Welcome to RightsLink

Royal Society of Chemistry has partnered with Copyright Clearance Center's RightsLink service to offer a variety of options for reusing Royal Society of Chemistry content. Select the "I would like to ..." drop-down menu to view the many reuse options available to you.

I would like to... reuse in a thesis/dissertation

Copyright © 2017 Copyright Clearance Center, Inc. All Rights Reserved. Privacy statement. Terms and Conditions.
Comments? We would like to hear from you. E-mail us at customercare@copyright.com

Appendix A6: permission to republish the "Optimization of electrochemical capacitors design parameters and operating conditions for high energy and power performances".

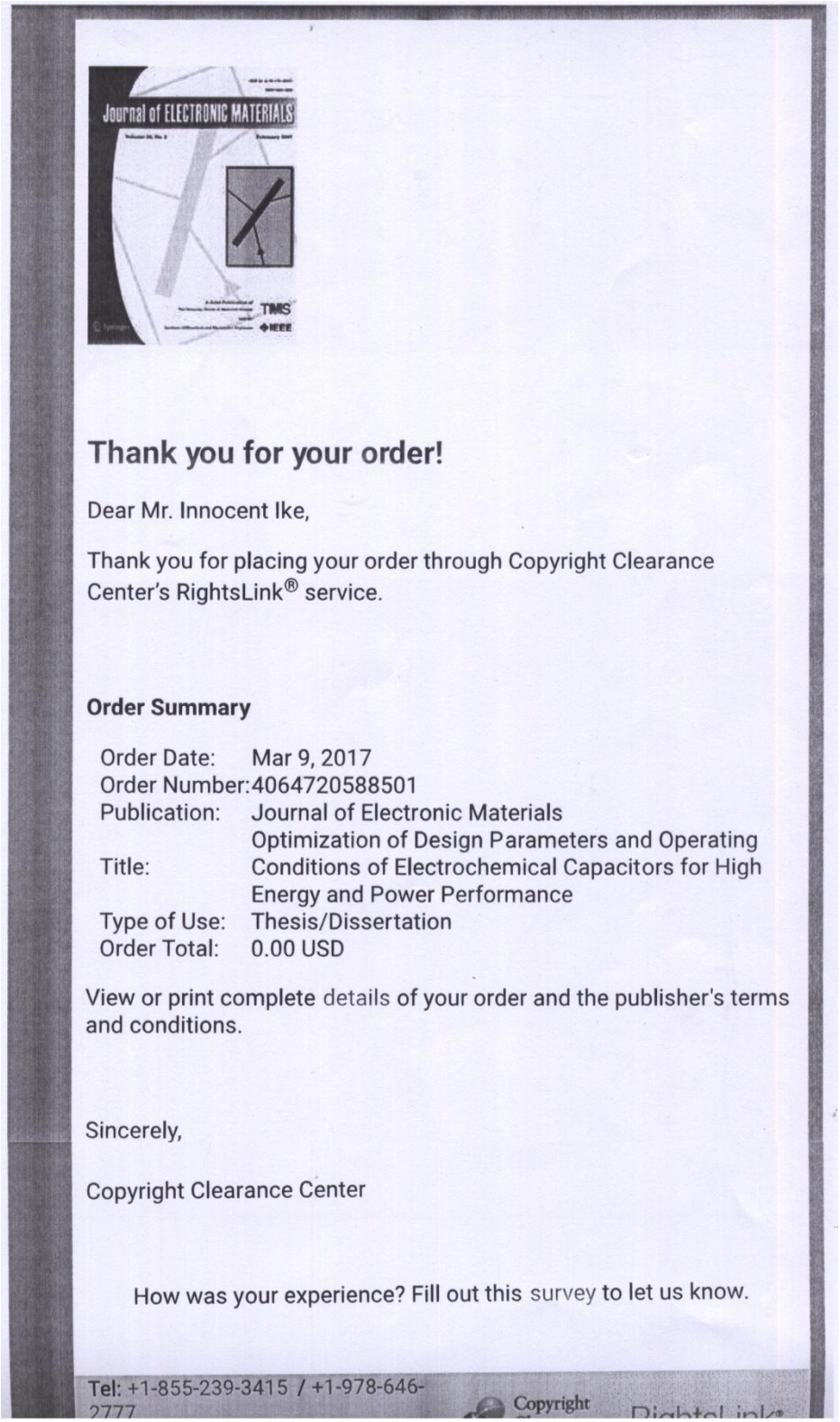

Appendix B

Homogeneous/symmetric electrochemical capacitors without self-discharge.

For the homogeneous equation $\frac{\partial \varphi_{ne}}{\partial t} = \beta^2 \frac{\partial^2 \varphi_{ne}}{\partial x^2}$, with the inhomogeneous boundary and initial conditions, it becomes $\frac{\partial \varphi_{ne}}{\partial t} - \beta^2 \frac{\partial^2 \varphi_{ne}}{\partial x^2} = 0$ B1

Using the Fourier Cosine series solution method, we seek a Fourier Cosine series solution of the form [289,290]: $\varphi_{ne}(x,t) = b_0(t) + \sum_{n=1}^{\infty} b_n(t)\, Cos\left(\frac{n\pi x}{w_{ne}}\right)$ B2

where $b_0(t) = \frac{1}{w_{ne}} \int_0^{w_{ne}} \varphi_{ne}(x,t)\, dx$ and $b_n(t) = \frac{2}{w_{ne}} \int_0^{w_{ne}} \varphi_{ne}(x,t)\, Cos\left(\frac{n\pi x}{w_{ne}}\right) dx$, $n = 1,2,3.....$

On differentiating equation B2 with respect to t and x once and twice respectively, we have

$$\frac{\partial \varphi_{ne}}{\partial t}(x,t) = \frac{db_0(t)}{dt} + \sum_{n=1}^{\infty} \frac{db_n(t)}{dt} Cos\left(\frac{n\pi x}{w_{ne}}\right)$$

and $$-\frac{\partial^2 \varphi_{ne}}{\partial x^2} = \sum_{1}^{\infty} \frac{n^2\pi^2}{w_{ne}^2} b_n(t) \cos\left(\frac{n\pi x}{w_{ne}}\right)$$

Writing the PDE in terms of the Fourier cosine series requires determining the formulas for Fourier cosine coefficients of $\partial \varphi_{ne} / \partial t(x,t)$ and $-\partial^2 \varphi_{ne} / \partial x^2(x,t)$ in terms of the Fourier coefficients of $\varphi_{ne}(x,t)$. Computing the Fourier coefficients of $-\beta^2 \frac{\partial^2 \varphi_{ne}(x,t)}{\partial x^2}$ needs integrating the term by parts twice as below:

$$-\frac{2\beta^2}{w_{ne}} \int_0^{w_{ne}} \frac{\partial^2 \varphi_{ne}}{\partial x^2}(x,t)\, Cos\left(\frac{n\pi x}{w_{ne}}\right) dx = -\frac{2\beta^2}{w_{ne}} \int_0^{w_{ne}} \frac{\partial^2 \varphi_{ne}}{\partial x^2}(x,t)\, Cos\left(\frac{n\pi x}{w_{ne}}\right) dx$$

$$= -\frac{2\beta^2}{w_{ne}} \left(\left[\frac{\partial \varphi_{ne}}{\partial x}(x,t) Cos\left(\frac{n\pi x}{w_{ne}}\right) \right]_0^{w_{ne}} + \frac{n\pi}{w_{ne}} \int_0^{w_{ne}} \frac{\partial \varphi_{ne}}{\partial x}(x,t) \sin\left(\frac{n\pi x}{w_{ne}}\right) dx \right)$$

$$= -\frac{2n\pi\beta^2}{w_{ne}^2} \int_0^{w_{ne}} \frac{\partial \varphi_{ne}}{\partial x}(x,t) \sin\left(\frac{n\pi x}{w_{ne}}\right) dx$$

$$= -\frac{2n\pi\beta^2}{w_{ne}^2}\left(\left[\varphi_{ne}(x,t)\sin\left(\frac{n\pi x}{w_{ne}}\right)\right]_0^{w_{ne}} - \frac{n\pi}{w_{ne}}\int_0^{w_{ne}}\varphi_{ne}(x,t)\cos\left(\frac{n\pi x}{w_{ne}}\right)dx\right)$$

$$= \frac{2n^2\pi^2\beta^2}{w_{ne}^3}\int_0^{w_{ne}}\varphi_{ne}(x,t)\cos\left(\frac{n\pi x}{w_{ne}}\right)dx$$

$$-\beta^2\frac{\partial^2\varphi_{ne}(x,t)}{\partial x^2} = \frac{n^2\pi^2\beta^2}{w_{ne}^2}b_n(t) \qquad \text{B3}$$

To compute the n = 0 Fourier coefficients, we just use direct integration:

$$-\frac{1}{w_{ne}}\int_0^{w_{ne}}\frac{\partial^2\varphi_{ne}}{\partial x^2}(x,t)\,dx = \frac{1}{w_{ne}}\left[\frac{\partial\varphi_{ne}}{\partial x}(x,t)\right]_{x=0}^{w_{ne}}$$

$$= \frac{1}{w_{ne}}\left[\frac{\partial\varphi_{ne}}{\partial x}(w_{ne},t) - \frac{\partial\varphi_{ne}}{\partial x}(0,t)\right] = \frac{J_0\beta^2}{w_{ne}}\left(\frac{1}{\alpha_2}+\frac{1}{\alpha_1}\right)$$

Since $\partial\varphi_{ne}/\partial x(w_{ne},t)$ and $\partial\varphi_{ne}/\partial x(0,t)$ are not equal to zero (non-zero), we obtain

$$-\beta^2\frac{\partial^2\varphi_{ne}(x,t)}{\partial x^2} = \frac{\beta^2 J_0}{w_{ne}}\left(\frac{1}{\alpha_2}+\frac{1}{\alpha_1}\right) + \sum_{n=1}^{\infty}\frac{\beta^2n^2\pi^2}{w_{ne}^2}b_n(t)Cos\left(\frac{n\pi x}{w_{ne}}\right)$$

Also computing the Fourier cosine coefficients of $\partial\varphi_{ne}/\partial t(x,t)$ as follows:

$$\frac{2}{w_{ne}}\int_0^{w_{ne}}\frac{\partial\varphi_{ne}}{\partial x}(x,t)\cos\left(\frac{n\pi x}{w_{ne}}\right)dx = \frac{d}{dt}\left[\frac{2}{w_{ne}}\int_0^{w_{ne}}\frac{\partial\varphi_{ne}}{\partial x}(x,t)\cos\left(\frac{n\pi x}{w_{ne}}\right)dx\right] = \frac{db_n}{dt}(t), \text{ when n=0}$$

Substituting the Fourier cosine coefficients of $\partial\varphi_{ne}/\partial t(x,t)$ and $-\partial^2\varphi_{ne}/\partial x^2(x,t)$ into equation A1, we have:

$$\frac{\partial\varphi_{ne}(x,t)}{\partial t} - \beta^2\frac{\partial^2\varphi_{ne}(x,t)}{\partial x^2} = \frac{db_0(t)}{dt} + \frac{\beta^2J_0}{w_{ne}}\left(\frac{1}{\alpha_2}+\frac{1}{\alpha_1}\right)$$
$$+\sum_{n=1}^{\infty}\left(\frac{db_n(t)}{dt} + \frac{\beta^2n^2\pi^2}{w_{ne}^2}b_n(t)\right)Cos\left(\frac{n\pi x}{w_{ne}}\right) \qquad \text{B4}$$

Since the right hand side of the PDE is zero, we obtain

$$\frac{db_0(t)}{dt} + \frac{\beta^2J_0}{w_{ne}}\left(\frac{1}{\alpha_2}+\frac{1}{\alpha_1}\right) = 0\,,\ \frac{db_n(t)}{dt} + \frac{\beta^2n^2\pi^2}{w_{ne}^2}b_n(t) = 0 \qquad \text{B5}$$

Again, since $\varphi_{ne}(x,t_0) = \varphi^{0^+} - \frac{J_0(\alpha_1+\alpha_2)x^2}{w_{ne}2\alpha_1\alpha_2} + \frac{J_0x}{\alpha_1}$, $0 < x < w_{ne}$, the function $\varphi_{ne}^{0^+}(x)$ can be

represented by Fourier cosine series as:

$$\varphi_{ne}(x,t_0)=\varphi^{0^+_-}-\frac{J_0(\alpha_1+\alpha_2)x^2}{w_{ne}2\alpha_1\alpha_2}+\frac{J_0x}{\alpha_1}=d_0+\sum_{n=1}^{\infty}d_nCos\left(\frac{n\pi x}{w_{ne}}\right) \quad \text{B6}$$

where $d_0=\frac{1}{w_{ne}}\int_0^{w_{ne}}\left(\varphi^{0^+_-}-\frac{J_0(\alpha_1+\alpha_2)x^2}{w_{ne}2\alpha_1\alpha_2}+\frac{J_0x}{\alpha_1}\right)dx$,

$$d_n=\frac{2}{w_{ne}}\int_0^{w_{ne}}\left(\varphi^{0^+_-}-\frac{J_0(\alpha_1+\alpha_2)x^2}{w_{ne}2\alpha_1\alpha_2}+\frac{J_0x}{\alpha_1}\right)Cos\left(\frac{n\pi x}{w_{ne}}\right)dx \quad n=1,2,3,....$$

Also, comparing equations B2 and B6 at t=0, we have

$$b_0(0)=d_0 \quad and \quad b_n(0)=d_n \quad \text{B7}$$

On solving equations B5 and B7 we have

$$b_0(t)-b_0(0)=-\frac{\beta^2J_0\,t}{w_{ne}}\left(\frac{1}{\alpha_2}+\frac{1}{\alpha_1}\right)$$

$$b_0(t)=b_0(0)-\frac{\beta^2J_0\,t}{w_{ne}}\left(\frac{1}{\alpha_2}+\frac{1}{\alpha_1}\right), \text{ Since } b_0(0)=d_0,$$

$$b_0(t)=d_0-\frac{\beta^2J_0\,t}{w_{ne}}\left(\frac{1}{\alpha_2}+\frac{1}{\alpha_1}\right) \quad \text{B8}$$

Recall that $d_0=\frac{1}{w_{ne}}\int_0^{w_{ne}}\left(\varphi^{0^+_-}-\frac{J_0(\alpha_1+\alpha_2)x^2}{w_{ne}2\alpha_1\alpha_2}+\frac{J_0x}{\alpha_1}\right)dx$ and integrating and taking limit

from 0 to w_{ne}, we obtain, $d_0=\frac{1}{w_{ne}}\left[\varphi^{0^+_-}x-\frac{J_0(\alpha_1+\alpha_2)x^3}{w_{ne}6\alpha_1\alpha_2}+\frac{J_0x^2}{2\alpha_1}\right]_0^{w_{ne}}$

$$d_0=\varphi^{0^+_-}-\frac{J_0(\alpha_1+\alpha_2)w_{ne}^2}{6\alpha_1\alpha_2}+\frac{J_0w_{ne}^2}{2\alpha_1}$$

$$d_0=\varphi^{0^+_-}+\frac{J_0(2\alpha_2-\alpha_1)w_{ne}^2}{6\alpha_1\alpha_2} \quad \text{B9}$$

Substituting equation B9 into equation B8 and using $\beta^2=\frac{\alpha_1\alpha_2}{C_V(\alpha_2+\alpha_1)}$, we obtain

$$b_0(t) = \varphi^{0^+} + \frac{J_0(2\alpha_2 - \alpha_1)w_{ne}^2}{6\alpha_1\alpha_2} - \frac{J_0\, t}{w_{ne}C_V} \quad \text{B10}$$

Again, $\frac{db_n(t)}{b_n(t)} = -\frac{\beta^2 n^2 \pi^2}{w_{ne}^2} dt$

$$\ln b_n(t) - \ln b_n(0) = -\frac{\beta^2 n^2 \pi^2}{w_{ne}^2} t$$

$b_n(t) = b_n(0)\, \ell^{-\frac{\beta^2 n^2 \pi^2}{w_{ne}^2} t} = d_n\, \ell^{-\frac{\beta^2 n^2 \pi^2}{w_{ne}^2} t}$, since $b_n(0) = d_n$

$$b_n(t) = d_n\, \ell^{-\frac{\beta^2 n^2 \pi^2}{w_{ne}^2} t} \quad \text{B11}$$

Recall that $d_n = \frac{2}{w_{ne}} \int_0^{w_{ne}} \left(\varphi^{0^+} - \frac{J_0(\alpha_1 + \alpha_2)x^2}{w_{ne} 2\alpha_1\alpha_2} + \frac{J_0 x}{\alpha_1} \right) Cos\left(\frac{n\pi x}{w_{ne}} \right) dx$.

Integrating $d_n = \frac{2}{w_{ne}} \int_0^{w_{ne}} \left(\varphi^{0^+} - \frac{J_0(\alpha_1 + \alpha_2)x^2}{w_{ne} 2\alpha_1\alpha_2} + \frac{J_0 x}{\alpha_1} \right) Cos\left(\frac{n\pi x}{w_{ne}} \right) dx$ by parts, we obtain

$$d_n = \frac{J_0}{w_{ne}} \left(\frac{(\alpha_2 + \alpha_1)}{2\alpha_1\alpha_2} x^2 - \frac{w_{ne} x}{\alpha_1} - \frac{2w_{ne}^{\ 2}}{n^2\pi^2} \left(\frac{1}{\alpha_1} + \frac{(-1)^n}{\alpha_2} \right) \right) \quad \text{B12}$$

Substituting equation B12 into equation B11, we obtain

$$b_n(t) = \frac{J_0}{w_{ne}} \left(\frac{(\alpha_2 + \alpha_1)}{2\alpha_1\alpha_2} x^2 - \frac{w_{ne} x}{\alpha_1} - \frac{2w_{ne}^2}{n^2\pi^2} \left(\frac{1}{\alpha_1} + \frac{(-1)^n}{\alpha_2} \right) \right) \ell^{-\frac{\beta^2 n^2 \pi^2}{w_{ne}^2} t} \quad \text{B13}$$

Substituting equations B10 and B13 into equation B3, we finally obtain

$$\varphi_{ne}(x,t) = \varphi_{ne}^{0^+} \pm \frac{J_0}{w_{ne}C_V} \left\{ t + C_V \left[\frac{(\alpha_2 + \alpha_1)}{2\alpha_1\alpha_2} x^2 - \frac{w_{ne} x}{\alpha_1} + \frac{w_{ne}^2(2\alpha_2 - \alpha_1)}{6\alpha_1\alpha_2} - \frac{2w_{ne}^2}{\pi^2} \right.\right.$$

$$\left.\left. \sum_{n=1}^{\infty} \left(\frac{1}{\alpha_1} + \frac{(-1)^n}{\alpha_2} \right) \frac{\ell^{-\frac{\beta^2 n^2 \pi^2 t}{w_{ne}^2}}}{n^2} Cos\left(\frac{n\pi x}{w_{ne}} \right) \right] \right\} \quad \text{B14}$$

$$\varphi_{ne}(x,t) = \varphi_{ne}^{pause} \pm \frac{J_0}{w_{ne}C_V} \left\{ t + C_V \left[\frac{(\alpha_2 + \alpha_1)}{2\alpha_1\alpha_2} x^2 - \frac{w_{ne} x}{\alpha_1} - \frac{2w_{ne}^2}{\pi^2} \right.\right.$$

$$\sum_{n=1}^{\infty}\left(\frac{1}{\alpha_1}+\frac{(-1)^n}{\alpha_2}\right)\frac{\ell^{-\frac{\beta^2 n^2\pi^2 t}{w_{ne}^2}}}{n^2}Cos\left(\frac{n\pi x}{w_{ne}}\right)\Bigg]\Bigg\} \qquad \text{B15}$$

$$where\ \ \varphi_{ne}^{pause}=\varphi_{ne}^{0^{\pm}}\pm\frac{J_0 w_{ne}(2\alpha_2-\alpha_1)}{6\alpha_1\alpha_2}$$

Appendix C

Homogeneous/Symmetric electrochemical capacitors with self-discharge.

For the negative electrode of supercapacitors with electric double layer electrode

For the inhomogeneous equation $\frac{\partial \varphi_{ne}(x,t)}{\partial t} = \beta^2 \frac{\partial^2 \varphi_{ne}(x,t)}{\partial x^2} + \frac{J_{VR}(x,t)}{C_V}$ having the self-discharge with inhomogeneous boundary conditions $\frac{\partial \varphi_{ne}}{\partial x}(0,t) = -\frac{J_0}{\alpha_1}$, $\frac{\partial \varphi_{ne}}{\partial x}(w_{ne},t) = \frac{J_0}{\alpha_2}$ and an inhomogeneous initial condition $\varphi_{ne}(t)\Big|_{t=0} = \varphi_{ne}^{0^+}$, the inhomogeneous equation becomes:

$$\frac{\partial \varphi_{ne}(x,t)}{\partial t} - \beta^2 \frac{\partial^2 \varphi_{ne}(x,t)}{\partial x^2} = \frac{J_{VR}(x,t)}{C_V} \qquad \text{C1}$$

Using the Fourier Cosine series solution method, we seek a Fourier Cosine series solution of the form [289,290]:

$$\varphi_{ne}(x,t) = b_0(t) + \sum_{n=1}^{\infty} b_n(t)\, Cos\left(\frac{n\pi x}{w_{ne}}\right) \qquad \text{C2}$$

where $b_0(t) = \frac{1}{w_{ne}} \int_0^{w_{ne}} \varphi_{ne}(x,t)\, dx$ and $b_n(t) = \frac{2}{w_{ne}} \int_0^{w_{ne}} \varphi_{ne}(x,t)\, Cos\left(\frac{n\pi x}{w_{ne}}\right) dx$, $n = 1,2,3.....$

On differentiating equation C2, we have

$$\frac{\partial \varphi_{ne}}{\partial t}(x,t) = \frac{db_0(t)}{dt} + \sum_{n=1}^{\infty} \frac{db_n(t)}{dt} Cos\left(\frac{n\pi x}{w_{ne}}\right) \text{ and } -\frac{\partial^2 \varphi_{ne}(x,t)}{\partial x^2} = \sum_{1}^{\infty} \frac{n^2\pi^2}{w_{ne}^2} b_n(t) \cos\left(\frac{n\pi x}{w_{ne}}\right)$$

Writing the PDE in terms of the Fourier cosine series requires determining the formulas for Fourier cosine coefficients of $\partial \varphi_{ne} / \partial t(x,t)$ and $-\partial^2 \varphi_{ne} / \partial x^2(x,t)$ in terms of the Fourier coefficients of $\varphi_{ne}(x,t)$. Computing the Fourier coefficients of $-\beta^2 \frac{\partial^2 \varphi_{ne}(x,t)}{\partial x^2}$ needs integrating the term by parts twice as below:

$$-\frac{2\beta^2}{w_{ne}} \int_0^{w_{ne}} \frac{\partial^2 \varphi_{ne}}{\partial x^2}(x,t)\, Cos\left(\frac{n\pi x}{w_{ne}}\right) dx = -\frac{2\beta^2}{w_{ne}} \int_0^{w_{ne}} \frac{\partial^2 \varphi_{ne}}{\partial x^2}(x,t)\, Cos\left(\frac{n\pi x}{w_{ne}}\right) dx$$

$$= -\frac{2\beta^2}{w_{ne}}\left(\left[\frac{\partial\varphi_{ne}}{\partial x}(x,t)Cos\left(\frac{n\pi x}{w_{ne}}\right)\right]_0^{w_{ne}} + \frac{n\pi}{w_{ne}}\int_0^{w_{ne}}\frac{\partial\varphi_{ne}}{\partial x}(x,t)\sin\left(\frac{n\pi x}{w_{ne}}\right)dx\right)$$

$$= -\frac{2n\pi\beta^2}{w_{ne}^2}\int_0^{w_{ne}}\frac{\partial\varphi_{ne}}{\partial x}(x,t)\sin\left(\frac{n\pi x}{w_{ne}}\right)dx$$

$$= -\frac{2n\pi\beta^2}{w_{ne}^2}\left(\left[\varphi_{ne}(x,t)\sin\left(\frac{n\pi x}{w_{ne}}\right)\right]_0^{w_{ne}} - \frac{n\pi}{w_{ne}}\int_0^{w_{ne}}\varphi_{ne}(x,t)\cos\left(\frac{n\pi x}{w_{ne}}\right)dx\right)$$

$$= \frac{2n^2\pi^2\beta^2}{w_{ne}^3}\int_0^{w_{ne}}\varphi_{ne}(x,t)\cos\left(\frac{n\pi x}{w_{ne}}\right)dx$$

$$= \frac{n^2\pi^2\beta^2}{w_{ne}^2}b_n(t)$$

To compute the n = 0 Fourier coefficients, we just use direct integration:

$$-\frac{1}{w_{ne}}\int_0^{w_{ne}}\frac{\partial^2\varphi_{ne}}{\partial x^2}(x,t)\,dx = \frac{1}{w_{ne}}\left[\frac{\partial\varphi_{ne}}{\partial x}(x,t)\right]_{x=0}^{w_{ne}}$$

$$= \frac{1}{w_{ne}}\left[\frac{\partial\varphi_{ne}}{\partial x}(w_{ne},t) - \frac{\partial\varphi_{ne}}{\partial x}(0,t)\right] = \frac{J_0\beta^2}{w_{ne}}\left(\frac{1}{\alpha_2}+\frac{1}{\alpha_1}\right)$$

Since $\partial\varphi_{ne}/\partial x(w_{ne},t)$ and $\partial\varphi_{ne}/\partial x(0,t)$ are not equal to zero (non-zero), we obtain

$$-\beta^2\frac{\partial^2\varphi_{ne}(x,t)}{\partial x^2} = \frac{\beta^2 J_0}{w_{ne}}\left(\frac{1}{\alpha_2}+\frac{1}{\alpha_1}\right) + \sum_{n=1}^{\infty}\frac{\beta^2 n^2\pi^2}{w_{ne}^2}b_n(t)Cos\left(\frac{n\pi x}{w_{ne}}\right)$$

Also computing the Fourier cosine coefficients of $\partial\varphi_{ne}/\partial t(x,t)$ as follows:

$$\frac{2}{w_{ne}}\int_0^{w_{ne}}\frac{\partial\varphi_{ne}}{\partial x}(x,t)\cos\left(\frac{n\pi x}{w_{ne}}\right)dx = \frac{d}{dt}\left[\frac{2}{w_{ne}}\int_0^{w_{ne}}\frac{\partial\varphi_{ne}}{\partial x}(x,t)\cos\left(\frac{n\pi x}{w_{ne}}\right)dx\right] = \frac{db_n}{dt}(t),\ \text{when n=0}$$

$$-\frac{1}{w_{ne}}\int_0^{w_{ne}}\frac{\partial^2\varphi_{ne}}{\partial x^2}(x,t)\,dx = \frac{1}{w_{ne}}\left[\frac{\partial\varphi_{ne}}{\partial x}(x,t)\right]_{x=0}^{w_{ne}}$$

$$= \frac{1}{w_{ne}}\left[\frac{\partial\varphi_{ne}}{\partial x}(w_{ne},t) - \frac{\partial\varphi_{ne}}{\partial x}(0,t)\right] = 0$$

Since $\partial\varphi_{ne}/\partial x(w_{ne},t) \neq 0 \quad and \quad \partial\varphi_{ne}/\partial x(0,t) = 0$, we obtain:

$$-\beta^2 \frac{\partial^2 \varphi_{ne}(x,t)}{\partial x^2} = \sum_{n=1}^{\infty} \frac{\beta^2 n^2 \pi^2}{w_{ne}^2} b_n(t) Cos\left(\frac{n\pi x}{w_{ne}}\right)$$

Substituting the Fourier cosine coefficients of $\partial\varphi_{ne}/\partial t(x,t)$ and $-\partial^2\varphi_{ne}/\partial x^2(x,t)$ into equation C2, we have: $\frac{\partial \varphi_{ne}(x,t)}{\partial t} - \beta^2 \frac{\partial^2 \varphi_{ne}(x,t)}{\partial x^2} = \frac{db_0(t)}{dt} + \frac{\beta^2 J_0}{w_{ne}}\left(\frac{1}{\alpha_2} + \frac{1}{\alpha_1}\right)$

$$+\sum_{n=1}^{\infty}\left(\frac{db_n(t)}{dt} + \frac{\beta^2 n^2 \pi^2}{w_{ne}^2} b_n(t)\right) Cos\left(\frac{n\pi x}{w_{ne}}\right) \qquad \text{C3}$$

Again, $\frac{J_{VR(x,t)}}{C_V} = C_0(t) + \sum_{n=1}^{\infty} C_n(t)\, Cos\left(\frac{n\pi x}{w_{ne}}\right)$, where $C_0(t) = \frac{1}{w_{ne}} \int_0^{w_{ne}} \frac{J_{VR}}{C_V}(x,t)\, dx$,

$C_n(t) = \frac{2}{w_{ne}} \int_0^{w_{ne}} \frac{J_{VR}}{C_V}(x,t)\, Cos\left(\frac{n\pi x}{w_{ne}}\right) dx$, $n = 1,2,3.....$

Since the right hand side of the PDE is not zero, we obtain:

$$\frac{db_0(t)}{dt} + \frac{\beta^2 J_0}{w_{ne}}\left(\frac{1}{\alpha_2} + \frac{1}{\alpha_1}\right) = C_0(t),\ \frac{db_n(t)}{dt} + \frac{\beta^2 n^2 \pi^2}{w_{ne}^2} b_n(t) = C_n(t) \qquad \text{C4}$$

Again, since $\varphi_{ne}(x,t_0) = \varphi^{0^+_-} - \frac{J_0(\alpha_1+\alpha_2)x^2}{w_{ne} 2\alpha_1\alpha_2} + \frac{J_0 x}{\alpha_1}$, $0 < x < w_{ne}$, the function $\varphi_{ne}^{0^+_-}(x)$ can be represented by Fourier cosine series as:

$$\varphi_{ne}(x,t_0) = \varphi^{0^+_-} - \frac{J_0(\alpha_1+\alpha_2)x^2}{w_{ne} 2\alpha_1\alpha_2} + \frac{J_0 x}{\alpha_1} = d_0 + \sum_{n=1}^{\infty} d_n Cos\left(\frac{n\pi x}{w_{ne}}\right) \qquad \text{C5}$$

where $d_0 = \frac{1}{w_{ne}} \int_0^{w_{ne}} \left(\varphi^{0^+_-} - \frac{J_0(\alpha_1+\alpha_2)x^2}{w_{ne} 2\alpha_1\alpha_2} + \frac{J_0 x}{\alpha_1}\right) dx$,

$d_n = \frac{2}{w_{ne}} \int_0^{w_{ne}} \left(\varphi^{0^+_-} - \frac{J_0(\alpha_1+\alpha_2)x^2}{w_{ne} 2\alpha_1\alpha_2} + \frac{J_0 x}{\alpha_1}\right) Cos\left(\frac{n\pi x}{w_{ne}}\right) dx \quad n = 1,2,3,....$

Also, comparing equations C2 and C5 at t=0, we have

$$b_0(0) = d_0 \quad and \quad b_n(0) = d_n \qquad \text{C6}$$

On solving equations C4 and C6 we have: $b_0(t) - b_0(0) = C_0(t)\, t - \frac{\beta^2 J_0\, t}{w_{ne}}\left(\frac{1}{\alpha_2} + \frac{1}{\alpha_1}\right)$

Since $b_0(0) = d_0$,

$$b_0(t) = d_0 + C_0(t)\,t - \frac{\beta^2 J_0\, t}{w_{ne}}\left(\frac{1}{\alpha_2} + \frac{1}{\alpha_1}\right) \qquad \text{C7}$$

Recall that $d_0 = \frac{1}{w_{ne}}\int_0^{w_{ne}}\left(\varphi^{0^+_-} - \frac{J_0(\alpha_1+\alpha_2)x^2}{w_{ne}2\alpha_1\alpha_2} + \frac{J_0 x}{\alpha_1}\right)dx$ and integrating and taking limit from 0 to w_{ne}, we obtains: $d_0 = \frac{1}{w_{ne}}\left[\varphi^{0^+_-}x - \frac{J_0(\alpha_1+\alpha_2)x^3}{w_{ne}6\alpha_1\alpha_2} + \frac{J_0 x^2}{2\alpha_1}\right]_0^{w_{ne}}$

$$d_0 = \varphi^{0^+_-} - \frac{J_0(\alpha_1+\alpha_2)w_{ne}^2}{6\alpha_1\alpha_2} + \frac{J_0 w_{ne}^2}{2\alpha_1}$$

$$d_0 = \varphi^{0^+_-} + \frac{J_0(2\alpha_2-\alpha_1)w_{ne}^2}{6\alpha_1\alpha_2} \qquad \text{C8}$$

Substituting equation C8 into equation C7 and using $\beta^2 = \frac{\alpha_1\alpha_2}{C_V(\alpha_2+\alpha_1)}$, we obtain

$$b_0(t) = \varphi^{0^+_-} + \frac{J_0(2\alpha_2-\alpha_1)w_{ne}^2}{6\alpha_1\alpha_2} + C_0(t)\,t - \frac{J_0\, t}{w_{ne}C_V} \qquad \text{C9}$$

Again, $\frac{db_n(t)}{dt} + \frac{\beta^2 n^2\pi^2}{w_{ne}^2}b_n(t) = C_n(t)$, $b_n(t) = b_n(0)\,\ell^{-\frac{\beta^2 n^2\pi^2}{w_{ne}^2}(t-t_0)} + \int_0^t \ell^{-\frac{\beta^2 n^2\pi^2}{w_{ne}^2}(t-t_0)}C_n(s)\,ds$,

since $b_n(0) = d_n$

$$b_n(t) = \left(d_n - \frac{C_n(t)w_{ne}^2}{\beta^2 n^2\pi^2}\right)\ell^{-\frac{\beta^2 n^2\pi^2}{w_{ne}^2}(t-t_0)} + \frac{C_n(t)w_{ne}^2}{\beta^2 n^2\pi^2} \qquad \text{C10}$$

Recall that $d_n = \frac{2}{w_{ne}}\int_0^{w_{ne}}\left(\varphi^{0^+_-} - \frac{J_0(\alpha_1+\alpha_2)x^2}{w_{ne}2\alpha_1\alpha_2} + \frac{J_0 x}{\alpha_1}\right)Cos\left(\frac{n\pi x}{w_{ne}}\right)dx$.

Integrating $d_n = \frac{2}{w_{ne}}\int_0^{w_{ne}}\left(\varphi^{0^+_-} - \frac{J_0(\alpha_1+\alpha_2)x^2}{w_{ne}2\alpha_1\alpha_2} + \frac{J_0 x}{\alpha_1}\right)Cos\left(\frac{n\pi x}{w_{ne}}\right)dx$ by parts, we obtain

$$d_n = \frac{J_0}{w_{ne}}\left(\frac{(\alpha_2+\alpha_1)}{2\alpha_1\alpha_2}x^2 - \frac{w_{ne}x}{\alpha_1} - \frac{2w_{ne}^{\,2}}{n^2\pi^2}\left(\frac{1}{\alpha_1} + \frac{(-1)^n}{\alpha_2}\right)\right) \qquad \text{C11}$$

Note again that $C_0(t) = \frac{1}{w_{ne}}\int_0^{w_{ne}}\frac{J_{VR}}{C_V}(x,t)\,dx$

Integrating the above, we obtain: $C_0(t) = \frac{1}{w_{ne}}\left[\frac{J_{VR}}{C_V}x\right]_0^{w_{ne}} = \frac{1}{w_{ne}}\left[\frac{J_{VR}}{C_V}w_{ne} - 0\right] = \frac{J_{VR}}{C_V}$

$$C_0(t) = \frac{J_{VR}}{C_V} \qquad \text{C12}$$

$$\text{And } C_n(t) = \frac{2}{w_{ne}} \int_0^{w_{ne}} \frac{J_{VR}}{C_V}(x,t)\, Cos\left(\frac{n\pi x}{w_{ne}}\right) dx \text{ , } n = 1,2,3..$$

$$= \frac{2}{w_{ne}}\left(\frac{J_{VR}}{C_V}\frac{w_{ne}}{n\pi}\sin\left(\frac{n\pi x}{w_{ne}}\right)\right)_0^{w_{ne}} = \frac{2}{w_{ne}}\left(\frac{J_{VR}}{C_V}\frac{w_{ne}}{n\pi}(-1)^n\right) = \frac{2J_{VR}}{C_V n\pi}(-1)^n$$

$$C_n(t) = \frac{2J_{VR}}{C_V n\pi}(-1)^n \qquad \text{C13}$$

Substituting equation C12 into equation C9 and equations C11 and C14 into equation C10, and using ($\beta^2 = \frac{\alpha_1\alpha_2}{C_V(\alpha_2+\alpha_1)}$), we obtain:

$$b_0(t) = \varphi^{0^+} + \frac{J_0(2\alpha_2 - \alpha_1)w_{ne}^2}{6\alpha_1\alpha_2} + \frac{J_{VR}}{C_V}t - \frac{J_0\, t}{w_{ne}C_V} \qquad \text{C14}$$

$$b_n(t) = \left\{\frac{J_0}{w_{ne}}\left(\frac{(\alpha_2+\alpha_1)}{2\alpha_1\alpha_2}x^2 - \frac{w_{ne}x}{\alpha_1} - \frac{2w_{ne}{}^2}{n^2\pi^2}\left(\frac{1}{\alpha_1} + \frac{(-1)^n}{\alpha_2}\right)\ell^{-\frac{\beta^2n^2\pi^2}{w_{ne}^2}(t-t_0)}\right)\right\}$$

$$- \frac{2J_{VR}w_{ne}^2(-1)^n}{C_V\beta^2n^3\pi^3}\ell^{-\frac{\beta^2n^2\pi^2}{w_{ne}^2}(t-t_0)} + \frac{2J_{VR}(-1)^n w_{ne}^2}{C_V\beta^2n^3\pi^3} \qquad \text{C15}$$

Substituting equations C14 and C15 into equation C12, using $\beta^2 = \frac{\alpha_1\alpha_2}{C_V(\alpha_2+\alpha_1)}$ and rearranging appropriately, we obtain the solution for negative electrode with self-discharge due to only electric double layer (EDL) instability:

$$\varphi_{ne}(x,t) = \varphi_{ne}^{0^+} \pm \frac{J_0}{w_{ne}C_V}\left\{t + C_V\left[\frac{(\alpha_2+\alpha_1)}{2\alpha_1\alpha_2}x^2 - \frac{w_{ne}\,x}{\alpha_1} + \frac{w_{ne}^2(2\alpha_2-\alpha_1)}{6\alpha_1\alpha_2} - \frac{2\,w_{ne}^2}{\pi^2}\right.\right.$$

$$\left.\left.\sum_{n=1}^{\infty}\left(\frac{1}{\alpha_1} + \frac{(-1)^n}{\alpha_2}\right)\frac{\ell^{-\frac{\beta^2n^2\pi^2t}{w_{ne}^2}}}{n^2}Cos\left(\frac{n\pi x}{w_{ne}}\right)\right]\right\} + \frac{J_{VR}\,t}{C_V} + \frac{2w_{ne}^2J_{VR}}{\pi^3}\sum_{n=1}^{\infty}\frac{(-1)^n(\alpha_2+\alpha_1)}{\alpha_1\alpha_2}$$

$$\left(\frac{1-\ell^{-\frac{\beta^2n^2\pi^2}{w_{ne}^2}(t-t_0)}}{n^3}\right)Cos\left(\frac{n\pi x}{w_{ne}}\right) \qquad \text{C16}$$

$$\varphi_{ne}(x,t) = \varphi_{ne}^{pause} \pm \frac{J_0}{w_{ne} C_V} \left\{ t + C_V \left[\frac{(\alpha_2 + \alpha_1)}{2\alpha_1\alpha_2} x^2 - \frac{w_{ne}\, x}{\alpha_1} - \frac{2\, w_{ne}^2}{\pi^2} \right.\right.$$

$$\left.\left. \sum_{n=1}^{\infty} \left(\frac{1}{\alpha_1} + \frac{(-1)^n}{\alpha_2} \right) \frac{\ell^{-\frac{\beta^2 n^2 \pi^2 t}{w_{ne}^2}}}{n^2} Cos\left(\frac{n\pi x}{w_{ne}} \right) \right] \right\} + \frac{J_{VR}\, t}{C_V} + \frac{2 w_{ne}^2 J_{VR}}{\pi^3} \sum_{n=1}^{\infty} \frac{(-1)^n (\alpha_2 + \alpha_1)}{\alpha_1\alpha_2}$$

$$\left(\frac{1 - \ell^{-\frac{\beta^2 n^2 \pi^2}{w_{ne}^2}(t - t_0)}}{n^3} \right) Cos\left(\frac{n\pi x}{w_{ne}} \right) \qquad \text{C17}$$

$$where \;\; \varphi_{ne}^{pause} = \varphi_{ne}^{0^+_-} \pm \frac{J_0 w_{ne} (2\alpha_2 - \alpha_1)}{6\alpha_1\alpha_2}$$

Appendix D

Homogeneous/Symmetric electrochemical capacitors with only faraday electrodes

For the negative electrode of supercapacitors with redox couple electrode

$$\frac{\partial C_s}{\partial t} = D_s \frac{\partial^2 C_s}{\partial x^2} + \frac{J_{Cell}}{D_s\left(1-\theta^0\right)} \quad \text{D1}$$

The boundary conditions of this negative electrode during the capacitor charge are as follows:

$$x = 0\,, \frac{\partial C_s}{\partial x} = 0 \quad \text{D2}$$

$$x = w_{ne}\,, \ \frac{\partial C_s}{\partial x} = \frac{J_{Cell}}{D_s\left(1-\theta^0\right)} \quad \text{D3}$$

and the initial condition is given as follow:

$$At\ t = 0,\ C_{t=0} = C^0 \quad \text{D4}$$

The boundary conditions of this negative electrode during the capacitor discharge are as follows:

$$x = 0\,, \frac{\partial C_s}{\partial x} = 0 \quad \text{D5}$$

$$x = w_{ne}\,, \ \frac{\partial C_s}{\partial x} = -\frac{J_{Cell}}{D_s\left(1-\theta^0\right)} \quad \text{D6}$$

and the initial condition is given as follow:

$$At\ t = 0,\ C_{t=0} = C^{0-} \quad \text{D7}$$

Using the Fourier Cosine series solution method, we seek a Fourier Cosine series solution of the form [289,290]:

$$C_s(x,t) = a_0(t) + \sum_{n=1}^{\infty} a_n(t)\, Cos\left(\frac{n\pi x}{w_{ne}}\right) \quad \text{D8}$$

where $a_0(t) = \frac{1}{w_{ne}} \int_0^{w_{ne}} C_s(x,t)\, dx$ and $a_n(t) = \frac{2}{w_{ne}} \int_0^{w_{ne}} C_s(x,t)\, Cos\left(\frac{n\pi x}{w_{ne}}\right) dx$, $n = 1,2,3.....$

On differentiating equation C3 with respect to t and x once and twice respectively, we have

$$\frac{\partial C_s}{\partial t}(x,t)=\frac{da_0(t)}{dt}+\sum_{n=1}^{\infty}\frac{da_n(t)}{dt}Cos\left(\frac{n\pi x}{w_{ne}}\right),\ \text{and}\ -\frac{\partial^2 C_s(x,t)}{\partial x^2}=\sum_{1}^{\infty}\frac{n^2\pi^2}{w_{ne}^2}a_n(t)\cos\left(\frac{n\pi x}{w_{ne}}\right)$$

Writing the PDE in terms of the Fourier cosine series requires determining the formulas for Fourier cosine coefficients of $\partial C_s/\partial t(x,t)$ and $-\partial^2 C_s/\partial x^2(x,t)$ in terms of the Fourier coefficients of $C_s(x,t)$.Computing the Fourier coefficients of $-D_s\frac{\partial^2 C_s(x,t)}{\partial x^2}$ needs integrating the term by parts twice as below:

$$-\frac{2D_s}{w_{ne}}\int_0^{w_{ne}}\frac{\partial^2\varphi_{ne}}{\partial x^2}(x,t)\,Cos\left(\frac{n\pi x}{w_{ne}}\right)dx=-\frac{2D_s}{w_{ne}}\int_0^{w_{ne}}\frac{\partial^2 \mathrm{C_s}}{\partial x^2}(x,t)\,Cos\left(\frac{n\pi x}{w_{ne}}\right)dx$$

$$-\frac{2D_s}{w_{ne}}\int_0^{w_{ne}}\frac{\partial^2 \mathrm{C_s}}{\partial x^2}(x,t)\,Cos\left(\frac{n\pi x}{w_{ne}}\right)dx=-\frac{2D_s}{w_{ne}}\int_0^{w_{ne}}\frac{\partial^2 \mathrm{C_s}}{\partial x^2}(x,t)\,Cos\left(\frac{n\pi x}{w_{ne}}\right)dx$$

$$=-\frac{2n\pi D_s}{w_{ne}^2}\int_0^{w_{ne}}\frac{\partial \mathrm{C_s}}{\partial x}(x,t)\sin\left(\frac{n\pi x}{w_{ne}}\right)dx$$

$$=-\frac{2n\pi D_s}{w_{ne}^2}\left(\left[\mathrm{C_s}(x,t)\sin\left(\frac{n\pi x}{w_{ne}}\right)\right]_0^{w_{ne}}-\frac{n\pi}{w_{ne}}\int_0^{w_{ne}}\mathrm{C_s}(x,t)\cos\left(\frac{n\pi x}{w_{ne}}\right)dx\right)$$

$$=\frac{2n^2\pi^2 D_s}{w_{ne}^3}\int_0^{w_{ne}}\mathrm{C_s}(x,t)\cos\left(\frac{n\pi x}{w_{ne}}\right)dx$$

$$=\frac{n^2\pi^2 D_s}{w_{ne}^2}a_n(t)$$

To compute the n = 0 Fourier coefficients, we just use direct integration:

$$-\frac{1}{w_{ne}}\int_0^{w_{ne}}\frac{\partial^2 C_s}{\partial x^2}(x,t)\,dx=\frac{1}{w_{ne}}\left[\frac{\partial C_s}{\partial x}(x,t)\right]_{x=0}^{w_{ne}}$$

$$=\frac{1}{w_{ne}}\left[\frac{\partial C_s}{\partial x}(w_{ne},t)-\frac{\partial C_s}{\partial x}(0,t)\right]=\frac{J_{Cell}}{D_s(1-\theta^0)w_{ne}}$$

Since $\partial C_s/\partial x(w_{ne},t)\neq 0$ *and* $\partial C_s/\partial x(0,t)=0$, we obtain

$$-D_s\frac{\partial^2 C_s(x,t)}{\partial x^2}=\frac{J_{Cell}}{D_s\left(1-\theta^0\right)w_{ne}}+\sum_{n=1}^{\infty}\frac{D_s n^2\pi^2}{w_{ne}^2}a_n(t)Cos\left(\frac{n\pi x}{w_{ne}}\right)$$

Also computing the Fourier cosine coefficients of $\partial C_s/\partial t(x,t)$ as follows:

$$\frac{2}{w_{ne}}\int_0^{w_{ne}}\frac{\partial C_s}{\partial x}(x,t)\cos\left(\frac{n\pi x}{w_{ne}}\right)dx=\frac{d}{dt}\left[\frac{2}{w_{ne}}\int_0^{w_{ne}}\frac{\partial C_s}{\partial x}(x,t)\cos\left(\frac{n\pi x}{w_{ne}}\right)dx\right]=\frac{da_n}{dt}(t),\text{ when n=0}$$

Substituting the Fourier cosine coefficients of $\partial C_s/\partial t(x,t)$ and $-\partial^2 C_s/\partial x^2(x,t)$ into equation D1, we have:

$$\frac{\partial C_s(x,t)}{\partial t}-D_s\frac{\partial^2 C_s(x,t)}{\partial x^2}=\frac{da_0(t)}{dt}+\frac{J_{Cell}}{D_s\left(1-\theta^0\right)w_{ne}}+\sum_{n=1}^{\infty}\left(\frac{da_n(t)}{dt}+\frac{D_s n^2\pi^2}{w_{ne}^2}a_n(t)\right)Cos\left(\frac{n\pi x}{w_{ne}}\right)\quad\text{D9}$$

$$\text{Again, }\frac{J_{Cell}}{D_s\left(1-\theta^0\right)}=b_0(t)+\sum_{n=1}^{\infty}b_n(t)\,Cos\left(\frac{n\pi x}{w_{ne}}\right)\quad\text{D10}$$

$$\text{Where }b_0(t)=\frac{1}{w_{ne}}\int_0^{w_{ne}}\left(\frac{J_{Cell}}{D_s\left(1-\theta^0\right)}\right)dx$$

$$b_n(t)=\frac{2}{w_{ne}}\int_0^{w_{ne}}\left(\frac{J_{Cell}}{D_s\left(1-\theta^0\right)}\right)Cos\left(\frac{n\pi x}{w_{ne}}\right)dx,\ n=1,2,3.....$$

Since the right hand side of the PDE is not zero, we obtain

$$\frac{da_0(t)}{dt}+\frac{J_{Cell}}{D_s\left(1-\theta^0\right)w_{ne}}=b_0(t),\ \frac{da_n(t)}{dt}+\frac{D_s n^2\pi^2}{w_{ne}^2}a_n(t)=b_n(t)\quad\text{D11}$$

Again, since $C_s(x,t_0)=C^0(x),0<x<w_{ne}$, the function $C_s(x,t_0)$ can be represented by Fourier cosine series as:

$$C^0=C_s(x,t_0)=C_0+\sum_{n=1}^{\infty}C_n\,Cos\left(\frac{n\pi x}{w_{ne}}\right)\quad\text{D12}$$

$$\text{where }C_0=\frac{1}{w_{ne}}\int_0^{w_{ne}}C^0dx,\ C_n=\frac{2}{w_{ne}}\int_0^{w_{ne}}C^0\,Cos\left(\frac{n\pi x}{w_{ne}}\right)dx,\ n=1,2,3.....$$

Also, comparing equations D9 and D12 at t=0, we have

$$a_0(0) = C_0 \quad and \quad a_n(0) = C_n \tag{D13}$$

On solving equations D8 and D6 we have

$$a_0(t) - a_0(0) = b_0(t)\,t - \frac{J_{Cell}\,t}{D_s\left(1-\theta^0\right)w_{ne}}, \text{ Since } a_0(0) = C_0,$$

$$a_0(t) = C_0 + b_0(t)\,t - \frac{J_{Cell}\,t}{D_s\left(1-\theta^0\right)w_{ne}} \tag{D14}$$

Recall that $C_0 = \frac{1}{w_{ne}}\int_0^{w_{ne}} C^0 dx$ and integrating and taking limit from 0 to w_{ne}, we obtain

$$C_0 = \left[\frac{1}{w_{ne}} C^0\, x\right]_0^{w_{ne}},\; C_0 = \frac{1}{w_{ne}}\left[C^0\; w_{ne} - C^0\; 0\right]$$

$$C_0 = C^0 \tag{D15}$$

Substituting equation D15 into equation D14, we obtain the expression below:

$$a_0(t) = C^0 + b_0(t)\,t - \frac{J_{Cell}\,t}{D_s\left(1-\theta^0\right)w_{ne}} \tag{D16}$$

Again, $\frac{a_n(t)}{dt} + \frac{D_s n^2\pi^2}{w_{ne}^2} a_n(t) = b_n(t)$

$$a_n(t) = a_n(0)\,\ell^{-\frac{D_s n^2\pi^2}{w_{ne}^2}(t-t_0)} + \int_0^t \ell^{-\frac{D_s n^2\pi^2}{w_{ne}^2}(t-t_0)} b_n(s)\,ds, \text{ since } a_n(0) = C_n$$

$$a_n(t) = \left(C_n - \frac{b_n(t)w_{ne}^2}{D_s n^2\pi^2}\right)\ell^{-\frac{Dn^2\pi^2}{w_{ne}^2}(t-t_0)} + \frac{b_n(t)w_{ne}^2}{D_s n^2\pi^2} \tag{D17}$$

Recall also that $C_n = \frac{2}{w_{ne}}\int_0^{w_{ne}} C^0\,(x,t)\,Cos\left(\frac{n\pi x}{w_{ne}}\right)dx$.

Integrating $C_n = \frac{2}{w_{ne}}\int_0^{w_{ne}} C^0\,(x,t)\,Cos\left(\frac{n\pi x}{w_{ne}}\right)dx$ twice with respect to x, we obtain

$$C_n = \frac{2w_{ne}C^0(-1)^n}{\pi^2 n^2} \qquad \text{D18}$$

Note again that $b_0(t) = \frac{1}{w_{ne}}\int_0^{w_{ne}}\left(\frac{J_{Cell}}{D_s(1-\theta^0)}\right)dx$

Integrating the above, we obtain

$$b_0(t) = \frac{1}{w_{ne}}\left[\frac{J_{Cell}}{D_s(1-\theta^0)}\right]_0^{w_{ne}} = \frac{1}{w_{ne}}\left[\frac{J_{Cell}}{D_s(1-\theta^0)} - 0\right] = \frac{J_{Cell}}{D_s(1-\theta^0)}$$

$$b_0(t) = \frac{J_{Cell}}{D_s(1-\theta^0)} \qquad \text{D19}$$

And again $b_n(t) = \frac{2}{w_{ne}}\int_0^{w_{ne}}\left(\frac{J_{Cell}}{D_s(1-\theta^0)}\right) Cos\left(\frac{n\pi x}{w_{ne}}\right)dx$, $n = 1,2,3..$

Integrating $b_n(t) = \frac{2}{w_{ne}}\int_0^{w_{ne}}\left(\frac{J_{Cell}}{D_s(1-\theta^0)}\right) Cos\left(\frac{n\pi x}{w_{ne}}\right)dx$, $n = 1,2,3..$ twice with respect to x, we obtain:

$$b_n(t) = \frac{2w_{ne}(-1)^n}{n^2\pi^2}\left(\frac{J_{Cell}}{D_s(1-\theta^0)}\right) \qquad \text{D20}$$

Substituting equation D18 and D20 into equation D17, we obtain

$$a_n(t) = \left(\frac{2w_{ne}C^0(-1)^n}{\pi^2 n^2} - \frac{2w_{ne}^3(-1)^n}{n^2\pi^2}\left(\frac{J_{Cell}}{n^2\pi^2 D_s(1-\theta^0)D_s}\right)\right)\ell^{-\frac{D_s n^2\pi^2}{w_{ne}^2}(t-t_0)} + \frac{2w_{ne}^3(-1)^n}{n^2\pi^2}$$
$$\left(\frac{J_{Cell}}{n^2\pi^2 D_s(1-\theta^0)D_s}\right) \qquad \text{D21}$$

Again, substituting equation D19 into equation D16, we obtain:

$$a_0(t) = C^0 + \frac{J_{Cell}\ t}{D_s(1-\theta^0)} - \frac{J_{Cell}\ t}{D_s(1-\theta^0)w_{ne}} \qquad \text{D22}$$

Substituting equation D21and D22 into equation D8, we obtain:

$$C_s(x,t) = C^0 + \frac{J_{Cell}\ t}{D_s\left(1-\theta^0\right)} - \frac{J_{Cell}\ t}{D_s\left(1-\theta^0\right)w_{ne}} +$$

$$\sum_{n=1}^{\infty}\left(\left(\frac{2w_{ne}C^0(-1)^n}{\pi^2 n^2} - \frac{2w_{ne}^3(-1)^n J_{Cell}}{D_s\left(1-\theta^0\right)D_s n^4\pi^4}\right)\ell^{-\frac{D_s n^2\pi^2}{w_{ne}^2}(t-t_0)} + \frac{2w_{ne}^3(-1)^n J_{Cell}}{D_s\left(1-\theta^0\right)D_s n^4\pi^4}\right)Cos\left(\frac{n\pi x}{w_{ne}}\right)$$

$$C_s(x,t) = C^0 + \frac{J_{Cell}}{D_s\left(1-\theta^0\right)}\left\{\left(1-\frac{1}{w_{ne}}\right)t + \frac{2w_{ne}^3}{\pi^2}\right.$$

$$\left.\sum_{n=1}^{\infty}\left(\left(\frac{D_s\left(1-\theta^0\right)}{J_{Cell}}\frac{C^0(-1)^n}{w_{ne}^2 n^2} - \frac{(-1)^n}{D_s n^4\pi^2}\right)\ell^{-\frac{D_s n^2\pi^2}{w_{ne}^2}(t-t_0)} + \frac{(-1)^n}{D_s n^4\pi^2}\right)Cos\left(\frac{n\pi x}{w_{ne}}\right)\right\} \qquad \text{D23}$$

Appendix E

Numerical solutions of the models for EDLCs without self-discharge effects

Finite difference scheme for Crank-Nicolson Method

$$\frac{\partial \varphi_{ne}(x,t)}{\partial t} = \beta^2 \frac{\partial^2 \varphi_{ne}(x,t)}{\partial x^2} + \frac{J_{VR}(x,t)}{C_V} \quad \text{E1}$$

$$\frac{\partial \varphi(x,t)}{\partial t} = \frac{\varphi_i^{n+1} - \varphi_i^n}{\Delta t} \quad \text{E2}$$

$$\frac{\partial^2 \varphi(x,t)}{\partial x^2} = \frac{1}{2} \frac{\left(\varphi_{i+1}^{n+1} - 2\varphi_i^{n+1} + \varphi_{i-1}^{n+1}\right) + \left(\varphi_{i+1}^{n} - 2\varphi_i^{n} + \varphi_{i-1}^{n}\right)}{(\Delta x)^2} \quad \text{E3}$$

The boundary conditions are

$$\frac{\partial \varphi(x=0,t)}{\partial x} = \frac{\varphi_{i+1}^{n+1} - \varphi_{i-1}^{n}}{2\Delta x}, \Rightarrow \frac{\varphi_{i+1}^{n+1} - \varphi_{i-1}^{n}}{2\Delta x} = \frac{-J_0}{\alpha_1}, \Rightarrow \frac{\varphi_2^{n+1} - \varphi_0^{n}}{2\Delta x} = \frac{J_0}{\alpha_1} \; at \quad i = 1 \quad \text{E4}$$

$$\frac{\partial \varphi(x=w,t)}{\partial x} = \frac{\varphi_{i+1}^{n+1} - \varphi_{i-1}^{n}}{2\Delta x}, \Rightarrow \frac{\varphi_{i+1}^{n+1} - \varphi_{i-1}^{n}}{2\Delta x} = \frac{J_0}{\alpha_2}, \Rightarrow \frac{\varphi_{nx+1}^{n+1} - \varphi_{nx-1}^{n}}{2\Delta x} = -\frac{J_0}{\alpha_2} \; at \quad i = nx \quad \text{E5}$$

Substitute equations E2 and E3 into equation E1 while assuming self-discharge to be zero ($\frac{J_{VR}(x,t)}{C_V} = 0$), we obtain:

$$\frac{\varphi_i^{n+1} - \varphi_i^n}{\Delta t} = \frac{\beta^2}{2}\left[\frac{\left(\varphi_{i+1}^{n+1} - 2\varphi_i^{n+1} + \varphi_{i-1}^{n+1}\right) + \left(\varphi_{i+1}^{n} - 2\varphi_i^{n} + \varphi_{i-1}^{n}\right)}{(\Delta x)^2}\right] \quad \text{E6}$$

From boundary equations E4 and E5, we obtain:

$$\varphi_{i-1}^{n+1} = \varphi_{i+1}^{n+1} - \frac{2\Delta x J_0}{\alpha_1} \quad \text{E7}$$

$$\varphi_{i-1}^{n} = \varphi_{i+1}^{n} - \frac{2\Delta x J_0}{\alpha_1} \quad \text{E8}$$

$$\varphi_{nx+1}^{n+1} = \varphi_{nx-1}^{n+1} + \frac{2\Delta x J_0}{\alpha_2} \quad \text{E9}$$

$$\varphi_{nx+1}^{n} = \varphi_{nx-1}^{n} + \frac{2\Delta x J_0}{\alpha_2} \quad \text{E10}$$

From equation E6, we obtain;

$$\varphi_i^{n+1} - \frac{r}{2}\left(\varphi_{i+1}^{n+1} - 2\varphi_i^{n+1} + \varphi_{i-1}^{n+1}\right) = \varphi_i^n + \frac{r}{2}\left(\varphi_{i+1}^n - 2\varphi_i^n + \varphi_{i-1}^n\right) \quad \text{E11}$$

$$-r\varphi_{i+1}^{n+1} + (2+2r)\varphi_i^{n+1} - r\varphi_{i-1}^{n+1} = r\varphi_{i+1}^n + (2-2r)\varphi_i^n + r\varphi_{i-1}^n \,, 1 \le n \le nx-1 \quad \text{E12}$$

$$where \quad r = \frac{\Delta t \beta^2}{(\Delta x)^2}$$

Substitute equations E7, E8, E9 and E10 into equations E11 and E12 separately for i and i=nx, and re-arrange to obtain the boundary conditions equations as:

$$2\varphi_i^{n+1} - r\left(2\varphi_{i-1}^{n+1} - 2\varphi_i^{n+1}\right) = 2\varphi_i^n + r\left(\varphi_{i-1}^n - 2\varphi_i^n + j\right) \quad \text{E13}$$

$$2\varphi_{nx}^{n+1} - r\left(k - 2\varphi_{nx}^{n+1} + \varphi_{nx-1}^{n+1}\right) = 2\varphi_{nx}^n + r\left(-2\varphi_{nx}^n + 2\varphi_{nx-1}^n\right) \quad \text{E14}$$

$$-2r\varphi_{i-1}^{n+1} + (2+2r)\varphi_i^{n+1} = 2r\varphi_{i-1}^n + (2-2r)\varphi_i^n - 2jr \quad \text{E15}$$

$$-2r\varphi_{nx-1}^{n+1} + (2+2r)\varphi_{nx}^{n+1} = 2r\varphi_{nx-1}^n + (2-2r)\varphi_{nx}^n + 2kr \quad \text{E16}$$

$$where \; j = \frac{2\Delta x J_0}{\alpha_1} \; and \; k = \frac{2\Delta x J_0}{\alpha_2}$$

Equation E12 can be written in matrix form as:

$$\begin{bmatrix} -r & 2+2r & -r & 0 & \bullet & \bullet & \bullet \\ 0 & -r & 2+2r & -r & \bullet & \bullet & \bullet \\ \bullet & 0 & \bullet & \bullet & \bullet & \bullet & \bullet \\ \bullet & \bullet & \bullet & \bullet & 2+2r & -r & 0 \\ \bullet & \bullet & \bullet & \bullet & -r & 2+2r & -r \end{bmatrix} \begin{bmatrix} \varphi_0^{n+1} \\ \varphi_1^{n+1} \\ \bullet \\ \bullet \\ \bullet \\ \varphi_{nx-1}^{n+1} \\ \varphi_{nx}^{n+1} \end{bmatrix} =$$

$$\begin{bmatrix} r & 2-2r & r & 0 & \bullet & \bullet & \bullet \\ 0 & r & 2-2r & r & \bullet & \bullet & \bullet \\ \bullet & 0 & \bullet & \bullet & \bullet & \bullet & \bullet \\ \bullet & \bullet & \bullet & \bullet & 2-2r & r & 0 \\ \bullet & \bullet & \bullet & \bullet & r & 2-2r & r \end{bmatrix} \begin{bmatrix} \varphi_0^n \\ \varphi_1^n \\ \bullet \\ \bullet \\ \bullet \\ \varphi_{nx-1}^n \\ \varphi_{nx}^n \end{bmatrix} \quad \text{E17}$$

This two matrices have nx-1 rows and nx+1 columns, which is a representation of the nx-1 equations and nx+1 unknowns. The two remaining equations come from the boundary conditions.

Using the boundary conditions equations E15 and E16, we can write a system of equations in the form:

$$A_i^{n+1}\varphi_i^{n+1} + a_i^{n+1} = A_i^n\varphi_i^n + a_i^n \quad \text{E18}$$

where A_i^{n+1} and A_i^n are known square matrices; and a_i^{n+1} and a_i^n are known vectors , where the details of the boundary conditions have been fully incorporated. In this case, we write:

$$\begin{bmatrix} -r & 2+2r & -r & 0 & \bullet & \bullet & \bullet \\ 0 & -r & 2+2r & -r & \bullet & \bullet & \bullet \\ \bullet & 0 & \bullet & \bullet & \bullet & \bullet & \bullet \\ \bullet & \bullet & \bullet & \bullet & 2+2r & -r & 0 \\ \bullet & \bullet & \bullet & \bullet & -r & 2+2r & -r \end{bmatrix} \begin{bmatrix} \varphi_0^{n+1} \\ \varphi_1^{n+1} \\ \bullet \\ \bullet \\ \bullet \\ \varphi_{nx-1}^{n+1} \\ \varphi_{nx}^{n+1} \end{bmatrix} \text{ as}$$

$$\begin{bmatrix} 2+2r & 0 & 0 & \bullet & 0 & 0 & 0 \\ -r & 2+2r & -r & \bullet & 0 & 0 & 0 \\ 0 & -r & 2+2r & \bullet & 0 & 0 & 0 \\ \bullet & \bullet & \bullet & \bullet & \bullet & \bullet & \bullet \\ 0 & 0 & 0 & \bullet & 2+2r & -r & 0 \\ 0 & 0 & 0 & \bullet & -r & 2+2r & -r \\ 0 & 0 & 0 & \bullet & 0 & -2r & 2+2r \end{bmatrix} \begin{bmatrix} \varphi_1^{n+1} \\ \varphi_2^{n+1} \\ \varphi_3^{n+1} \\ \bullet \\ \varphi_{nx-2}^{n+1} \\ \varphi_{nx-1}^{n+1} \\ \varphi_{nx}^{n+1} \end{bmatrix} + \begin{bmatrix} -2r\varphi_0^{n+1} - rj \\ 0 \\ 0 \\ \bullet \\ 0 \\ 0 \\ -rk \end{bmatrix} =$$

$$A_i^{n+1}\varphi_i^{n+1} + a_i^{n+1} \qquad \text{E19}$$

and similarly

$$\begin{bmatrix} 2-2r & 0 & 0 & \bullet & 0 & 0 & 0 \\ r & 2-2r & r & \bullet & 0 & 0 & 0 \\ 0 & r & 2-2r & \bullet & 0 & 0 & 0 \\ \bullet & \bullet & \bullet & \bullet & \bullet & \bullet & \bullet \\ 0 & 0 & 0 & \bullet & 2-2r & r & 0 \\ 0 & 0 & 0 & \bullet & r & 2-2r & r \\ 0 & 0 & 0 & \bullet & 0 & 2r & 2-2r \end{bmatrix} \begin{bmatrix} \varphi_1^{n} \\ \varphi_2^{n} \\ \varphi_3^{n} \\ \bullet \\ \varphi_{nx-2}^{n} \\ \varphi_{nx-1}^{n} \\ \varphi_{nx}^{n} \end{bmatrix} + \begin{bmatrix} 2r\varphi_0^{n} + rj \\ 0 \\ 0 \\ \bullet \\ 0 \\ 0 \\ rk \end{bmatrix} =$$

$$A_i^{n}\varphi_i^{n} + a_i^{n} \qquad \text{E20}$$

Equation E18 is then written as

$$A_i^{n+1}\varphi_i^{n+1} = a_i^{n} - a_i^{n+1} + A_i^{n}\varphi_i^{n} \qquad \text{E21}$$

$$\begin{bmatrix} 2+2r & 0 & 0 & \bullet & 0 & 0 & 0 \\ -r & 2+2r & -r & \bullet & 0 & 0 & 0 \\ 0 & -r & 2+2r & \bullet & 0 & 0 & 0 \\ \bullet & \bullet & \bullet & \bullet & \bullet & \bullet & \bullet \\ 0 & 0 & 0 & \bullet & 2+2r & -r & 0 \\ 0 & 0 & 0 & \bullet & -r & 2+2r & -r \\ 0 & 0 & 0 & \bullet & 0 & -2r & 2+2r \end{bmatrix} \begin{bmatrix} \varphi_1^{n+1} \\ \varphi_2^{n+1} \\ \varphi_3^{n+1} \\ \bullet \\ \varphi_{nx-2}^{n+1} \\ \varphi_{nx-1}^{n+1} \\ \varphi_{nx}^{n+1} \end{bmatrix} =$$

$$\begin{bmatrix} 2-2r & 0 & 0 & \bullet & 0 & 0 & 0 \\ r & 2-2r & r & \bullet & 0 & 0 & 0 \\ 0 & r & 2-2r & \bullet & 0 & 0 & 0 \\ \bullet & \bullet & \bullet & \bullet & \bullet & \bullet & \bullet \\ 0 & 0 & 0 & \bullet & 2-2r & r & 0 \\ 0 & 0 & 0 & \bullet & r & 2-2r & r \\ 0 & 0 & 0 & \bullet & 0 & 2r & 2-2r \end{bmatrix} \begin{bmatrix} \varphi_1^{n} \\ \varphi_2^{n} \\ \varphi_3^{n} \\ \bullet \\ \varphi_{nx-2}^{n} \\ \varphi_{nx-1}^{n} \\ \varphi_{nx}^{n} \end{bmatrix} + \begin{bmatrix} 2r\left(\varphi_0^{n+1} + \varphi_0^{n} + j\right) \\ 0 \\ 0 \\ \bullet \\ 0 \\ 0 \\ 2rk \end{bmatrix} \qquad \text{E22}$$

$$\text{Andfinally } \varphi_i^{n+1} = \left(A_i^{n+1}\right)^{-1}\left(a_i^{n} - a_i^{n+1} + A_i^{n}\varphi_i^{n}\right) \qquad \text{E23}$$

But the matrix inversion is very time consuming and computationally inefficient. The matrix A_i^{n+1} is tridiagonal and can be decomposed into the product of two other matrices such that A=LU

$$\begin{bmatrix} 2+2r & 0 & 0 & \bullet & 0 & 0 & 0 \\ -r & 2+2r & -r & \bullet & 0 & 0 & 0 \\ 0 & -r & 2+2r & \bullet & 0 & 0 & 0 \\ \bullet & \bullet & \bullet & \bullet & \bullet & \bullet & \bullet \\ 0 & 0 & 0 & \bullet & 2+2r & -r & 0 \\ 0 & 0 & 0 & \bullet & -r & 2+2r & -r \\ 0 & 0 & 0 & \bullet & 0 & -2r & 2+2r \end{bmatrix} = \begin{bmatrix} 1 & 0 & 0 & 0 & 0 & 0 & 0 \\ l_2 & 1 & 0 & 0 & 0 & 0 & 0 \\ 0 & l_3 & 1 & \bullet & 0 & 0 & 0 \\ 0 & 0 & l_4 & \bullet & 0 & 0 & 0 \\ 0 & 0 & 0 & \bullet & 1 & 0 & 0 \\ 0 & 0 & 0 & 0 & l_{nx-2} & 1 & 0 \\ 0 & 0 & 0 & 0 & 0 & l_{nx-1} & 1 \end{bmatrix}$$

$$\begin{bmatrix} d_1 & p_1 & 0 & 0 & 0 & 0 & 0 \\ 0 & d_2 & p_2 & 0 & 0 & 0 & 0 \\ 0 & 0 & d_3 & \bullet & 0 & 0 & 0 \\ 0 & 0 & 0 & \bullet & p_{nx-4} & 0 & 0 \\ 0 & 0 & 0 & \bullet & d_{nx-2} & p_{nx-3} & 0 \\ 0 & 0 & 0 & 0 & 0 & d_{nx-1} & p_{nx-2} \\ 0 & 0 & 0 & 0 & 0 & 0 & d_{nx} \end{bmatrix} \qquad \text{E24}$$

where $d_1=2+2r$, $l_n d_{n-1}=p_{n-1}=-r$ and $d_n=2+2r-l_n p^{n-1}$ for $2 \le n \le nx-1$.

Notice that we work from n=1 to n= nx sequentially.

Let $A_i^{n+1}\varphi_i^{n+1} = A\varphi \; and \; a_i^n - a_i^{n+1} + A_i^n\varphi_i^n = q, then \; A\varphi = q$, $LU\varphi = q$, $Lw = q$, $U\varphi = w$

First step gives:

$w_1=q_1$ and $w_n = q_n - l_n w_{n-1} \quad for \quad 2 \le n \le n_{x-1}$.

Second step involves working backwards from n=nx-2 to n=1:

$$\varphi_{nx-1} = \frac{w_{nx-1}}{d_{nx-1}} \quad and \quad \varphi_n = \frac{w_n - p_n\varphi_{n+1}}{d_n} \quad for \quad n_{x-2} \ge 2 \ge 1$$

Appendix F

Numerical solutions of the models for EDLCs with self-discharge effects

Substitute equations E2 and E3 into equation E1, we obtain with self-discharge term:

$$\frac{\varphi_i^{n+1}-\varphi_i^n}{\Delta t}=\frac{\beta^2}{2}\left[\frac{\left(\varphi_{i+1}^{n+1}-2\varphi_i^{n+1}+\varphi_{i-1}^{n+1}\right)+\left(\varphi_{i+1}^{n}-2\varphi_i^{n}+\varphi_{i-1}^{n}\right)}{(\Delta x)^2}\right]+\frac{J_{VRi}^n}{C_V} \qquad \text{F1}$$

From equation E22, we obtain;

$$\varphi_i^{n+1}-\frac{r}{2}\left(\varphi_{i+1}^{n+1}-2\varphi_i^{n+1}+\varphi_{i-1}^{n+1}\right)=\varphi_i^n+\frac{r}{2}\left(\varphi_{i+1}^{n}-2\varphi_i^{n}+\varphi_{i-1}^{n}\right)+\frac{\Delta t J_{VRi}^n}{C_V} \qquad \text{F2}$$

$$-r\varphi_{i+1}^{n+1}+(2+2r)\varphi_i^{n+1}-r\varphi_{i-1}^{n+1}=r\varphi_{i+1}^{n}+(2-2r)\varphi_i^{n}+r\varphi_{i-1}^{n}+\frac{\Delta t J_{VRi}^n}{C_V},\ 1\le n\le nx-1 \qquad \text{F3}$$

$$where \quad r=\frac{\Delta t\beta^2}{(\Delta x)^2}$$

Substitute equations E7, E8, E9 and E10 into equations F2 and F3 separately for i and i=nx, and re-arrange to obtain the boundary conditions equations as:

$$2\varphi_i^{n+1}-r\left(2\varphi_{i+1}^{n+1}-2\varphi_i^{n+1}+\varphi_{i-1}^{n+1}\right)=2\varphi_i^n+r\left(\varphi_{i+1}^{n}-2\varphi_i^{n}+j\right)+s\,J_{VRi}^n \qquad \text{F4}$$

$$2\varphi_{nx}^{n+1}-r\left(k-2\varphi_{nx}^{n+1}+\varphi_{nx-1}^{n+1}\right)=2\varphi_{nx}^n+r\left(\varphi_{nx+1}^{n}-2\varphi_{nx}^{n}+\varphi_{nx-1}^{n}\right)+s\,J_{VRnx}^n \qquad \text{F5}$$

or

$$-2r\varphi_{i+1}^{n+1}+(2+2r)\varphi_i^{n+1}=2r\varphi_{i+1}^{n}+(2-2r)\varphi_i^{n}-2jr+s\,J_{VRi}^n \qquad \text{F6}$$

$$-2r\varphi_{nx-1}^{n+1}+(2+2r)\varphi_{nx}^{n+1}=2r\varphi_{nx-1}^{n}+(2-2r)\varphi_{nx}^{n}+2kr+s\,J_{VRnx}^n \qquad \text{F7}$$

$$where\ j=\frac{2\Delta x J_0}{\alpha_1}\ and\ k=\frac{2\Delta x J_0}{\alpha_2},\ s=\frac{\Delta t}{C_V}.$$

Equation F6 can be written in matrix form as:

$$\begin{bmatrix} -r & 2+2r & -r & 0 & \bullet & \bullet & \bullet \\ 0 & -r & 2+2r & -r & \bullet & \bullet & \bullet \\ \bullet & 0 & \bullet & \bullet & \bullet & \bullet & \bullet \\ \bullet & \bullet & \bullet & \bullet & 2+2r & -r & 0 \\ \bullet & \bullet & \bullet & \bullet & -r & 2+2r & -r \end{bmatrix} \begin{bmatrix} \varphi_0^{n+1} \\ \varphi_1^{n+1} \\ \bullet \\ \bullet \\ \bullet \\ \varphi_{nx-1}^{n+1} \\ \varphi_{nx}^{n+1} \end{bmatrix} =$$

$$\begin{bmatrix} r & 2-2r & r & 0 & \bullet & \bullet & \bullet \\ 0 & r & 2-2r & r & \bullet & \bullet & \bullet \\ \bullet & 0 & \bullet & \bullet & \bullet & \bullet & \bullet \\ \bullet & \bullet & \bullet & \bullet & 2-2r & r & 0 \\ \bullet & \bullet & \bullet & \bullet & r & 2-2r & r \end{bmatrix} \begin{bmatrix} \varphi_0^n \\ \varphi_1^n \\ \bullet \\ \bullet \\ \bullet \\ \varphi_{nx-1}^n \\ \varphi_{nx}^n \end{bmatrix} + b \begin{bmatrix} J_{VR0}^n \\ J_{VR1}^n \\ \bullet \\ \bullet \\ \bullet \\ J_{VRnx-1}^n \\ J_{VRnx}^n \end{bmatrix} \qquad \text{F8}$$

These two matrices have nx-1 rows and nx+1 column, which is a representation of the nx-1 equations and nx+1 unknown. The two remaining equations come from the boundary conditions. Using the boundary conditions equations F6 and F7, we can write a system of equations in the form:

$$A_i^{n+1}\varphi_i^{n+1} + a_i^{n+1} = A_i^n\varphi_i^n + a_i^n + bJ_{VRi}^n \qquad \text{F9}$$

where A_i^{n+1} and A_i^n are known square matrices; b is a constant; and a_i^{n+1}, a_i^n and J_{VRi}^n are known vectors , where the details of the boundary conditions have been fully incorporated. In this case, we write:

$$\begin{bmatrix} -r & 2+2r & -r & 0 & \bullet & \bullet & \bullet \\ 0 & -r & 2+2r & -r & \bullet & \bullet & \bullet \\ \bullet & 0 & \bullet & \bullet & \bullet & \bullet & \bullet \\ \bullet & \bullet & \bullet & \bullet & 2+2r & -r & 0 \\ \bullet & \bullet & \bullet & \bullet & -r & 2+2r & -r \end{bmatrix} \begin{bmatrix} \varphi_0^{n+1} \\ \varphi_1^{n+1} \\ \bullet \\ \bullet \\ \bullet \\ \varphi_{nx-1}^{n+1} \\ \varphi_{nx}^{n+1} \end{bmatrix} \quad \text{as}$$

$$\begin{bmatrix} 2+2r & 0 & 0 & \bullet & 0 & 0 & 0 \\ -r & 2+2r & -r & \bullet & 0 & 0 & 0 \\ 0 & -r & 2+2r & \bullet & 0 & 0 & 0 \\ \bullet & \bullet & \bullet & \bullet & \bullet & \bullet & \bullet \\ 0 & 0 & 0 & \bullet & 2+2r & -r & 0 \\ 0 & 0 & 0 & \bullet & -r & 2+2r & -r \\ 0 & 0 & 0 & \bullet & 0 & -2r & 2+2r \end{bmatrix} \begin{bmatrix} \varphi_1^{n+1} \\ \varphi_2^{n+1} \\ \varphi_3^{n+1} \\ \bullet \\ \varphi_{nx-2}^{n+1} \\ \varphi_{nx-1}^{n+1} \\ \varphi_{nx}^{n+1} \end{bmatrix} + \begin{bmatrix} -2r\varphi_0^{n+1} - rj \\ 0 \\ 0 \\ \bullet \\ 0 \\ 0 \\ -rk \end{bmatrix} =$$

$$A_i^{n+1}\varphi_i^{n+1} + a_i^{n+1} \qquad \text{F10}$$

and similarly

$$\begin{bmatrix} 2-2r & 0 & 0 & \bullet & 0 & 0 & 0 \\ r & 2-2r & r & \bullet & 0 & 0 & 0 \\ 0 & r & 2-2r & \bullet & 0 & 0 & 0 \\ \bullet & \bullet & \bullet & \bullet & \bullet & \bullet & \bullet \\ 0 & 0 & 0 & \bullet & 2-2r & r & 0 \\ 0 & 0 & 0 & \bullet & r & 2-2r & r \\ 0 & 0 & 0 & \bullet & 0 & 2r & 2-2r \end{bmatrix} \begin{bmatrix} \varphi_1^n \\ \varphi_2^n \\ \varphi_3^n \\ \bullet \\ \varphi_{nx-2}^n \\ \varphi_{nx-1}^n \\ \varphi_{nx}^n \end{bmatrix} + \begin{bmatrix} 2r\varphi_0^n + rj \\ 0 \\ 0 \\ \bullet \\ 0 \\ 0 \\ rk \end{bmatrix} + \text{b} \begin{bmatrix} J_{VR0}^n \\ J_{VR1}^n \\ \bullet \\ \bullet \\ \bullet \\ J_{VRnx-1}^n \\ J_{VRnx}^n \end{bmatrix} =$$

$$A_i^n \varphi_i^n + a_i^n + bJ_{VRi}^n \qquad \text{F11}$$

Equation F9 is then written as

$$A_i^{n+1} \varphi_i^{n+1} = a_i^n - a_i^{n+1} + A_i^n \varphi_i^n + bJ_{VRi}^n \qquad \text{F12}$$

$$\begin{bmatrix} 2+2r & 0 & 0 & \bullet & 0 & 0 & 0 \\ -r & 2+2r & -r & \bullet & 0 & 0 & 0 \\ 0 & -r & 2+2r & \bullet & 0 & 0 & 0 \\ \bullet & \bullet & \bullet & \bullet & \bullet & \bullet & \bullet \\ 0 & 0 & 0 & \bullet & 2+2r & -r & 0 \\ 0 & 0 & 0 & \bullet & -r & 2+2r & -r \\ 0 & 0 & 0 & \bullet & 0 & -2r & 2+2r \end{bmatrix} \begin{bmatrix} \varphi_1^{n+1} \\ \varphi_2^{n+1} \\ \varphi_3^{n+1} \\ \bullet \\ \varphi_{nx-2}^{n+1} \\ \varphi_{nx-1}^{n+1} \\ \varphi_{nx}^{n+1} \end{bmatrix} =$$

$$\begin{bmatrix} 2-2r & 0 & 0 & \bullet & 0 & 0 & 0 \\ r & 2-2r & r & \bullet & 0 & 0 & 0 \\ 0 & r & 2-2r & \bullet & 0 & 0 & 0 \\ \bullet & \bullet & \bullet & \bullet & \bullet & \bullet & \bullet \\ 0 & 0 & 0 & \bullet & 2-2r & r & 0 \\ 0 & 0 & 0 & \bullet & r & 2-2r & r \\ 0 & 0 & 0 & \bullet & 0 & 2r & 2-2r \end{bmatrix} \begin{bmatrix} \varphi_1^n \\ \varphi_2^n \\ \varphi_3^n \\ \bullet \\ \varphi_{nx-2}^n \\ \varphi_{nx-1}^n \\ \varphi_{nx}^n \end{bmatrix} + \begin{bmatrix} 2r\left(\varphi_0^{n+1} + \varphi_0^n + j\right) \\ 0 \\ 0 \\ \bullet \\ 0 \\ 0 \\ 2rk \end{bmatrix} + \text{b}$$

$$\begin{bmatrix} J_{VR0}^n \\ J_{VR1}^n \\ \bullet \\ \bullet \\ \bullet \\ J_{VRnx-1}^n \\ J_{VRnx}^n \end{bmatrix} \qquad \text{F13}$$

and finally $\varphi_i^{n+1} = \left(A_i^{n+1}\right)^{-1}\left(a_i^n - a_i^{n+1} + A_i^n \varphi_i^n + bJ_{VRi}^n\right)$ F14

But the matrix inversion is very time consuming and computationally inefficient. The matrix

A_i^{n+1} is tridiagonal and can be decomposed into the product of two other matrices such that A=LU

$$\begin{bmatrix} 2+2r & 0 & 0 & \bullet & 0 & 0 & 0 \\ -r & 2+2r & -r & \bullet & 0 & 0 & 0 \\ 0 & -r & 2+2r & \bullet & 0 & 0 & 0 \\ \bullet & \bullet & \bullet & \bullet & \bullet & \bullet & \bullet \\ 0 & 0 & 0 & \bullet & 2+2r & -r & 0 \\ 0 & 0 & 0 & \bullet & -r & 2+2r & -r \\ 0 & 0 & 0 & \bullet & 0 & -2r & 2+2r \end{bmatrix} = \begin{bmatrix} 1 & 0 & 0 & 0 & 0 & 0 & 0 \\ l_2 & 1 & 0 & 0 & 0 & 0 & 0 \\ 0 & l_3 & 1 & \bullet & 0 & 0 & 0 \\ 0 & 0 & l_4 & \bullet & 0 & 0 & 0 \\ 0 & 0 & 0 & \bullet & 1 & 0 & 0 \\ 0 & 0 & 0 & 0 & l_{nx-2} & 1 & 0 \\ 0 & 0 & 0 & 0 & 0 & l_{nx-1} & 1 \end{bmatrix}$$

$$\begin{bmatrix} d_1 & p_1 & 0 & 0 & 0 & 0 & 0 \\ 0 & d_2 & p_2 & 0 & 0 & 0 & 0 \\ 0 & 0 & d_3 & \bullet & 0 & 0 & 0 \\ 0 & 0 & 0 & \bullet & p_{nx-4} & 0 & 0 \\ 0 & 0 & 0 & \bullet & d_{nx-2} & p_{nx-3} & 0 \\ 0 & 0 & 0 & 0 & 0 & d_{nx-1} & p_{nx-2} \\ 0 & 0 & 0 & 0 & 0 & 0 & d_{nx} \end{bmatrix} \qquad \text{F15}$$

where $d_1 = 2+2r$, $l_n d_{n-1} = p_{n-1} = -r$ and $d_n = 2+2r-l_n p_{n-1}$ *for* $2 \le n \le nx-1$.

Notice that we work from $n=1$ *to* $n=nx$ sequentially.

Let $A_i^{n+1}\varphi_i^{n+1} = A\varphi$ *and* $a_i^n - a_i^{n+1} + A_i^n\varphi_i^n = q$, *then* $A\varphi = q$, $LU\varphi = q$, $Lw = q$, $U\varphi = w$

First step gives:

$w_1=q_1$ and $w_n = q_n - l_n w_{n-1}$ *for* $2 \le n \le n_{x-1}$.

Second step involves working backwards from $n = nx-2$ *to* $n=1$:

$$\varphi_{nx-1} = \frac{w_{nx-1}}{d_{nx-1}} \quad and \quad \varphi_n = \frac{w_n - p_n\varphi_{n+1}}{d_n} \quad for \quad n_{x-2} \ge 2 \ge 1$$

Appendix G

Numerical solutions of the models with composite electrode and self-discharge effects

$$\frac{\partial \varphi_{ne}(x,t)}{\partial t} = \beta^2 \frac{\partial^2 \varphi_{ne}(x,t)}{\partial x^2} - \frac{S_f J_f(x,t)}{C_V} - \gamma \frac{\partial^2 (\ln C(x,t))}{\partial x^2} + \frac{J_{VR}(x,t)}{C_V} \quad \text{G1}$$

$$\beta^2 = \frac{\alpha_1 \alpha_2}{C_V(\alpha_2 + \alpha_1)} \quad \text{G2}$$

$$\gamma = \frac{\sigma_{ne}^l RT}{C_V F}\left(\frac{s_+}{n\nu_+} + \frac{t_+^0}{z_+ \nu_+}\right) \quad \text{G3}$$

$$J_f(x,t) = i_0\{\exp[\alpha_a f \varphi_{ne}(x,t) - U_1] - \exp[-\alpha_c f \varphi_{ne}(x,t) - U_1]\} \quad \text{G4}$$

$$J_{VR}(x,t) = J_{VR} + J_{VR1}(t) = \frac{eZN}{w_{sp}\left(\frac{s_+ + s_-}{s_+ s_-} + \frac{D_+ + D_-}{D_+ D_-}\right)} + \frac{\frac{8nFVD_{Ox}C_{Ox}}{l^2}\exp\left(\frac{-\pi^2 D_{Ox} t}{l^2}\right)}{A} \quad \text{G5}$$

$$J_{VR} = \frac{eZN}{w_{sp}\left(\frac{s_+ + s_-}{s_+ s_-} + \frac{D_+ + D_-}{D_+ D_-}\right)} \quad \text{G6}$$

$$J_{VR1}(t) = \frac{\frac{8nFVD_{Ox}C_{Ox}}{l^2}\exp\left(\frac{-\pi^2 D_{Ox} t}{l^2}\right)}{A} \quad \text{G7}$$

$$\frac{\partial \theta(x,t)}{\partial t} = \frac{S_f J_f}{Q_{f,oxd} - Q_{f,red}} \quad \text{G8}$$

$$where\ f = \frac{F}{RT}$$

$$\frac{\partial C_s(x,t)}{\partial t} = D_s \frac{\partial^2 C_s(x,t)}{\partial x^2} + \frac{S_d C_d (1 - t_+^0)}{2\varepsilon F}\frac{\partial \varphi_{ne}(x,t)}{\partial t} + \frac{S_f (1 - t_+^0)}{2\varepsilon F} J_f(x,t) \quad \text{G9}$$

The boundary conditions of this task during the capacitor discharge are as follows:

$$J_1(0,t) = -\alpha_1 \frac{\partial \varphi_{ne}(x,t)}{\partial x}\Big|_{x=0} = J_0 \qquad \text{G10}$$

$$J_2(w,t) = \alpha_2 \frac{\partial \varphi_{ne}(x,t)}{\partial x}\Big|_{x=w_{ne}} = J_0 \qquad \text{G11}$$

$$\frac{\partial C(x,t)}{\partial x}\Big|_{x=0} = 0 \qquad \text{G12}$$

$$\frac{\partial C(x,t)}{\partial x}\Big|_{x=w} = \frac{\left(1-t_+^0\right)J_0}{2\varepsilon_{sp}D_{sp}F} \qquad \text{G13}$$

and the initial condition is as follows:

$$\varphi_{ne}(x,t_{=0}) = \varphi_{ne}^{0^-} - \frac{J_0\, x}{\alpha_1} + \frac{J_0(\alpha_1+\alpha_2)x^2}{2w_{ne}\alpha_1\alpha_2}$$

$$\varphi_{ne}(x_{=0},t_{=0}) = \varphi_{ne}^{0^-} \qquad \text{G14}$$

$$\theta(x.t=0) = 1, \quad C(x,t=0) = C_{so^-} + \frac{\left(1-t_0^+\right)J_0}{2\varepsilon_{sp}D_{ssp}F}\frac{1\,x^2}{2w_{ne}}$$

$$C(x_{=0},t_{=0}) = C_{so^-} \qquad \text{G15}$$

Finite difference scheme for Crank-Nicolson Method

$$\frac{\partial \varphi(x,t)}{\partial t} = \frac{\varphi_i^{n+1} - \varphi_i^n}{\Delta t} \qquad \text{G16}$$

$$\frac{\partial^2 \varphi(x,t)}{\partial x^2} = \frac{1}{2}\frac{\left(\varphi_{i+1}^{n+1} - 2\varphi_i^{n+1} + \varphi_{i-1}^{n+1}\right) + \left(\varphi_{i+1}^{n} - 2\varphi_i^{n} + \varphi_{i-1}^{n}\right)}{(\Delta x)^2} \qquad \text{G17}$$

$$\frac{\partial^2 \ln C(x,t)}{\partial x^2} = \frac{1}{2}\frac{\left(\ln C_{i+1}^{n+1} - 2\ln C_i^{n+1} + \ln C_{i-1}^{n+1}\right) + \left(\ln C_{i+1}^{n} - 2\ln C_i^{n} + \ln C_{i-1}^{n}\right)}{(\Delta x)^2} \qquad \text{G18}$$

$$\varphi(x,t) = \frac{1}{2}\left(\varphi_{i+1}^n + \varphi_i^n\right) \qquad \text{G19}$$

$$\frac{\partial \theta(x,t)}{\partial t} = \frac{\theta_i^{n+1} - \theta_i^n}{\Delta t} \qquad \text{G20}$$

$$\frac{\partial C(x,t)}{\partial t} = \frac{C_i^{n+1} - C_i^n}{\Delta t} \qquad \text{G21}$$

$$\frac{\partial^2 C(x,t)}{\partial x^2} = \frac{1}{2}\frac{\left(C_{i+1}^{n+1} - 2C_i^{n+1} + C_{i-1}^{n+1}\right) + \left(C_{i+1}^{n} - 2C_i^{n} + C_{i-1}^{n}\right)}{(\Delta x)^2} \qquad \text{G22}$$

The boundary conditions equations G10, G11, G12 and G13 are

$$\frac{\partial \varphi(x=0,t)}{\partial x} = \frac{\varphi_{i+1}^{n+1} - \varphi_{i-1}^{n}}{2\Delta x}, \Rightarrow \frac{\varphi_{i+1}^{n+1} - \varphi_{i-1}^{n}}{2\Delta x} = \frac{-J_0}{\alpha_1}, \Rightarrow \frac{\varphi_2^{n+1} - \varphi_0^{n}}{2\Delta x} = \frac{-J_0}{\alpha_1} \; at \quad i=1 \qquad \text{G23}$$

$$\frac{\partial\varphi(x=w,t)}{\partial x}=\frac{\varphi_{i+1}^{n+1}-\varphi_{i-1}^{n}}{2\Delta x},\Rightarrow\frac{\varphi_{i+1}^{n+1}-\varphi_{i-1}^{n}}{2\Delta x}=\frac{J_0}{\alpha_2},\Rightarrow\frac{\varphi_{nx+1}^{n+1}-\varphi_{nx-1}^{n}}{2\Delta x}=\frac{J_0}{\alpha_2}\ at\quad i=nx \tag{G24}$$

$$\frac{\partial C(x=0,t)}{\partial x}=\frac{C_{i+1}^{n+1}-C_{i-1}^{n}}{2\Delta x},\Rightarrow\frac{C_{i+1}^{n+1}-C_{i-1}^{n}}{2\Delta x}=0,\Rightarrow\frac{C_{2}^{n+1}-C_{0}^{n}}{2\Delta x}=0\ at\quad i=1 \tag{G25}$$

$$\frac{\partial C(x=w,t)}{\partial x}=\frac{C_{i+1}^{n+1}-C_{i-1}^{n}}{2\Delta x},\Rightarrow\frac{C_{i+1}^{n+1}-C_{i-1}^{n}}{2\Delta x}=\frac{\left(1-t_+^0\right)J_0}{2\varepsilon_{sp}D_{sp}F},\Rightarrow\frac{C_{nx+1}^{n+1}-C_{nx-1}^{n}}{2\Delta x}=\frac{\left(1-t_+^0\right)J_0}{2\varepsilon_{sp}D_{sp}F} \tag{G26}$$

$at\quad i=nx$

Substitute equations G16, G17 and G18 into G3; equation G20 into G8; and equations G16, G21 and G22 into G9 respectively to obtain:

$$\frac{\varphi_i^{n+1}-\varphi_i^{n}}{\Delta t}=\frac{\beta^2}{2}\left[\frac{\left(\varphi_{i+1}^{n+1}-2\varphi_i^{n+1}+\varphi_{i-1}^{n+1}\right)+\left(\varphi_{i+1}^{n}-2\varphi_i^{n}+\varphi_{i-1}^{n}\right)}{(\Delta x)^2}\right]-\frac{S_f J_{f\,i}^{n}}{C_V}-$$

$$\frac{\gamma}{2}\left[\frac{\left(\ln C_{i+1}^{n+1}-2\ln C_i^{n+1}+\ln C_{i-1}^{n+1}\right)+\left(\ln C_{i+1}^{n}-2\ln C_i^{n}+\ln C_{i-1}^{n}\right)}{(\Delta x)^2}\right]+\frac{J_{VRi}^{n}}{C_V} \tag{G27}$$

$$\frac{\theta_i^{n+1}-\theta_i^{n}}{\Delta t}=b\,J_{f\,i}^{n} \tag{G28}$$

$$\frac{C_i^{n+1}-C_i^{n}}{\Delta t}=\frac{D}{2}\left[\frac{\left(C_{i+1}^{n+1}-2C_i^{n+1}+C_{i-1}^{n+1}\right)+\left(C_{i+1}^{n}-2C_i^{n}+C_{i-1}^{n}\right)}{(\Delta x)^2}\right]+\frac{d\left(\varphi_i^{n+1}-\varphi_i^{n}\right)}{\Delta t}+eJ_{f\,i}^{n} \tag{G29}$$

$$where\quad z=\frac{S_f}{Q_{f,oxd}-Q_{f,red}},\ d=\frac{S_d C_d\left(1-t_+^0\right)}{2\varepsilon F},\ and\quad e=\frac{S_f\left(1-t_+^0\right)}{2\varepsilon F}$$

From the boundary equations G23, G24, G25 and G26, respectively we obtain:

$$\varphi_{i-1}^{n+1}=\varphi_{i+1}^{n+1}-\frac{2\Delta x J_0}{\alpha_1} \tag{G30}$$

$$\varphi_{i-1}^{n}=\varphi_{i+1}^{n}-\frac{2\Delta x J_0}{\alpha_1} \tag{G31}$$

$$\varphi_{nx+1}^{n+1}=\varphi_{nx-1}^{n+1}+\frac{2\Delta x J_0}{\alpha_2} \tag{G32}$$

$$\varphi_{nx+1}^{n}=\varphi_{nx-1}^{n}+\frac{2\Delta x J_0}{\alpha_2} \tag{G33}$$

$$C_{nx+1}^{n+1}=C_{nx-1}^{n}+f_1 2\Delta x J_0 \tag{G34}$$

$$C_{nx+1}^{n}=C_{nx-1}^{n}+f_1 2\Delta x J_0 \tag{G35}$$

$$where\quad f_1=\frac{\left(1-t_+^0\right)}{2\varepsilon_{sp}D_{sp}F}$$

From equations G27, G28 and G29 respectively, we obtain:

$$\varphi_i^{n+1} - \frac{r}{2}\left(\varphi_{i+1}^{n+1} - 2\varphi_i^{n+1} + \varphi_{i-1}^{n+1}\right) + \frac{m}{2}\left(\ln C_{i+1}^{n+1} - 2\ln C_i^{n+1} + \ln C_{i-1}^{n+1}\right) = \varphi_i^n + \frac{r}{2}\left(\varphi_{i+1}^n - 2\varphi_i^n + \varphi_{i-1}^n\right)$$

$$- \frac{m}{2}\left(\ln C_{i+1}^n - 2\ln C_i^n + \ln C_{i-1}^n\right) - u\, J_{f\,i}^n + s\, J_{VRi}^n \qquad \text{G36}$$

$$\theta_i^{n+1} = \theta_i^n + z\Delta t\, J_{f\,i}^n \qquad \text{G37}$$

$$C_i^{n+1} - \frac{\eta}{2}\left(C_{i+1}^{n+1} - 2C_i^{n+1} + C_{i-1}^{n+1}\right) - d\,\varphi_i^{n+1} = C_i^n + \frac{\eta}{2}\left(C_{i+1}^n - 2C_i^n + C_{i-1}^n\right) - d\,\varphi_i^n + e\, J_{f\,i}^n \qquad \text{G38}$$

or

$$-r\varphi_{i+1}^{n+1} + (2+2r)\varphi_i^{n+1} - r\varphi_{i-1}^{n+1} + m\ln C_{i+1}^{n+1} - 2m\ln C_i^{n+1} + m\ln C_{i-1}^{n+1} = r\varphi_{i+1}^n + (2-2r)\varphi_i^n$$

$$+ r\varphi_{i-1}^n - m\ln C_{i+1}^n + 2m\ln C_i^n - m\ln C_{i-1}^{n+1} - u\, J_{f\,i}^n + s\, J_{VRi}^n \qquad \text{G39}$$

$$-\eta C_{i+1}^{n+1} + (2+2\eta)C_i^{n+1} - \eta C_{i-1}^{n+1} - d\,\varphi_i^{n+1} = \eta C_{i+1}^n + (2-2\eta)C_i^n + \eta C_{i-1}^n - d\,\varphi_i^n + e\, J_{f\,i}^n \qquad \text{G40}$$

where $r = \dfrac{\Delta t\beta^2}{(\Delta x)^2}$, $m = \dfrac{\Delta t\gamma}{(\Delta x)^2}$, $\eta = \dfrac{\Delta tD}{(\Delta x)^2}$, $u = \dfrac{\Delta tS_f}{C_V}$, $s = \dfrac{\Delta t}{C_V}$.

Substitute equations G30, G31, G32, G33, G34 and G35 into equations G36 and G37 separately and re-arrange to obtain for i and i=nx:

$$2\varphi_i^{n+1} - r\left(\varphi_{i+1}^{n+1} - 2\varphi_i^{n+1} + \varphi_{i-1}^{n+1}\right) + m\left(\ln C_{i+1}^{n+1} - 2\ln C_i^{n+1} + \ln C_{i-1}^{n+1}\right) = 2\varphi_i^n + r\left(\varphi_{i+1}^n - 2\varphi_i^n + j\right)$$

$$- m\left(\ln C_{i+1}^n - 2\ln C_i^n\right) - u\, J_{f\,i}^n + s\, J_{VRi}^n \qquad \text{G41}$$

$$2\varphi_{nx}^{n+1} - r\left(k - 2\varphi_{nx}^{n+1} + \varphi_{nx-1}^{n+1}\right) + m\left(v - 2\ln C_{nx}^{n+1} + \ln C_{nx-1}^{n+1}\right) = 2\varphi_{nx}^n + r\left(\varphi_{nx+1}^n - 2\varphi_{nx}^n + 2\varphi_{nx-1}^n\right)$$

$$- m\left(\ln C_{i+1}^n - 2\ln C_i^n + \ln C_{i-1}^n\right) - u\, J_{f\,i}^n + s\, J_{VRi}^n \qquad \text{G42}$$

$$2C_i^{n+1} - \eta\left(2C_{i+1}^{n+1} - 2C_i^{n+1} + C_{i-1}^{n+1}\right) - d\,\varphi_i^{n+1} = 2C_i^n + \eta\left(C_{i+1}^n - 2C_i^n\right) - d\,\varphi_i^n + e\, J_{f\,i}^n \qquad \text{G43}$$

$$2C_{nx}^{n+1} - \eta\left(v - 2C_{nx}^{n+1} + C_{nx-1}^{n+1}\right) - d\,\varphi_{nx}^{n+1} = 2C_{nx}^n + \eta\left(C_{nx+1}^n - 2C_{nx}^n + 2C_{nx-1}^n\right) - d\,\varphi_{nx}^n + e\, J_{f\,nx}^n \qquad \text{G44}$$

where $v = f_1 2\Delta x J_0$

Equations G41, G42, G43 and G44 can be re-written as:

$$-2r\varphi_{i-1}^{n+1} + (2+2r)\varphi_i^{n+1} + 2m\ln C_{i-1}^{n+1} - 2m\ln C_i^{n+1} = 2r\varphi_{i-1}^n + (2-2r)\varphi_i^n$$

$$-2j\,r - 2m\ln C_{i-1}^n + 2m\ln C_i^n - u\, J_{f\,i}^n + s\, J_{VRi}^n \qquad \text{G45}$$

$$-2r\varphi_{nx-1}^{n+1} + (2+2r)\varphi_{nx}^{n+1} + 2m\ln C_{nx-1}^{n+1} - 2m\ln C_{nx}^{n+1} = r\varphi_{nx-1}^n + (2-2r)\varphi_{nx}^n$$

$$+ 2k\,r - 2vm - 2m\ln C_{nx-1}^n + 2m\ln C_{nx}^n - u\, J_{f\,nx}^n + s\, J_{VRnx}^n \qquad \text{G46}$$

$$-2\eta C_{i-1}^{n+1}+(2+2\eta)C_i^{n+1}-d\ \varphi_i^{n+1}=2\eta C_{i-1}^{n}+(2-2\eta)C_i^{n}-d\ \varphi_i^{n}+e\,J_{f\,i}^{n} \quad \text{G47}$$

$$-\eta C_{nx-1}^{n+1}+(2+2\eta)C_{nx}^{n+1}-d\ \varphi_{nx}^{n+1}=2\eta C_{nx-1}^{n}+(2-2\eta)C_{nx}^{n}+2vm-d\ \varphi_{nx}^{n}+e\,J_{f\,nx}^{n} \quad \text{G48}$$

$$where\ j=\frac{2\Delta x J_0}{\alpha_1}\quad and\quad k=\frac{2\Delta x J_0}{\alpha_2}$$

From equation G47, we can write in the matrix form that:

$$\begin{bmatrix} r & 2-2r & r & 0 & \bullet & \bullet & \bullet \\ 0 & r & 2-2r & r & \bullet & \bullet & \bullet \\ \bullet & 0 & \bullet & \bullet & \bullet & \bullet & \bullet \\ \bullet & \bullet & \bullet & \bullet & 2-2r & r & 0 \\ \bullet & \bullet & \bullet & \bullet & r & 2-2r & r \end{bmatrix} \begin{bmatrix} \varphi_0^{n+1} \\ \varphi_1^{n+1} \\ \bullet \\ \bullet \\ \bullet \\ \varphi_{nx-1}^{n+1} \\ \varphi_{0nx}^{n+1} \end{bmatrix}$$

$$\begin{bmatrix} -m & 2m & -m & 0 & \bullet & \bullet & \bullet \\ 0 & -m & 2m & -m & \bullet & \bullet & \bullet \\ \bullet & 0 & \bullet & \bullet & \bullet & \bullet & \bullet \\ \bullet & \bullet & \bullet & \bullet & 2r & -m & 0 \\ \bullet & \bullet & \bullet & \bullet & -m & 2r & -m \end{bmatrix} \begin{bmatrix} \ln C_0^{n+1} \\ \ln C_1^{n+1} \\ \bullet \\ \bullet \\ \bullet \\ \ln C_{nx-1}^{n+1} \\ \ln C_{0nx}^{n+1} \end{bmatrix} - u \begin{bmatrix} J_{f0}^{n} \\ J_{f1}^{n} \\ \bullet \\ \bullet \\ \bullet \\ J_{f\,nx-1}^{n+1} \\ J_{f\,nx}^{n+1} \end{bmatrix} + \text{s} \begin{bmatrix} J_{VR0}^{n} \\ J_{VR1}^{n} \\ \bullet \\ \bullet \\ \bullet \\ J_{VR\,nx-1}^{n+1} \\ J_{VR\,nx}^{n+1} \end{bmatrix} \quad \text{G49}$$

Also, we can write from equation G48 in matrix form as:

$$\begin{bmatrix} -\eta & 2+2\eta & -\eta & 0 & \bullet & \bullet & \bullet \\ 0 & -\eta & 2+2\eta & -\eta & \bullet & \bullet & \bullet \\ \bullet & 0 & \bullet & \bullet & \bullet & \bullet & \bullet \\ \bullet & \bullet & \bullet & \bullet & 2+2\eta & -\eta & 0 \\ \bullet & \bullet & \bullet & \bullet & -\eta & 2+2\eta & -\eta \end{bmatrix} \begin{bmatrix} C_0^{n+1} \\ C_1^{n+1} \\ \bullet \\ \bullet \\ \bullet \\ C_{nx-1}^{n+1} \\ C_{nx}^{n+1} \end{bmatrix} + \text{d} \begin{bmatrix} \varphi_0^{n+1} \\ \varphi_1^{n+1} \\ \bullet \\ \bullet \\ \bullet \\ \varphi_{nx-1}^{n+1} \\ \varphi_{nx}^{n+1} \end{bmatrix} =$$

$$\begin{bmatrix} \eta & 2-2\eta & \eta & 0 & \bullet & \bullet & \bullet \\ 0 & \eta & 2-2\eta & \eta & \bullet & \bullet & \bullet \\ \bullet & 0 & \bullet & \bullet & \bullet & \bullet & \bullet \\ \bullet & \bullet & \bullet & \bullet & 2-2\eta & \eta & 0 \\ \bullet & \bullet & \bullet & \bullet & \eta & 2-2\eta & \eta \end{bmatrix} \begin{bmatrix} C_0^{n} \\ C_1^{n} \\ \bullet \\ \bullet \\ \bullet \\ C_{nx-1}^{n} \\ C_{nx}^{n} \end{bmatrix} - d \begin{bmatrix} \varphi_0^{n} \\ \varphi_1^{n} \\ \bullet \\ \bullet \\ \bullet \\ \varphi_{nx-1}^{n} \\ \varphi_{nx}^{n} \end{bmatrix} + \text{e} \begin{bmatrix} J_{f0}^{n} \\ J_{f1}^{n} \\ \bullet \\ \bullet \\ \bullet \\ J_{f\,nx-1}^{n} \\ J_{f\,nx}^{n} \end{bmatrix} \quad \text{G50}$$

Using the boundary conditions equations G45, G46, G47 and G48, we can write system of equations for equations G49 and G50 respectively in the form:

$$A_i^{n+1}\varphi_i^{n+1} + a_i^{n+1} + G_i^{n+1}\ln C_i^{n+1} + g_i^{n+1} = B_i^n\varphi_i^n + b_i^n + H_i^n \ln C_i^n + h_i^n - u\, J_{f\,i}^n + s\, J_{VR\,i}^n \qquad \text{G51}$$

$$Q_i^{n+1}C_i^{n+1} + q_i^{n+1} + d\ \varphi_i^{n+1} = V_i^n C_i^n + v_i^n - d\ \varphi_i^n + e\, J_{f\,i}^n \qquad \text{G52}$$

where $A_i^{n+1}, G_i^{n+1}, B_i^n, H_i^n, Q_i^{n+1}$ and V_i^n are known square matrices, $a_i^{n+1}, g_i^{n+1}, b_i^{n+1}, h_i^{n+1}, q_i^n$ and v_i^n are known vectors where the details of the boundary conditions have been fully incorporated in this case.

LHS of equation G49 is now written as:

$$\begin{bmatrix} 2+2r & 0 & 0 & \bullet & 0 & 0 & 0 \\ -r & 2+2r & -r & \bullet & 0 & 0 & 0 \\ 0 & -r & 2+2r & \bullet & 0 & 0 & 0 \\ \bullet & \bullet & \bullet & \bullet & \bullet & \bullet & \bullet \\ 0 & 0 & 0 & \bullet & 2+2r & -r & 0 \\ 0 & 0 & 0 & \bullet & -r & 2+2r & -r \\ 0 & 0 & 0 & \bullet & 0 & -2r & 2+2r \end{bmatrix} \begin{bmatrix} \varphi_1^{n+1} \\ \varphi_2^{n+1} \\ \varphi_3^{n+1} \\ \bullet \\ \varphi_{nx-2}^{n+1} \\ \varphi_{nx-1}^{n+1} \\ \varphi_{nx}^{n+1} \end{bmatrix} + \begin{bmatrix} -2r\varphi_0^{n+1} - rj \\ 0 \\ 0 \\ \bullet \\ 0 \\ 0 \\ -rk \end{bmatrix} +$$

$$\begin{bmatrix} -2m & 0 & 0 & \bullet & 0 & 0 & 0 \\ m & -2m & m & \bullet & 0 & 0 & 0 \\ 0 & m & -2m & \bullet & 0 & 0 & 0 \\ \bullet & \bullet & \bullet & \bullet & \bullet & \bullet & \bullet \\ 0 & 0 & 0 & \bullet & -2m & m & 0 \\ 0 & 0 & 0 & \bullet & m & -2m & m \\ 0 & 0 & 0 & \bullet & 0 & 2m & -2m \end{bmatrix} \begin{bmatrix} \ln C_1^{n+1} \\ \ln C_2^{n+1} \\ \ln C_3^{n+1} \\ \bullet \\ \ln C_{nx-2}^{n+1} \\ \ln C_{nx-1}^{n+1} \\ \ln C_{nx}^{n+1} \end{bmatrix} + \begin{bmatrix} -2r\ln C_0^{n+1} - rj \\ 0 \\ 0 \\ \bullet \\ 0 \\ 0 \\ -rk \end{bmatrix}$$

$$A_i^{n+1}\varphi_i^{n+1} + a_i^{n+1} + G_i^{n+1}\ln C_i^{n+1} + g_i^{n+1} \qquad \text{G53}$$

Similarly the RHS of equation G49 is written as:

$$\begin{bmatrix} 2-2r & 0 & 0 & \bullet & 0 & 0 & 0 \\ r & 2-2r & r & \bullet & 0 & 0 & 0 \\ 0 & r & 2-2r & \bullet & 0 & 0 & 0 \\ \bullet & \bullet & \bullet & \bullet & \bullet & \bullet & \bullet \\ 0 & 0 & 0 & \bullet & 2-2r & r & 0 \\ 0 & 0 & 0 & \bullet & r & 2-2r & r \\ 0 & 0 & 0 & \bullet & 0 & 2r & 2-2r \end{bmatrix} \begin{bmatrix} \varphi_1^n \\ \varphi_2^n \\ \varphi_3^n \\ \bullet \\ \varphi_{nx-2}^n \\ \varphi_{nx-1}^n \\ \varphi_{nx}^n \end{bmatrix} + \begin{bmatrix} 2r\varphi_0^n + rj \\ 0 \\ 0 \\ \bullet \\ 0 \\ 0 \\ rk \end{bmatrix} +$$

$$\begin{bmatrix} 2m & 0 & 0 & \bullet & 0 & 0 & 0 \\ -m & 2m & -m & \bullet & 0 & 0 & 0 \\ 0 & -m & 2m & \bullet & 0 & 0 & 0 \\ \bullet & \bullet & \bullet & \bullet & \bullet & \bullet & \bullet \\ 0 & 0 & 0 & \bullet & 2m & -m & 0 \\ 0 & 0 & 0 & \bullet & -m & 2m & -m \\ 0 & 0 & 0 & \bullet & 0 & -2m & 2m \end{bmatrix} \begin{bmatrix} \ln C_1^n \\ \ln C_2^n \\ \ln C_3^n \\ \bullet \\ \ln C_{nx-2}^n \\ \ln C_{nx-1}^n \\ \ln C_{nx}^n \end{bmatrix} + \begin{bmatrix} -2r \ln C_0^n - rj \\ 0 \\ 0 \\ \bullet \\ 0 \\ 0 \\ -rk \end{bmatrix} - u \begin{bmatrix} J_{f0}^n \\ J_{f1}^n \\ \bullet \\ \bullet \\ \bullet \\ J_{f\,nx-1}^n \\ J_{f\,nx}^n \end{bmatrix} +$$

$$s \begin{bmatrix} J_{VR0}^n \\ J_{VR1}^n \\ \bullet \\ \bullet \\ \bullet \\ J_{VRnx-1}^n \\ J_{VRnx}^n \end{bmatrix} = B_i^n \varphi_i^n + b_i^n + H_i^n \ln C_i^n + h_i^n - u\, J_{f\,i}^n + s\, J_{VR\,i}^n \qquad \text{G54}$$

Also LHS of equation G50 can be written as:

$$\begin{bmatrix} 2+2\eta & 0 & 0 & \bullet & 0 & 0 & 0 \\ -\eta & 2+2\eta & -\eta & \bullet & 0 & 0 & 0 \\ 0 & -\eta & 2+2\eta & \bullet & 0 & 0 & 0 \\ \bullet & \bullet & \bullet & \bullet & \bullet & \bullet & \bullet \\ 0 & 0 & 0 & \bullet & 2+2\eta & -\eta & 0 \\ 0 & 0 & 0 & \bullet & -\eta & 2+2\eta & -\eta \\ 0 & 0 & 0 & \bullet & 0 & -2\eta & 2+2\eta \end{bmatrix} \begin{bmatrix} C_1^{n+1} \\ C_2^{n+1} \\ C_3^{n+1} \\ \bullet \\ C_{nx-2}^{n+1} \\ C_{nx-1}^{n+1} \\ C_{nx}^{n+1} \end{bmatrix} + \begin{bmatrix} -2rC_0^{n+1} - rj \\ 0 \\ 0 \\ \bullet \\ 0 \\ 0 \\ -rk \end{bmatrix} + d \begin{bmatrix} \varphi_0^{n+1} \\ \varphi_1^{n+1} \\ \varphi_1^{n+1} \\ \bullet \\ \bullet \\ \varphi_{nx-1}^{n+1} \\ \varphi_{nx}^{n+1} \end{bmatrix}$$

$$= Q_i^{n+1} C_i^{n+1} + q_i^{n+1} + d\, \varphi_i^{n+1} \qquad \text{G55}$$

Similarly the RHS of equation G50 will be written as:

$$\begin{bmatrix} 2-2\eta & 0 & 0 & \bullet & 0 & 0 & 0 \\ \eta & 2-2\eta & \eta & \bullet & 0 & 0 & 0 \\ 0 & \eta & 2-2\eta & \bullet & 0 & 0 & 0 \\ \bullet & \bullet & \bullet & \bullet & \bullet & \bullet & \bullet \\ 0 & 0 & 0 & \bullet & 2-2\eta & \eta & 0 \\ 0 & 0 & 0 & \bullet & \eta & 2-2\eta & \eta \\ 0 & 0 & 0 & \bullet & 0 & -2\eta & 2+2\eta \end{bmatrix} \begin{bmatrix} C_1^n \\ C_2^n \\ C_3^n \\ \bullet \\ C_{nx-2}^n \\ C_{nx-1}^n \\ C_{nx}^n \end{bmatrix} + \begin{bmatrix} -2rC_0^n - rj \\ 0 \\ 0 \\ \bullet \\ 0 \\ 0 \\ -rk \end{bmatrix} - d \begin{bmatrix} \varphi_0^n \\ \varphi_1^n \\ \varphi_2^1 \\ \bullet \\ \varphi_{nx}^n \\ \varphi_{nx}^n \\ \varphi_{nx}^n \end{bmatrix}$$

$$+e\begin{bmatrix} J^n_{f\,0} \\ J^n_{f\,1} \\ \bullet \\ \bullet \\ \bullet \\ J^n_{f\,nx-1} \\ J^n_{f\,nx} \end{bmatrix} = V_i^n C_i^n + v_i^n - d\ \varphi_i^n + e\ J^n_{f\,i} \qquad \text{G56}$$

Equations G50 and G51 are then written respectively as:

$$A_i^{n+1}\varphi_i^{n+1} = B_i^n\varphi_i^n + b_i^n + H_i^n \ln C_i^n + h_i^n - G_i^{n+1}\ln C_i^{n+1} - g_i^{n+1} - a_i^{n+1} - u\ J^n_{f\,i} + s\ J^n_{VR\,i} \qquad \text{G57}$$

$$Q_i^{n+1}C_i^{n+1} = V_i^n C_i^n + v_i^n - q_i^{n+1} - d\ \varphi_i^{n+1} - d\ \varphi_i^n + e\ J^n_{f\,i} \qquad \text{G58}$$

$$\begin{bmatrix} 2+2r & 0 & 0 & \bullet & 0 & 0 & 0 \\ -r & 2+2r & -r & \bullet & 0 & 0 & 0 \\ 0 & -r & 2+2r & \bullet & 0 & 0 & 0 \\ \bullet & \bullet & \bullet & \bullet & \bullet & \bullet & \bullet \\ 0 & 0 & 0 & \bullet & 2+2r & -r & 0 \\ 0 & 0 & 0 & \bullet & -r & 2+2r & -r \\ 0 & 0 & 0 & \bullet & 0 & -2r & 2+2r \end{bmatrix}\begin{bmatrix} \varphi_1^{n+1} \\ \varphi_2^{n+1} \\ \varphi_3^{n+1} \\ \bullet \\ \varphi_{nx-2}^{n+1} \\ \varphi_{nx-1}^{n+1} \\ \varphi_{nx}^{n+1} \end{bmatrix} =$$

$$\begin{bmatrix} 2-2r & 0 & 0 & \bullet & 0 & 0 & 0 \\ r & 2-2r & r & \bullet & 0 & 0 & 0 \\ 0 & r & 2-2r & \bullet & 0 & 0 & 0 \\ \bullet & \bullet & \bullet & \bullet & \bullet & \bullet & \bullet \\ 0 & 0 & 0 & \bullet & 2-2r & r & 0 \\ 0 & 0 & 0 & \bullet & r & 2-2r & r \\ 0 & 0 & 0 & \bullet & 0 & 2r & 2-2r \end{bmatrix}\begin{bmatrix} \varphi_1^n \\ \varphi_2^n \\ \varphi_3^n \\ \bullet \\ \varphi_{nx-2}^n \\ \varphi_{nx-1}^n \\ \varphi_{nx}^n \end{bmatrix} + \begin{bmatrix} 2r\left(\varphi_0^{n+1} + \varphi_0^n + j\right) \\ 0 \\ 0 \\ \bullet \\ 0 \\ 0 \\ 2rk \end{bmatrix} +$$

$$\begin{bmatrix} 2m & 0 & 0 & \bullet & 0 & 0 & 0 \\ -m & 2m & -m & \bullet & 0 & 0 & 0 \\ 0 & -m & 2m & \bullet & 0 & 0 & 0 \\ \bullet & \bullet & \bullet & \bullet & \bullet & \bullet & \bullet \\ 0 & 0 & 0 & \bullet & 2m & -m & 0 \\ 0 & 0 & 0 & \bullet & -m & 2m & -m \\ 0 & 0 & 0 & \bullet & 0 & -2m & 2m \end{bmatrix}\begin{bmatrix} \ln C_1^n \\ \ln C_2^n \\ \ln C_3^n \\ \bullet \\ \ln C_{nx-2}^n \\ \ln C_{nx-1}^n \\ \ln C_{nx}^n \end{bmatrix} -$$

$$\begin{bmatrix} -2m & 0 & 0 & \bullet & 0 & 0 & 0 \\ m & -2m & m & \bullet & 0 & 0 & 0 \\ 0 & m & -2m & \bullet & 0 & 0 & 0 \\ \bullet & \bullet & \bullet & \bullet & \bullet & \bullet & \bullet \\ 0 & 0 & 0 & \bullet & -2m & m & 0 \\ 0 & 0 & 0 & \bullet & m & -2m & m \\ 0 & 0 & 0 & \bullet & 0 & 2m & -2m \end{bmatrix} \begin{bmatrix} \ln C_1^{n+1} \\ \ln C_2^{n+1} \\ \ln C_3^{n+1} \\ \bullet \\ \ln C_{nx-2}^{n+1} \\ \ln C_{nx-1}^{n+1} \\ \ln C_{nx}^{n+1} \end{bmatrix} + \begin{bmatrix} -2r\left(\ln C_0^{n+1} + \ln C_0^n - j\right) \\ 0 \\ 0 \\ \bullet \\ 0 \\ 0 \\ 2rk \end{bmatrix}$$

$$-u \begin{bmatrix} J_{f0}^n \\ J_{f1}^n \\ \bullet \\ \bullet \\ \bullet \\ J_{f\,nx-1}^n \\ J_{f\,nx}^n \end{bmatrix} + s \begin{bmatrix} J_{VR0}^n \\ J_{VR1}^n \\ \bullet \\ \bullet \\ \bullet \\ J_{VRnx-1}^n \\ J_{VRnx}^n \end{bmatrix} \qquad \textbf{G}59$$

$$\begin{bmatrix} 2+2\eta & 0 & 0 & \bullet & 0 & 0 & 0 \\ -\eta & 2+2\eta & -\eta & \bullet & 0 & 0 & 0 \\ 0 & -\eta & 2+2\eta & \bullet & 0 & 0 & 0 \\ \bullet & \bullet & \bullet & \bullet & \bullet & \bullet & \bullet \\ 0 & 0 & 0 & \bullet & 2+2\eta & -\eta & 0 \\ 0 & 0 & 0 & \bullet & -\eta & 2+2\eta & -\eta \\ 0 & 0 & 0 & \bullet & 0 & -2\eta & 2+2\eta \end{bmatrix} \begin{bmatrix} C_1^{n+1} \\ C_2^{n+1} \\ C_3^{n+1} \\ \bullet \\ C_{nx-2}^{n+1} \\ C_{nx-1}^{n+1} \\ C_{nx}^{n+1} \end{bmatrix} =$$

$$\begin{bmatrix} 2-2\eta & 0 & 0 & \bullet & 0 & 0 & 0 \\ \eta & 2-2\eta & \eta & \bullet & 0 & 0 & 0 \\ 0 & \eta & 2-2\eta & \bullet & 0 & 0 & 0 \\ \bullet & \bullet & \bullet & \bullet & \bullet & \bullet & \bullet \\ 0 & 0 & 0 & \bullet & 2-2\eta & \eta & 0 \\ 0 & 0 & 0 & \bullet & \eta & 2-2\eta & \eta \\ 0 & 0 & 0 & \bullet & 0 & -2\eta & 2+2\eta \end{bmatrix} \begin{bmatrix} C_1^n \\ C_2^n \\ C_3^n \\ \bullet \\ C_{nx-2}^n \\ C_{nx-1}^n \\ C_{nx}^n \end{bmatrix} + \begin{bmatrix} 2r\left(C_0^{n+1} + C_0^n + j\right) \\ 0 \\ 0 \\ \bullet \\ 0 \\ 0 \\ 2rk \end{bmatrix}$$

$$-d \begin{bmatrix} \varphi_0^n \\ \varphi_1^n \\ \varphi_2^1 \\ \bullet \\ \varphi_{nx}^n \\ \varphi_{nx}^n \\ \varphi_{nx}^n \end{bmatrix} - d \begin{bmatrix} \varphi_0^{n+1} \\ \varphi_1^{n+1} \\ \varphi_1^{n+1} \\ \bullet \\ \bullet \\ \varphi_{nx-1}^{n+1} \\ \varphi_{nx}^{n+1} \end{bmatrix} + e \begin{bmatrix} J_{f0}^n \\ J_{f1}^n \\ \bullet \\ \bullet \\ \bullet \\ J_{f\,nx-1}^n \\ J_{f\,nx}^n \end{bmatrix} \qquad \text{G}60$$

And finally we have,

$$\varphi_i^{n+1} = \left(A_i^{n+1}\right)^{-1}\left(B_i^n \varphi_i^n + b_i^n + H_i^n \ln C_i^n + h_i^n - G_i^{n+1} \ln C_i^{n+1} - g_i^{n+1} - a_i^{n+1} - u\, J_{f\,i}^n + s\, J_{VR\,i}^n\right) \quad \text{G61}$$

$$C_i^{n+1} = \left(Q_i^{n+1}\right)^{-1}\left(V_i^n C_i^n + v_i^n - q_i^{n+1} - d\, \varphi_i^{n+1} - d\, \varphi_i^n + e\, J_{f\,i}^n\right) \quad \text{G62}$$

Also, recall that equation G37 is given as:

$$\theta_i^{n+1} = \theta_i^n + z\Delta t\, J_{f\,i}^n \quad \text{G37}$$

But the matrix inversion is very time consuming and computationally inefficient. The matrices A_i^{n+1} and Q_i^{n+1} are tridiagonal and can be decomposed into the product of two other matrices such that A=LU. There the matrices A_i^{n+1} and Q_i^{n+1} are now written respectively as:

$$\begin{bmatrix} 2+2r & 0 & 0 & \bullet & 0 & 0 & 0 \\ -r & 2+2r & -r & \bullet & 0 & 0 & 0 \\ 0 & -r & 2+2r & \bullet & 0 & 0 & 0 \\ \bullet & \bullet & \bullet & \bullet & \bullet & \bullet & \bullet \\ 0 & 0 & 0 & \bullet & 2+2r & -r & 0 \\ 0 & 0 & 0 & \bullet & -r & 2+2r & -r \\ 0 & 0 & 0 & \bullet & 0 & -2r & 2+2r \end{bmatrix} = \begin{bmatrix} 1 & 0 & 0 & 0 & 0 & 0 & 0 \\ l_2 & 1 & 0 & 0 & 0 & 0 & 0 \\ 0 & l_3 & 1 & \bullet & 0 & 0 & 0 \\ 0 & 0 & l_4 & \bullet & 0 & 0 & 0 \\ 0 & 0 & 0 & \bullet & 1 & 0 & 0 \\ 0 & 0 & 0 & 0 & l_{nx-2} & 1 & 0 \\ 0 & 0 & 0 & 0 & 0 & l_{nx-1} & 1 \end{bmatrix}$$

$$\begin{bmatrix} d_1 & p_1 & 0 & 0 & 0 & 0 & 0 \\ 0 & d_2 & p_2 & 0 & 0 & 0 & 0 \\ 0 & 0 & d_3 & \bullet & 0 & 0 & 0 \\ 0 & 0 & 0 & \bullet & p_{nx-4} & 0 & 0 \\ 0 & 0 & 0 & \bullet & d_{nx-2} & p_{nx-3} & 0 \\ 0 & 0 & 0 & 0 & 0 & d_{nx-1} & p_{nx-2} \\ 0 & 0 & 0 & 0 & 0 & 0 & d_{nx} \end{bmatrix} \quad \text{G63}$$

$$\begin{bmatrix} 2+2\eta & 0 & 0 & \bullet & 0 & 0 & 0 \\ -\eta & 2+2\eta & -\eta & \bullet & 0 & 0 & 0 \\ 0 & -\eta & 2+2\eta & \bullet & 0 & 0 & 0 \\ \bullet & \bullet & \bullet & \bullet & \bullet & \bullet & \bullet \\ 0 & 0 & 0 & \bullet & 2+2\eta & -\eta & 0 \\ 0 & 0 & 0 & \bullet & -\eta & 2+2\eta & -\eta \\ 0 & 0 & 0 & \bullet & 0 & -2\eta & 2+2\eta \end{bmatrix} = \begin{bmatrix} 1 & 0 & 0 & 0 & 0 & 0 & 0 \\ l_2 & 1 & 0 & 0 & 0 & 0 & 0 \\ 0 & l_3 & 1 & \bullet & 0 & 0 & 0 \\ 0 & 0 & l_4 & \bullet & 0 & 0 & 0 \\ 0 & 0 & 0 & \bullet & 1 & 0 & 0 \\ 0 & 0 & 0 & 0 & l_{nx-2} & 1 & 0 \\ 0 & 0 & 0 & 0 & 0 & l_{nx-1} & 1 \end{bmatrix}$$

$$\begin{bmatrix} d_1 & p_1 & 0 & 0 & 0 & 0 & 0 \\ 0 & d_2 & p_2 & 0 & 0 & 0 & 0 \\ 0 & 0 & d_3 & \bullet & 0 & 0 & 0 \\ 0 & 0 & 0 & \bullet & p_{nx-4} & 0 & 0 \\ 0 & 0 & 0 & \bullet & d_{nx-2} & p_{nx-3} & 0 \\ 0 & 0 & 0 & 0 & 0 & d_{nx-1} & p_{nx-2} \\ 0 & 0 & 0 & 0 & 0 & 0 & d_{nx} \end{bmatrix} \quad \text{G64}$$

For equation G63, $d_1 = 2 + 2r$, $l_n d_{n-1} = p_{n-1} = -r$ and $d_n = 2 + 2r - l_n p_{n-1}$ *for* $2 \le n \le nx - 1$,

and for equation G64, $d_1 = 2 + 2\eta$, $l_n d_{n-1} = p_{n-1} = -\eta$ and $d_n = 2 + 2\eta - l_n p_{n-1}$ *for* $2 \le n \le nx - 1$

.

Notice that we work from $n = 1$ *to* $n = nx$ sequentially. Let

$A_i^{n+1}\varphi_i^{n+1} = A\varphi$ *and* $B_i^n \varphi_i^n + b_i^n + H_i^n \ln C_i^n + h_i^n - G_i^{n+1} \ln C_i^{n+1} - g_i^{n+1} - a_i^{n+1} - uJ_{fi}^n + sJ_{VRi}^n = q$,
then $A\varphi = q$, $LU\varphi = q$, $Lw = q$, $U\varphi = w$ *for equation* $F63$

Also, let

$A_i^{n+1}\varphi_i^{n+1} = A\varphi$ *and* $V_i^n C_i^n + v_i^n - q_i^{n+1} - d\varphi_i^{n+1} - d\varphi_i^n + uJ_{fi}^n = q$, *then* $A\varphi = q$, $LU\varphi = q$,
$Lw = q$, $U\varphi = w$ *for equation* $F64$

First step gives:

$w_1 = q_1$ and $w_n = q_n - l_n w_{n-1}$ *for* $2 \le n \le n_{x-1}$.

Second step involves working backwards from $n = nx - 2$ *to* $n = 1$:

$$\varphi_{nx-1} = \frac{w_{nx-1}}{d_{nx-1}} \text{ and } \varphi_n = \frac{w_n - p_n \varphi_{n+1}}{d_n} \text{ for } n_{x-2} \ge 2 \ge 1$$

Appendix H

Appendix H1: MATLAB scripts for analytical numerical solutions of EDLCs models with and without self-discharge

```
phine_charge=0.6;phine_discharge=-0.6;cv=400;t0=0;Jvr=0.00125;t=18000;
wne=0.2;J0=0.00533;alpha1a=0.0005;alpha2a=alpha1a;alpha1b=0.001;alpha2b=alp
ha1b;alpha1c=0.005;alpha2c=alpha1c;alpha1d=0.01;alpha2d=alpha1d;alpha1e=0.0
5;alpha2e=alpha1e;phi0=0.6;phip=1.4;V_0=0.8;V_1=2.0;n1=2;F=96487;c=3e-4;
l=0.25;A=6290;C=400;D=1.8e-5;la=0.2;lb=0.05;va=A.*la;vb=A.*lb;V=10e-1;
q=(n1.*A.*F.*V.*c).*(1-(8./pi.^2).*exp(-(pi.^2.*D.*t)./l^2))*1/3600;
J=q/A.*t;Jvr1=(2.*F.*V.*c)./t.*(1-(8./pi.^2).*exp(-(pi.^2.*D.*t)./l^2));
phi=phi0-Jvr1.*t./cv;
betaa=(alpha1a*alpha2a)/(cv*(alpha2a+alpha1a));
betab=(alpha1b*alpha2b)/(cv*(alpha2b+alpha1b));
betac=(alpha1c*alpha2c)/(cv*(alpha2c+alpha1c));
betad=(alpha1d*alpha2d)/(cv*(alpha2d+alpha1d));
betae=(alpha1e*alpha2e)/(cv*(alpha2e+alpha1e));
Aa=sqrt(betaa);Ab=sqrt(betab);Ac=sqrt(betac);
Ad=sqrt(betad);Ae=sqrt(betae);a=J0/(wne*cv);
h=Jvr/cv;
syms n x pi t s
ba=cv*x.^2*(alpha2a+alpha1a)/(2*alpha1a*alpha2a);
bb=cv*x.^2*(alpha2b+alpha1b)/(2*alpha1b*alpha2b);
bc=cv*x.^2*(alpha2c+alpha1c)/(2*alpha1c*alpha2c);
bd=cv*x.^2*(alpha2d+alpha1d)/(2*alpha1d*alpha2d);
be=cv*x.^2*(alpha2e+alpha1e)/(2*alpha1e*alpha2e);
ca=cv*x*wne/alpha1a;
cb=cv*x*wne/alpha1b;
cc=cv*x*wne/alpha1c;
cd=cv*x*wne/alpha1d;
ce=cv*x*wne/alpha1e;
da=cv*wne.^2*(2*alpha2a-alpha1a)/(6*alpha1a*alpha2a);
db=cv*wne.^2*(2*alpha2b-alpha1b)/(6*alpha1b*alpha2b);
dc=cv*wne.^2*(2*alpha2c-alpha1c)/(6*alpha1c*alpha2c);
dd=cv*wne.^2*(2*alpha2d-alpha1d)/(6*alpha1d*alpha2d);
de=cv*wne.^2*(2*alpha2e-alpha1e)/(6*alpha1e*alpha2e);
e=2*cv*wne.^2/pi.^2;
fa=(1/alpha1a+(-1).^n/alpha2a);
fb=(1/alpha1b+(-1).^n/alpha2b);
fc=(1/alpha1c+(-1).^n/alpha2c);
fd=(1/alpha1d+(-1).^n/alpha2d);
fe=(1/alpha1e+(-1).^n/alpha2e);
ia=((-1).^n*(alpha2a+alpha1a))/(alpha1a*alpha2a);
ib=((-1).^n*(alpha2b+alpha1b))/(alpha1b*alpha2b);
ic=((-1).^n*(alpha2c+alpha1c))/(alpha1c*alpha2c);
id=((-1).^n*(alpha2d+alpha1d))/(alpha1d*alpha2d);
ie=((-1).^n*(alpha2e+alpha1e))/(alpha1e*alpha2e);
ga=exp(-(pi.*n.*Aa./wne).^2.*t./n.^2);
gb=exp(-(pi.*n.*Ab./wne).^2.*t./n.^2);
gc=exp(-(pi.*n.*Ac./wne).^2.*t./n.^2);
gd=exp(-(pi.*n.*Ad./wne).^2.*t./n.^2);
ge=exp(-(pi.*n.*Ae./wne).^2.*t./n.^2);
ja=ia*((1-exp(-(pi.*n.*Aa./wne).^2.*t-t0))./n.^3);
jb=ib*((1-exp(-(pi.*n.*Ab./wne).^2.*t-t0))./n.^3);
```

```
jc=ic*((1-exp(-(pi.*n.*Ac./wne).^2.*t-t0))./n.^3);
jd=id*((1-exp(-(pi.*n.*Ad./wne).^2.*t-t0))./n.^3);
je=ie*((1-exp(-(pi.*n.*Ae./wne).^2.*t-t0))./n.^3);
phinea=phine_charge-a*(t+ba-ca+da-
e*symsum(fa*ga*cos(n.*pi.*x./wne),n,1,1));
phineb=phine_charge-a*(t+bb-cb+db-
e*symsum(fb*gb*cos(n.*pi.*x./wne),n,1,1));
phinec=phine_charge-a*(t+bc-cc+dc-
e*symsum(fc*gc*cos(n.*pi.*x./wne),n,1,1));
phined=phine_charge-a*(t+bd-cd+dd-
e*symsum(fd*gd*cos(n.*pi.*x./wne),n,1,1));
phinee=phine_charge-a*(t+be-ce+de-
e*symsum(fe*ge*cos(n.*pi.*x./wne),n,1,1));
phinea18000=subs(phinea,t,18000);
phineb18000=subs(phineb,t,18000);
phinec18000=subs(phinec,t,18000);
phined18000=subs(phined,t,18000);
phinee18000=subs(phinee,t,18000);
phinea1=phine_charge-a*(t+ba-ca+da-
e*symsum(fa*ga*cos(n.*pi.*x./wne),n,1,1))+h*t+(h*e)./pi*symsum(ja*cos(n.*pi
.*x./wne),n,1,1);
phineb1=phine_charge-a*(t+bb-cb+db-
e*symsum(fb*gb*cos(n.*pi.*x./wne),n,1,1))+h*t+(h*e)./pi*symsum(jb*cos(n.*pi
.*x./wne),n,1,1);
phinec1=phine_charge-a*(t+bc-cc+dc-
e*symsum(fc*gc*cos(n.*pi.*x./wne),n,1,1))+h*t+(h*e)./pi*symsum(jc*cos(n.*pi
.*x./wne),n,1,1);
phined1=phine_charge-a*(t+bd-cd+dd-
e*symsum(fd*gd*cos(n.*pi.*x./wne),n,1,1))+h*t+(h*e)./pi*symsum(jd*cos(n.*pi
.*x./wne),n,1,1);
phinee1=phine_charge-a*(t+be-ce+de-
e*symsum(fe*ge*cos(n.*pi.*x./wne),n,1,1))+h*t+(h*e)./pi*symsum(je*cos(n.*pi
.*x./wne),n,1,1);
phinea118000=subs(phinea1,t,18000);
phineb118000=subs(phineb1,t,18000);
phinec118000=subs(phinec1,t,18000);
phined118000=subs(phined1,t,18000);
phinee118000=subs(phinee1,t,18000);
phinea2=phine_charge-a*(t+ba-ca+da-
e*symsum(fa*ga*cos(n.*pi.*x./wne),n,1,1))+h*t+(h*e)./pi*symsum(ja*cos(n.*pi
.*x./wne),n,1,1)+Jvr1.*t./cv;
phineb2=phine_charge-a*(t+bb-cb+db-
e*symsum(fb*gb*cos(n.*pi.*x./wne),n,1,1))+h*t+(h*e)./pi*symsum(jb*cos(n.*pi
.*x./wne),n,1,1)+Jvr1.*t./cv;
phinec2=phine_charge-a*(t+bc-cc+dc-
e*symsum(fc*gc*cos(n.*pi.*x./wne),n,1,1))+h*t+(h*e)./pi*symsum(jc*cos(n.*pi
.*x./wne),n,1,1)+Jvr1.*t./cv;
phined2=phine_charge-a*(t+bd-cd+dd-
e*symsum(fd*gd*cos(n.*pi.*x./wne),n,1,1))+h*t+(h*e)./pi*symsum(jd*cos(n.*pi
.*x./wne),n,1,1)+Jvr1.*t./cv;
phinee2=phine_charge-a*(t+be-ce+de-
e*symsum(fe*ge*cos(n.*pi.*x./wne),n,1,1))+h*t+(h*e)./pi*symsum(je*cos(n.*pi
.*x./wne),n,1,1)+Jvr1.*t./cv;
phinea218000=subs(phinea2,t,18000);
phineb218000=subs(phineb2,t,18000);
phinec218000=subs(phinec2,t,18000);
phined218000=subs(phined2,t,18000);
phinee218000=subs(phinee2,t,18000);
xx=linspace(0,0.2,201);
subplot(2,2,1)
```

```
plot(xx,subs(phinea18000,x,xx),'r',xx,subs(phineb18000,x,xx),'b',xx,subs(ph
inec18000,x,xx),'g',xx,subs(phinee18000,x,xx),'k'),xlabel('Thickness,wne
,cm'),ylabel('Potential,phine,V'),title('a'),legend('phinea18000(alpha1a=al
pha2a=0.0005S/cm)','phineb18000(alpha1b=alpha2b=0.001S/cm)','phinec18000(al
pha1c=alpha2c=0.005S/cm)','phinea18000(alpha1e=alpha2e=0.05S/cm)')
grid on,
subplot(2,2,2)
plot(xx,subs(phinea118000,x,xx),'r',xx,subs(phineb118000,x,xx),'b',xx,subs(
phinec118000,x,xx),'g',xx,subs(phinee118000,x,xx),'k'),xlabel('Thickness,wn
e
,cm'),ylabel('Potential,phine,V'),title('b'),legend('phinea18000(alpha1a=al
pha2a=0.0005S/cm)','phineb18000(alpha1b=alpha2b=0.001S/cm)','phinec18000(al
pha1c=alpha2c=0.005S/cm)','phinea18000(alpha1e=alpha2e=0.05S/cm)')
grid on,
subplot(2,2,3)
plot(xx,subs(phinea218000,x,xx),'r',xx,subs(phineb218000,x,xx),'b',xx,subs(
phinec218000,x,xx),'g',xx,subs(phinee218000,x,xx),'k'),xlabel('Thickness,wn
e
,cm'),ylabel('Potential,phine,V'),title('c'),legend('phinea18000(alpha1a=al
pha2a=0.0005S/cm)','phineb18000(alpha1b=alpha2b=0.001S/cm)','phinec18000(al
pha1c=alpha2c=0.005S/cm)','phinea18000(alpha1e=alpha2e=0.05S/cm)')
grid on,
```

Appendix H2: MATLAB scripts for the numerical solutions of EDLCs models without self-discharge

```
function model_without_self-discharge
clear all
clc
tf = 18000;
x0 = 0;
xf = 0.2;
n = 50;
x = linspace(x0, xf, n+1);
dx = x(2) - x(1);
c_v = 400;
alp_1 = 0.05;
alp_2 = alp_1;
bta = alp_1*alp_2/(c_v*(alp_1 + alp_2));
r = 0.3906;
J0 = 0.00533;
phi_0 = 0.9;
w_n = 0.2;
dt = r*dx^2/(bta);
m = round(tf/dt);
e = ones(n+1,1);
dia= (2 + 2*r)*e;
ofd = -r*e;
A = spdiags([ofd dia ofd],-1:1,n+1,n+1);
A(1,1:2) = [2+2*r -2*r];
A(end,end-1:end) = [-2*r 2+2*r];

dia_2 = (2 - 2*r)*e;
A_rh = spdiags([-ofd dia_2 -ofd],-1:1,n+1,n+1);
A_rh(1,1:2) = [2-2*r 2*r];
A_rh(end,end-1:end) = [2*r 2-2*r];
e2 = zeros(n-1,1);
```

```
b1 = 4*r*J0*dx;
b_r = [-b1/alp_1; e2; -b1/alp_2];
f = @(y)phi_0 - J0*y/alp_1 + J0*(alp_1+alp_2)*y.^2/(2*w_n*alp_1*alp_2);
phi(:,1) = f(x);

for j = 2:m+1
    v0 = phi(:,j-1);
    rhs = A_rh*v0 + b_r;
    vn = A\rhs;
    phi(:,j) = vn;
end
        set( 0, 'DefaultTextFontName', 'times' );
        set( 0, 'DefaultAxesFontName', 'times' );
        set( 0, 'DefaultTextFontSize', 20 );
        set( 0, 'DefaultAxesFontSize', 20 );
        set( 0, 'DefaultLineLineWidth', 2 ); % default is 1
        set( 0, 'DefaultLineMarkerSize',8 ); % default is 6
 subplot(2,1,1)
 plot(x, phi(:,end))
 t = linspace(0,tf,m+1);
 subplot(2,1,2)
 mesh(x,t,phi')
print -depsc 'energy'
```

Appendix H3: MATLAB scripts for the numerical solutions of EDLCs models with self-discharge

```
function model_with_self-discharge
clear all
clc
tf = 18000;x0 = 0;xf = 0.2;n = 50;
x = linspace(x0, xf, n+1);
dx = x(2) - x(1);
c_v = 400;
alp_1 = 0.05;
alp_2 = alp_1;
bta = alp_1*alp_2/(c_v*(alp_1 + alp_2));
r = 0.3906;
J0 = 0.00533;
phi_0 = 0.9;
w_n = 0.2;
Jc = 0.00393125;
dt = r*dx^2/(bta);
m = round(tf/dt);
e = ones(n+1,1);
dia= (2 + 2*r)*e;
ofd = -r*e;
A = spdiags([ofd dia ofd],-1:1,n+1,n+1);
A(1,1:2) = [2+2*r -2*r];
A(end,end-1:end) = [-2*r 2+2*r];
 dia_2 = (2 - 2*r)*e;
A_rh = spdiags([-ofd dia_2 -ofd],-1:1,n+1,n+1);
A_rh(1,1:2) = [2-2*r 2*r];
A_rh(end,end-1:end) = [2*r 2-2*r];
e2 = zeros(n-1,1);
```

```
b1 = 4*r*J0*dx;
b2 = 2*dt*Jc/c_v;
b_r = [-b1/alp_1; e2; -b1/alp_2] + b2;
f = @(y)phi_0 - J0*y/alp_1 + J0*(alp_1+alp_2)*y.^2/(2*w_n*alp_1*alp_2);
phi(:,1) = f(x);
 for j = 2:m+1
    v0 = phi(:,j-1);
    rhs = A_rh*v0 + b_r;
    vn = A\rhs;
    phi(:,j) = vn;
end
        set( 0, 'DefaultTextFontName', 'times' );
        set( 0, 'DefaultAxesFontName', 'times' );
        set( 0, 'DefaultTextFontSize', 20 );
        set( 0, 'DefaultAxesFontSize', 20 );
        set( 0, 'DefaultLineLineWidth', 2 ); % default is 1
        set( 0, 'DefaultLineMarkerSize',8 ); % default is 6
subplot(2,1,1)
 plot(x, phi(:,end))
 t = linspace(0,tf,m+1);
 subplot(2,1,2)
 mesh(x,t,phi')
%print -depsc 'case1'
```

Appendix H4: MATLAB script for optimization of coefficient associated to battery-kind material, K_{BM}

```
x_1=0:0.1:1;
x_2=0:0.1:1;
[x1,x2]=meshgrid(0:0.1:1);
[x1a,x2a]=meshgrid(0:0.05:0.5,0:0.07:0.7);
y1=(1-x1).*(1-x2.^2);
y1a=(1-x1a).*(1-x2a.^2);
a=1-x_1;
b=1-x2.^2;
subplot(2,2,3)
surf(x1a, x2a, y1a),xlabel('Mass ratio (x1a) '),ylabel('Voltage ratio
(x2a)'),zlabel('Constant of Battery Mat (Kbm)'),title('c')
subplot(2,2,1)
surf(x1, x2, y1),xlabel('Mass ratio (x1) '),ylabel('Voltage ratio
(x2)'),zlabel('Constant of Battery Mat (Kbm)'),title('a')
subplot(2,2,4)
surf(x1a, x2a, y1a),xlabel('Mass ratio (x1a) '),ylabel('Voltage ratio
(x2a)'),zlabel('Constant of Battery Mat (Kbm)'),title('d')
subplot(2,2,2)
surf(x1, x2, y1),xlabel('Mass ratio (x1) '),ylabel('Voltage ratio
(x2)'),zlabel('Constant of Battery Mat (Kbm)'),title('b')
```

Appendix H5: MATLAB script for optimization of coefficient associated to electrolyte-kind material, K_E

```
x3=0:0.05:1;x4=x3.^2;x3a=0:0.1:1;x4a=0:0.1:1;
x_3=0:0.015:0.3;
x_4=0:0.025:0.5;
y=meshgrid(x_4.*(x_3.^2).^-1);
[y2]=meshgrid(x4a.*(x3a.^2).^-1);
subplot(2,2,2)
surf(x4a, x3a, y2),xlabel('Voltage ratio (x3)'),ylabel('Capacitance ratio
(x4)'),zlabel('Electrolyte Mat. constant (KE)'),title('b')
subplot(2,2,3)
surf(x3a, x4a, y2),ylabel('Voltage ratio (x3)'),xlabel('Capacitance ratio
(x4)'),zlabel('Electrolyte Mat. constant (KE)'),title('b')
subplot(2,2,1)
plot(x4, x3,'b'),ylabel('Voltage ratio (K3)'),xlabel('Capacitance ratio
(K4)'),title('a')
grid on
```

Appendix H6: MATLAB script for optimization of coefficient associated to electrolyte-kind material, K_E

```
k1=0:0.05:0.5;
k2=0:0.07:0.7;
k3=0.3:0.1:1;
k4=0.5:0.07142857:1;
y1=(1-k1).*(1-k2.^2);
y2=k4./k3.^2;
[y2]=meshgrid(k4.*(k3.^2).^-1);
subplot(1,2,1)
surf(k3, k4, y2),xlabel('Voltage ratio (k3)'),ylabel('Capacitance ratio
(k4)'),zlabel('Electrolyte Mat. constant (KE)'),title('a')
subplot(1,2,2)
surf(k3, k4, y2),xlabel('Voltage ratio (k3)'),ylabel('Capacitance ratio
(k4)'),zlabel('Electrolyte Mat. constant (KE)'),title('b')
```

Appendix H7: MATLAB script for determing effective electrodes thickness in supercapacitors [we]

```
alpha1=50;alpha2=0.05;wne=0.2;e=1.2;cv=400;epselon=0.25;wsp=0.05;wne0=0:0.0
01886:0.2;alpha1a=50;alpha1b=5;alpha1c=0.5;alpha1d=0.05;alpha2a=0.5;alpha2b
=0.05;alpha2c=0.005;alpha2d=0.0005;J0=0:0.11320755:12.00;ea=1.5;
alpha2s=5;alpha21=0.075;J01=0.00533;J02=0.0533;J03=0.533;J04=5.33;J05=6.50;
w1=(alpha2a*e)./(2.*J0);w2=(alpha2b*e)./(2.*J0);
w3=(alpha2c*e)./(2.*J0);w4=(alpha2d*e)./(2.*J0);
subplot(2,2,1)
plot(J0,w1,'b'),xlabel('Current density J0 (A/cm^2)'),ylabel('Effective
electrode thickness [w](cm)'),title('a'),legend('(\alpha2 = 0.5 S/c m )')
grid on
```

```
subplot(2,2,2)
plot(J0,w2,'r'),xlabel('Current density J0 (A/cm^2)'),ylabel('Effective
electrode thickness [w](cm)'),title('b'),legend('(\alpha2 = 0.05 S/c m )')
grid on
subplot(2,2,3)
plot(J0,w3,'k'),xlabel('Current density J0 (A/cm^2)'),ylabel('Effective
electrode thickness [w](cm)'),title('c'),legend('(\alpha2 = 0.005 S/c m )')
grid on
subplot(2,2,4)
plot(J0,w4,'g'),xlabel('Current density J0 (A/cm^2)'),ylabel('Effective
electrode thickness [w](cm)'),title('d'),legend('(\alpha2 = 0.0005 S/c m
)')
grid on
```

Appendix H8 : MATLAB script for determing electrodes utilization in supercapacitors [*u*]

```
alpha1=50;alpha2=0.05;wne=0.2;e=1.2;cv=400;epselon=0.25;wsp=0.05;wne0=0:0.0
01886:0.2;alpha1a=50;alpha1b=5;alpha1c=0.5;alpha1d=0.05;alpha2a=0.5;
alpha2b=0.05;alpha2c=0.005;alpha2d=0.0005;J0=0:0.11320755:12.00;ea=1.5;
J01=0.00533;J02=0.0533;J03=0.533;J04=5.33;J05=6.50;
w1=(alpha2a*e)./(2.*J0);
w2=(alpha2b*e)./(2.*J0);
w3=(alpha2c*e)./(2.*J0);
w4=(alpha2d*e)./(2.*J0);
J01a=[0.1132 0.2264 0.4528 0.566 1.0 1.5 2.0 3.0 4.0 5.0 6.0 7.0 8.0 9.0
10.0 11.0 12.0];
w1b=[13.25 6.625 3.3125 2.65 1.5 1.0 0.75 0.50 0.37 0.30 0.25 0.215 0.19
0.165 0.15 0.135 0.126];
w2b=[1.325 0.6625 0.33125 0.265 0.15 0.10 0.075 0.050 0.037 0.030 0.025
0.0215 0.019 0.0165 0.015 0.0135 0.0126];
w3b=[0.1325 0.06625 0.033125 0.0265 0.015 0.010 0.0075 0.0050 0.0037 0.0030
0.0025 0.00215 0.0019 0.00165 0.0015 0.00135 0.00126];
w4b=[0.01325 0.006625 0.0033125 0.00265 0.0015 0.0010 0.00075 0.00050
0.00037 0.00030 0.00025 0.000215 0.00019 0.000165 0.00015 0.000135
0.000126];
u1=w1b*100;
u2=w2b*100;
u3=w3b*100;
u4=w4b*100;
subplot(2,2,1)
plot(J01a,u1,'b'),xlabel('Current density J0 (A/cm^2)'),ylabel('Electrode
utilization, u (%)'),title('a'),legend('(\alpha2 = 0.5 S/c m )')
grid on
subplot(2,2,2)
plot(J01a,u2,'r'),xlabel('Current density J0 (A/cm^2)'),ylabel('Electrode
utilization, u (%)'),title('b'),legend('(\alpha2 = 0.05 S/c m )')
grid on
subplot(2,2,3)
plot(J01a,u3,'k'),xlabel('Current density J0 (A/cm^2)'),ylabel('Electrode
utilization, u (%)'),title('c'),legend('(\alpha2 = 0.005 S/c m )')
grid on
subplot(2,2,4)
plot(J01a,u4,'g'),xlabel('Current density J0 (A/cm^2)'),ylabel('Electrode
utilization, u (%)'),title('d'),legend('(\alpha2 = 0.0005 S/c m )')
grid on
```